Le rôle de la SUMOylation dans la différenciation du cortex surrénalien

Damien Dufour

UNIVERSITÉ Clermont Auvergne

ECOLE DOCTORALE SCIENCES DE LA VIE, SANTE, AGRONOMIE, ENVIRONNEMENT

Thèse présentée à l'Université Clermont Auvergne

Pour l'obtention du grade de

DOCTEUR D'UNIVERSITE

Spécialité : Biologie Santé

Présentée et soutenue publiquement par

Damien DUFOUR

le 23/09/2022

Le rôle de la SUMOylation dans la différenciation du cortex surrénalien

---

Rapporteurs:

Pr. Jérôme BERTHERAT	Institut Cochin
Pr. Pierre CHYMKOWITCH	Université d'Oslo
Dr. Valérie LALLEMAND-BREITENBACH	Collège de France

Examinateurs:

Dr. Mathilde BONNET	Université Clermont Auvergne
Dr. Estelle LOUISET	Université de Rouen

Directeur de thèse:

Antoine MARTINEZ	*i*GReD Clermont-Ferrand

Institut GReD - Université Clermont Auvergne UMR CNRS 6293 INSERM U1103
Équipe Physiopathologie moléculaire de la surrénale & des tissus endocrines

Je tiens à exprimer toute ma reconnaissance au Professeur Jérôme Bertherat, au Professeur Pierre Chymkowitch et au Docteur Valérie Lallemand-Breitenbach pour m'avoir fait l'honneur de juger ce travail et je remercie très sincèrement les Docteurs Mathilde Bonnet et Estelle Louiset d'avoir accepté de faire partie de ce jury.

Ce travail de thèse a été réalisé sous la direction du Dr Antoine Martinez dans l'équipe « Physiopathologie moléculaire de la surrénale & des tissus endocrines» au sein de l'institut Génétique, Reproduction et Développement (*i*GReD) de Clermont-Ferrand, unité mixte de recherche Université Clermont Auvergne CNRS 6293 INSERM U1103. Les trois premières années de thèse ont été financées par le Ministère de l'Enseignement Supérieur, de la Recherche et de l'Innovation. L'obtention d'aides individuelles de l'école doctorale Sciences Vie Santé, Agronomie et Environnement de l'université Clermont Auvergne et de la société Française d'Endocrinologie a permis la poursuite des travaux de recherche au cours d'une quatrième année de thèse.

L'obtention de certains résultats présentés dans ce manuscrit a été le fruit de collaborations établies avec :

Le Dr David T. Breault (Boston Children's Hospital, Boston, Etats-Unis) pour l'obtention de la lignée AS^{Cre}

Le Dr Edward T.H. Yeh (University of Arkansas for Medical Science, Little Rock, Etats-Unis) pour l'obtention de la lignée $Senp2^{fl/fl}$

Le Pr Eric Pussard (Hopital de Kremlin-Bicêtre, France) pour les dosages en spectrométrie de masse

Le Dr Guillaume Bossis (Institut de Génétique Moléculaire de Montpellier, France) pour les anticorps SUMO et les conseils méthodologiques

Les Dr Françoise Muscatelli et Clément Menuet (Institut de Neurobiologie de Méditerranée, Marseille, France) pour l'obtention des échantillons de souris *Ndn-KO* et *Ndn/Magel2-dKO*

Liste des communications

Une partie de ces travaux a été présentée aux congrès suivants :

Communications orales à des congrès ou conférences avec comité de lecture :

Society of Experimental Biology's annual conference Satellite - SUMO modification in cell signalling, Montpellier, le 4 juillet 2022
Loss of SUMO-specific protease 2 blocks adrenocortex transdifferentiation

24e European Congress of Endocrinology, Milan, le 24 Mai 2022
Loss of SUMO-specific protease 2 leads to adrenal insufficiency limited to glucocorticoids

37e congrès de la Société Française d'Endocrinologie, Le Havre, le 15 octobre 2021
L'hyperSUMOylation altère l'homéostasie post-natale du cortex surrénalien et induit un déficit isolé en glucocorticoïdes

eSymposium Nucléotides cycliques, le 31 mai 2021
La déSUMOylase Senp2 est nécessaire à la zonation du cortex surrénalien et à la réponse à l'ACTH

23es journées scientifiques de l'École Doctorale SVSAE, Clermont-Ferrand, le 15 octobre 2020
The role of SUMOylation in endocrine differentiation

36e congrès de la Société Française d'Endocrinologie, Marseille, le 6 octobre 2020
La déSUMOylase SENP2 est nécessaire à la zonation fonctionnelle du cortex surrénalien

1e réunion du projet Sex-Specs, Valrose institute, Nice, le 10 février 2020
Impact of cortex hyperSUMOylation in the conversion of zG to zF identity

Réseau CARNEY, 5e réunion du projet DevMiCar, GReD institute, Clermont-Ferrand, le 26 septembre 2019
The SUMO isopeptidase SENP2 controls the setting-up of zona fasciculata & alters stress response

Réseau COMETE Bio, 27e réunion plénière, Cochin Institute, Paris, le 28 juin 2019
SUMO's weight in adrenal homeostasis: glucocorticoid insufficiency and bypass

Réseau CARNEY, 4e réunion du projet DevMiCar, Cochin Institute, Paris, le 16 novembre 2018
Invalidation of the SUMO-specific protease SENP2 impairs zona fasciculata differentiation & maintenance leading to isolated glucocorticoid deficiency

Liste des articles

Une partie de ces travaux fait l'objet d'articles en cours de publication :

Article 1 (soumis à Nature Communications)

Dufour, D., Dumontet, T., Sahut-Barnola, I., Onzon, M., Pussard, E., Wilmouth, J., Olabe, J., Lucas, C., Levasseur, A., Pointud, J.-C., Roucher-Boulez, F., Tauveron, I., Bossis, G., Yeh, E.T.H, Breault, D.T., Val, P., Lefrançois-Martinez, A.-M. and Martinez, A. (2022). Loss of SUMO-specific protease 2 causes isolated glucocorticoid deficiency by blocking adrenal cortex zonal transdifferentiation.

Article 2 (en préparation)

Dufour, D., Menuet, C., Muscatelli, F., Val, P., Lefrançois-Martinez, A.-M. and Martinez, A. (2022). Prader-Willi syndrome proteins NECDIN and MAGEL2 are implicated in hypothalamic-pituitary-adrenal axis regulation.

Contributions présentées en annexes

Wilmouth, J., Olabe, J., Garcia-Garcia, D., Lucas C., Guiton, R., Roucher-Boulez, F, **Dufour, D.**, et al. (2022) Sexually dimorphic activation of innate antitumour immunity prevents adrenocortical carcinoma development. (Preprint sur BioRxiv)

Sahut-Barnola, I., Lefrancois-Martinez, A.-M., **Dufour, D.**, Botto, J.M., Kamilaris, C., Faucz, F.R., Stratakis, C.A., Val, P., and Martinez, A. (2022). Steroidogenic factor-1 lineage origin of skin lesions in Carney complex syndrome. Journal of Investigative Dermatology S0022202X22003773.

Djari, C., Sahut-Barnola, I., Septier, A., Plotton, I., Montanier, N., **Dufour, D.**, Levasseur, A., Wilmouth, J., Pointud, J.-C., Faucz, F.R., et al. (2021). Protein kinase A drives paracrine crisis and WNT4-dependent testis tumor in Carney complex. Journal of Clinical Investigation 131, e146910.

Dumontet, T., Sahut-Barnola, I., **Dufour, D.**, Lefrançois-Martinez, A., Berthon, A., Montanier, N., Ragazzon, B., Djari, C., Pointud, J., Roucher-Boulez, F., et al. (2019). Hormonal and spatial control of SUMOylation in the human and mouse adrenal cortex. FASEB j. 33, 10218–10230.

Ishaq, A.#, **Dufour, D.#**, Cameron, K., von Zglinicki, T., and Saretzki, G. (2018). Metabolic memory of dietary restriction ameliorates DNA damage and adipocyte size in mouse visceral adipose tissue. Experimental Gerontology 113, 228–236. #Co-auteurs

RESUME

Le cortex surrénalien, au centre de la réponse au stress, synthétise les corticostéroïdes essentiels pour l'homéostasie hydrominérale et métabolique. Chez la souris, il est organisé en deux zones concentriques : la zone glomérulée (zG) et la zone fasciculée (zF), issues de progéniteurs situés dans et sous la capsule. Le renouvellement centripète et le maintien de la zonation corticale sont sous la dépendance d'un équilibre entre les voies de signalisation WNT/β-caténine et ACTH/PKA qui permettent le recrutement et la différenciation des progéniteurs.

La SUMOylation est une modification post-traductionnelle des protéines particulièrement dynamique permettant de réguler finement la fonction de protéines impliquées dans la réponse au stress cellulaire, la différenciation et l'ontogénèse tissulaire. Dans le cortex surrénalien, la SUMOylation suit un gradient inversement corrélé au stade de différenciation des cellules, ce qui pose la question de son rôle dans la zonation fonctionnelle du cortex et dans la réponse au stress. Etant donné que la signalisation ACTH/PKA induit la surexpression de la déSUMOylase SENP2, nous avons généré un modèle d'invalidation de SENP2 spécifiquement dans la surrénale. Deux modèles ont été développés, l'un ciblant toutes les cellules du cortex pendant la vie embryonnaire (*Sf1-cre::Senp2*$^{fl/fl}$) et l'autre le cortex post-natal (*AS*^{cre}*::Senp2*$^{fl/fl}$).

L'inactivation de SENP2 dans les cellules stéroïdogènes provoque une atrophie majeure de la zone fasciculée, une perte de réponse à l'ACTH et une insuffisance en glucocorticoïdes isolée. Les mécanismes qui sous tendent ces effets mettent en jeu une dérégulation de la balance entre les signalisations WNT/β-caténine et ACTH/PKA en réprimant l'activité kinase de la PKA et en promouvant l'activation ectopique de la β-caténine. Ceci se traduit par une impossibilité pour les cellules glomérulées de se transdifférencier en cellules fasciculées et favorise l'apoptose à la jonction de ces deux zones. Nos données suggèrent que la SUMOylation est un acteur capital de l'homéostasie de la glande et de la réponse au stress.

La perte de SENP2 induit également une accumulation des transcrits codant NECDIN et MAGEL2, deux protéines impliquées dans étiologie du syndrome de Prader-Willi. Nous avons montré que NECDIN est exprimée dans la zone glomérulée et réprimée transcriptionnellement par l'ACTH suggérant un rôle dans la réponse au stress. Pour explorer le rôle de ces deux protéines, nous avons étudier le statut d'activation de l'axe hypothalamo-hypophysaire-surrénalien dans des souris invalidés pour NECDIN et MAGEL2 (*Ndn/Magel2-KO*). Ces dernières répondent moins bien au stress que les sauvages et possèdent une accumulation des transcrits *Pomc*, le précurseur de l'ACTH, dans l'hypophyse. Cette accumulation laisse penser que NDN/MAGEL2 pourraient exercer un rôle dans la maturation de l'ACTH et le contrôle de la réponse au stress.

ABSTRACT

The adrenal cortex, the endocrine centre of the stress response, produces corticosteroids essential for hydromineral and metabolic homeostasis. It is organised, in mice, in two concentric layers. The *zona glomerulosa* (zG) and *fasciculata* (zF), renewed from progenitors located in the capsular periphery. Centripetal renewal and maintenance of cortical zonation are dependant of a balance between WNT/β-catenin and ACTH/PKA signalling pathways. They provide recruitment and consecutive differentiation of progenitors into zG and zF.

SUMOylation is a dynamic posttranslational modification, that provides fine-tuning of protein function involved in cellular response to stress, differentiation, and tissue development. In the adrenal cortex, the SUMOylation gradient is inversely correlated with the differentiation flow. This raises the question of its role on functional zonation and stress response. Considering that SUMO-specific protease 2 (SENP2), a deSUMOylating enzyme, is upregulated by ACTH/PKA signalling, we generated mice with adrenal-specific SENP2 invalidation. We compared two models of embryonnic (*Sf1-cre::Senp2*$^{fl/fl}$) and post-natal (*AS*^{cre}*::Senp2*$^{fl/fl}$) deletion of SENP2 to decipher the effects happening before and after birth.

SENP2 activity disruption in steroidogenic cells leads to specific hypoplasia of the *zona fasciculata*, blunted cortical ACTH responsiveness and isolated glucocorticoid deficiency. Mechanistically, overSUMOylation upon SENP2 loss shifts the balance between ACTH/PKA and WNT/β-catenin antagonistic pathways by repressing PKA catalytic activity and promoting ectopic β-catenin activation. This results in blocking the ability of *zona glomerulosa* cells to transdifferentiate into *fasciculata* and sensitises the latter to premature apoptosis happening between the two zones. Our findings suggest that the SUMO pathway is instrumental for adrenal zone homeostasis and stress response.

Loss of SENP2 also leads to an increase in Prader-Willi imprinted genes NDN and MAGEL2. We demonstrated that NECDIN is expressed in the *zona glomerulosa* and transcriptionnaly repressed by ACTH suggesting a role in stress response. To unravel the effects of those proteins in this context, we explored HPA-axis status of *Ndn/Magel2-KO* mice. They showed blunted stress response and accumulation of ACTH precursor *Pomc* in the pituitary, suggesting a role of NDN/MAGEL2 in ACTH maturation and proper stress adaptation.

ABREVIATIONS

ACE : *Angiotensin Converting Enzyme*

ACTH : *AdrenoCorticoTropic Hormone*

ADN : Acide DésoxyriboNucléique

AGP : Primordium AdrénoGonadique

AKAP : *A-Kinase Anchor Proteins*

AKR1B7 : Aldose Keto Reductase B7

AMH : hormone anti-mullérienne

AMPc : Adénosine monophosphate cyclique

AngII : Angiotensine II

APC : *Adenomatosis Polyposis Coli*

ApoA : Apolipoprotéine A

ARIP4 : *Androgen Receptor-Interacting Protein 4*

ARN : Acide RiboNucléique

ATF3 : *cAMP-dependent Transcription Factor 3*

ATP : Adénosine TriPhosphate

BAT : *Brown Adipose Tissue*

BDNF : *Brain-Derived Neurotrophic Factor*

BMP : *Bone Morphogenetic Protein*

CAI : *Central Adrenal Insufficiency*

CaMK : Ca^{2+}*/CalModulin-dependent protein Kinase*

CCDC80 : *Coiled-Coil Domain Containing 80*

CB1 : *Cannabinoid receptor type 1*

CBX4 : *ChromoBoX homolog 4 (Pc2)*

CDK7 : *Cyclin-Dependent Kinase 7*

C/EBP : *CCAAT/Enhancer-Binding Protein*

CITED2 : *CBP/p300 Interacting Transactivator with ED-rich tail 2*

CK1 : Caséine Kinase 1

CLP : *Common Lymphoid Protein*

CMP : *Common Myeloid Protein*

COPII : *Coat Protein Complex II*

COS-1 : *CV-1 (simian) in Origin, and carrying the SV40 genetic material cells*

COUPTF : *Chicken Ovalbumin Upstream Promoter Transcription Factor (NR2F2)*

CREB : *cAMP Response Element-Binding protein*

CRH : *Corticotropin Releasing Hormone*

CRHR1 : *CRH Receptor 1*

CRM1 : *Chromosomal Maintenance 1 (Exportin 1)*

DAB2 : *Disabled2*

DAX-1 : *Dose sensitive sex reversal, Adrenal hypoplasia congenital critical region on the X chromosome, gene 1 (NR0B1)*

DBH : Dopamine β-Hydroxylase

DeSI : *DeSUMOylating Isopeptidase 1*

DHEAS : DeHydroEpiAndrosterone Sulfate

DHH : *Desert HedgeHog*

DLK1 : *Delta Homolog 1 (PREF-1)*

DNMT : *DNA Methyl Transferase*

DOC : DéOxyCorticostérone

DPPA : *Developmental Pluripotency Associated*

DRP1 : *Dynamin Related Protein 1*

DUX : *DoUble homeoboX protein*

DVL : *Dishevelled*

EGR2 : *Early Growth Response protein 2*

EPAC : *Exchange Protein Activated by CAMP*

EPO : ErythroPOïétine

ERK : *Extracellular signal-Regulated Kinase*

ESC : *Embryonnic Stem Cell*

FAdE : *Fetal Adrenal Enhancer*

FGD : *Familial Glucocorticoid Deficiency*

FGF : *Fibroblast Growth Factor*

FGFR : *FGF Receptor*

FKBP5 : *FK506 Binding Protein 5*

FOXL2 : *Forkhead bOX L2*

FOXM1 : *Forkhead bOX M1*

FOXP3 : *Forkhead bOX P3*

GATA4/6

GC : GlucoCorticoïde

GDP : Guanosine DiPhosphate

GED : *GTPase effector domain*

GNAS : *Guanine Nucleotide binding protein, Alpha Stimulating activity polypeptide*

GLI1 : *GLIoma-associated oncogene 1*

GPL1 : *Glucagon-like peptide 1*

GR : *Glucocorticoid Receptor (NR3C1)*

GSK3β : *Glycogen synthase kinase 3 β*

GTP : Guanosine TriPhosphate

H3K9me3 : Lysine 9 de l'histone 3 triméthylée

HDL : *High Density Lipoprotein*

HDST : *High Dose Synacthene Test*

HEK293 : *Human Embryonnic Kidney cell line 293*

HIF1-α : *Hypoxia-inducible factor 1-a*

HMG-CoA : β-Hydroxy β-methylglutaryl-CoA

HP1 : *Hetereochromatin Protein 1*

HPA : *Hypothalamo-Pituitary Axis*

HSC : *Hematopoietic Stem Cell*

HSL : *Hormone Sensitive-neutral Lipase*

HSP70/90 : *Heat Shock Protein*

IHH : *Indian HedgeHog*

IMM : *Inner mitochondrial membrane*

INHα : Inhibine α

INSIG : *INSulin-Induced Gene protein*

ITT : *Insulin Tolerance Test*

KLF : Krüppel-Like Factor

LAMB1 : LAMinine B1

LDL : *Low Density Lipoprotein*

LDL-R : *LDL Receptor*

LDST : *Low Dose Synacthene Test*

LEF : *Lymphoid Enhancer-binding Factor 1*

LGR : *Leucine-rich repeat-containing G-protein coupled Receptor*

LINC : *Linker of Nucleoskeleton and Cytoskeleton*

MAGE : *Melanoma Antigen GEne*

MAM : *Mitochondria-Associated Membrane*

MAPK : *Mitogen-Activated Protein Kinase*

MAPL : *Mitochondrial E3 ubiquitin Protein Ligase 1*

MC2R : *MelaCortin-2 Receptor*

MDM2 : *Mouse Double Minute 2 homolog*

MEF : *Mouse Embryonnic Factor*

MFF : *Mitochondrial Fission Factor*

MFN : MitoFusiNe

MHD : *MAGE Homology Domain*

MKRN3 : *MaKorin Ring finger proteiN 3*

MR : *Mineralocorticoid Receptor (NR3C2)*

MRAP : *Melanocortin 2 Receptor Accessory Protein*

mTOR : *mouse Target Of Rapamycin*

NBRE : *NGFI-β Response Element*

NECDIN : *Neurally differentiated EC cell-Derived proteIN*

NESTIN : *NeuroEpithelial STem cell proteIN*

NES : *Nuclear Export Signal*

NLS : *Nuclear Localisation Signal*

NNT : *Nicotinamide Nucleotide Transhydrogenase*

NPAP1 : *Nuclear Pore Associated Protein 1*

NPC : *Nuclear Pore Complex*

NPC1L1 : *Niemann-Pick disease C1 Like 1*

NRIP1 : *Nuclear Receptor-Interacting Protein 1*

NURR1 : *NUclear Receptor related-1 protein (NR4A2)*

NUR77 : *NUclear Receptor 77 (NR4A1)*

OCT3/4 : *OCTamer-binding transcription factor 3/4*

OMM : *Outer Mitochondrial Membrane*

OMT : *Overnight Metyrapone Test*

OPA1 : *OPtic Atrophy protein 1*

PC1/3 : Prohormone Convertase 1/3

Pc2 : *Polycomb 2 Homolog (CBX4)*

PCSK : *Proprotein Convertase Subtilisin Kexin*

PDE : Phosphodiestérase

PI3K : PhosphoInositide 3-Kinase

PIAS : *Protein Inhibitor of Activatated STAT*

PKA : Protéine Kinase A

PLA : *Proximity Ligation Assay*

PLC : PhosphoLipase C

PML : *ProMyelocytic Leukemia*

PMSG : *Pregnant Mare's Serum Gonadotropin*

PNMT : *Phénylethanolamine-N-MethylTransferase*

PPNAD : *Primary Pigmented Nodular Adrenal Disease*

POMC : ProOpioMélanoCortine

PP2A : Protéine Phosphatase 2A

PPARγ : *Peroxisome Proliferator-Activated Receptor γ*

PRC2 : *Polycomb Repressive Complex 2*

PREF1 : *PREadipocyte Factor 1*

PWS : *Prader-Willi Syndrome*

RanBP2 : *Ran Binding Protein 2*

RanGAP1 : *Ran GTPase-Activating Protein 1*

RE : Réticulum Endoplasmique

RNF4/111 : *Ring Finger Protein 4/111*

ROS : *Reactive Oxygen Species*

RSPO3 : *R-SPOndin 3*

S1P : *Site-1 Protease*

S2P : *Site-2 Protease*

SAE1 : *SUMO Activating Enzyme 1*

SAM : *Site of Alterned Modification*

SCAP : *SREBP Cleavage-Activating Protein*

SENP : *SENtrin Protease*

SF1 : *Steroidogenic Factor 1 (NR5A1)*

SFRP2 : *Secreted Frizzled-Related Protein 2*

SHH : *Sonic HedgeHog*

SIM : *SUMO Interacting Motif*

SNAP25 : *Synaptosomal-Associated Protein of 25 kDa*

SNARE : *Soluble N-ethylmaleimide-sensitive-factor Attachement protein REceptor*

SNRPN : *Small Nuclear RiboNucleoProtein N*

SNURF : *Small NUclear Ring Finger*

SOX2/9 : *SRY-bOX transcription Factor 2/9*

SRA : Système Rénine-Angiotensine

SR-B1 : *Scavenger Receptor class B type 1*

SREBP : *Sterol Regulatory Element Binding Protein*

StAR : *Steroidogenic Acute Regulatory protein*

STUbL : *SUMO Targeted Ubiquitine Ligase*

STX5 : *Syntaxin-5*

SUMO : *Small Ubiquitin-Like Modifier*

SUV39H1 : *SUppressor of Variegation 3-9 Homolog 1*

TASK1 : *TWIK-related Acid Sensitive* K^+

TBL1 : *Transducin β-Like protein 1*

TBLR1 : *TBL1 Receptor*

TCF7 : *Transcription Factor 7*

TGF-β : *Transforming Growth Factor β*

TH : Tyrosine Hydroxylase

TOPORS : *TOP1 Binding Arginine/Serine Rich Protein, E3 Ubiquitin Ligase*

TRIM : *TRIpartite Motif containing*

TSPO : *TranSlocator Protein*

UCP1 : *UnCoupling Protein 1*

UBA2 : *Ubiquitin-like Activating protein 1*

UBC9 : *Ubiquitin Carrier protein 9*

USPL1 : *Ubiquitin Specific Peptidase Like 1*

WAT : *White Adipose Tissue*

WNT : *Wingless-related integration site*

WT1 : *Wilm's Tumour 1*

WWOX : *WW domain-containing OXidoreductase*

YAP : *Yes-Associated Protein 1*

zG : zone Glomérulée

zF : zone Fasciculée

ZNRF3 : *Zinc and Ring Finger 3*

β-TRCP : *β-Transducin Repeat Containing E3 ubiquitin Protein ligase*

Sommaire

LA GLANDE SURRENALE

1 Anatomie et fonction

1.1 Un organe au coeur de la réponse au stress

Selon la tradition Hippocratique, la santé était définie par l'harmonie, en opposition à la maladie qui se traduisait par une perte d'équilibre (Valles, 2020). De manière générale, la vue qui prédominait durant la Grèce antique était que la vie, les écosystèmes et, les organismes eux mêmes étaient régis par un équilibre entre des forces qui se repoussent et se neutralisent. Les travaux de Claude Bernard et Walter Cannon au 19e siècle, ont permis de théoriser le concept d'homéostasie : le maintien de l'état basal du corps (Le Moal, 2007).

C'est en se basant sur ces concepts, que Hans Selye décrivit, en 1936 le stress comme le résultat non spécifique d'une demande aiguë au corps, qui peut avoir des effets somatiques ou mentaux et dont la nature importe peu. Il divise son syndrome en trois phase : la phase d'alerte, l'adaptation et la phase d'épuisement où le corps ne peut plus adapter son fonctionnement aux *stimuli* (Selye, 1936).

Désormais, le stress peut être défini comme la perception de l'individu face à un élément physiquement ou émotionnellement perturbant tandis que l'ensemble des adaptations mises en place pour répondre à ce *stimulus* et maintenir l'homéostasie est appelée allostasie (Joels et al., 2007).

Chez l'Homme, cette adaptation engage principalement deux systèmes : le système sympatho-médullaire et l'axe hypothalamo-hypophysaire-surrénalien. Lors d'un élément perçu comme stressant par le cortex préfrontal, l'information transite directement par voie nerveuse jusqu'à la medullo-surrénale qui produit de l'adrénaline et de la noradrénaline afin de répondre de façon la plus rapide possible au stresseur. Ces catécholamines permettent à l'individu de réagir vite et d'éliminer le stresseur *via* une réponse dite

"fight or flight" [1].

Parallèlement, l'hypothalamus produit du CRH, induisant une réponse comportementale *via* des connexions avec l'amygdale et le *locus coereleus*, et induisant la sécrétion d'ACTH par l'hypophyse. L'ACTH transite *via* la circulation sanguine pour induire une stimulation du cortex surrénalien enclenchant la production de corticostéroïdes [2]. Le rôle de ces stéroïdes est l'adaptation du corps au stresseurs notamment grâce à la mobilisation de nutriments dans la circulation sanguine [3].

Les surrénales sont ainsi le centre effecteur de la réponse au stress ce qui les rend nécessaires à la vie de l'individu et à la capacité d'adaptation de l'espèce. En effet, le koala (*Phascolarctos cinereus*) qui a évolué dans un environnement sans prédateur possède des glandes surrénales vestigiales et atteint un état de choc lorsqu'il rentre en contact avec un être humain (Marik and Levitov, 2010).

[1] voir paragraphe 1.3.1 - Production de catécholamines par la médulla
[2] voir paragraphe 1.3.3.4 - Régulation de la stéroïdogénèse fasciculée
[3] voir paragraphe 1.3.3.3 - Effets physiologique des glucocorticoïdes

1.2 Anatomie et histologie de la glande

Les surrénales sont de petites glandes paires endocrines situées juste au dessus des reins. Elles ont pour la première fois été décrites par Bartholomeo Eustachio en 1563 dans la *Tabula Anatomicae* publiée en 1714 (Eustachio B, 1714) (Figure 1). Elles sont composées de deux tissus, la médullo-surrénale au centre et le cortex surrénalien en périphérie, lui même entouré d'une capsule fibroblastique.

La médulla est composée de cellules chromaffines (productrices de catécholamines), ganglionnaires et des cellules sustentaculaires qui ont une morphologie similaires aux cellules gliales mais dont on ignore le rôle (Bechmann et al., 2021).

Le cortex est principalement composé de cellules stéroïdogènes. Il est divisé en deux zones chez la souris : la zone glomérulée en périphérie et la zone fasciculée plus interne (Figure 2).

La zone glomérulée se caractérise par la présence de cellules qui possèdent un cytoplasme relativement petit et basophile. Elles sont organisées en rosettes, structures principalement retrouvées au cours du développement, se caractérisant par 5 cellules ou plus qui se rejoignent en un point unique (Harding et al., 2014). Les cellules glomérulées se distinguent par l'expression de marqueurs tels que DAB2 (Romero et al., 2007) et $G\alpha_q$ dans leur cytoplasme, β-caténine à leur membrane et Lamb1 à l'extérieur des rosettes (Leng et al., 2020).

Au sein de la zone fasciculée, les cellules sont organisées en cordons de façon parallèle à l'axe diamétrale. Elles possèdent un cytoplasme développé et fortement éosinophile, témoin de la présence de nombreuses mitochondries. Moléculairement, elles se caractérisent par l'expression de CYP11B1 et AKR1B7. Enfin, chez l'être humain, le gorille, le chimpanzé et le bonobo, on peut distinguer une troisième zone, la zone réticulée, qui apparaît au cours de la période prépubertaire, lors de l'adrénarche (Campbell, 2020).

Cette zonation est soutenue par la vascularisation du cortex très riche pour la taille de la glande. Les artérioles issues de artère phrénique inférieure, de l'artère rénale ou

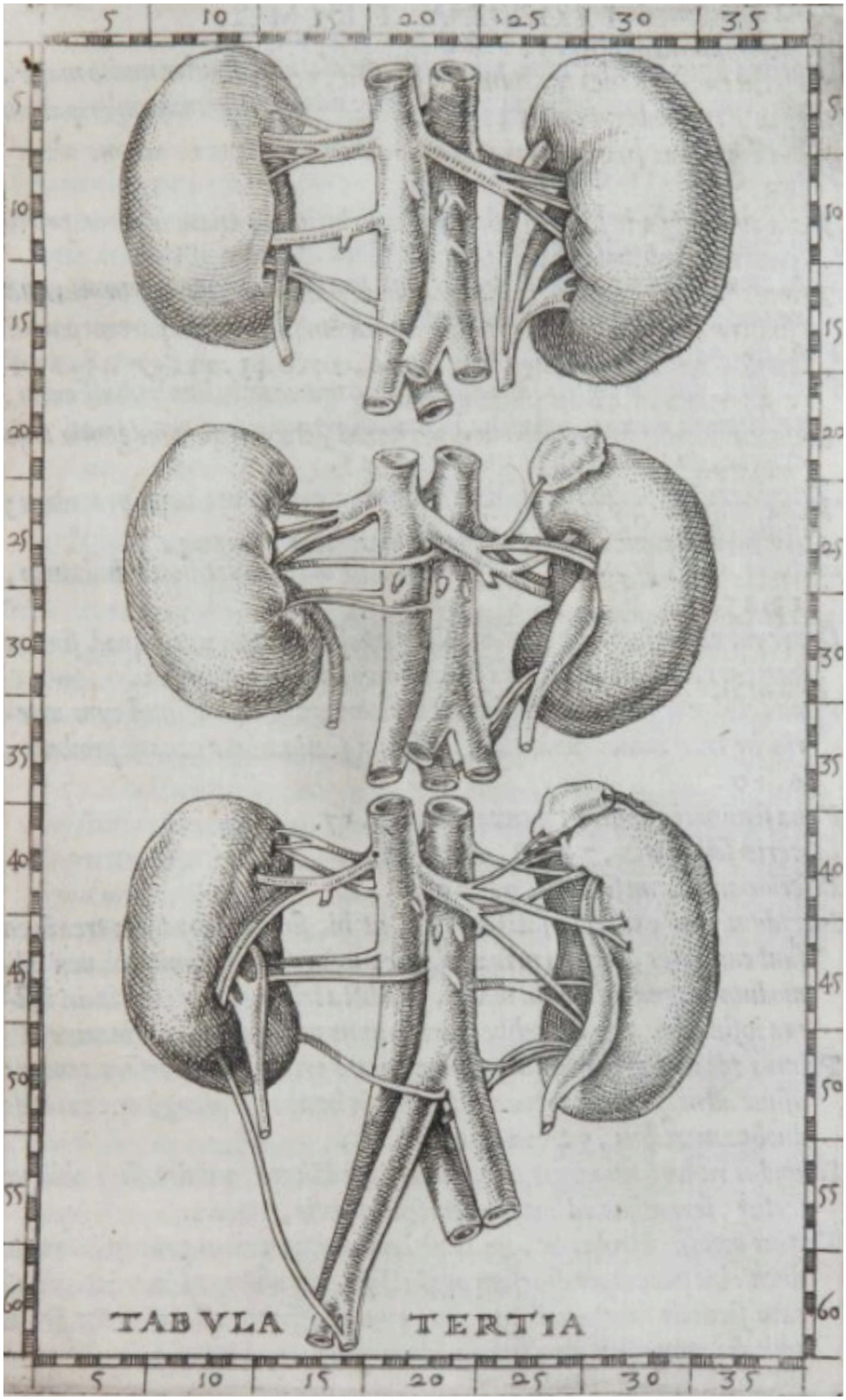

Figure 1: **Dessin original des glandes surrénales issu de la Tabula Anatomicae**

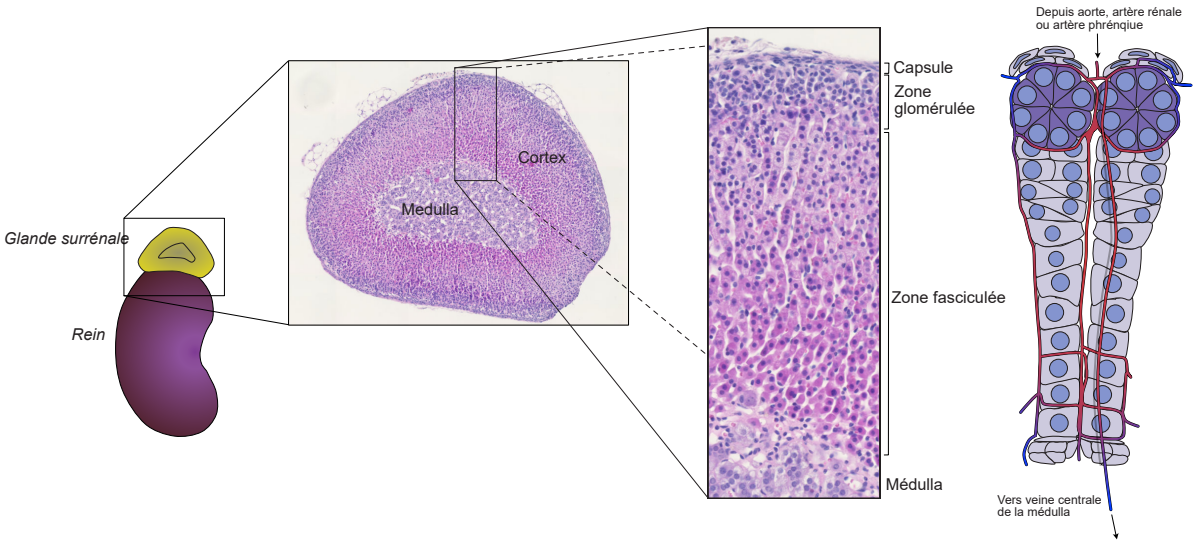

Figure 2: **Localisation, structure histologique et vascularisation de la glande surrénale**

de l'aorte se rejoignent au niveau du plexus sous-capsulaire. Des branches issues de ce plexus, s'enroulent autour des glomérules sans les pénétrer puis plongent le long des colonnes de cellules fasciculées pour créer un réseau de capillaires dans le cortex profond et entrer dans la médulla. D'autres branches issues du plexus sous capsulaire longent la capsule pour l'alimenter en oxygène ou vont directement dans la médulla (Figure 2). Ces deux sources de sang pour la médulla permettent l'apport de glucocorticoïdes aux cellules chromaffines d'une part [4] et l'apport de sang riche en oxygène d'autre part. Le sang est drainé jusqu'à la veine centrale dans la médulla qui se jette dans la veine rénale gauche ou la veine cave à droite (Inomata and Sasano, 2015).

Les cellules stéroïdogènes cohabitent avec un microenvironnement complexe composé de cellules immunitaires (Lopez et al., 2021a) qui vont coordonner la fonction surrénalienne:

- les mastocytes présents au niveau de la zone glomérulée contrôlent la production d'aldostérone *via* la production de sérotonine.
- les macrophages présents dans le cortex surrénalien assurent la clairance des cellules apoptotiques et jouent un rôle dans l'homéostasie lipidique (Dolfi et al., 2022)
- les lymphocytes auraient un impact sur la régulation de l'activité stéroïdogène et

[4] voir paragraphe 1.3.3.3 - Effets physiologique des glucocorticoïdes

l'élimination de cellules corticales

Enfin, un réseau de fibres nerveuse provenant de la médulla ou de ganglions ortho- et parasympathiques innervent le cortex. Une partie de ces fibres produit de la substance-P qui est capable de stimuler la production d'aldostérone, probablement en agissant directement sur les cellules glomérulées (Hinson et al., 1994; Wils et al., 2020)

1.3 Activité endocrine

1.3.1 Production de catécholamines par la médulla

Lors d'un stress aiguë, l'activation du système orthosympathique amène, *via* les nerfs splanchniques au relargage d'acétylcholine qui induit l'entrée de Ca^{2+} dans les cellules chromaffines et la libération d'adrénaline et de noradrénaline dans la circulation. Ces catécholamines sont produites à partir de tyrosine, qui est hydroxylée sous l'action de la tyrosine hydroxylase (TH) en L-DOPA que la L-DOPA-carboxylase convertit en dopamine. La dopamine est ensuite prise en charge par la dopamine-β-hydroxylase (DBH) et la phenyléthanolamine-N-méthyltransferase (PNMT) pour produire successivement de la noradrénaline et de l'adrénaline.

Celles-ci agissent sur une variété de tissus assurant la réponse rapide au stress, *via* la mobilisation des récepteurs adrénergiques (Bechmann et al., 2021). L'augmentation de la tension artérielle, de la fréquence et de la force des battements cardiaques, de la perfusion des muscles et de l'ouverture des bronches sont autant de paramètres contrôlés par l'adrénaline qui permettent à l'individu d'adapter rapidement son comportement face à un éventuel danger.

1.3.2 Stéroidogénèse

La zonation histologique du cortex est le reflet d'une zonation fonctionnelle : la zone glomérulée, en périphérie, produit des minéralocorticoïdes et la zone fasciculée, plus au centre produit des glucocorticoïdes. Tandis que la zone réticulée produit des précurseurs des androgènes.

1.3.2.1 Origine du cholestérol

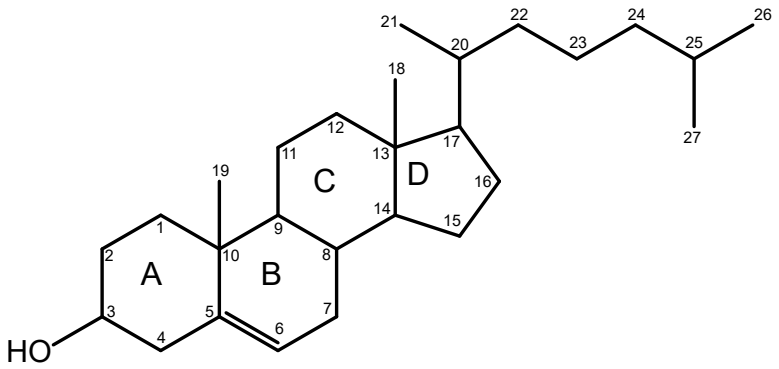

Figure 3: **Structure du cholestérol**

L'unique précurseur stéroïdien est le cholestérol, une molécule liposoluble cyclique composée de 27 carbones répartis en quatre cycles formant le noyau stérol (Figure 3). Il est stocké dans le cytoplasme avec les triglycérides sous forme de gouttelettes lipidiques ou au sein des membranes. Les concentrations de cholestérol dans la cellule dépendent en majorité de son apport exogène et de sa synthèse endogène.

- L'apport exogène

Lors d'une prise alimentaire le cholestérol est absorbé par les entérocytes principalement grâce à la protéine Niemann–Pick C1 Like 1 (NPC1L1) (Altmann et al., 2004). Le cholestérol est alors incorporé dans des lipoprotéines de haut poids moléculaires : les chylomicrons, permettant son transport *via* le système lymphatique vers la circulation sanguine au niveau de la veine sous-claviculaire. Le cholestérol est ensuite métabolisé par le foie et relargué sous forme de LDL (Low Density Lipoprotein) ou absorbé par les cellules périphériques. Celles-ci relarguent dans le sang le cholestérol en excès, qui se lie à la protéine ApoA, produite par le foie et l'intestin grêle formant des HDL (High Density Lipoprotein). Ces deux lipoprotéines possèdent leurs récepteurs respectifs : le LDL-R pour les LDL et SR-B1 (Scavenger receptor class B, type I) pour les HDL. Chez l'Homme, la grande majorité du cholestérol est transporté sous forme de LDL, à l'inverse de la souris où le cholestérol est principalement retrouvé sous forme de HDL.

- Entrée du cholestérol dans la cellule

Chez la souris, la glande surrénale dépend principalement du récepteur SR-B1. En effet, l'absence de LDL-R dans des cultures primaires de cellules corticosurrénalienne n'affecte pas leur capacité à produire de la corticostérone (Kraemer et al., 2007). Ainsi, la restauration du LDL-R spécifiquement dans les surrénales de souris déficientes pour LDL-R n'améliore pas la réponse stéroïdogénique à un stress (van der Sluis et al., 2015).

La délétion concomitante du récepteur au LDL et de la protéine ApoA [5] a permis d'explorer l'implication des LDL dans la stéroïdogénèse surrénalienne. Ces souris transportent la majorité du cholestérol dans les LDL. Contrairement aux souris sauvages, elles ne stockent pas de cholestérol dans les cellules fasciculées mais présentent une forte surexpression génique de la HMG-CoA reductase, enzyme limitante de la synthèse *de novo* du cholestérol. Cette dernière caractéristique pourrait expliquer pourquoi ces souris restent capables de répondre à un stress en dépit de l'absence de cholestérol stocké dans les cellules stéroïdogènes (Hoekstra and Van Eck, 2016).

A l'inverse, les souris dépourvues de SR-B1, uniquement dans la surrénales (Hoekstra et al., 2013) ou dans l'ensemble des cellules (Cai et al., 2008; Hoekstra et al., 2008; Rigotti et al., 1997) présentent une réponse stéroïdogénique fortement réduite lors d'un stress infectieux, thermique ou nutritionnel et ce peu importe le profil sanguin en LDL/HDL (Ito et al., 2020).

Absence de LDL-R	Stéroïdogénèse normale	Van der Luis et al., 2015; Hoekstra et al., 2016
Absence de LDL-R sauf dans surrénale	Stéroïdogénèse normale	Van der Luis et al., 2015
Absence de HDL	Stéroïdogénèse normale	Hoekstra et al., 2016; Ito et al., 2020
Absence de LDL-R et de HDL	Stéroïdogénèse normale mais pas de stockage du cholestérol dans la surrénale	Hoekstra et al., 2016
Absence de SR-B1	Déficit de réponse au stress	Rigotti et al., 1997; Hoekstra et al., 2013; Ito et al., 2020
Absence de SR-B1 uniquement dans la surrénale	Déficit de réponse au stress	Cai et al., 2008; Hoekstra et al., 2008
Absence de SR-B1 et de HDL	Déficit de réponse au stress	Ito et al., 2020

Table 1: **Tableau récapitulatif du phénotypes des modèles murins affectant le transport sanguin et l'import du cholestérol**

L'ensemble de ces résultats montrent que le principal moyen pour la surrénale d'obtenir

[5] ApoA est nécessaire à la formation des HDL et permet aux souris d'avoir un profil lipidique enrichi en LDL, similaire à celui des humains

du cholestérol est l'internalisation *via* SR-B1 des lipoprotéines peu importe leur nature (Table 1). SR-B1 permet ainsi l'import du cholestérol dans la membrane plasmique (Shen et al., 2018) qui est alors transporté dans le réticulum endoplasmique ou les gouttelettes lipidiques par les protéines ASTER (Sandhu et al., 2018) qui forment un pont entre la membrane plasmique et le réticulum endoplasmique (Besprozvannaya et al., 2018).

- Synthèse *de novo* du cholestérol

Lorsque les apports exogènes en cholestérol sont insuffisants ou dans le cas de la perte du LDL-R et des HDL chez la souris (Hoekstra and Van Eck, 2016), la cellule peut elle-même produire du cholestérol *via* la voie du mévalonate, à partir d'acétyl-CoA et d'acétoacétyl-CoA.

Cette synthèse est régulée par le facteur de transcription SREBP-1 [6] ou SREBP-2 (Sterol Regulatory Element Binding Protein), constitutivement liés à la protéine SCAP (SREBP cleavage-activating protein). Lorsque les stocks de cholestérols sont suffisants, la protéine INSIG maintient le complexe SCAP/SREBP dans la membrane du réticulum endoplasmique. Cette interaction est possible grâce à la fixation du cholestérol sur SCAP qui permet sa reconnaissance par INSIG (Xu et al., 2020; Yang et al., 2002). Lors d'une diminution du stock de cholestérol, le complexe SREBP/SCAP est transporté dans des vésicules [7], de la membrane du réticulum endoplasmique vers l'appareil de Golgi pour être clivée par les protéases S1P et S2P, permettant à la partie N-terminale de SREBP de transloquer dans le noyau (Goldstein et al., 2006). Une fois dans le noyau, il induit l'expression de gènes de la synthèse *de novo* du cholestérol comme *Hmgcr* (Espenshade and Hughes, 2007; Goldstein et al., 2006) (Figure 4). Cette dernière est l'enzyme limitante de la synthèse *de novo* du cholestérol. Elle catalyse la réaction de réduction de l'HMG-CoA (3-Hydroxy-3-Methylglutaryl Coenzyme A) issue de la condensation d'acétyl-CoA et d'acétoacétyl-CoA, en mévalonate. Le mévalonate rentre ensuite dans une cascade enzymatique aboutissant à la synthèse de cholestérol.

[6] Il existe en fait deux isoformes de SREBP-1 générées par épissage alternatif: SREBP-1c dont la forme est prédominante dans la surrénale (Shimomura et al., 1997) et SREBP-1a

[7] Ces vésicules sont formées par des complexes COPII. La capacité de SCAP à recruter ce complexe est bloquée par INSIG, empêchant ainsi le transport de SREBP vers le Golgi (Sun et al., 2007b)

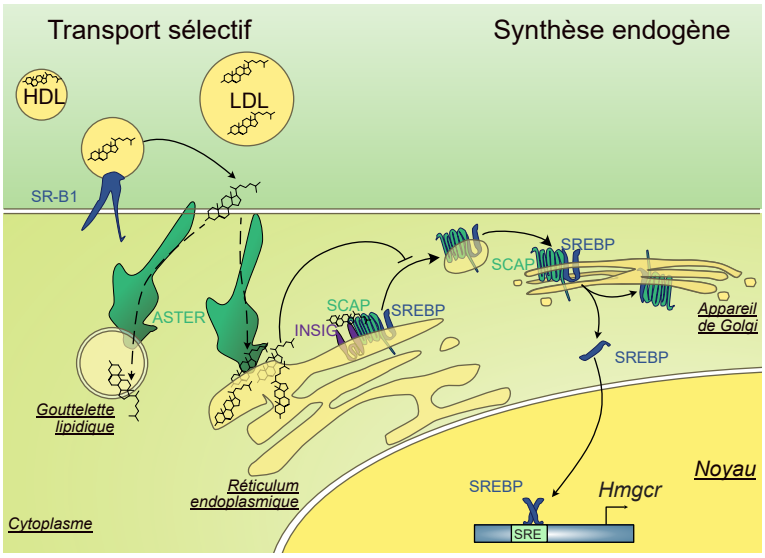

Figure 4: **Entrée du cholestérol dans la cellule**

La nécessité de la voie de synthèse *de novo* dans la stéroïdogénèse surrénalienne n'a pas été testée directement. Cependant, dans un mutant total de SREBP-1, SREBP-2 est fortement surexprimé dans le foie et y augmente la production d'acide gras et de stérol. Les taux d'ARNm codant SREBP-2 n'ont pas été mesurés dans la surrénale mais sa synthèse de cholestérol est augmentée d'un facteur 3 (Shimano et al., 1997). En outre, dans la surrénale, la synthèse *de novo* du cholestérol est stimulée en cas de stress (Hoekstra and Van Eck, 2016) ou d'activation de la PKA (Dumontet et al., 2018; Rainey et al., 1986; Wellman et al., 2021), on peut donc imaginer que dans la surrénale, la synthèse du cholestérol est un moyen de compenser un déficit de stéroïdogénèse.

1.3.2.2 Transport du cholestérol vers la mitochondrie

Pour la production de stéroïdes, le cholestérol, stocké principalement sous la forme de cholesteryl-ester dans des gouttelettes lipidiques ou dans les membranes doit être acheminé au niveau des mitochondries où auront lieu les premières étapes de la stéroïdogénèse. Le cholestérol est tout d'abord désestérifié grâce à l'action de l'hormone sensitive lipase (HSL) (Hu et al., 2010).

Le mécanisme de transport du cholestérol jusqu'à la membrane externe de la mitochondrie semblerait impliquer - au moins en partie - les protéines de la famille SNARE (Soluble

N-ethylmaleimide sensitive factor Attachment protein receptor). En effet, au sein de cette famille, les protéines α-SNAP et SNAP25 sont surexprimées suite à un traitement ACTH et interviennent dans le mouvement du cholestérol jusqu'aux mitochondries depuis les goutelettes lipidiques *in vitro* (Lin et al., 2016) tandis que STX5 et α-SNAP sont impliquées dans le transport des membranes plasmiques aux mitochondries *in vitro* (Deng et al., 2019). Les protéines ASTER, sembleraient capables de faire transiter le cholestérol du réticulum endoplasmique vers la mitochondrie au niveau de zones d'interactions entre le RE et la mitochondrie appelées MAM (mitochondria associated membranes) (Andersen et al., 2020).

Une fois au niveau de la mitochondrie, le cholestérol est transloqué de la membrane mitochondriale externe (OMM) vers la membrane mitochondriale interne (IMM) où a lieu la première étape de la stéroïdogénèse. Le cholestérol étant liposoluble, il ne peut transiter dans l'espace hydrophile séparant les deux membranes, ce qui fait de cette étape un facteur limitant de la stéroïdogénèse (Black et al., 1994). La protéine permettant ce transfert est StAR (Steroid Acute Regulatory protein) (Kallen et al., 1998).

Chez l'être humain, des mutations dans le gène codant StAR causent une hyperplasie congénitale lipoïde des surrénales (OMIM #600617) (Lin et al., 1995; Tee et al., 1995) qui consiste en l'accumulation du cholestérol dans les surrénales, associée à une forte diminution voire une absence de stéroïdes circulant. L'absence de StAR et donc de transfert du cholestérol vers la mitochondrie aboutit à une accumulation de gouttelettes lipidiques. Parallèlement, l'absence de glucocorticoïdes stimule la production d'ACTH [8] qui, exerçant un effet trophique sur la surrénale, entraîne son hyperplasie.

De façon similaire, la perte de StAR chez la souris conduit à une accumulation de gouttelettes lipidiques dans la surrénale (Caron et al., 1997; Hasegawa et al., 2000) et une incapacité à maintenir des taux de stéroïdes adéquats (Hasegawa et al., 2000; Ishii et al., 2012)

Le mécanisme exact par lequel StAR permet le transfert du cholestérol de la membrane

[8] voir paragraphe 1.3.3.4 - Régulation de la stéroïdogénèse fasciculée

externe à la membrane interne reste peu connu et est sujet à controverses notamment concernant l'implication de la protéine TSPO (Papadopoulos et al., 2018; Selvaraj et al., 2018) [9].

StAR est synthetisé sous la forme d'une protéine de 37 kDa puis clivé en une protéine de 30 kDa avant d'être adressé à la membrane externe de la mitochondrie. Des expériences de surexpression de StAR dans des cellules COS-1 mettent en exergue l'importance de sa localisation au niveau de l'OMM et le rôle secondaire de son clivage. En effet, la surexpression d'une forme adressée a la membrane interne ne stimule pas la production basale de prégnénolone par les cellules tandis que la surexpression à la membrane externe d'une forme totale ou clivée aboutit dans les deux cas à une forte induction de la stéroïdogénèse (Bose et al., 2002) (Figure 5).

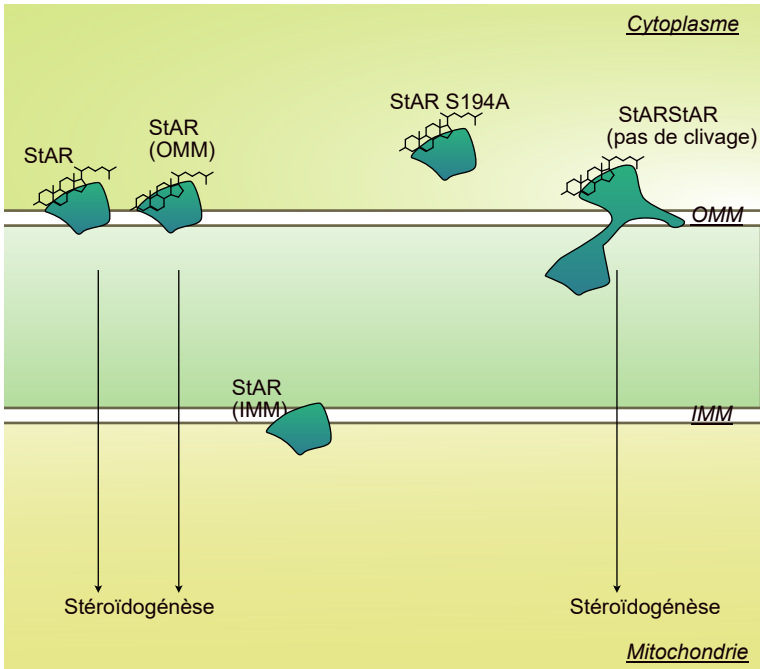

Figure 5: **Régulation de l'activité de StAR dans le transfert du cholestérol de la membrane externe (OMM) à la membrane interne (IMM) de la mitochondrie**
Seul StAR ancré à la membrane externe de la mitochondrie est capable de lier le cholestérol et d'induire la stéroïdogénèse. Sa phosphorylation n'est pas nécessaire à sa liaison au cholestérol mais est requise pour son recrutement à l'OMM. L'absence de clivage de la partie N-terminale de StAR (de 37 kDa à 30 kDa) n'a aucun effet sur son activité

L'un des leviers capitaux de la fonction de StAR est sa phosphorylation sur la sérine 194

[9]Certains résultats suggèrent que TSPO ainsi que plusieurs autres protéines mitochondriales formeraient un complexe permettant la translocation du cholestérol. Mais ces résultats sont contestés notamment car les modèles de délétion de TSPO aboutissent, selon les études, à une diminution de la stéroïdogénèse globale (Owen et al., 2017), un effet sur la corticostérone uniquement (Barron et al., 2018; Fan et al., 2015), sur la testostérone uniquement (Fan et al., 2020) ou une absence totale d'effet sur la stéroïdogénèse (Banati et al., 2014; Tu et al., 2014)

dont l'absence bloque considérablement son activité (Arakane et al., 1997; Fleury et al., 2004) et altère son recrutement à l'OMM (Duarte et al., 2014) sans modifier sa capacité de liaison au cholestérol (Baker et al., 2007). En effet, la surexpression de StAR dans des souris déficientes pour la protéine rétablit des taux de stéroïdes normaux tandis que la surexpression d'une forme mutée S194A non phosphorylable ne parvient pas à restaurer la stérodoïgénèse (Sasaki et al., 2014) (Figure 5).

1.3.2.3 Etapes de la stéroïdogénèse surrénalienne

Une fois parvenu à l'IMM, le cholestérol est clivé par le cytochrome P450 de clivage de la chaîne latérale du cholestérol (P450-SCC ou CYP11A1). Ce clivage produit d'une part de la prégnénolone et d'autre part de l'isocaproaldehyde. Ce dernier étant délétère pour les cellules surrénaliennes, est détoxifié par réduction en alcool isocaprylique suite à l'action de l'enzyme AKR1B7 (Aldose Keto Reductase B7) (Lefrançois-Martinez et al., 1999) fortement exprimée dans la zone fasciculée. La prégnénolone étant plus hydrophile que les autres stéroïdes, celle-ci diffuse passivement à travers la membrane mitochondriale pour attendre le réticulum endoplasmique (McManus et al., 2019). Là, elle y est convertie en progestérone, le premier stéroïde actif, grâce à l'action de la 3β-HSD (3β-hydroxystéroïde déshydrogénase/Δ5-Δ4 isomérase) puis en 11-deoxycorticostérone (DOC) par le P450C21 (CYP21A2 chez l'Homme, CYP21A1 chez la souris). Ce dernier possède un intérêt particulier en clinique, car *CYP21A2* est fortement sujet aux recombinaisons ce qui provoque des mutations perte de fonction avec une incidence estimée à un cas pour 5000 à 15000 naissances (Witchel, 2017). Ces mutations sont à l'origine de l'hyperplasie congénitale des surrénales CYP21-dépendante (OMIM #20190) qui se traduit par un tableau clinique similaire à l'hyperplasie lipoïde des surrénales [10] et s'accompagne en plus d'une virilisation des individus XX. [11]

[10] voir paragraphe 1.3.2.2 - Transport du cholestérol vers la mitochondrie

[11] En effet, contrairement aux rongeurs, les êtres humains expriment CYP17 (P450C17) dans la zone réticulée, permettant l'hydroxylation de la prégnénolone, la progestérone et la DOC en 17α-hydroxyprégnénolone, 17α-hydroxyprogestérone ou 11-deoxycortisol respectivement. Lors d'une déficience en CYP21, la prégnénolone et la progestérone s'accumulent et sont utilisées pour produire des androgènes surrénaliens, ce qui amène les patientes à développer des appareils genitaux externes masculinisés malgré un développement normal des ovaires, des trompes de Fallope et de l'utérus (Speiser and White, 2003; Witchel, 2017).

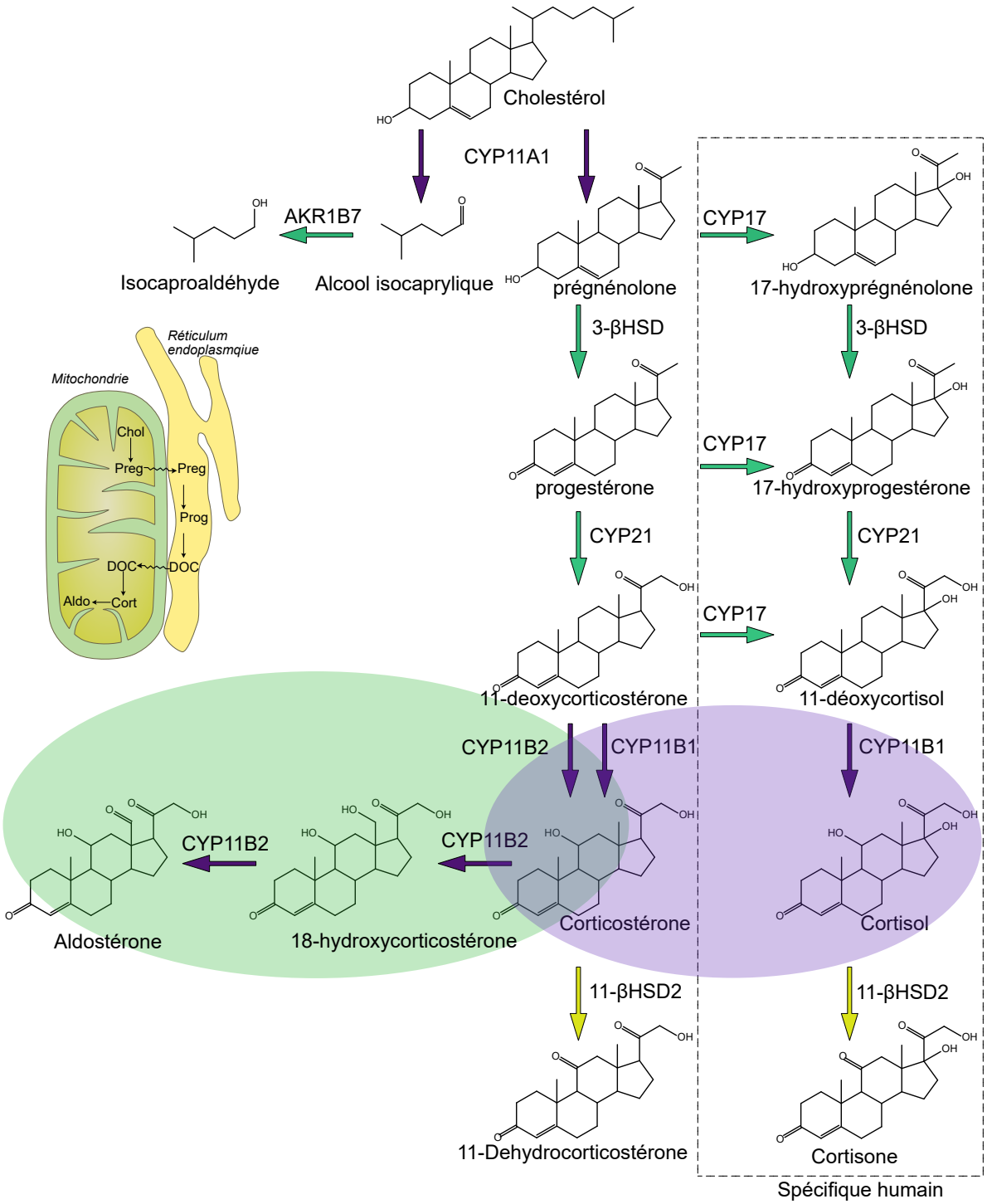

Figure 6: **Schéma de la stéroïdogénèse surrénalienne.**
La zone verte représente les étapes uniquement prises en charge par la zG. La zone violette représente les étapes spécifiques de la zF.
Les flèches violettes répresentent les étapes qui ont lieu dans la mitochondrie alors que les vertes représentent les étapes qui ont lieu en dehors. Les flèches jaunes représentent les réactions qui ont lieu au niveau des organes périphériques

La dernière étape a lieu dans la mitochondrie où la DOC est prise en charge. Dans la zone glomérulée, sous l'action de l'adostérone synthase (CYP11B2), la DOC est hydroxylée à deux reprises en corticostérone, puis en 18-hydroxycorticostérone pour enfin être oxydée en aldostérone. CYP11B1, en revanche, est présent dans la zone fasciculée uniquement et catalyse l'hydroxylation de la DOC en corticostérone. La corticostérone et l'aldostérone représentent les deux stéroïdes principaux produits par la surrénale.

1.3.3 Rôle et régulation des stéroïdes surrénaliens

Les stéroïdes surrénaliens sont les principaux effecteurs de la réponse au stress, leurs effets sont puissants et pléiotropes. Ainsi leurs régulations doivent être fines sans quoi, leur excès ou leur manque peuvent provoquer des pathologies graves.

1.3.3.1 Mode d'action pharmacologique

Les stéroïdes surrénaliens agissent à travers deux récepteurs nucléaires : le récepteur aux glucocorticoïdes (GR codé par *NR3C1*) et le récepteur aux minéralocorticoïdes (MR codé par *NR3C2*) (Bradbury et al., 1991).

MR et GR sont des récepteurs nucléaires, ils sont séquestrés dans le cytoplasme, en absence de ligand, par un complexe de protéines co-chaperones (HSP90, HSP70 et p23) et d'immunophilines (FKBP51/52). Lors de la liaison à un ligand, ils changent de conformation, sont hyperphosphorylés, les libérant du complexe et transloquent dans le noyau. Une fois au niveau de la chromatine, ils se fixent en dimères, à des éléments de réponse et induisent ou répriment l'expression de gènes cibles.

Ils peuvent également exercer des effets non génomiques, intéressants car beaucoup plus rapides. Ces effets non-génomiques peuvent mettre en jeu des voies de signalisation cellulaire comme celle des MAPKs ou de PI3K/AKT (Ramamoorthy and Cidlowski, 2016).

1.3.3.2 Effets physiologiques et régulation de la synthèse d'aldostérone

Le principal effet des minéralocorticoïdes, est le maintien de l'équilibre hydrosodé. L'aldostérone agit au niveau des tubes contournés distaux du rein pour réabsorber le sodium, l'eau et sécréter le potassium. A cet effet périphérique, se joint un effet central stimulant l'appétit pour le sel et une stimulation de la vasoconstriction générale liée à un effet direct sur l'endothélium et le système nerveux sympathique (Gomez-Sanchez and Gomez-Sanchez, 2014). Ces actions combinées permettent le maintien de la volémie et de la pression artérielle.

La régulation de la synthèse d'aldostérone est principalement régie par le système rénine angiotensine (SRA). Lors de la détection d'une baisse de la pression artérielle ou de la concentration en sodium, le rein libère de la rénine dans la circulation. L'angiotensinogène, produit par le foie est alors clivé par la rénine en angiotensine I puis en angiotensine II (AngII) par l'enzyme de conversion (ACE) au niveau des poumons (Figure 7).

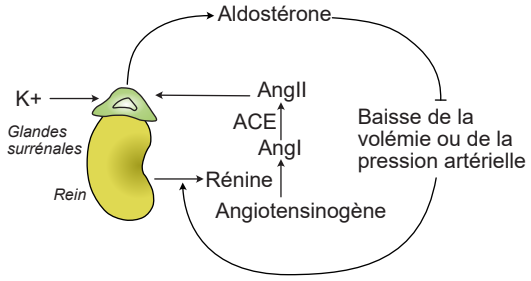

Figure 7: **Fonctionnement du système rénine angiotensine**

L'AngII se fixe à son récepteur à protéines G AT1R dans les cellules glomérulées. Cette liaison, à travers l'activation de la protéine $G\alpha_q$ (Taylor et al., 2019) conduit à l'activation de la phospholipase C (PLC) amenant *in fine* à une augmentation du calcium intracellulaire (MacKenzie et al., 2019). Cette augmentation est possible grâce à la mobilisation des stocks intracellulaires de Ca^{2+} mais également grâce à la dépolarisation des cellules et l'ouverture des canaux calciques voltage-dépendant $CA_v3.2$. La zG subit alors des oscillations de voltage et de concentrations en Ca^{2+} (Guagliardo et al., 2020) (Figure 8).

L'augmentation de la concentration en Ca^{2+} permet l'activation de la CaMK (calmodulin-dependant protein Kinase) nécessaire à la production d'aldostérone (Pezzi et al., 1996).

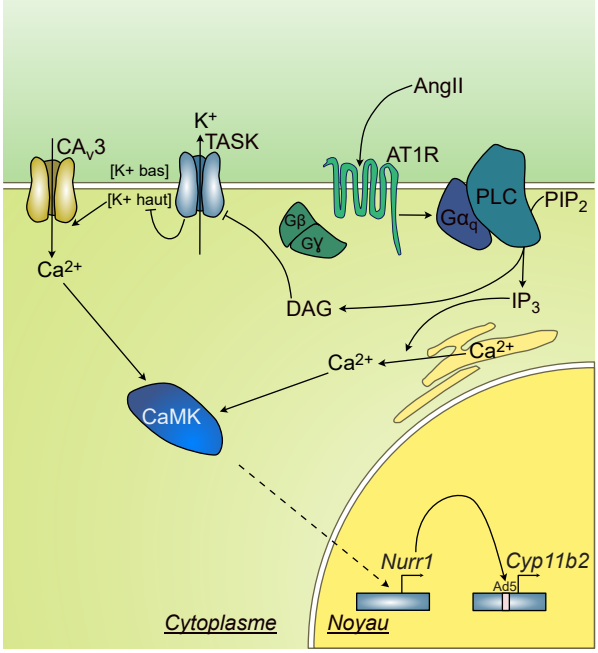

Figure 8: **Régulation de l'expression de l'aldostérone synthase (*(*Cyp11b2)) par l'angiotensine II et les ions potassium**

L'activation de la CaMK conduit à l'augmentation de l'expression de l'aldostérone synthase (Condon et al., 2002; Uruno et al., 2011) *via* l'augmentation de l'expression de NURR1 se fixant à un élément de réponse *Ad5* sur le promoteur de *Cyp11b2* (Matsuda et al., 2014).

Un autre acteur important de la régulation de l'activité de la zG est l'ion potassium K^+. En condition basale, la concentration en K^+ dans le milieu extracellulaire est plus faible qu'au sein de la cellule, notamment grâce à l'action de la pompe NA^+/K^+ ATP dépendante maintenant la différence de potentiel. Cette différence permet la diffusion du K^+ intracellulaire vers l'extérieur de la cellule, *via* les transporteurs TWIK-related acid-sensitive K^+ (TASK). Diffusion qui est bloquée lorsque la concentration en K^+ dans le milieu extracellulaire augmente ce qui induit une augmentation de voltage propice à l'ouverture des canaux calciques voltage-dépendant (MacKenzie et al., 2019). L'absence du canal TASK1 chez la souris induit chez la femelle uniquement, une augmentation des taux plasmatiques d'aldostérone illustrant la nécessité de la mobilité du potassium dans la fonction glomérulée (Heitzmann et al., 2008).

1.3.3.3 Effets physiologique des glucocorticoïdes

La principale fonction des glucocorticoïdes (GC) est la réponse aiguë au stress, notamment à travers la mobilisation de nutriments dans la circulation sanguine. Cependant, leur action s'étend également au système immunitaire (Cruz-Topete and Cidlowski, 2015), cardiovasculaire (Cruz-Topete et al., 2016), osseux (Seibel et al., 2013) et nerveux.

- Rôle dans la mobilisation des nutriments

Les GC augmentent la glycémie en agissant au niveau du foie et des muscles pour stimuler la néoglucogénèse, la glycogénolyse et bloquer l'import du glucose dans les tissus. Parallèlement, ils inhibent la production de l'insuline, hypoglycémiante, par les cellules β du pancréas.
La lipolyse est stimulée dans les adipocytes alors que la lipogénèse est promue dans le foie ce qui aboutit à une hypertriglycéridémie. Enfin les GC vont mobiliser des nutriments sous la forme de protéines dans le muscle en bloquant la synthèse protéique et stimulant sa dégradation (Vegiopoulos and Herzig, 2007).

- Rôle au niveau de la médulla

Bien qu'étant deux tissus d'origine différente, le cortex et la médulla sont fonctionnellement interconnectés. En effet, le sang circule dans le cortex avant d'irriguer la médulla, se chargeant ainsi de GC. Dans un modèle de souris $GR^{-/-}$, la médulla n'exprime pas PNMT et produit moins de catécholamines (Finotto et al., 1999), de plus la présence de glucocorticoïdes permettrait aux précurseurs de la médulla provenant de la crête neurale d'acquérir leur phénotype de cellules chromaffines (Anderson and Axel, 1986). Toutefois, les modèles ne produisant pas de corticostérone, KO totaux pour MC2R (Melanocortin-2 receptor) (Chida et al., 2007) ou dans une moindre mesure son co-récepteur MRAP (Melanocortin-2 receptor accesory protein) (Novoselova et al., 2018) [12] produisent moins d'adrénaline sans que la structure de la médulla ne soit affectée. Par ailleurs, les modèles

[12] détaillé dans le paragraphe 2.2.4.2 - Effet de l'absence de stimulation ACTH

génétiques d'insuffisance corticosurrénalienne ne ciblant que les cellules stéroïdogènes impactent la structure de la médulla sans affecter sa fonction endocrine (Huang et al., 2012; Mathieu et al., 2018).

Ainsi il semblerait que les GC exercent un léger impact sur la fonction médullaire, en régulant l'expression des enzymes responsables de la biogénèse des catécholamines comme il a été montré *in vitro* pour TH et PNMT (Evinger et al., 1992; Fossom et al., 1992).

- Impact sur la fonction cognitive

L'exposition a un stresseur nécessite une réponse comportementale rapide et adaptée pour la survie de l'individu, il est donc peu surprenant d'observer une modulation des capacités cognitives par les GC.

En effet, l'absence de GR chez des souris ou l'ablation des surrénales réduisent la mémoire spatiale des souris. Cette capacité de mémoire est restaurée lorsque les souris surrénalectomisées sont traités avec de la corticostérone (Oitzl et al., 2001). Par ailleurs, les souris traitées avec de la corticostérone pendant une période d'apprentissage voient leur capacité à discriminer les objets, améliorée (Buurstede et al., 2021), tandis qu'à l'inverse un stress traumatisant de séparation maternelle altère leur capacité de discrimination des objets de façon dépendante du récepteur aux glucocorticoïdes (Loi et al., 2017). Enfin, l'administration de GC sur des souris soumises à un protocole de stress post-traumatique module leur réaction de peur face au stresseur initial (Kaouane et al., 2012; Yang et al., 2006b).

Ces effets touchent à la fois l'hippocampe qui possède une forte expression de MR et GR (Buurstede et al., 2021; Viho et al., 2021) ainsi que l'amygdale (Kaouane et al., 2012; Yang et al., 2006b). Ces résultats montrent qu'un dosage fin des GC permet de moduler la capacité de mémorisation des évènements, et qu'au delà des aspects strictement biochimiques, les GC induisent des atteintes comportementales à long terme [13].

[13] Cette dimension comportementale se voit particulièrement chez les patients ayant souffert d'un excès chronique en GC, qui, même après traitement, sont plus sujets aux troubles anxieux et dépressifs (Frimodt-Møller et al., 2019)

- Métabolisme périphérique des glucocorticoïdes

Les glucocorticoïdes sont présents en grande quantité par rapport aux minéralocorticoïdes et ne sont pas régulés de la même façon. En outre, ils ont une affinité plus importante pour MR que pour GR. La corticostérone a un $K_d = 0.8$ nM pour MR contre un $K_d = 2.5$ nM pour GR (Reul and Kloet, 1985). L'aldostérone, cependant n'agit qu'à travers sa liaison au MR avec un K_d 3-5 nM (Agarwal and Mirshahi, 1999). Ainsi, en condition basale, les GC occupent la majorité des MR, il est donc important pour les tissus répondant aux minéralocorticoïdes de pouvoir ressentir les variations de ces derniers.

C'est possible, grâce à la présence au niveau des tissus périphériques, de deux enzymes : la 11βHSD1 et 11βHSD2. Ces deux enzymes catalysent les réactions de conversion entre la corticostérone et la 11-déhydrocorticostérone (ou entre le cortisol et la cortisone) permettant de rendre la corticostérone inactive (Abramovitz et al., 1982) (Figure 9).

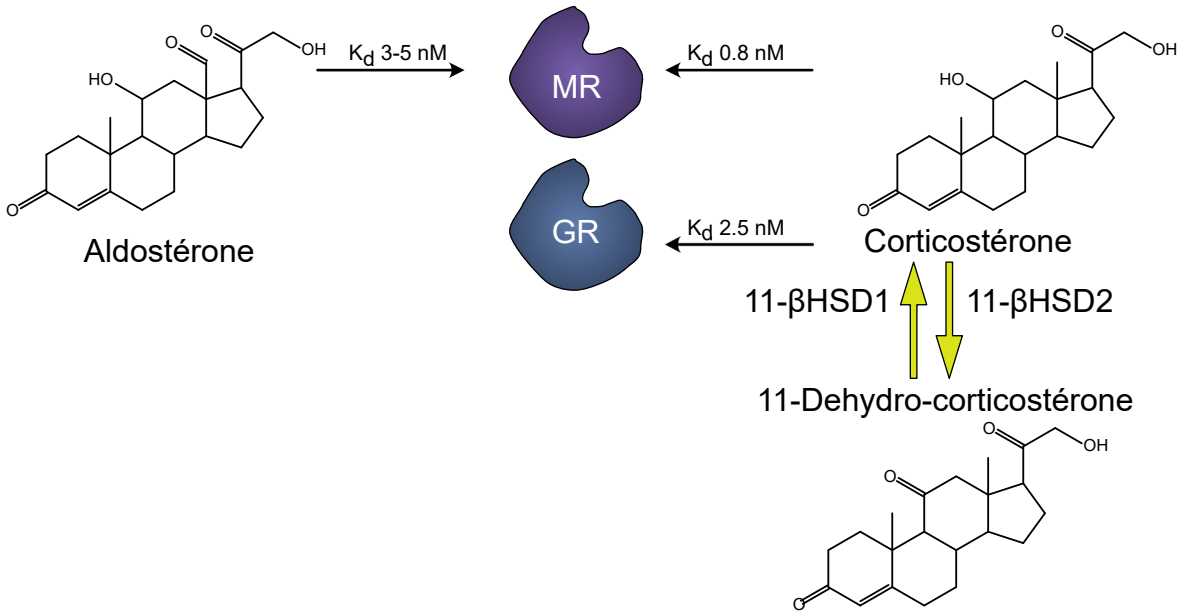

Figure 9: **Affinités différentielles pour MR et GR des stéroïdes surrénaliens**

La perte de l'activité de 11βHSD2 provoque chez l'être humain le syndrome d'excès de minéralocorticoïde apparent (OMIM #218030). Ce dernier produit une hypertension avec hypoaldostéronémie et rénine basse, symptômes retrouvés dans les souris déficientes pour 11βHSD2 (Kotelevtsev et al., 1999). Dans ce syndrome, les GC exercent une activité

minéralo-mimétique constante indépendamment de la régulation par le SRA ou les taux de K^+.

Ainsi, en conditions physiologiques, les GC sont inactivés de façon locale pour permettre aux minéralococorticoïdes d'agir de façon ciblée et permettre un contrôle précis de l'activité des tissus (Seckl, 2004).

1.3.3.4 Régulation de la stéroïdogénèse fasciculée

- Régulation centrale et signalisation AMPc/PKA

La principale voie de signalisation permettant la régulation de l'activité stéroïdogène est la signalisation PKA. Les effets puissants et pléiotropes des GC nécessitent une régulation fine, rapide et permettant une adaptation effective au stress. Ainsi la PKA est au cœur d'une boucle de régulation nommée axe hypothalamo-hypophysaire-surrénalien (Hypothalamo-pituitary-adrenal axis, HPA). Ainsi lors d'un stress, les neurones présents au sein du noyau paraventriculaire de l'hypothalamus relarguent du CRH (Corticotropin Releasing Hormone) dans le système porte hypothalamo-hypophysaire. Ce CRH se lie au récepteur CRHR1 présent au sein des cellules corticotrophes de l'hypophyse antérieure et stimule l'expression de la prohormone *Pomc*. POMC est ensuite clivé en ACTH dans l'hypophyse, par l'enzyme PC1/3 et relargué dans la circulation sanguine (Stevens and White, 2009).

Une fois au niveau surrénalien, l'ACTH se lie au récepteur couplé des protéines G trimériques, MC2R [14] ce qui provoque la libération de la protéine $G\alpha_S$ après dissociation des protéines $G\beta$ et $G\gamma$, une activation de l'adénylyl cyclase et une accumulation d'adénosine monophosphate cyclique (AMPc) dans le cytoplasme, permettant *in fine* l'activation de la Protéine Kinase AMPc dépendante (PKA) (Figure 10.A.B.).

En effet, la PKA est une kinase à régulation allostérique, permettant à de faibles variations en concentrations d'AMPc d'induire des changements d'activité globale du

[14] Cette liaison est possible grâce au corécepteur MRAP qui permet l'adressage de MC2R à la membrane (Sebag and Hinkle, 2009) mais aussi l'activation de la signalisation (Malik et al., 2015)

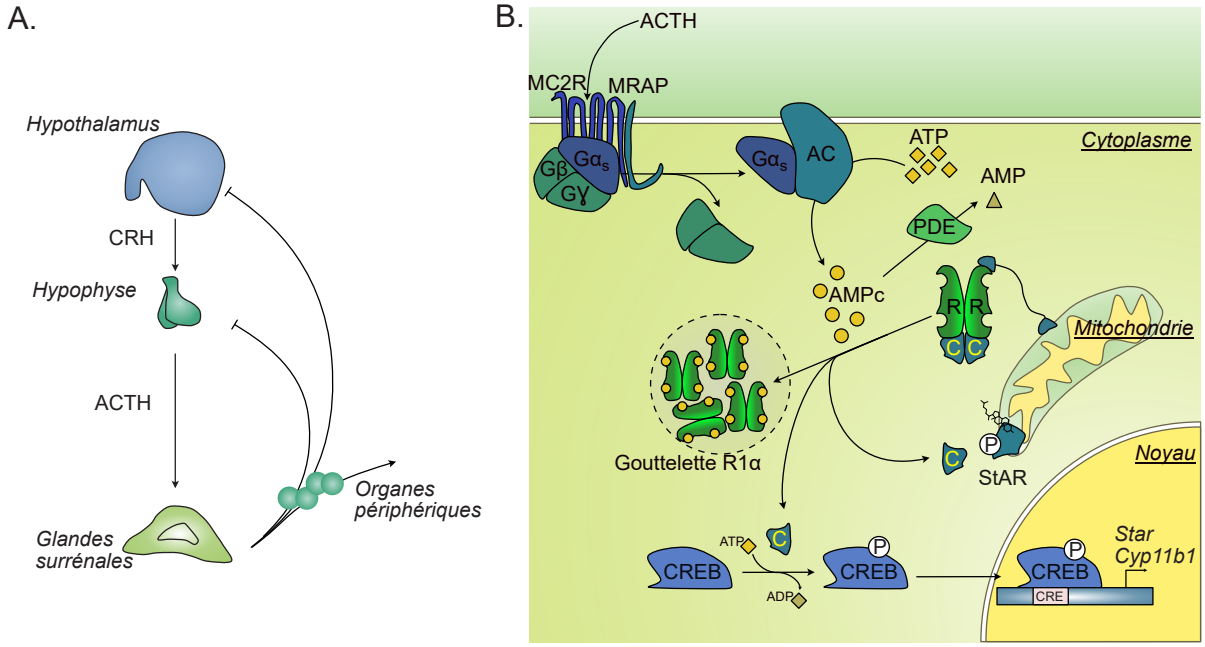

Figure 10: **A. Fonctionnement de l'axe Hypothalamique-hypophysaire-surrénalien**
B. Signalisation AMPc/PKA dans le cortex surrénalien

pool de PKA (Monod et al., 1965). Elle est composée de deux sous unités régulatrices et deux catalytiques. Ces deux monomères comportent plusieurs isoformes dont les principales sont pour les sous unités régulatrices R1α (retrouvée dans la majorité des tissus (Cadd and Stanley McKnight, 1989)), R1β, R2α et R2β et pour les catalytiques Cα et Cβ (Barradeau et al., 2000; Skalhegg and Tasken, 2000; Weigand et al., 2017).
La fixation de l'AMPc sur les sous unités régulatrices, induit une séparation de phase liquide-liquide produisant des gouttelettes séquestrant le complexe R1α/AMPc (Zhang et al., 2020) [15] et la libération des sous unités catalytiques de la PKA qui peuvent alors phosphoryler des protéines cibles telles que StAR ou le facteur de transcription CREB (cAMP Responive Element Binding protein) qui en conséquence induit l'expression de gènes stimulant la stéroïdogénèse.

Les GC ainsi produits exercent leurs effets sur les différents tissus mais vont également exercer un rétrocontrôle négatif au niveau central. En effet, les GC entraînent, par différents mécanismes convergents, la répression transcriptionnelle de *Pomc* et *Crhr1* au

[15] Cette séparation permet d'expliquer les mécanismes de compartimentalisation de l'AMPc afin qu'il n'interfère pas avec d'autres voies de signalisation. En effet, l'AMPc diffuse rapidement dans le cytoplasme et sa dégradation en AMP par les PDEs (phosphodiesterases) est relativement lente (Zhang et al., 2021a)

niveau de l'hypophyse et de *Crh* au niveau hypothalamique (Keller-Wood, 2015) (Figure 10). Ce rétrocontrôle permet d'adapter la réponse au stress en évitant une surproduction de stéroïdes pouvant avoir des conséquences néfastes sur l'organisme. Il permet également la sécrétion pulsatile de l'ACTH [16], nécessaire à l'activité stéroïdogénique correcte de la glande (Hazell et al., 2019).

- Cinétique de la stimulation de la stéroïdogénèse

La réponse à l'ACTH se divise en deux étapes, une réponse aiguë qui se déroule dans les minutes suivant la stimulation et une réponse chronique qui dure plusieurs heures après le début de la stimulation.

Ainsi après quelques minutes, on détecte la phosphorylation de StAR sur la sérine 194 (Hazell et al., 2019) [17] permettant l'entrée du cholestérol dans la mitochondrie et le départ presque immédiat de la stéroïdogénèse. Parallèlement, la PKA phosphoryle HSL (Trzeciak and Boyd, 1974) qui permet la désestérification du cholestérol, nécessaire à son entrée dans la mitochondrie, et phosphoryle CREB qui va stimuler la transcription des gènes stéroïdogènes. Cette réponse aiguë permet d'observer une augmentation des taux de corticostérone une dizaine de minutes après l'augmentation des taux d'ACTH (Walker et al., 2012).

Dans les heures suivant l'induction, *Mc2r*, *Mrap*, *Star*, les gènes de la synthèse *de novo* du cholestérol, les gènes codant pour les enzymes de la stéroïdogénèse sont stimulés (Menzies et al., 2017; Spiga et al., 2017; Wellman et al., 2021) ce qui permet de maintenir une réponse importante. [18]

[16] Les concentrations de glucocorticoïdes suivent un cycle circadien dicté par le CRH avec un pic au lever mais aussi un rythme ultradien avec une période d'environ une heure possible grâce au dialogue GC/ACTH indépendamment du CRH (Walker et al., 2010, 2012)

[17] voir paragraphe 1.3.2.2 - Transport du cholestérol vers la mitochondrie

[18] Il est à noter que bien que ces effets ciblent principalement la zone fasciculée, la stéroïdogénèse glomérulée est elle aussi en partie stimulée par l'ACTH (Gallo-Payet et al., 1996).

2 Développement et renouvellement du cortex surrénalien de souris

2.1 Développement embryonnaire de la glande surrénale

Au stade embryonnaire E9 [19], la cavité cœlomique, qui deviendra les futures séreuses et où vont se développer la plupart des organes, possède un épithélium riche en cellules exprimant le facteur WT1 (Wilms tumour suppressor gene).

A partir de E9.5, l'épithélium cœlomique s'épaissit donnant naissance au primordium adrénoganodique (AGP). En effet, la présence concomittante de WT1 et Cited2 permet l'expression du facteur de transcription SF-1 (Steroidogenic Factor 1, codé par *Nr5a1*) dès E9.5 (Bandiera et al., 2013; Hatano et al., 1996; Val et al., 2007; Wilhelm and Englert, 2002) [20]. L'expression de WT1 s'éteint ensuite (Bandiera et al., 2013) tandis que deux populations se forment dans le primordium adrénogonadique [21]. Une population de cellules exprimant des taux faibles de SF-1 donneront naissance au primordium gonadique (PG) et les cellules exprimant de forts taux de SF-1 deviendront le primordium surrénalien (PS) (Hatano et al., 1996). La séparation a lieu autour de E12.5 (Hatano et al., 1996), moment où le cortex surrénalien est envahi par des cellules provenant de la crête neurale et qui donneront naissance à la médulla (Anderson and Axel, 1986; Zubair et al., 2008).

Pendant cette période (entre E10.5 et E13.5), l'expression de SF-1 est contrôlée dans le primoridum surrénalien, par un élément activateur fœtal nommé FAdE (Foetal Adrenal Enhancer) présent dans l'intron 4 du gène (Zubair et al., 2006). A partir de E12.5, une partie de ces cellules situées en périphérie, perdent l'expression de SF-1 [22], expriment

[19] Le 9^{e} jour embryonnaire chez la souris correspond au stade de Carnegie 9 et au 20^{e} jour post-conception chez l'être humain (Hill, 2010)

[20] Le rôle de SF-1 dans le développement et le maintien du cortex surrénalien est développé dans le paragraphe 6 - La SUMOylation de SF-1 gardienne de l'identité surrénalienne

[21] Chez l'être humain et le macaque, la partie la plus antérieure de l'épithélium cœlomique exprime WT1 et SF-1 et deviendra le primordium surrénalien tandis que la partie postérieure exprimant WT1 et GATA4 deviendra le primordium gonadique et exprimera à son tour SF-1. Ainsi la séparation est plus précoce et n'implique pas la structure commune qu'est le primordium adrénoganodique. (Cheng et al., 2022)

[22] Cette extinction de FAdE est probablement due au facteur DAX-1 (Dosage-sensitive sex reversal, Adrenal hypoplasia congenita critical region, on the X chromosome, gene 1 codé par *Nr0b1*) dont

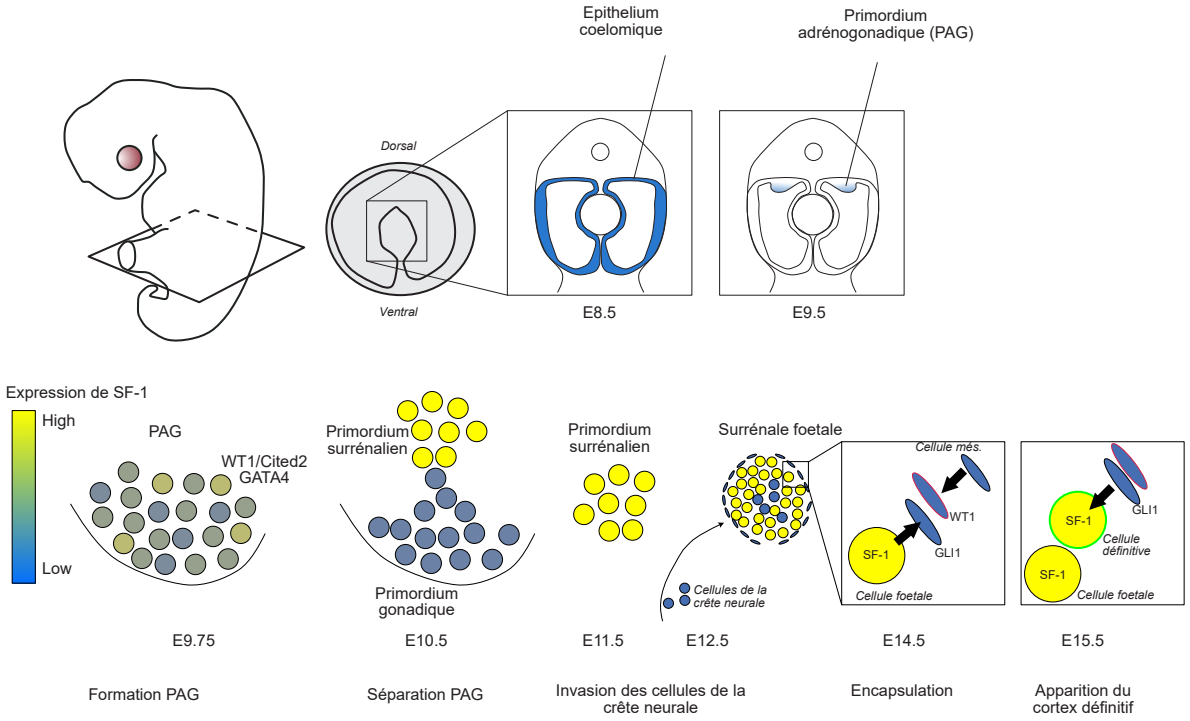

Figure 11: **Développement embryonnaire de la glande surrénale murine**

GLI1 (Glioma-associated oncogene homolog 1) et/ou COUPTFII (codé par *Nr2f2*) et vont participer à peupler la capsule (Wood et al., 2013). Les quelques cellules GL1+ présentes dans la capsule, possèdent la capacité de se différencier et sont à l'origine de cellules SF-1 positives qui émergent à partir de E14.5 et constitueront le cortex définitif (King et al., 2009; Wood et al., 2013; Zubair et al., 2008) (Figure 11.).

A la naissance, le cortex comprend donc des cellules issues des progéniteurs exprimant GLI1 ce qui correspond au cortex définitif et des cellules situées à proximité de la médulla, qui ont conservé l'expression de SF-1 sous le contrôle de FAdE après E14.5 et qui constitueront une zone transitoire appelée zone X. Cette dernière disparaît à la puberté chez le mâle et pendant la gestation chez la femelle (Bielohuby et al., 2007; Hershkovitz et al., 2007), son maintien est régulé par différents facteurs incluant la signalisation androgénique (Gannon et al., 2019; Gannon et al., 2021; Hershkovitz et al., 2007), GATA6 (Pihlajoki et al., 2013) et DAX-1 (Xing et al., 2017). Sa fonction ainsi que les mécanismes aboutissant à son maintien ou sa disparition dépendante du

l'apparition corrèle avec l'extinction de FAdE et qui possède la capacité de réprimer son activité *in vitro* (Xing et al., 2017; Zubair et al., 2008)

sexe restent à explorer (Huang and Kang, 2019) [23].

[23]Les travaux récents du laboratoire suggèrent que la signalisation androgéniques dans les cellules du cortex définitif est un acteur de cette disparition et que les macrophages sont impliqués dans sa clairance

2.2 Renouvellement post natal du cortex

2.2.1 Le modèle centripète

Les données amassées jusque dans les années 80 par études des mitoses (situées principalement en périphérie), observations développementales et expériences d'énucléation des glandes surrénales aboutissant à une régénération avaient permis de dégager trois hypothèses sur l'origine des cellules du cortex surrénalien (Figure 12.A.) (Hyatt, 1987).

- ① La théorie de la migration cellulaire ou modèle centripète. Les cellules sont toutes issues de la zone périphériques et migrent vers le centre pour mourir au niveau de la jonction corticomédullaire.
- ② La théorie zonale. Chaque zone contient ses propres progéniteurs et est indépendante des autres.
- ③ L'hypothèse de la zone intermédiaire proliférative. Les cellules sont issus d'une zone intermédiaire entre la zG et la zF.

Ce n'est que plus récemment, avec les méthodes de perte dirigée de gène et de lignage cellulaire que le modèle centripète a pu être adopté comme modèle standard. Dès 1996, des observations suggéraient fortement la présence d'une migration centripète (Morley et al., 1996). Puis, en 2009, l'implication de cellules exprimant la protéine SHH (Sonic HedgeHog) comme précurseurs des cellules du cortex surrénalien a été démontrée.

Au sein de la surrénale l'expression de SHH est localisée dès E10.5 en périphérie de la glande et au niveau sous-capsulaire après la naissance (Ching and Vilain, 2009; Huang et al., 2010; King et al., 2009). Ces cellules sont *a priori* dépourvues d'activité stéroïdogène mais expriment SF-1, et sont ainsi engagées dans le devenir stéroïdogène. Le suivi du lignage des cellules SHH+ grâce au transgène *Shh-CreERT2* a permis de démontrer qu'après la naissance, la descendance de ces cellules contribue à la formation des zones glomérulée puis fasciculée (King et al., 2009). Elles constituent donc une population de

progéniteurs stéroïdogènes.

Ce résultat est en accord avec le co marquage de Shh^{LacZ} et *Cyp11b2* qui révèle qu'une partie des cellules SHH positives expriment également l'aldostérone synthase et sont donc en voie de différenciation (Walczak et al., 2014).

L'origine glomérulée des cellules fasciculées a été mise en évidence par une approche similaire utilisant cette fois AS^{Cre}. L'expression de cette Cre est limitée aux cellules exprimant *Cyp11b2* codant l'aldostérone synthase, enzyme spécifiquement exprimée dans la zone glomérulée à partir de la naissance de la souris. Le suivi du lignage de ces cellules révèle une contribution des cellules AS positives à l'entièreté du cortex (Freedman et al., 2013).

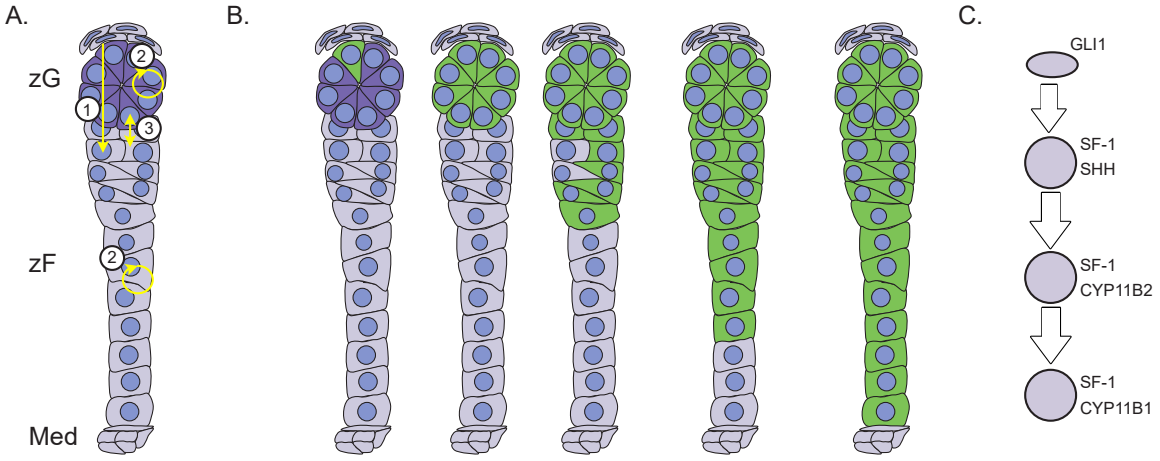

Figure 12: **Le modèle standard de renouvellement post-natal centripète du cortex surrénalien**
A. Les différentes hypothèses concernant le renouvellement post-natal du cortex surrénalien
B. Suivi du devenir d'une cellule SHH+ au cours du temps
C. Schéma représentant les marqueurs exprimés par les différentes cellules

Ces travaux, ainsi que d'autres confirmant ces résultats (Dumontet et al., 2018; Grabek et al., 2019), permettent de valider le modèle centripète chez la souris (Figure 12.A.). Cependant, il semblerait que ce chemin de différenciation ne soit pas l'unique voie possible. En effet, alors que l'absence de SF-1 induit une agénésie de la glande surrénale (Luo et al., 1994), l'invalidation de SF-1 limitée aux cellules glomérulées par AS^{Cre} induit une dédifférenciation de cette zone mais sans aucune conséquence sur l'intégrité de la zone fasciculée (Freedman et al., 2013). Les cellules fasciculées, dans ce cas, ne dérivent pas des cellules glomérulées suggérant qu'il existe une voie alternative au modèle centripète

canonique ou tout au moins, la possibilité par des progéniteurs de repeupler le cortex sans passer par une identité glomérulée. Par ailleurs, la prolifération cellulaire n'est pas limitée - bien qu'enrichie - dans la zone glomérulée, suggérant que les cellules fasciculées sont également capables de se multiplier.

2.2.2 Progéniteurs corticaux

2.2.2.1 Rôle de la signalisation HH

SHH (Sonic HedgeHog) fait partie des ligands sécrétés de la signalisation HedgeHog avec IHH (Indian HedgeHog) et DHH (Desert HedgeHog). Dans la surrénale, ce ligand agit de façon paracrine à courte distance [24]. La spécificité de cette interaction paracrine est rendue possible par la présence de cils primaires nécessaires à l'activation de la voie (Goetz and Anderson, 2010), uniquement dans certaines cellules de la capsule (Mateska et al., 2020). Suite à la liaison entre le ligand HH et son récepteur PTCH1, la dégradation du récepteur SMO est inhibée induisant son adressage à la membrane et l'activation de la voie. Cette dernière passe par l'arrêt de la protéolyse de GLI2 et GLI3 et l'expression de GLI1 (Laufer et al., 2012) (Figure 13.).

La contribution de la signalisation HH à l'homéostasie du cortex surrénalien est révélée par l'invalidation génique de SHH dans le cortex surrénalien dépendante du transgène *Sf1-Cre*. La perte partielle de SHH, produit à l'état hétérozygote une forte hypoplasie (Huang et al., 2010; King et al., 2009) tandis que son invalidation totale induit une agénésie de la surrénale droite et une atrophie de la surrénale gauche (Ching and Vilain, 2009).

Cette implication est en accord avec les effets observés suite à un traitement à la dexaméthasone, qui bloque l'axe corticotrope et induit une atrophie transitoire de la zF [25]. En effet, lors de la régénération suivant l'arrêt du traitement, les transcrits

[24] La signalisation HH à plus longue distance est possible grâce à la sécrétion de SHH associé à des lipoprotéines mais il semblerait que les lipoprotéines produite par les cellules corticosurrénaliennes contiennent SHH et une molécule inhibitrice empêchant son action. Ainsi la signalisation HH n'a lieu qu'à courte distance dans la surrénale (Mateska et al., 2020)

[25] voir paragraphe 2.2.4.2 - Effet de l'absence de stimulation ACTH

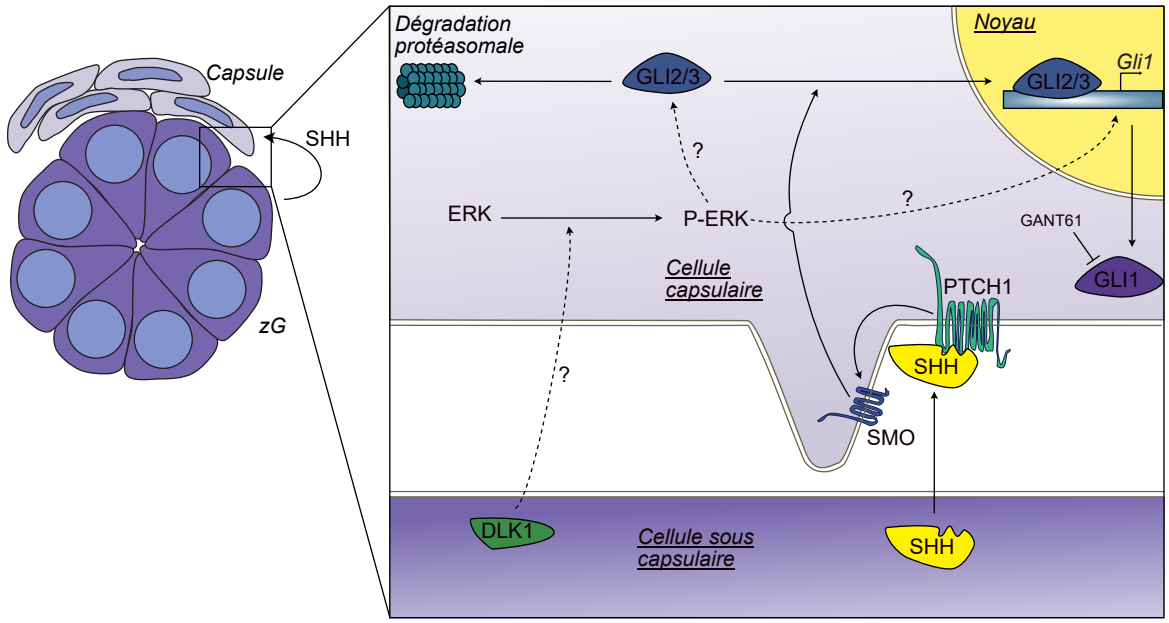

Figure 13: **Schéma de la signalisation SHH dans les progéniteurs surrénaliens**
La liaison de SHH à son récepteur PTCH1 permet la stabilisation de SMO, ce qui aboutit au blocage de la dégradation et GLI2/3 et à l'expression de GLI1. DLK1 stimule également l'expression de GLI1 en mettant en jeu la phosphorylation de ERK1/2 mais par des mécanismes inconnus pour le moment.

/

des différents acteurs en aval de la voie HH sont surexprimés tandis que le blocage pharmacologique de la voie (GANT61), ralentit la reconstitution de la zF (Finco et al., 2018).

La capsule surrénalienne est constitué de cellules fibroblastiques, exprimant GLI1 mais pas SF-1, dont le nombre diminue suite à la perte de SHH dans le cortex (Huang et al., 2010; King et al., 2009). Le lien entre les cellules SHH+ et les cellules capsulaires GLI1+ dépend de deux interactions paracrines (Figure 13.) :

- La présence de cils primaires au niveau des cellules GLI1, leur permettant de recevoir le signal SHH (Mateska et al., 2020).
- Les cellules SHH de rat (Guasti et al., 2013a) et humaines (Hadjidemetriou et al., 2019) produisent également DLK1/PREF1 (δ-like homologue 1/preadipocyte factor-1), facteur sécrété qui, à travers l'activation de la signalisation ERK stimulerait l'expression de GLI1 dans les cellules capsulaires (Guasti et al., 2013a).

Ces résultats illustrent le rôle prépondérant de la signalisation HH dans le renouvellement et le maintien dans le cortex. Toutefois, il est surprenant qu'une signalisation ne touchant

que la capsule puisse affecter tout le cortex. En effet, les cellules GLI1+ sont peu nombreuses et sont à l'origine de peu de cellules stéroïdogènes après la naissance (Finco et al., 2018; King et al., 2009). L'hypothèse la plus probable est que la signalisation SHH contrôle la survie du *pool* de cellules GLI1+ (Huang et al., 2010; King et al., 2009) tandis que les cellules GLI1+ permettraient le maintien de l'identité glomérulée *via* la production de facteurs paracrines induisant l'activation de la signalisation WNT (Vidal et al., 2016).

2.2.2.2 Autres populations progénitrices

Les cellules GLI1 et SHH sont les principales cellules responsables du renouvellement du cortex, cependant des cellules exprimant WT1 sont présentes dans la capsule et possèdent une certaine capacité de différenciation. En effet, des expériences de lignages ont montré que des cellules WT1 pouvaient se différencier en cellules stéroïdogènes pendant la vie fœtale (Bandiera et al., 2013). Cependant, après la naissance, les cellules WT1+ contribuent très peu au renouvellement du cortex en condition physiologique. Toutefois, lors d'une demande supraphysiologique comme une castration (Bandiera et al., 2013; Dorner et al., 2017), lors du vieillissement (Dorner et al., 2017; Petterino et al., 2015) ou dans certains modèles génétiques (Berthon et al., 2010; Mathieu et al., 2018), des cellules à morphologie allongée exprimant GATA4 et TCF21 forment des amas qui s'insinuent entre les glomérules et affichent certaines caractéristiques gonadiques. Ces cellules peuvent être issues des cellules GLI1+ (Dorner et al., 2017) ou WT1+ (Bandiera et al., 2013) et provenir de la dédifférenciation de cellules SF-1+ embryonnaires (Mathieu et al., 2018).

Une étude récente a proposé que certaines cellules exprimant le marqueur de progéniteur neuronal NESTIN (neuroepithelial stem cell protein), pourraient contribuer au cortex dans des conditions de stress. En effet, des expériences de lignages semblent montrer que de rares cellules issues de cellules NESTIN positives se retrouvent dans le cortex ou dans la capsule et dont une faible proportion exprime la protéine StAR ou CYP11B2, témoins

d'une différenciation stéroïdogène (Steenblock et al., 2018) [26].

2.2.2.3 Dimorphisme sexuel du recrutement des progéniteurs

La glande surrénale de souris est un organe fortement influencé par les hormones sexuelles (Levasseur et al., 2019). En effet, les surrénales des deux sexes possèdent des signatures transcriptomiques différentes (El Wakil et al., 2013; Jopek et al., 2017) et les femelles possèdent des surrénales plus grosses tout en produisant plus de glucocorticoïdes (Bielohuby et al., 2007). Enfin, la vitesse de renouvellement des cellules du cortex est 2.5 fois plus rapide chez la femelle (Dumontet et al., 2018; Grabek et al., 2019). Le suivi du lignage AS^{Cre} au cours de temps montre que les cellules fasciculées descendantes des cellules glomérulées mettent environ 3 mois pour atteindre la jonction corticomédullaire chez les femelles adultes, tandis qu'elles en mettent 7 chez le mâle. Pour cette raison, le phénotype d'hypersecrétion hormonale induit par la perte de *Prkar1a* sous le contrôle d'AS^{Cre} survient après 3 mois chez la femelle et après 10 chez le mâle. De même, la castration des mâles à 5 mois permet d'observer des effets dès 7 mois, ceci étant abrogé par un traitement à la dihydrotestostérone (Dumontet et al., 2018). L'utilisation de souris castrées, ou de souris mâles XX (*Tg(WT1:Sox9)*) confirme que cette différence de dynamique cellulaire est principalement due aux androgènes (Grabek et al., 2019). Ces résultats sont d'ailleurs corroborés par l'invalidation du récepteur aux androgènes (AR codé par *Nr3c4*) dans les cellules surrénaliennes qui induit une hyperplasie des surrénales chez les mâles (Gannon et al., 2019; Gannon et al., 2021; Levasseur, non publié).

Les mécanismes de l'effet des androgènes sur l'homéostasie corticale ne sont que partiellement connus. Le suivi du lignage GLI1+ grâce au transgène *Gli1-creERT2*, révèle qu'après la puberté, les mâles sont incapables de recruter ces progéniteurs contrairement aux femelles (Grabek et al., 2019). Par conséquent, celles-ci renouvellent leur cortex en mobilisant à la fois des progéniteurs SHH+ et GLI1+. Enfin, les androgènes stimulent la signalisation WNT/β-caténine, ce qui inhibe probablement la signalisation PKA et entrave l'acquisition de l'identité fasciculée (Dumontet et al., 2018).

[26] Ces résultats sont toutefois techniquement discutables et n'ont pas été répliqués

Questions et perspectives

Les androgènes exercent un effet ralentisseur sur le renouvellement du cortex surrénalien murin, qui pourrait expliquer en partie une activité endocrine fasciculée plus importante et une meilleure réponse au stress chez la femelle. La question se pose desormais de savoir si ce mécanisme est conservé chez l'être humain et s'il pourrait être la cause du dimorphisme sexuel concernant l'incidence des pathologies surrénaliennes. En effet, les femmes sont plus touchées par les carcinomes corticosurrénaliens (1.5-2.5:1), les adénomes corticosurrénaliens sécrétant (4-8:1), les hyperplasies primaires bilatérales des surrénales (2-3:1) (Levasseur et al., 2019) . Les réponses à cette question pourraient alors permettre le développement de thérapies ou au moins de prise en charge adaptées en fonction du sexe des patients.

2.2.3 La voie WNT/β-caténine : maintien du pool de progéniteurs et différenciation du cortex externe

La β-caténine est une protéine de 98 kDa impliquée dans la formation de jonctions adhérentes de par sa capacité à se lier avec l'α-caténine et la E-cadhérine. Elle joue également un rôle de coactivateur transcriptionnel au sein de la signalisation WNT (Wingless-related integration site) dite canonique. Cette signalisation, très conservée, est impliquée dans de nombreux processus tels que la prolifération, la morphogenèse tissulaire et la différenciation cellulaire. Des dérégulations de la signalisation WNT/β-caténine sont fréquemment impliquées dans l'étiologie de tumeurs surrénaliennes (Wilmouth et al., 2019). Par ailleurs, dans la surrénale, la signalisation WNT est principalement présente dans la zone glomérulée. En effet, les immuno-marquages β-caténine ou WNT4 sont limités à la zG et 80% des cellules qui expriment CYP11B2 possèdent une activité *Lef/Tcf:H2B-GFP* (témoin de l'activité transcriptionnelle de la β-caténine) (Walczak et al., 2014).

2.2.3.1 Fonctionnement et régulation de la voie WNT/β-caténine

En l'absence de ligand WNT, la β-caténine, est phosphorylée par un complexe de destruction amenant à sa dégradation par le protéasome. Ce complexe de destruction est organisé autour de l'axine qui interagit avec la β-caténine, DVL (Dishevelled), CK1 (Casein Kinase 1), GSK3β (glycogen synthase kinase 3b) et APC (adenomatosis polyposis coli) (Ikeda et al., 1998). GSK3β et CK1 phosphorylent la β-caténine sur des sérines et thréonines codées par l'exon 3, ce qui induit sa reconnaissance par l'E3 ubiquitine ligase β-TrCP (beta-transducin repeat containing) et sa dégradation par le protéasome (Hart et al., 1999). Parallèlement, l'E3 ubiquitine ligase, ZNRF3 (Zinc And Ring Finger 3) promeut l'ubiquitination de Frizzled, le récepteur aux ligands WNT, et donc sa dégradation (Hao et al., 2012).

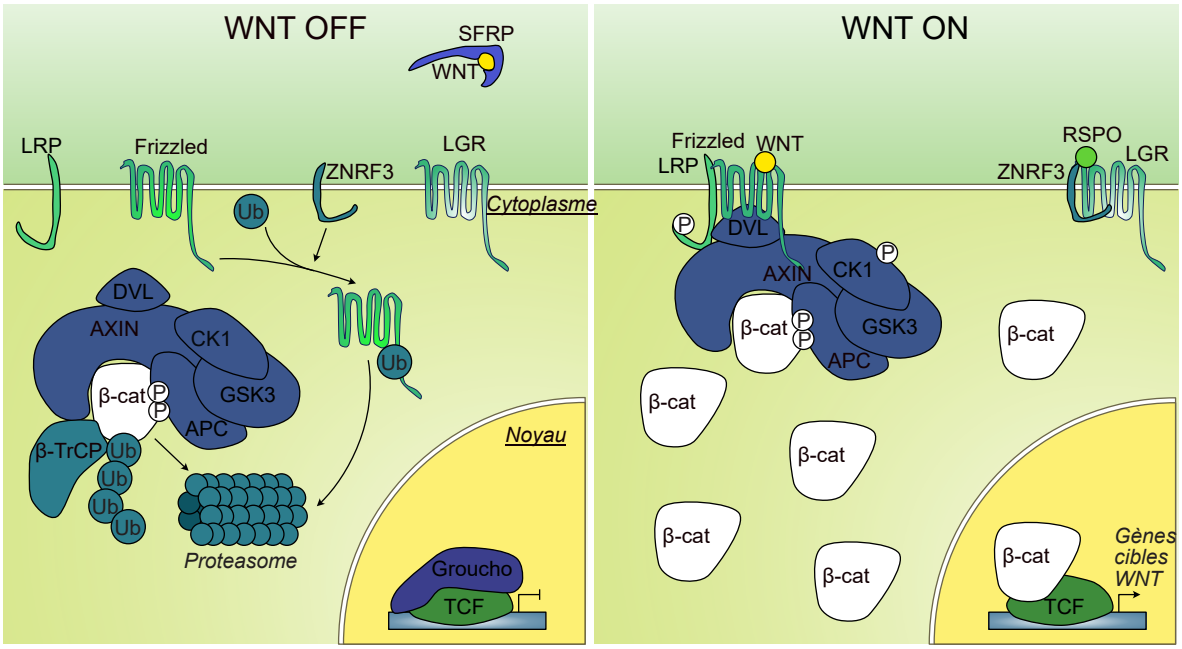

Figure 14: **Vue d'ensemble du fonctionnement de la signalisation WNT canonique**

Lors de la fixation d'un ligand WNT sur son récepteur, le complexe de destruction se lie à Frizzled par l'intermédiaire de DVL (Gao and Chen, 2010) et ne recrute plus β-TrCP ce qui amène la β-caténine phosphorylée à s'accumuler, saturant le complexe tandis que la β-caténine non phosphorylée, nouvellement synthétisée s'accumule dans le cytoplasme (Li et al., 2012). Cet effet est potentialisé par la présence de ligands RSPO (R-Spondin). Ces derniers activent leurs récepteurs LGRs qui recrutent ZNRF3, bloquant son action E3 ubiquitine ligase et permettant d'augmenter *in fine*, la disponibilité de Frizzled à

la membrane (Hao et al., 2012). La β-caténine accumulée dans le cytoplasme sous l'action conjuguée de tous ces mécanismes, est transférée dans le noyau où elle se fixe aux facteurs de transcription TCF/LEF (T cell factor/lymphoid enhancing factor) et induit l'expression de gènes cibles de la voie WNT canonique (Korinek et al., 1997) (Figure 14).

2.2.3.2 Transfert nucléaire de la β-caténine

Pour transloquer dans le noyau, une protéine de plus de 40 kDa doit passer à travers le NPC (nuclear pore complex), constitué d'une quarantaine de protéines nommées nucléoporines (Adams and Wente, 2013). Ce transport se fait *via* la reconnaissance d'un signal de localisation nucléaire (NLS) par des protéines de la famille des importines qui accompagnent la protéine à travers le NPC vers le noyau ou des exportines qui reconnaissent le signal d'export nucléaire (NES) et permettent la sortie du noyau. Ces protéines possèdent des domaines hydrophobes leur permettant de reconnaître les nucléoporines et d'assurer le passage à travers les NPC (Wing et al., 2022). La β-caténine ne possède pas de NLS ou de NES, cependant elle navigue rapidement entre le noyau et le cytoplasme (Krieghoff et al., 2006) et s'accumule dans le noyau lors de l'activation de la voie.

Les travaux réalisés jusque là ne permettent pas de comprendre quels sont les mécanismes exacts de la translocation de la β-caténine dans les noyaux, mais différentes hypothèses non exclusives existent.

- Interaction avec des protéines du port nucléaire indépendant du système importine/exportine

En absence d'activation de la voie, une partie du pool de β-caténine est localisé au niveau de la membrane nucléaire (Fagotto et al., 1998). La β-caténine interagit avec des nucléoporines telles que RanBP2, RanBP3 et RanGAP1 dont l'activité est directement associée à la localisation de la β-caténine ainsi qu'avec Nup358 et Nup153 avec qui elle interagit grâce à des acide aminés hydrophobes situés en N- et C-terminal (Sharma

et al., 2016). En effet, la délétion de RanBP2 ou RanGAP1 dans des cellules HCT-116 ou DLD1 diminue la proportion de β-caténine nucléaire (Shitashige et al., 2008) tandis que la perte de RanBP3 augmente cette proportion (Hendriksen et al., 2005). De plus, la mutations des résidus hydrophobes contenus dans les parties terminales de la β-caténine, diminuent sa capacité à interagir avec Nup358 et Nup153 réduisuant, par la même, sa capacité d'import et d'export nucléaire (Sharma et al., 2016). Ces résultats suggèrent que la β-caténine pourrait traverser le NPC, sans être prise en charge par les importines/exportines, mais en interagissant directement avec les nucléoporines. Cette conclusion est en accord avec l'absence d'effet de l'inhibition de l'exportine CRM1 sur l'export nucléaire de la β-caténine (Krieghoff et al., 2006).

- Import induit par les tensions mécaniques

Récemment, des travaux ont mis en évidence l'importance du cytosquelette et du nucléosquelette dans la translocation nucléaire de la β-caténine. En effet, l'application de contraintes mécaniques dynamiques induit l'inhibition de la GSK3β et l'accumulation de β-caténine dans le noyau (Sen et al., 2022). Cette accumulation est dépendante des protéines SUN, appartenant au LINC (Linker of Nucleoskeleton and Cytoskeleton) (Méjat, 2010) avec lequel la β-caténine intéragit (Uzer et al., 2018). Plus précisemment, Cofilin-1 et Importin-9, dont la présence est strictement nécessaire pour l'import de la β-actine dans le noyau agissent de la même façon sur la β-caténine (Sen et al., 2022). Ces résultats sont similaires à des données obtenues concernant la translocation du facteur de transcription YAP, qui traverse les NPC suite à une contrainte mécanique. Cette dernière produit une augmentation de la taille des pores nucléaires, facilitant l'import des protéines (Elosegui-Artola et al., 2017). Dans la zone glomérulée, les rosettes possèdent un centre enrichie en protéines impliquées dans la formation des jonctions adhérentes (Leng et al., 2020). Or, ces jonctions induisent de fortes tensions de contractions lors de la formation des rosettes (Harding et al., 2014), on peut ainsi émettre l'hypothèse que ces tensions favorisent l'import nucléaire de la β-caténine dans la zG.

- Rétention par des protéines nucléaires

Un dernier mécanismes est le maintien de la β-caténine dans le noyau grâce à son interaction avec des protéines nucléaires (Jamieson et al., 2016; Shitashige et al., 2008; Zhang et al., 2011). En effet les cellules de cancer mammaire MCF7 qui expriment peu LEF1 et TCFs ont des taux faibles de β-caténine dans leur noyau même en cas d'activation de la voie, tandis que ce déficit est aboli lors de la surexpression de LEF1 (Jamieson et al., 2016). Dans le cytoplasme, la β-caténine peut se lier au facteur de transcription FOXM1 (Zhang et al., 2011) ou à DVL-3 (Gan et al., 2008) suite à l'activation de la voie, ce qui permet à la β-caténine d'être transférée dans le noyau grâce à leur NLS et de favorise la formation et le maintien d'un complexe avec TCF4. La β-caténine est également capable de se lier à plusieurs autres protéines nucléaires contenant des NLS (Hwang et al., 2017), par exemple sa liaison avec AXIN2, APC ou TCF4 ralentit sa capacité à naviguer entre le noyau et le cytoplasme (Krieghoff et al., 2006). Sa capacité à interagir avec des protéines nucléaires est donc un facteur important de son maintien dans le noyau.

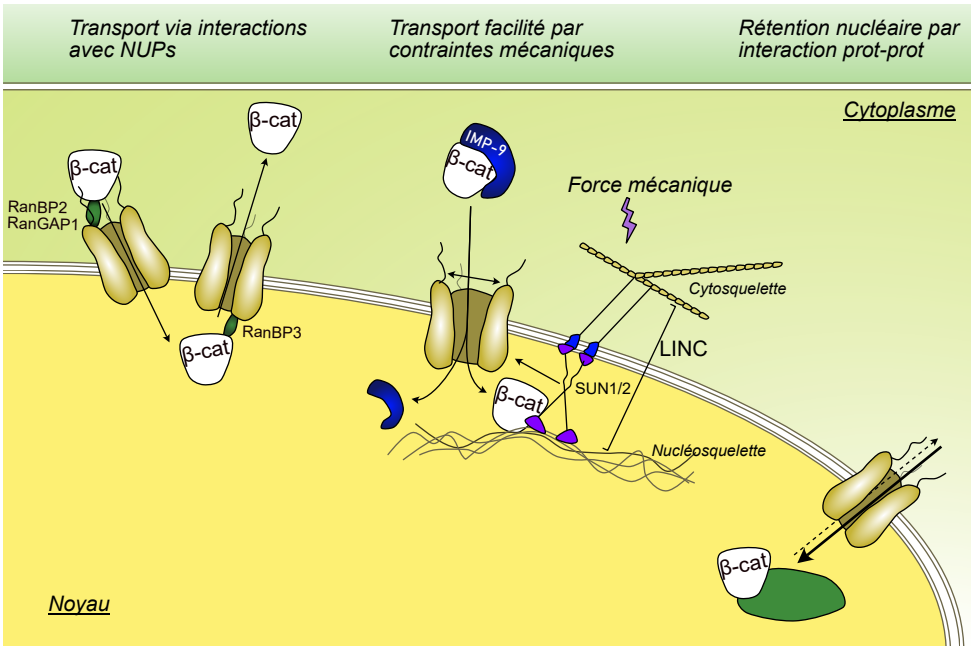

Figure 15: **Schéma des différents moyens permettant à la β-caténine de naviguer entre le cytoplasme et le noyau**

2.2.3.3 Stimulation de la voie WNT dans la surrénale

Aussi bien chez les patients que dans des modèles murins, des mutations activatrices

de la β-caténine aboutissent à un hyperaldostéronisme primaire (Berthon et al., 2010, 2014; Pignatti et al., 2020). Des résultats obtenus sur des lignées surrénaliennes humaines et des souris transgéniques montrent que la β-caténine est capable d'induire l'expression de *CYP11B2/Cyp11b2* de façon indirecte. Elle induit dans un premier temps, l'expression des récepteurs nucléaires NURR1 (*NR4A2/Nr4a2*) *via* un site *LEF* et NUR77 (*NR4A1/Nr4a1*) *via* un site *AP1* (Berthon et al., 2014). En retour, NURR1 et NUR77 se fixent sur le promoteur de *CYP11B2/Cyp11b2* et activent sa transcription *via* des sites *NBRE*, *Ad1* et *Ad5* (Bassett et al., 2004; Berthon et al., 2014)

Outre l'hyperactivité endocrine, les souris présentant une stabilisation de la β-caténine, causée par la perte du domaine phosphorylable codé par l'exon 3 ($Catnb1^{lox(ex3)}$), montrent des défauts de différenciation. En effet, lorsque cette mutation gain de fonction cible les cellules du cortex en général (0.5 *Akr1b7:Cre* nommées ΔCat), elle aboutit à une hyperplasie liée à une hyperprolifération et une dédifférenciation des cellules fasciculées qui perdent l'expression de leurs marqueurs au profit de marqueurs glomérulés comme CYP11B2 (Berthon et al., 2010). Lorsqu'elle cible uniquement les cellules glomérulées (AS^{Cre}), la mutation provoque un blocage de la conversion glomérulée vers fasciculée mais n'affecte pas la prolifération (Pignatti et al., 2020).

D'autres modèles d'activation supposés de la signalisation WNT/β-caténine montrent des résultats partiellement similaires. Le récepteur WNT secrété SFRP2 (secreted frizzled related protein) inhibe l'activation de la signalisation en empêchant les ligands WNT d'interagir avec le récepteur Frizzled (figure 14). Ainsi, la perte de SFRP2 augmente le nombre de cellules glomérulées et la secrétion d'aldostérone (Berthon et al., 2014). La perte de l'E3 ubiquitine ligase ZNRF3 dans les cellules stéroïdogènes ($Sf1\text{-}Cre::Znrf3^{fl/fl}$) induit quant à elle, une hyperplasie des surrénales mais sans blocage de la différenciation malgré une légère activation ectopique de la signalisation dans les cellules fasciculées et une absence d'effet lorsque la sécrétion des ligands WNT est bloquée (Basham et al., 2019) (figure 16).

De plus, ces différents modèles ont permis de mettre en évidence un effet inhibiteur de la signalisation WNT sur la stéroïdogénèse dépendante de la signalisation PKA. La β-

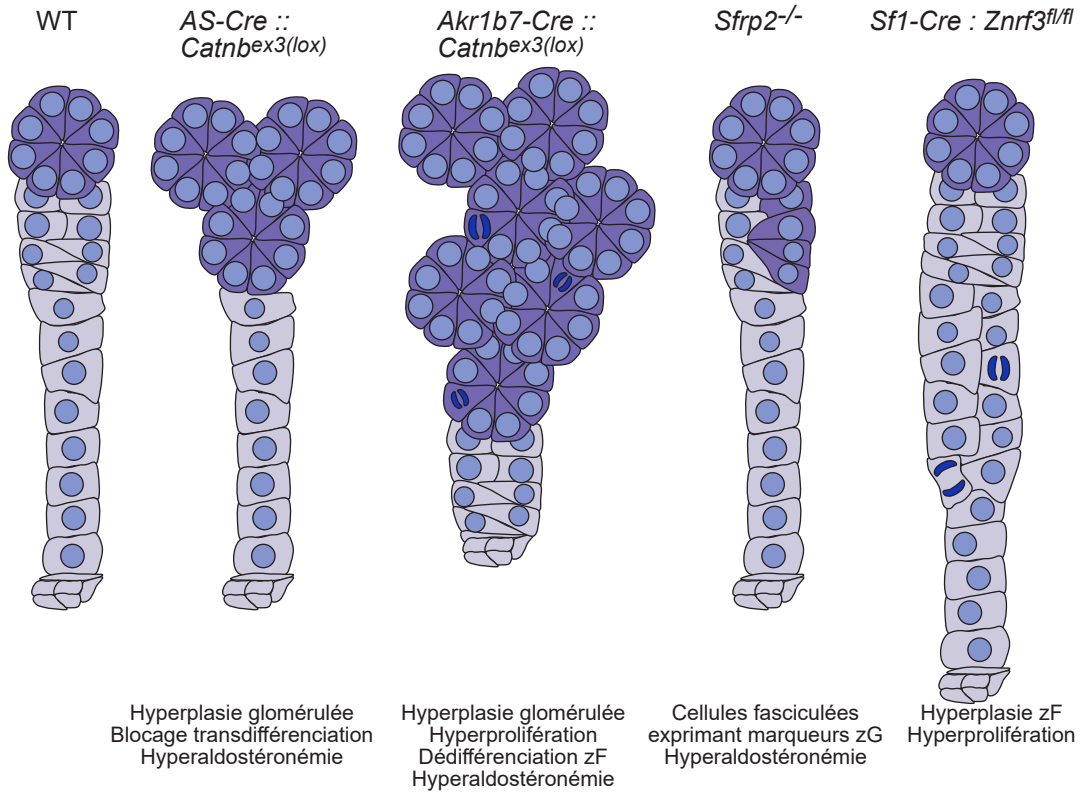

Figure 16: **Effets des modèles d'activation de la signalisation WNT/β-caténine sur le renouvellement du cortex surrénalien**
Les cellules violettes représentent les cellules présentant des caractéristiques glomérulées tandis que les cellules roses représentent les cellules fasciculées.

caténine stimule directement l'expression de la phosphodiestérase PDE2A dans la zG accroissant ainsi la dégradation de l'AMPc (Pignatti et al., 2020). Elle induit également l'expression de *Ccdc80* en se fixant sur des sites *Lef/Tcf* en amont du gène. CCDC80 exerce alors une répression de l'expression de *Star*, *Cyp11b1* et *Cyp11a1.* (Walczak et al., 2014).

Ces résultats montrent que la signalisation WNT canonique permet le maintien de l'identité glomérulée en partie en réprimant la signalisation PKA. L'hyperprolifération observée uniquement dans les souris ΔCat et *Sf1-Cre::Znrf3*$^{fl/fl}$ suggère que ce phénotype n'est possible que lors de l'activation ectopique de la signalisation WNT/β-caténine dans la zF.

2.2.3.4 Absence de signalisation WNT

L'un des phénotypes les plus marquants touchant la signalisation WNT dans la surrénale

est la perte de la β-caténine sous le contrôle du promoteur de SF-1 (*Sf1-cre:: Ctnnb1$^{fl/fl}$*), qui aboutit à une agénésie totale de la glande (Huang et al., 2012; Kim et al., 2008). Ce même modèle utilisant un promoteur de SF-1 moins efficace (*Sf1^{low}-cre:: Ctnnb1$^{fl/fl}$*) provoque une hypoplasie due à une perte progressive du renouvellement des cellules corticales (Kim et al., 2008). De façon similaire, la perte de WNT4, exprimé dans les cellules glomérulées, n'a aucun effet sur les étapes précoces du développement surrénalien (Heikkilä et al., 2002; Zubair et al., 2008) mais aboutit, après la naissance, à une perte des marqueurs glomérulés comme DAB2, CYP11B2, et DLK1, associé à un hypoaldostéronisme (Drelon et al., 2016; Heikkilä et al., 2002).

Parallèlement, la signalisation WNT/β-caténine est impliquée dans la formation de la structure des glomérules en rosettes [27]. En effet, la formation des rosettes, qui a lieu dans les six semaines suivant la naissance, est retardée chez des souris *AS^{cre}::Ctnnb1$^{fl/fl}$* alors qu'elle est à l'inverse stimulée dans les souris *AS^{cre}::Catnb1$^{lox(ex3)}$* qui comportent plus de rosettes que des sauvages (Leng et al., 2020; Pignatti et al., 2020). Cet effet de la β-caténine dépend notamment de la stimulation de l'expression de *Fgfr2* dont l'activité est nécessaire à la formation des rosettes (Guasti et al., 2013b; Leng et al., 2020) et au développement du cortex surrénalien (Häfner et al., 2015; Kim et al., 2007). En effet, l'inactivation de *Fgfr2* dans l'épithélium cœlomique (*Tbx18^{cre}*)(Kim et al., 2007) ou les cellules stéroïdogènes (*Sf1-cre*) (Kim et al., 2007) provoque une hypoplasie majeure du cortex surrénalien.

L'un des régulateurs de l'activité WNT dans la surrénale est le facteur sécrété RSPO3 produit par les cellules de la capsule GLI1 positives. Sa délétion aboutit à une perte des marqueurs glomérulés, mais aussi SHH et GLI1 ainsi qu'à une hypoplasie du cortex (Vidal et al., 2016) (figure 17). Ce phénotype est cohérent avec les effets de la perte de ZNRF3 dans les cellules stéroïdogènes qui induit une hyper prolifération fasciculée (Basham et al., 2019) suggérant que les ligands RSPOs produits par la capsule, ont

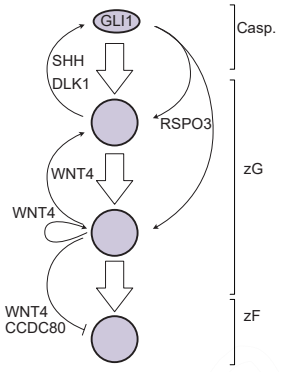

Figure 17: **Modèle d'interactions paracrine entre la capsule et les cellules stéroïdogènes**

[27] voir paragraphe 1.2 - Anatomie et histologie de la glande

la capacité de potentialiser l'effet prolifératif induit par la β-caténine.

2.2.4 La voie ACTH/PKA/AMPc : renouvellement cortical et différenciation du cortex interne

Le rôle de la signalisation ACTH sur le remodelage du cortex surrénalien est illustré en pathologies humaines par des mutations perte ou gain de fonction et attesté expérimentalement par des modèles de souris génétiquement modifiées reproduisant certaines de ces mutations au sein de la surrénale.

Ces mutations peuvent affecter les différents composants de la voie de signalisation et aboutir à une activation ou une inhibition de la signalisation PKA [28]

2.2.4.1 Excès d'activité PKA

Chez l'Homme, la perte de la sous unité régulatrice de la PKA, R1α induit une activité constitutive de la signalisation et se traduit par un syndrome héréditaire rare, le complexe de Carney (OMIM #160980). C'est un syndrome multinéoplasique qui induit entre autres des hyperfonctions endocrines au niveau hypophysaire, thyroïdien, gonadique et surrénalien (Espiard et al., 2020; Kamilaris et al., 2019). A l'échelle surrénalienne, il se manifeste par une hyperplasie modérée du cortex ou PPNAD (Primary Pigmented Nodular Adrenal Disease) dans 25 à 60% des cas. Le PPNAD se caractérise par l'apparition de petits nodules pigmentés de moins d'un cm de diamètre entourés de tissu cortical atrophié. Ces nodules sont responsables d'une sécrétion autonome de glucocorticoïdes qui se manifeste par un syndrome de Cushing et par un effondrement des taux circulant d'ACTH expliquant l'atrophie du cortex "sain" internodulaire. Le

[28] Différentes mutations sont associées à une activation de la signalisation ACTH mais ne seront pas traitées dans ce paragraphe. Par exemple des mutations gain de fonction de la protéine G activatrice α_s (*GNAS*) qui produit le syndrome de McCune Albright (OMIM #174800) (Carney et al., 2011) ou la duplication du gène codant la sous unité catalytique de la PKA (*PRKACA*) qui provoque des adénomes corticosurrénaliens unilatéraux ou des hyperplasie bilatérales des surrénales (Kamilaris et al., 2021) pour lesquels aucun modèle murin n'a été développé, des mutations perte de fonction des phosphodiestérases 11A qui sont associées au syndrome de Carney chez l'Homme (Szarek and Stratakis, 2014) mais dont la délétion chez la souris ne produit pas de phénotype surrénalien (Seftel, 2005).

syndrome de Cushing provoque chez les patients, une hyperglycémie une résistance à l'insuline, un redistribution du tissu adipeux au niveau viscéral, une fonte musculaire, une ostéoporose, des troubles anxieux et cognitifs et une absence d'inflammation (Lacroix et al., 2015).

Le rôle causal des mutations perte de fonction affectant R1α a pu être établi dans divers modèles de souris. En effet, les souris portant une délétion homozygote de R1α dans le cortex embryonnaire (*0.5Akr1b7-cre* ou *Sf1-Cre::Prkar1a*$^{fl/fl}$) (Drelon et al., 2016; Sahut-Barnola et al., 2010), ou post-natal (*Cyp11b2*^{Cre}*/+::Prkar1a*$^{fl/fl}$) (Dumontet et al., 2018) produisent un excès de GC indépendamment de la stimulation ACTH et présentent les manifestations métaboliques et morphologiques des patients atteints du syndrome de Cushing (Amaya et al., 2021; Amaya et al., 2022; Dumontet et al., 2018; Sahut-Barnola et al., 2010).

Par ailleurs le cortex surrénalien de ces souris présente une hyperplasie fasciculée associée à une perte d'identité des cellules glomérulées (Drelon et al., 2016; Dumontet et al., 2018). Cette dédifférenciation s'explique par l'effet répresseur de la PKA sur la signalisation WNT/β-caténine nécessaire au maintien de l'identité glomérulée et notamment par une dérégulation de la phosphorylation de la β-caténine qui favorise sa dégradation (Drelon et al., 2016; Dumontet et al., 2018).

En outre, l'activation postnatale de la PKA stimule le renouvellement cellulaire du cortex comme l'attestent les expériences de lignage cellulaire et l'épuisement concomitant des progéniteurs capsulaires (GLI1+) et sous capsulaires (SHH+) chez les souris mutantes (Dumontet et al., 2018). Ces résultats démontrent le rôle de la PKA sur le recrutement et la différenciation des progéniteurs et des cellules glomérulées vers l'identité fasciculée, les mécanismes sous-jacents restent toutefois incompris.

L'autre impact de l'activation constitutive de la PKA suite à la perte de R1α est le remodelage du cortex profond qui acquiert une identité et une fonction de zone réticulée, normalement absente chez la souris (Dumontet et al., 2018; Sahut-Barnola et al., 2010). La zone réticulée, qui apparaît chez l'Homme entre 8 et 9 ans au cours de l'adrénarche,

produit, sous la dépendance de l'ACTH, des précurseurs androgéniques tels que la DHEAS (Dehydroepiandrosterone sulfate), responsable de l'apparition de la pilosité axillaire et du changement d'odeur corporelle (Rosenfield, 2021). Ainsi, la PKA stimule la différenciation de la zF en une zone similaire à la zone réticulée humaine, qui exprime également CYP17, enzyme nécessaire à la conversion des stéroïdes en leur équivalent hydroxylés sur le carbone 17 [29] et qui produit des androgènes surrénaliens comme la DHEAS. [30].

Des mutations perte de fonction de la PDE8B sont retrouvées chez des patients atteints de PPNAD ou d'hyperplasie bilatérale des surrénales (Wilmot Roussel et al., 2013) et la perte de la PDE8B chez la souris aboutit à une augmentation des taux plasmatique de corticostérone et une diminution des taux d'ACTH. Toutefois, ces souris ne développent pas de syndrome de Cushing ni d'hyperplasie surrénalienne et la présence d'une zone pseudo réticulée n'a pas été rapportée (Tsai et al., 2011).

2.2.4.2 Effet de l'absence de stimulation ACTH

- Perte des récepteurs à l'ACTH

Chez l'Homme, le déficit familial en glucocorticoïdes (FGD) (OMIM #202200) se caractérise par une insuffisance surrénalienne et une atrophie du cortex (Migeon et al., 1968). Il est causé dans 25 % des cas par des mutations perte de fonction de *MC2R* (FGD1) (Clark et al., 1993; Naville et al., 1996; Tsigos et al., 1993; Weber et al., 1995), dans le reste des cas (FGD2), il peut toucher *MRAP*, codant le co-récepteur de MC2R (Buonocore and Achermann, 2020; Metherell et al., 2005).

Afin d'évaluer le rôle causal de ces mutations, des modèles murins de délétion de MC2R et MRAP ont été développés (Chida et al., 2007; Novoselova et al., 2018).

[29] voir paragraphe 1.3.2.3 - Etapes de la stéroïdogénèse surrénalienne

[30] De façon intéressante, des travaux réalisés au laboratoire montrent que la perte de la signalisation androgénique induit également la différenciation des cellules fasciculées en cellules apparentées à des cellules réticulées. Cependant, bien que ces cellules expriment la 20α-HSD, elles n'expriment pas CYP17 et ne produisent pas de précurseurs androgéniques

Comme attendu, ces deux modèles comportent de nombreux traits phénotypiques communs. Dans les deux cas, la mutation provoque une forte mortalité périnatale. Cette mortalité, due aux altérations du métabolisme du glucose hépatique et de la maturation des poumons peut être compensée par une supplémentation en glucocorticoïdes (Chida et al., 2007; Novoselova et al., 2018).

En ce qui concerne le cortex surrénalien, ces deux modèles induisent une hypoplasie drastique aboutissant à une absence totale de corticostérone et de réponse à l'ACTH. L'aldostérone est quand à elle fortement réduite chez les souris déficientes pour MC2R mais pas pour MRAP. L'absence de signalisation PKA semble ainsi cibler préférentiellement la zF, ceci est confirmé par l'analyse histologique de la glande qui dans les deux cas, présente une zone fasciculée atrophiée tandis que la zone glomérulée est peu touchée.

Ces deux modèles présentent également un épaississement de la capsule ainsi qu'une expansion du domaine d'expression de *Shh* dans le cortex des souris déficientes pour MRAP suggérant une accumulation des progéniteurs [31].

Le croisement des données humaines et des souris confirme le rôle central de la signalisation ACTH pour la mise en place de la zone fasciculée [32], le recrutement des progéniteurs et la fonction stéroïdogène du cortex surrénalien.

- Signalisation PKA et apoptose

L'atrophie observée en cas d'absence des récepteurs a l'ACTH suggèrent une augmentation de l'apoptose. Dans des conditions physiologiques, l'apoptose a lieu au niveau de la jonction corticomédullaire et est stimulée par un blocage de l'axe hypophysaire-surrénalien induit par la prédnisolone (Wyllie et al., 1973) ou la déxaméthasone (Thomas et al., 2004), une hypophysectomie (Carsia et al., 1996;

[31] Ce résultat pourrait être dû à un effet négatif direct de la PKA sur la signalisation HH ayant lieu dans les cellules capsulaires, qui serait en l'occurrence aboli (Liu, 2019)

[32] Des résultats récents montrent que dans un contexte de perte de MC2R, l'injection d'ostéocalcine permettrait de restaurer en partie les fonctions de la surrénale et de limiter la mortalité périnatale, suggérant que l'ostéocalcine exerce un rôle sur l'acquisition des fonctions fasciculée et agirait en parallèle ou en aval da signalisation PKA (Yadav et al., 2022)

Ceccatelli et al., 1995). A l'inverse, elle est prévenue par un traitement par de l'ACTH (Carsia et al., 1996; Ceccatelli et al., 1995; Thomas et al., 2004; Wyllie et al., 1973) impliquant directement sa signalisation dans l'inhibition de l'apoptose surrénalienne.

L'implication de la signalisation PKA dans la prévention de l'apoptose a été confirmé *in vitro* et *in vivo* par l'invalidation de *PRKAR1A* [33]. Dans des cellules corticosurrénaliennes humaines H295R, la diminution de l'expression de *PRKAR1A via* une approche d'ARN interférant aboutit à une protection partielle des cellules face à l'apoptose induite par le TGFβ (Ragazzon et al., 2009). De façon similaire, le traitement par du H89, un inhibiteur pharmacologique de la PKA, induit une augmentation de l'apoptose des cellules corticosurrénaliennes murines ATC7 (de Joussineau et al., 2014). *In vivo*, la perte de PRKAR1A dans le cortex surrénalien (AdKO) protège les cellules stéroïdogènes de l'apoptose induite par un traitement à la déxaméthasone (de Joussineau et al., 2014; Sahut-Barnola et al., 2010) tout comme la perfusion d'ACTH en continu (Menzies et al., 2017).

Un des mécanismes proposés pour expliquer cette apoptose est l'activation de la voie de signalisation mTOR par la PKA. En effet, la perte de PRKAR1A chez les souris et le traitement par l'AMPc des cellules, induisent une stimulation de la voie mTOR tandis qu'un inhibiteur de mTOR, la rapamycine, lève en partie la protection face à l'apoptose conférée par la signalisation PKA (de Joussineau et al., 2014).

L'apoptose surrénalienne est donc un phénomène physiologique survenant au niveau de la jonction corticomédullaire dont l'occurrence est limitée par l'ACTH et la signalisation PKA. Cette apoptose semble mettre en jeu la signalisation mTOR néanmoins les causes et les mécanismes de cette apoptose restent encore à préciser.

Questions et perspectives

En s'opposant à la signalisation WNT, la signalisation PKA, stimulée par l'ACTH hypophysaire, facilite le recrutement des progéniteurs puis leur différenciation. Parallèlement, elle exerce un effet d'accélération du renouvellement cortical. Mais

[33] voir paragraphe 2.2.4.1 - Excès d'activité PKA

alors que les cellules glomérulées expriment *Mc2r* et *Mrap* (Lopez et al., 2021b), comment expliquer que les cellules glomérulées maintiennent leur identité?
Une hypothèse, énoncée en 1987 (Hyatt, 1987), serait que le sang a tendance a s'accumuler au niveau du cortex profond augmentant le contact entre ces cellules et l'ACTH. Cette hypothèse est cohérente avec l'expression différentielle de *Mc2r*, *Cyp11b2* et *Cyp11b1* en fonction de leur position dans un modèle *in vitro* de cellules corticales dans un flot de milieu avec un gradient de concentration en forskoline ou AngII (Friedrich et al., 2021). Il est également possible que d'autres signaux favorisent ou défavorisent la capacité des cellules à se différencier.

LA SUMOYLATION

3 La SUMOylation, une modification en partie similaire à l'ubiquitination

TOUTES les cellules d'un organisme possèdent le même génome, ainsi pour permettre aux cellules d'assurer leurs fonctions et de s'adapter, l'expression et l'activité des protéines doivent être régulées. L'un des moyens pour atteindre ce but est la modification post-traductionnelle des protéines. Les modifications post-traductionnelles sont variées et comptent par exemple la phosphorylation, l'acétylation, l'ubiquitination ou encore la SUMOylation.

Le processus de SUMOylation a été découvert simultanément par deux équipes. Ces équipes ont identifié que la protéine du pore nucléaire RanGAP1, possédait deux formes différant d'environ 20 kDa, due à la liaison à un autre polypeptide. Celui-ci, qui forme un *smear* en western blot, indiquant son association à de multiples protéines, correspond à SUMO1 (Mahajan et al., 1997; Matunis et al., 1996).

3.1 Mécanismes moléculaire de la SUMOylation

La famille SUMO (Small Ubiquitin-like Modifier), est composée chez la souris de trois protéines : SUMO1, 2 et 3 [34]. SUMO2 et SUMO3 ne diffèrent que par 3 acides aminés (Figure 18.A.), ce qui les rend indistinguables lors de l'utilisation d'anticorps. SUMO1 partage 43 et 42 % d'identité avec SUMO2 et SUMO3, respectivement. Les protéines SUMO possèdent une séquence primaire peu similaire à l'ubiquitine (16% d'identité pour SUMO1) (Bayer et al., 1998) mais partagent une structure tridimensionnelle, le repliement ββαββαβ (Jin et al., 2001), l'un des neufs "super-repliements" (Kiel and

[34]Chez l'Homme, il existe deux autres SUMOs (Bouchard et al., 2021) : SUMO4, dont des mutations seraient potentiellement associées à des prédispositions au diabète de type 1 (Bohren et al., 2004; Guo et al., 2004) ou à la sclérose latérale amyotrophique (OMIM # 105400) (Osmanovic et al., 2022) et SUMO5 qui favoriserait la formation des corps PML (Liang et al., 2016)

Serrano, 2006; Orengo et al., 1994) (Figure 18.A.B.) permettant d'expliquer certaines similarités fonctionnelles.

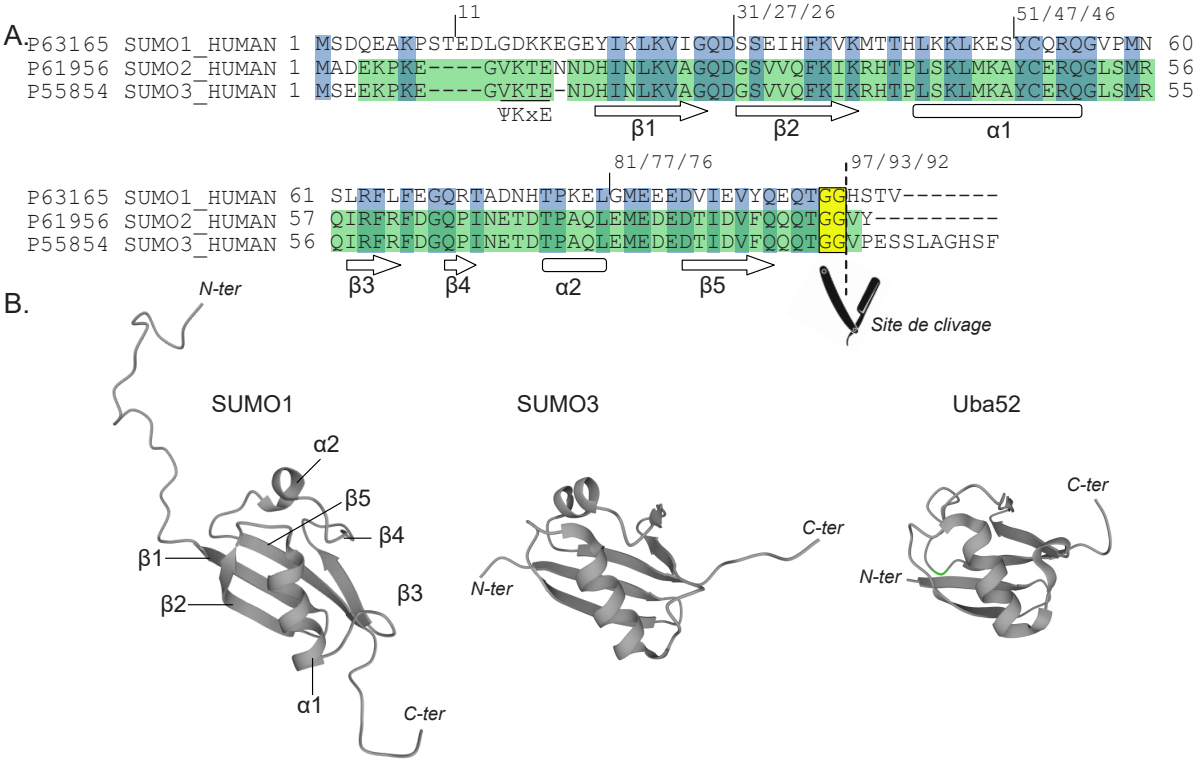

Figure 18: **Séquence des différents peptides SUMO et similarités avec l'Ubiquitine**
A. Séquence des 3 peptides SUMO humains. Les résidus bleus sont conservés dans les 3 protéines tandis que les verts sont spécifiques à SUMO2 et SUMO3. B. Comparaison des structures tertiaires de SUMO1, SUMO3 et de l'ubiquitine humains. Les feuillets β sont représentés par des flèches tandis que les hélices α sont représentés par des vrilles

En effet, la SUMOylation partage avec l'ubiquitination, sa cascade enzymatique en trois étapes et amenant à la liaison covalente d'un peptide SUMO sur une protéine cible.

- L'enzyme d'activation E1, formé de l'hétérodimère SAE1/UBA2 (Desterro et al., 1999; Okuma et al., 1999)
- L'unique enzyme de conjugaison UBC9 (Okuma et al., 1999)
- les multiples E3 SUMO ligases

Avant la conjugaison, les derniers acides aminés de la queue C-terminal de SUMO, sont clivés pour exposer les résidus Gly-Gly, nécessaires à la conjugaison (Johnson, 1997) [35]. Après cette étape, SAE1/UBA2 forme une liaison thioester avec le motif GG de SUMO

[35]SUMO4 possède une proline en aval du motif GG qui prévient sa maturation et ainsi son utilisation en tant que substrat pour la SUMOylation (Owerbach et al., 2005)

suite à une réaction ATP-dépendante (Desterro et al., 1999). SUMO est ensuite transféré à UBC9, formant à nouveau une liaison thioester (Okuma et al., 1999). Enfin, UBC9 crée la liaison covalente entre la queue C-terminale du peptide SUMO et une lysine de la protéine cible (Figure 19). L'étape de ligation est possible *in vitro* en présence de UBC9 et de son substrat uniquement, mais est catalysée par la présence de E3 SUMO ligases (Kahyo et al., 2001; Potts and Yu, 2005).

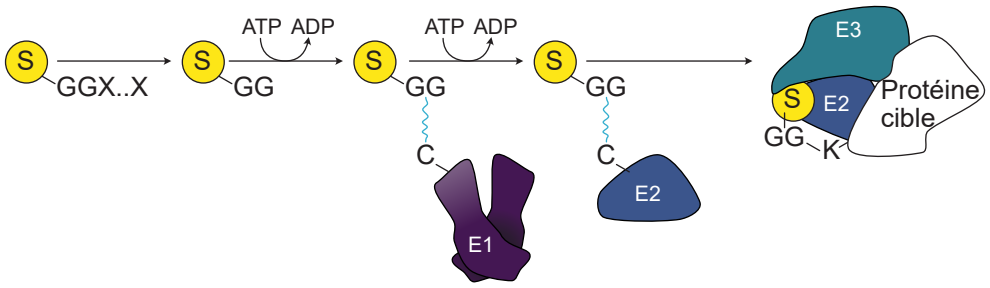

Figure 19: **Schéma détaillé de la SUMOylation d'une protéine cible** G : Glycine, C : Cystéine, K : Lysine, X : n'importe quel acide aminé

La majorité des E3 SUMO ligases comportent un domaine doigt de zinc de type SP-RING (Siz/PIAS RING) similaire au domaine RING des E3 ubiquitine ligases MDM2 et c-CBL (Kahyo et al., 2001). Ces E3 sont composées des protéines ZMIZ1 (Sharma, 2003), NSE2 (Potts and Yu, 2005) mais surtout de la famille PIAS (protein inhibitors of activated STAT) qui sont au nombre de 4 chez la souris (PIAS1, PIAS2, PIAS3 et PIAS4) (Abdelaleem et al., 2017; Kahyo et al., 2001; Kotaja et al., 2002; Nishida and Yasuda, 2002; Sachdev, 2001). D'autres E3 SUMO ligases ne comportent pas de domaine SP-RING comme RanBP2 (Pichler et al., 2002), TRIM28 (Li et al., 2020), TRIM38 (Hu et al., 2016), TOPORS (Weger et al., 2005), EGR2 (García-Gutiérrez et al., 2011), HDAC4 (Zhao et al., 2005), P19 (Tago et al., 2005), MAPL (Braschi et al., 2009; Prudent et al., 2015) ou CBX4/PC2 (Kagey et al., 2003).

La SUMOylation a lieu sur une lysine, afin de déterminer les lysines acceptrices, il a été émis l'hypothèse d'une séquence commune à tous les sites de SUMOylation. L'étude par mutagénèse des séquences de RanGAP1, IκBα et P53 a permis de mettre en évidence une séquence consensus de SUMOylation : ΨKx[D/E] [36] (Rodriguez et al.,

[36] Ψ est un acide aminé hydrophobe comme la leucine ou la valine, l'isoleucine, la méthionine ou la phénylalanine, K est une lysine, D l'aspartate, E le glutamate et x n'importe quel acide aminé

2001). Cette spécificité de site consensus est illustrée par la capacité que possèdent SUMO2 et SUMO3 à former des chaînes poly-SUMOs sur leur lysine 11 présente au sein d'un site consensus et absente chez SUMO1 (Tatham et al., 2001) (Figure 18.A.). Ce site consensus permettant d'interagir avec UBC9 (Lin et al., 2002), a été élargit par la présence de résidus acides en aval du site (Yang et al., 2006a). Ces résidus acides, négativement chargés favoriseraient la liaison avec UBC9, *via* la présence dans celui-ci, d'un domaine basique (Yang et al., 2006a). Ce mécanisme est cohérent avec l'idée d'un site phospho-dépendant ΨKxD/ExxSP [37] où le phosphate apporté sur la sérine ajouterait une charge négative contribuant au recrutement d'UBC9 (Hietakangas et al., 2006).

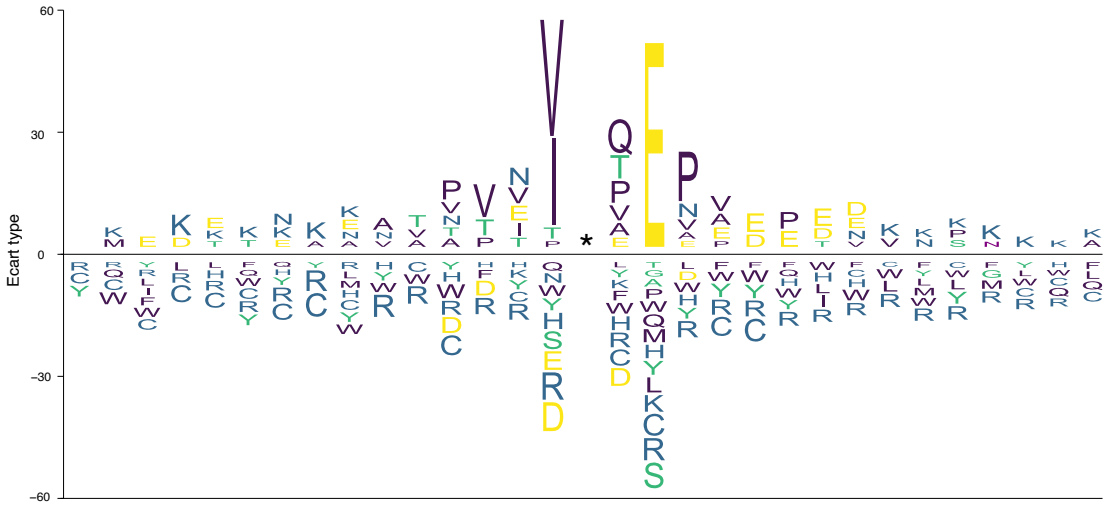

Figure 20: **IceLogo des sites de SUMOylation**
Peptides issues des 10% de lysines les plus SUMOylées chez la souris. Les residus au dessus de la ligne sont enrichis et ceux en dessous sont deplétés par rapport à un jeu de protéine aléatoire (Hendriks and Vertegaal, 2016). La lysine cible est représentée par un astérisque.

Cependant, bien que SUMO2 et SUMO3, ne possèdent qu'un site consensus sur la lysine 11, ils sont capables de constituer des chaînes poly-SUMOs branchées en se liant à la lysine 32/33 (Bruderer et al., 2011; Hendriks et al., 2018; Matic et al., 2008) (Figure 18). En outre, des protéines comme DRP1 [38] (Figueroa-Romero et al., 2009) ou CREB (Comerford et al., 2003) sont SUMOylés sur des sites non consensus. Des études plus récentes de

[37] S est une sérine et P une proline
[38] Voir paragraphe 9.2 - Des régulations post-traductionnelles capitales

spectrométrie de masse, ont montré une grande diversité de sites accepteurs (Hendriks and Vertegaal, 2016) (Figure 20.A.) et ont estimé que les sites consensus (ou consensus inversés [E/D]xKΨ) ne représentent qu'environ 35% des sites accepteurs (Hendriks et al., 2018; Ulman et al., 2021). Par ailleurs, bien que les protéines SUMOs varient peu au cours de l'évolution (Figure 21.), les sites de SUMOylation comptent parmi les sites de modifications post-traductionnelles les moins conservées (Minguez et al., 2012).

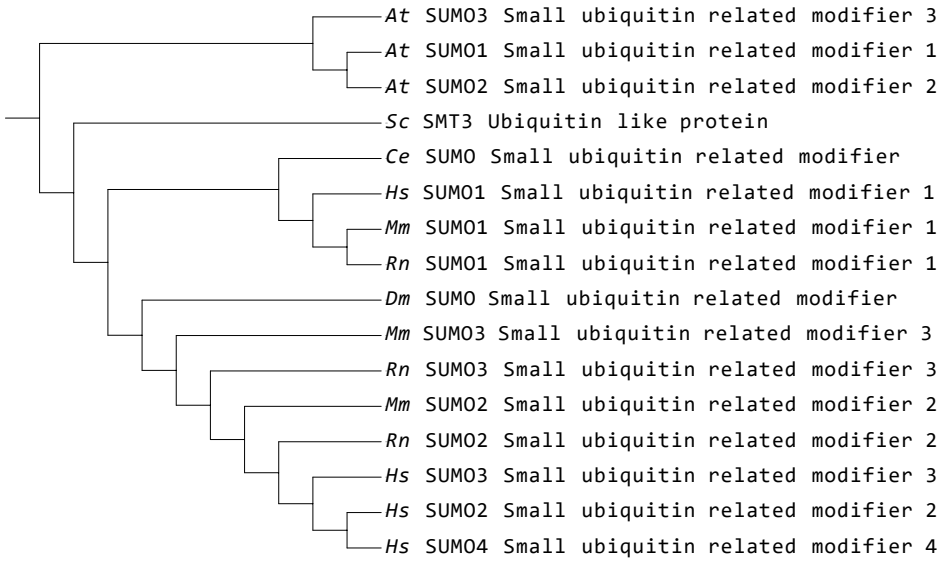

Figure 21: **Arbre phylogénique des séquences SUMO** *At : Arabidopsis thaliana, Ce : caenorhabditis Elegans, Dm : Drosophilia melanogaster, Hs : Homo Sapiens, Mm : Mus musculus, Rv : Rattus norvegicus, Sc : Saccharomyces cerevisiae* Arbre construit avec iTOL (Letunic and Bork, 2021)

3.2 DéSUMOylation et SENP2

Contrairement à l'ubiquitination qui amène généralement les protéines vers un destin inéluctable, la SUMOylation est un processus dynamique et réversible. En effet, une protéine SUMOylée peut être déconjuguée par une action enzymatique. Les enzymes impliquées dans ce clivage sont DeSI1/2 (DeSumoylating Isopeptidase) (Shin et al., 2012; Suh et al., 2012) USPL1 (Ubiquitin-Specific Protease-Like 1) (Li et al., 2022; Schulz et al., 2012) ou les protéines de la famille des SENPs (Sentrin specific protease).

Cette famille est composée de six protéines [39] qui peuvent être classées en trois catégories

[39]Il existe également une protéine SENP8 qui catalyse la déconjugaison de NEDD8, modification similaire à la SUMOylation (Mendoza et al., 2003)

en fonction de leur activité (Figure 22) :

- SENP1 et SENP2 qui catalysent la déSUMOylation de SUMO1 et SUMO2/3 (Best et al., 2002; Itahana et al., 2006; Nishida et al., 2001) bien que SENP1 possède une forte préférence pour SUMO1 *in vivo* (Sharma et al., 2013).
- SENP3 et SENP5 qui prennent en charge préférentiellement SUMO2/3 (Gong and Yeh, 2006; Nishida et al., 2000).
- SENP6 et SENP7 qui ciblent préférentiellement les chaînes de polySUMOs (Lima and Reverter, 2008; Mukhopadhyay et al., 2006) bien que SENP6 soit capable de déSUMO1-yler RANGAP1 *in vitro* (Kim et al., 2000)

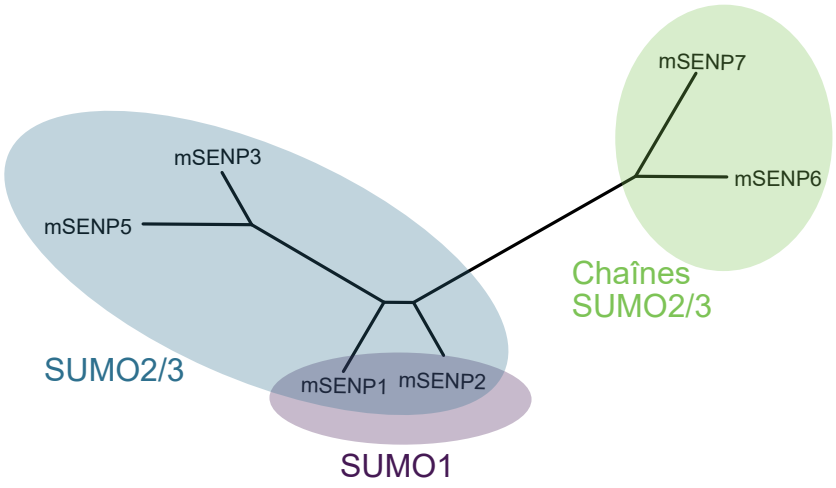

Figure 22: **Arbre phylogénique des SENPs murines**
Arbre construit avec iTOL (Letunic and Bork, 2021)

En plus de ces actions de déSUMOylation, USPL1 et SENP1-5 sont responsables de la maturation des peptides SUMO révélant le motif Gly-Gly (Lima and Reverter, 2008; Schulz et al., 2012) (Figure 19).

Au sein de la surrénale murine, les transcrits de SENP3 et SENP6 sont les plus abondants (Figure 23) mais l'expression de SENP2 est stimulée par la signalisation PKA (Dumontet et al., 2019) de manière analogue au tissu adipeux où cela s'explique par l'interaction de CREB en amont du promoteur de *Senp2* (Chung et al., 2010).

SENP2 est une déSUMOylase de 589 acides aminés (Nishida et al., 2001) nécessaire au

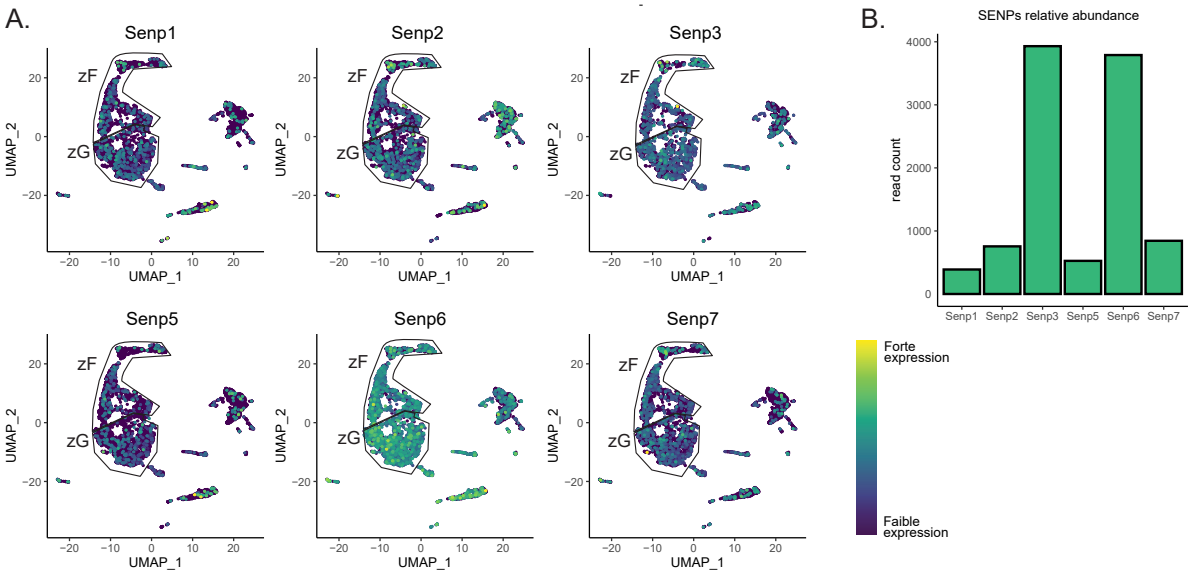

Figure 23: **Expression des différentes SENPs dans le cortex surrénalien murin**
A. UMAP représentant l'expression relative des SENPs en fonction du type cellulaire, données issues de séquençage ARN en cellule unique (Lopez et al., 2021)
B. Histogramme représentant les niveaux d'expression des SENPs dans la surrénales, données issues de séquençage ARN (GEO : GSE193480)

développement embryonnaire [40] (Maruyama et al., 2016; Yu et al., 2020). Elle contient en N-terminale, une hélice amphiphile (Figure 24), lui permettant de se localiser au niveau des membranes nucléaires mais aussi de l'appareil de Golgi, du réticulum endoplasmique (Odeh et al., 2018) et de la mitochondrie (Fu et al., 2014). SENP2 possède également un domaine de localisation nucléaire et un domaine d'export nucléaire qui permettent le contrôle dynamique de sa localisation subcellulaire (Itahana et al., 2006) contrairement à SENP1 retrouvé au niveau de *foci* nucléaires (Bailey and O'Hare, 2002), SENP3 dans les nucléoles (Nishida et al., 2000) et SENP6 dans le cytoplasme (Kim et al., 2000). Par ailleurs, SENP2 possède des variants d'épissage (Nishida et al., 2001) utilisant des sites d'initiation de traduction différents. Alors que la forme longue de SENP2 (589 AA) est principalement localisée au niveau de la membrane nucléaire et de la chromatine (Garvin et al., 2019), SENP2M (542 AA) est localisé principalement dans les vésicules cytoplasmiques et la région périnucléaire tandis que SENP2S (511 AA) est cytoplasmique (Fu et al., 2014; Jiang et al., 2011) (Figure 24).

[40] voir paragraphe 4.2.3.3 - Perte des SENPs

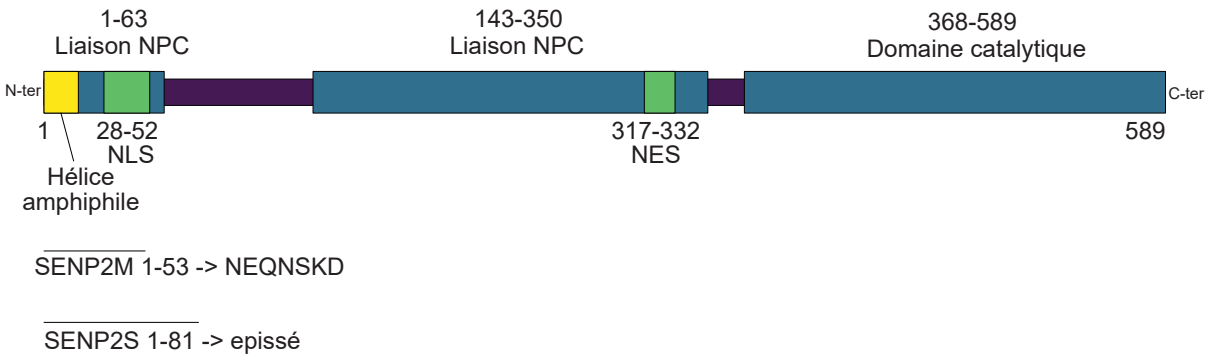

Figure 24: **Domaines protéiques et variants d'épissage de SENP2**

3.3 Interactions protéines-protéines et spécificité de substrat

La spécificité de l'ubiquitination se fait grâce à la myriade d'E3 ubiquitine ligases qui reconnaissent un substrat particulier. A l'inverse, on connaît à l'heure actuelle presque 6000 protéines SUMOylables (Ulman et al., 2021) et une quinzaine d'E3 SUMO ligases, ce qui questionne sur les mécanismes permettant la spécificité de substrats de la SUMOylation.

Les E3 SUMO ligases peuvent reconnaître les peptides SUMO grâce à la présence d'une séquence de reconnaissance de SUMO appelée SIM (SUMO interacting motif) qui permet de créer une liaison non covalente [41] (Minty et al., 2000; Song et al., 2004). Le motif SIM se compose d'un cœur de résidus hydrophobes ΨΨΨΨ, ΨΨxΨ ou ΨxΨΨ formant un feuillet β qui interagit avec le feuillet β2 de SUMO (Hecker et al., 2006; Song et al., 2004). Les acides aminés de part et d'autre du cœur permettent de créer une interaction avec l'hélice α1 de SUMO. Les protéines interagissant préférentiellement avec SUMO2/3 possèdent des acides aminés acides (aspartate ou glutamate) (Hecker et al., 2006) ou phosphorylables (sérine ou thréonine) (Cappadocia et al., 2015) tandis que le cœur est plutôt entouré de prolines et de lysines dans les protéines interagissant avec SUMO1 (González-Prieto et al., 2021). Le choix entre la modification par SUMO1 ou SUMO2/3 semble donc reposer en partie sur la capacité des SIMs présents sur les E3 à reconnaître un paralogue SUMO plutôt qu'un autre. Des travaux récents montrent que ce choix pourrait

[41] Il existe d'autres motifs permettant la liaison à SUMO, comme sur DPP9 qui interagit avec le feuillet β3 de SUMO1 et recrute alors SUMO1 uniquement (Pilla et al., 2012)

être également dicté par l'acétylation de UBA2 qui permet à ce dernier de favoriser la modification par SUMO2 par rapport à SUMO1 (Walker et al., 2022).

Un autre moyen de modifier spécifiquement un substrat passe par la localisation subcellulaire des E3 et des SENPs. En effet, la plupart des substrats de la SUMOylation sont nucléaires (Hendriks et al., 2018) alors que les SENPs sont localisées dans différents compartiments subcellulaires ou sous compartiments [42]. Par exemple, la mutation du NLS de SENP2 (mais pas du NES) entraîne une accumulation de protéines SUMOylées par SUMO3, suggérant que l'activité de déSUMOylation de SUMO3 par SENP2 a lieu principalement au niveau du noyau (Itahana et al., 2006).

Cette sensibilité peut permettre d'aboutir à une spécificité relative de substrat. En effet certaines protéines ne sont SUMOylables que par une combinaison particulière d'acteurs, ainsi la protéine DBC est prise en charge par PIAS3 (mais pas PIAS1, 2 ou 4), SUMOylée uniquement par SUMO2 et 3 et déSUMOylée par SENP1 (Park et al., 2014) (Figure 25).

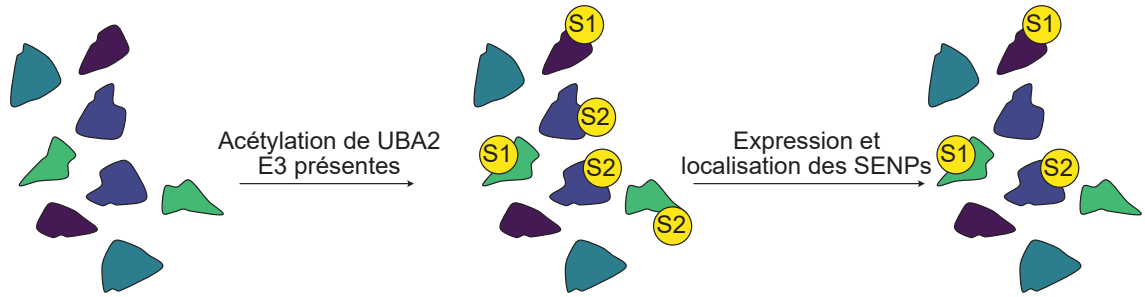

Figure 25: **Hypothèse concernant les mécanismes de spécificité de la SUMOylation** Pour un pool de protéine donnée, seules certaines comportent des lysines SUMOylables. Ces dernières seront SUMOylées par SUMO1 ou SUMO2/3 selon l'état d'acétylation de UBA2 et les E3 exprimées dans le compartiment subcellulaire. Enfin, les SENPs présentent reconnaitront certaines protéines cibles et certains SUMOs.

3.4 Interaction avec l'ubiquitination

Parmis les 5847 protéines connues pour être SUMOylées, 1087 sont ubiquitinées sur une autre lysine et 4188 sur la même lysine appelée SAM (Site of Alternate Modification) (Ulman et al., 2021), il est alors aisé d'imaginer que ces deux modifications interagissent

[42] voir paragraphe 3.2 - DéSUMOylation et SENP2

entre elles. En effet, le couple de modification post-traductionnelles co-ocurrant le plus fréquemment sur le même résidu est ubiquitination/SUMOylation (Ulman et al., 2021). Il semblerait toutefois que les SAMs ne possèdent pas de séquence spécifique par rapport aux sites de SUMOylation exclusifs (Ulman et al., 2021; Xu et al., 2021). La présence de ces lysines ambivalentes est associée à une plus forte probabilité de posséder un NLS et un NES ainsi qu'à une stabilité plus élevée en accord avec les rôles connus de la SUMOylation et l'ubiquitination (Ulman et al., 2021).

Le mécanisme le plus simple permettant d'expliquer la stabilité relative des protéines possédant un SAM est que la SUMOylation d'un SAM prévient son ubiquitination et ainsi empêche la dégradation de la protéine. C'est le cas de IκBα qui est SUMOylée et ubiquitinée sur la lysine K21 (Desterro et al., 1998) et qui est stabilisée par sa SUMOylation.

Un autre mécanisme de compétition entre SUMOylation et Ubiquitination, affectant cette fois plusieurs protéines, concerne l'E3 ubiquitine ligase MDM2 dont l'activité est réprimée par la SUMOylation. Lorsqu'elle est déSUMOylée par SENP2, elle peut ubiquitiner la protéine suppresseur de tumeur, P53, induisant sa dégradation (Jiang et al., 2011).

A l'inverse, ubiquitination et SUMOylation peuvent agir de concert. C'est notamment le cas pour les STUbLs (SUMO-targeted ubiquitin ligase) RNF4 (Sun et al., 2007a) et RNF111 (Sun and Hunter, 2012) chez les mammifères. Ce sont des E3 ubiquitine ligases qui possèdent un ou plusieurs SIMs ce qui leur permet de reconnaître les chaînes de SUMOs sur une protéine, qui sera alors polyubiquitinée et dégradée par le protéasome.

A l'échelle de la cellule, inhiber l'ubiquitination [43], provoque une augmentation de la SUMOylation des protéines nouvellement synthétisées (Sha et al., 2019). Cet effet peut s'expliquer par la stabilisation des protéines nouvellement synthétisées qui deviennent alors cibles de la SUMOylation mais aussi par une stabilisation des E3 SUMO ligases qui peuvent alors exercer leur activité sans être dégradées. A l'inverse, la perte du NLS de SENP2, comportant un site d'ubiquitination, amène à sa stabilisation et à une diminution de la SUMOylation (Itahana et al., 2006) (Figure 26).

[43]Le TAK-243 utilisé ici bloque le transfert de l'ubiquitine activé par l'enzyme E1 sur l'enzyme E2

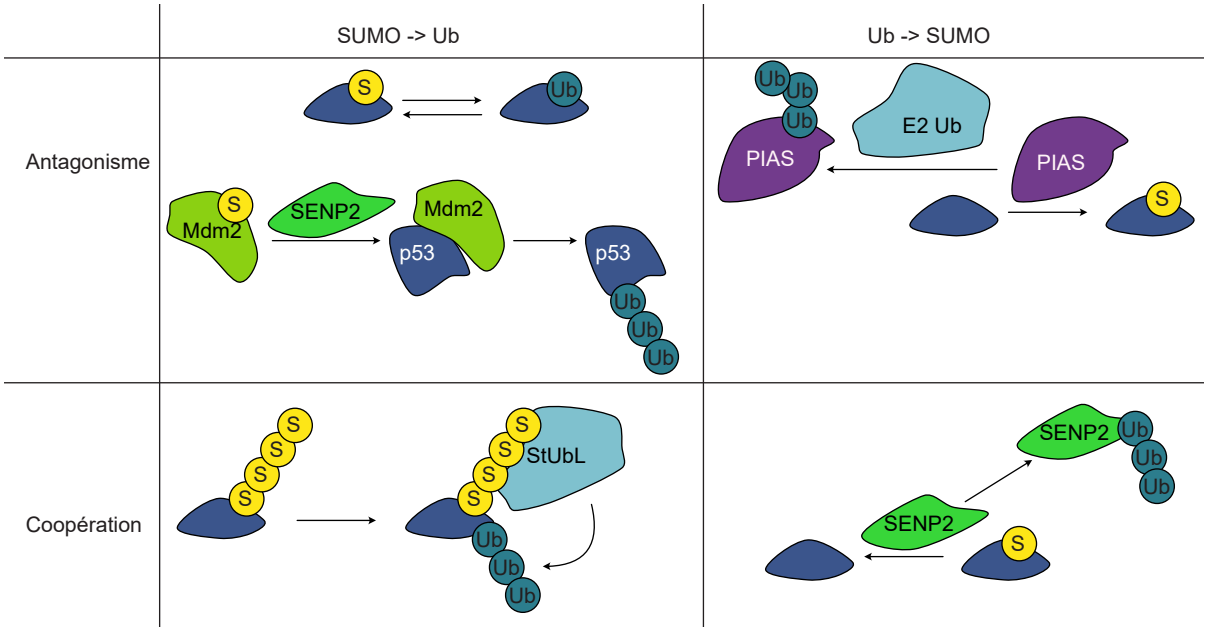

Figure 26: **Schéma des différentes interactions entre la SUMOylation et l'ubiquitination**

4 Fonctions biologiques de la SUMOylation

La SUMOylation, de par sa présence dans toutes les cellules et la multiplicité de ses cibles (Hendriks and Vertegaal, 2016; Hendriks et al., 2018) exerce de nombreuses fonctions au niveau de la cellule qui se répercutent sur les tissus et les organismes. A l'échelle moléculaire, la SUMOylation peut entre autre empêcher une interaction avec une autre protéine en masquant un site d'interaction, elle peut également créer une interaction grâce à la présence de SIMs, ou encore permettre un transfert dans un autre compartiment subcellulaire.

La diversité des cibles de la SUMOylation ne permet pas de faire la liste exhaustive de ses actions, en effet la SUMOylation exerce par exemple un rôle capital dans le contrôle de la mitose (Hanel et al., 2022; Mukhopadhyay and Dasso, 2017; Nacerddine et al., 2005) et est directement impliquée dans la réparation de l'ADN suite à une cassure double brins (Garvin et al., 2019).

Alors que la surrénale est l'organe au centre de la réponse au stress à l'échelle de l'organisme et, est elle-même fortement productrice de déchets oxydants pouvant altérer sa fonction (Meimaridou et al., 2018), il est important d'explorer le rôle de la SUMOylation dans la réponse au stress cellulaire pour pouvoir comprendre son rôle dans

le cortex surrénalien.

4.1 Senseur du stress oxydant

La SUMOylation répond à différents stresseurs cellulaires : génotoxique lorsque l'ADN est atteint, protéotoxique lors de l'accumulation de protéines mal repliées, la déficience en nutriment, le stress induit par une réponse immunitaire et enfin le stress oxydant qui sera l'objet de ce paragraphe.

Le stress oxydant est causé par un déséquilibre entre la production d'espèces oxygénées réactives (ROS) et les anti-oxydants. Ce déséquilibre peut être modélisé par l'utilisation de peroxyde d'hydrogène (H_2O_2). L'application de doses variables d'H_2O_2 induit des effets complexes sur la SUMOylation. En effet, alors que des fortes doses d'H_2O_2 provoquent une augmentation de la SUMOylation générale (Bossis and Melchior, 2006; Manza et al., 2004; Saitoh and Hinchey, 2000; Zhou et al., 2004) des doses entre 1 et 10 mM induisent une diminution de la SUMOylation générale.

La réponse de la SUMOylation face au stress oxydant est composée de trois phases selon le potentiel redox (Figure 27) :

- A des doses faibles d'H_2O_2 (0.01 à 0.5 mM), l'ubiquitination de SENP3 est inhibée amenant à sa stabilisation et sa relocalisation des nucléoles vers le nucléoplasme (Cai et al., 2021; Huang et al., 2009; Yan et al., 2010; Zhang et al., 2021b)
- Entre 1mM et 10 mM, les ROS induisent la formation d'une liaison thioesther entre UBC9 et UBA2 empêchant la formation d'une liaison entre ces derniers et le peptide SUMO et donc la SUMOylation (Bossis and Melchior, 2006). Parallèlement, l'expression génique de SENP1 est stimulée causant une déSUMOylation générale (Ma et al., 2020).
- Au dessus de 10 mM, l'H_2O_2 inhibe la fonction des SENPs aboutissant à une augmentation de la SUMOylation par déficit en déSUMOylation (Bossis and Melchior, 2006). Cette inhibition est causée par l'homodimérisation de SENP1 *via*

la création d'un pont disulfure entre les cystéines 603 et 613 (Xu et al., 2008) [44].

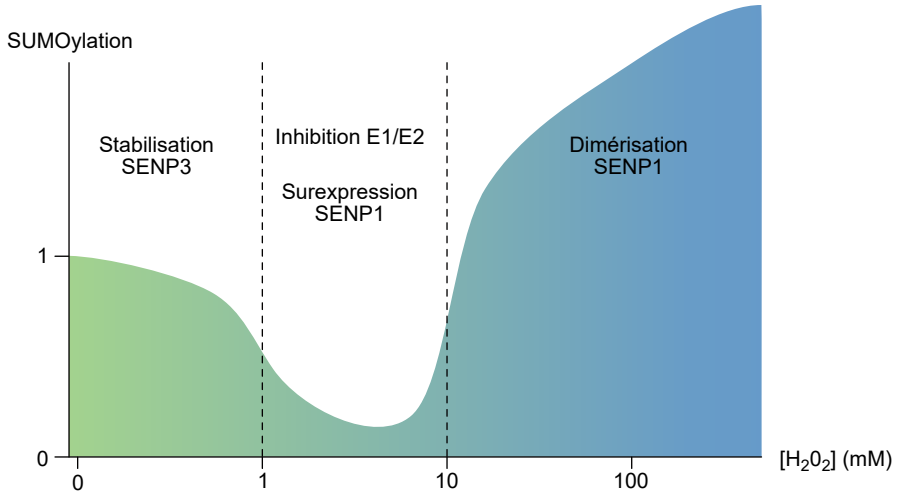

Figure 27: **Hypothèses sur les causes des variations de SUMOylations provoquées par le stress oxydant**

L'une des conséquences de la stabilisation de SENP3 suite à un stress oxydant léger est la stimulation de la prolifération. En effet, SENP3 déSUMOyle les protéines PMLs (promyelocytic leukemia) associées aux corps nucléaires. Ces derniers sont des organites sans membrane particulièrement sensibles à leur environnement et composés d'une couche de PMLs entourant d'autres protéines de nature variable. Ils agissent comme des *hubs* de modifications post-traductionnelles ce qui peut aboutir à des conséquences sur l'apoptose, l'autophagie, la prolifération et la tumorigénèse [45] (Lallemand-Breitenbach and de Thé, 2018). Dans un contexte de stress oxydant, la déSUMOylation des PMLs par SENP3, réduit le nombre de corps nucléaires PML et stimule la prolifération (Han et al., 2010). A l'inverse, une augmentation plus importante du stress oxydant *via* l'utilisation d'anhydride arsénieux (As_2O_3) promeut la formation de corps PML. Ces corps PML exercent alors des rôles complexes, ils sont nécessaires à l'activation de la signalisation de P53 et protègent des ROS tout en favorisant l'apoptose induite par ces derniers (Niwa-Kawakita et al., 2017).

[44] De façon intéressante, SENP2 ne se dimérise pas dans les mêmes conditions ce qui suggère un maintien de son activité de déSUMOylation et donc certains substrats qui restent potentiellement SUMOylés (Xu et al., 2008)

[45] La protéine PML a été nommée ainsi de par son rôle oncogénique dans la leucémie myéloïde aiguë (Grisolano et al., 1997)

Questions et perspectives :

Malgré cette capacité de la SUMOylation à répondre au stress oxydant, l'expression génique des acteurs de la SUMOylation n'est pas affectée par la hausse du stress oxydant observée dans le cortex des souris déficientes pour NNT (nicotinamide nucleotide transhydrogenase) (Meimaridou et al., 2018). Il serait intéressant d'observer le niveau de SUMOylation générale dans les surrénales de ces souris afin de pouvoir observer les effets du stress oxydant *in vivo*.

4.2 Dans les mécanismes développementaux et d'ontogénèse

4.2.1 La SUMOylation contrôle la mitose

Le traitement de cellules de cancer colorectal HCT116 avec un inhibiteur de SAE1 (ML-792) induit un arrêt de la prolifération avec des défauts de ségrégation lors de la mitose (He et al., 2017) suggérant que dans un organisme, il est capital de contrôler les niveaux de SUMOylation dès la première division cellulaire. En effet, les embryons déficients pour UBC9, présentent une mauvaise ségrégation en anaphase et une décondensation de la chromatine en métaphase empêchant tout développement consécutif (Nacerddine et al., 2005). Cette perte de condensation est cohérente avec une présence importante de SUMOs et des acteurs de la SUMOylation sur la chromatine, exerçant un rôle de contrôle transcriptionnel des caractéristiques de sénéscence [46] (Neyret-Kahn et al., 2013). De manière analogue à l'hypoSUMOylation, l'hyperSUMOylation aboutit *in fine* à un blocage de la mitose bien que le mécanisme soit probablement différent. Les cellules souches embryonnaires deplétées de l'ARNm maternel codant SENP7 n'atteignant le stade "deux-cellules" que dans 20% des cas (Huang et al., 2017).

[46] La perte de UBC9 induit l'apparition de caractéristiques de sénescence telles que l'arrêt de la prolifération, l'expression de la β-galactosidase acide et de *foci* associés à l'hétérochromatine tandis que des cellules sénéscentes comportent des faibles taux de SUMOylation au niveau de la chromatine (Neyret-Kahn et al., 2013)

4.2.2 Activation zygotique

Dans des conditions physiologiques, lorsque l'embryon atteint le stade "deux-cellules", le génome provenant de l'embryon va commencer à s'exprimer pour pouvoir progressivement remplacer les ARNm et les protéines de l'ovocyte, c'est l'activation zygotique. Ce processus implique de nombreux phénomènes dont notamment une modification de l'environnement chromatinien pour favoriser la transcription. Chez les mammifères, l'acteur maternel principal de cette activation est DUX (Jukam et al., 2017).

Au stade "deux-cellules", PIAS4 dont l'origine est maternelle, doit être dégradé afin de permettre l'activation zygotique. Cette nécessité s'illustre par deux mécanismes, le premier implique la stabilisation par PIAS4, de l'histone méthyl transférase SUV39H1 (suppressor of variegation 3-9 homolog 1) responsable du dépôt des marques H3K9me3 (Higuchi et al., 2019), or l'effacement de cette marque est nécessaire à l'activation du génome (Ancelin et al., 2016).
Le second mécanisme est le blocage de l'activité de DPPA2 dû à sa SUMOylation par PIAS4. Ce facteur, lorsque non SUMOylé, agit en tant qu'activateur transcriptionnel de DUX et est donc l'un des premiers acteurs de la cascade aboutissant à l'activation du génome zygotique (Yan et al., 2019). Ces résultats sont en accord avec les effets de la perte d'UBC9 dans des cellules souches embryonnaires qui induit une diminution des marques H3K9me3, l'expression de DUX et la transition des cellules souches embryonnaires en un état "2C-like" très similaire au stade "deux-cellules" pendant lequel a lieu l'activation du génome zygotique (Cossec et al., 2018).

4.2.3 Modèles génétiques d'altération générale de la SUMOylation

Afin d'étudier le rôle de la SUMOylation dans le développement embryonnaire et post-natal, des modèles génétiques de délétions totales ont été mis en place. Ces derniers peuvent cibler les protéines SUMO elles mêmes, les enzymes responsables de la SUMOylation, aboutissant dans les deux cas à une hypoSUMOylation théorique, ou les déSUMOylases provoquant cette fois une hyperSUMOylation. De plus, l'utilisation

d'allèles conditionnels et de transgènes spécifiques permet d'induire la délétion à un moment précis du développement de l'organisme.

4.2.3.1 Délétion des protéines SUMO

La première étude concernant le rôle de SUMO1 dans le développement embryonnaire rapporte une augmentation de la proportion de décès embryonnaire ou périnatal (Alkuraya, 2006). Cependant, ce résultat a été mis en perspective par des travaux ne liant la perte de SUMO1 à aucun effet sur le développement embryonnaire, la fertilité ou encore la fonction adipogénique (Evdokimov et al., 2008; Wang et al., 2014; Zhang et al., 2008). Cette absence d'effet, malgré le caractère ubiquiste de SUMO1, s'explique par une compensation de la SUMO1-ylation vers une SUMO2/3-ylation illustrée par la cible canonique de SUMO1, RanGAP1 qui devient SUMOylé par SUMO2/3 lors de la perte de SUMO1 (Evdokimov et al., 2008). Une autre étude a toutefois retrouvé une augmentation de la mortalité pré- et post-natale dans un contexte de perte de SUMO1. Cet effet semble être dû à une septogénèse ventriculaire déficiente étant donné qu'une ré expression de SUMO1 dans les cardiomyocytes permet de prévenir cette surmortalité (Wang et al., 2011).

Modèle	Phénotype développemental	Référence
$SUMO1^{-/-}$	Mortalité embryonnaire et périnatale Fente labio-palatine	Alkuraya et al., 2006
$SUMO1^{-/-}$	Développement normal	Evkodimov et al., 2008
$SUMO1^{-/-}$	Développement normal	Zhang et al., 2008
$SUMO1^{-/-}$	Mortalité embryonnaire Développement cardiaque anormal	Wang et al., 2011
$SUMO2^{-/-}$	Mortalité embryonnaire à E10.5	Wang et al., 2014
$SUMO3^{-/-}$	Développement normal	Wang et al., 2014
$SUMO3^{-/-}$	Développement normal	Yu et al., 2020
$SUMO2^{+/-}$ $SUMO3^{-/-}$	Mortalité embryonnaire à E18.5	Wang et al., 2014

Figure 28: **Synthèse des phénotypes causés par la délétion des différents SUMOs**

Bien que la perte de SUMO3 ou l'hétérozygotie de SUMO2 n'affecte pas le développement embryonnaire, la perte de SUMO2 provoque une létalité embryonnaire dès E10.5. Cette dernière est causée par une forte diminution de la prolifération et une augmentation de l'apoptose à partir de E7.5 chez les souris déficientes pour SUMO2 (Wang et al., 2014; Yu et al., 2020). De façon intéressante, la perte totale de SUMO3 associée à l'hétérozygotie

de SUMO2, aboutit à une létalité embryonnaire autour de E18.5 (Wang et al., 2014) (Figure 28).

Questions et perspectives :

Ces résultats suggèrent que SUMO1 ne permet pas de compenser la perte de SUMO2 ou SUMO3 mais que ces derniers sont fonctionnellement comparables. En effet, la modification par SUMO1 ou SUMO2/3 peut aboutir à des effets différents sur certaines protéines mais aussi à l'échelle de la cellule, où la perte de SUMO1 ou de SUMO2 entraînent des profils transcriptionnels différents, se traduisant par un rôle spécifique de SUMO2 dans la morphologie des fibroblastes (Bouchard et al., 2021). Par ailleurs, les effets différents de la perte de SUMO2 et SUMO3, peuvent s'expliquer par la représentation plus importante de SUMO2 dans la majorité des tissus comme le cœur, le pancréas, le cerveau ou les ovaires (Wang et al., 2014; Bouchard et al., 2021). Néanmoins, ce n'est pas le cas de tous les organes et notamment de la surrénale (Figure 29) (Bouchard et al., 2021), il serait ainsi intéressant d'étudier les effets de la perte de SUMO3 dans ces tissus.

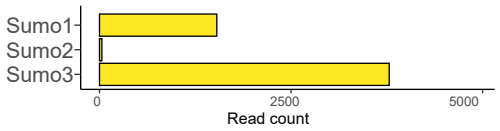

Figure 29: **Expression des transcrits codant les différentes formes de SUMO dans la surrénale murine**
Sonnées issues de séquençage ARN (GEO : GSE193480)

4.2.3.2 Délétion des enzymes de la SUMOylation

En accord avec ses effets pendant les étapes précoces du développement embryonnaire (Nacerddine et al., 2005), la délétion post natale totale de UBC9 produit un décès des souris après 6 jours dû à une altération de la survie, la prolifération et la différenciation des cellules souches intestinales (Demarque et al., 2011). De façon similaire, chez le ver planaire, l'ingestion de RNAi contre UBC9 provoque une disparition de la queue et la mort des vers après 25 jours. Ce phénotype est causé par un arrêt de la prolifération associé à une induction de l'apoptose (Thiruvalluvan et al., 2018).

En ce qui concerne les E3 SUMO ligases, les pertes de PIAS2 (Santti et al., 2005), PIAS3 (Campla et al., 2017) ou PIAS4 (Wong et al., 2004) ne causent aucun problème développemental tandis que la délétion de PIAS1 (Liu et al., 2004) provoque une légère augmentation de la mortalité périnatale [47]. De façon intéressante, l'invalidation simultanée de PIAS1 et PIAS4 provoque une létalité embryonnaire totale avant E11.5 (Tahk et al., 2007). TRIM28, est quant à lui nécessaire au processus de gastrulation, ne permettant à aucun embryon de dépasser le stade E8.5 (Cammas et al., 2000) alors qu'il semble en partie [48] dispensable en post-natal (Rousseaux et al., 2018). Ces différences peuvent s'expliquer par des différences d'expression tissu-spécifique des différentes E3 (Figure 30). En effet, les PIAS sont relativement peu exprimés pendant la vie embryonnaire contrairement à TRIM28 dont l'expression est particulièrement importante à E10.5 puis décroit progressivement (Cardoso-Moreira et al., 2019)

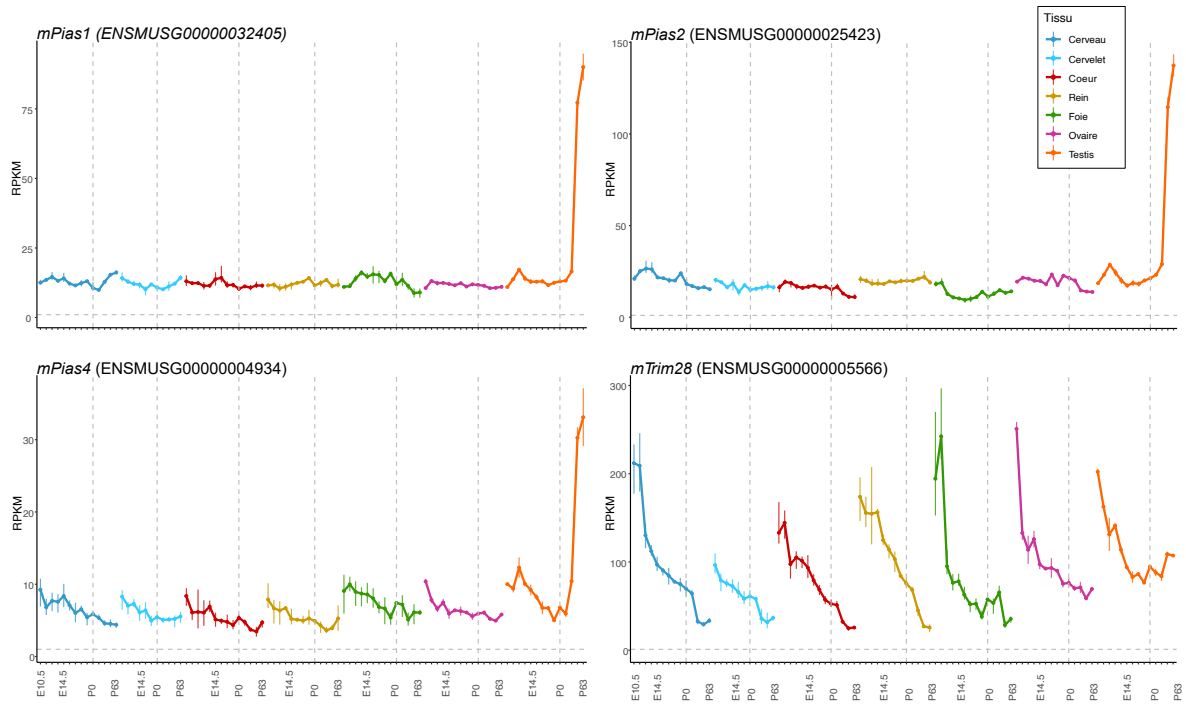

Figure 30: **Expression des transcrits codant les E3 SUMO ligases PIAS1, PIAS2, PIAS4 et TRIM28 entre E10.5 et P63 dans cerveau, cervelt, coeur, rein, foie, ovaire et testis de souris. Données issues de Cardoso-Moreira et al., 2019**

[47] Ces différents modèles ne semblent pas modifier les niveaux de SUMOylations généraux suggérant que soit les PIAS exercent des fonctions redondantes soit que les protéines différenciellement SUMOylés ne sont pas assez représentées pour induire un effet visible en western blot

[48] Les effets de la perte de TRIM28 dans la différenciation gonadique sont évoqués dans le paragraphe 5.4 - Gonades

4.2.3.3 Perte des SENPs

Des niveaux suffisant de SUMOylation sont capitaux pour le développement physiologique, mais des niveaux trop importants peuvent également se révéler néfastes. En effet, la perte totale de SENP1 provoque une forte létalité entre E13 et E15 due à des malformations du réseau vasculaire du placenta (Yamaguchi et al., 2005) ou un défaut d'érythropoïèse (Cheng et al., 2007; Yu et al., 2010). Cet effet est principalement médié par l'augmentation spécifique de SUMO1 [49] et est donc compensé par l'hémizygotie de SUMO1 (Sharma et al., 2013).

De façon similaire, la perte de SENP2 ou de son domaine catalytique produit dès E10.5 des malformations cardiaques (Kang et al., 2010; Maruyama et al., 2016; Yu et al., 2020) aboutissant à la mort rapide de la majorité des embryons.

Il a été proposé que cette invalidation affectait directement le développement cardiaque, la perte de SENP2 aboutissant à une diminution de l'expression de GATA6, facteur nécessaire au développement cardiaque (Kang et al., 2010), cependant l'invalidation de SENP2 dans l'épiblaste [50] n'induit pas de phénotype embryonnaire. En fait, la perte de SENP2 entraîne des altérations du cycle cellulaire dans les trophoblastes. L'hyperSUMO1-ylation de MDM2 l'empêche de reconnaître P53 et amène à la stabilisation de P53 et l'arrêt de la prolifération (Chiu et al., 2008). C'est alors l'altération du développement du placenta qui affecte le développement cardiaque. Bien que ce mécanisme mette en jeu SUMO1, la délétion de SUMO3 ou l'hémizygotie de SUMO2 concomitantes à la perte de SENP2 permettent de sauver le phénotype, impliquant SUMO2/3 dans la mortalité induite par la perte de SENP2 dans les tissus extra-embryonnaires (Yu et al., 2020)

La régulation des chaînes SUMO2/3 semble également un paramètre important pour le développement murin, la perte de SENP6 induisant une mort *in utero*. Les mécanismes n'ont pas été explorés mais la perte de SENP6 induite à l'âge de deux mois, provoque

[49] Seul le modèle utilisé par Cheng et al. provoque en plus de la perte de SENP1, une diminution de l'expression de SENP2 qui induit une augmentation de la SUMO2/3-ylation

[50] L'utilisation d'une *Sox2-cre* permet de ne cibler que l'épiblaste, et donc d'exclure les tissus extra-embryonnaires

un vieillissement prématuré du squelette causé par une apoptose et une sénéscence P53 dépendantes (Li et al., 2018).

Maintenir des niveaux de SUMOylation appropriés semble donc être un levier important dans le développement des organismes comme en témoignent les effets dramatiques observés très tôt dans le développement suite à la déstabilisation des voies de contrôle de la SUMOylation. Il est désormais important de s'intéresser aux effets de la SUMOylation à l'échelle de l'organe pendant le développement embryonnaire et après la naissance afin de mesurer la nécessité du contrôle de la SUMOylation et de comprendre les mécanismes mis en jeu.

5 La SUMOylation un acteur clé de la différenciation

La différenciation cellulaire est un mécanisme nécessitant le contrôle précis de programmes génétiques, la SUMOylation, capable de réguler l'activité de nombreuses cibles principalement nucléaires apparaît alors comme un candidat légitime dans le contrôle de la différenciation cellulaire.

5.1 La SUMOylation comme régulateur de pluripotence

La SUMOylation des facteurs de pluripotence OCT3/4, KLF4, SOX2 et c-MYC [51] (Hendriks and Vertegaal, 2016) laisse penser que la SUMOylation pourrait être un des moyens permettant de réguler le maintien de la pluripotence. Ce constat a été mis à l'épreuve par l'utilisation de cellules souches pluripotentes induites (IPSC).

En effet, la SUMOylation de OCT4, KLF4 ou SOX2 réduit leur activité transcriptionnelle et défavorise la reprogrammation de MEFs (fibroblastes embryonnaires murins) en ESCs (cellules souches embryonnaires) (Tahmasebi et al., 2013). De façon intéressante, la reprogrammation des MEFs induit de façon stochastique une différenciation adipocytaire dont la fréquence est diminuée lorsque KLF4 est non SUMOylable ($KLF4^{F269R}$) (Tahmasebi et al., 2013). Enfin, le récepteur nucléaire LRH1 (codé par *Nr5a2*) peut prendre la place de OCT3/4 dans le processus de reprogrammation et voit également son activité transcriptionnelle altérée par la SUMOylation (Heng et al., 2010), renforçant l'hypothèse d'un rôle promoteur de la SUMOylation dans l'acquisition d'une identité non différenciée.

Par ailleurs, l'expression d'*Ubc9* augmente au cours de la reprogrammation, et sa délétion dans des ESCs empêche cette reprogrammation et induit une apoptose (Tahmasebi et al., 2014). Ces résultats ont été nuancés dans des travaux montrant que la réduction de la SUMOylation pharmacologiquement ou *via* l'invalidation d'UBC9 facilite la reprogrammation de MEF en ESC. Cette reprogrammation est associée à une

[51] Ces facteurs, quand surexprimés, sont nécessaires et suffisants pour induire une reprogrammation de n'importe quelle cellule vers un état de pluripotence (Takahashi and Yamanaka, 2006)

redistribution des facteurs de pluripotence d'élements activateurs fibroblastiques vers des éléments activateurs de gènes de pluripotence (Cossec et al., 2018). Ces résultats bien que discordant témoignent d'un rôle important de la SUMOylation dans l'acquisition de la pluripotence.

Questions et perspectives :

Bien que les techniques de reprogrammation cellulaire avancent, la génération de cellules adrénocorticales reste peu efficace (Yazawa et al., 2014) or cette dernière pourrait apporter une avancée thérapeutique majeure. L'utilisation de ces cellules pour traiter des pathologies comme l'hyperplasie congénitale des surrénales où uniquement un gène est muté, permettrait de restaurer un *pool* de cellules stéroïdogènes fonctionelles. Au vu du rôle de la SUMOylation dans le maintien de la pluripotence, il pourrait être intéressant de tester l'impact de modulations de la SUMOylations dans les protocoles de différenciation de cellules stéroïdogènes.

5.2 Cellules souches hématopoïétiques

L'hématopoïèse adulte est le processus permettant la formation et le renouvellement des cellules sanguines à partir des cellules souches hématopoïétiques (HSC). Les HSC donnent naissance à 3 lignages : la lignée lymphoïde, issue des progéniteurs communs lymphoïdes (CLP), la lignée myéloïde et la lignée mégacaryocyte/érythrocyte toutes deux issues des progéniteurs communs myéloïdes (CMP) (Figure 31). Ces différenciations consécutives qui ont lieu en permanence dans la moelle osseuse offrent un modèle *in vivo* permettant d'étudier les impacts de la SUMOylation dans les processus de différenciation.

Le rôle de la SUMOylation dans l'hématopoïèse a été étudié dans les souris déficientes pour l'E3 SUMO ligase PIAS1. Ces souris sont plus résistantes aux infections virales ou bactériennes mais plus sujettes au chocs génotoxiques (Liu et al., 2004). Cet effet est dû à une augmentation de la prolifération des HSC, du nombre de lymphocytes T régulateurs et une diminution des CMP. PIAS1 coopère avec DNMT3A/B qui déméthyle

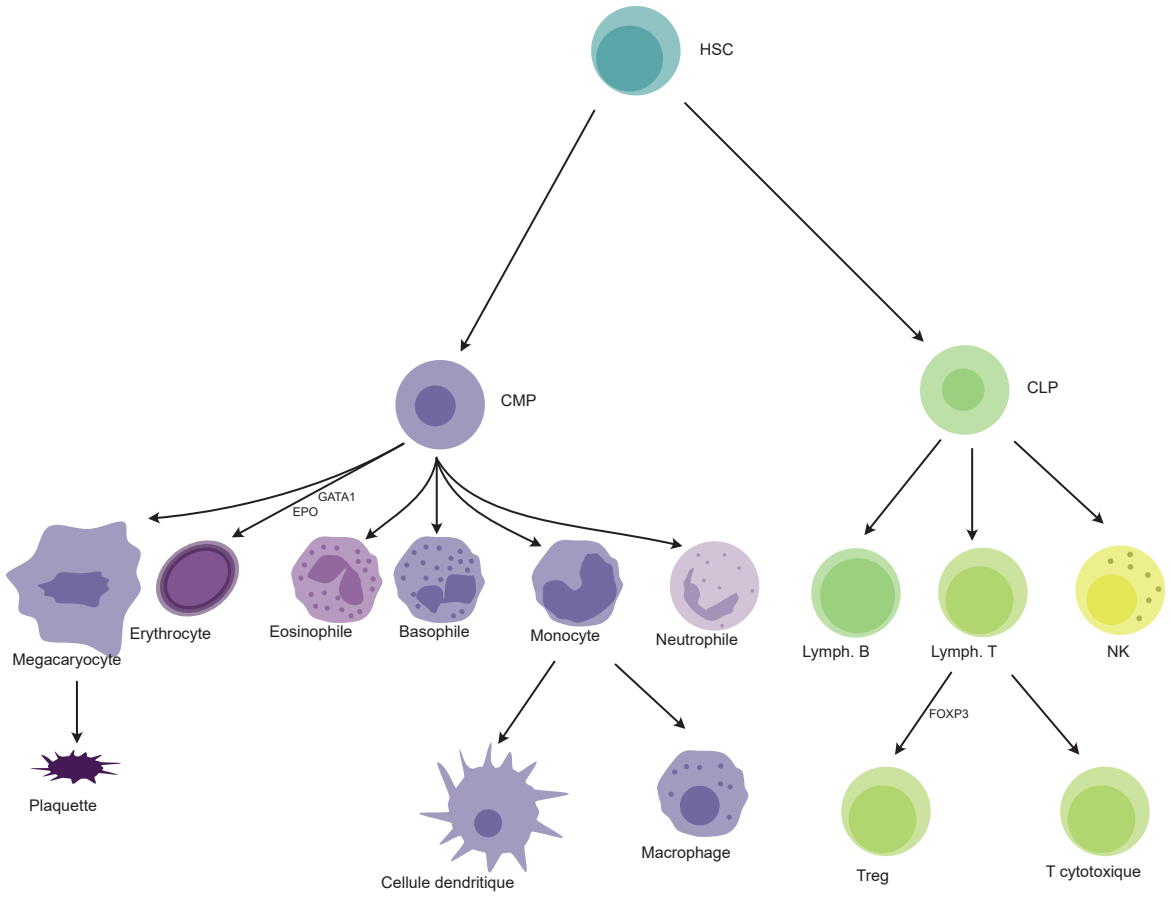

Figure 31: **Schéma de l'hématopoïèse adulte** HSC : hematopoietic stem cells, CLP : common lymphoid progenitor, CMP : common myeloid progenitors

l'ADN ce qui aboutit à l'expression de gènes importants pour la différenciation des cellules hématopoïétiques comme GATA1 ou FOXP3 [52] (Liu et al., 2010; Liu et al., 2014a).

FOXP3 est le facteur au centre de la différenciation des lymphocytes T régulateurs (Hori et al., 2003), qui exercent une activité immunomodulatrice évitant notamment l'autoimmunité [53]. Augmenter (*Foxp3-cre::Senp3*$^{fl/fl}$) ou diminuer (*Foxp3-cre::Ubc9*$^{fl/fl}$) la SUMOylation dans ces cellules altère leur fonction et induit une augmentation de l'inflammation et des désordres autoimmuns (Ding et al., 2016; Yu et al., 2018) montrant un rôle non binaire de la SUMOylation dans le maintien de l'identité de ces cellules. Les mécanismes en cause impliquent la SUMOylation de BACH2 qui réprime les programmes transcriptionnels associés aux lymphocytes T (Yu et al., 2018) et IRF4, un partenaire de

[52] Cependant, rien n'indique avec certitude que cet effet est dû à une variation de la SUMOylation et pas à d'autres fonctions de PIAS1 comme rapporté pour PIASy (Gross et al., 2004)

[53] L'utilisation de *Foxp3-cre* permet ainsi de cibler ces cellules

FOXP3, dont la SUMOylation stimule l'activité transcriptionnelle (Ding et al., 2016).

En ce qui concerne la lignée mégacaryocyte/érythrocyte, la perte de SENP1 totale aboutit à un blocage de l'érythropoïèse foetale, c'est à dire la production de globule rouges (Cheng et al., 2007; Yu et al., 2010). Ce phénotype s'explique par l'augmentation de la SUMOylation de HIF1α, responsable de l'expression d'EPO [54], amenant à sa dégradation (Cheng et al., 2007) et à l'hyperSUMOylation du facteur de transcription GATA1 diminuant sa capacité à se lier à l'ADN (Yu et al., 2010)

Enfin la SUMOylation permet de contrôler les fonctions des macrophages. En effet, la délétion de SENP3 dans les macrophages favorise une activité plutôt anti-inflammatoire (Xiao et al., 2021) alors qu'à l'inverse la perte de UBC9 dans les macrophages pancréatiques promeut une activité pro-inflammatoire (Wang et al., 2019).

Ces résultats témoignent d'une nécessité du contrôle de la SUMOylation, pas seulement générale, mais à l'échelle de certains acteurs spécifiques pour réguler la différenciation et le maintien de l'identité des cellules hématopoïétiques.

5.3 Tissu adipeux

Le tissu adipeux assure la régulation de la balance énergétique en exerçant sa fonction principale qui est le stockage de l'excès de triglycérides sanguins, permettant également de protéger les autres tissus de l'accumulation ectopique des lipides. En plus, de cette fonction, c'est également un organe endocrine régulant, *via* diverses sécrétions, le système immunitaire ou l'appétit. Le tissu adipeux est généralement séparé en deux catégories : le tissu adipeux blanc (WAT) exerçant plutôt une fonction de stockage dans des gouttelettes lipidiques occupant la majorité du cytoplasme et le tissu adipeux brun (BAT) dont la fonction principale est la thermogénèse notamment *via* l'action de UCP1 (uncoupling protein 1).

Les cellules précurseurs des adipocytes sont appelées préadipocytes. Il existe des lignées

[54] L'érythropoïétine ou EPO, est un facteur de croissance produit dans le foie fœtal puis les reins, nécessaire à la survie, la prolifération et la différenciation des progéniteurs érythroïdes en globules rouges (Wu et al., 1995)

cellulaires de préadipocytes qui peuvent être différenciées *in vitro* en tissu adipeux brun ou blanc via un cocktail d'agents. Enfin, les adipocytes blancs possèdent la propriété de "brunir" et devenir des adipocytes beiges en acquérant des propriétés d'adipocytes bruns.

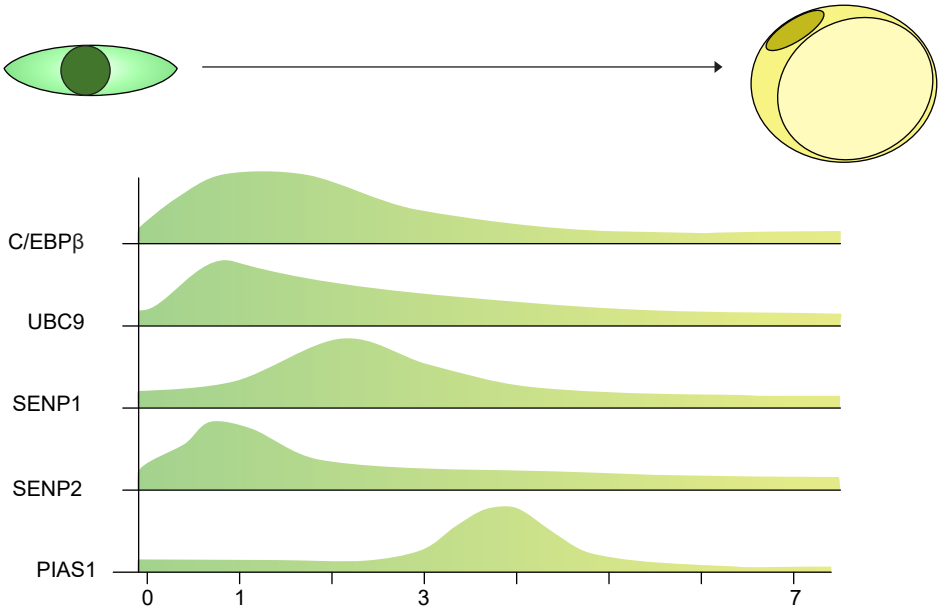

Figure 32: Evolution de l'accumulation des différents acteurs de la SUMOylation pendant l'adipogénèse

La différenciation adipogénique met en scène plusieurs acteurs transcriptionnels mais les principaux sont C/EBPα et PPARγ dont l'expression est régulée par C/EBPβ. Au cours de cette différenciation, des acteurs de la SUMOylation sont modulés selon des cinétiques différentes (Figure 32).

Lors du premier jour de différenciation, *Senp2* est surexprimé ce qui induit une déSUMOylation de C/EBPβ. La SUMOylation de C/EBPβ aboutissant à son ubiquitination et sa dégradation, C/EBPβ va être stabilisé par SENP2 (Figure 33), ce qui en fait un acteur nécessaire à la différenciation adipogénique (Chung et al., 2010; Lee et al., 2022; Mitani et al., 2017; Yu et al., 2021). C/EBPβ est à nouveau SUMOylé à partir du 4^{e} jour de différenciation grâce à l'action de PIAS1 ce qui va entraîner sa dégradation et la régulation fine et dynamique de l'adipogénèse (Liu et al., 2013b).

SENP1 est également exprimé au cours de la différenciation adipogénique, cependant son pic d'expression est atteint plus tardivement, autour du deuxième jour. Son action aussi va être différente, en effet, SENP1 lève une inhibition en déSUMOylant SHARP1 qui est

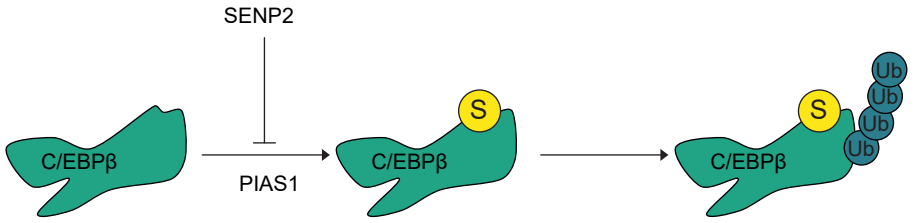

Figure 33: Régulation de CEBPβ par la SUMOylation au cours de l'adipogénèse

un régulateur négatif de l'adipogénèse (Liu et al., 2014b).

Par ailleurs, l'inhibition de la SUMOylation induite par le ML-792 (Zhao et al., 2022) ou par la perte de SUMO1 (Mikkonen et al., 2013) altère l'adipogénèse confirmant le besoin d'une SUMOylation *de novo* au cours de l'adipogénèse en parallèle des déSUMOylations exercées par SENP1 et SENP2. L'une des cibles de cette SUMOylation *de novo* pourrait être KLF4, dont l'activité promotrice de l'adipogénèse est fortement réduite lors de l'utilisation d'une forme non SUMOylable (Tahmasebi et al., 2013).

UBC9, est surexprimé chez les patients atteints de diabète de type 2 et les souris nourries avec un régime riche en graisse. De plus, son expression augmente pendant le premier jour de différenciation puis diminue (Cignarelli et al., 2010). Ainsi, son invalidation au cours de l'adipogénèse empêche la différenciation en adipocytes (Cignarelli et al., 2010) tandis que son invalidation dans des adipocytes blancs provoque une augmentation des marqueurs de tissu adipeux brun indiquant un rôle de la SUMOylation dans l'adipogènese puis dans l'inhibition du brunissement et donc le maintien de l'identité d'adipocyte blanc (Hartig et al., 2015).

Ces résultats traduisent d'une nécessité *in vitro*, d'une modification dynamique du profil de SUMOylation pour la différenciation des préadipocytes en adipocytes blanc qui aboutit à un maintien de niveaux de SUMOylations importants pour conserver cette identité. Cet effet se traduit par un rôle de la SUMOylation dans la répression des gènes de préadipocytes aux stades précoces de l'adipogénèse puis par l'induction de gènes nécessaires à la fonction adipogénique (Zhao et al., 2022).

L'importance de la SUMOylation dans le processus d'adipogénèse est illustré *in vivo* par

différents modèles animaux de modulation de la SUMOylation dans le tissu adipeux ou ses précurseurs.

Comme attendu, l'hypoSUMOylation des adipocytes provoque une lipoatrophie lorsqu'elle est causée par la perte de UBC9 dans le WAT (*Adipoq-cre::Ubc9$^{fl/fl}$*) (Cox et al., 2021) et une résistance au régime riche en acide gras lorsqu'elle est due à la perte générale de SUMO1 (Mikkonen et al., 2013).

L'hyperSUMOylation induite par la perte de SENP2 dans les adipocytes blancs (*Adipoq-cre::Senp2$^{fl/fl}$*) provoque également une atrophie du tissu adipeux notamment suite à un régime riche en graisse (Lee et al., 2022; Zheng et al., 2018) et promeut le brunissement du WAT *in vivo* et *in vitro* (Lee et al., 2022). Cet effet est concomitant à une réduction de la masse du BAT, en accord avec les effets de la perte de SENP2 dans les préadipocytes bruns (*Myf5-cre::Senp2$^{fl/fl}$*) (Liang et al., 2019). Elle induit un blocage de la différenciation des précurseurs en adipocytes bruns *in vivo* et *in vitro* en induisant l'expression de la NECDIN [55], protéine bloquant la différenciation brune.

5.4 Gonades

Les gonades (ovaires et testicules) sont des organes stéroïdogènes dont les cellules somatiques partagent leur origine embryonnaire avec le cortex surrénalien [56] et présentent une forte expression de SENP6 (Kim et al., 2000) et pour le testicule *a minima*, de SUMO1 (Vigodner and Morris, 2005) et des PIAS (Tan et al., 2002) (Figure 30).

Les tissus somatiques des gonades sont composés de cellules stéroïdogènes exerçant l'activité endocrine (cellules de Leydig dans le testicule et de la thèque dans l'ovaire), de cellules de soutien permettant la maturation des cellules germinales (Sertoli pour le testicule et *granulosa* pour l'ovaire) ainsi que d'un stroma.

Bien que le testicule présente des taux importants de SUMOylation, la perte de PIAS2

[55] Le mécanisme de cette induction et le rôle potentiel de la NECDIN dans la physiologie de l'HPA sont développés dans le paragraphe 10 - Le syndrome de Prader-Willi

[56] Voir paragraphe 2.1 - Développement embryonnaire de la glande surrénale

n'induit que des effets minimes sur la masse des testicules et altère légèrement la spermatogenèse sans effet sur la fertilité et aucun effet dans l'ovaire (Santti et al., 2005).

En revanche, la perte de TRIM28 dans les cellules de Sertoli induite par l'utilisation du transgène *Amh-cre* [57] provoque un défaut de spermatogénèse alors que son hémizygotie (Tan et al., 2020) ou la perte de son interaction avec HP1 (Herzog et al., 2011) n'a pas d'effet sur la physiologie testiculaire, suggérant que la perte de SUMOylation est en cause dans ce phénotype.

De façon similaire, la perte de l'activité de SUMOylation de TRIM28 dans les cellules de l'ovaire (*Sf1-cre::Trim28*^{PHD}) aboutit à une différenciation anormale du tissu qui acquiert des caractéristiques mâles telles que la production de testostérone, l'expression de gènes d'identité sertolienne ou leydigienne et la formation de pseudotubes séminifères (Rossitto et al., 2022) [58]. Cet phénotype peut être en partie dû à FOXL2 (Forkhead Box L2), facteur central à la régulation de la différenciation de la *granulosa* et dont la perte provoque une réversion sexuelle (Tucker, 2021). Il interagit avec TRIM28 (Rossitto et al., 2022) et sa SUMOylation favorise sa stabilité et son activité de répresseur transcriptionnel des régulateurs du programme de différenciation masculin (Marongiu et al., 2010).

Par ailleurs d'autres facteurs importants pour la différenciation des cellules de *granulosa* sont régulés par leur SUMOylation. Des mutations de NRIP1 ont été retrouvées chez une patiente atteinte d'insuffisance ovarienne primaire. Cette mutation produit une forme tronquée en C-terminale qui ne contient plus la lysine SUMOylable 1154 et a une capacité à réprimer la signalisation induite par les estrogènes plus faible que la forme sauvage (Jaillard et al., 2020). De la même façon, AuroraB est une protéine dont l'absence de SUMOylation diminue *in vitro* la capacité proliférative des cellules primaires de *granulosa* et augmente leur apoptose (Cao et al., 2018).

Enfin, la SUMOylation agit également sur le compartiment stromal, la perte de

[57] L'Anti-Mullerian Hormone est exprimée spécifiquement dans les cellules de Sertoli fœtales chez le mâle et de *granulosa* post-natales chez la femelle (Behringer R et al., 1995)

[58] Cette différenciation incomplète des cellules possédant une identité mixte entre mâle et femelle rappelle le phénotype des souris *Sf1*$^{2KR/2KR}$ décrite dans le paragraphe 6 - La SUMOylation de SF-1 gardienne de l'identité surrénalienne où les programmes transcriptionnels surrénaliens et gonadiques se chevauchent.

SENP1 dans les cellules stromales (*Sm22-cre::Senp1*$^{fl/fl}$) aboutit à une diminution de la folliculogénèse néonatale due à une altération de la signalisation paracrine BMP entre le stroma et les follicules (Tan et al., 2017).

Questions et perspectives :

La SUMOylation exerce des actions importantes à diverses échelles : en agissant à l'échelle de l'ADN pour affecter l'expression de gènes amenant à des conséquences sur les capacités prolifératives, la survie et l'identité des cellules. C'est sans surprise que les modèles génétiques altérant le contrôle de la SUMOylation aboutissent à des conséquences dramatiques sur le développement des organismes et la différenciation des tissus. Néanmoins la majorité de ces modèles provoquent des déréglements généraux de la SUMOylation ce qui complexifient l'investigation des mécanismes mis en jeu. Les prochains travaux devront systématiser l'analyse des SUMOylomes mutants et essayer de comprendre le rôle qu'exerce la SUMOylation sur des protéines particulières.

HOMEOSTASIE SURRENALIENNE ET SUMOYLATION

Le cortex surrénalien est un organe au renouvellement constant où les mécanismes qui permettent les différenciations successives des zones fonctionnelles restent seulement en partie explorés. De multiples voies de signalisation et facteurs de transcriptions mis en jeu comme acteurs du développement physiologique du tissu sont potentiellement modulés par la SUMOylation.

Au vu de ces connaissances notamment le rôle prépondérant du facteur de transcription SF-1 et l'équilibre entre les signalisations WNT/β-caténine et PKA, il convient de se poser la question du rôle de la SUMOylation dans la mise en place, le maintien et les fonctions du cortex surrénalien.

6 La SUMOylation de SF-1 gardienne de l'identité surrénalienne

6.1 Le facteur de transcription SF-1

Le facteur de transcription SF-1, codé par le gène *Nr5a1* est un récepteur nucléaire orphelin de la famille NR5A (qu'il partage avec LRH1). Il est exprimé dans l'AGP [59] et est nécessaire au développement des gonades et des surrénales (Luo et al., 1994). De la même façon, chez l'être humain, des mutations diminuant ou abolissant sa capacité à se lier à l'ADN provoquent une insuffisance surrénalienne (Achermann et al., 1999, 2002).

Son importance en tant qu'inducteur de la différenciation des lignages stéroïdogènes surrénaliens est illustrée par des expériences de différenciation *ex vivo*. En effet, la surexpression de SF-1 en présence d'un traitement à l'AMPc permet à des cellules souches mésenchymateuses d'exprimer des marqueurs de différenciation stéroïdogènes et de produire des glucocorticoïdes (Yazawa et al., 2006, 2011).

[59] voir paragraphe 2.1 - Développement embryonnaire de la glande surrénale

6.2 Régulation de l'activité transcriptionnelle de SF-1 par la SUMOylation

SF-1 est SUMOylable par SUMO1 (Chen et al., 2004) et SUMO2/3 (Komatsu et al., 2004). Cette réaction peut être permise *in vitro* par PIAS1, PIAS2, PIAS3 et PIAS4 Lee et al. (2005) et déconjuguée par SENP1 (Lee et al., 2005) ou SENP2 (Yang et al., 2009b).

La SUMOylation de SF-1 a lieu sur les lysines 119 et 194, la SUMOylation sur la lysine 194 semblant conditionner celle de la 119 (Chen et al., 2004; Komatsu et al., 2004).

La mutation de ces deux lysines en arginine (SF-1^{2KR}) a permis d'explorer l'impact de la perte de la SUMOylation sur l'activité de SF-1.

Il a d'abord été rapporté une augmentation de l'activité transcriptionnelle du SF-1^{2KR} indépendamment de son recrutement à l'ADN (Chen et al., 2004; Komatsu et al., 2004; Lee et al., 2005) confirmée par la co-transfection de SF-1 sauvage avec les déconjugases SENP1 (Lee et al., 2005) ou SENP2 (Yang et al., 2009b) qui induisent les mêmes effets. Cette action transactivatrice a lieu sur les gènes cibles de SF-1 tels que *Cyp19a1*, *Star* et *Mc2r* (Wang et al., 2013) mais seule la forme non-SUMOylée de SF1 est capable de se fixer sur le promoteur de certains gènes comme *Inha* (Campbell et al., 2008). La SUMOylation de SF-1 impacterait donc son activité de deux façons : en diminuant son activité transcriptionnelle au niveau de promoteurs de gènes cibles canoniques et en réprimant son recrutement sur des sites "non canoniques" qualifiés alors de "SUMO-sensibles".

6.3 Effet de la perte de SUMOylation de SF-1 *in vivo*

Les effets de la SUMOylation de SF-1 *in vivo* ont été explorer grâce à un modèle murin de *knock-in* exprimant un SF-1 non SUMOylable ($Sf1^{2KR/2KR}$). Au lieu de développer une agénésie adrénogonadique ou de révéler simplement un gain de fonction comme attendu d'un facteur plus actif transcriptionnellement, comme en cas de délétion totale de SF-1

(Luo et al., 1994), les anomalies observées chez ces souris, touchent à l'identité des glandes stéroïdogènes. En effet les souris SF-1^{2KR} sont stériles, leurs testicules hypomorphes (due à une perte des cellules germinales) affichant des marqueurs d'identité surrénalienne dans le compartiment leydigien tandis qu'à l'inverse leurs surrénales expriment des associés à une identité testiculaire comme *Sox9*, *Hsd17b3* ou *Wnt5a* (Lee et al., 2011). De plus, chez les mutants, le domaine d'expression de *Shh* s'étend dans le cortex des surrénales et remplace celui de DHH dans le testicule, suggérant qu'il est un gène SUMO-sensible. En effet, des expériences de culture cellulaire démontrent que la SUMOylation de SF-1 empêche son recrutement au niveau du promoteur de *Shh* (mais pas *Cyp11b1*) tandis que la surexpression de SENP1 mime les effets du mutants SF-1^{2KR} (Lee et al., 2011).

Un des mécanismes pouvant expliquer l'effet négatif de la SUMOylation sur l'activité transcriptionnelle de SF-1, est le recrutement de co-represseurs. En effet, SF-1 SUMOylé recrute ARIP4, ce qui induit une répression transitoire de son activité transcriptionnelle au niveau des promoteurs de *Inha*, *Star* et *Cyp11a1* (Ogawa et al., 2009). Un autre co-répresseur possiblement impliqué est le récepteur nucléaire orphelin DAX-1 (codé par *Nr0b1*) connu pour s'hétérodimériser avec SF-1. Lors de co-transfection SF1/DAX-1 dans des cellules HEK293, l'interaction avec DAX-1 est plus importante lorsque SF-1 est SUMOylé et réduite avec SF-1^{2KR} (Xing et al., 2017). Ce résultat pourrait expliquer certains traits phénotypiques des souris SF-1^{2KR} comme la maintenance de la zone-X après la puberté chez les mâles (Lee et al., 2011) retrouvée de façon similaire en cas de perte de DAX-1 (souris DAX-$1^{-/Y}$) (Scheys et al., 2011; Xing et al., 2017). Ainsi, l'interaction renforcée de DAX-1 avec SF-1 SUMOylé expliquerait la répression de l'enhancer fœtal FAdE nécessaire à la regression physiologique de la zone X (Xing et al., 2017).

6.4 Interaction de la SUMOylation de SF-1 avec d'autres modifications post-traductionnelles

Une autre explication de l'effet répresseur de la SUMOylation de SF-1 est l'interaction avec d'autres modifications post-traductionnelles.

La SUMOylation et l'ubiquitination sont fortement interconnectées [60]. La lysine 119, en plus d'être SUMOylable, est l'unique lysine de SF-1 sujette à l'ubiquitination (Luo et al., 2010). Cependant, SF-1^{K194R} comporte le même niveau d'ubiquitination que la forme sauvage (Luo et al., 2010), bien que la SUMOylation y soit abolie (Chen et al., 2004; Komatsu et al., 2004). La SUMOylation de SF-1, ne semble donc pas, en soit, affecter son ubiquitination. Pourtant, dans un contexte de restriction énergétique, la SUMOylation semble nécessaire à l'ubiquitination de SF-1. En effet, la co-transfection de SF-1 et SUMOs dans des cellules HEK293 privées de sérum aboutit à la dégradation ubiquitine-dépendante de SF-1 alors que les formes SF-1^{K194R} et SF-1^{2KR} résistent à la privation de sérum (Lee et al., 2016).

SF-1 est également phosphorylé sur la sérine 203, ce qui stimule son activité transcriptionnelle (Hammer et al., 1999). L'incapacité de SF-1 à être phosphorylé ($SF1^{S203A}$) prévient son ubiquitination (Luo et al., 2010) mais ne semble pas avoir d'effet sur sa SUMOylation (Lee et al., 2005; Luo et al., 2010; Yang et al., 2009b). Cependant, la perte de SUMOylation de SF-1 permet à SF-1 d'être phosphorylé par CDK7 (Yang et al., 2009b) et stimule sa phosphorylation par ERK1/2 (Campbell et al., 2008).

Bien que la plupart des études montrent un effet négatif de la SUMOylation sur l'activité transcriptionnelle de SF-1, la transfection de SF-1^{K194R} provoque une diminution de l'activité des promoteurs luciferase de *CB1*, *BDNF* (Lee et al., 2016) ou *ATF3* (Emura et al., 2020) par rapport à SF-1 sauvage. Cet effet est associé à un recrutement moins important de SF-1^{K194R} au niveau du promoteur de *CB1*. De façon intéressante, BDNF et CB1 sont exprimés dans l'hypothalamus mais pas dans la surrénale, ce qui pourrait indiquer un effet tissu-dépendant.

SF-1 est un des acteurs majeurs du développement de la surrénale. Il est modifié par la SUMOylation, la phosphorylation et l'ubiquitination qui intéragissent entre elles, régulant finement l'activité de SF-1. Les modèles murins de perte de SUMOylation révèlent un rôle capital de la SUMOylation de SF-1 dans la différenciation normale

[60] voir paragraphe 3.4 - Interaction avec l'ubiquitination

du cortex surrénalien. Ce résultat pourrait être dû à un défaut de séparation des ébauches adrénogonadiques, à la différenciation de cellules d'identité gonadique dans les surrénales ou la dédifférenciation des cellules surrénaliennes. Les résultats actuels montrent en effet, que des mécanismes actifs sont à l'œuvre afin de maintenir l'identité différenciée de la surrénale comme des gonades, et sont contrôlés par la SUMOylation notamment dans l'ovaire (Rossitto et al., 2022). Il semblerait que la SUMOylation soit l'un des mécanismes principaux permettant l'acquisition et le maintien des identités stéroïdogènes (Figure 34).

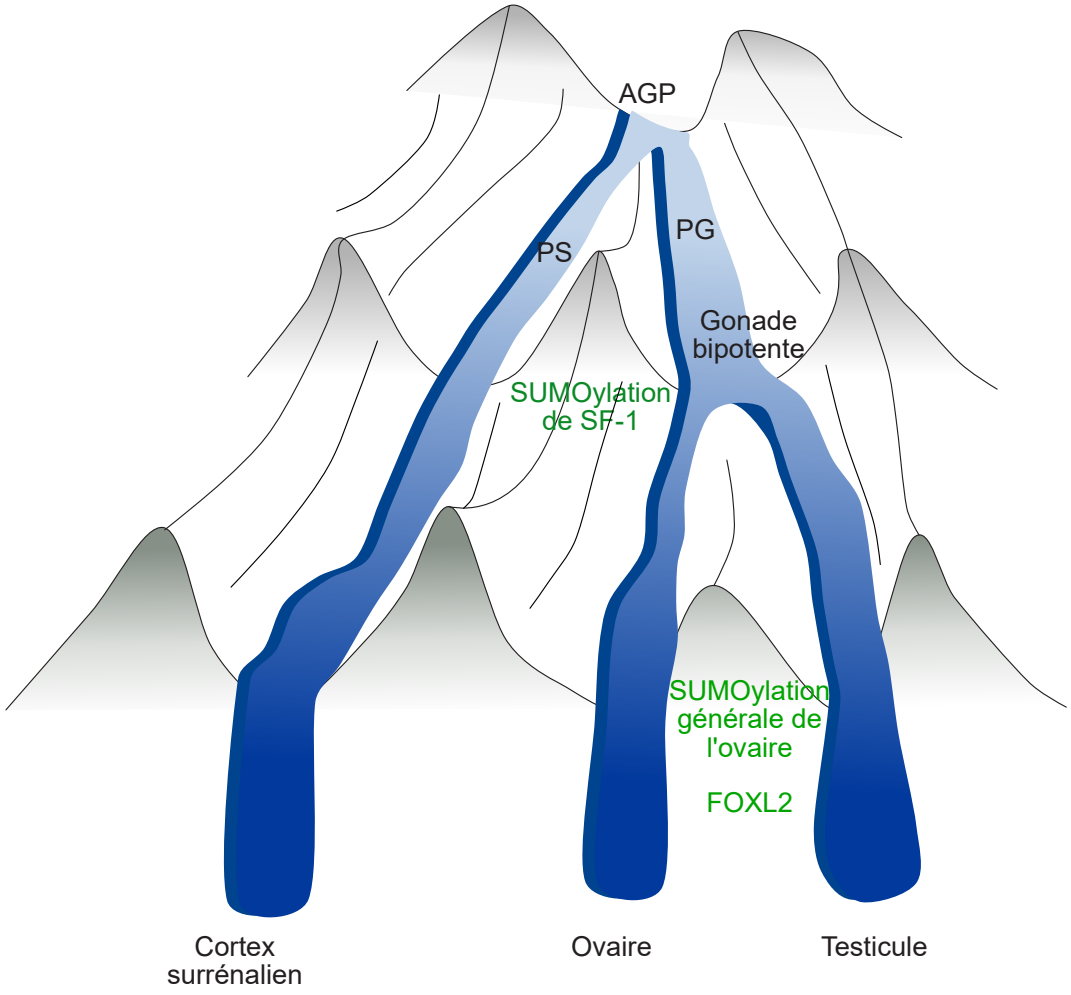

Figure 34: Lors de la séparation du primordium adrénogonadique (AGP) en primordium gonadique (PG) et surrénalien (PS), SF-1 est un des principaux facteurs discriminant, sa SUMOylation permet de diriger et/ou maintenir les cellules vers leur identité surrénalienne ou gonadique (Lee et al., 2011). Plus tard, lorsque la gonade bipotente a acquis son identité femelle, la SUMOylation contrôlée en amont par TRIM28 permet de maintenir la gonade femelle dans cet état, probablement en affectant la SUMOylation de FOXL2 (Rossitto et al., 2022). Adapté de Waddington, C. H. (1957). The Strategy Of The Genes

7 La régulation de la voie WNT/β-caténine par la SUMOylation

L'étude de l'activité de la voie WNT canonique dans des MEFs issues de souris déficientes pour PIAS4 indique que cette E3 SUMO ligase et par extension probablement la SUMOylation est nécessaire à l'activation optimale de la voie (Roth et al., 2004).

En accord avec ce résultat, SENP2 a été initialement caractérisé comme une protéine interagissant avec AXIN et induisant la dégradation de la β-caténine (Kadoya et al., 2000; Nishida et al., 2000). Cette activité de dégradation, initialement pensée comme indépendante de l'activité catalytique de SENP2 (Nishida et al., 2000), semble en fait majoritairement due à son activité de déSUMOylation (Kadoya et al., 2002; Shen et al., 2012). Cet effet négatif de SENP2 sur la stabilité de la β-caténine a été reproduit dans les cellules hépatiques HepG2 (Jiang et al., 2014; Shen et al., 2012), rénales HEK293T (Jiang et al., 2014), les lymphocytes (Chen et al., 2018) et des cellules stellaires hépatiques (Bu et al., 2018).

7.1 SUMOylation de la β-caténine

L'un des mécanismes proposés serait l'interférence de la SUMOylation de la β-caténine [61] avec son ubiquination. En effet l'invalidation de *Sumo1* par une approche d'ARN interférant induit une diminution de la SUMO1-yation et une dégradation de la β-caténine dans des cellules de myélome (Huang et al., 2015) tandis que l'invalidation de SENP7S dans des cellules mammaires provoque son hyperSUMO2/3-ylation et diminue son ubiquitination suite à la perte d'interaction avec AXIN1 (Karami et al., 2017). L'hypothèse du rôle stabilisateur de la SUMOylation sur la β-caténine est d'autre part soutenu par les effets de l'inactivation de l'enzyme E1 UBA2, qui induit la dégradation de la β-caténine dans des cellules coliques HT29 et DLD-1 (Cheng et al., 2018). De façon surprenante, la surexpression de SENP3 dans des cellules HEK293T déSUMOyle

[61] Cette SUMOylation a lieu sur la lysine 21 (Hendriks et al., 2018) qui est également une des deux lysines ciblées par β-TRCP amenant à la dégradation de la β-caténine (Winer et al., 2006)

la β-caténine et cependant inhibe sa dégradation protéasomale (Cai et al., 2021). Ce résultat inattendu pourrait être dû à des interactions entre la SUMOylation de la β-caténine et sa phosphorylation ou son ubiquitination ou à la déSUMOylation d'autres protéines responsables de sa dégradation.

7.2 WWOX

Un autre biais par lequel SENP2 contrôlerait la stabilité de la β-caténine est *via* la protéine WWOX (WW domain-containing oxidoreductase). Les transcrits codant *Wwox* sont surexprimés lors de la transfection de SENP2 dans des cellules hépatiques HepG2 et son expression est nécessaire à la répression exercée par SENP2 sur la signalisation WNT canonique (Jiang et al., 2014). Les effets exercés par WWOX semblent indépendants de sa SUMOylation, car cette dernière, catalysée par CBX4 prévient sa dégradation (Choi et al., 2015). SENP2 agirait donc sur d'autres acteurs pour stimuler l'expression de WWOX. WWOX agit en inhibant la translocation nucléaire de DVL-3 et par conséquent de la β-caténine ainsi qu'en favorisant sa dégradation (Bouteille et al., 2009; Itoh et al., 2005).

7.3 TCF4

TCF4 interagit avec de nombreuses protéines du NPC ainsi qu'avec UBC9 et RANBP2 (Shitashige et al., 2008). Ces dernières favorisent sa SUMOylation, ce qui est associé à une activation de la signalisation WNT canonique (Li et al., 2019; Shitashige et al., 2008; Yamamoto, 2003). En fait, la SUMOylation de TCF4 favorise sa capacité à interagir avec la β-caténine et son transfert nucléaire (Li et al., 2019; Shitashige et al., 2008; Yamamoto, 2003). L'un des régulateurs positifs de cette SUMOylation est la protéine NUSAP (Nucleolar and spindle associated protein 1) qui est surexprimée dans le cancer cervical et qui interagit avec l'E3 SUMO ligase RanBP2 pour modifier TCF4 (Li et al., 2019), à l'inverse SENP2 déSUMOyle TCF4 et empêche l'activation de la signalisation WNT/β-caténine (Shitashige et al., 2008; Yamamoto, 2003)

7.4 TBL1/TBL1R

TBL1 (transducin β-like protein 1) et TBLR1 (TBL1 receptor) sont des protéines qui interagissent avec la β-caténine dans le noyau formant un complexe avec TCF qui est ensuite recruté aux promoteurs des gènes cibles (Li and Wang, 2008). La SUMOylation de ces protéines favorise l'accumulation nucléaire de la β-caténine (Tan et al., 2015), la formation du complexe avec TCF4 et l'activité transactivatrice de la β-caténine (Choi et al., 2011). A l'inverse, la surexpression de SENP1 (Choi et al., 2011) ou SENP2 (Tan et al., 2015) empêche cet effet exercé par TBL/TBLR1 confirmant le rôle promoteur de la SUMOylation sur la signalisation WNT canonique.

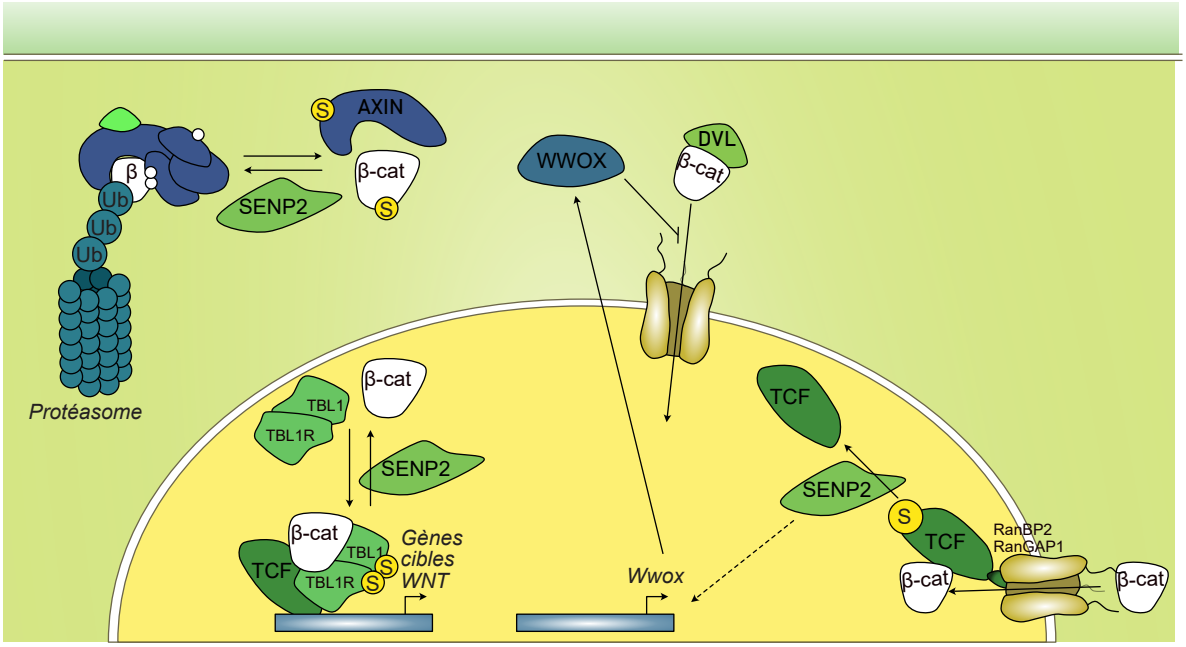

Figure 35: Hypothétiques mécanismes expliquant l'effet de SENP2 et de la SUMOylation sur la signalisation WNT canonique

8 PKA et SUMOylation, un dialogue complexe

8.1 La signalisation AMPc comme modulateur de la SUMOylation

Le stimulation de la signalisation AMPc dans l'ovaire (ou directement dans les cellules de *granulosa*) par la PMSG (Pregnant Mare Serum Gonadotropin) [62] induit une diminution de la quantité totale de SUMO1 (Shao et al., 2004). De façon analogue, le traitement à la forskoline, un activateur de l'adénylate cyclase, exclue le récepteur nucléaire LRH1 des corps nucléaires où la SUMOylation le dirige, suggérant que la signalisation AMPc réduit sa SUMOylation (Yang et al., 2009a).

Cet effet négatif est retrouvé dans les cellules stromales endométriales primaires (Jones et al., 2006) et dans le cortex surrénalien sain et des pathologies surrénaliennes de la PKA (Dumontet et al., 2019). Il est causé par un effet principalement transcriptionnel affectant SAE1, UBC9, différentes E3 [63] mais aussi SENP6 et SENP2 (Dumontet et al., 2019; Jones et al., 2006; Yang et al., 2009a). Concernant SENP2, il a été démontré dans le tissu adipeux que sa régulation par l'AMPc passait par le recrutement de CREB au niveau d'un site *CRE* du promoteur de *Senp2* (Chung et al., 2010). CREB induit également l'expression de *Pias1* dans l'hippocampe, en se fixant sur son promoteur (Liu et al., 2013a).

A l'inverse, l'AMPc peut activer EPAC1 (exchange protein directly activated by cyclic AMP) et aboutir à une augmentation générale de la SUMOylation. Cet effet est médié par la séparation de phase produite par la liaison entre l'AMPc et EPAC1. Les corps nucléaires ainsi créés sont enrichies en SUMO2/3 et en SAE1 favorisant la SUMOylation de protéines présentes dans ces corps (Yang et al., 2022).

Ainsi la signalisation AMPc semble exercer un effet hypoSUMOylant lorsqu'elle passe par la PKA tandis qu'elle induit une hyperSUMOylation lorsqu'elle est relayée par EPAC1.

[62] La PMSG est une hormone reproduisant les effets des hormones gonadotropes produites par l'hypophyse, qui stimule la signalisation AMPc/PKA dans les cellules somatiques de l'ovaire

[63] La régulation de ces E3 diffère selon les tissus ce qui signe une spécificité de substrat selon le tissu permettant d'adapter les réponses à l'AMPc

8.2 Impact de la SUMOylation sur la signalisation AMPc/PKA

Une hypoxie prolongée sur 24h induit la SUMOylation de CREB. Cette SUMOylation a deux effets : CREB est stabilisé et son activité transcriptionnelle est stimulée (Chen et al., 2014; Comerford et al., 2003; Liang et al., 2019). En effet, la transfection d'un mutant CREB non SUMOylable ($CREB^{K285R,K304R}$) a une activité transcriptionnelle réduite sur un promoteur *CRE* dépendant (Liang et al., 2019) ou sur l'expression de *Bdnf* (Chen et al., 2014). Par ailleurs, pour être SUMOylé, CREB doit d'abord être phosphorylé (Chen et al., 2014), mais cette modification est transitoire car CREB SUMOylé recrute PP2A amenant *in fine* à sa déphosphorylation (Liang et al., 2019).

La SUMOylation cible d'autres acteurs de la signalisation AMPc/PKA comme les PDE 4A4 et 5D5 dont la SUMOylation stimule l'activité enzymatique (Li et al., 2010) ou le récepteur au GLP-1, qui est séquestré par sa SUMOylation dans le cytoplasme des cellules β pancréatiques empêchant l'activation de la signalisation PKA en aval (Rajan et al., 2012).

Questions et perspectives :

Ces résultats laissent penser que la signalisation AMPc et la SUMOylation sont interconnectées. On peut alors se demander si la baisse de SUMOylation dans le cortex surrénalien induite par la signalisation PKA est un médiateur incontournable des effets de celle-ci et ainsi si moduler les capacités de SUMOylation entraînerait des altération de l'homéostasie corticale et de la réponse au stress

9 DRP1, un lien entre apoptose et SUMOylation au sein de la surrénale

9.1 DRP1 et dynamique mitochondriale

La mitochondrie est le siège de la stéroïdogénèse [64], elle exerce donc un rôle prépondérant au sein des cellules du cortex surrénalien. En fonction des besoins de la cellule, le réseau mitochondrial doit s'adapter et subit une réorganisation dictée par l'équilibre entre fusion et fission des mitochondries. Cette balance est importante dans de multiples phénomènes tels que la division cellulaire, la différenciation, la production d'énergie ou l'apoptose et doit en conséquence être finement régulée (Westermann, 2008).

Une protéine clé de cette régulation est DRP1 (Dynamin Related Protein 1), une GTPase cytoplasmique codée par le gène *Dnm1l* (Smirnova et al., 1998). Son rôle lors de l'apoptose a été explorée par des expériences *in vitro* de culture de cellules (Frank et al., 2001). Une apoptose induite par un traitement à la staurosporine entraîne un recrutement de DRP1 à la mitochondrie et un changement de morphologie de ces dernières vers un phénotype punctiforme, conséquence d'une fragmentation mitochondriale. La surexpression d'un mutant dominant négatif $DRP1^{K38A}$ empêche le changement de morphologie des mitochondries, la libération du cytochrome C dans le cytoplasme et en conséquence inhibe l'apoptose. Ainsi, DRP1 est une protéine nécessaire à la fission mitochondriale permettant d'aboutir à l'initiation de l'apoptose.

9.2 Des régulations post-traductionnelles capitales

DRP1 est une enzyme constituée d'un domaine catalytique de type dynamine, en N-terminal, possédant une activité de liaison et d'hydrolysation du GTP en GDP (Wenger et al., 2013). Cette activité, également présente dans les autres protéines de la famille des dynamines, est nécessaire et suffisante pour la fission des membranes (Roy and Pucadyil,

[64] voir paragraphe 1.3.2.3 - Etapes de la stéroïdogénèse surrénalienne

2022). Une autre caractéristique de cette famille est la capacité à s'oligomériser et à former une structure quaternaire comprimant les membranes pour permettre leur fission (Antonny et al., 2016) [65]. L'oligomérisation de DRP1 est observée lors de l'apoptose (Prudent et al., 2015; Yoon et al., 2001) et est rendue possible par la capacité du domaine GED (GTPase effector domain) présent en C-terminal à se lier au domaine *middle* de DRP1 (Fröhlich et al., 2013; Zhu et al., 2004). Enfin, DRP1 possède un domaine B ou domaine variable, absent des autres dynamines, lui permettant d'être recruté au niveau des membranes plasmiques (Fröhlich et al., 2013) (Figure 36.A.B.C.). Cette liaison nécessite l'interaction avec des protéines adaptatrices telles que MFF, MiD49 ou MiD51 (Koirala et al., 2013; Losón et al., 2013) (Figure 36.B.).

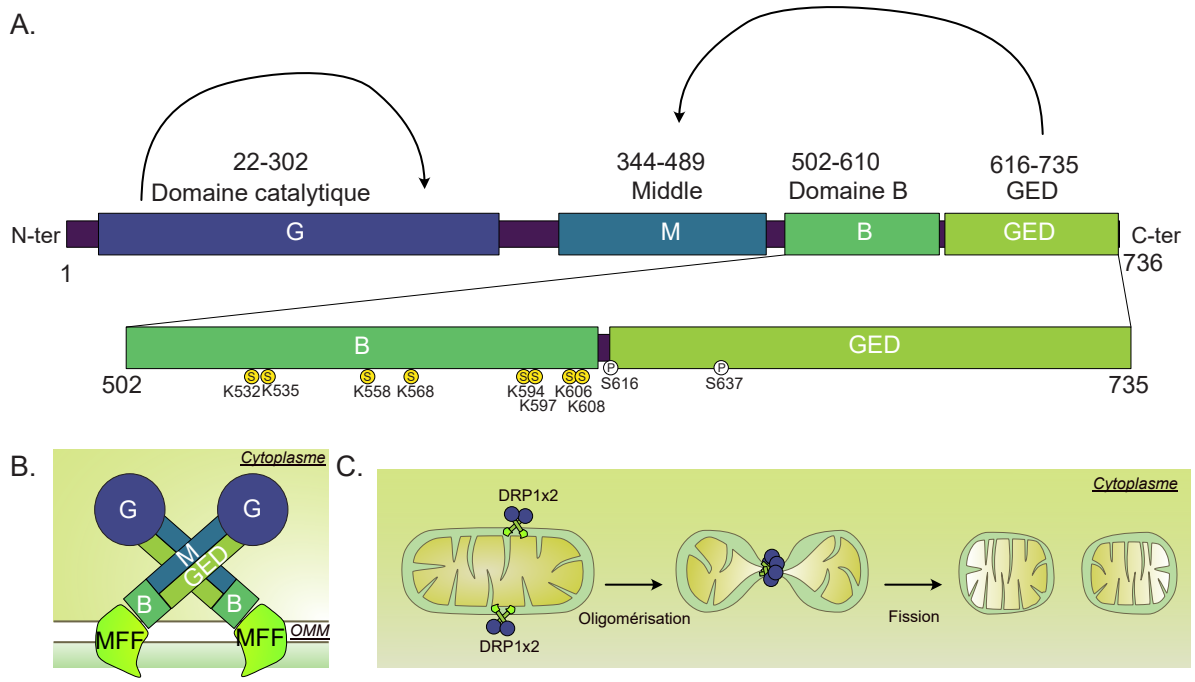

Figure 36: **Vue d'ensemble de la protéine DRP1**
A. Domaine protéique de DRP1 et localisation des modifications post-traductionneles
B. Schéma de la dimérisation de DRP1 et son recrutement à l'OMM
C. Schéma de la fission mitochondriale
D'après Zhu et al., 2004, Fröhlich et al., 2013

Un des leviers majeurs de la régulation de l'activité de DRP1 est la variation de la

[65] Les mécanismes permettant d'aboutir à cette fission sont débattus, dégageant deux hypothèse. Dans la première, une fois les membranes assez serrées, DRP1 se désassemblent induisant une fission des membranes, dans la seconde les oligomères de DRP1 aboutissent à une constriction telle que que les membranes s'hémifissionnent (fusion de deux doubles membranes en une seule double membrane) ce qui demande une force relativement importante (Antonny et al., 2016). Une étude récente a permis de valider la possibilité et l'existence de la deuxième hypothèse montrant que les dynamines sont capables de produire une force suffisante pour aboutir à la fission des membranes (Ganichkin et al., 2021)

phosphorylation de ses sérines 616 et 637. L'activation de la signalisation PKA provoque une augmentation de la phosphorylation de DRP1 sur la sérine 637 (Chang and Blackstone, 2007; Cribbs and Strack, 2007). Cet effet s'accompagne d'une diminution de l'activité GTPase et une augmentation de la taille des mitochondries (Chang and Blackstone, 2007). A l'inverse la déphosphorylation de cette sérine par la calcineurine, amène DRP1 à la mitochondrie et provoque une augmentation de la fragmentation mitochondriale (Cereghetti et al., 2008). Ceci s'illustre par une augmentation de la sensibilité aux agents pro-apoptotiques comme la staurosporine (STS) lors de l'expression d'une forme de DRP1 non phosphorylable ($DRP1^{S637A}$) et, à l'inverse, une résistance face à l'apoptose avec un DRP1 phosphomimétique ($DRP1^{S637D}$) (Cribbs and Strack, 2007). *A contrario*, la sérine 616 est phosphorylée lors de la mitose par la CDK1 (Cyclin dependant kinase) dans des cellules HeLa et promeut la fission mitochondriale *via* le recrutement de DRP1 au niveau de la membrane mitochondriale (Taguchi et al., 2007) tandis que sa déphosphorylation par DUSP6 protège de l'apoptose induite par le stress oxydant (Ma et al., 2020) (Figure 37).

De façon surprenante, la phosphorylation de DRP1 en sérine 637 dans des adipocytes bruns aboutit à une augmentation de la fission mitochondriale (Wikstrom et al., 2014). L'utilisation de cellules et de souris où la sérine 637 est remplacée par une alanine, acide aminé non-phosphorylable montre que la phosphorylation en sérine 637 est nécessaire pour la phosphorylation de la sérine 616 (Valera-Alberni et al., 2021). En effet, les auteurs observent une augmentation concomitante de la phosphorylation en 616 et en 637 dans les adipocytes bruns, le foie et les muscles squelettiques ce qui contraste avec les résultats observés dans les cellules stéroïdogènes (Park et al., 2019; Plewes et al., 2020), les HeLa ou dans le cerveau (Ma et al., 2020). Cette différence pourrait être due à des isoformes différentes en fonction des organes, l'isoforme 1, comportant 2 exons de plus que l'isoforme 3 (exprimée dans tous les tissus), étant très fortement exprimée dans les neurones (Valera-Alberni et al., 2021).

DRP1 est également modifiable par SUMO1, 2 et 3. La SUMO1-ylation de DRP1 a été mise en évidence en 2004 (Harder et al., 2004) et est associée à un recrutement de

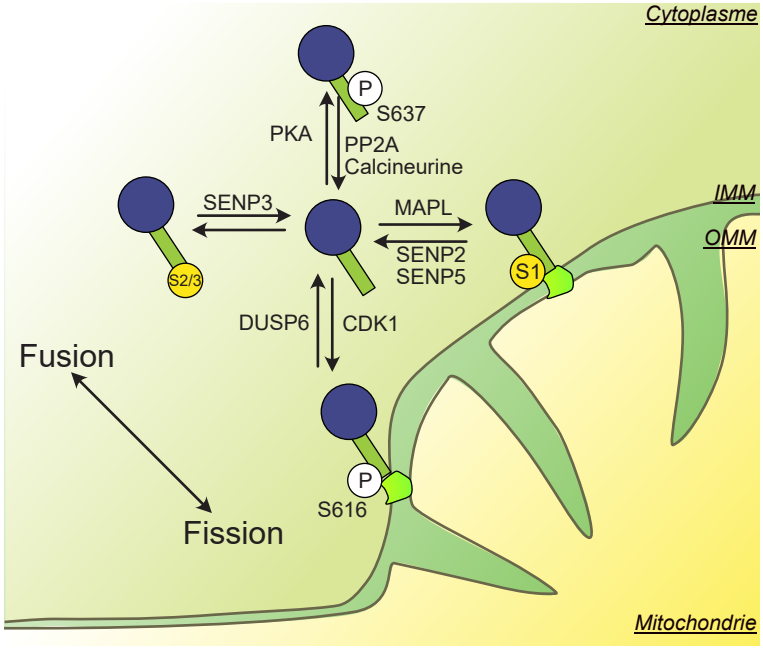

Figure 37: **Effet des modifications post-traductionnelles de DRP1 sur sa fonction**
La phosphorylation sur la sérine 637 et la SUMO2/3-ylation de DRP1 sont associées à une localisation cytoplasmique de DRP1 et une fusion mitochondriale tandis que la phosphorylation de la sérine 616 et la SUMO1-ylation sont corrélées au recrutement de DRP1 à la membrane mitochondriale, la fission et l'apoptose

DRP1 à la mitochondrie et une augmentation de la fission mitochondriale. Cet effet a ensuite été confirmé par plusieurs travaux (Wasiak et al., 2007) mettant en exergue la contribution de la protéine MAPL comme E3 SUMO ligase (Braschi et al., 2009; Prudent et al., 2015) ainsi que SENP2 (Fu et al., 2014) et SENP5 (Prudent et al., 2015; Zunino et al., 2007; Zunino et al., 2009) comme deSUMOylases. Des travaux de mutagénèse dirigée sur DRP1 ont révélé la présence de 8 lysines SUMOylables par SUMO1, 2 et 3 dans des cellules COS7, présentes sur le domaine B de DRP1 (Figure 36.A.) (Figueroa-Romero et al., 2009) [66].

La SUMO2/3-ylation de DRP1 a également été décrite dans des cellules primaires de neurones de rat privées d'oxygène. Cette SUMO2/3-ylation est causée par la diminution de l'expression de SENP3 et associée à une réduction de la fission mitochondriale et de l'apoptose (Guo et al., 2013). Le traitement de souris avec du sévoflurane (un anesthésique gazeux) induit une diminution du profil de SUMO2/3-ylation générale dû à un enrichissement de la protéine SENP3. Cette diminution est accompagnée d'une réduction de la SUMO2/3-ylation de DRP1 et une altération de la structure

[66] De façon remarquable, seuls SUMO2 et 3 semblent capables de se lier a DRP1 dans des cellules HEK293T (Figueroa-Romero et al., 2009)

mitochondriale (Zheng et al., 2020). Le mécanisme proposé pour expliquer l'induction de la fission mitochondriale lorsque DRP1 est déSUMOylé serait que la SUMO2/3-ylation de DRP1 sur le domaine B, bloque sa capacité à reconnaître MFF et en conséquence à être recruté au niveau de la membrane mitochondriale (Guo et al., 2017; Guo et al., 2021). Ces résultats pointent vers un rôle pro apoptotique de la SUMO1-ylation de DRP1 et anti apoptotique de sa SUMO2/3-ylation (Figure 37). Néanmoins, dans des cellules HeLa, l'inactivation par ARN interférant de SENP3, induit une augmentation de la SUMO2/3-ylation totale sans effet sur l'apoptose (Prudent et al., 2015).

Pour que la fission mitochondriale ait lieu, la sérine 637 de DRP1 doit être déphosphorylée, notamment par PP2A (Dickey and Strack, 2011). Ceci est possible grâce à l'ubiquitination et la dégradation de AKAP121 (A-kinase Anchoring Protein 121) [67] qui permet à la PKA d'être localisée au niveau de la membrane mitochondriale (Kim et al., 2011). Le blocage de la SUMO1-ylation de DRP1 par un *si-MAPL* n'affecte pas cette phosphorylation, suggérant que la déSUMOylation n'est pas nécessaire à la déphosphorylation de DRP1 (Prudent et al., 2015). Nénamoins, une étude récente a mis en évidence une diminution de la phosphorylation de la sérine 616 associée à une augmentation de la SUMO2/3-ylation dans des cellules pancréatiques β suggérant un rôle de la SUMO2/3-ylation de DRP1 sur sa phosphorylation (Nan et al., 2022) [68].

La mutation de la sérine 637 en alanine, quant à elle, ne modifie pas les niveaux de SUMO2/3-ylation de DRP1 ce qui montrerait que la SUMOylation est indépendante de l'état de phosphorylation de la sérine 637 (Guo et al., 2013). Toutefois, le niveau de phosphorylation de la sérine 616 ($DRP1^{S616D}$ ou $DRP1^{S616A}$) est inversement corrélé à sa SUMO1-ylation tandis que le blocage de la SUMOylation de DRP1 ($DRP1^{4KR}$) augmente la phosphorylation en sérine 616 sans affecter la sérine 637 (Huang et al., 2020).

[67] Les AKAPs sont une large famille de protéines situées dans les membranes qui reconnaissent les sous unités régulatrices de la PKA et permettent ainsi de régionaliser l'activité PKA (Omar and Scott, 2020)

[68] Il est possible que cet effet ne soit pas direct mais mette en jeu la SUMOylation d'autres protéines affectant la phosphorylation de DRP1 tel que DUSP6 (Ma et al., 2020)

Questions et perspectives

Les interactions entre les différentes modifications post-traductionnelles de DRP1 sont complexes et restent encore à clarifier. Des expériences de surexpression de mutants non phosphorylables, phosphomimétiques ou non SUMOylables couplées à des expériences de co-immunoprécipitations permettraient d'investiguer le rôle qu'exerce une modification sur une autre et la possibilité pour DRP1 de porter simultanément plusieurs modifications.

9.3 La morphologie mitochondriale, un aspect capital de la stéroïdogénèse

La fusion mitochondriale est orchestrée par MFN1/2 (mitofusin) et OPA1 (Optic atrophy 1), GTPases de la famille des dynamines. MFN1/2 permettent la fusion des membranes externes de la mitochondrie grâce à leur capacité de dimérisation tandis que OPA1 permet la fusion de l'IMM (Gao and Hu, 2021).

Dans des cellules stéroïdogènes de Leydig (MA-10) ou de corticosurrénale (Y1) la signalisation PKA augmente la fusion mitochondriale (Duarte et al., 2012) ainsi que le recrutement de StAR au niveau de la mitochondrie (Duarte et al., 2014; Park et al., 2019). De façon similaire, le traitement par l'angiotensine II ou le K^+ des cellules corticosurrélaniennes H295R, induit une élongation des mitochondries (Helfenberger et al., 2019).

Ces effets se traduisent par une augmentation de la production de stéroïdes et sont dépendants de la présence de MFN2. En effet, l'utilisation de *sh-Mfn* induit une diminution de la fusion mitochondriale, du recrutement de StAR à l'OMM et de la stéroïdogénèse (Duarte et al., 2012; Helfenberger et al., 2019)

De récents travaux ont montré que la signalisation PKA favorise la phosphorylation sur la sérine 637 de DRP1 dans des cellules de Leydig (Park et al., 2019) ou de placenta (Plewes et al., 2020). Cette modification provoquée par le traitement par AMPc ou LH

induit le transfert de DRP1 hors de la mitochondrie, l'élongation des mitochondries et favorise la production de stéroïdes.

En conclusion, l'équilibre entre la fusion et la fission mitochondriale permet l'induction de l'apoptose dans le cas de la fission ou la stimulation de la stéroïdogénèse lorsque les mitochondries sont élargies. La fission est dépendante de la protéine DRP1 dont l'activité est régulée de façon post-traductionnelle par sa SUMOylation et sa phosphorylation. Son implication dans l'apoptose et la stéroïdogénèse ainsi que sa régulation par SENP2 et la PKA font de DRP1 un candidat sérieux en tant que régulateur de la physiologie du cortex surrénalien

LA NECDIN, UN POTENTIEL ACTEUR DE L'INSUFFISANCE SURRENALIENNE

10 Le syndrome de Prader-Willi

10.1 Causes et manifestations cliniques

Le syndrome de Prader-Willi (PWS) (OMIM #176270) est un syndrome neuro-développemental affectant de nombreuses fonctions. Les patients naissent en sous-poids, présentent une hypotonie et un déficit d'activité de succion. L'apprentissage général est fortement ralenti et est associé à des troubles de la cognition. A partir de 8 ans, les patients entrent dans une phase d'hyperphagie et d'absence de satiété menant à une obésité (Cassidy et al., 2012).

Le syndrome de Prader-Willi est associé au *locus 15q11.2-q13* localisé sur le chromosome 15 chez l'Homme (sur le chromosome 7 chez la souris). Une partie de ce *locus* est soumise à empreinte parentale (appelé région Prader-Willi), c'est-à-dire que l'allèle provenant d'un seul des deux parents est exprimé, en l'occurrence, l'allèle paternel. Des changements génomiques ou épigénétiques aboutissant à la perte d'expression de ces gènes aboutit au

PWS. Ces changements peuvent être dus à une microdélétion génique (65-75% des cas), une disomie uniparentale, c'est à dire deux allèles maternelles (20-30 % des cas) ou plus rarement, une empreinte maternelle sur les deux allèles et donc une absence d'expression génique (1-3% des cas). Les gènes codants présents au sein de cette région sont *MKRN3*, *MAGEL2* (Boccaccio et al., 1999; Lee, 2000), *NDN* (MacDonald and Wevrick, 1997), *NPAP1* [69] et *SNURF/SNRPN* et sont accompagnés de clusters de gènes non codants *PWRN* et *SNORDs* (Cassidy et al., 2012; Tauber and Hoybye, 2021) (Figure 38).

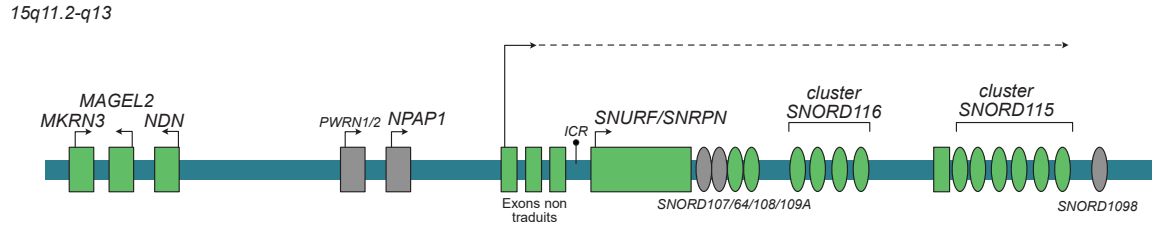

Figure 38: **Schéma de la région 15q11.2-q13 humaine**
Les parties vertes représentent les régions conservées chez la souris tandis que les parties grises ne sont présentes que chez les êtres humains. Les SNORDs sont représentés par des ovales. D'après Tauber & Hoybye, 2021.

10.2 La NECDIN et les protéines MAGE

La NECDIN (neurally differentiated EC cell-derived protein) est une protéine qui a été découverte en 1991, enrichie lors de la différenciation *in vitro* de cellules fibroblastiques en neurones (Maruyama et al., 1991). C'est une protéine de 42 kDa exprimée dans le système nerveux central, les préadipocytes blancs et bruns, les cellules souches hématopoïétiques, les cellules musculaires satellites et les cellules stellaires hépatiques (Liang et al., 2019; Yoshikawa, 2021). Elle appartient à la famille MAGE (melanoma antigen). Cette famille se caractérise par la présence d'un domaine d'homologie MAGE (MHD) généralement positionné en position C-terminale. Ces protéines exercent leurs fonctions principalement par la liaison à d'autres protéines notamment des E3 ubiquitine ligases [70] (Florke Gee et al., 2020).

[69] *NPAP1* est absent chez les souris mais elles possèdent un autre gène codant dans ce *locus*, *Frat3*

[70] Par exemple, l'ubiquitine & SUMO E3 ligase TRIM28, est capable de réguler la stabilité de p53 et agit comme un puissant répresseur chromatinien (Doyle et al., 2010). Les protéines MAGE-A2 et MAGE-C2 ont la capacité de se lier à TRIM28 et d'augmenter son activité E3 ubiquitine ligase stimulant la dégradation de p53 par le protéasome (Doyle et al., 2010; Xiao et al., 2011, 2014).

Les protéines de la familles MAGE sont classées en 2 catégories : le type 1 (comprenant MAGE A, B et C) correspond a des protéines exprimées principalement dans les cellules germinales et les tissus fœtaux et dont l'expression dans les autres tissus ne se réactive que lors de tumorigénèse (Florke Gee et al., 2020). Le type 2 quant à lui, comprend les protéines MAGE D, E, F, G, H, L et la NECDIN. Elles sont exprimées dans une variété de tissus et ne sont pas spécialement liés à l'apparition de cancers.

10.3 Implications de NECDIN et MAGEL2 dans le syndrome de Prader-Willi : modèles animaux

Un premier modèle animal de perte de la NECDIN n'a révélé aucune atteinte sur la fertilité, le poids et la physiologie générale des souris $Ndn^{-/-}$ (Tsai et al., 1999). Néanmoins, deux autres modèles de délétion de NECDIN ont aboutit à des conclusions opposées. L'un est produit par remplacement du gène *Ndn* par *LacZ* (Ndn^{tm2Stw})(Gerard et al., 1999) alors que le second (Ndn^{tm1Mus}) est produit en introduisant une cassette néomycine à la place des deux premiers tiers du gène codant la NECDIN (Muscatelli, 2000). Ces deux modèles induisent une forte mortalité post-natale et une détresse respiratoire (Gerard et al., 1999; Muscatelli, 2000). Par ailleurs, les souris Ndn^{tm1Mus} présentent moins de neurones à GnRH et à ocytocine au niveau de l'hypothalamus, elles se toilettent plus et performent mieux en terme d'apprentissage que des souris sauvages (Muscatelli, 2000). Ces résultats, bien qu'en partie discordants, permettent de conclure à l'implication de la NECDIN dans une partie de l'étiologie du PWS. Plus tard, d'autres modèles ciblés mettront en évidence l'importance de la NECDIN pour la maturation de nombreux neurones (Yoshikawa, 2021).

Les modèles de délétion de MAGEL2 décrivent une forte létalité post-natale (Kozlov et al., 2007; Mercer and Wevrick, 2009; Schaller et al., 2010) due à un défaut de succion des nouveaux-nés, qui peut être corrigé par une injection unique d'ocytocine (Schaller et al., 2010). Les souris ne développent pas d'obésité (Bischof et al., 2007; Kozlov et al., 2007; Schaller et al., 2010) mais ont une légère hyperphagie à l'âge adulte associée

à une diminution de la production d'orexine A et B (Kozlov et al., 2007), une légère augmentation du rapport masse grasse/masse maigre et des taux d'insuline et de leptine (Bischof et al., 2007). De plus, les souris *Magel2*$^{-/-}$ des deux sexes deviennent infertiles à 24 semaines. Les mâles présentent une diminution des concentrations plasmatiques de testostérone mais pas de réduction du poids ou de la morphologie des testicules ou de l'épididyme ni d'altération de la spermatogénèse. Les femelles, quant à elles, présentent une absence de corps jaune entre 10 et 24 semaines et une dérégulation de l'œstrus dès 10 semaines (Mercer and Wevrick, 2009).

Ces modèles animaux impliquent la NECDIN et MAGEL2 dans l'étiologie du PWS, cependant l'ensemble des atteintes du PWS ne sont pas reproduites et les effets varient de façon assez importante d'un modèle à l'autre. La contribution de MAGEL2 dans la physiopathologie du PWS est d'autant plus probable que le syndrome de Schaaf-Yang, causé par la perte de fonction de MAGEL2 (OMIM #615547) décrit en 2013 (Schaaf et al., 2013) reproduit une grande partie des atteintes du syndrome de Prader-Willi, telles que les difficultés d'alimentation, les déficits développementaux, l'hypogonadisme ou les déficits cognitifs.

10.4 Atteintes endocrines du PWS

En plus des atteintes comportementales, le syndrome de Prader-willi est associé à de nombreuses atteintes endocrines. Les patients souffrent d'obésité sous cutanée causée par une hyperphagie et impactant drastiquement leur qualité de vie. Une grande partie des atteintes du PWS touchent l'hypothalamus, les patients sont ainsi atteints d'hypothyroïdisme, de déficit en hormone de croissance et d'hypogonadisme, tous les trois d'origine centrale (Moscogiuri et al., 2019).

En 2004, une étude a mis en évidence une hypoplasie bilatérale des surrénales chez 3 patients atteints de PWS sur 4 patients autopsiés (Stevenson et al., 2004) ce qui a amené à se poser la question de l'insuffisance surrénalienne. L'insuffisance surrénalienne est une maladie endocrine rare (Arlt and Allolio, 2003). Elle peut être périphérique, c'est-à-dire

qu'elle vient de l'incapacité de la surrénale à produire des stéroïdes convenablement ou centrale (CAI) lorsque l'hypophyse ou l'hypothalamus sont touchés ce qui aboutit à une production d'ACTH défaillante.

Méthode	Age	ACTH basal <1.8 pmol/l	Pic ACTH <33 pmol/l	DOC <200nmol/l	cortisol <500nmol/l ou 0.47 pg/mg pour HCC	Publication
OMT	Enfants	0/25	15/25	7/25	_	De Lind et al., 2008
ITT	Enfants	_	_	_	1/15	Connell et al., 2010
HDST (250 µg)		_	_	_	0/6	
LDST (1µg)		_	_	_	0/4	
LDST (1µg)	Enfants	11/41	_	_	0/41	Nyunt et al., 2010
ITT	Enfants & adultes	_	_	_	0/8	Farholt et al., 2011
HDST (250 µg)		_	_	_	1/57	
LDST (1µg)	Enfants	7/84	_	_	12/84	Corrias et al., 2012
hDST (250µg)		_	_	_	6/12	
LDST (1µg)	Adultes	_	_	_	8/53	Grugni et al., 2013
hDST (250µg)		2/8	_	_	4/7	
ITT	Enfants	_	_	_	1/7	Beauloye et al., 2015
GT		_	_	_	0/13	
ITT	Enfants	5/36	3/36	_	0/36	Oto et al., 2018
OMT	Enfants	_	5/20	1/21	_	Obrynba et al., 2018
LDST (1µg)		_	_	_	6/21	
OMT	Adultes	_	21/46	0/46	_	Rosenberg et al., 2020
ITT		_	_	_	1/36	
HCC	Adultes	_	_	_	0/31	Shukur et al., 2021
HCC	Enfants & adultes	_	_	_	13/41	Damen et al., 2021
OMT		_	2/2	2/2	_	
LDST (1µg)	Enfants	_	_	_	2/52	Dağdeviren Çakır et al., 2021

Table 2: **Tableau synthétique des atteintes de l'HPA chez les patients atteints du syndrome de Prader-Willi** OMT : Test à la métyrapone sur la nuit, ITT : test de tolérance à l'insuline, LDST/HDST : test à l'ACTH synthétique (synacthen) à basse/haute dose, GT : test au glucagon, HCC : concentration en cortisol dans les cheveux

Une étude réalisée sur 24 enfants atteints de Prader-Willi soumis à un test à la métyrapone [71] a révélé une réponse insuffisante chez 60% des patients atteints de PWS (de Lind van Wijngaarden et al., 2008). Suite à ce travail différentes études ont remis en perspective ces résultats en utilisant des tests à la métyrapone, à l'insuline, au

[71]La métyrapone inhibe l'enzyme terminale de production du cortisol CYP11B1. Les patients sont traités avant le coucher et on mesure au réveil l'accumulation de DOC (due à l'absence de sa conversion en corticostérone) et d'ACTH (due à l'absence de rétrocontrôle par les GC)

glucagon ou à l'ACTH [72] (Beauloye et al., 2015; Connell et al., 2010; Corrias et al., 2012; Farholt et al., 2011; Grugni et al., 2013; Nyunt et al., 2010; Obrynba et al., 2018; Oto et al., 2018; Rosenberg et al., 2020) (Table 2). Lorsque l'on regarde les taux de cortisol après stimulation, une prévalence d'insuffisance surrénalienne de 0-15% est rapportée. L'absence de crise surrénalienne pendant les opérations des patients atteints de PWS indique que la prévalence de la CAI chez les patients atteints du PWS est rare (Rosenberg et al., 2020). Néanmoins, lorsque l'on s'intéresse à l'accumulation de l'ACTH suite à un blocage à la métyrapone, les taux sont inférieurs au seuil de 33 pmol/l dans 60% (de Lind van Wijngaarden et al., 2008), 25% (Obrynba et al., 2018) et 46% (Rosenberg et al., 2020) respectivement [73].

On peut donc supposer que, bien qu'il n'y ait pas de d'insuffisance surrénalienne clinique, il existe un défaut de production d'ACTH chez les patients atteints du syndrome de Prader-Willi [74]. Ce caractère serait cohérent avec un déficit en enzyme de conversion PC1/3 [75] retrouvé chez les patients (Burnett et al., 2017; Polex-Wolf et al., 2016) et dans certains modèles murins de PWS (Burnett et al., 2017; Chen et al., 2020) ainsi qu'une accumulation des transcrits codant *Pomc* dans le cerveau de souris dont le *locus* PWS est inactif (Bittel et al., 2007). Il est donc, à l'heure actuelle, difficile de conclure quant à l'association entre syndrome de Prader-willi et insuffisance surrénalienne d'origine centrale.

[72] Les test à l'insuline ou au glucagon font fortement varier la glycémie ce qui active la sécrétion d'ACTH par l'hypophyse et permet de tester l'intégrité de l'axe HPA en entier. Le test à l'ACTH quant à lui ne mesure que la capacité de la surrénale à répondre à une stimulation

[73] De façon surprenante, une étude s'intéressant au taux de cortisol dans les cheveux, permettant d'avoir une mesure des taux sur le long terme observe des taux plus importants chez les patients atteints du PWS (Shukur et al., 2020)

[74] La mesure de l'ACTH avec un seuil à 33pmol/l suite à un test à la métyrapone reste toutefois une méthode avec une forte sensibilité mais une spécificité relativement faible augmentant la proportion de faux positifs (Giordano et al., 2008).

[75] voir paragraphe 1.3.3.4 - Régulation de la stéroïdogénèse fasciculée

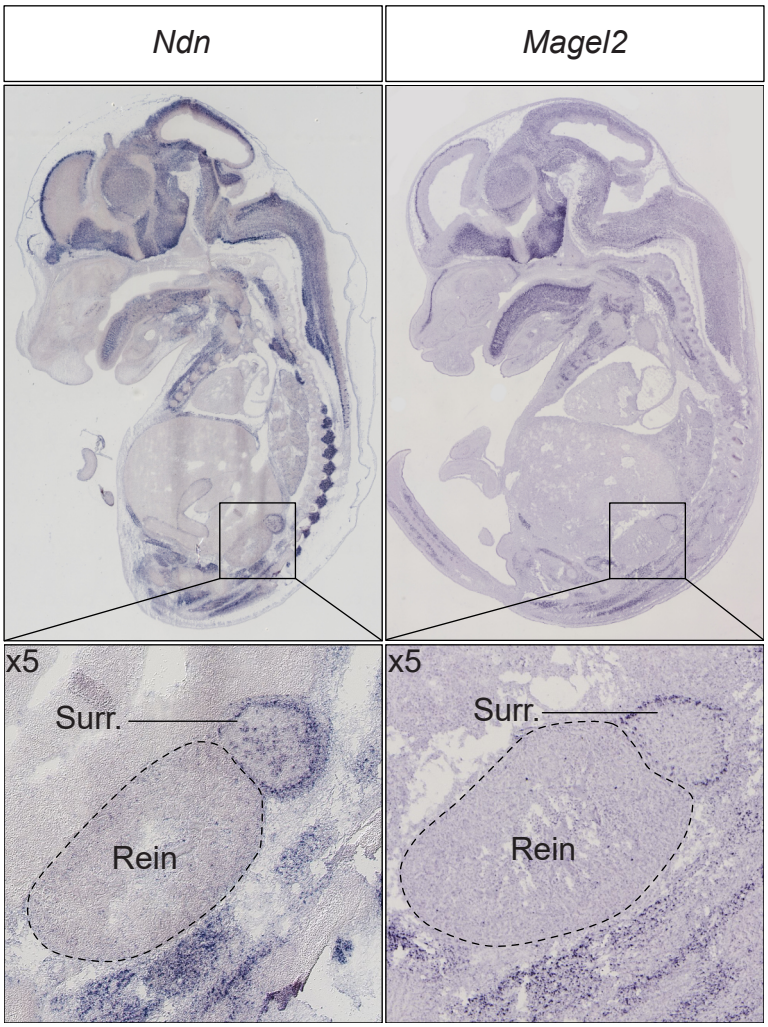

Figure 39: **Localisation des ARNm de *Ndn* et *Magel2* sur des embryons à E14.5**
Données issues de genepaint (Visel, 2004)

11 Intêrét dans l'homéostasie du cortex surrénalien

Les analyses réalisées en hybridation *in-situ* sur embryons à E14.5 révèlent une expression régionalisée de *Ndn* et *Magel2* en périphérie des glandes surrénales (Figure 39) (Visel, 2004).

De plus, dans une analyse des gènes différentiellement exprimés entre la zone fasciculée et glomérulée de rat par *micro-array*, *Ndn* est le 17e gène le plus enrichi dans la zG par rapport à la zF (Nishimoto et al., 2012). Enfin dans une analyse en *single-cell RNAseq* de surrénales murines adultes, *Ndn* est enrichi spécifiquement dans les cellules glomérulées (Lopez et al., 2021b).

Par ailleurs, l'expression génique de *Ndn* est directement régulée par le facteur CREB qui

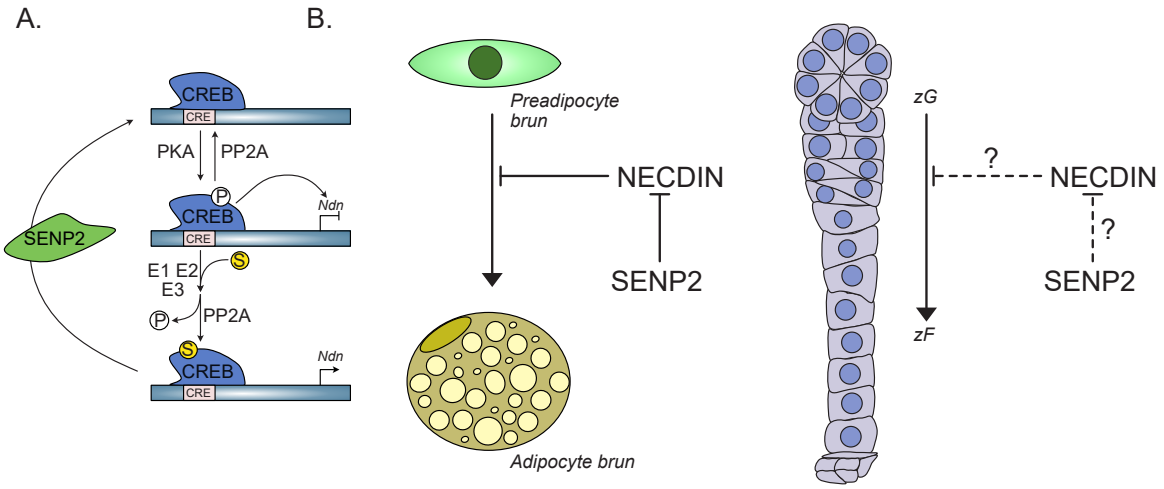

Figure 40: **Hypothèse concernant le rôle de la NECDIN dans le cortex surrénalien**
A. Cinétique hypothétique des modifications post-traductionnelles de CREB et de leur effet sur la transcription
B. Hypothèse quant aux effets de la NECDIN sur la différenciation corticosurrénalienne

se fixe sur le promoteur de *Ndn* et réprime son expression en réponse à la phsophorylation par la PKA (Cypess et al., 2011). Dans un modèle de souris portant une délétion de *Senp2* dans les préadipocytes bruns, l'accroissement de la SUMOylation réprime l'adipogénèse (Liang et al., 2019). Ce déficit en adipocytes bruns serait la conséquence de la levée de répression du gène *Ndn* par un CREB dont la SUMOylation va conduire à sa déphosphorylation par PP2A [76] (Figure 40.A.). Ainsi, dans les préadipocytes bruns, la perte de SENP2 bloque la différenciation adipogénique *via* la répression de certains effecteurs de la signalisation PKA et la surexpression de la NECDIN. Dans le cortex surrénalien, la NECDIN n'est présente que dans le zG et est absente de la zF, où la signalisation PKA est la plus active. On peut donc imaginer un mécanismes commun de blocage de la différenciation à travers un axe SUMO-PKA-NECDIN (Figure 40.B.).

En ce qui concerne MAGEL2, une insuffisance surrénalienne a été retrouvée dans 15% des cas chez les patients atteints du syndrome de Schaaf-Yang (Halloun et al., 2021). A l'inverse, les souris déficientes pour MAGEL2, présentent une augmentation des taux circulant de corticostérone, résistant au traitement dexaméthasone chez les femelles (Tennese and Wevrick, 2011). Ce phénotype rappelle celui retrouvé chez les souris déficientes pour le *locus* Prader-Willi entier qui présentent une hypercorticostéronémie

[76] Voir paragraphe 8.2 - Impact de la SUMOylation sur la signalisation AMPc/PKA

périnatale (Stefan et al., 2005) [77].

[77] Ces résultats sont à nuancer notamment à cause de l'hypoglycémie présente chez ces souris qui provoque un stress et peut faire augmenter la production de corticostérone sans atteintes de l'HPA

RESULTATS

Objectifs du travail de thèse

Le cortex surrénalien est un organe complexe qui nécessite de s'adapter rapidement et convenablement pour assurer la pérennité de l'individu. On ne connaît à l'heure actuelle, que partiellement les mécanismes permettant la régulation de sa fonction et du renouvellement des cellules stéroïdogènes, incluant leurs différenciation, prolifération et apoptose. Il y a donc une nécessité de mettre en évidence de nouveaux acteurs permettant de comprendre la physiologie du cortex pour mieux comprendre ses pathologies.

Caractérisation d'un modèle d'hyperSUMOylation du cortex surrénalien

Les modèles murins de modifications de la SUMOylation ont montré que cette modification post-traductionnellle assumait un rôle particulièrement important dans les processus d'ontogénèse tissulaire et de différenciation. Dans la surrénale, l'intensité de SUMOylation suit les zones fonctionnelles du cortex, en effet, on observe des taux élevés de SUMOylation dans la zone glomérulée alors que la SUMOylation dans la zone fasciculée est relativement faible. En outre, la SUMOylation est régulée négativement par la signalisation PKA notamment *via* la surexpression de la déSUMOylase SENP2.

Pour investiguer l'effet de la SUMOylation dans la physiologie et la différenciation cellulaire du cortex surrénalien, nous avons généré des modèles d'hyperSUMOylation en invalidant la déSUMOylase SENP2 dans le cortex surrénalien. Deux modèles ont été développés, l'un ciblant toutes les cellules du cortex dès la vie embryonnaire (*Sf1-Cre::Senp2*$^{fl/fl}$) l'autre agissant uniquement dans la zone glomérulée autour de la naissance (*AS*^{Cre}*::Senp2*$^{fl/fl}$) et ciblant donc l'entièreté du cortex uniquement à l'âge adulte. De plus, afin de déterminer l'implication de la SUMOylation dans les effets causés par la signalisation AMPc/PKA sur le cortex, un modèle double transgénique d'hyperSUMOylation associée à une activation de la PKA (*Sf1-Cre::Senp2*$^{fl/fl}$*::Prkar1a*$^{fl/fl}$) a été étudié.

Ces modèles visent à déterminer l'impact d'un excès de SUMOylation sur le cortex surrénalien et notamment sur la zone fasciculée où la SUMOylation est faible ainsi que ses interactions avec la signalisation PKA.

Exploration de la physiologie surrénalienne dans des modèles de PWS

L'exploration des atteintes associées à la perte de SENP2 dans le cortex a permis de mettre en évidence la surexpression de deux protéines de la famille MAGE : NECDIN et MAGEL2. Ainsi, le deuxième projet s'est focalisé sur le rôle de ces protéines dans la fonction surrénalienne et notamment de la NECDIN qui est surexprimée dans un modèle de préadipocytes bruns déficients pour SENP2 (*Myf5-Cre::Senp2*$^{fl/fl}$) et qui bloque l'adipogénèse brune. Cette hypothèse est supportée par les atteintes surrénaliennes suspectées dans le syndrome de Prader-Willi et de Schaaf-Yang causés respectivement par la perte du *locus* contenant *NECDIN* et *MAGEL2* ou des mutations inactivatrices de *MAGEL2*. L'étude des modèles de délétion totale de NECDIN (*Ndn-KO*) et de MAGEL2 (*Ndn/Magel2-dKO*) a permis d'explorer le rôle de ces deux protéines dans la réponse au stress notamment aux niveaux surrénalien et hypophysaire.

Article 1

Graphical abstract

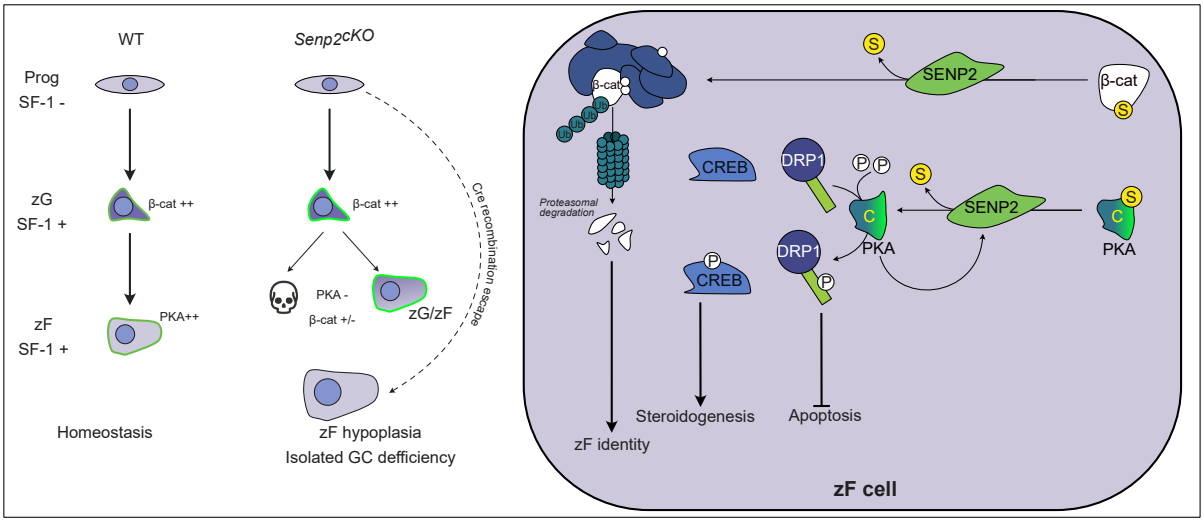

Loss of SUMO-specific protease 2 causes isolated glucocorticoid deficiency by blocking adrenal cortex zonal transdifferentiation

Damien Dufour [1], Typhanie Dumontet [1,2,3], Isabelle Sahut-Barnola [1], Meline Onzon [1], Eric Pussard [4], James Jr Wilmouth [1], Julie Olabe [1], Cecily Lucas [1,5], Adrien Levasseur [1], Christelle Soubeyrand-Damon [1], Jean-Christophe Pointud [1], Florence Roucher-Boulez [1,5], Igor Tauveron [1,6], Guillaume Bossis [7], Edward T.Yeh [8], David T. Breault [9,10], Pierre Val [1], Anne-Marie Lefrançois-Martinez [1] and Antoine Martinez [1*]

[1] institut Génétique, Reproduction & Développement (iGReD), CNRS, INSERM, Université Clermont Auvergne, Clermont–Ferrand, F-63000, France. [2] Department of Internal Medicine, Division of Metabolism, Endocrinology, and Diabetes, University of Michigan, Ann Arbor, Michigan, USA. [3] Training Program in Organogenesis, Center for Cell Plasticity and Organ Design, University of Michigan, Ann Arbor, Michigan, USA. [4] Service de Génétique Moléculaire, Pharmacogénétique et Hormonologie, Hôpital de Bicêtre, Assistance Publique-Hôpitaux de Paris (APHP), Physiologie et Physiopathologie Endocriniennes, INSERM, Université Paris-Saclay, Le Kremlin-Bicêtre, France. [5] Endocrinologie Moléculaire et Maladies Rares, Centre Hospitalier Universitaire, Université Claude Bernard Lyon 1, Bron, France. [6] Service d'Endocrinologie, Centre Hospitalier Universitaire Gabriel Montpied, Université Clermont Auvergne, Clermont-Ferrand, France. [7] IGMM, Université de Montpellier, CNRS, Montpellier, France. [8] Department of Internal Medicine, University of Arkansas for Medical Sciences, Little Rock, Arkansas, USA. [9] Division of Endocrinology, Boston Children's Hospital, Department of Pediatrics, Harvard Medical School, Boston, Massachusetts, USA. [10] Harvard Stem Cell Institute, Harvard University, Cambridge, Massachusetts, USA.

*Corresponding author. E-mail(s): antoine.martinez@uca.fr;

Abstract

SUMOylation is a dynamic posttranslational modification, that provides fine-tuning of protein function involved in the cellular response to stress, differentiation, and tissue development. In the adrenal cortex, an emblematic endocrine organ that mediates adaptation to physiological demands, the SUMOylation gradient is inversely correlated with the gradient of cellular differentiation raising important questions about its role in functional zonation and the response to stress. Considering that SUMO-specific protease 2 (SENP2), a deSUMOylating enzyme, is upregulated by ACTH/PKA signalling within the zona *Fasciculata* (zF), we generated mice with adrenal-specific *Senp2* loss to address these questions. Disruption of SENP2 activity in steroidogenic cells leads to specific hypoplasia of the zF, a blunted reponses to ACTH and isolated glucocorticoid deficiency. Mechanistically, overSUMOylation resulting from SENP2 loss shifts the balance between ACTH/PKA and WNT/β-catenin signalling leading to repression of PKA activity and ectopic activation of β-catenin. At the cellular level, this blocks transdifferentiation of β-catenin-positive zona *Glomerulosa* cells into zF cells and sensitises them to premature apoptosis. Our findings indicate that the SUMO pathway is critical for adrenal homeostasis and stress responsiveness.

Keywords: Adrenal, SUMO, SENP2, β-catenin, PKA, DRP1

The mouse adrenal cortex is a constantly self-renewed endocrine organ composed of concentric zones, including the outermost *zona glomerulosa* (zG) layer producing mineralocorticoids and the innermost *zona fasciculata* (zF) layer producing glucocorticoids. According to the centripetal migration model occurring during postnatal development, progenitors cell populations located in the adrenal capsule (characterised by GLI1 expression) or within the zG (characterised by SHH expression) consecutively differentiate into steroid-producing zG cells, then through a process of zonal transdifferentiation, convert into zF cells before eventually undergoing apoptosis at the corticomedullary junction[1–3].

Genetic models and *in vitro* approaches have identified two important signalling pathways for adrenal cortex homeostasis. On the one hand, the WNT/Rspondin/β-catenin pathway is necessary for the maintenance of progenitor pools and the acquisition of zG identity[4–6]. On the other hand, cAMP/PKA signalling, stimulated by pituitary ACTH, triggers the recruitment of progenitors by inducing the transdifferentiation of zG cells into zF cells and stimulates glucocorticoids production[7,8]. We and others have previously shown that these two signalling pathways antagonise each other by modulating various actors such as WNT4, PDE2A or CCDC80[3,6,9]. Optimal response to PKA signalling and therefore zF differentiation is also subject to epigenetic programming by the histone methyl transferase EZH2[10]. Nonetheless, the mechanisms that maintain adrenal cortex zonation and balance between these two pathways are yet to be discovered.

SUMOylation is a dynamic and one of the fastest evolving[11] posttranslational modification consisting in the covalent addition of SUMO peptides on a target protein. This modification can affect various processes such as protein stability, interactions or subcellular localisation[12]. There are three main SUMO peptides in rodents, namely SUMO1, which shares around 50% of identity with SUMO2 and SUMO3, the two latter differing by only three amino acids. SUMOylation is achieved through an enzymatic cascade involving activation by the E1 heterodimer (SAE1/UBA2), conjugation by the sole E2 enzyme UBC9 (encoded by *Ube2i*) and final ligation by various E3 SUMO ligases such as members of the PIAS and TRIM families as well as RANBP2 and CBX4[13,14]. SUMO peptides can be removed from SUMO-conjugated substrates by deSUMOylases belonging mainly to the Sentrin-specific proteases family (SENPs) or by the more recently discovered DeSI-1 and USPL1 making this posttranslational modification highly dynamic (Figure S1.A.B.). Several *in vitro* and *in vivo* studies have highlighted the importance of controlling SUMOylation levels to enable differentiation or maintain cellular identity[15–17] and tissue homeostasis *in vivo* in various cell lineages[18,19]. The adrenal gland could provide a paradigm to study how SUMOylation dynamics can interact with the function and homeostasis of an organ, in charge of constant adaptation to stress.

We have previously shown that protein SUMOylation follows a decreasing centripetal gradient in human and mouse normal adrenal cortices. Moreover, this gradient is altered in genetic endocrine diseases with deregulated PKA or WNT signalling pathways[20]. Remarkably, SUMOylation is negatively and acutely regulated by ACTH in both adrenal cortex and adrenocortical cell cultures through transcriptional control of key enzymes, especially SENP2 whose upregulation by PKA correlates with transient hypoSUMOylation in zF.

Interestingly, PKA-mediated up-regulation of *Senp2* was previously shown to promote the progression of preadipocytes into the adipogenic program[15]. Taken together, these studies suggest that limiting SUMOylation may facilitate or be a prerequisite for any change in differentiation states. Conversely, an excess of WNT/β-catenin signalling in the adrenal cortex induces an expansion of zG identity that is correlated with a high SUMOylation state[20]. Finally, preventing *in vivo* SUMOylation of the transcription factor SF-1 (*SF-1*$^{2KR/2KR}$ mice), the main driver of adrenogonadal cell fate, disturbs endocrine development by maintaining discrete gonadal traits in the cortex and adrenal traits in the testis[21]. This highlights the need to control SUMOylation during cell fate decisions leading to adrenal cortex identity.

We hypothesise that disruption of the SUMOylation gradient in the adrenal cortex may disrupt zonation and impair adaptive response to stress. In order to understand the implication of SUMO pathway on homeostatic maintenance and endocrine function, we have developed mouse models of adrenal hyperSUMOylation by conditional ablation of *Senp2* in the cortex (*Senp2*^{cKO}). Our report reveals that *Senp2*^{cKO} mice show zone-specific adrenal atrophy, isolated glucocorticoid deficiency and blunted response to ACTH. Progressive atrophy of zF evoked by SENP2 deficiency results from a blockade of zonal transdifferentiation, early apoptosis and impaired PKA catalytic activity that cannot be rescued by genetic de-repression of the PKA holoenzyme. SENP2-deficient adrenals also show increased β-catenin SUMOylation and activity that may help to antagonise PKA signalling, thus maintaining the suppression of zF identity. As *Senp2* expression is itself under the control of ACTH/PKA, our data identify SUMOylation as a feedforward mechanism that readies the adrenal cortex to respond to stress and maintain functional zonation.

Results

Senp2 invalidation in the adrenal cortex leads to zF hypoplasia and adrenal dysplasia

To assess the role of SUMOylation in the adrenal cortex, we have developed a mouse model with specific deletion of the ACTH-regulated deSUMOylase SENP2[20] in steroidogenic cells by mating *Senp2*$^{fl/fl}$ mice[22] with *SF-1(Nr5a1)*-Cre mice[23]. *Senp2* conditional knock-out mice are later referred to as *Senp2*^{cKO}. *Senp2* deletion was confirmed in 4-week-old mouse adrenals by RT-qPCR analyses showing reduced *Senp2* mRNA accumulation in both genders and by genomic PCR, confirming adrenal-specific recombination at the *Senp2 locus* (Figure S1.C.D.).

Monitoring of adrenal mass from 4 to 40 weeks of age revealed significant adrenal hypoplasia in mutants, occurring between 4 and 8 weeks in both sexes. After this time point, overall adrenal weight in *Senp2*^{cKO} remained below that of controls in females only because of sex differences in the kinetics of adrenal mass gain (almost continuous growth in WT females contrasting with a progressive decrease in WT males over time) (Figure 1.A.). To investigate the causes of this hypoplasia, we performed H&E staining, which revealed two different histological phenotypes: either homogeneous atrophy of the cortex leaving medulla centrally located, or cortical atrophy accompanied by dysplasia due to clusters of large eosinophilic cells, usually at one pole of the gland and pushing the medulla toward the other pole (Figure

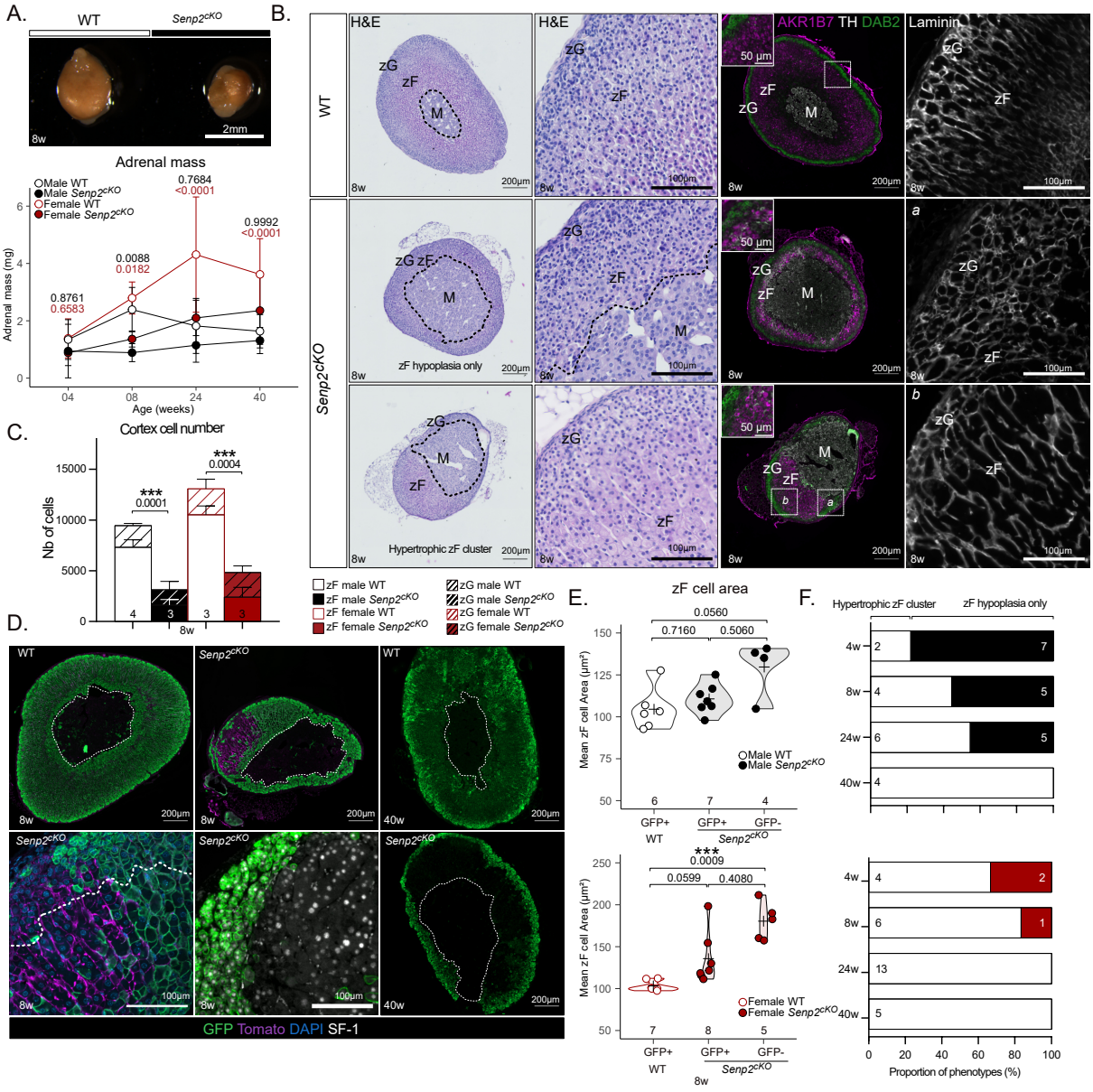

Figure 1: **Deletion of the deSUMOylase *Senp2* in embryonic steroidogenic cells induces adrenal dysplasia and zF hypoplasia in adult mice.**

A. Top : Representative picture of an 8-week-old WT (left) and a $Senp2^{cKO}$ (right) adrenal.
Bottom : Absolute adrenal mass follow-up of male and female mice WT and $Senp2^{cKO}$ (mean) from 4 to 40 weeks of age. *P*-values represent difference between genotypes within the same age and sex group.

B. Morphological analysis of the phenotypes on 8-week-old males' adrenals. Left : H&E staining of WT or $Senp2^{cKO}$ adrenals with or without dysplasia. Center : Coimmunofluorescence labelling of AKR1B7 (green), TH/Tyrosine Hydroxylase (white) and DAB2/Disabled2 (Purple) in WT and $Senp2^{cKO}$ adrenals. Right : Immunofluorescence analysis of laminin (white) revealing the vascular network in WT and cKO adrenals.

C. 2D cell number counting in male and female adrenals at 8 weeks of age.

D. Coimmunofluorescence labelling of GFP (green) with Tomato (purple) and SF-1 (white) at 8 (left and center) and 40 weeks of age (right) WT and $Senp2^{cKO}$ adrenals.

E. Morphometric analysis of zF cells area in WT (GFP+) adrenals and recombined (GFP+) or non recombined (GFP-) zones of $Senp2^{cKO}$ adrenals at 8 weeks of age.

F. Prevalence of phenotypes in cKO adrenals at different ages. Black (male) or red (female) bars represent hypoplastic adrenals without any gross morphological change and white bar represents hypoplastic and dysplastic adrenals harbouring hypertrophic zF clusters.

zG, *zona glomerulosa*; zF, *zona fasciculata*; WT, wild-type; cKO, conditional Knock-Out.

1.B. left panel).

Immunofluorescence co-staining for zonal markers showed that, compared to WT, the integrity of zG (DAB2+) did not seem affected in *Senp2*^{cKO} adrenals of 8-week-old mice, while zF (AKR1B7+) was atrophic and sometimes mislocated together with the medulla (TH+) in dysplastic glands (Figure 1.B. right panels). To confirm that the zF was the most affected by *Senp2* invalidation, the number of cells in each cortical zones and medulla was counted on 2D sections. This showed a dramatic and specific reduction in total cortical cell number regardless of sex, solely attributable to the 75-80% loss of zF cells (Figures 1.C. & S1.E). Laminin immunostaining was then used to examine vascular architecture in WT and mutant adrenal sections. Typical capillaries surrounding the "rosette" structures in the zG and delimiting the zF cells columns were evidenced in WT adrenal sections. Consistent with zonal markers immunostaining, a rosette-like pattern of vascularisation, typical of zG, was found in areas with atrophic zF (Figure 1.B.a.), whereas large columnar structures surrounding clusters of hypertrophic zF cells were evidenced in dysplastic *Senp2*-deficient glands (Figure 1.B.b.).

To further characterise the origin of adrenal dysplasia, we introduced the *Rosa26RmTmG* reporter transgene[24] (Figure S1.F.) into *Senp2*^{cKO} background to trace *Senp2* recombination using GFP immunostaining and non-recombined cells using Tomato immunostaining. WT adrenals (from *Sf1-Cre/+::Senp2*$^{fl/+}$*::R26R*$^{mTmG/mTmG}$ triple transgenic mice) presented full recombined cortex, while in dysplastic *Senp2*^{cKO} adrenals (*Sf1-Cre/+::Senp2*$^{fl/fl}$*::R26R*$^{mTmG/mTmG}$), most of the cells belonging to the mislocated zF were GFP-negative/Tomato-positive, hence non recombined (Figure 1.D.). To address the identity of these cells escaping recombination, we performed co-staining of GFP with the canonical steroidogenic marker SF-1. Surprisingly, GFP-negative cells expressed SF-1, implying that they kept full steroidogenic identity (Figure 1.D. bottom centre panel) as also suggested by detection of zonal markers (Figure 1.B. right panels, bottom). To confirm that these cells were hypertrophic as H&E and Laminin staining suggested, we measured 2D cell areas in the zF of WT and *Senp2*^{cKO} adrenal sections. This showed that in females, although GFP-positive and GFP-negative zF cell areas did not differ in the mutant, GFP-negative cells were larger than zF cells from WT adrenals (Figure 1.E.). Similar observations were made in males but with a *P*-value of 0.0560. Next, we assessed global SUMOylation status by western blot and found no variation in the profile of SUMO1 or SUMO2/3 conjugates as a function of the genotype (Figure S1.G.H.). However, GFP-positive zF cells retained nuclear SUMO2/3 staining whereas GFP-negative had diffuse staining in the cytoplasm (Figure S1.I.J.). Together, these results indicate that the clusters of cellular hypertrophy found in dysplastic *Senp2*^{cKO} adrenals are predominantly composed of zF cells that have escaped *Senp2* ablation and that this phenotype (hypertrophic zF clusters) seems more likely to occur in females. To examine further this sexual dimorphism, we assessed the proportion of mutant adrenals presenting with hypertrophic zF clusters from 4 to 40 weeks of age in both genders (Figure 1.F.). Throughout time, the frequency of adrenals with hypertrophic zF clusters increased in a sexually dimorphic fashion: indeed, for these clusters to develop in all adrenals, it took 40 weeks in males and only 24 in females. Thus, in 40-week-old mice, *Senp2*^{cKO} adrenal cortex contained, compared to WT, very few GFP-positive zF cells, with GFP staining

limited to zG and non-recombined cells constituting the entire zF (Figures 1.D. right panel & S1.K.).

Altogether, these results show that SENP2 is necessary for proper adrenal cortex zonation and homeostatic maintenance. Indeed, its inactivation initially leads, to zF atrophy, which is compensated over time by the recruitment of cells escaping *Senp2* recombination allowing them to maintain a wild-type *Senp2* zF in otherwise mutant adrenals. Importantly, we show that females more efficiently overcome zF atrophy induced by *Senp2* loss. This further highlights the sexually dimorphic traits of adrenal homeostasis[25,26].

Loss of SENP2 is associated with isolated glucocorticoid deficiency

Given the profound alterations and notably, the time and sex-dependant remodelling of adrenal cortex zonation in *Senp2*^{cKO}, we measured changes in circulating steroid levels and assessed steroidogenic gene expression. Steroid hormones are synthesised from cholesterol through enzymatic processes resulting in corticosterone production by zF cells and aldosterone by zG cells (Figure 2.A.). Since zF was the most impacted zone by the *Senp2* mutation, we anticipated a reduction in plasmatic corticosterone levels, the main glucocorticoid in rodents. Indeed, compared to control males, corticosterone levels were dramatically reduced in *Senp2*^{cKO} at 4 weeks and remained lower at 8 weeks of age. Interestingly, levels normalised over time to be indistinguishable from controls by 24 weeks (Figure 2.B. top). In contrast, *Senp2* inactivation had no impact on corticosterone concentrations in females, at any time point (Figure 2.B. bottom). The integrity of the zF and the corticosterone production are under the strict control of pituitary ACTH that maintains homeostasis through a negative feedback loop mediated by the glucocorticoids on the hypothalamic-pituitary-adrenals (HPA) axis. Therefore, we measured circulating ACTH in *Senp2*^{cKO} and found a 8- 10-fold increase at 24 weeks in both sexes. This is consistent with a dysfunction of the zF cells, resulting in a subclinical insufficiency over time (Figure 2.C.).

For insights into the mechanisms of this insufficiency, we analysed the expression of steroidogenic genes in adrenals of 4-week-old mice. RT-qPCR analyses showed that mRNA levels of *Star* and *Cyp11a1* encoding rate limiting step proteins in steroidogenesis, were decreased in both male and female *Senp2*^{cKO} adrenals (Figure 2.D.). Interestingly, *Cyp21a1*, *Hsd3b1* and *Cyp11b1* transcripts were specifically downregulated in female *Senp2*^{cKO} adrenals (Figure 2.D). To assess the impact of *Senp2* loss on zG function, we measured mineralocorticoids plasma levels and *Cyp11b2* expression. Consistently with histological observations, we did not find any negative effect of *Senp2* ablation on aldosterone levels, but rather a positive trend with an increase in 18-hydroxy-corticosterone plasmatic concentration in *Senp2*^{cKO} males at 24 weeks and a trend toward upregulation of *Cyp11b2* expression in *Senp2*^{cKO} female adrenals at 4 weeks (Figure S2.A.B.C.).

To go further into details on steroidogenesis, we assessed enrichment of neutral lipids in steroidogenic cells from 40 week-old adrenals. Bodipy staining revealed strong staining in zF cells from WT adrenals and GFP negative cells from *Senp2*^{cKO} adrenals whereas lipid accumulation was lower in GFP positive cells (Figure 2.E.).

In conclusion, these results draw a picture of

the differential role of *Senp2* in the zonation of the adrenal cortex. While it is dispensable for the zG, its absence leads to a deficient zF struggling to produce enough corticosterone to maintain homeostasis. This effort is illustrated by elevated circulating ACTH and hypertrophic zF cells, hallmarks of isolated glucocorticoid deficiency.

Adrenal cortex lacking *Senp2* shows blunted ACTH response

To understand the underpinnings of the adrenal phenotype in $Senp2^{cKO}$ mice, knowing that ACTH is a regulator of SUMOylation in the adrenal cortex[20], we assessed the endocrine and transcriptional steroidogenic responses to acute ACTH stimulation. Plasma concentrations of steroids associated with glucocorticoid metabolism (Figure 2.A.) were determined by LC-MS/MS, in 24-week-old mice injected 2 hours before with ACTH and compared to vehicle (Figure 3.A. & Table 1.). We confirmed that, at this age, there were no differences in plasma levels of all steroids measured in basal conditions (vehicle) between WT and $Senp2^{cKO}$ mice. As expected, ACTH treatment induced a strong increase in adrenal steroids (*e.g.* corticosterone levels were 3- to 7-fold induced in females and males, respectively) in plasma from WT mice (except progesterone in females, which comes mainly from the ovaries). However, the ACTH-stimulated endocrine response was heavily blunted and at least halved in $Senp2^{cKO}$ mice (Table 1.). To determine whether alteration of endocrine response correlated with changes in gene expression, we measured mRNA levels of ACTH-responsive genes involved in initial steps of steroidogenesis (*i.e. Scarb1* and *Star*) by RT-qPCR (Figure 3.B.). In males, *Senp2* mutation did not alter *Scarb1* and *Star* transcriptional responsiveness to ACTH (1.5- to 2-fold induction after 2h) but impaired their basal expression, so that mRNA levels in ACTH-treated mutant adrenals barely reached basal expression in controls. By contrast in females, although their basal expression remained unchanged, both *Scarb1* and *Star* genes entirely failed to respond to ACTH in $Senp2^{cKO}$ adrenals (Figure 3.B.). To test whether this blunted transcriptional response relied on changes in phosphorylation of PKA substrates (Figure S3.A.), we performed western blots on trans-acting factor CREB and SUMO E3 ligase TRIM28, in response to 30 min ACTH treatment, in WT and mutant mice. Ser133 CREB and Ser473 TRIM28 phosphorylation levels were similar in basal conditions, increased in WT upon ACTH stimulation but failed to respond to treatment in $Senp2^{cKO}$ adrenals (Figure 3.C.). This impaired response to ACTH/PKA-mediated phosphorylation was unlikely caused by altered expression of ACTH receptor and co-receptor (*Mc2r* and *Mrap*, respectively) that were unaltered by *Senp2* loss (Figure S3.B.).

To determine whether the deficiency in ACTH response involved PKA holoenzyme or occurred upstream of the kinase, we assessed the capacity of genetic activation of PKA to rescue adrenal insufficiency in $Senp2^{cKO}$ mice by removing the RIα subunit (*Prkar1a* floxed allele) known to repress PKA catalytic activity[7,9,27]. As expected, 4-week-old $Prkar1a^{cKO}$ mice developed large adrenals with hyperplastic zF and atrophic zG (Figure S3.C.D.). Adrenals from $Senp2,Prkar1a^{dcKO}$ and $Senp2^{cKO}$ mice were both dysplastic and showed reduction in cortical cell numbers. However, *dcKO* adrenals showed an atrophic zG (loss of DAB2 staining) presumably resulting from the antagonistic action of PKA signalling on zG identity (Figures 3.D.

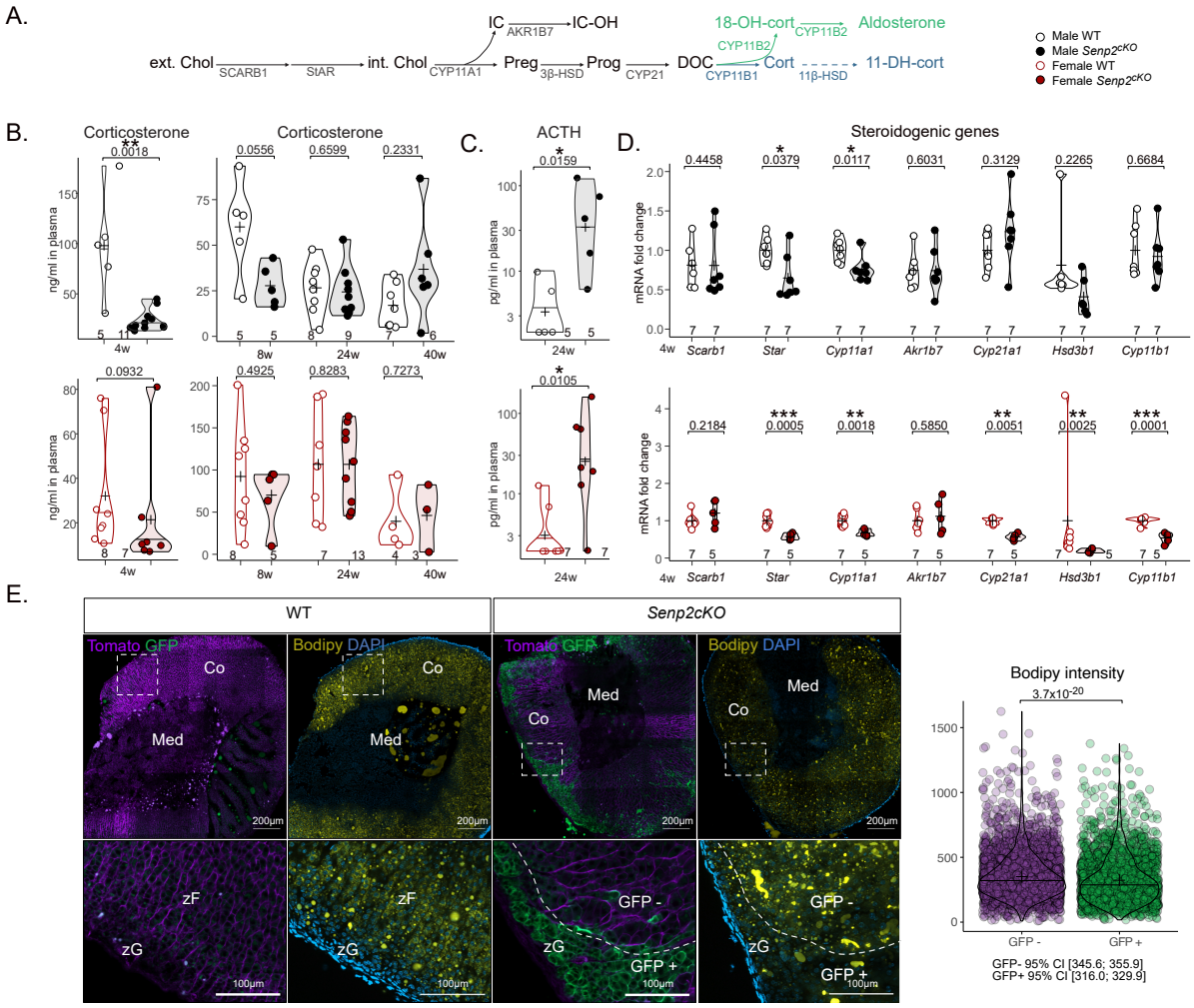

Figure 2: ***Senp2* invalidation induces isolated glucocorticoid insufficiency.**
A. Schematic representation of gluco- (blue) and mineralo- (green) corticoids synthesis : ext.Chol/int.Chol, extra/intracellular cholesterol; Preg, pregnenolone; Prog, progesterone; DOC, 11-deoxy-corticosterone; cort, corticosterone; 18-OH-cort, 18-hydroxycorticosterone; including detoxication of cholesterol side-chain clivage IC (Isocaproaldehyde) into IC-OH (isocapryl alcohol) and inactivation of corticosterone into 11-DH-cort (11-dehydrocorticosterone).
B. Plasmatic concentration of corticosterone in WT and $Senp2^{cKO}$ at 4 (determined by ELISA), 8, 24 and 40 weeks of age (determined by LC-MS/MS).
C. ACTH plasmatic levels of 24-week-old WT and $Senp2^{cKO}$ mice.
D. qPCR analyses of steroidogenic genes mRNA accumulation in 4-week-old WT and $Senp2^{cKO}$ mice.
E. Endogenous expression of GFP (green) and Tomato (purple) with Bodipy staining on WT and $Senp2^{cKO}$ adrenal cortices at 40 weeks of age.

& S3.C.D.)[7,9]. As a result, in the absence of NaCl supplementation, $Senp2,Prkar1a^{dcKO}$ mice died prematurely from salt wasting (Figure S3.E.), whereas $Senp2^{cKO}$ mice only suffered from isolated glucocorticoid deficiency. Thus, genetic derepression of PKA was unable to overcome cortical atrophy and dysplasia imparted by *Senp2* deficiency. This suggested that consequences of *Senp2* loss, including the excess of SUMOylation, had a dominant impact on the zF homeostasis over PKA constitutive activation. Then, we explored endocrine activity of double KO mice. Although

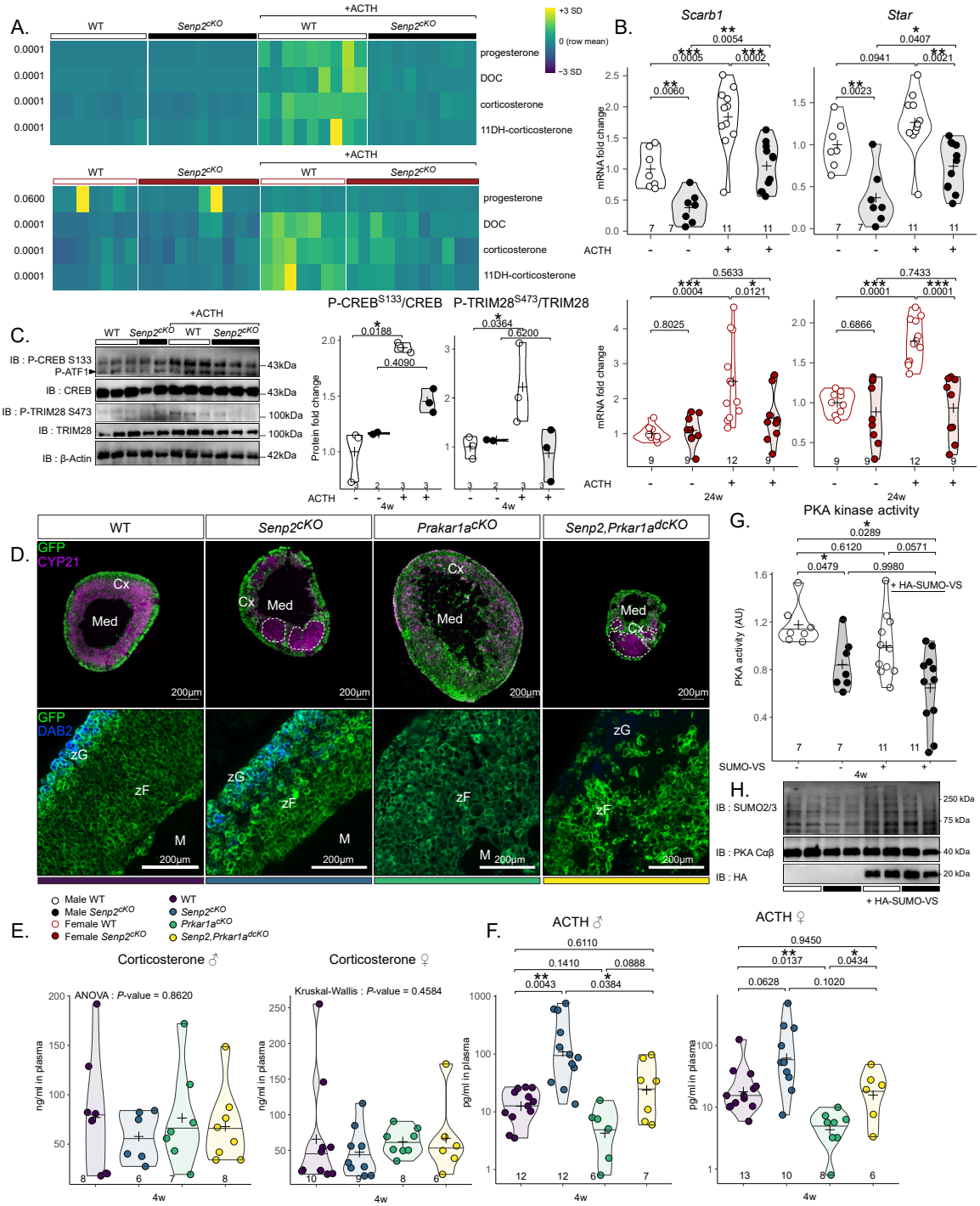

Figure 3: ***Senp2* is necessary for proper ACTH response**.
A. Heatmap representing the plasmatic concentration of progesterone, DOC, corticosterone and 11-dehydrocorticosterone after treatment with PBS or ACTH for 2 h determined by LC-MS/MS in WT or *Senp2*^{cKO} 24-week-old mice.
B. qPCR analysis of ACTH responsive genes mRNA accumulation in 24-week-old WT and *Senp2*^{cKO} mice after treatment with PBS or ACTH for 2 h.
C. Western blot analysis of phosphorylated CREB (Ser133) and TRIM28 (Ser473) in 4-week-old mice treated with PBS or ACTH for 30 minutes. Graphs represent phosphorylated form over total form
D. Coimmunofluorescent labelling of GFP (green) with CYP21 (purple) or DAB2 (blue) on WT, *Senp2*^{cKO}, *Prkar1a*^{cKO} or double knock-out adrenals.
E. Plasmatic concentration of corticosterone in 4-week-old WT, *Senp2*^{cKO}, *Prkar1a*^{cKO} or double knock-out male and female mice
F. Plasmatic concentration of ACTH in 4-week-old WT, *Senp2*^{cKO}, *Prkar1a*^{cKO} or double knock-out male and female mice
G. PKA kinase activity measurements in WT and *Senp2*^{cKO} 4-week-old adrenals in presence or absence of 5µM SUMO vinyl sufone
H. Western blot analysis of global SUMOylation and PKA catalytic subunits protein accumulation 4-week-old adrenals from WT and *Senp2*^{cKO} mice

			ACTH	
	Mean concentration +/- SD (*P*-value compared to vehicle counterpart)			
Male	WT	*Senp2* cKO	WT	*Senp2* cKO
Progesterone	0.15 +/- 0.09	0.30 +/- 0.39	9.23 +/- 4.03 (**0.0001**)	1.70 +/- 0.88 (**0.0457**)
DOC	0.31 +/- 0.29	0.43 +/- 0.17	24.02 +/- 18.9 (**0.0001**)	5.26 +/- 3.53 (**0.0401**)
Corticosterone	26.6 +/- 13.89	24.39 +/- 13.36	202.3 +/- 40.96 (**0.0001**)	75.53 +/- 22.10 (**0.0267**)
11-DH-cort	0.13 +/- 0.11	0.12 +/- 0.06	0.89 +/- 0.68 (**0.0004**)	0.18 +/- 0.06 (0.3815)

			ACTH	
	Mean concentration +/- SD (*P*-value compared to vehicle counterpart)			
Female	WT	*Senp2* cKO	WT	*Senp2* cKO
Progesterone	7.31 +/- 15.52	5.56 +/- 11.57	3.55 +/- 1.62 (0.9999)	2.60 +/- 1.08 (0.2182)
DOC	4.91 +/- 4.20	9.65 +/- 11.53	55.75 +/- 14.29 (**0.0001**)	28.02 +/- 13.62 (0.0896)
Corticosterone	106.70 +/- 65.69	112.80 +/- 47.87	334.20 +/- 67.24 (**0.0001**)	200.00 +/- 81.52 (**0.0113**)
11-DH-cort	0.49 +/- 0.33	0.45 +/- 0.18	2.30 +/- 1.01 (**0.0001**)	0.85 +/- 0.36 (0.1544)

Kruskal-Wallis with multiple comparisons using Dunn's test to determine the genotype or treatment effect

Table 1: **Mean steroids plasmatic concentrations after 2 hours ACTH treatment**

plasma corticosterone dosage showed no differences among the four genotypes, plasma ACTH concentrations were elevated in $Senp2^{cKO}$ and reduced in $Prkar1a^{cKO}$, consistent with the corresponding associated disorders *i.e.* glucocorticoid deficiency and ACTH-independent glucocorticoid excess, respectively (Figure 3.E.F.). By contrast, *Senp2-Prkar1a* double ablation restored ACTH levels to control values. This strongly suggested that the lack of *Senp2* resulted, among other things, in the repression of PKA catalytic activity that the deletion of RIα regulatory subunits could partially overcome. Indeed, PKA kinase activity was decreased by 30% in $Senp2^{cKO}$ adrenal extracts compared to WT without affecting Cαβ protein levels (Figure 3.G.H.). To test a possible direct repressive effect of SUMOylation, we measured kinase activity in the presence of a mix of SUMO1/2 modified with vinyl sulfone (SUMOs-VS) acting as specific trap and potent inhibitors of SENPs SUMO proteases present in the extracts[28]. Under these conditions enhancing SUMOylation in adrenal extracts, PKA kinase activity was further decreased in $Senp2^{cKO}$, reaching a 50% inhibition (Figure 3.G.H.). Together, these results present SENP2 as a mandatory actor of proper ACTH response acting most likely by limiting repressive action of SUMOylation on the catalytic activity of the PKA holoenzyme.

Senp2 is necessary for the acquisition of zF identity

Based on the blunted response to ACTH, we decided to assess the differentiation status of the zF in $Senp2^{cKO}$ mice. We took

advantage of cortical cells' capacity to escape recombination to compare the intensity of differentiation markers in neighbouring cells, differing only by their recombination status. We performed triple staining for GFP, used as a proxy of *Senp2* recombination, with DAB2 and AKR1B7 labelling zG and zF, respectively. We observed a consistent lower AKR1B7 staining intensity in GFP-positive cells, indicating that loss of *Senp2* hinders cells from expressing zF markers compared to neighbouring GFP-negative cells (Figures 4.A.B. & S4.A.). RT-qPCR analysis revealed an increased accumulation of progenitors' markers and higher number of NR2F2-positive capsular cells in males (Figure S4.B.C.) implying a default in cortical cell turnover which, together with the downregulated AKR1B7 expression, suggests a block in centripetal differentiation. This hypothesis was further supported by an increased proportion of cells coexpressing DAB2 and AKR1B7 in the cortex of $Senp2^{cKO}$, suggesting altered zG to zF transdifferentiation (Figure 4.C.). To examine this hypothesis, we performed functional lineage tracing analysis of *Senp2*-deficient cells using mTmG reporter mice and AS^{Cre} driver[2], which allowed to delete *Senp2* in zG cells after birth ($AS^{Cre}/+::Senp2^{fl/fl}::R26R^{mTmG/mTmG}$). This Cre driver enabled to assess cortex cellular turnover through the percentage of GFP-stained cells progressing centripetally. As previously shown[7,29], complete cortical cell took around 12 weeks in female and 40 weeks in male WT mice (Figure 4.D.). Interestingly, whereas GFP immunostaining marked the first third of the cortex (zG and upper zF) in 4 weeks WT females, GFP staining was confined to the zG and some rare stripes projecting into the zF in $AS^{Cre}/+$ $Senp2^{cKO}$ littermates (Figure 4.E.).

To accelerate lineage tracing, we mated Cre homozygosity, and thus deleted the Aldosterone Synthase gene ($AS^{Cre/Cre}::Senp2^{fl/fl}::R26R^{mTmG/mTmG}$). Consistent with previous reports[2], this enhanced trophic drive through renin-angiotensin signalling, and increased recombination rate, leading to almost full recombination cortex by 4 weeks of age in $AS^{Cre/Cre}$ *Senp2* heterozygous female adrenal. In sharp contrast, GFP staining was almost confined to the zG in $AS^{Cre/Cre}$ $Senp2^{cKO}$ even though the zG was slightly expanded because of trophic stimulation by angiotensin (Figure 4.E.). A similar phenotype was observed in $AS^{Cre/+}$ $Senp2^{cKO}$ at 40 weeks of age with a recombined zF consisting of scattered stripes of GFP-positive cells (Figure 4.E.). We next quantified AKR1B7 protein accumulation in zF cells of $AS^{Cre/+}$ $Senp2^{cKO}$ of 24 weeks of age and again observed lower AKR1B7 staining in GFP-positive than in GFP-negative cells (GFP- 95% CI [6887;7164] AU, GFP+95% CI [5427;5582] AU, P-value = 10^{-16}) (Figure 4.F.G.). In contrast with *Sf1-Cre* mediated inactivation of *Senp2*, AS^{Cre} mediated deletion did not alter adrenal weight at 24 weeks of age (Figure 4.H.). However, when ACTH responsiveness was assessed over time, plasma corticosterone peaked 2 hours after ACTH treatment in WT, whereas the response was slower in $AS^{Cre/+}$ $Senp2^{cKO}$ and never reached statistical threshold (Figure 4.I.). This shows that even in the absence of adrenal hypoplasia, *Senp2* ablation results in a block of zF transdifferentiation from zG cells. This causes incomplete zF differentiation in recombined cells and allows competitive selection of non-recombined cells, which cannot completely overcome the endocrine phenotype.

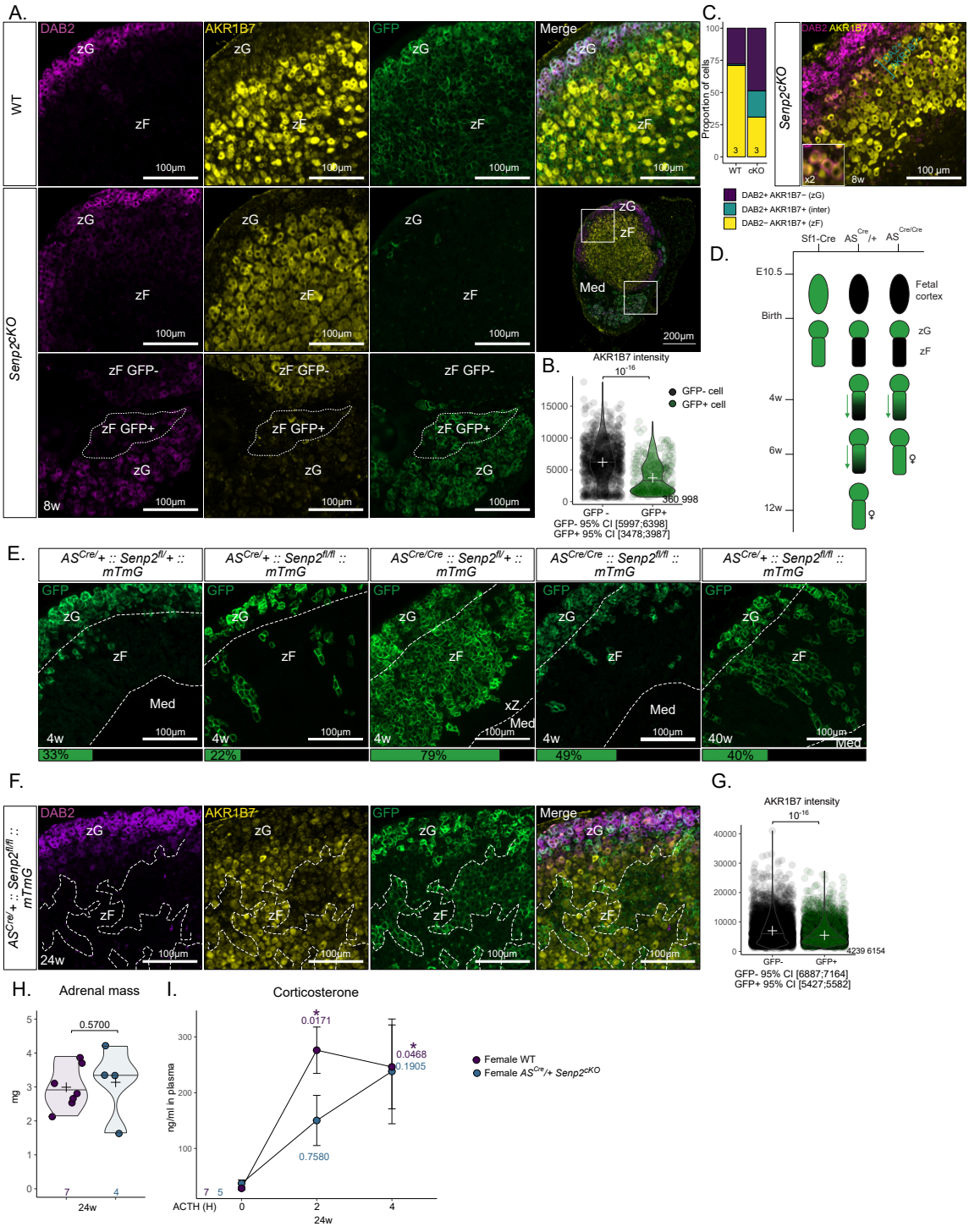

Figure 4: ***Senp2* ablation prevents proper zF differentiation**

A. Coimmunofluorescence labelling of AKR1B7 (yellow), GFP (green) and Disabled2/DAB2 (purple) on 8-week-old WT and $Senp2^{cKO}$ male adrenals

B. Quantification of AKR1B7 intensity in GFP+ and GFP- $Senp2^{cKO}$ male adrenal cells

C. Quantification and representative image of cells expressing DAB2 (purple), AKR1B7 (yellow) or both (blue) in WT and $Senp2^{cKO}$ 8-week-old adrenals

D. Scheme representing the differences in recombination kinetics between cre drivers used in genetic models

E. Immunofluorescence labelling with mean percentage of GFP-positive cells in 4w and 40w cortex

F. Coimmunofluorescence labelling of AKR1B7 (yellow), GFP (green) and Disabled2/DAB2 (purple) on female 24-week-old $AS^{Cre}/+$ $Senp2^{cKO}$ adrenals

G. Quantification of AKR1B7 intensity in GFP+ and GFP- 24-week-old $AS^{Cre}/+$ $Senp2^{cKO}$ adrenal cells

H. Mean adrenal mass of 24-week-old female $AS^{Cre}/+$ *Senp2* and WT

I. Kinetics of ACTH response of 24-week-old female $AS^{Cre}/+$ *Senp2* and WT. *P*-values represent difference between samples from the same mice before treatment compared to after 2 hours or after 4 hours of treatment.

Senp2 deficient cells undergo apoptosis associated with DRP1 phosphorylation

We next examined the cellular mechanisms underlying the development of zF atrophy in $Senp2^{cKO}$ mice, by analysing the proliferation/apoptosis balance. The cortical proliferation index determined by scoring the number of Ki67- or BrdU-positive cells ruled out the contribution of a decreased proliferation rate to the hypoplastic phenotype, but rather showed a trend toward increased cell division in mutant adrenals (Figure S5.A.B.). Nonetheless, cleaved caspase-3 staining showed that the numbers of cells undergoing apoptosis was dramatically increased in $Senp2^{cKO}$ adrenals at 4 and 8 weeks of age in both sexes (Figure 5.A.). Whereas, according to the standard model, apoptosis is normally found at the corticomedullary junction (where adrenal cells die after centripetal migration[30]), in the $Senp2^{cKO}$ cortex, apoptosis occurred prematurely at the border between the zG and zF (Figure 5.A.).

DRP1 (Dynamin Related Protein 1) is considered the primary driver of mitochondrial fission and mitochondrial-dependant cell death[31,32]. Phosphorylation of DRP1 on Ser616 activates mitochondrial fission while that on Ser637 prevents the fission. The dysregulation of DRP1 phosphorylations on these two residues will result in imbalanced mitochondrial fission/fusion, a major cause of apoptotic cell death. Phosphorylation on Ser637 particularly raised our attention since it is catalysed by PKA[33]. Besides its participation to inhibition of mitochondrial fission, studies have shown that phosphorylated DRP1-Ser637 promotes steroidogenesis in Leydig cells[34] and *corpus luteum*[35]. To assess the impact of ACTH/PKA on DRP1 activity in adrenal glands, we performed western blotting of DRP1 and its Ser637 phosphorylated form in WT or $Senp2^{cKO}$ adrenal treated with vehicle or ACTH for 30 min. We found no difference in total or phosphorylated DRP1 in vehicle treated mice. In constrast, ACTH treatment induced DRP1 Ser637 phosphorylation solely in WT mice whereas this response was abolished in $Senp2^{cKO}$ adrenals (Figure 5.B.).

We then took an *in vitro* approach to determine whether PKA-induced changes in DRP1 phosphorylation were involved in the apoptotic response of adrenocortical cells. The *fasciculata*-like ATC7 cells[36] were treated with forskolin (FSK), a pharmacological activator of PKA (through increased cAMP cellular levels), one hour before a 2 hours-incubation with the proapoptotic drug staurosporine (STS). As expected, FSK alone resulted in increased Ser637 phosphorylation of DRP1, while STS alone induced caspase-3 cleavage. When combined, FSK limited STS-driven apoptosis, as depicted by the reduced accumulation of cleaved caspase-3 (Figure 5.C.). Of note, Ser616 proapoptotic phosphorylation of DRP1 showed a trend to be regulated in the exact opposite way to Ser637 (Figure 5.C.). To specifically assess the contribution of DRP1 in STS-induced apoptosis, we pretreated cells with the DRP1 specific inhibitor (Mdivi-1) before inducing apoptosis with STS[37]. Similar to FSK, pretreatment with Mdivi-1 resulted in protection against apoptosis as shown by reduced accumulation of cleaved caspase-3 (Figure S5.C.). Consistently *in vivo*, we observed an inverse correlation (τ = -0.3823, P-value = 0.0341) between cortical apoptosis rate and DRP1 Ser637 phosphorylation in *Senp2*, *Prkar1a* single and double knock-outs (Figure 5.D.E.F S5.D). Altogether, these results strongly suggest that increased

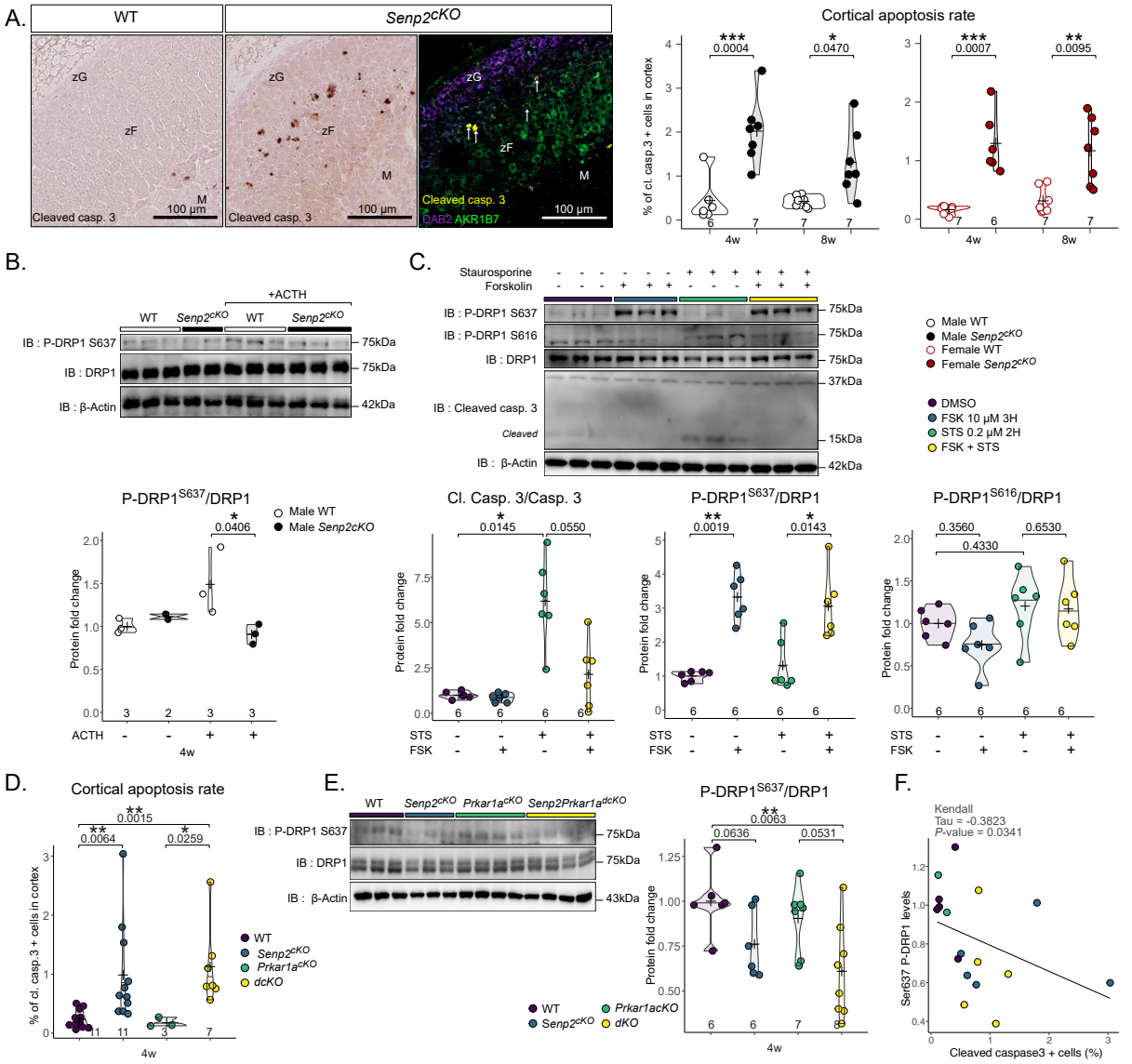

Figure 5: ***Senp2* loss triggers apoptosis at the zG-zF boundary**
A. Representative image of cleaved caspase-3 immunostaining and immunofluorescence labelling of cleaved caspase-3 (yellow), zG marker Disabled2/DAB2 (purple) and zF marker AKR1B7 (green). Quantification of apoptosis in WT and cKO through measurement of the percentage of cells positive for cleaved caspase3 at 4 and 8 weeks of age
B. Western blot analysis of S637 phosphorylated and total DRP1 in adrenal after 30 minutes ACTH I.P. treatment of WT and $Senp2^{cKO}$ male mice
C. Western blot analysis of phosphorylated and total DRP1 in cells treated with DMSO, Forskolin (10 µM) and/or Staurosporine (0.2 µM).
D. Quantification of cleaved caspase-3 positive cells in the cortex (E) of WT, $Senp2^{cKO}$, $Prkar1a^{cKO}$ and double knock-out male adrenals
E. Western blot analysis of S637 phosphorylated and total DRP1 in the cortex (E) of WT, $Senp2^{cKO}$, $Prkar1a^{cKO}$ and double knock-out males adrenals
F. Correlation plot between Ser637 DRP1 phosphorylation and proportion of cleaved caspase-3 positive cells in the adrenal cortex across genotypes

apoptosis seen at the zG-zF boundary in $Senp2^{cKO}$ adrenals results from a deficient ability of ACTH/PKA signalling to properly phosphorylate DRP1 Ser637.

Senp2 deficiency leads to β-catenin hyperSUMOylation and mild activation of WNT pathway

To unravel new SUMOylation-sensitive pathways that could explain further the

adrenal insufficiency of mice lacking SUMO protease SENP2, we performed bulk RNA sequencing on four-week-old male and female WT and *Senp2*^{cKO}. We found 1337 genes to be differentially expressed in male (1115 up and 222 down) and 1235 in female (960 up and 275 down) (Figure 6.A.B.). Unsupervised clustering and principal component analysis discriminated samples based on genotype but not on sex (Figure S6.A.B.), implying that at 4 weeks of age, sex has a low impact on gene transcription. Since most of the genes were co-regulated in males and females, we chose to focus on these subsets of genes. We performed Gene Ontology (GO) functional enrichment analysis on upregulated or downregulated genes in *Senp2*^{cKO} adrenals of both sexes (Figure 6.C.). The top GO terms associated with the upregulated genes were linked to neuron cells and function, which may be due to over representation of medullar chromaffin cells resulting from cortical hypoplasia. Pathways related to steroid processing were enriched in downregulated genes, consistent with the endocrine deficiency phenotype of *Senp2*^{cKO} mice.

We performed Get Set Enrichment Analysis (GSEA) on the Kyoto Encyclopedia of Genes and Genomes (KEGG) database and selected only the enriched pathways that were present in both males and females (Figure 6.D.). This confirmed negative enrichment of the gene signature for steroid hormone biosynthesis pathway, in accordance with GO analysis and hormonal insufficiency characterised in *Senp2*^{cKO} mice (Figure 2.). Moreover, we found negative enrichment of signatures associated with nucleotide excision repair, aminoacyl tRNA biosynthesis, ribosome, pyrimidine metabolism and spliceosome, indicating that *Senp2* loss in the adrenal cortex altered basic cellular processes known to be regulated by SUMOylation[12]. Interestingly, among the positively enriched pathways, WNT signalling caught our attention as it is mandatory for adrenocortical maintenance and proper zonation[38–40] (Figure 6.D.E.)

Based on RNA-Seq analyses and given that SENP2 has first been described as a negative regulator of β-catenin[41–43], we sought out to see if the WNT/β-catenin pathway was altered in *Senp2*^{cKO} adrenals. We evaluated the activation of the pathway by running RT-qPCR on its target genes. At 24 weeks of age, we observed a consistent ~1.5 fold induction of *Axin2*, *Lef1*, *Apcdd1* and *Ccdc80* in the adrenals of *Senp2*^{cKO} females, whereas in mutant males, only *Ccdc80* was upregulated by about 3 fold (Figure 7.A.). To gain more insight into the modulation of the WNT signalling pathway, we extracted expression levels of 48 WNT target genes from RNA-seq data (Figure 7.B.). Among these genes, 31 were upregulated mainly in males *Senp2*^{cKO} and 7 mainly in females while 10 genes were downregulated in both sexes.

We next carried out immunostaining on adrenal sections that revealed a nuclear localisation of non-phospho (active) β-catenin specifically in the inner cortex of mutant adrenals regardless of sex (Figure 7.C. top). Co-staining of total β-catenin with zF marker AKR1B7 confirmed zF identity of these cells, which were also GFP-positive and hence, had been targeted by Cre recombination (Figure 7.C. bottom).

Given that β-catenin can be SUMOylated by both SUMO1[44] and SUMO2/3[45], we hypothesised that it was SUMOylated in the adrenal cortex. We performed immunoprecipitation of both SUMO1 or SUMO2/3 and blotted β-catenin. We observed a doublet between 120 and 150 kDa for SUMO2/3 consistent with a previous

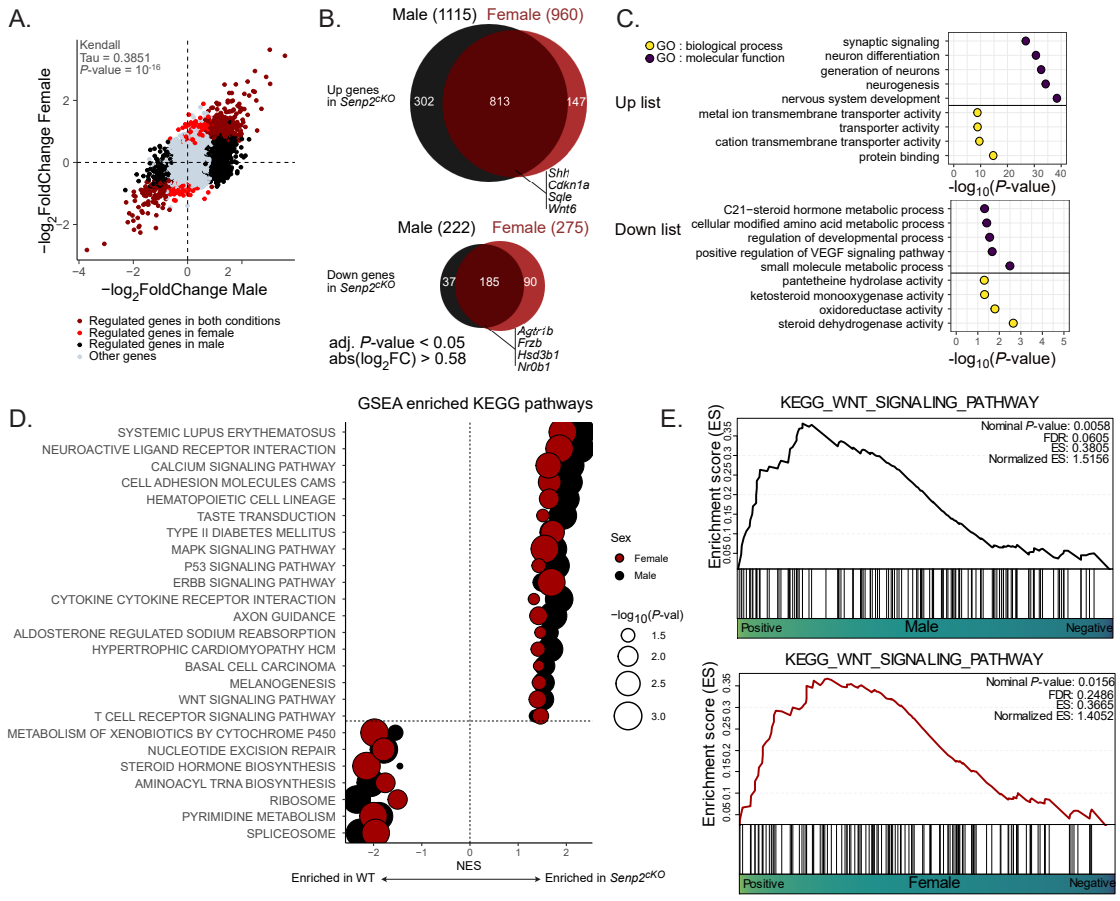

Figure 6: **RNA-seq analysis of male and female *Senp2*^{cKO} adrenals**
A. Scatter plot showing the correlation between dysregulated genes (adjusted P-value < 0.05 and absolute $\log_2$ fold change > 0.58) in male and female *Senp2*^{cKO} adrenals at 4 weeks of age
B. Euler diagrams illustrating the commonly up or downregulated genes in both sexes *Senp2*^{cKO} adrenals at 4 weeks of age
C. Top GO terms from Gene Ontology functional enrichment analysis based on the up or downregulated genes lists
D. Gene set enrichment analysis (GSEA) pathways from the KEGG database that are commonly affected in male and female *Senp2*^{cKO} adrenals
E. Gene set enrichment analysis (GSEA) plots of WNT pathway on male and female WT versus *Senp2*^{cKO} adrenals

report[45] but no evidence for significant SUMO1 conjugation (Figure 7.D.). To evaluate if β-catenin SUMO2/3-ylation was affected upon *Senp2* deletion, we immunoprecipitated β-catenin and blotted SUMO2/3. Although we did not see any difference in the amount of SUMOylated β-catenin, the accumulation of its native form was reduced in mutant adrenals whereas global SUMOylation by SUMO2/3 was unchanged (Figure 7.E.). Reciprocally, by immunoprecipitating SUMO2/3 and blotting β-catenin, we observed a slight but reproducible accumulation of SUMOylated β-catenin compared to native form (Figure 7.F.). To confirm this increase in β-catenin SUMO2/3-ylation, we used Proximity Ligation Assay (PLA) which enables to visualise *in situ* the close proximity of two proteins (Figure 7.G.). As a negative control, we first ran PLA between β-catenin and GATA6, a transcription factor present in the nucleus of all adrenocortical cells and which is not known to interact with β-catenin. As expected, there were no *foci* of β-catenin/GATA6 interaction in adrenal

sections of all genotypes. In contrast, PLA between β-catenin and SUMO2/3 showed specific *foci* in the zG with similar density in both genotypes. However, in the zF of *Senp2*^{cKO}, there was an increase in cells containing 2 or more β-catenin/SUMO2/3 dots per nucleus (Figure 7.G.).

In conclusion, loss of SENP2 leads to ectopic nuclear accumulation of β-catenin in the zF associated with its increased conjugation to SUMO2/3. This accumulation is correlated with a mild activation of WNT pathway targeting genes in a partially sexually dimorphic pattern.

Discussion

We have previously established that the overall SUMOylation of proteins in the adrenal cortex displays two remarkable properties: it gradually decreases as the centripetal transdifferentiation of zG cells into zF cells progresses and it is acutely downregulated by stress through ACTH/PKA signalling[20]. The present study was initiated to address the hypothesis that this posttranslational mechanism involved in the cellular response to various environmental stressors[46] may be an integral part of the adrenal gland's toolbox to produce steroid hormones critical for body homeostasis and stress adaptation. Adrenal-specific KO mouse models of SENP2 deSUMOylase and of PKA regulators established that this is indeed the case. Foetal or postnatal SENP2 dependent deSUMOylation is necessary for initial zF differentiation, its maintenance throughout life and for ACTH/PKA-stimulated glucocorticoid production. As a result, foetal or postnatal deletion of *Senp2* in adrenal steroidogenic cells causes postnatal hypoplasia limited to the zF or incomplete zF formation respectively, which can lead to isolated glucocorticoid deficiency. This selective atrophy and associated endocrine deficit result both from a blockage of zonal transdifferentiation preventing the switch from zG to zF identity, and from a repression of ACTH/PKA responsiveness. Interestingly, overt corticosterone deficiency is only measurable in males at 4 weeks of age, even though ACTH levels are higher at all ages tested in both genders. This implies that a subclinical deficiency is permanently established in the mutants, despite setting up compensation. This compensation to maintain physiological plasma glucocorticoid levels, which occurs in both sexes but with delay in males, most likely relies on the emergence of a population of cells that has escaped recombination and helps the mutant cortex to overcome zF atrophy. Indeed, their hypertrophy indicates that they are overreacting to the high levels of circulating ACTH, to compensate for the lack of corticosterone due to the dramatic atrophy of the *Senp2*-deficient zF cell population.

We hypothesise that steroidogenic progenitor cells, which do not express the Cre recombinase for a still unknown reason, must gain a selective advantage over *Senp2*-deficient cells, either by being able to proliferate more or by being less prone to death upon differentiation. Similar observations have been made in adrenals following SF-1 loss driven by *AS*^{Cre2} or *Cyp11a1-Cre*[47], where a majority of cells escaped recombination. How cells manage to express a protein but not the Cre while both genes depend on the same promoter is still unknown. One possibility could be methylation of the promoter. For instance, *Ins1-Cre* transgene is shown to be a poor quality driver to target β cells in the pancreas as its expression is silenced by *de novo* methylation even though *Ins1* gene is normally expressed[48]. In any

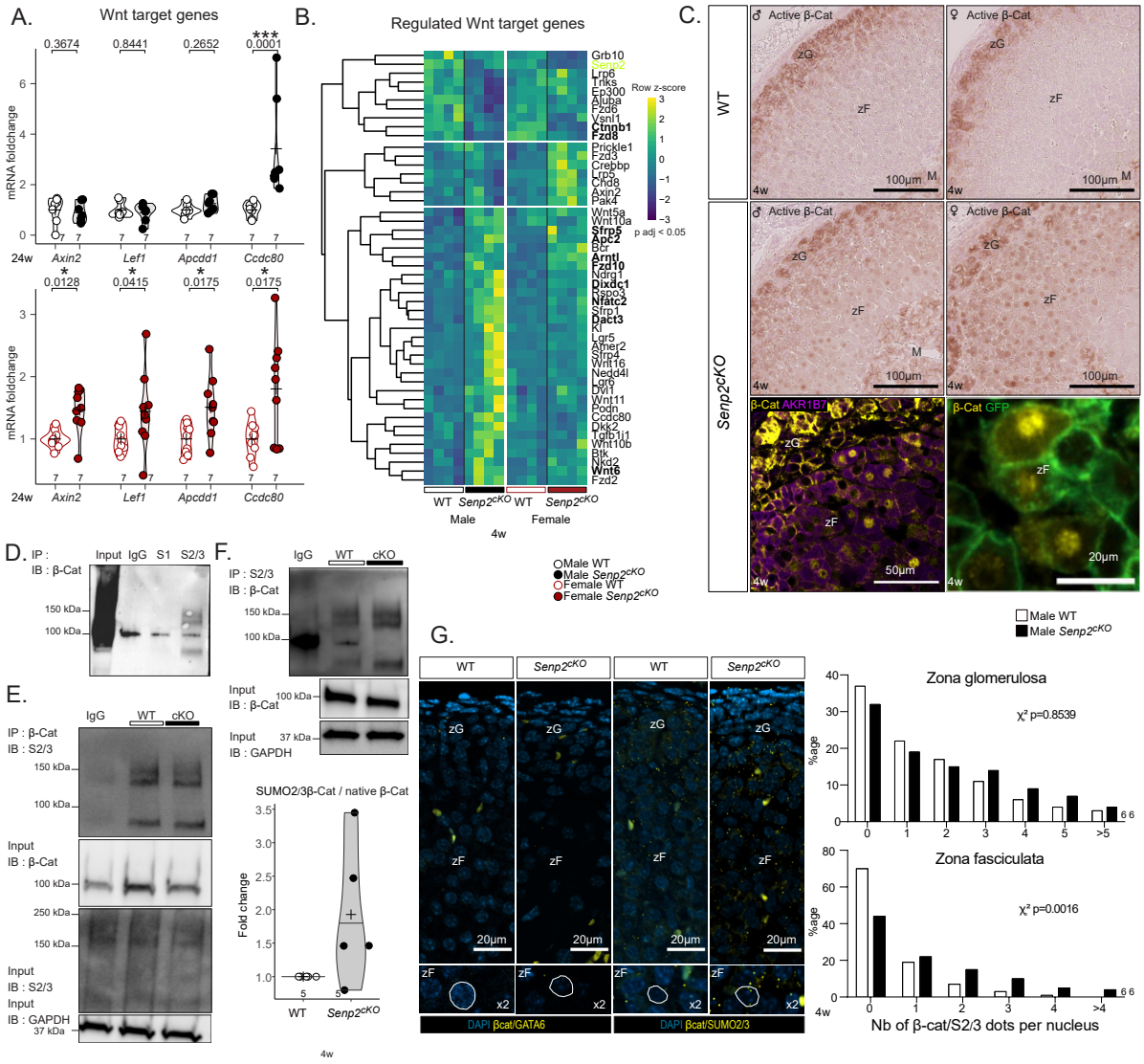

Figure 7: ***Senp2* loss promotes β-catenin SUMOylation and activates the WNT signalling pathway**
A. qPCR analysis of β-catenin target genes *Axin2*, *Lef1*, *Apcdd1* and *Ccdc80* mRNA accumulation in 24-week-old WT and $Senp2^{cKO}$ mice.
B. Heatmap of dysregulated WNT target genes in $Senp2^{cKO}$ male or female adrenals RNA-seq (adjusted P-value < 0.05). Commonly dysregulated genes in males and females are represented in bold characters.
C. Top : Immunohistochemistry analysis of active (non-phospho) β-catenin on WT and $Senp2^{cKO}$ male (left) and female (right) adrenals.
Bottom : immunofluorescence staining of β-catenin (yellow) with zF marker AKR1B7 (purple) and GFP (green).
D. Immunoprecipitation assay depicting the interaction between β-catenin and SUMO1 or SUMO2/3 in WT adrenals.
E. & F. Immunoprecipitation assay depicting the interaction between β-catenin and SUMO2/3 in adrenals of 4-week-old WT and $Senp2^{cKO}$ male mice. Extracts were immunoprecipated with β-catenin (D) or SUMO2/3 antibodies (E). SUMOylated β-catenin was quantified relative to its native form.
G. Proximity ligation assay (PLA) of β-catenin and GATA6 (negative control) or β-catenin and SUMO2/3 in nuclei of 4-week-old WT and $Senp2^{cKO}$ male mice's adrenals. Histograms represent proportion of cells in each zone containing the specified number of dots per nucleus of WT and $Senp2^{cKO}$ male adrenals. n = 6 per genotype
Ca, capsule; zG, *zona glomerulosa*; zF, *zona fasciculata*.

case, the triggering of a compensatory mechanism underlines the absolute necessity

of maintaining *Senp2* expression (and thus the possibility of reducing SUMOylation), in order to build a functional *zona Fasciculata* to maintain the individual's ability to adapt to stress.

The fact that *Senp2*-deficiency preferentially affects the zF while being expressed in all cortical areas[49] can be explained by two non-mutually exclusive mechanisms. First, the zG already harbours high levels of nuclear SUMOylation compared to the zF[20], therefore the expected increase in SUMOylation conjugates consecutive to lowered deconjugase pools will preferentially affect hypoSUMOylated regions. Moreover, we showed that SENP2 loss alters the PKA/WNT balance toward WNT signalling. The latter being already highly active in the zG[4,6,38], it is not surprising to find an altered phenotype only in the zF where WNT/β-catenin signalling is naturally repressed[9]. The second reason is that low SUMOylation seems to be a prerequisite for adequate PKA signalling. Indeed, in our model, ACTH response is blunted and the zF atrophy phenotype is reminiscent, at least partially, of mouse models lacking ACTH receptor and its co-receptor *i.e.* *Mc2r*$^{-/-}$ or *Mrap*$^{-/-}$ whole-body knock-outs[50,51]. Although various mechanisms could be simultaneously affected and remain to be explored, there are converging pieces of evidence that SENP2 deletion-dependant SUMOylation alters PKA responsiveness. Indeed, first, our data show that SENP2 deletion decreases overall PKA activity in the adrenal glands and prevents the phosphorylation of specific targets (CREB$^{\text{Ser133}}$, DRP1$^{\text{Ser637}}$, TRIM28$^{\text{Ser473}}$). Secondly, since *Senp2*^{cKO} phenotype is not rescued by concomitant deletion of PKA regulatory subunit (*Prkar1a*), it is very likely that SENP2 loss directly affects the PKA catalytic subunits function. This is in line with 1) the presence of conserved K169 lysine in the major subunits (PRKACA and PRKACB) amino acid sequence, predicted as a SUMO consensus motif (ψKxD/E where ψ is a hydrophobic residue) and 2) the decreased PKA activity caused by SUMO vinyl sulfone derivatives (figure 3.G.H.). Further studies will assess the SUMOylation of the catalytic subunits and their potential in fine-tuning PKA kinase activity.

SENP2 has first been described as a negative regulator of β-catenin stability[43] but this effect was independent of SUMOylation. Our model showed increased β-catenin SUMO2/3ylation along with ectopic nuclear β-catenin localisation associated with a gene signature indicative of the canonical WNT signalling. Similar observations have been reported following direct SUMOy2/3lation of β-catenin in mammary epithelial cells[45] or SUMOylation of TBL1/TBLR1 that in turn increased chromatin recruitment of β-catenin and its oncogenic activity in colon cancer[52]. However, the picture is not as clear since β-catenin SUMO2/3ylation can trigger its degradation in vascular smooth muscle cells[53] or prevent it in mammary epithelial cells[45]. Targeting gain-of-function mutation of β-catenin in aldosterone-synthase expressing cells caused hyperplasia by blocking *glomerulosa* cells transdifferentiation into *fasciculata* cells[3]. However, in contrast to *Senp2*^{cKO} mice, zF cells never became atrophic in β-catenin gain-of-function. It was thus proposed that when physiological transdifferentiation is unachievable, the zF can be maintained by an alternative cellular pathway involving progenitor cells that bypass the zG state[2]. Here, we report the first occurrence of β-catenin SUMOylation associated with its nuclear translocation which takes place ectopically in *Senp2*-deficient zF. This leads to moderate WNT

target genes activation and together with blunted PKA activity, impairs acquisition of *fasciculata* identity. In this context where zG-to-zF zonal transdifferentiation is impaired, the deficit in PKA signalling alters the phosphorylation profile of the major mitochondrial fission GTPase, DRP1, leading to premature apoptosis of the neoformed mutant *fasciculata* cells, reinforcing the atrophy of the zone over time. The block in zonal transdifferentiation induced by zG-targeted stabilised β-catenin has been ascribed to increased rosette formation (the basal cellular organisation of zG cells forming flower-like structures) and/or impaired rosette resolution (the moment when zG cells exit the rosette to form a single column of cells typical of zF)[54]. Conversely, adrenal cortex lacking *Senp2* do not exhibit zG hyperplasia and thus should not display enhanced rosette formation. Our data indicate that mechanisms by which zG undergoes resolution during normal homeostatic turnover could be controlled by SUMOylation. Identifying what targets of *Senp2*-dependent SUMOylation directly contribute to zG resolution and whether this is coupled to zF transdifferentiation will require extensive studies.

SUMOylation has already proven a role in adrenocortical development with the unSUMOylatable *SF-1*$^{2KR/2KR}$ model, which results in adrenal cells expressing gonadal markers[21]. In ovaries which share a common foetal origin with adrenals, SUMOylation by the E3 SUMO ligase activity of TRIM28, is essential for maintenance of granulosa cell fate at the expense of Sertoli-like identity[55], whereas SENP1 presence in stromal cells is necessary for proper oocyte maturation and ovulation[56]. From a broader perspective, our study belongs to a growing corpus of evidence associating SUMOylation with coordination of differentiation in different tissues and cell types such as white and brown adipose tissue[15,17,57], induced pluripotent stem cells[16], or intestine[18]. Seemingly counter-intuitively, the induction of the adrenal phenotype of *Senp2*^{cKO} mice does not rely on an overall increase in SUMO conjugates levels but rather on specific overSUMOylation of certain cell populations (Figure S1.I.J.) or substrates belonging to signalling pathways crucial for adrenal homeostasis. These findings are consistent with recent studies exploring the consequences of increased SUMOylation in the uterine stroma (by *Senp1* deletion) or decreased SUMOylation (by *Ubc9* haploinsufficiency) in the intestine of *Apc* mutant mice that showed strong phenotypes in the absence of global changes in visible SUMO conjugate levels[58,59]. This illustrates the great versatility of this posttranslational modification pathway. Changes in SUMOylation capacity can have specific effects *in vivo*, especially when targeted steps are catalysed by various members of the same enzymatic family, such as E3 SUMO-ligases or SUMO-specific proteases, which can therefore differ in their substrate specificity. With this in mind, we speculate that specific over-SUMOylated substrates produced in *Senp2*-deficient adrenals should result from the primary loss of the SUMO-protease. Their SUMOylation could be reinforced by the unrepressed (hypo-phosphorylated) E3 SUMO-ligase activity of TRIM28[60,61], secondary to the blunted ACTH/PKA signalling.

Overall, the present paper demonstrates that preventing deSUMOylation by adrenocortical specific SENP2 ablation induces zF hypoplasia associated with increased premature apoptosis along the lineage conversion zG-zF process, ultimately resulting in a blockage of the physiological differentiation process, translating to isolated glucocorticoid deficiency. This

is linked to dysregulation of WNT/PKA balance in favour of WNT signalling. This shift highlights the central role of SUMOylation in physiological processes such as differentiation, tissue maintenance, and stress response. Furthermore, our data could broaden the scope of expected impacts of SUMOylation alterations to endocrine pathogenesis. Although pathogenic associations have been made with alterations in SUMO enzymes or substrates, direct causal links to pathologies have very rarely been established[13,62]. Our work suggests that genetic alterations leading to excessive SUMOylation could be associated with isolated glucocorticoid deficiency in patients.

Methods

Cell culture

Adrenocortical tumour cell line 7 (ATC7) cells were established from an adrenal tumour derived from a mouse expressing the Simian Virus 40 large T (SV40 T) antigen under the control of the aldo-keto reductase 1b7 (*Akr1b7*) gene promoter specific to the adrenal cortex[36,63]. Cells were cultured on poly-D-lysine–coated 10 cm cell culture dishes (MilliporeSigma, Burlington, MA) in a DMEM-F12 medium (Thermo Fisher Scientific, Waltham, MA) at 37°C in the presence of 5% CO2, insulin (10 mg/mL), transferrin (5.5 mg/mL), selenium (6.7 ng/mL) (Thermo Fisher Scientific), L-glutamine (2 mM), penicillin 0.1 U/mL), streptomycin (0.1 mg/mL), 2.5% horse serum, and 2.5% foetal calf serum. Cells were seeded in 12-well plates and cultures to subconfluence and then starved by replacing medium by serum-free medium the day before the addition of forskolin (Sigma-Aldrich), staurosporine (Sigma-Aldrich) or Mdivi-1 (Merck) at the times and concentrations indicated in the figure's legends.

Mice

Mice bred in-house and maintained on a mixed sv129-C57Bl/6 genetic background were housed on a 12-hour light/12-hour dark cycle (lights on at 7:00 am). Mice were fed normal, commercial rodent chow and provided with water *ad libitum*. After weaning, mice were kept in siblings with a maximum of 4 animals per cage.

Hormonal measurements

Mice were killed by decapitation around 8:30 am and blood was collected in vacuum blood collection tubes (VF-053STK, Terumo). For ACTH treatments mice were injected intraperitoneally with 0.05 mg/30g Synacthene (0.25 mg/mL, Novartis, Basel, Switzerland) 2 hours or 30 minutes prior the euthanasia. ACTH response kinetics in Figure4.I., was done with collection of the blood from the tail of the mice at 8 am, 10 am and 12 pm.

Corticosterone was measured from serum with ELISA kit (AR E-8100, LDN), ACTH was measured with Milliplex Map Kit (MPTMAG-49K, Millipore) and other steroids were measured by LC-MS/MS[64].

Histology and Proximity ligation assay

Adrenals were fixed in 4% PFA for 6 hours and embedded in paraffin. 5µm sections were deparaffinised and processed for H&E. For immunohistochemistry or immunofluorescence, deparaffinised slides were submerged in antigen retrieval buffer and microwaved for 8 minutes. After being rinsed with 1X PBS, they were blocked for an hour with 2.5% horse serum (Vector) and incubated overnight at 4°C with primary antibody. After rinsing, they were incubated with ImmPRESS polymer for 30

minutes at room temperature. HRP activity was detected with NOVAred (Vector) or Alexafluor (Thermo Fisher). Primary antibodies are listed in supplementary table S1.

For PLA, blocked slides were incubated overnight at 4°C with indicated antibodies followed by Duolink *in situ* PLA (Sigma-Aldrich) anti-mouse (minus) and anti-rabbit (plus) probes and detection reagents according to manufacturer's instructions.

Images were acquired with Zeiss Axioscan Z1 or Zeiss Imager M2 and analysed with QuPath software[65].

Lipid droplet analysis on cryosections

For frozen sections, adrenal were fixed in 4% PFA for 6 hours and immersed into 10% and 15% PBS-sucrose solutions for 20 minutes each, then 20% PBS-sucrose solution for 1 hour, and in 50/50 OCT-Sucrose 20% solution overnight. They were subsequently placed in embedding molds and with pure OCT and frozen to be stored at -80°C.

To detect lipid droplet, 14 µm sections were cut from OCT embedded adrenals. Sections were washed thrice in PBS 1x and incubated for 30 min in the dark with 10 µg/ml Bodipy 493/503 solution. After staining, sections were washed thrice in PBS 1x and mounted with VECTASHIELD® Antifade Mounting Medium with DAPI (Vector) to stain nuclei.

RT-qPCR

Adrenal glands were removed, flash frozen on dry ice, and RNA was extracted using RNeasy micro kit from QIAGEN. After reverse transcription, PCR reaction was conducted using SYBR qPCR Premix Ex Taq II Tli RNase H+ (TAKRR820W, Takara). Primer pairs are listed in supplementary table S2.

RNA-Seq

For each sex, adrenal gene expression profiles for four 4-week-old *Sf1-Cre/+::Senp2*$^{fl/fl}$ and four WT littermates were analysed using RNA-seq. RNA-sequencing, library generation and differential expression genes analysis were performed by the GenomEast platform (IGBMC, Illkirch, France).

Image analysis and base calling were performed using RTA 2.7.3 and bcl2fastq 2.17.1.14. Adapter dimer reads were removed using DimerRemover Reads were mapped onto the mm10 assembly of *Mus musculus* genome using STAR version 2.5.3a. Gene expression quantification was performed from uniquely aligned reads using htseq-count version 0.6.1p1. Read counts have been normalised across samples with the median-of-ratios method proposed by Anders and Huber. Differential expression have been implemented using the Bioconductor package DESeq2 version 1.16.1. Raw and processed data have been deposited in NCBI's GEO database (GSE193480).

Gene Set Enrichement Analysis was performed using the GSEA software[66] and plotted using the replotGSEA function from the Rtoolbox package (https://github.com/PeeperLab/Rtoolbox). Gene ontology analysis was performed using g:Profiler[67]. Data visualisation was carried out using R software (v4.1.0)[68], Pheatmap package was used for heatmaps, Vennerable for Euler diagrams and ggplot2 for plots. PCA analysis was produced on read counts matrix using prcomp function from the stats package and plotted using ggplot2.

Western blot and immunoprecipitation

Proteins were extracted from snap frozen adrenals in RIPA buffer (TRIS 25 mM, EDTA 1 mM, $MgCl_2$ 5 mM, NP40 1%, glycerol 10%, NaCl 150 mM supplemented extemporaneously with phosphatase inhibitors (1 mM Na_3VO_4, 0.5 mM

NaF), protease inhibitors (Roche, Basel, Switzerland), and SUMO proteases inhibitor N-ethylmaleimide (MilliporeSigma) (3.13 mg/mL).

For western blot, thirty µg of total denatured proteins were loaded on 10% SDS-page gel, transferred on nitrocellulose and detected with primary antibodies (Supplementary table 2). Signals were quantified with ChemiDoc MP Imaging System camera system (Bio-Rad) and Image Lab software (Bio-Rad). Expression of phosphorylated or SUMOylated proteins was normalised to the expression of the corresponding unmodified protein.

Immunoprecipitation was carried out using Automag Solution (AdemTech). 500-1000 µg of total proteins were precleared with 50 µL of beads for 30 minutes at room temperature. 10 µL of antibodies (Supplementary table 2) were crosslinked with 50 µL of beads in 20 mM DMP for 30 minutes. Precleared samples were immunoprecipitated with crosslinked antibodies for 60 minutes at room temperature, washed thrice in RIPA buffer and eluted with 50 µL of 50 mM glycine pH3. pH was brought back to neutral with 1 µL of TRIS buffer pH9 and samples were denatured in Laemmli buffer (Bio-Rad) at 95°C for 5 minutes and loaded for SDS-PAGE.

PKA activity

Proteins were extracted from snap frozen adrenals in lysis buffer (MOPS 20 mM, Betaglycerol-phosphate 50 mM, NP40 1%, DTT 1 mM, EDTA 2 mM, EGTA 5 mM supplemented extemporaneously with phosphatase inhibitors (1 mM Na_3VO_4, 50 mM NaF), protease inhibitors (Roche, Basel, Switzerland). HA-SUMO vinyl sulfone (R&D Systems, Minneapolis, MN) was added for the SUMO-VS condition to the concentration of 5 µM for both SUMO1 and SUMO2.

10 µg of protein from 4-week-old adrenals were used for measurement with PKA kinase activity kit (ab139435, Abcam).

Statistics

Statistics were conducted using R language[68] and Comp3Moy function from sumo package (https://github.com/Damien-Dufour/sumo). Normality of populations distribution was assessed with Shapiro & Wilk test for $n \in [7,5000]$ or otherwise Kolmogorof- Smirnov normality test.

If data followed a normal distribution, homoscedasticity was estimated with a Barlett test. To compare two populations, unpaired, two tailed t-test was used for normally distributed data with the same variance, Mann-Whitney for non normal distributions and Welch t-test for normally distributed data but with different variances. To compare three or more distributions : one way ANOVA for normally distributed samples with pairwise multiple t.tests or Kruskal-Wallis for non normally distributed samples with planned comparisons using Dunn's test to determine the genotype effect or the treatment effect

Crosses on the violin plots represent the mean and lines represent the median. Error bars in barplot represent the SD unless otherwise stated. The number of samples per condition is indicated at the bottom of each plot. Corticosterone response to ACTH in Figure 4.I. was analysed with paired 2 way ANOVA to compare the effect of treatment for each genotype. Correlations in Figure 5.F. and 6.A. have been conducted using cor.test function from stat package and Kendall method as distributions did not follow normality and contained ties.

Ethical approval declarations

Mouse experiments were conducted according to French and European directives for the use and care of animals for research purposes and were approved by the Comité d'Éthique pour l'Expérimentation Animale en Auvergne (project agreement #21152-2019061912052883), C2EA-02, at Institut National de Recherche pour l'Agriculture, l'Alimentation et l'Environnement, Research Centre Clermont-Theix, France (C2E2A).

Data availability

Sequencing data has been deposited in GEO with the accession code GSE193480. All other data that supports the findings of this study is provided in the article or supplementary data. Source data is provided with this paper.

Code availability

All code for data cleaning and analysis associated with the current submission is available upon request.

Supplementary information

Acknowledgements

We thank K. Ouchen, S. Plantade, and P. Mazuel for animal care, A. Dehaze and J.P. Saru for their technical assistance, and Y. Renaud for management of the bioinformatic platform.

Authors' contributions

DD, TD, GB and AM designed research. DTB and ETY provided AS^{Cre}-expressing and *Senp2*-floxed mice, respectively. DD, ISB, MO, EP, JJW, JO, CL, AL, CSD, JCP and FRB performed experiments. DD and AM analysed data. DD and AM wrote the paper. GB, IT, DTB, PV and AMLM edited the paper.

Funding

This work was funded through institutional support from CNRS, INSERM, Université Clermont-Auvergne, the French government IDEX-ISITE initiative 16-IDEX-0001 (CAP 20-25), and grants from Ministère de l'Enseignement Supérieur, de la Recherche et de l'Innovation (to DD), Société Française d'Endocrinologie (to DD and AM), Fondation Association pour la Recherche sur le Cancer (to JW and JO), and Agence Nationale pour la Recherche (ANR-18-CE14-0012-02 Sex-Specs to AL and AM).

Competing interests

The authors declare no conflict of interest.

Supplementary figures

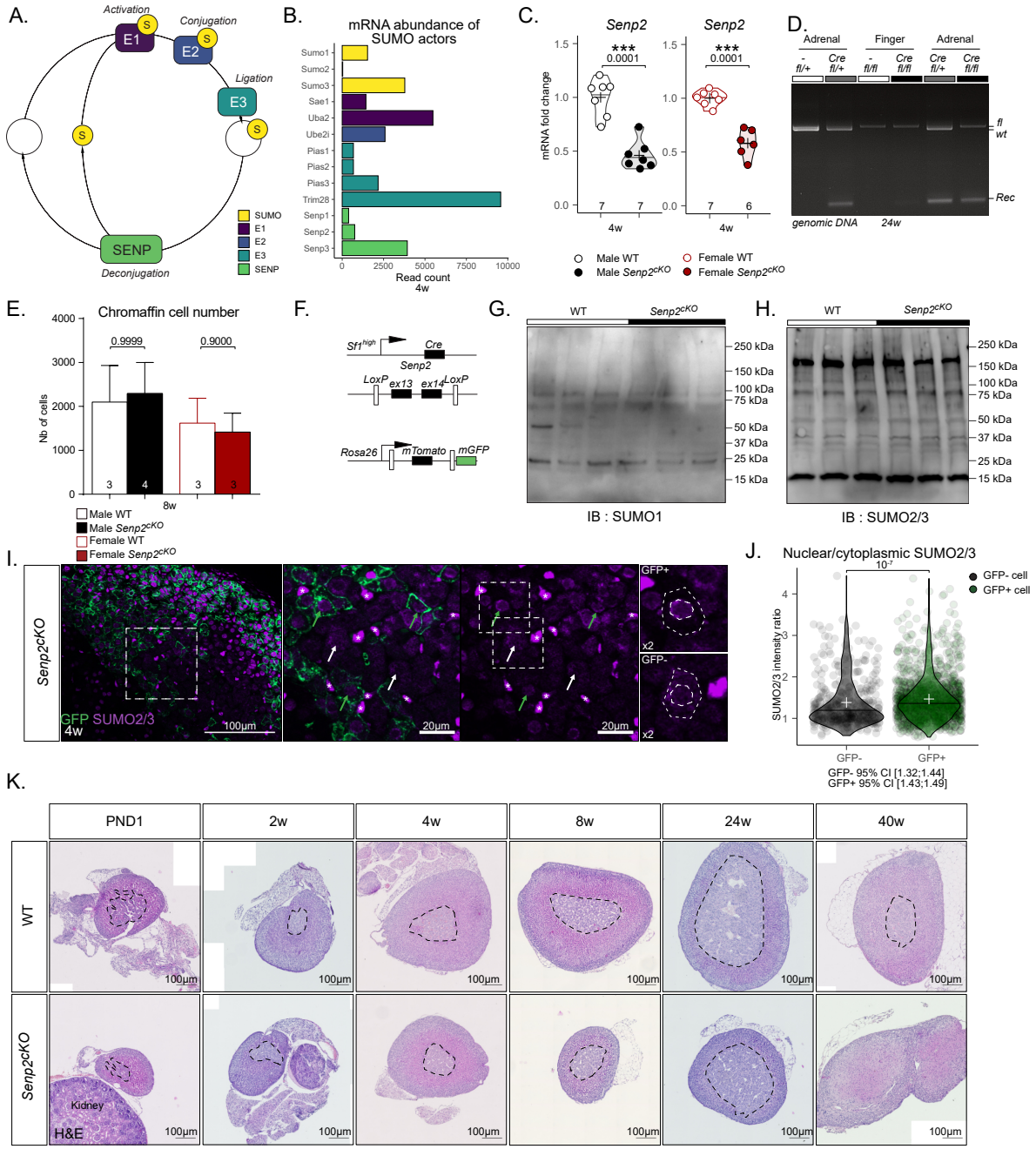

Fig.S 1: **Related to figure 1**
A. Schematic representation of the SUMOylation process
B. Relative abundance of the main actors of SUMOylation in the adrenal gland
C. qPCR analysis of *Senp2* mRNA accumulation in 4-week-old adrenals
D. Genomic PCR of *Senp2* gene showing specific recombination in *cKO* adrenals
E. 2D cell counting number in male and female medulla of WT and $Senp2^{cKO}$ mice
F. Scheme representing genetic model of $Senp2^{cKO}$ and reporter gene *Rosa26RmTmG*
G. Western blot analysis of SUMO1 in WT and $Senp2^{cKO}$ 4-week-old adrenals
H. Western blot analysis of SUMO2/3 in WT and $Senp2^{cKO}$ 4-week-old adrenals
I. Coimmunofluorescent labelling of GFP (green) and SUMO2/3 (purple) in $Senp2^{cKO}$ adrenal cortex at 4 weeks of age. Asterisks represent endothelial cells
J. Quantification of the ratio of nuclear vs cytoplasmic intensity of SUMO2/3 in GFP-negative cells vs GFP-positive cells in $Senp2^{cKO}$ adrenal cortex
K. Ontogenic analysis of adrenal morphology with H&E staining. Dotted lines represent the boundaries of the medulla.

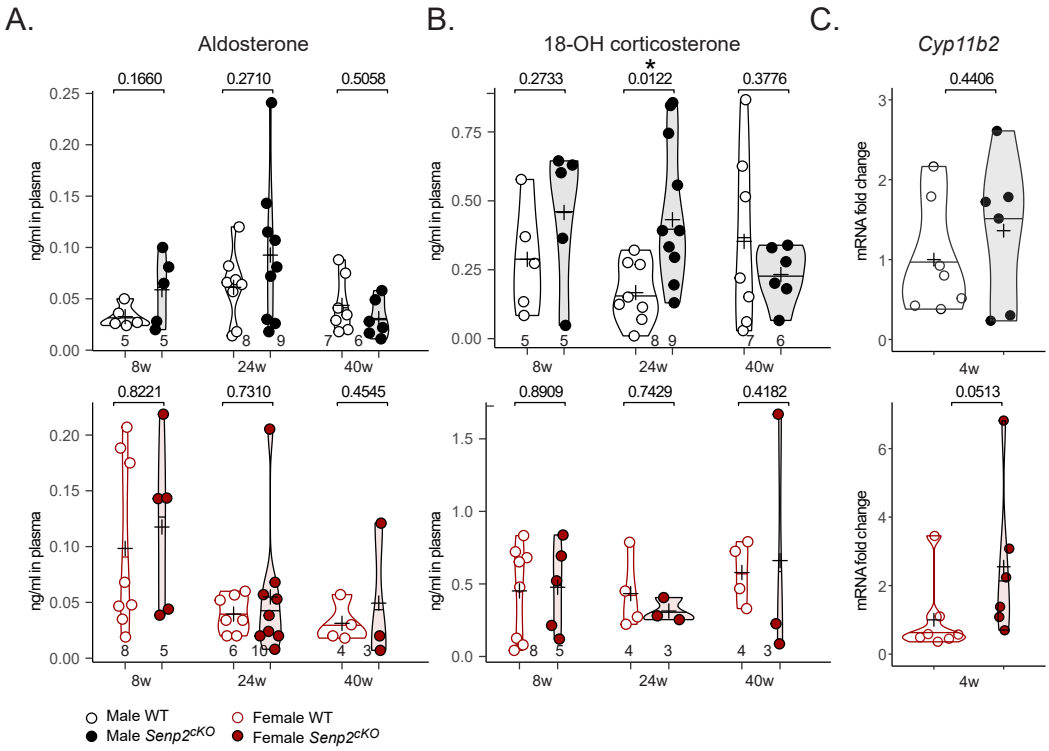

Fig.S 2: **Related to figure 2**
A. Plasmatic concentration of aldosterone in WT and $Senp2^{cKO}$ at 8, 24and 40 weeks of age (determined by LC-MS/MS).
B. Plasmatic concentration of 18-hydroxy-corticosterone in WT and $Senp2^{cKO}$ at 8, 24and 40 weeks of age (determined by LC-MS/MS).
C. qPCR analysis of aldosterone synthase coding gene *Cyp11b2* mRNA accumulation in 4-week-old WT and $Senp2^{cKO}$ adrenals.

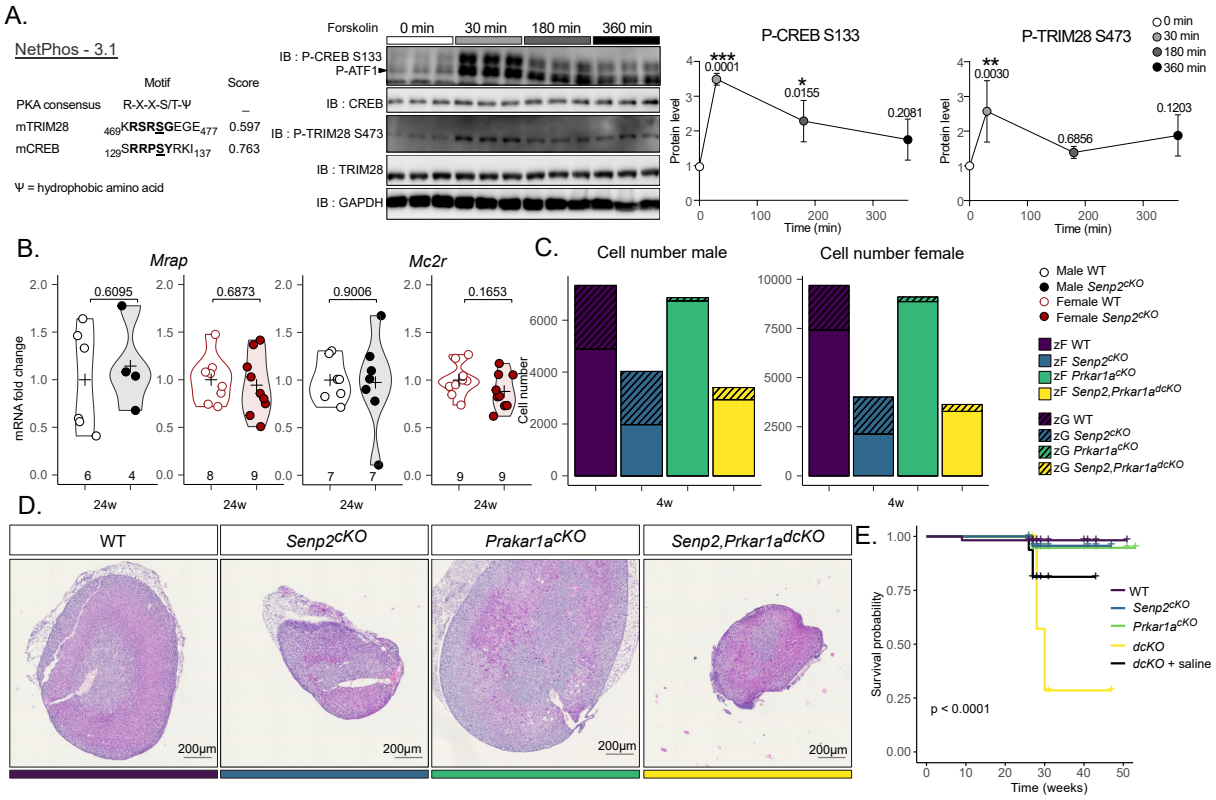

Fig.S 3: **Related to figure 3**
A. Left : PKA phosphorylation motifs on CREB and TRIM28 proteins as determined by NetPhos.3.1.
Right : Western blot analysis of the kinetics of CREB and TRIM28 phosphorylation after forskolin treatment in ATC7 cells. *P*-values represent difference between wells treated with vehicle compared to 30, 180 and 360 minutes of forskolin.
B. qPCR analysis of ACTH receptor and co-receptor mRNA accumulation in 24-week-old WT and $Senp2^{cKO}$ mice.
C. 2D cell counting number the adrenal cortex of male and female
D. Representative H&E staining of WT, $Senp2^{cKO}$, $Prkar1a^{cKO}$ or $Senp2,Prkar1a^{dcKO}$ adrenals
E. Kaplan-Meier curve of double-knockout mice with or without 0.9 % NaCl treatment

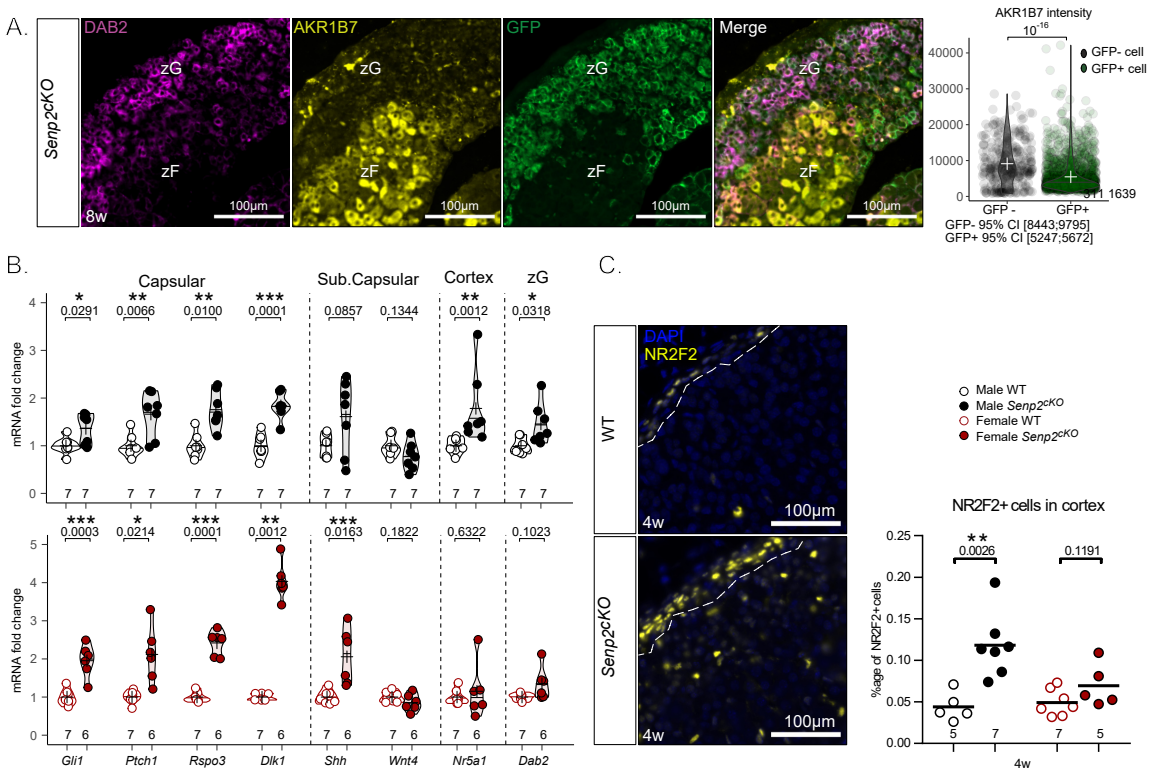

Fig.S 4: **Related to figure 4**
A. Coimmunofluorescent labelling of AKR1B7 (yellow), GFP (green) and Disabled2 (purple) on 8-week-old $Senp2^{cKO}$ female adrenal. Quantification of AKR1B7 intensity in GFP+ and GFP- $Senp2^{cKO}$ female adrenal cells
B. qPCR analysis of zonal marker mRNA accumulation in 4-week-old WT and $Senp2^{cKO}$ adrenals
C. Immunofluorescent labelling of capsular marker NR2F2 (yellow) with nuclei staining with DAPI (blue) and quantification of the proportion of NR2F2+ cells in the adrenal cortex of WT and $Senp2^{cKO}$ male and female adrenal cortices

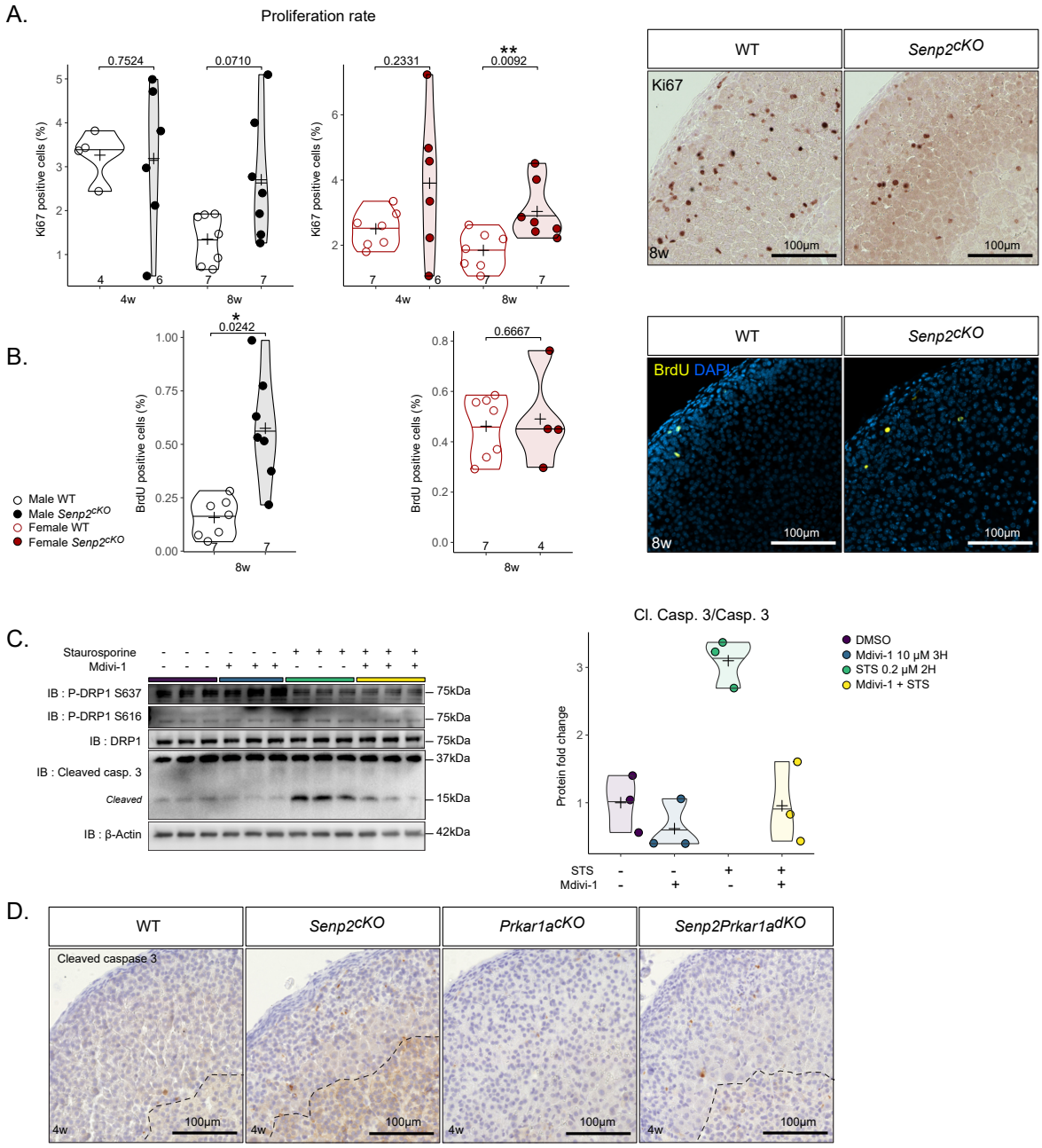

Fig.S 5: **Related to figure 5**
A. Quantification and representative picture of Ki67 staining on WT and *Senp2*^{cKO} 4- and 8-week-old adrenal cortices
B.Quantification and representative picture of 2 hours BrdU incorporation staining on WT and *Senp2*^{cKO} 8-week-old adrenal cortices
C. Western blot analysis of phosphorylated and total DRP1 in cells treated with DMSO, DRP1 inhibitor M-divi1 (10 µM) and/or Staurosporine (0.2 µM).
D. Immunostaining of cleaved caspase3 staining of WT, *Senp2*^{cKO}, *Prkar1a*^{cKO} or *Senp2,Prkar1a*^{dcKO} adrenals

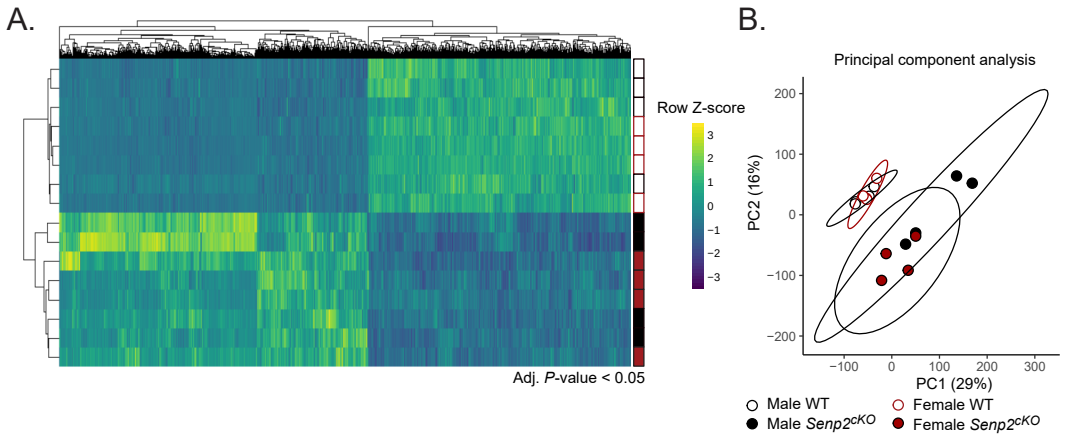

Fig.S 6: **Related to figure 6**
A. Heatmap representing the median centred expression of dysregulated genes (adjusted P-value < 0.05 between WT and $Senp2^{cKO}$ male or female) in 4-week-old male and female, WT and $Senp2^{cKO}$ adrenals
B. Principal component analysis of gene expression in WT and $Senp2^{cKO}$ 4-week-old male and female adrenals

References

1. King, P., Paul, A. & Laufer, E. Shh signaling regulates adrenocortical development and identifies progenitors of steroidogenic lineages. *Proceedings of the National Academy of Sciences* **106**, 21185–21190 (2009).
2. Freedman, B. D. *et al.* Adrenocortical Zonation Results from Lineage Conversion of Differentiated Zona Glomerulosa Cells. *Developmental Cell* **26**, 666–673 (2013).
3. Pignatti, E. *et al.* Beta-Catenin Causes Adrenal Hyperplasia by Blocking Zonal Transdifferentiation. *Cell Reports* **31**, 107524 (2020).
4. Berthon, A. *et al.* Constitutive beta-catenin activation induces adrenal hyperplasia and promotes adrenal cancer development. *Human Molecular Genetics* **19**, 1561–1576 (2010).
5. Berthon, A. *et al.* WNT/beta-catenin signalling is activated in aldosterone-producing adenomas and controls aldosterone production. *Human Molecular Genetics* **23**, 889–905 (2014).
6. Walczak, E. M. *et al.* Wnt Signaling Inhibits Adrenal Steroidogenesis by Cell-Autonomous and NonCell-Autonomous Mechanisms. *Molecular Endocrinology* **28**, 1471–1486 (2014).
7. Dumontet, T. *et al.* PKA signaling drives reticularis differentiation and sexually dimorphic adrenal cortex renewal. *JCI Insight* **3**, (2018).
8. Novoselova, T. V. *et al.* ACTH signalling and adrenal development: Lessons from mouse models. *Endocrine Connections* **8**, R122–R130 (2019).
9. Drelon, C. *et al.* PKA inhibits WNT signalling in adrenal cortex zonation and prevents malignant tumour development. *Nature Communications* **7**, 12751 (2016).
10. Mathieu, M. *et al.* Steroidogenic differentiation and PKA signaling are programmed by histone methyltransferase EZH2 in the adrenal cortex. *Proc Natl Acad Sci USA* **115**, E12265–E12274 (2018).
11. Minguez, P. *et al.* Deciphering a global network of functionally associated post-translational modifications. *Mol Syst Biol* **8**, 599 (2012).
12. *SUMO Regulation of Cellular Processes*. vol. 963 (Springer International Publishing, 2017).
13. Chang, H.-M. & Yeh, E. T. H. SUMO: From Bench to Bedside. *Physiological Reviews* **100**, 1599–1619 (2020).
14. Talamillo, A. *et al.* The role of SUMOylation during development. *Biochemical Society Transactions* **48**, 463–478 (2020).
15. Chung, S. S. *et al.* Control of Adipogenesis by the SUMO-Specific Protease SENP2. *Molecular and Cellular Biology* **30**, 2135–2146 (2010).
16. Cossec, J.-C. *et al.* SUMO Safeguards Somatic and Pluripotent Cell Identities by Enforcing Distinct Chromatin States. *Cell Stem Cell* **23**, 742–757.e8 (2018).
17. Liang, Q. *et al.* SENP2 Suppresses Necdin Expression to Promote Brown Adipocyte Differentiation. *Cell Reports* **28**, 2004–2011.e4 (2019).
18. Demarque, M. D. *et al.* Sumoylation by Ubc9 Regulates the Stem Cell Compartment and Structure and Function of the Intestinal Epithelium in Mice. *Gastroenterology* **140**, 286–296 (2011).
19. Ding, X. *et al.* Protein SUMOylation Is Required for Regulatory T Cell Expansion and Function. *Cell Reports* **16**, 1055–1066 (2016).
20. Dumontet, T. *et al.* Hormonal and spatial control of SUMOylation in the human and mouse adrenal cortex. *FASEB j.* **33**, 10218–10230 (2019).
21. Lee, F. Y. *et al.* Eliminating SF-1 (NR5A1) Sumoylation In Vivo Results in Ectopic Hedgehog Signaling and Disruption of Endocrine Development. *Developmental Cell* **21**, 315–327 (2011).
22. Qi, Y. *et al.* Hyper-SUMOylation of the Kv7 Potassium Channel Diminishes the M-Current Leading to Seizures and Sudden Death. *Neuron* **83**, 1159–1171 (2014).

23. Bingham, N. C., Verma-Kurvari, S., Parada, L. F. & Parker, K. L. Development of a steroidogenic factor 1/Cre transgenic mouse line. *genesis* **44**, 419–424 (2006).

24. Muzumdar, M. D., Tasic, B., Miyamichi, K., Li, L. & Luo, L. A global double-fluorescent Cre reporter mouse. *genesis* **45**, 593–605 (2007).

25. Levasseur, A., Dumontet, T. & Martinez, A. Sexual dimorphism in adrenal gland development and tumorigenesis. *Current Opinion in Endocrine and Metabolic Research* **8**, 60–65 (2019).

26. Lyraki, R. & Schedl, A. The Sexually Dimorphic Adrenal Cortex: Implications for Adrenal Disease. *IJMS* **22**, 4889 (2021).

27. Sahut-Barnola, I. *et al.* Cushing's Syndrome and Fetal Features Resurgence in Adrenal Cortex-Specific Prkar1a Knockout Mice. *PLoS Genetics* **6**, e1000980 (2010).

28. Kunz, K., Muller, S. & Mendler, L. Assays of SUMO protease/isopeptidase activity and function in mammalian cells and tissues. in *Methods in Enzymology* vol. 618 389–410 (Elsevier, 2019).

29. Grabek, A. *et al.* The Adult Adrenal Cortex Undergoes Rapid Tissue Renewal in a Sex-Specific Manner. *Cell Stem Cell* **25**, 290–296.e2 (2019).

30. Vinson, G. P. Functional Zonation of the Adult Mammalian Adrenal Cortex. *Front. Neurosci.* **10**, (2016).

31. Frank, S. *et al.* The Role of Dynamin-Related Protein 1, a Mediator of Mitochondrial Fission, in Apoptosis. *Developmental Cell* **1**, 515–525 (2001).

32. Sabouny, R. & Shutt, T. E. Reciprocal Regulation of Mitochondrial Fission and Fusion. *Trends in Biochemical Sciences* **45**, 564–577 (2020).

33. Chang, C.-R. & Blackstone, C. Cyclic AMP-dependent Protein Kinase Phosphorylation of Drp1 Regulates Its GTPase Activity and Mitochondrial Morphology. *J. Biol. Chem.* **282**, 21583–21587 (2007).

34. Park, J.-E. *et al.* Drp1 Phosphorylation Is Indispensable for Steroidogenesis in Leydig Cells. *Endocrinology* **160**, 729–743 (2019).

35. Plewes, M. R. *et al.* Luteinizing hormone regulates the phosphorylation and localization of the mitochondrial effector dynamin-related Protein1 (DRP1) and steroidogenesis in the bovine corpus luteum. *FASEB j.* fj.201902958R (2020) doi:10.1096/fj.201902958R.

36. Ragazzon, B. *et al.* Adrenocorticotropin-Dependent Changes in SF-1/DAX-1 Ratio Influence Steroidogenic Genes Expression in a Novel Model of Glucocorticoid-Producing Adrenocortical Cell Lines Derived from Targeted Tumorigenesis. *Endocrinology* **147**, 1805–1818 (2006).

37. Manczak, M., Kandimalla, R., Yin, X. & Reddy, P. H. Mitochondrial division inhibitor 1 reduces dynamin-related protein 1 and mitochondrial fission activity. *Human Molecular Genetics* **28**, 177–199 (2019).

38. Berthon, A., Martinez, A., Bertherat, J. & Val, P. Wnt/beta-catenin signalling in adrenal physiology and tumour development. *Molecular and Cellular Endocrinology* **351**, 87–95 (2012).

39. Kim, A. C. *et al.* Targeted disruption of beta-catenin in Sf1-expressing cells impairs development and maintenance of the adrenal cortex. *Development* **135**, 2593–2602 (2008).

40. Little, D. W., Dumontet, T., LaPensee, C. R. & Hammer, G. D. Beta-catenin in adrenal zonation and disease. *Molecular and Cellular Endocrinology* **522**, 111120 (2021).

41. Kadoya, T. *et al.* Desumoylation Activity of Axam, a Novel Axin-Binding Protein, Is Involved in Downregulation of beta-Catenin. *Mol Cell Biol* **22**, 3803–3819 (2002).

42. Kadoya, T. *et al.* Inhibition of Wnt Signaling Pathway by a Novel Axin-binding Protein. *Journal of Biological Chemistry* **275**, 37030–37037 (2000).

43. Nishida, T., Kaneko, F., Kitagawa, M. & Yasuda, H. Characterization of a Novel Mammalian SUMO-1/Smt3-specific Isopeptidase, a Homologue of Rat Axam, Which Is an Axin-binding Protein Promoting beta-Catenin Degradation. *J. Biol. Chem.* **276**, 39060–39066 (2001).

44. Huang, H.-J. *et al.* Beta-catenin SUMOylation is involved in the dysregulated proliferation of myeloma cells. *Am J Cancer Res* **5**, 309–320 (2015).

45. Karami, S. *et al.* Novel SUMO-Protease SENP7S Regulates beta-catenin Signaling and Mammary Epithelial Cell Transformation. *Scientific Reports* **7**, 46477 (2017).

46. Enserink, J. M. Sumo and the cellular stress response. *Cell Div* **10**, 4 (2015).

47. Buaas, F. W., Gardiner, J. R., Clayton, S., Val, P. & Swain, A. In vivo evidence for the crucial role of SF1 in steroid-producing cells of the testis, ovary and adrenal gland. *Development* **139**, 4561–4570 (2012).

48. Mosleh, E. *et al.* Ins1-Cre and Ins1-CreER Gene Replacement Alleles Are Susceptible To Silencing By DNA Hypermethylation. *Endocrinology* **161**, bqaa054 (2020).

49. Lopez, J. P. *et al.* Single-cell molecular profiling of all three components of the HPA axis reveals adrenal ABCB1 as a regulator of stress adaptation. *Sci. Adv.* **7**, eabe4497 (2021).

50. Chida, D. *et al.* Melanocortin 2 receptor is required for adrenal gland development, steroidogenesis, and neonatal gluconeogenesis. *Proceedings of the National Academy of Sciences* **104**, 18205–18210 (2007).

51. Novoselova, T. V. *et al.* MRAP deficiency impairs adrenal progenitor cell differentiation and gland zonation. *FASEB j.* **32**, 6186–6196 (2018).

52. Choi, H.-K. *et al.* Reversible SUMOylation of TBL1-TBLR1 Regulates beta-Catenin-Mediated Wnt Signaling. *Molecular Cell* **43**, 203–216 (2011).

53. Cai, Z. *et al.* Redox-sensitive enzyme SENP3 mediates vascular remodeling via de-SUMOylation of beta-catenin and regulation of its stability. *EBioMedicine* **67**, 103386 (2021).

54. Leng, S. *et al.* Beta-Catenin and FGFR2 regulate postnatal rosette-based adrenocortical morphogenesis. *Nat Commun* **11**, 1680 (2020).

55. Rossitto, M. *et al. TRIM28-dependent SUMOylation protects the adult ovary from the male pathway.* http://biorxiv.org/lookup/doi/10.1101/2021.03.24.436749 (2021) doi:10.1101/2021.03.24.436749.

56. Tan, S. *et al.* Stromal Senp1 promotes mouse early folliculogenesis by regulating BMP4 expression. *Cell Biosci* **7**, 36 (2017).

57. Lee, J. S. *et al. SUMO-specific protease 2 (SENP2) suppresses browning of white adipose tissue through C/EBPbeta modulation.* http://biorxiv.org/lookup/doi/10.1101/2020.12.16.422969 (2020) doi:10.1101/2020.12.16.422969.

58. Lopez, I. *et al.* An unanticipated tumor-suppressive role of the SUMO pathway in the intestine unveiled by Ubc9 haploinsufficiency. *Oncogene* **39**, 6692–6703 (2020).

59. Yin, M. *et al.* CD34+KLF4+ Stromal Stem Cells Contribute to Endometrial Regeneration and Repair. *Cell Reports* **27**, 2709–2724.e3 (2019).

60. Jang, S. M. *et al.* KAP1 facilitates reinstatement of heterochromatin after DNA replication. *Nucleic Acids Research* **46**, 8788–8802 (2018).

61. Li, M., Xu, X., Chang, C.-W. & Liu, Y. TRIM28 functions as the SUMO E3 ligase for PCNA in prevention of transcription induced DNA breaks. *Proc Natl Acad Sci USA* **117**, 23588–23596 (2020).

62. Leclerc, J., Ballotti, R. & Bertolotto, C. Pathways from senescence to melanoma: Focus on MITF sumoylation. *Oncogene* **36**, 6659–6667 (2017).

63. Batisse-Lignier, M. *et al.* P53/Rb inhibition induces metastatic adrenocortical carcinomas in a preclinical transgenic model. *Oncogene* **36**, 4445–4456 (2017).

64. Travers, S. *et al.* Multiplexed steroid profiling of gluco- and mineralocorticoids pathways using a liquid chromatography tandem mass spectrometry method. *The Journal of Steroid Biochemistry and Molecular Biology* **165**, 202–211 (2017).

65. Bankhead, P. *et al.* QuPath: Open source software for digital pathology image analysis. *Sci Rep* **7**, 16878 (2017).

66. Subramanian, A. *et al.* Gene set enrichment analysis: A knowledge-based approach for interpreting genome-wide expression profiles. *Proceedings of the National Academy of Sciences* **102**, 15545–15550 (2005).

67. Raudvere, U. *et al.* G:Profiler: A web server for functional enrichment analysis and conversions of gene lists (2019 update). *Nucleic Acids Research* **47**, W191–W198 (2019).

68. R Core Team. *R: A language and environment for statistical computing.* (R Foundation for Statistical Computing, 2018).

Article 2

Graphical abstract

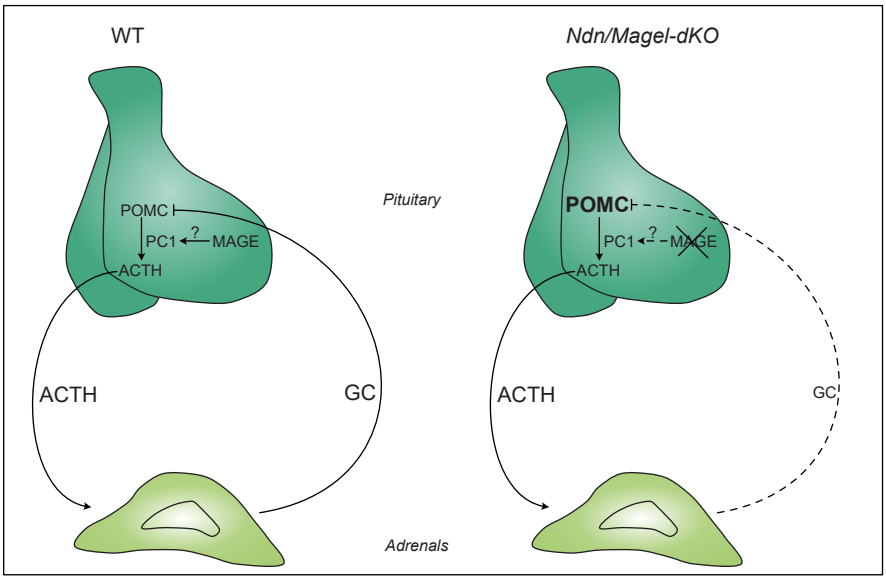

Prader-Willi syndrome proteins NECDIN and MAGEL2 are implicated in hypothalamic-pituitary-adrenal axis regulation

Damien Dufour [1], Clément Menuet [2], Anne-Marie Lefrançois-Martinez [1], Pierre Val [1], Françoise Muscatelli [2] and Antoine Martinez [1*]

[1] institut Génétique, Reproduction & Développement (*i*GReD), CNRS, INSERM, Université Clermont Auvergne, Clermont–Ferrand, F-63000, France.

[2] Institut de Neurobiologie de la Méditerranée (INMED) UMR1249, INSERM, Aix-Marseille Université, Marseille, France.

*Corresponding author(s). E-mail(s): antoine.martinez@uca.fr; Contributing authors: damien.dufour@doctorant.uca.fr

Abstract

NECDIN and MAGEL2 are proteins of the MAGE family implicated in the aetiology of Prader-Willi syndrome (PWS). Patients affected by this syndrome suffer from multiple metabolic and endocrine disorders including obesity, hypothyroidism or hypogonadism. While some studies have reported high prevalence of central adrenal insufficiency in PWS patients, there is no consensus on this aspect. Adrenal cortex response to stress is controlled by pituitary ACTH surge which itself depends on hypothalamic CRH. Glucocorticoids produced by the adrenal cortex inhibit ACTH production through a negative feedback ensuring fine tuning of steroidogenesis and adaptation to stress. In order to decipher the role of NECDIN and MAGEL2 in hypothalamic-pituitary-adrenal axis, we have studied the stress response of NDN/MAGEL2 knockout mice. We show that NECDIN expression is specifically enriched in the *zona glomerulosa* of the adrenal cortex and negatively regulated by ACTH. *Ndn/Magel2* double KO mice show intact adrenal glands but impaired corticosterone response to stress and increased *Pomc* expression in the pituitary despite unaltered ACTH plasmatic levels. These preliminary results suggest that MAGE proteins are involved in adrenal stress response by affecting POMC maturation into ACTH, thus arguing for central adrenal insufficiency and better exploration of the HPA axis in PWS patients.

Keywords: Adrenal, Prader-Willi syndrome, Necdin, Magel2

The adrenal cortex is an endocrine organ at the centre of stress response through the hypothalamic-pituitary-adrenal (HPA) axis. Following a perceived stress, the hypothalamus produces CRH (corticotropin realeasing factor) to the pituitary which synthesises POMC (Proopio melanocortin) in response. POMC is then cleaved by PC1/3 (proprotein convertase 1) into ACTH which is released into the bloodstream[1]. ACTH stimulates, *via* PKA signalling, the release of glucocorticoids which in turn signal to the pituitary to stop ACTH production resulting in a real-time adjustment to physiological demand[2,3].

We have showed that SENP2 is a central protein in adrenal cortex physiology since its deletion prevents proper centripetal cellular transdifferenciation of cortical zones[4]. Interestingly, loss of SENP2 has been shown to block brown preadipocytes differentiation into fully fonctionning brown adipocytes through increased expression of NECDIN (neurally differentiated EC cell-derived protein)[5].

NECDIN is part of the MAGE protein family and is expressed mainly in neurons. It can act as an E3 ubiquitin ligase, but also as a scaffold protein or as a transcription cofactor[6]. The *Ndn* gene is located on the 15q13-11 *locus* with genes such as *Magel2* or *Snord116*. This *locus* is implicated in Prader-willi syndrome (PWS), a genomic imprinting-associated neurodevelopmental disorder consisting of symptoms varying from short stature, cognitive defects, hyperphagia to endocrine disorders. The latter include central hypogonadism, hypothyroidism and GH insufficiency[7]. Several reports have suggested that adrenal function might be affected in PWS[8–12] while other did not[13,14] raising the question of the implication of NECDIN or other PWS proteins on adrenal function directly or on the HPA axis. To answer this question we explored HPA axis function in *Ndn*-KO ($Ndn^{-/-}$)[15] and *Ndn/Magel2-dKO* ($Ndn^{-/-}/Magel2^{-/-}$) mice[16]. We show that NECDIN is expressed in the *zona glomerulosa* (zG) of the adrenal cortex and negatively regulated by ACTH. Surprisingly, female but not male *Ndn-KO* mice have hypocorticosteronemia and present normal ACTH plasmatic levels and adrenocortical morphology. *Ndn/Magel2-dKO* have reduced response to stress independant of ACTH plasmatic concentration but males harbours higher levels of *Pomc* transcripts in the pituitary suggesting impaired ACTH maturation.

Results

Necdin is overexpressed in a mouse model of adrenal hyper-SUMOylation

Since the loss of *Senp2* in BAT preadipocytes leads to overexpression of *Ndn*, blocking adipogenic differentiation, we wondered if a similar mechansim could be at stake in the adrenal cortex acting on zonal transdifferentiation[17]. Immunofluorescent staining revealed cytoplasmic staining of NECDIN limited to the zG of WT mice, whereas $Senp2^{cKO}$ adrenals showed staining extending additionally (but with less intensity) to the *zona fasciculata* (zF) (Figure 1.A.). RT-qPCR analyses showed increased accumulation of *Ndn* transcripts as well as its target genes *Wnt10b* and *Dlk1*, and the co-upregulation of PWS-*locus* gene *Magel2* (Figure 1.B.).

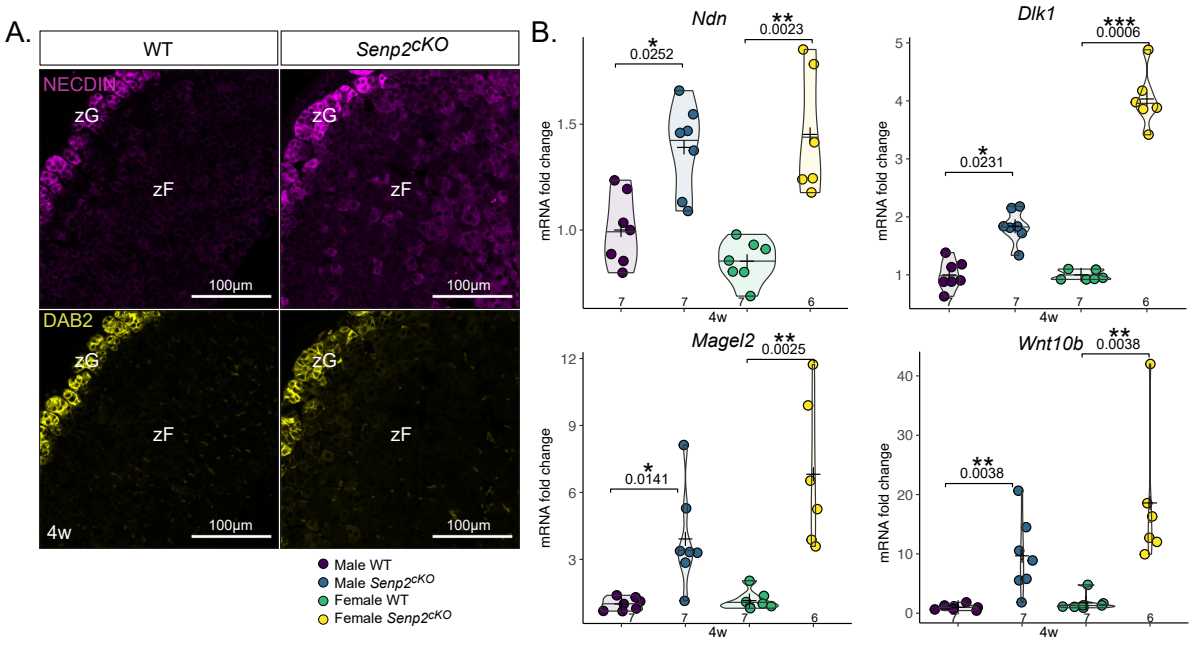

Figure 1: ***Necdin* is overexpressed in a mouse model of isolated glucocorticoid insufficiency**
A. Immunofluorescence labelling of NECDIN (pink) and DAB2/Disabled2 (yellow) in WT and $Senp2^{cKO}$ 4-week-old adrenals. B. qPCR analyses of *Ndn*, *Magel2* and NECDIN target genes *Wnt10b* and *Dlk1* mRNA accumulation in 4-week-old WT and $Senp2^{cKO}$ adrenals.

NECDIN expression is restricted to zG and controlled by PKA signalling in the adrenal cortex

In order to delve into the implication of NECDIN in adrenal homeostasis, we used publicly available single cell RNA-seq data, to locate the cells expressing *Ndn*[18]. In agreement with immunohistofluorescent staining, *Ndn* mRNA expression is enriched in the zG in WT adrenals (Figures 1.A. and 2.B.). To confirm that NECDIN is indeed a reliable zG marker, we used mouse models of either zG hyperplasia due to stabilised β-catenin (*0.5Akr1b7-cre::Catnb*$^{lox(ex3)}$ or Δ-cat)[19] or zG hypoplasia due to constitutive PKA signalling ($AS^{Cre}/+$ :: $Prkar1a^{fl/fl}$ or DAdKO)[20]. As expected, NECDIN expression domain followed zG, being expended in Δ-cat mice and strongly reduced in DAdKO mice (Figure 2.C.).

During brown adipocyte differentiation, *Ndn* expression is repressed by P-CREB^{S133} recruitment to its promoter[5,21]. Based on this data and the fact that NECDIN is expressed in *glomerulosa* cells where PKA signalling is low, we hypothesised that PKA signalling could control *Ndn* expression in the adrenal. In adrenals, the main stimulator of PKA signalling is pituitary ACTH that binds to its receptor MC2R leading to increased cAMP concentrations and subsequent phosphorylation of CREB on Ser 133. We treated mice for 2 hours with ACTH and measured *Ndn* transcript accumulation in the adrenals. ACTH treatment led to a 70% decrease in males and 40% decrease in females (albeit with a *P*-value of 0.0908) (Figure 2.D.).

To explore the kinetics of *Ndn* regulation , we treated adrenocortical cell line ATC7 with adenylyl cyclase activator Forskolin. Treatment led to a transient 50% decrease after six

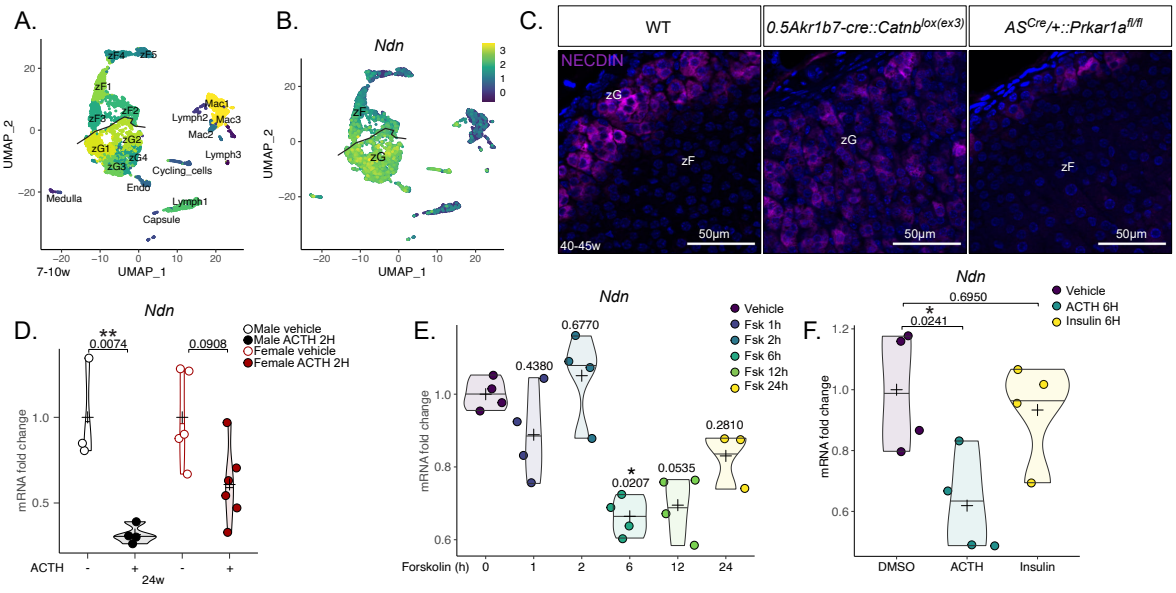

Figure 2: ***Necdin* expression is restricted to zG and controlled by PKA signalling in the adrenal.**
A. Dimensional reduction (UMAP) representation of adrenal cortex cells clustered by gene expression profiles and assigned to specific cell types
B. UMAP representation of *Ndn* normalised mRNA expression per cell
C. Immunofluorescence analysis of NECDIN on WT, ΔCat and DAdKO 40-45 week-old cortices
D. qPCR analyses of *Ndn* mRNA accumulation in adrenals from 24-week-old WT and $Senp2^{cKO}$ treated with ACTH.
E. Kinetics of *Ndn* expression in ATC7 cells treated with 10 µM forskolin, determined by qPCR
F. qPCR analyses of *Ndn* mRNA accumulation in ATC7 cells treated with 10 µM forskolin or insulin 200µg/l for 6 hours
Mac : Macrophages; Endo : endothelial cells; Lymph : lymphocytes; zG : zona glomerulosa; zF : zona fasciculata

hours (Figure 2.E.). As *Ndn* has been shown to be regulated by both PKA and insulin signalisation[21], we treated cells with ACTH or insulin for 6 hours and observed a 40% decrease in *Ndn* expression with ACTH while insulin had no effect (Figure 2.F.).

Ndn-KO have mild adrenal insufficiency but show overexpression of *Magel2*

To know if NECDIN is implicated in adrenal cortex physiology, we used *Ndn* deficient mice (*Ndn-KO*)[15]. *Ndn* gene invalidation was confirmed in the adrenal by RT-qPCR (Figure S1.) and immunofluorescence (Figure 3.C. right panel) Male and female *Ndn-KO* mice had the same body mass and showed no difference in adrenal mass, histology or zonation (Figure 3.A.B.C.). Hormonal measurements revealed no difference in plasma aldosterone concentration but female *Ndn-KO* had lower circulating corticosterone without any difference in ACTH (Figure 2.D.). Since MAGEL2 can also be responsible for a part of PWS symptoms[22–24], we measured the accumulation of *Magel2* transcripts. *Magel2* expression in *Ndn* deficient mice adrenals was indeed higher than in WT male (Figure 3.E.) which could compensate for *Ndn* loss as both genes appeared coregulated in $Senp2^{cKO}$ adrenals (Figure 1.B).

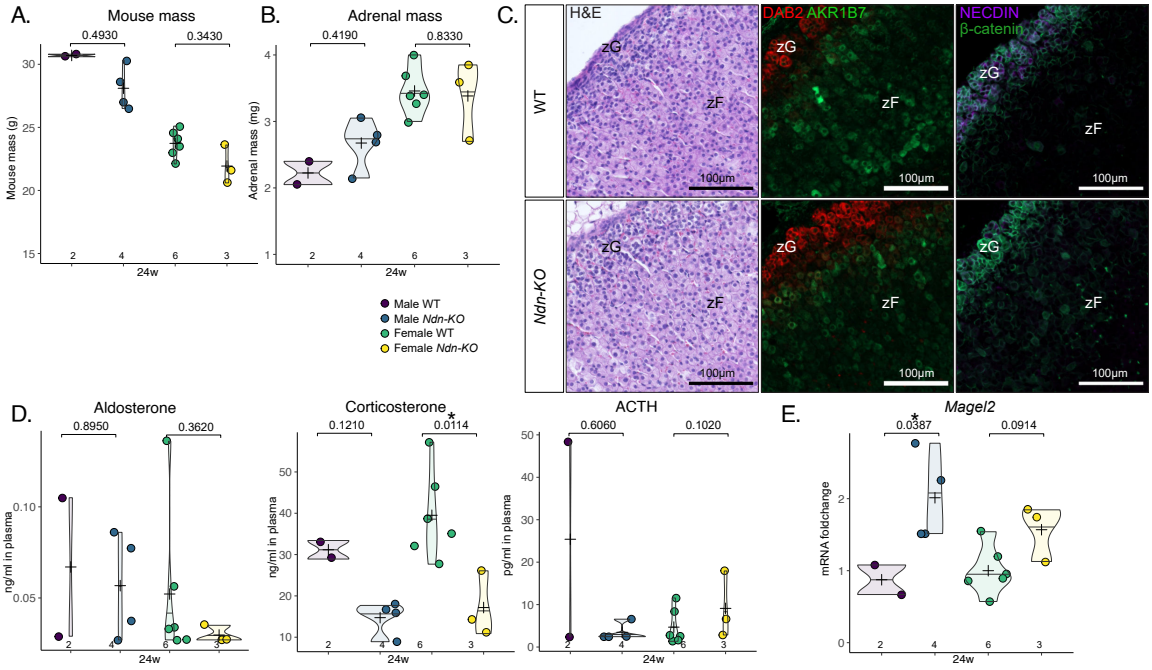

Figure 3: ***Ndn*-KO female mice have corticosterone unsufficiency synthesis without change in ACTH**.
A. WT and *Ndn-KO* body mass at 24 weeks of age
B. Absolute adrenal mass of male and female mice WT and *Ndn-KO* (mean) at 24 weeks of age.
C. Left : H&E staining of WT or *Ndn-KO* 24-week-old adrenals.
Center : Coimmunofluorescence labelling of AKR1B7 (green) and DAB2/Disabled2 (red) in WT and *Ndn-KO* adrenals.
Right : Coimmunofluorescence analysis of NECDIN (purple) and β-catenine (green) in WT and KO adrenals.
D. Plasmatic concentration of aldosterone (left) (determined by LC-MS/MS), corticosterone (centre) and ACTH (right) in WT and *Ndn-KO* at 24 weeks of age (determined by ELISA).
E. qPCR analyses of *Magel2* mRNA accumulation in adrenals from 24-week-old WT and *Ndn-KO*

Concomitant deletion of NECDIN and MAGEL2 leads to deficit in stress response

Since NECDIN and MAGEL2 exert similar functions, we decided to study *Ndn/Magel2-dKO*. These mice were smaller than their WT counterpart (Figure S2.G.). In order to evaluate adrenal function, we measured corticosterone at 5pm and submitted mice to a mild stress by injecting them intra peritonealy with PBS at 9am the next day. Corticosterone measurements revealed higher corticosterone levels after the stress, in 7/8 WT male and 5/8 WT female mice whereas in dKO, only 4/8 mice responded in male and 4/8 in female (Figure 4.A.B.). Corticosterone secretion is stimulated by pituitary ACTH, itself negatively regulated by corticosterone (Figure 5.A.). Despite their blunted response to stress, *Ndn/Magel2-dKO* mice had normal ACTH concentration compared to WT (Figure 4.C.). These mice had normal sized adrenals (Figure 4.F.), H&E staining did not reveal any structural defects (Figure 4.D.) while 3β-HSD immunofluorescence showed modest reduction in male dKO cortices (Figure 4.E.).

NDN/MAGEL2 effect on hypothalamus and pituitary

Since the *Ndn/Magel2* deletion affects the whole organism, we decided to focus on the hypothalamus and pituitary. Sc-RNA seq revealed strong expression of *Ndn* and

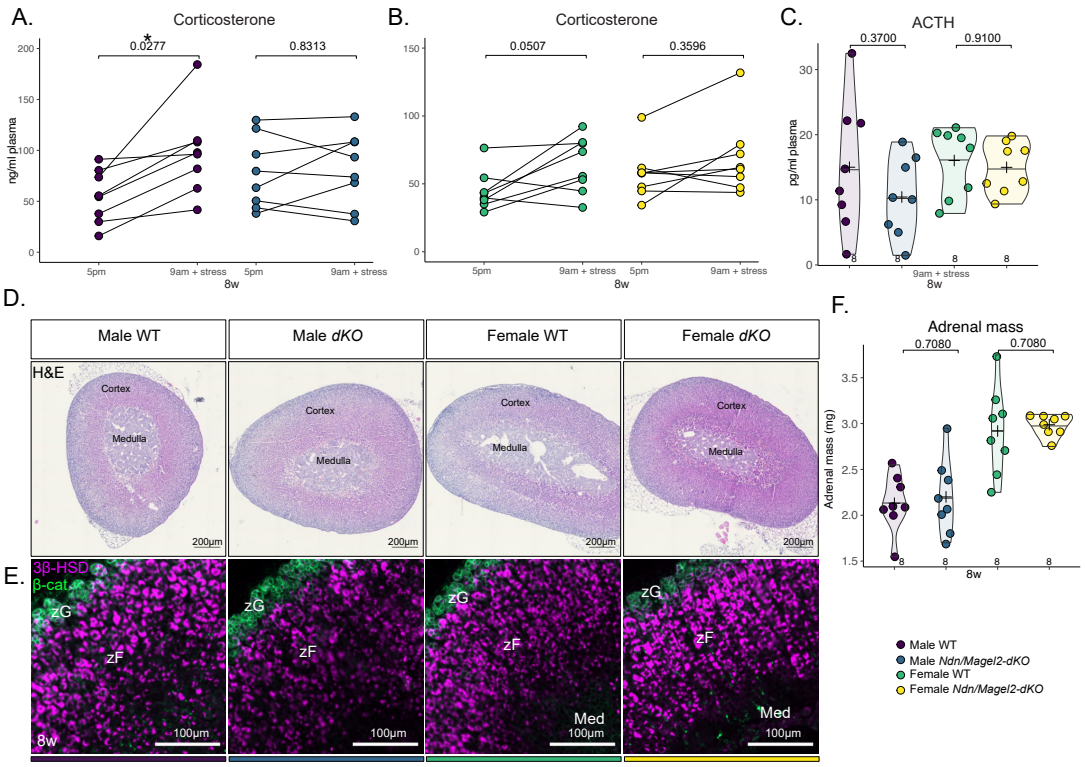

Figure 4: **Concomitant deletion of NECDIN and MAGEL2 leads to deficit in stress response**
A. Plasmatic concentration of corticosterone in WT and *Ndn/Magel2-dKO* males at 8 weeks of age at 5pm and the subsequent day at 9am after a mild stress caused by I.P. injection of PBS (determined by ELISA).
B. Plasmatic concentration of corticosterone in WT and *Ndn/Magel2-dKO* females at 8 weeks of age at 5pm and the subsequent day at 9am after a mild stress caused by I.P. injection of PBS (determined by ELISA). C. Post stress plasmatic concentration of ACTH in WT and *Ndn/Magel2-dKO* males and females at 8 weeks of age
D. H&E staining of WT or *Ndn/Magel2-dKO* 8-week-old adrenals.
E. Coimmunofluorescence analysis of 3β-HSD (pink) and β-catenine (green) in WT and KO adrenals.
F. Absolute adrenal mass of male and female mice WT and *Ndn/Magel2-dKO* (mean) at 8 weeks of age.

Magel2 in neurons from the hypothalamus and of *Ndn* in endocrine cells of the anterior pituitary including the corticotrophs (Figure S2.A.B.D.E.) while *Magel2* did not seem to be expressed at this age in any cell of the pituitary (Figure S2.E.). qPCR analyses confirmed deletion of *Ndn* and *Magel2* in pituitary and hypothalamus (Figure S2.C.F.)

The hypothalamus produces CRH which circulates through the door vein to the pituitary gland where it induces the expression of *Pomc via* binding to CRH1R. POMC is then cleaved by PC1/3 (*Pcsk1*) in the pituitary gland and released in the blood as mature ACTH. ACTH, through binding to MC2R/MRAP receptors stimulates PKA signalling and induces steroidogenesis to produce GCs. Finally, GCs bind to GR (*Nr3c1*) and stimulates the expression of *Fkbp5* while downregulating *Crh1* in the hypothalamus and *Pomc* in the pituitary (Figure 5.A.).

RT-qPCR analyses revealed no alteration of *Fkbp5* nor *Nr3c1* in the hypothalamus (Figure 5.C.D.) or pituitary (Figure 5.G.H.) meaning that there were no difference in chronic corticosterone concentration[25] or sensibility. Consistantly, *Crh1* in the hypothalamus and *Crh1r* in the pituitary were not altered by loss of *Ndn* and *Magel2* (Figure 5.B.F.).

Based on ACTH concentrations, we expected no change in POMC expression, however we found an increased in *Pomc* transcripts in male dKO compared to WT pituitaries (Figure 5.E.). To explain this surprising finding, we analysed expression of *Pcsk1* coding PC1/3, the enzyme responsible for POMC cleavage in the pituitary and its upstream transcriptional regulator *Nhlh2*. RT-qPCR analysis however revealed no differences in the expression of *Pcsk1* nor *Nhlh2* between males or females WT and dKO pituitaries (Figure 5.I.J.).

Discussion

Based on findings from a brown adipocyte differentiation system[5], we have explored expression of NECDIN and related protein MAGEL2 in adrenal and relevance in hypothalamic-pituitary-adrenal axis physiology. We have shown that NECDIN is restricted to zG cells in the adrenal, upregulated by *Senp2* loss and downregulated by activation of PKA signalling. This finding is consistent with previous reports showing that *Necdin* expression is directly repressed by PKA[26] though binding of CREB on its promoter[5,21].

Ndn deficiency alone or with *Magel2* produced defects in HPA axis. *Ndn-KO* female mice had lower corticosterone than WT mice while their plasmatic ACTH levels were not affected, dKO mice, on the other hand showed blunted to mild stress in both sexes, which could suggest mild adrenal insufficiency. Normal plasmactic ACTH concentrations in both models could be explained by presence of immature and mature forms of ACTH that are not detected by standard ELISA detection[27]. Central adrenal insufficiency is rarely found in patients with PWS[28] yet with a higher prevalence than in the general population[29,30]. A recent study estimated that Schaaf-Yang patients, who suffer from *MAGEL2* inactivation, have a rate of adrenal insufficiency of around 15%[31]. On the other hand, a previous mouse model of *Magel2* deficiency, presented with dexamethasone resistant hypercorticosteronemia in female[32]. The difference between the model from Tennese et al and ours could be explained by different mouse strains, gene inactivation strategy and concomitant deletion of *Ndn* in our case which could compensate for effects of *Magel2* loss.

An interesting finding of the study is the sexual dimorphism. Only females show adrenal insufficiency in *Ndn-KO* mice while only male have higher *Pomc* in *Ndn/Magel2-dKO* pituitary. Adrenal cortex show strong sexual dimorphism in term of function[33] and renewal[20,34,35], we can hypothesise that genetic alteration would hit male and female differently as it had been shown in *Magel2* deficient mice[32]. In the pituitary, males show higher PC1/3 levels than females and have a higher ratio of ACTH over POMC[36] which could explain why they are affected and not females. In depth studies, involving targeted disruption of *Magel2* and/or *Ndn* and sexual hormones manipulation would help decipher the causes of the observed sexual dimorphism.

PWS patients share common features with patients harbouring inactivating mutations of *PCSK1*[37] and PC1/3 protein accumulation is decreased in *Magel2* deficient mice's hypothalamus[38] or *Snord116* deficient mice stomach and pancreas[39,40]. We found no differences in mRNA coding *Pcsk1* however we can expect to see a difference in protein accumulation as had been shown in *Magel2* deficient mice's hypothalami[38] by proteomic approach. Interestingly, Chen et al. did not found any difference in PC1/3 protein in the pituitary, but these mice produced more

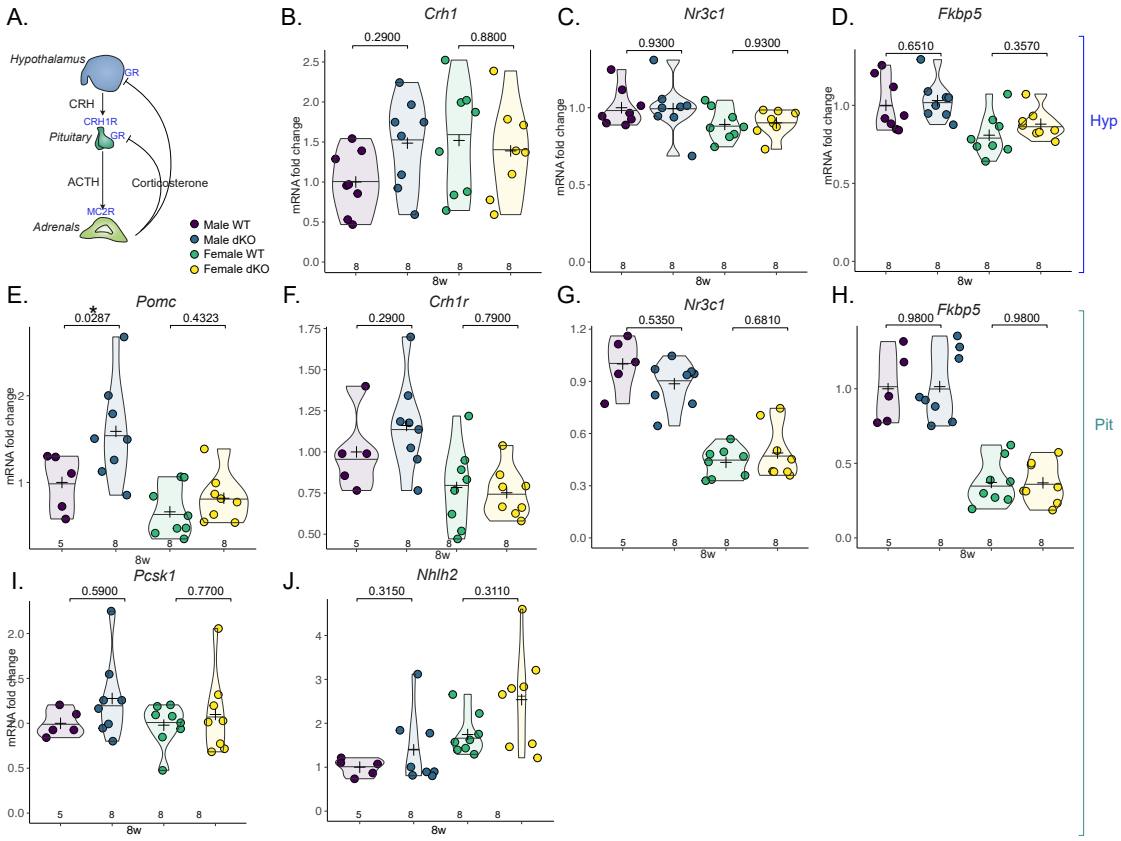

Figure 5: **NECDIN/MAGEL2 loss induces accumulation of *Pomc* in the pituitary**
A. Schematic representation of the hypothalamic-pituitary-adrenal axis
B.C.D. qPCR analyses of *Crh1* (B.), *Nr3c1* (C.) and *Fkbp5* (D.) mRNA accumulation in hypothalami from 8-week-old WT and *Magel2/Ndn-dKO*
E.-J. qPCR analyses of *Pomc* (E.), *Crh1r* (F.), *Nr3c1* (G.), *Fkbp5* (H.), *Pcsk1* (I.) and *Nhlh2* (J.) mRNA accumulation in pituitaries from 8-week-old WT and *Magel2/Ndn-dKO*

GC[32] decreasing the relevance compared to our double inactivation model.

Overall, our data shows that NECDIN and MAGEL2 could be implicated in ACTH maturation hence response to stress. These results provide a reason to explore HPA function in Prader-willi patients especially regarding ACTH to adapt treatment accordingly.

Methods

Cell culture

Adrenocortical tumour cell line 7 (ATC7) cells were established from an adrenal tumour derived from a mouse expressing the Simian Virus 40 large T (SV40 T) antigen under the control of the aldo-keto reductase 1b7 (*Akr1b7*) gene promoter specific to the adrenal cortex[41,42]. Cells were cultured on poly-D-lysine–coated 10 cm cell culture dishes (MilliporeSigma, Burlington, MA) in a DMEM-F12 medium (Thermo Fisher Scientific, Waltham, MA) at 37°C in the presence of 5% CO2, insulin (10 mg/mL), transferrin (5.5 mg/mL), selenium (6.7 ng/mL) (Thermo Fisher Scientific), L-glutamine (2 mM), penicillin 0.1 U/mL), streptomycin (0.1 mg/mL), 2.5% horse serum, and 2.5% foetal calf serum. Cells were seeded in 12-well plates and cultures to subconfluence

and then starved by replacing medium by serum-free medium the day before the addition of forskolin (Sigma-Aldrich), ACTH (Novartis, Basel, Switzerland) or insulin at the times and concentrations indicated in the figure's legends.

Mice

Mice bred in-house and maintained on a mixed sv129-C57Bl/6 genetic background were housed on a 12-hour light/12-hour dark cycle (lights on at 7:00 am). Mice were fed normal, commercial rodent chow and provided with water *ad libitum*. After weaning, mice were kept in siblings with a maximum of 4 animals per cage.

Hormonal measurements

Mice were killed by decapitation around 9 am and blood was collected in vacuum blood collection tubes (VF-053STK, Terumo). For stress response, blood was collected at 5pm from the tail, the day after mice were injected intraperitoneally with PBS at 8/30am to induce a mild stress 30 minutes prior the euthanasia. For ACTH treatments mice were injected intraperitoneally with 0.05 mg/30g Synacthene (0.25 mg/mL, Novartis, Basel, Switzerland) prior the euthanasia.

Corticosterone was measured from serum with ELISA kit (AR E-8100, LDN), ACTH was measured with Milliplex Map Kit (MPTMAG-49K, Millipore).

Histology

Organs were fixed in 4% PFA for 6 hours and embedded in paraffin. 5µm sections were deparaffinised and processed for H&E. For immunohistochemistry or immunofluorescence, deparaffinised slides were submerged in antigen retrieval buffer and microwaved for 8 minutes. After being rinsed thrice with 1X PBS, they were blocked for an hour with 2.5% horse serum (Vector) and incubated overnight at 4°C with primary antibody. After rinsing, they were incubated with ImmPRESS polymer for 30 minutes at room temperature. HRP activity was detected with NOVAred (Vector) or Alexafluor (Thermo Fisher). Primary antibodies are listed in supplementary table S1.

Images were acquired with Zeiss Axioscan Z1 or Zeiss Imager M2 and analysed with QuPath software[43].

RT-qPCR

Organs were removed, flash frozen on dry ice, and RNA was extracted using RNeasy micro kit from QIAGEN. After reverse transcription, PCR reaction was conducted using SYBR qPCR Premix Ex Taq II Tli RNase H+ (TAKRR820W, Takara). Primer pairs are listed in supplementary table S2.

scRNA-seq data resources, data metrics and pre-processing

The present study is based on the 10x scRNA-seq dataset published by Lopez et al[18].

scRNA-seq data from the regions of interest were generated using 10x Genomics Chromium. For downstream processing, cells with <1500 detected genes as well as doublets were filtered out. The data was then clustered, and cluster names were assigned based on litterature.

The final gene count matrix consisted of 27998 genes for 5375, 9197, 7221 cells for hypothalamus, pituitary and adrenal respectively and was pre-processed in R, version 4.1.0 ([44]) according to the Seurat, version 4.0.5 (https://satijalab.org/seurat) pipeline for quality control, normalisation and analysis of scRNA-seq data using the following criteria: min.Feature_RNA = 1000 maxpercent.mt = 25, minCount = 400. The gene counts were normalised and log-transformed across all cells, which allowed for statistical comparison between

cells and cell types. We performed principal component analysis and we selected the top 50 PCs as input for the UMAP dimensional reduction with 15 neighbours.

Statistics

Statistics were conducted using R language[44] and Comp3Moy function from sumo package (https://github.com/Damien-Dufour/sumo). Normality of populations distribution was assessed with Shapiro & Wilk test for n $\in$ [7,5000] or otherwise Kolmogorof- Smirnov normality test.

If data followed a normal distribution, homoscedasticity was estimated with a Barlett test. To compare two populations, unpaired, two tailed t-test was used for normally distributed data with the same variance, Mann-Whitney for non normal distributions and Welch t-test for normally distributed data but with different variances. To compare three or more distributions : one way ANOVA for normally distributed samples with pairwise multiple t.tests or Kruskal-Wallis for non normally distributed samples with planned comparisons using Dunn's tests. Stress response in figure was evaluated with paired one way ANOVA for each sex and genotype.

Crosses on the violin plots represent the mean and lines represent the median.

Ethical approval declarations

Mouse experiments were conducted according to French and European directives for the use and care of animals for research purposes and were approved by the Comité d'Éthique pour l'Expérimentation Animale en Auvergne (project agreement #21152-2019061912052883), C2EA-02, at Institut National de Recherche pour l'Agriculture, l'Alimentation et l'Environnement, Research Centre Clermont-Theix, France (C2E2A).

Data availability

All data that supports the findings of this study is provided in the article or supplementary data. Source data is provided with this paper.

Code availability

All code for data cleaning and analysis associated with the current submission is available upon request.

Supplementary information

Acknowledgements

We thank K. Ouchen, S. Plantade, and P. Mazuel for animal care, A. Dehaze and J.P. Saru for their technical assistance, and Y. Renaud for management of the bioinformatic platform.

Authors' contributions

DD and AM designed research.

Funding

This work was funded through institutional support from CNRS, INSERM, Université

Clermont-Auvergne, the French government IDEX-ISITE initiative 16-IDEX-0001 (CAP 20-25), and grants from Ministère de l'Enseignement Supérieur, de la Recherche et de l'Innovation (to DD) and Société Française d'Endocrinologie (to DD and AM)

Competing interests

The authors declare no conflict of interest.

Supplementary figures

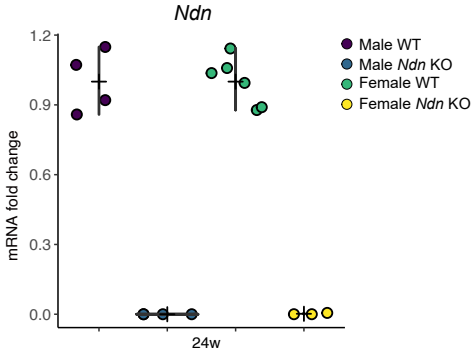

Fig.S 1: **related to Figure3**
A. qPCR analysis of *Ndn* mRNA accumulation in 24-week-old *Ndn-KO* and WT adrenals

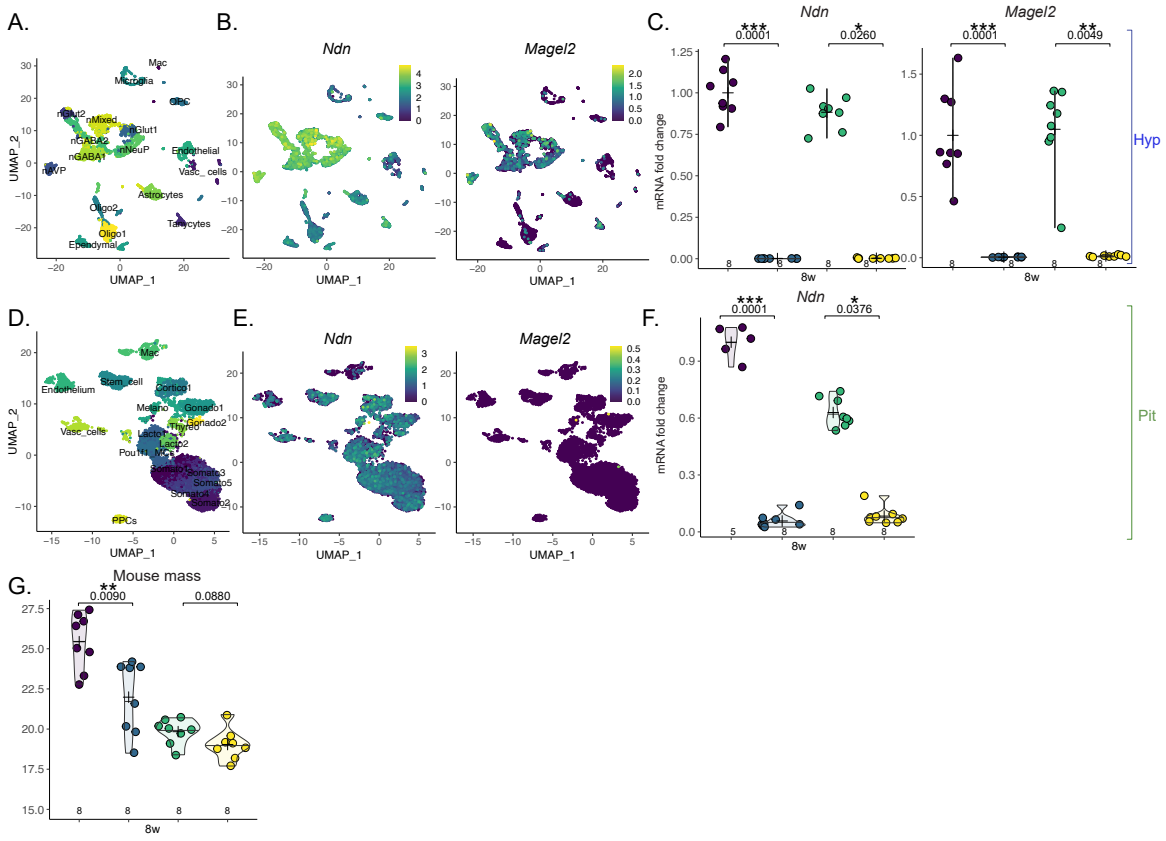

Fig.S 2: **related to Figure5**
A. Dimensional reduction (UMAP) representation of hypothalamus cells clustered by gene expression profiles and assigned to specific cell types (left)
B. UMAP representation of *Ndn* and *Magel2* normalised mRNA expression per cell of the hypothalamus
C. qPCR analysis of *Ndn* and *Magel2* mRNA accumulation in 8-week-old WT and dKO hypothalami
D. Dimensional reduction (UMAP) representation of pituitary cells clustered by gene expression profiles and assigned to specific cell types (left)
E. UMAP representation of *Ndn* and *Magel2* normalised mRNA expression per cell of the pituitary
F. qPCR analysis of *Ndn* mRNA accumulation in 8-week-old WT and dKO pituitaries
G. WT and *Ndn/Magel2-dKO* body mass at 8 weeks of age
Mac : Macrophages; OPC : oligodendrocyte progenitor cells;nGLUT : Glutamatergic neurones; nGABA : GABAergic neurons; nNeuP : Neuropetides neurones; nAVP : vasopressin neurons; nMixed : mixed neurons; Vasc cells : vascular cells; Melano : melanotrophs; cortico : corticotrophs; lacto : lactotrophs; somato : somatotrophs; Pou1f1 MCs : Pou1f1 mixed cells; thyreo : threotrophs; PPCs : posterior pituitary cells.

References

1. Cawley, N. X., Li, Z. & Loh, Y. P. 60 YEARS OF POMC: Biosynthesis, trafficking, and secretion of pro-opiomelanocortin-derived peptides. *Journal of Molecular Endocrinology* **56**, T77–T97 (2016).
2. Walker, J. J. *et al.* The Origin of Glucocorticoid Hormone Oscillations. *PLoS Biol* **10**, e1001341 (2012).
3. Walker, J. J., Terry, J. R. & Lightman, S. L. Origin of ultradian pulsatility in the hypothalamic–pituitary–adrenal axis. *Proc. R. Soc. B.* **277**, 1627–1633 (2010).
4. Dufour, D. *et al. Loss of SUMO-specific protease 2 causes isolated glucocorticoid deficiency by blocking zonal transdifferentiation.* http://biorxiv.org/lookup/doi/10.1101/2022.02.08.479354 (2022) doi:10.1101/2022.02.08.479354.
5. Liang, Q. *et al.* SENP2 Suppresses Necdin Expression to Promote Brown Adipocyte Differentiation. *Cell Reports* **28**, 2004–2011.e4 (2019).
6. Yoshikawa, K. Necdin: A purposive integrator of molecular interaction networks for mammalian neuron vitality. *Genes Cells* **26**, 641–683 (2021).
7. Moscogiuri, G. *et al.* Prader- Willi syndrome: An uptodate on endocrine and metabolic complications. *Rev Endocr Metab Disord* **20**, 239–250 (2019).
8. Connell, N. A., Paterson, W. F., Wallace, A. M. & Donaldson, M. D. Adrenal function and mortality in children and adolescents with Prader-Willi syndrome attending a single centre from 1991-2009: Letter to the Editor. *Clinical Endocrinology* **73**, 686–688 (2010).
9. Corrias, A. *et al.* Assessment of central adrenal insufficiency in children and adolescents with Prader-Willi syndrome: ACTH test in paediatric Prader-Willi syndrome. *Clin Endocrinol* **76**, 843–850 (2012).
10. de Lind van Wijngaarden, R. F. A. *et al.* High Prevalence of Central Adrenal Insufficiency in Patients with Prader-Willi Syndrome. *The Journal of Clinical Endocrinology & Metabolism* **93**, 1649–1654 (2008).
11. Grugni, G. *et al.* Central adrenal insufficiency in young adults with Prader-Willi Syndrome. *Clin Endocrinol* **79**, 371–378 (2013).
12. Stevenson, D. A. *et al.* Unexpected death and critical illness in Prader-Willi syndrome: Report of ten individuals. *Am. J. Med. Genet.* **124A**, 158–164 (2004).
13. Farholt, S., Sode-Carlsen, R., Christiansen, J. S., Østergaard, J. R. & Høybye, C. Normal Cortisol Response to High-Dose Synacthen and Insulin Tolerance Test in Children and Adults with Prader-Willi Syndrome. *The Journal of Clinical Endocrinology & Metabolism* **96**, E173–E180 (2011).
14. Nyunt, O. *et al.* Normal Cortisol Response on Low-Dose Synacthen (1 Mg) Test in Children with Prader Willi Syndrome. *The Journal of Clinical Endocrinology & Metabolism* **95**, E464–E467 (2010).
15. Muscatelli, F. Disruption of the mouse Necdin gene results in hypothalamic and behavioral alterations reminiscent of the human Prader-Willi syndrome. *Human Molecular Genetics* **9**, 3101–3110 (2000).
16. Schaller, F. *et al.* A single postnatal injection of oxytocin rescues the lethal feeding behaviour in mouse newborns deficient for the imprinted Magel2 gene. *Human Molecular Genetics* **19**, 4895–4905 (2010).
17. Freedman, B. D. *et al.* Adrenocortical Zonation Results from Lineage Conversion of Differentiated Zona Glomerulosa Cells. *Developmental Cell* **26**, 666–673 (2013).
18. Lopez, J. P. *et al.* Single-cell molecular profiling of all three components of the HPA axis reveals adrenal ABCB1 as a regulator of stress adaptation. *Sci. Adv.* **7**, eabe4497 (2021).
19. Berthon, A. *et al.* Constitutive β-catenin activation induces adrenal hyperplasia and promotes adrenal cancer development. *Human Molecular Genetics* **19**, 1561–1576 (2010).
20. Dumontet, T. *et al.* PKA signaling drives reticularis differentiation and sexually dimorphic adrenal cortex renewal. *JCI Insight* **3**, (2018).

21. Cypess, A. M. *et al.* Insulin/IGF-I Regulation of Necdin and Brown Adipocyte Differentiation Via CREB- and FoxO1-Associated Pathways. *Endocrinology* **152**, 3680–3689 (2011).

22. Bischof, J. M., Stewart, C. L. & Wevrick, R. Inactivation of the mouse Magel2 gene results in growth abnormalities similar to Prader-Willi syndrome. *Human Molecular Genetics* **16**, 2713–2719 (2007).

23. Lee, S. Expression and imprinting of MAGEL2 suggest a role in Prader-Willi syndrome and the homologous murine imprinting phenotype. *Human Molecular Genetics* **9**, 1813–1819 (2000).

24. Schaaf, C. P. *et al.* Truncating mutations of MAGEL2 cause Prader-Willi phenotypes and autism. *Nat Genet* **45**, 1405–1408 (2013).

25. Scharf, S. H., Liebl, C., Binder, E. B., Schmidt, M. V. & Müller, M. B. Expression and Regulation of the Fkbp5 Gene in the Adult Mouse Brain. *PLoS ONE* **6**, e16883 (2011).

26. Tseng, Y.-H. *et al.* Prediction of preadipocyte differentiation by gene expression reveals role of insulin receptor substrates and necdin. *Nat Cell Biol* **7**, 601–611 (2005).

27. Matsuno, A., Okazaki, R., Oki, Y. & Nagashima, T. Secretion of high-molecular-weight adrenocorticotropic hormone from a pituitary adenoma in a patient without Cushing stigmata: Case report. *Journal of Neurosurgery* **101**, 874–877 (2004).

28. Rosenberg, A. G. W. *et al.* Central Adrenal Insufficiency Is Rare in Adults With Prader–Willi Syndrome. *The Journal of Clinical Endocrinology & Metabolism* **105**, e2563–e2571 (2020).

29. Arlt, W. & Allolio, B. Adrenal insufficiency. *The Lancet* **361**, 1881–1893 (2003).

30. Patti, G. *et al.* Central adrenal insufficiency in children and adolescents. *Best Practice & Research Clinical Endocrinology & Metabolism* **32**, 425–444 (2018).

31. Halloun, R. *et al.* Expanding the spectrum of endocrinopathies identified in Schaaf-Yang syndrome - A case report and review of the literature. *European Journal of Medical Genetics* **64**, 104252 (2021).

32. Tennese, A. A. & Wevrick, R. Impaired Hypothalamic Regulation of Endocrine Function and Delayed Counterregulatory Response to Hypoglycemia in Magel2-Null Mice. *Endocrinology* **152**, 967–978 (2011).

33. Bielohuby, M. *et al.* Growth analysis of the mouse adrenal gland from weaning to adulthood: Time- and gender-dependent alterations of cell size and number in the cortical compartment. *American Journal of Physiology-Endocrinology and Metabolism* **293**, E139–E146 (2007).

34. Grabek, A. *et al.* The Adult Adrenal Cortex Undergoes Rapid Tissue Renewal in a Sex-Specific Manner. *Cell Stem Cell* **25**, 290–296.e2 (2019).

35. Levasseur, A., Dumontet, T. & Martinez, A. 'Sexual dimorphism in adrenal gland development and tumorigenesis'. *Current Opinion in Endocrine and Metabolic Research* **8**, 60–65 (2019).

36. Shakya, M. *et al.* Mice lacking PC1/3 expression in POMC-expressing cells do not develop obesity. *Endocrinology* bqab055 (2021) doi:10.1210/endocr/bqab055.

37. Polex-Wolf, J., Yeo, G. S. H. & O'Rahilly, S. Impaired prohormone processing: A grand unified theory for features of Prader-Willi syndrome? *Journal of Clinical Investigation* **127**, 98–99 (2016).

38. Chen, H. *et al.* Loss of MAGEL2 in Prader-Willi syndrome leads to decreased secretory granule and neuropeptide production. *JCI Insight* **5**, (2020).

39. Burnett, L. C. *et al.* Deficiency in prohormone convertase PC1 impairs prohormone processing in Prader-Willi syndrome. https://www.jci.org/articles/view/88648/figure/2 (2017) doi:10.1172/JCI88648.

40. Chen, H. *et al.* Modification of cardiac transcription factor Gata6 by SUMO. *Biochimie* **170**, 212–218 (2020).

41. Batisse-Lignier, M. *et al.* P53/Rb inhibition induces metastatic adrenocortical carcinomas in a preclinical transgenic model. *Oncogene* **36**, 4445–4456 (2017).

42. Ragazzon, B. *et al.* Adrenocorticotropin-Dependent Changes in SF-1/DAX-1 Ratio Influence Steroidogenic Genes Expression in a Novel Model of Glucocorticoid-Producing Adrenocortical Cell Lines Derived from Targeted Tumorigenesis. *Endocrinology* **147**, 1805–1818 (2006).

43. Bankhead, P. *et al.* QuPath: Open source software for digital pathology image analysis. *Sci Rep* **7**, 16878 (2017).

44. R Core Team. *R: A language and environment for statistical computing.* (R Foundation for Statistical Computing, 2018).

DISCUSSION ET PERSPECTIVES

11.1 Effets de la perte de SENP2 sur le cortex surrénalien

Les donnés précédentes de l'équipe ont démontré l'existence d'un profil de SUMOylation singulier dans la glande surrénale murine et humaine avec une SUMOylation inversement corrélée au flux de la différenciation cellulaire corticale et négativement contrôlée par l'ACTH *via* la signalisation PKA. Mon projet de thèse a eu pour objectif de tester l'hypothèse d'un rôle majeur de cette modification post-traductionnelle dans l'homéostasie surrénalienne et la réponse au stress en explorant les conséquences de l'inactivation corticale de SENP2, la seule SUMO protéase dont l'expression est contrôlée par l'ACTH. La perte de SENP2 dans la corticosurrénale aboutit aux conséquences suivantes :

- un accroissement du niveau de SUMOylation limité à certains acteurs ou compartiments cellulaires sans sans hyperSUMOylation générale
- une atrophie du cortex associée à un déficit isolé en glucocorticoïdes
- un blocage de la réponse à l'ACTH ciblant probablement directement les sous unités catalytiques de la PKA
- un arrêt progressif de la différenciation de la zG en zF
- une apoptose prématurée des cellules fasciculées néoformées qui est associée à un déficit de phosphorylation de la protéine mitochondriale DRP1
- une accumulation nucléaire ectopique de la β-caténine associée à son hyperSUMOylation et à une activation modérée de la signalisation WNT canonique

11.1.1 SENP2 absent mais une SUMOylation intacte

L'un des résultats inattendus de la perte de SENP2 dans le cortex est l'absence de modification de la SUMOylation générale (Article 1 Figure S1.). En effet, la

recombinaison du même allèle conditionnel *Senp2*^{flox} induit une hypoSUMOylation dans le cerveau (Qi et al., 2014) et le tissu adipeux blanc (Zheng et al., 2018). Cette "incohérence" pourrait avoir plusieurs causes :

- La cellularité : le transgène *Sf1-cre* permet la recombinaison uniquement dans les cellules stéroïdogènes qui ne représentent qu'une partie des cellules de la glande.
- Les niveaux d'expression relatifs des autres SUMO protéases : les transcrits de SENP1 et SENP3 sont plus abondants que ceux de SENP2 dans la surrénale en condition basale (Figure 23) et s'accumulent (Figure 41) suite à la délétion de SENP2; on peut donc s'attendre à un phénomène de compensation.
- L'émergence d'une zone non recombinée compensant la perte de la zone fasciculée mutante : de nombreuses cellules échappent à la recombinaison dépendante du transgène *Sf1-cre* et sont donc fortement exposées à l'ACTH qui exerce un effet déSUMOylant dans le cortex surrénalien (Dumontet et al., 2019)
- La représentation des protéines SUMOylées : la détection des SUMOs conjugués par western blot ne révèle qu'un nombre réduit de protéines, cells qui sont majoritaires et/ou le plus fortement SUMOylées. Il est possible que ces protéines ne soient pas des cibles privilégiées de SENP2 dans la surrénale

Enfin, bien que la SUMOylation générale ne paraisse pas affectée, certains substrats spécifiques sont hyperSUMOylés. En effet, les analyses en *Proximity Ligation Assay* révèlent une hyperSUMOylation de SF-1 (Figure 46), Cα (Figure 42) et β-caténine (Article 1 Figure 7).

Ce constat illustre bien la difficulté à appréhender les effets biologiques de la SUMOylation qui a été associé à un blocage de la différenciation (Cossec et al., 2018) et à une répression transcriptionnelle (Girdwood et al., 2004). Cependant, au vu de la multitude de substrats et d'effets, les expérimentations *in vivo* montrent qu'il est difficile d'associer un état de SUMOylation global à un état transcriptionnel ou phénotypique. En effet la SUMOylation peut exercer un effet répresseur ou activateur selon le facteur de transcription (Chymkowitch et al., 2015). La perte de l'E3 ligase TRIM28 dans

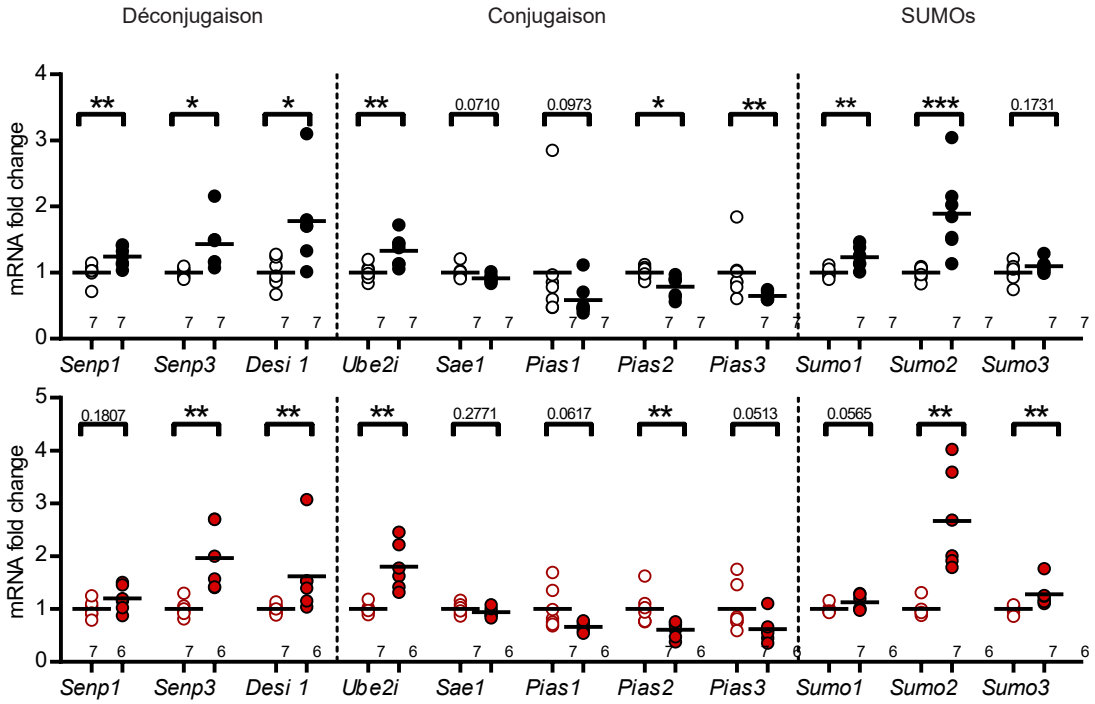

Figure 41: RT-qPCR mesurant l'expression des transcrits codant les différents enzymes de SUMOylation et déSUMOylation ainsi que les peptides SUMO dans des surrénales sauvages et *Senp2*^{cKO} de 4 semaines

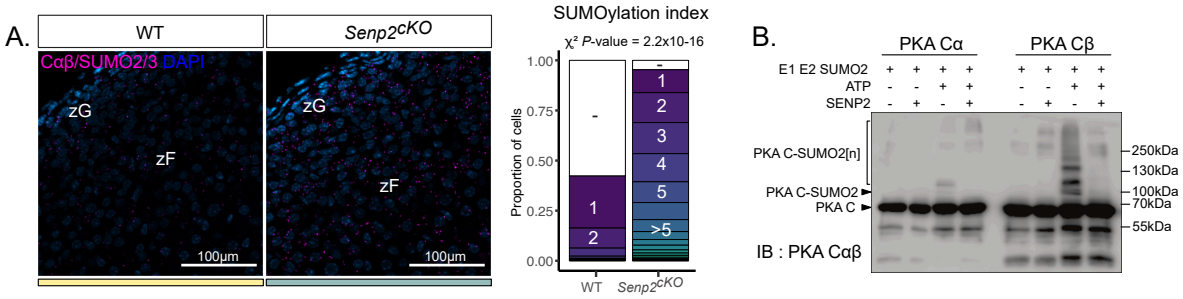

Figure 42: ***Proximity ligation assay* révélant la SUMOylation de Cα dans des surrénales sauvages et *Senp2*^{cKO} de 4 semaines** L'histogramme représente la proportion de cellules ne contenant aucun *focus*, 1, 2, 3, 4, 5 ou plus de 5 *foci* Cα/SUMO2/3 dans les cortex de souris WT ou *Senp2*^{cKO}

l'ovaire (*Sf1-cre::Trim28*$^{fl/fl}$), provoque une hypoSUMOylation générale mais l'analyse chromatinienne montre que les modules SUMOs sont redistribués et l'expression des gènes ciblés corrèle faiblement avec le niveau de SUMOylation (Rossitto et al., 2022). De façon analogue, les protéines SUMOylées sont redistribués au niveau de la chromatine lors de l'adipogénèse mais ne corrèlent pas systématiquement avec une répression ou une activation de la transcription au niveau de ces *loci* (Zhao et al., 2022).

Ainsi, au delà des niveaux de SUMOylation générale, il faut considérer les variations de SUMOylation à l'échelle des protéines ou des groupes de protéines (Ali et al., 2021; Shyu

et al., 2022). Le meilleur moyen d'avoir une représentation fidèle de la SUMOylation générale d'un organe est de réaliser une immuno-précipitation avec lyse partielle suivie de chromatographie associée à la spectrométrie de masse, ce qui permet de recenser de façon quantitative et qualitative les sites naturels de SUMO2/3-ylation (Hendriks et al., 2018). Dans le cas de la détermination du SUMOylome de la surrénale, il pourra être enrichi en SUMO-conjugués propre au cortex grâce à une approche génétique permettant d'étiqueter les différents SUMOs (*CAG-loxP-STOP-loxP-SUMO*) sous le contrôle de *Sf1-cre* (Yang et al., 2014). Cette approche pourra s'appliquer à l'étude du SUMOylome lors d'un stress, ou de conditions affectant l'homéostasie corticale comme la perte de SENP2.

11.1.2 Le contrôle de la SUMOylation est garant de la différenciation tissulaire

Les variations de SUMOylation sont associées à des impacts positifs ou négatifs sur la différenciation. Dans le cortex surrénalien, l'hyperSUMOylation spécifique induite parl'inactivation de SENP2 provoque un blocage de la conversion de l'identité cellulaire glomérulée vers fasciculée (Article 1 Figure 4). Cependant, une hyperSUMOylation consécutive à la perte d'une autre SUMO protéase pourrait avoir un effet différent en hyperSUMOylant d'autres cibles. A l'inverse, les hypoSUMOylations attendues suite à la perte de d'UBC9 ou de TRIM28 n'aboutiront pas forcément à une différenciation excessive de la zone fasciculée comme c'est le cas lors de l'activation constitutive de la PKA où la zone glomérulée disparaît au profit d'une zone fasciculée hyperplasique (Dumontet et al., 2018; Sahut-Barnola et al., 2010). C'est pourquoi il serait important d'étudier l'effet de la SUMOylation en affectant différents acteurs de la voie, à différents temps et dans différentes populations cellulaires. Par exemple, l'importance de contrôler la SUMOylation dans l'homéostasie des progéniteurs capsulaires pourrait être testée grâce à des souris *Gli-Cre^{ERT2}::Senp2$^{fl/fl}$* ou *Gli-Cre^{ERT2}::Ubc9$^{fl/fl}$*.

Nos expériences préliminaires suggèrent que limiter pharmacologiquement la SUMOylation permet d'amoindrir les effets de l'inactivation de SENP2 dans la surrénale. En effet, un traitement de 5 semaines des souris par TAK-981, inhibiteur

pharmacologique de SAE1 (Langston et al., 2021) (7.5 mg/kg I.P. 2x/semaine) réduit sensiblement le déficit de réponse à l'ACTH des souris *Senp2*^{cKO} et potentialise cette réponse chez les souris sauvages (Figure 43.A.B.C). Par ailleurs, ces souris ont un léger déficit pondéral dû à une diminution de la masse du tissu adipeux inguinal et de la taille des adipocytes (Figure 43.D.E.F.) en accord avec le rôle capital de la SUMOylation dans l'adipogénèse [78].

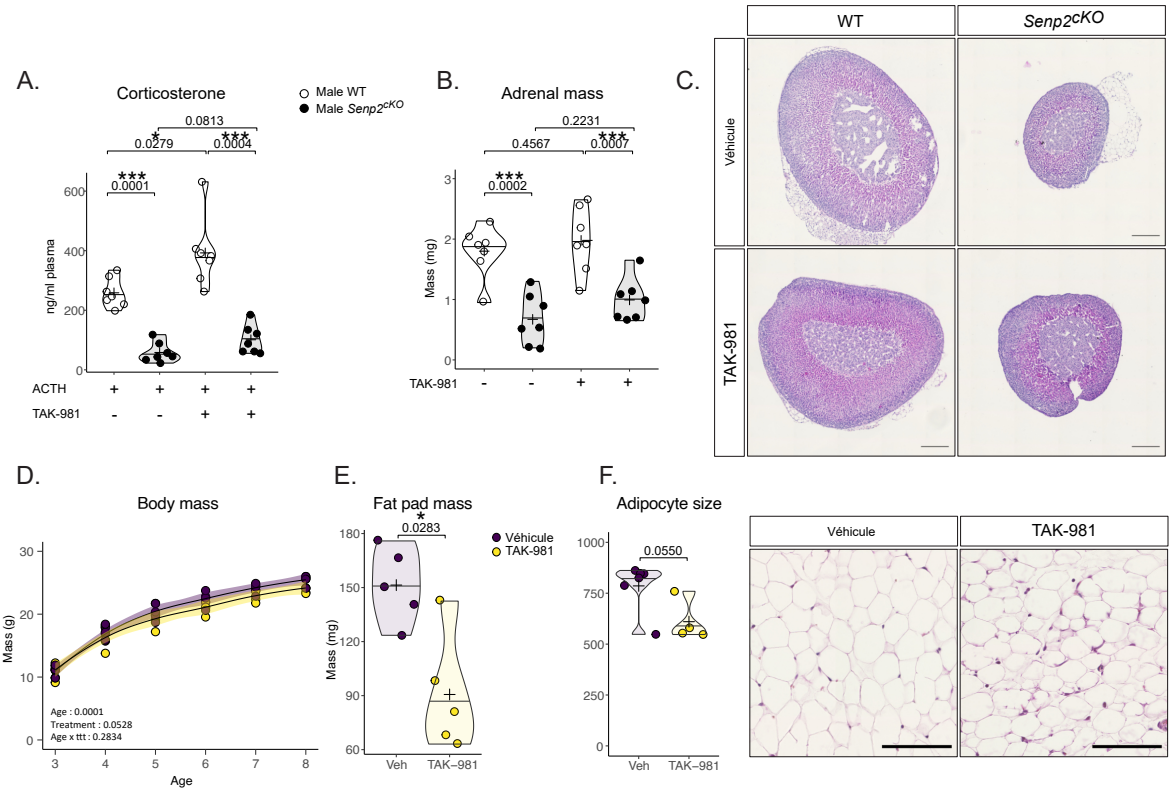

Figure 43: **Effet de l'inhibition pharmacologique de la SUMOylation sur la surrénale et le tissu adipeux**
A. Concentrations de corticostérone dans le plasma des souris sauvages et *Senp2*^{cKO} de 8 semaines traitées au TAK-981 5 semaines et à l'ACTH 30 minutes avant le sacrifice, déterminée par ELISA
B. Masse des surrénales des souris sauvages et *Senp2*^{cKO} de 8 semaines traitées au TAK-981
C. Coloration éosine héamtoxyline des surrénales sauvages et *Senp2*^{cKO} de 8 semaines traitées au TAK-981 5 semaines
D. Evolution de la masse des souris au cours du traitement au TAK-981
E. Masse des dépots de tissu adipeux inguinal après 5 semaines de traitement TAK-981
F. Coloration au trichrome de masson du tissu adipeux inguinal après 5 semaines de traitement TAK-981

En plus de la surrénale, le transgène *Sf1-cre* cible également les cellules somatiques des gonades et les cellules gonadotropes de l'hypophyse (Figure 44.G.H.). Compte tenu de l'impact de la modulation de la SUMOylation dans les cellules somatiques des gonades [79], il sera important d'explorer les effets de la perte de SENP2 dans ces tissus. Nos analyses préliminaires révèlent une hypoplasie des gonades mâles et femelles (Figure 44.D.E.),

[78] voir paragraphe 5.3 - Tissu adipeux
[79] voir paragraphe 5.4 - Gonades

une chute de la FSH chez les mâles et une élévation de la LH chez les femelles (Figure 44.A.B.C.) signant une atteinte de l'axe hypothalamo-pituitaire-gonadique sans atteinte évidente de l'hypophyse (Figure 44.G.H.). En effet, les souris *Senp2*^{cKO} femelles sont hypofertiles et ne présentent pas de corps jaunes (Figure 44.E.F.). En effet, les altérations gonadiques des souris *Senp2*^{cKO} pourront être comparées aux effets de l'inactivation de TRIM28 (Rossitto et al., 2022) et de R1α afin de mieux comprendre les interactions entre SUMOylation et signalisation AMPc/PKA dans ces organes. Ce travail soutenu par une ANR2021 *Ovary Protect* fera l'objet du projet de thèse de Florian Chaleil.

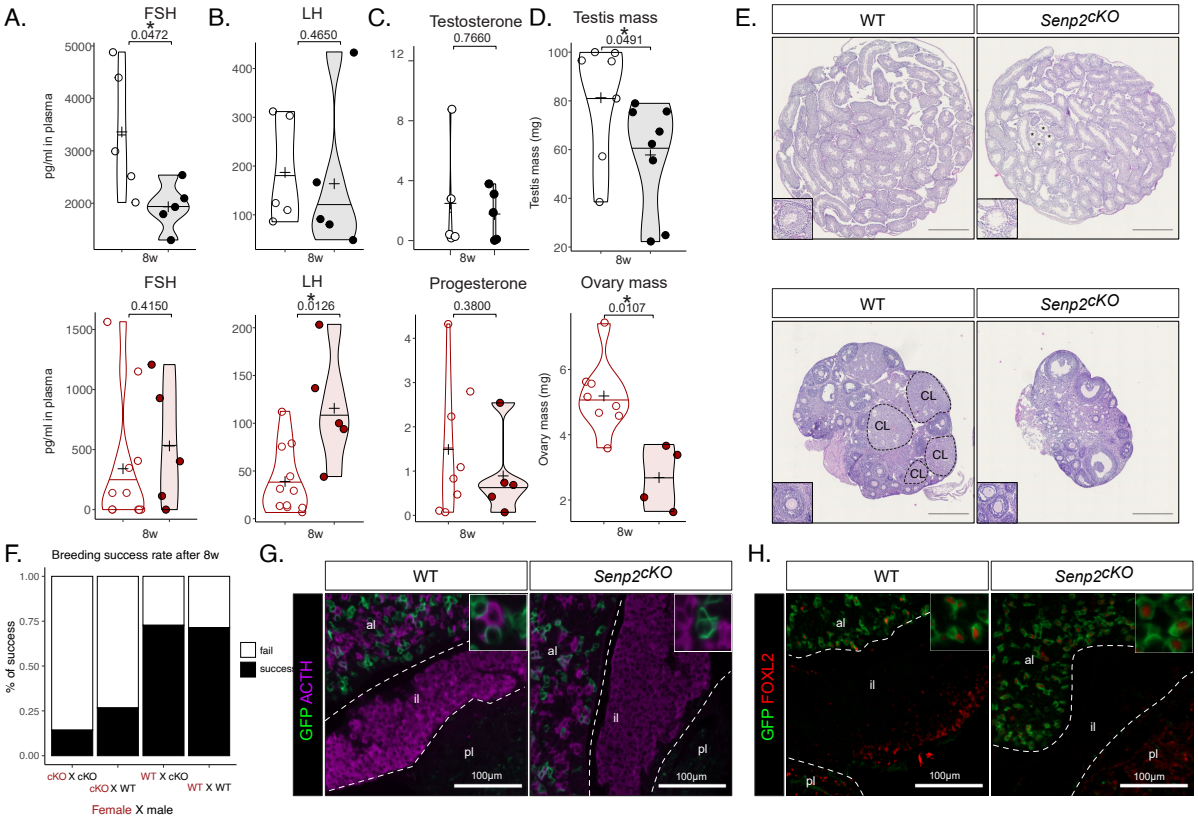

Figure 44: **Effet de la perte de SENP2 dans les cellules de lignage SF-1 sur l'axe hypothalamo-pituitaire-gonadique**
A. Dosage plasmatique des niveaux de FSH chez des souris sauvages et *Senp2*^{cKO} de 8 semaines, déterminé par ELISA
B. Dosage plasmatique des niveaux de LH chez des souris sauvages et *Senp2*^{cKO} de 8 semaines, déterminé par ELISA
C. Dosage plasmatique des niveaux de testostérone (mâle) et de progestérone (femelle) chez des souris sauvages et *Senp2*^{cKO} de 8 semaines, déterminé par LC-MS/MS
D. Masse des gonades sauvages et *Senp2*^{cKO} de 8 semaines
E. Coloration éosine héamtoxyline des gonades sauvages et *Senp2*^{cKO} de 8 semaines
F. Succès reproductif après 8 semaines des croisements de souris commencés dès 5 semaines
G. Co-immuno fluorescence de GFP (lignage SF-1 ciblé par la perte de SENP2) et ACTH (cellules corticotropes) dans l'hypophyse de souris sauvages et *Senp2*^{cKO} de 4 semaines
H. Co-immuno fluorescence de GFP (lignage SF-1 ciblé par la perte de SENP2) et FOXL2 (cellules gonadotropes) dans l'hypophyse de souris sauvages et *Senp2*^{cKO} de 4 semaines
al : lobe antérieur; il : lobe intermédiaire; pl : lobe postérieur; * : tubules présentant des vacuoles; CL : *Corpus Luteum*

11.1.3 La perte de SENP2 inhibe la réponse à l'ACTH

Suite à un traitement aigu à l'ACTH, les phosphorylations de CREB, TRIM28 et DRP1 dans la surrénale ainsi que les concentrations plasmatiques de corticostérone sont moins importantes chez les *Senp2*^{cKO} que les chez les sauvages (article 1 Figure 3). De plus, les souris mutantes présentent une forte hypoplasie de la glande similaire à celle causée par la perte de signalisation ACTH (MC2R$^{-/-}$ ou MRAP$^{-/-}$) (Chida et al., 2007; Novoselova et al., 2018). De manière importante, l'hypoplasie des *Senp2*^{cKo} n'est pas compensée par l'activation génétique constitutive de la PKA (*Sf1-cre::Senp2*$^{fl/fl}$*::Prkar1a*$^{fl/fl}$). La SUMOylation semble donc agir en amont des substrats de la phosphorylation et en aval de la sous unité régulatrice de la PKA donc probablement sur les sous unité catalytiques elles-mêmes. L'hypothèse la plus probable est que Cα et/ou Cβ sont SUMOylées et que cette SUMOylation affecte leur activité enzymatique.

Cette hypothèse est corroborée par la présence d'un site de SUMOylation consensus conservé sur la lysine 169 de Cα et Cβ contenue dans le domaine catalytique (Figure 45). L'analyse par PLA révèle un marquage important entre Cα et SUMO2/3 qui est enrichi chez les mutants (Figure 42) ce qui suggère fortement une SUMOylation accrue de Cα qui devra être confirmée par des approches d'immuno-précipitation.

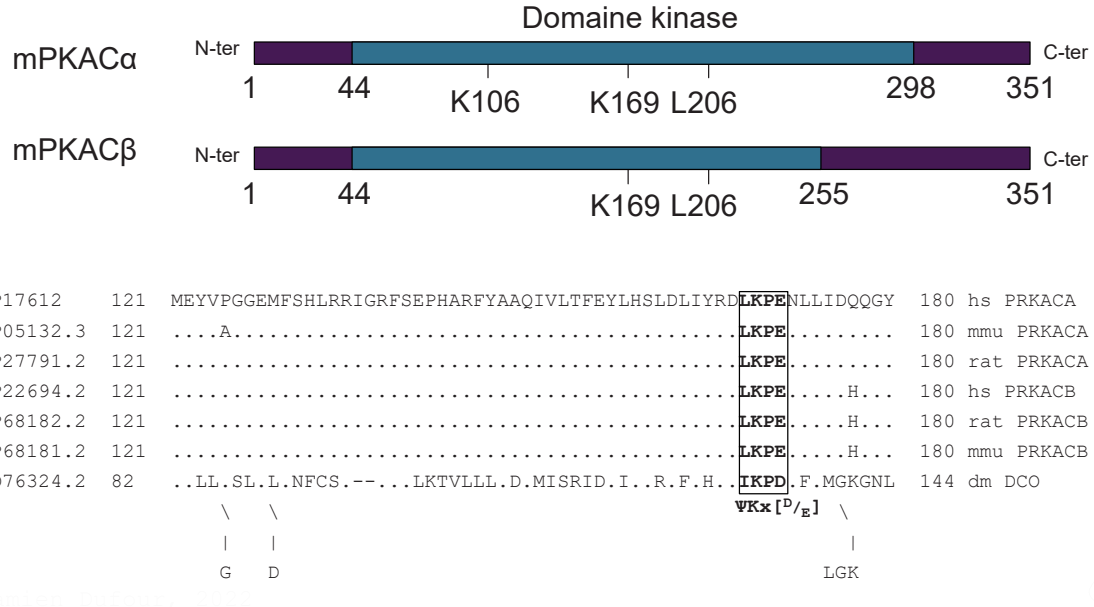

Figure 45: **Structure et alignements des sous unités catalytiques de la PKA Cαet Cβ**

Il sera alors intéressant d'explorer l'impact de la SUMOylation des sous-unités catalytiques sur leur activité kinase mais aussi sur leur localisation subcellulaire, leur stabilité et leur capacité à reconnaître les sous unité régulatrices. Cette SUMOylation pourra être modulée par l'ajout de la machinerie de SUMOylation ou de déSUMOylation *in vitro* ou par transfection cellulaire ainsi que par l'introduction d'une arginine en place de la lysine ($C\alpha^{K169R}$). L'impact de la SUMOylation sur l'activité du mutant naturel de $C\alpha^{L206R}$ qui n'est plus régulée par les sous unités régulatrices (Calebiro et al., 2014) et est responsable de syndromes de Cushing surrénaliens sera également instructive et potentiellement pourrait constituer une cible thérapeutique basée sur des activateurs de la SUMOylation (Bernstock et al., 2018).

11.1.4 La β-caténine, une stabilisation indépendante de son rôle oncogénique

La β-caténine est une protéine clé dans l'homéostasie surrénalienne mais exerce aussi un rôle oncogénique majeur dans l'étiologie des cancers corticosurrénaliens (Wilmouth et al., 2019). Ainsi, il est surprenant de retrouver une accumulation nucléaire ectopique de la β-caténine (Article 1 Figure 7) dans les surrénales $Senp2^{cKO}$ non oncogénique alors que la délétion de l'exon 3 de *Ctnnb1* induit une forte hyperplasie et une expansion glomérulée (Berthon et al., 2010; Pignatti et al., 2020).

Cette absence d'effet oncogénique pourrait être due à la forte induction de l'apoptose qui en éliminant les cellules (Article 1 Figure 5) pourrait empêcher l'acquisition d'un phénotype tumoral. Alternativement, la SUMOylation de co-facteurs transcriptionnels de la β-caténine pourraient empêcher l'activation de programmes tumorigènes. L'exploration des effets de la SUMOylation de la β-caténine *in cellulo* pourrait permettre de mieux comprendre les mécanismes de bascule entre différenciation et effets oncogéniques. Notamment, l'utilisation de mutants K29R non SUMOylables, de protéines de fusion CTNNB1-SUMO, de β-caténine non dégradable ($Catnb1^{lox(ex3)}$) permettront de comprendre comment la SUMOylation régule sa translocation nucléaire et les différents programmes cellulaire.

Une explication possible de l'effet non oncogénique de cette modification de la β-caténine pourriat mettre en jeu sa capacité à se complexer avec SF-1. Ce complexe β-caténine/SF-1 est recruté au niveau de "super activateurs" sur la chromatine des cellules du cortex surrénalien pour induire l'expression de gènes de différenciation et nécessite l'action de EZH2 pour être maintenu à la chromatine (Mohan et al., 2022). EZH2 et les protéines du PRC2 (Polycomb Repressive Complex 2) (Riising et al., 2008), SF-1 (Chen et al., 2004; Komatsu et al., 2004) et la β-caténine (Huang et al., 2015; Karami et al., 2017) étant SUMOylables, on peut imaginer que leur capacité à interagir est altérée par la perte de SENP2. Des expériences de PLA et d'immuno-précipitation permettront de déterminer le statut de ces complexes dans les surrénales *Senp2*^{cKO}.

11.1.5 Quel rôle de la SUMOylation de SF-1 dans le phénotype des surrénales *Senp2*^{cKO}?

SF-1 est l'une des protéines centrales contrôlant le développement et la fonction du cortex surrénalien et la restriction de sa SUMOylation aboutit à des effets intriguant [80]. L'atteinte générale de la mutation *Sf1*$^{2KR/2KR}$ ne permet pas de déterminer si les effets observés sont dus à une reprogrammation des cellules, une dédifférenciation ou encore un défaut de ségrégation des ébauches surrénaliennes et gonadiques, phénomène qui a déjà été décrit pour un petit nombre de cellules ayant une identité surrénalienne dans le testicule (Val et al., 2006).

Dans les surrénales, les expériences de PLA révèlent une SUMOylation de SF-1 relativement faible (Figure 46). en accord avec les expériences d'immuno-précipitation qui révèlent également une faible représentation des espèces SF-1 SUMOylées [81] (Lee et al., 2011). Suite à la perte de *Senp2*, la SUMO1-ylation de SF-1 est très légèrement

[80] voir paragraphe 6 - La SUMOylation de SF-1 gardienne de l'identité surrénalienne

[81] Cette faible représentation ne signifie pas forcément faible impact. Le paradoxe de la SUMOylation est qu'une très faible représentation des protéines SUMOylées par rapport aux formes natives aboutit à des impacts majeurs (Hay, 2005). Bien que cela pourrait être dû à des problèmes techniques ou une activité des déSUMOylases particulièrement importante, le concept de SUMOylation de groupe permettrait d'expliquer ce paradoxe apparent (Jentsch and Psakhye, 2013). Le principe est que les E3 SUMO ligases cibleraient un groupe de protéines localement permettant de favoriser leur interaction *via* les SIMs, la SUMOylation agirait alors comme une sorte de colle entre ces protéines sans affecter les autres copies de ces protéines

augmentée, sans cependant affecter son expression tandis qu'à l'inverse, les gènes surexprimés dans le modèle $Sf1^{2KR/2KR}$, dit "SUMO sensibles", le sont également dans les surrénales $Senp2^{cKO}$ (Figure 46) ce qui serait plutôt en faveur d'une déSUMOylation de SF-1. Il semble donc peu probable que cette variation de SUMOylation se traduise par un effet important sur l'activité de SF-1 dans ce contexte.

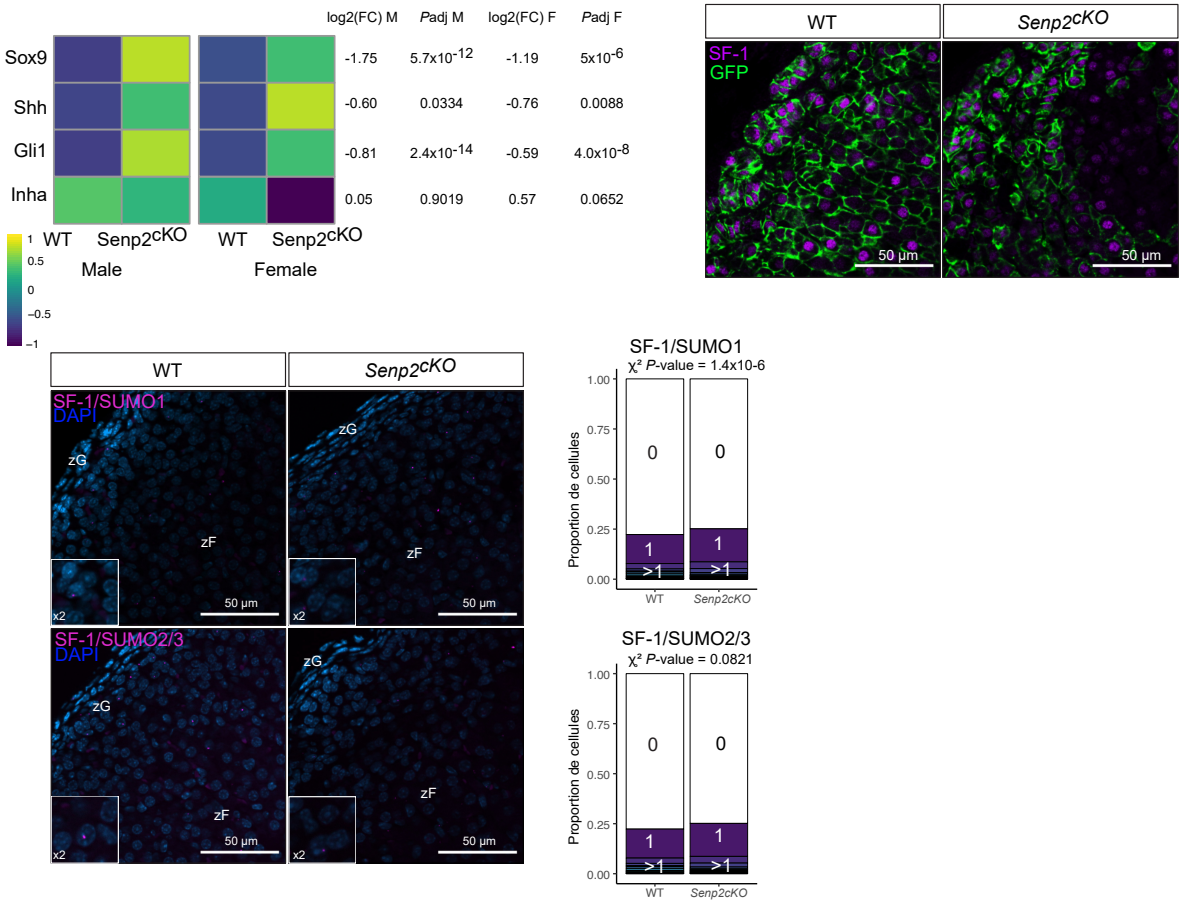

Figure 46: **Effet de la perte de SENP2 dans les surrénales sur la SUMOylation de SF-1**
Heatmap représentant l'expression des gènes "SUMO sensibles" dans les surrénales sauvages et $Senp2^{cKO}$ de 4 semaines
Co-immuno fluorescence de SF-1 et GFP dans des surrénales sauvages et $Senp2^{cKO}$ de 4 semaines
PLA entre SF-1 et SUMO1 (haut) ou SUMO2/3 (bas)

11.1.6 La mitochondrie dans les organes stéroïdogènes

La mitochondrie est un organite nécessaire à de nombreuses fonctions de la cellule incluant la stéroïdogénèse et l'apoptose. Plutôt que de simples organites dérivant dans le cytoplasme, elle s'organisent en un véritable réseau dont la réticulation dépend de l'équilibre entre fusion et fission mitochondriales. Dans le cortex surrénalien, les

mitochondries de la zone fasciculée sont beaucoup plus larges que dans la glomérulée (Farkash et al., 1986). Il est donc pertinent d'étudier la dynamique du réseau mitochondrial par rapport à l'apoptose mais également à la stéroïdogénèse.

Dans les cellules corticosurrénaliennes ATC7, DRP1 est un médiateur important de l'apoptose induite par la staurosporine (Article 1 Figure S5). Néanmoins, cet effet est inhibé par l'activation de la signalisation PKA et est corrélée avec sa phosphorylation sur la sérine 637 (Article 1 Figure 5).

Etant donné que la fonction et la localisation de DRP1 sont également régulées par sa SUMOylation, il serait intéressant d'étudier l'impact de cette variation de SUMOylation dans les cellules ATC et les surrénales $Senp2^{cKO}$. Les expériences d'immuno-précipitation sur cellules et sur organes n'ont cependant pas permis de mettre en évidence de forme SUMOylée de DRP1. La réduction de la SUMOylation *via* l'utilisation d'un inhibiteur de SAE1, le ML-792 n'a révélé aucun effet sur l'apoptose induite par la STS, ni sur la phosphorylation de DRP1 (Figure 47) suggérant un rôle minime de la SUMOylation dans la régulation de l'activité de DRP1 dans la surrénale. Toutefois, les cellules ATC ayant un phénotype fasciculé, leurs capacités de SUMOylation doivent être relativement basses. Il serait probablement nécessaire d'augmenter la SUMOylation dans ces cellules, *via* l'utilisation d'ARN interférents ciblant les SENPs par exemple et de tester la sensibilité à l'apoptose.

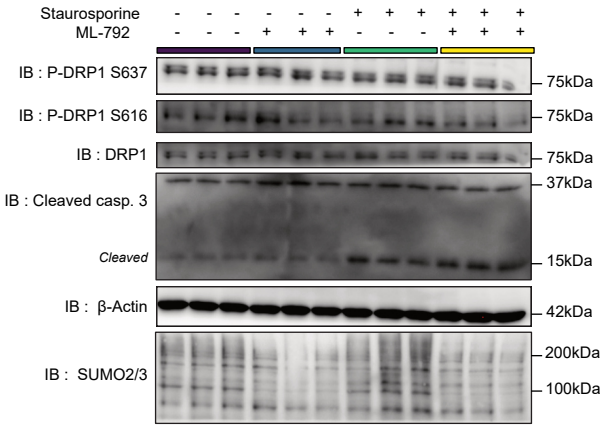

Figure 47: Western Blot représentant l'effet de l'inducteur d'apoptose staurosporine et de l'inhibiteur de SUMOylation ML-792 sur les phosphorylations de dans des cellules ATC7

Outre son rôle dans l'apoptose, DRP1 participe activement aux capacités stéroïdogènes des cellules de Leydig et lutéales (Park et al., 2019; Plewes et al., 2020). L'inhibition pharmacologique de l'activité enzymatique de DRP1 dans les cellules ATC potentialise l'effet de la forskoline sur la stéroïdogénèse (Figure 48) ce qui démontre que DRP1 exerce également un rôle moteur dans la stéroïdogénèse surrénalienne.

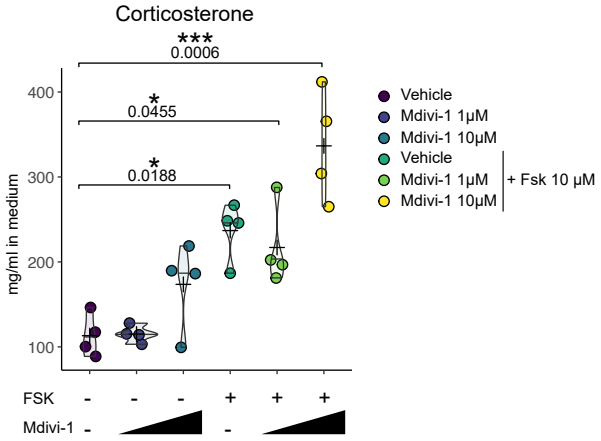

Figure 48: Concentration de corticostérone dans le milieu de cellules ATC7 traitées avec un inhibiteur de DRP1 (Mdivi-1) ou un activateur de l'adénylate cyclase (Forskoline)

Ces résultats encouragent à étudier l'ultrastructure mitochondriale et l'état de phosphorylation de DRP1 dans les différents modèles génétiques notamment vérifier si dans les souris $AS^{cre}::Prkar1a^{fl/fl}$ qui possèdent une activation constitutive de la PKA, DRP1 est hyperphosphorylé et les mitochondries élargies. Par ailleurs, pour confirmer l'impact de DRP1 dans la fonction stéroïdogène et pro apoptotique, il serait informatif d'étudier les surrénales des souris $DRP1^{KI}$ dont la sérine 637 est non phosphorylable (Valera-Alberni et al., 2021). L'étude de l'apoptose et des capacités stéroïdogènes de ces souris permettra de confirmer le rôle de DRP1 dans la fission mitochondriale *in vivo* et d'établir un lien de cause à effet entre la morphologie du réseau mitochondrial et la fonction surrénalienne.

11.2 Quelle implication des protéines MAGE dans l'insuffisance surrénalienne?

L'origine de ce projet de ma thèse est partie du constat que dans les préadipocytes bruns, la perte de SENP2 induit une augmentation de l'expression de la NECDIN, elle même responsable d'un blocage de l'adipogénèse brune (Liang et al., 2019). Le parallèle entre l'analyse des souris *Senp2*^{cKO} (*Sf1-Senp2*$^{fl/fl}$) et des souris *Ndn/Magel2-KO* révèle que:

- Les transcrits codant NECDIN et MAGEL2 sont accumulés dans les surrénales *Senp2*^{cKO}
- l'ACTH contrôle négativement l'expression de *Necdin* dans la surrénale
- les souris *Ndn/Magel2-KO* présentent un déficit de réponse au stress
- le transcrit codant POMC est accumulé dans l'hypophyse sans impact sur l'ACTH plasmatique

11.2.1 Implication de NECDIN et MAGEL2 dans l'axe hypothalamo-hypophysaire-surrénalien

Les résultats du deuxième article montrent une expression de *Ndn* dans les 3 composants de l'axe HPA et de *Magel2* dans l'hypothalamus [82]

Chez l'être humain, la perte du *locus* contenant *MAGEL2* et *NECDIN* se traduit par le syndrome de Prader-Willi tandis que la perte de *MAGEL2* uniquement conduit à un syndrome apparenté, celui de Schaaf-Yang. La synthèse des données cliniques sur ces syndromes semble indiquer une plus forte prévalence de l'insuffisance surrénale centrale chez ces patients [83].

A l'inverse, il serait intéressant de regarder chez des patients atteints de désordre de l'axe HPA tels que les insuffisances surrénales centralesle statut mutationnel de *MAGEL2* et

[82] Il semblerait que l'expression de *Magel2* ait lieu de façon transitoire dans l'hypophyse fœtale (Scagliotti et al., 2021), ce qui pourrait également être le cas dans le surrénale

[83] voir paragraphe 10.4 - Atteintes endocrines du PWS

NECDIN, car bien que la majorité des insuffisances en ACTH isolées sont associées à des mutations du gène *TBX19*, certaines restent idiopathiques (Patti et al., 2018).

11.2.2 Prader-Willi, un déficit de conversion?

Les patients atteints de Prader-Willi partagent des points communs avec les patients atteints de mutation perte de fonction de *PCSK1* qui code la prohormone convertase 1, responsable de la maturation de nombreuses pro-hormones. Des cellules souches reprogrammés (IPSC) ou des souris comportant une microdélétion dans le *locus* Prader-Willi, entourant la région *SNORD116*, présentent une diminution de l'expression de PC1/3 dont l'effet est visible pour les souris dans l'hypothalamus et le pancréas (Burnett et al., 2017).

Les patients atteints de mutations de *PCSK1* ont dans la majorité des cas de cette atteinte particulièrement rare, une accumulation de POMC et un ACTH plasmatiques normal (Mart'ın et al., 2013; Stijnen et al., 2016) tandis que les souris *Pcsk1-KO* ont un ACTH effondré mais des taux de corticostérone normaux (Zhu et al., 2002). Il sera intéressant d'explorer plus en détail la fonction surrénalienne des patients atteints du syndrome de Prader-Willi, en s'intéressant notamment aux taux d'ACTH. En effet, une étude récente a mis en évidence un seul patient présentant une insuffisance surrénalienne sur 84 patients atteints du syndrome de Prader-Willi. Cependant, parmi les 46 patients qui ont été soumis à un test à la métyrapone sur la nuit, 21 ont un ACTH en dessous de 33 pmol/l (Rosenberg et al., 2020) suggérant que la maturation de l'ACTH pourrait être affectée malgré un eucortisolisme apparent.

Il sera alors d'autant plus intéressant d'explorer les causes de l'accumulation de *Pomc* dans les souris *Ndn/Magel2-KO*. Tout d'abord en confirmant par western blot dans les hypophyses le renversement du rapport POMC/ACTH puis en mesurant l'accumulation de PC1/3 dans ce même tissu. Par ailleurs, l'implication d'un désordre d'origine hypophysaire pourrait être précisé par l'utilisation de transgène ciblant uniquement les cellules productrices de POMC (*Pomc-CreERT2*) (Berglund et al., 2013) ou toutes

les cellules de l'hypophyse, mais aussi le muscle squelettique et cardiaque (*aGSU-cre*) (Cushman et al., 2000). Tandis que la délétion ciblée dans la surrénale (*0.5Akr1b7-cre* (Lambert-Langlais et al., 2009) ou AS^{cre} (Freedman et al., 2013)) permettrait de s'assurer de l'absence d'effet de la NECDIN et de MAGEL2 dans le cortex surrénalien.

References bibliographiques

Abdelaleem, S.A., Hassan, O.A., Ahmed, R.F., Zenhom, N.M., Rifaai, R.A., and El-Tahawy, N.F. (2017). Tramadol Induced Adrenal Insufficiency: Histological, Immunohistochemical, Ultrastructural, and Biochemical Genetic Experimental Study. Journal of Toxicology *2017*, 1–14.

Abramovitz, M., Branchaud, C.L., and Murphy, B.E.P. (1982). Cortisol-Cortisone Interconversion in Human Fetal Lung: Contrasting Results Using Explant and Monolayer Cultures Suggest That 11-β-Hydroxysteroid Dehydrogenase (EC 1.1.1.146) Comprises Two Enzymes. The Journal of Clinical Endocrinology & Metabolism *54*, 563–568.

Achermann, J.C., Ito, M., Ito, M., Hindmarsh, P.C., and Jameson, J.L. (1999). A mutation in the gene encoding steroidogenic factor-1 causes XY sex reversal and adrenal failure in humans. Nat Genet *22*, 125–126.

Achermann, J.C., Ozisik, G., Ito, M., Orun, U.A., Harmanci, K., Gurakan, B., and Jameson, J.L. (2002). Gonadal Determination and Adrenal Development Are Regulated by the Orphan Nuclear Receptor Steroidogenic Factor-1, in a Dose-Dependent Manner. The Journal of Clinical Endocrinology & Metabolism *87*, 1829–1833.

Adams, R.L., and Wente, S.R. (2013). Uncovering Nuclear Pore Complexity with Innovation. Cell *152*, 1218–1221.

Agarwal, M.K., and Mirshahi, M. (1999). General overview of mineralocorticoid hormone action. Pharmacology & Therapeutics *84*, 273–326.

Ali, R.G., Bellchambers, H.M., Warr, N., Ahmed, J.N., Barratt, K.S., Neill, K., Diamand, K.E.M., and Arkell, R.M. (2021). WNT responsive SUMOylation of ZIC5 promotes murine neural crest cell development via multiple effects on transcription. J Cell Sci jcs.256792.

Alkuraya, F.S. (2006). SUMO1 Haploinsufficiency Leads to Cleft Lip and Palate. Science *313*, 1751–1751.

Altmann, S.W., Davis, H.R., Zhu, L., Yao, X., Hoos, L.M., Tetzloff, G., Iyer, S.P.N., Maguire, M., Golovko, A., Zeng, M., et al. (2004). Niemann-Pick C1 Like 1 Protein Is Critical for Intestinal Cholesterol Absorption. Science *303*, 1201–1204.

Amaya, J.M., Suidgeest, E., Sahut-Barnola, I., Dumontet, T., Montanier, N., Pag‘es, G., Keller, C., van der Weerd, L., Pereira, A.M., Martinez, A., et al. (2021). Effects of Long-Term Endogenous Corticosteroid Exposure on Brain Volume and Glial Cells in the AdKO Mouse. Front. Neurosci. *15*, 604103.

Amaya, J.M., Viho, E.M.G., Sips, H.C.M., Lalai, R.A., Sahut-Barnola, I., Dumontet, T., Montanier, N., Pereira, A.M., Martinez, A., and Meijer, O.C. (2022). Gene expression changes in the brain of a Cushing's syndrome mouse model. J Neuroendocrinology *34*.

Ancelin, K., Syx, L., Borensztein, M., Ranisavljevic, N., Vassilev, I., Briseño-Roa, L., Liu, T., Metzger, E., Servant, N., Barillot, E., et al. (2016). Maternal LSD1/KDM1A is an essential regulator of chromatin and transcription landscapes during zygotic genome activation. eLife *5*, e08851.

Andersen, J.-P., Zhang, J., Sun, H., Liu, X., Liu, J., Nie, J., and Shi, Y. (2020). Aster-B coordinates with Arf1 to regulate mitochondrial cholesterol

transport. Molecular Metabolism *42*, 101055.

Anderson, D.J., and Axel, R. (1986). A bipotential neuroendocrine precursor whose choice of cell fate is determined by NGF and glucocorticoids. Cell *47*, 1079–1090.

Antonny, B., Burd, C., De Camilli, P., Chen, E., Daumke, O., Faelber, K., Ford, M., Frolov, V.A., Frost, A., Hinshaw, J.E., et al. (2016). Membrane fission by dynamin: What we know and what we need to know. EMBO J *35*, 2270–2284.

Arakane, F., King, S.R., Du, Y., Kallen, C.B., Walsh, L.P., Watari, H., Stocco, D.M., and Strauss, J.F. (1997). Phosphorylation of Steroidogenic Acute Regulatory Protein (StAR) Modulates Its Steroidogenic Activity. Journal of Biological Chemistry *272*, 32656–32662.

Arlt, W., and Allolio, B. (2003). Adrenal insufficiency. The Lancet *361*, 1881–1893.

Bailey, D., and O'Hare, P. (2002). Herpes simplex virus 1 ICP0 co-localizes with a SUMO-specific protease. Journal of General Virology *83*, 2951–2964.

Baker, B.Y., Epand, R.F., Epand, R.M., and Miller, W.L. (2007). Cholesterol Binding Does Not Predict Activity of the Steroidogenic Acute Regulatory Protein, StAR. Journal of Biological Chemistry *282*, 10223–10232.

Banati, R.B., Middleton, R.J., Chan, R., Hatty, C.R., Wai-Ying Kam, W., Quin, C., Graeber, M.B., Parmar, A., Zahra, D., Callaghan, P., et al. (2014). Positron emission tomography and functional characterization of a complete PBR/TSPO knockout. Nat Commun *5*, 5452.

Bandiera, R., Vidal, V.P.I., Motamedi, F.J., Clarkson, M., Sahut-Barnola, I., Gise, A. von, Pu, W.T., Hohenstein, P., Martinez, A., and Schedl, A. (2013). WT1 Maintains Adrenal-Gonadal Primordium Identity and Marks a Population of AGP-like Progenitors within the Adrenal Gland. Developmental Cell *27*, 5–18.

Barradeau, S., Imaizumi-Scherrer, T., Weiss, M.C., and Faust, D.M. (2000). Alternative 5'-exons of the mouse cAMP-dependent protein kinase subunit RIa gene are conserved and expressed in both a ubiquitous and tissue-restricted fashion. FEBS Letters *476*, 272–276.

Barron, A.M., Ji, B., Kito, S., Suhara, T., and Higuchi, M. (2018). Steroidogenic abnormalities in translocator protein knockout mice and significance in the aging male. Biochemical Journal *475*, 75–85.

Basham, K.J., Rodriguez, S., Turcu, A.F., Lerario, A.M., Logan, C.Y., Rysztak, M.R., Gomez-Sanchez, C.E., Breault, D.T., Koo, B.-K., Clevers, H., et al. (2019). A ZNRF3-dependent Wnt/β-catenin signaling gradient is required for adrenal homeostasis. Genes Dev. *33*, 209–220.

Bassett, M.H., Suzuki, T., Sasano, H., White, P.C., and Rainey, W.E. (2004). The Orphan Nuclear Receptors NURR1 and NGFIB Regulate Adrenal Aldosterone Production. Molecular Endocrinology *18*, 279–290.

Bayer, P., Arndt, A., Metzger, S., Mahajan, R., Melchior, F., Jaenicke, R., and Becker, J. (1998). Structure determination of the small ubiquitin-related modifier SUMO-1. Journal of Molecular Biology *280*, 275–286.

Beauloye, V., Dhondt, K., Buysse, W., Nyakasane, A., Zech, F., De Schepper, J., Van Aken, S., De Waele, K., Craen, M., Gies, I., et al. (2015). Evaluation of the hypothalamic-pituitary-adrenal

axis and its relationship with central respiratory dysfunction in children with Prader-Willi syndrome. Orphanet J Rare Dis *10*, 106.

Bechmann, N., Berger, I., Bornstein, S.R., and Steenblock, C. (2021). Adrenal medulla development and medullary-cortical interactions. Molecular and Cellular Endocrinology *528*, 111258.

Behringer R, R., McLaren, A., and Josso, N. (1995). The Müllerian inhibitor and mammalian sexual development. Phil. Trans. R. Soc. Lond. B *350*, 285–289.

Berglund, E.D., Liu, C., Sohn, J.-W., Liu, T., Kim, M.H., Lee, C.E., Vianna, C.R., Williams, K.W., Xu, Y., and Elmquist, J.K. (2013). Serotonin 2C receptors in pro-opiomelanocortin neurons regulate energy and glucose homeostasis. J Clin Invest *123*, 5061–5070.

Bernstock, J.D., Ye, D., Smith, J.A., Lee, Y.-J., Gessler, F.A., Yasgar, A., Kouznetsova, J., Jadhav, A., Wang, Z., Pluchino, S., et al. (2018). Quantitative high-throughput screening identifies cytoprotective molecules that enhance SUMO conjugation *via* the inhibition of SUMO-specific protease (SENP)2. FASEB j. *32*, 1677–1691.

Berthon, A., Sahut-Barnola, I., Lambert-Langlais, S., de Joussineau, C., Damon-Soubeyrand, C., Louiset, E., Taketo, M.M., Tissier, F., Bertherat, J., Lefrançois-Martinez, A.-M., et al. (2010). Constitutive β-catenin activation induces adrenal hyperplasia and promotes adrenal cancer development. Human Molecular Genetics *19*, 1561–1576.

Berthon, A., Drelon, C., Ragazzon, B., Boulkroun, S., Tissier, F., Amar, L., Samson-Couterie, B., Zennaro, M.-C., Plouin, P.-F., Skah, S., et al. (2014). WNT/β-catenin signalling is activated in aldosterone-producing adenomas and controls aldosterone production. Human Molecular Genetics *23*, 889–905.

Besprozvannaya, M., Dickson, E., Li, H., Ginburg, K.S., Bers, D.M., Auwerx, J., and Nunnari, J. (2018). GRAM domain proteins specialize functionally distinct ER-PM contact sites in human cells. Elife *7*, e31019.

Best, J.L., Ganiatsas, S., Agarwal, S., Changou, A., Salomoni, P., Shirihai, O., Meluh, P.B., Pandolfi, P.P., and Zon, L.I. (2002). SUMO-1 Protease-1 Regulates Gene Transcription through PML. Molecular Cell *10*, 843–855.

Bielohuby, M., Herbach, N., Wanke, R., Maser-Gluth, C., Beuschlein, F., Wolf, E., and Hoeflich, A. (2007). Growth analysis of the mouse adrenal gland from weaning to adulthood: Time- and gender-dependent alterations of cell size and number in the cortical compartment. American Journal of Physiology-Endocrinology and Metabolism *293*, E139–E146.

Bischof, J.M., Stewart, C.L., and Wevrick, R. (2007). Inactivation of the mouse Magel2 gene results in growth abnormalities similar to Prader-Willi syndrome. Human Molecular Genetics *16*, 2713–2719.

Bittel, D.C., Kibiryeva, N., McNulty, S.G., Driscoll, D.J., Butler, M.G., and White, R.A. (2007). Whole genome microarray analysis of gene expression in an imprinting center deletion mouse model of Prader–Willi syndrome. Am. J. Med. Genet. *143A*, 422–429.

Black, S.M., Harikrishna, J.A., Szklarz, G.D., and Miller, W.L. (1994). The mitochondrial

environment is required for activity of the cholesterol side-chain cleavage enzyme, cytochrome P450scc. Proc. Natl. Acad. Sci. U.S.A. *91*, 7247–7251.

Boccaccio, I., Glatt-Deeley, H., Watrin, F., Roeckel, N., Lalande, M., and Muscatelli, F. (1999). The Human Magel2 Gene and Its Mouse Homologue Are Paternally Expressed and Mapped to the Prader-Willi Region. Human Molecular Genetics *8*, 2497–2505.

Bohren, K.M., Nadkarni, V., Song, J.H., Gabbay, K.H., and Owerbach, D. (2004). A M55V Polymorphism in a Novel *SUMO* Gene (*SUMO-4*) Differentially Activates Heat Shock Transcription Factors and Is Associated with Susceptibility to Type I Diabetes Mellitus. J. Biol. Chem. *279*, 27233–27238.

Bose, H.S., Lingappa, V.R., and Miller, W.L. (2002). Rapid regulation of steroidogenesis by mitochondrial protein import. Nature *417*, 87–91.

Bossis, G., and Melchior, F. (2006). Regulation of SUMOylation by Reversible Oxidation of SUMO Conjugating Enzymes. Molecular Cell *21*, 349–357.

Bouchard, D., Wang, W., Yang, W.-C., He, S., Garcia, A., and Matunis, M.J. (2021). SUMO paralogue–specific functions revealed through systematic analysis of human knockout cell lines and gene expression data. MBoC *32*, 1849–1866.

Bouteille, N., Driouch, K., Hage, P.E., Sin, S., Formstecher, E., Camonis, J., Lidereau, R., and Lallemand, F. (2009). Inhibition of the Wnt/β-catenin pathway by the WWOX tumor suppressor protein. Oncogene *28*, 2569–2580.

Bradbury, M.J., Akana, S.F., Cascio, C.S., Levin, N., Jacobson, L., and Dallman, M.F. (1991). Regulation of basal ACTH secretion by corticosterone is mediated by both type I (MR) and type II (GR) receptors in rat brain. The Journal of Steroid Biochemistry and Molecular Biology *40*, 133–142.

Braschi, E., Zunino, R., and McBride, H.M. (2009). MAPL is a new mitochondrial SUMO E3 ligase that regulates mitochondrial fission. EMBO Rep *10*, 748–754.

Bruderer, R., Tatham, M.H., Plechanovova, A., Matic, I., Garg, A.K., and Hay, R.T. (2011). Purification and identification of endogenous polySUMO conjugates. EMBO Rep *12*, 142–148.

Bu, F.-T., Chen, Y., Yu, H.-X., Chen, X., Yang, Y., Pan, X.-Y., Wang, Q., Wu, Y.-T., Huang, C., Meng, X.-M., et al. (2018). SENP2 alleviates CCl4-induced liver fibrosis by promoting activated hepatic stellate cell apoptosis and reversion. Toxicology Letters *289*, 86–98.

Buonocore, F., and Achermann, J.C. (2020). Primary adrenal insufficiency: New genetic causes and their long-term consequences. Clin Endocrinol *92*, 11–20.

Burnett, L.C., LeDuc, C.A., Sulsona, C.R., Paull, D., Rausch, R., Eddiry, S., Carli, J.F.M., Morabito, M.V., Skowronski, A.A., Hubner, G., et al. (2017). Deficiency in prohormone convertase PC1 impairs prohormone processing in Prader-Willi syndrome (American Society for Clinical Investigation).

Buurstede, J.C., Weert, L.T.C.M., Colucci, P., Gentenaar, M., Viho, E.M.G., Koorneef, L.L., Schoonderwoerd, R.A., Lanooij, S.D., Moustakas, I., Balog, J., et al. (2021). Hippocampal glucocorticoid target genes associated with enhancement of memory consolidation. Eur J

Neurosci ejn.15226.

Cadd, G., and Stanley McKnight, G. (1989). Distinct patterns of cAMP-dependent protein kinase gene expression in mouse brain. Neuron *3*, 71–79.

Cai, L., Ji, A., de Beer, F.C., Tannock, L.R., and van der Westhuyzen, D.R. (2008). SR-BI protects against endotoxemia in mice through its roles in glucocorticoid production and hepatic clearance. J. Clin. Invest. *118*, 364–375.

Cai, Z., Wang, Z., Yuan, R., Cui, M., Lao, Y., Wang, Y., Nie, P., Shen, L., Yi, J., and He, B. (2021). Redox-sensitive enzyme SENP3 mediates vascular remodeling via de-SUMOylation of β-catenin and regulation of its stability. EBioMedicine *67*, 103386.

Calebiro, D., Hannawacker, A., Lyga, S., Bathon, K., Zabel, U., Ronchi, C., Beuschlein, F., Reincke, M., Lorenz, K., Allolio, B., et al. (2014). PKA catalytic subunit mutations in adrenocortical Cushing's adenoma impair association with the regulatory subunit. Nat Commun *5*, 5680.

Cammas, F., Mark, M., Dolle, P., Dierich, A., Chambon, P., and Losson, R. (2000). Mice lacking the transcriptional corepressor TIF1beta are defective in early postimplantation development. Development *127*, 2955–2963.

Campbell, B. (2020). DHEAS and Human Development: An Evolutionary Perspective. Front. Endocrinol. *11*, 101.

Campbell, L.A., Faivre, E.J., Show, M.D., Ingraham, J.G., Flinders, J., Gross, J.D., and Ingraham, H.A. (2008). Decreased Recognition of SUMO-Sensitive Target Genes following Modification of SF-1 (NR5A1). Molecular and Cellular Biology *28*, 7476–7486.

Campla, C.K., Breit, H., Dong, L., Gumerson, J.D., Roger, J.E., and Swaroop, A. (2017). Pias3 is necessary for dorso-ventral patterning and visual response of retinal cones but is not required for rod photoreceptor differentiation. Biology Open bio.024679.

Cao, J., Liu, X.-M., Huang, L.-L., Wang, L., Jiao, X.-F., and Huo, L.-J. (2018). SUMO2 modification of Aurora B and its impact on follicular development and atresia in the mouse ovary. Int J Mol Med.

Cappadocia, L., Mascle, X.H., Bourdeau, V., Tremblay-Belzile, S., Chaker-Margot, M., Lussier-Price, M., Wada, J., Sakaguchi, K., Aubry, M., Ferbeyre, G., et al. (2015). Structural and Functional Characterization of the Phosphorylation-Dependent Interaction between PML and SUMO1. Structure *23*, 126–138.

Cardoso-Moreira, M., Halbert, J., Valloton, D., Velten, B., Chen, C., Shao, Y., Liechti, A., Ascenção, K., Rummel, C., Ovchinnikova, S., et al. (2019). Gene expression across mammalian organ development. Nature *571*, 505–509.

Carney, J.A., Young, W.F., and Stratakis, C.A. (2011). Primary Bimorphic Adrenocortical Disease: Cause of Hypercortisolism in McCune-Albright Syndrome. American Journal of Surgical Pathology *35*, 1311–1326.

Caron, K.M., Soo, S.-C., Wetsel, W.C., Stocco, D.M., Clark, B.J., and Parker, K.L. (1997). Targeted disruption of the mouse gene encoding steroidogenic acute regulatory protein provides insights into congenital lipoid adrenal hyperplasia. Proc. Natl. Acad. Sci. U.S.A. *94*, 11540–11545.

Carsia, R.V., Macdonald, G.J., Gibney, J.A., Tilly, K.I., and Tilly, J.L. (1996). Apoptotic cell death in the rat adrenal gland: An in vivo and in vitro investigation. Cell Tissue Res *283*, 247–254.

Cassidy, S.B., Schwartz, S., Miller, J.L., and Driscoll, D.J. (2012). Prader-Willi syndrome. Genetics in Medicine *14*, 10–26.

Ceccatelli, S., Diana, A., Villar, M.J., and Nicotera, P. (1995). Adrenocortical apoptosis in hypophysectomized rats is selectively reduced by ACTH. Neuroreport *6*, 342–344.

Cereghetti, G.M., Stangherlin, A., de Brito, O.M., Chang, C.R., Blackstone, C., Bernardi, P., and Scorrano, L. (2008). Dephosphorylation by calcineurin regulates translocation of Drp1 to mitochondria. Proc. Natl. Acad. Sci. U.S.A. *105*, 15803–15808.

Chang, C.-R., and Blackstone, C. (2007). Cyclic AMP-dependent Protein Kinase Phosphorylation of Drp1 Regulates Its GTPase Activity and Mitochondrial Morphology. J. Biol. Chem. *282*, 21583–21587.

Chen, H., Victor, A.K., Klein, J., Tacer, K.F., Tai, D.J.C., de Esch, C., Nuttle, A., Temirov, J., Burnett, L.C., Rosenbaum, M., et al. (2020). Loss of MAGEL2 in Prader-Willi syndrome leads to decreased secretory granule and neuropeptide production. JCI Insight *5*.

Chen, W.-Y., Lee, W.-C., Hsu, N.-C., Huang, F., and Chung, B. (2004). SUMO Modification of Repression Domains Modulates Function of Nuclear Receptor 5A1 (Steroidogenic Factor-1). J. Biol. Chem. *279*, 38730–38735.

Chen, X.-L., Wang, S.-F., Liang, X.-T., Liang, H.-X., Wang, T.-T., Wu, S.-Q., Qiu, Z.-J., Zhan, R., and Xu, Z.-S. (2018). SENP2 exerts an anti-tumor effect on chronic lymphocytic leukemia cells through the inhibition of the Notch and NF-κB signaling pathways. Int J Oncol.

Chen, Y.-C., Hsu, W.-L., Ma, Y.-L., Tai, D.J.C., and Lee, E.H.Y. (2014). CREB SUMOylation by the E3 Ligase PIAS1 Enhances Spatial Memory. Journal of Neuroscience *34*, 9574–9589.

Cheng, H., Sun, X., Li, J., He, P., Liu, W., and Meng, X. (2018). Knockdown of Uba2 inhibits colorectal cancer cell invasion and migration through downregulation of the Wnt/β-catenin signaling pathway. J. Cell. Biochem. *119*, 6914–6925.

Cheng, J., Kang, X., Zhang, S., and Yeh, E.T.H. (2007). SUMO-Specific Protease 1 Is Essential for Stabilization of HIF1α during Hypoxia. Cell *131*, 584–595.

Cheng, K., Seita, Y., Moriwaki, T., Noshiro, K., Sakata, Y., Hwang, Y.S., Torigoe, T., Saitou, M., Tsuchiya, H., Iwatani, C., et al. (2022). The developmental origin and the specification of the adrenal cortex in humans and cynomolgus monkeys (Developmental Biology).

Chida, D., Nakagawa, S., Nagai, S., Sagara, H., Katsumata, H., Imaki, T., Suzuki, H., Mitani, F., Ogishima, T., Shimizu, C., et al. (2007). Melanocortin 2 receptor is required for adrenal gland development, steroidogenesis, and neonatal gluconeogenesis. Proceedings of the National Academy of Sciences *104*, 18205–18210.

Ching, S., and Vilain, E. (2009). Targeted disruption of Sonic Hedgehog in the mouse adrenal leads to adrenocortical hypoplasia. Genesis *47*, 628–637.

Chiu, S.-Y., Asai, N., Costantini, F., and Hsu, W. (2008). SUMO-Specific Protease 2 Is Essential for Modulating P53-Mdm2 in Development of Trophoblast Stem Cell Niches and Lineages. PLoS Biol *6*, e310.

Choi, H.-J., Park, J.-H., Park, J.-H., Lee, K.B., and Oh, S.-M. (2015). Pc2-mediated SUMOylation of WWOX is essential for its suppression of DU145 prostate tumorigenesis. FEBS Letters *589*, 3977–3988.

Choi, H.-K., Choi, K.-C., Yoo, J.-Y., Song, M., Ko, S.J., Kim, C.H., Ahn, J.-H., Chun, K.-H., Yook, J.I., and Yoon, H.-G. (2011). Reversible SUMOylation of TBL1-TBLR1 Regulates β-Catenin-Mediated Wnt Signaling. Molecular Cell *43*, 203–216.

Chung, S.S., Ahn, B.Y., Kim, M., Choi, H.H., Park, H.S., Kang, S., Park, S.G., Kim, Y.B., Cho, Y.M., Lee, H.K., et al. (2010). Control of Adipogenesis by the SUMO-Specific Protease SENP2. Molecular and Cellular Biology *30*, 2135–2146.

Chymkowitch, P., Ngu'ea P, A., and Enserink, J.M. (2015). SUMO-regulated transcription: Challenging the dogma. BioEssays *37*, 1095–1105.

Cignarelli, A., Melchiorre, M., Peschechera, A., Conserva, A., Renna, L.A., Miccoli, S., Natalicchio, A., Perrini, S., Laviola, L., and Giorgino, F. (2010). Role of UBC9 in the Regulation of the Adipogenic Program in 3T3-L1 Adipocytes. Endocrinology *151*, 5255–5266.

Clark, A.J.L., Grossman, A., and McLoughlin, L. (1993). Familial glucocorticoid deficiency associated with point mutation in the adrenocorticotropin receptor. The Lancet *341*, 461–462.

Comerford, K.M., Leonard, M.O., Karhausen, J., Carey, R., Colgan, S.P., and Taylor, C.T. (2003). Small ubiquitin-related modifier-1 modification mediates resolution of CREB-dependent responses to hypoxia. Proceedings of the National Academy of Sciences *100*, 986–991.

Condon, J.C., Pezzi, V., Drummond, B.M., Yin, S., and Rainey, W.E. (2002). Calmodulin-Dependent Kinase I Regulates Adrenal Cell Expression of Aldosterone Synthase. Endocrinology *143*, 3651–3657.

Connell, N.A., Paterson, W.F., Wallace, A.M., and Donaldson, M.D. (2010). Adrenal function and mortality in children and adolescents with Prader-Willi syndrome attending a single centre from 1991-2009: Letter to the Editor. Clinical Endocrinology *73*, 686–688.

Corrias, A., Grugni, G., Crino, A., Di Candia, S., Chiabotto, P., Cogliardi, A., Chiumello, G., De Medici, C., Spera, S., Gargantini, L., et al. (2012). Assessment of central adrenal insufficiency in children and adolescents with Prader-Willi syndrome: ACTH test in paediatric Prader-Willi syndrome. Clin Endocrinol *76*, 843–850.

Cossec, J.-C., Theurillat, I., Chica, C., Búa Aguín, S., Gaume, X., Andrieux, A., Iturbide, A., Jouvion, G., Li, H., Bossis, G., et al. (2018). SUMO Safeguards Somatic and Pluripotent Cell Identities by Enforcing Distinct Chromatin States. Cell Stem Cell *23*, 742–757.e8.

Cox, A.R., Chernis, N., Kim, K.H., Masschelin, P.M., Saha, P.K., Briley, S.M., Sharp, R., Li, X., Felix, J.B., Sun, Z., et al. (2021). Ube2i deletion in adipocytes causes lipoatrophy in mice. Molecular Metabolism *48*, 101221.

Cribbs, J.T., and Strack, S. (2007). Reversible

phosphorylation of Drp1 by cyclic AMP-dependent protein kinase and calcineurin regulates mitochondrial fission and cell death. EMBO Rep *8*, 939–944.

Cruz-Topete, D., and Cidlowski, J.A. (2015). One Hormone, Two Actions: Anti- and Pro-Inflammatory Effects of Glucocorticoids. Neuroimmunomodulation *22*, 20–32.

Cruz-Topete, D., Myers, P.H., Foley, J.F., Willis, M.S., and Cidlowski, J.A. (2016). Corticosteroids Are Essential for Maintaining Cardiovascular Function in Male Mice. Endocrinology *157*, 2759–2771.

Cushman, L.J., Burrows, H.L., Seasholtz, A.F., Lewandoski, M., Muzyczka, N., and Camper, S.A. (2000). Cre-mediated recombination in the pituitary gland. Genesis *28*, 167–174.

Cypess, A.M., Zhang, H., Schulz, T.J., Huang, T.L., Espinoza, D.O., Kristiansen, K., Unterman, T.G., and Tseng, Y.-H. (2011). Insulin/IGF-I Regulation of Necdin and Brown Adipocyte Differentiation Via CREB- and FoxO1-Associated Pathways. Endocrinology *152*, 3680–3689.

de Joussineau, C., Sahut-Barnola, I., Tissier, F., Dumontet, T., Drelon, C., Batisse-Lignier, M., Tauveron, I., Pointud, J.-C., Lefrançois-Martinez, A.-M., Stratakis, C.A., et al. (2014). mTOR pathway is activated by PKA in adrenocortical cells and participates in vivo to apoptosis resistance in primary pigmented nodular adrenocortical disease (PPNAD). Human Molecular Genetics *23*, 5418–5428.

de Lind van Wijngaarden, R.F.A., Otten, B.J., Festen, D.A.M., Joosten, K.F.M., de Jong, F.H., Sweep, F.C.G.J., and Hokken-Koelega, A.C.S. (2008). High Prevalence of Central Adrenal Insufficiency in Patients with Prader-Willi Syndrome. The Journal of Clinical Endocrinology & Metabolism *93*, 1649–1654.

Demarque, M.D., Nacerddine, K., NeyretKahn, H., Andrieux, A., Danenberg, E., Jouvion, G., Bomme, P., Hamard, G., Romagnolo, B., Terris, B., et al. (2011). Sumoylation by Ubc9 Regulates the Stem Cell Compartment and Structure and Function of the Intestinal Epithelium in Mice. Gastroenterology *140*, 286–296.

Deng, B., Shen, W.-J., Dong, D., Azhar, S., and Kraemer, F.B. (2019). Plasma membrane cholesterol trafficking in steroidogenesis. FASEB j. *33*, 1389–1400.

Desterro, J.M.P., Rodriguez, M.S., and Hay, R.T. (1998). SUMO-1 Modification of IκBα Inhibits NF-κB Activation. Molecular Cell *2*, 233–239.

Desterro, J.M.P., Rodriguez, M.S., Kemp, G.D., and Hay, R.T. (1999). Identification of the Enzyme Required for Activation of the Small Ubiquitin-like Protein SUMO-1. J. Biol. Chem. *274*, 10618–10624.

Dickey, A.S., and Strack, S. (2011). PKA/AKAP1 and PP2A/B 2 Regulate Neuronal Morphogenesis via Drp1 Phosphorylation and Mitochondrial Bioenergetics. Journal of Neuroscience *31*, 15716–15726.

Ding, X., Wang, A., Ma, X., Demarque, M., Jin, W., Xin, H., Dejean, A., and Dong, C. (2016). Protein SUMOylation Is Required for Regulatory T Cell Expansion and Function. Cell Reports *16*, 1055–1066.

Dolfi, B., Gallerand, A., Firulyova, M.M., Xu, Y., Merlin, J., Dumont, A., Castiglione, A., Vaillant,

N., Quemener, S., Gerke, H., et al. (2022). Unravelling the sex-specific diversity and functions of adrenal gland macrophages. Cell Reports *39*, 110949.

Dorner, J., Martinez Rodriguez, V., Ziegler, R., Rohrig, T., Cochran, R.S., Gotz, R.M., Levin, M.D., Pihlajoki, M., Heikinheimo, M., and Wilson, D.B. (2017). GLI1+ progenitor cells in the adrenal capsule of the adult mouse give rise to heterotopic gonadal-like tissue. Molecular and Cellular Endocrinology *441*, 164–175.

Doyle, J.M., Gao, J., Wang, J., Yang, M., and Potts, P.R. (2010). MAGE-RING Protein Complexes Comprise a Family of E3 Ubiquitin Ligases. Molecular Cell *39*, 963–974.

Drelon, C., Berthon, A., Sahut-Barnola, I., Mathieu, M., Dumontet, T., Rodriguez, S., Batisse-Lignier, M., Tabbal, H., Tauveron, I., Lefrançois-Martinez, A.-M., et al. (2016). PKA inhibits WNT signalling in adrenal cortex zonation and prevents malignant tumour development. Nature Communications *7*, 12751.

Duarte, A., Poderoso, C., Cooke, M., Soria, G., Cornejo Maciel, F., Gottifredi, V., and Podest'a, E.J. (2012). Mitochondrial Fusion Is Essential for Steroid Biosynthesis. PLoS ONE *7*, e45829.

Duarte, A., Castillo, A.F., Podest'a, E.J., and Poderoso, C. (2014). Mitochondrial Fusion and ERK Activity Regulate Steroidogenic Acute Regulatory Protein Localization in Mitochondria. PLoS ONE *9*, e100387.

Dumontet, T., Sahut-Barnola, I., Septier, A., Montanier, N., Plotton, I., Roucher-Boulez, F., Ducros, V., Lefrançois-Martinez, A.-M., Pointud, J.-C., Zubair, M., et al. (2018). PKA signaling drives reticularis differentiation and sexually dimorphic adrenal cortex renewal. JCI Insight *3*.

Dumontet, T., Sahut-Barnola, I., Dufour, D., Lefrançois-Martinez, A.-M., Berthon, A., Montanier, N., Ragazzon, B., Djari, C., Pointud, J.-C., Roucher-Boulez, F., et al. (2019). Hormonal and spatial control of SUMOylation in the human and mouse adrenal cortex. FASEB j. *33*, 10218–10230.

El Wakil, A., Mari, B., Barhanin, J., and Lalli, E. (2013). Genomic Analysis of Sexual Dimorphism of Gene Expression in the Mouse Adrenal Gland. Hormone and Metabolic Research *45*, 870–873.

Elosegui-Artola, A., Andreu, I., Beedle, A.E.M., Lezamiz, A., Uroz, M., Kosmalska, A.J., Oria, R., Kechagia, J.Z., Rico-Lastres, P., Le Roux, A.-L., et al. (2017). Force Triggers YAP Nuclear Entry by Regulating Transport across Nuclear Pores. Cell *171*, 1397–1410.e14.

Emura, N., Wang, C.-M., Yang, W.H., and Yang, W.-H. (2020). Steroidogenic Factor 1 (NR5A1) Activates ATF3 Transcriptional Activity. IJMS *21*, 1429.

Espenshade, P.J., and Hughes, A.L. (2007). Regulation of Sterol Synthesis in Eukaryotes. Annu. Rev. Genet. *41*, 401–427.

Espiard, S., Vantyghem, M.-C., Assié, G., Cardot-Bauters, C., Raverot, G., Brucker-Davis, F., Archambeaud-Mouveroux, F., Lefebvre, H., Nunes, M.-L., Tabarin, A., et al. (2020). Frequency and Incidence of Carney Complex Manifestations: A Prospective Multicenter Study With a Three-Year Follow-Up. The Journal of Clinical Endocrinology & Metabolism *105*, e436–e446.

Eustachio B, L.G. (1714). Tabulae anatomicae clarissimi viri bartholomaei eustachii quas è tenebris tandem vindicatis.

Evdokimov, E., Sharma, P., Lockett, S.J., Lualdi, M., and Kuehn, M.R. (2008). Loss of SUMO1 in mice affects RanGAP1 localization and formation of PML nuclear bodies, but is not lethal as it can be compensated by SUMO2 or SUMO3. Journal of Cell Science *121*, 4106–4113.

Evinger, M.J., Towle, A.C., Park, D.H., Lee, P., and Joh, T.H. (1992). Glucocorticoids stimulate transcription of the rat phenylethanolamine N-methyltransferase (PNMT) gene in vivo and in vitro. Cell Mol Neurobiol *12*, 193–215.

Fagotto, F., Glück, U., and Gumbiner, B.M. (1998). Nuclear localization signal-independent and importin/karyopherin-independent nuclear import of β-catenin. Current Biology *8*, 181–190.

Fan, J., Campioli, E., Midzak, A., Culty, M., and Papadopoulos, V. (2015). Conditional steroidogenic cell-targeted deletion of TSPO unveils a crucial role in viability and hormone-dependent steroid formation. Proc. Natl. Acad. Sci. U.S.A. *112*, 7261–7266.

Fan, J., Campioli, E., Sottas, C., Zirkin, B., and Papadopoulos, V. (2020). Amhr2-Cre–Mediated Global Tspo Knockout. Journal of the Endocrine Society *4*, bvaa001.

Farholt, S., Sode-Carlsen, R., Christiansen, J.S., Ostergaard, J.R., and Hoybye, C. (2011). Normal Cortisol Response to High-Dose Synacthen and Insulin Tolerance Test in Children and Adults with Prader-Willi Syndrome. The Journal of Clinical Endocrinology & Metabolism *96*, E173–E180.

Farkash, Y., Timberg, R., and Orly, J. (1986). Preparation of Antiserum to Rat Cytochrome P-450 Cholesterol Side Chain Cleavage, and Its Use for Ultrastructural Localization of the Immunoreactive Enzyme by Protein A-Gold Technique*. Endocrinology *118*, 1353–1365.

Figueroa-Romero, C., Iñiguez-Lluh'ı, J.A., Stadler, J., Chang, C.-R., Arnoult, D., Keller, P.J., Hong, Y., Blackstone, C., and Feldman, E.L. (2009). SUMOylation of the mitochondrial fission protein Drpl occurs at multiple nonconsensus sites within the B domain and is linked to its activity cycle. FASEB j. *23*, 3917–3927.

Finco, I., Lerario, A.M., and Hammer, G.D. (2018). Sonic Hedgehog and WNT Signaling Promote Adrenal Gland Regeneration in Male Mice. Endocrinology *159*, 579–596.

Finotto, S., Krieglstein, K., Schober, A., Deimling, F., Lindner, K., Bruhl, B., Beier, K., Metz, J., Garcia-Arraras, J.E., Roig-Lopez, J.L., et al. (1999). Analysis of mice carrying targeted mutations of the glucocorticoid receptor gene argues against an essential role of glucocorticoid signalling for generating adrenal chromaffin cells. Development *126*, 2935–2944.

Fleury, A., Mathieu, A.P., Ducharme, L., Hales, D.B., and LeHoux, J.-G. (2004). Phosphorylation and function of the hamster adrenal steroidogenic acute regulatory protein (StAR). The Journal of Steroid Biochemistry and Molecular Biology *91*, 259–271.

Florke Gee, R.R., Chen, H., Lee, A.K., Daly, C.A., Wilander, B.A., Fon Tacer, K., and Potts, P.R. (2020). Emerging roles of the MAGE protein family in stress response pathways. Journal of Biological Chemistry *295*, 16121–16155.

Fossom, L.H., Sterling, C.R., and Tank, A.W. (1992). Regulation of tyrosine hydroxylase gene transcription rate and tyrosine hydroxylase mRNA stability by cyclic AMP and glucocorticoid. Mol Pharmacol *42*, 898–908.

Frank, S., Gaume, B., Bergmann-Leitner, E.S., Leitner, W.W., Robert, E.G., Catez, F., Smith, C.L., and Youle, R.J. (2001). The Role of Dynamin-Related Protein 1, a Mediator of Mitochondrial Fission, in Apoptosis. Developmental Cell *1*, 515–525.

Freedman, B.D., Kempna, P.B., Carlone, D.L., Shah, M.S., Guagliardo, N.A., Barrett, P.Q., Gomez-Sanchez, C.E., Majzoub, J.A., and Breault, D.T. (2013). Adrenocortical Zonation Results from Lineage Conversion of Differentiated Zona Glomerulosa Cells. Developmental Cell *26*, 666–673.

Frimodt-Møller, K.E., Møllegaard Jepsen, J.R., Feldt-Rasmussen, U., and Krogh, J. (2019). Hippocampal Volume, Cognitive Functions, Depression, Anxiety, and Quality of Life in Patients With Cushing Syndrome. The Journal of Clinical Endocrinology & Metabolism *104*, 4563–4577.

Fröhlich, C., Grabiger, S., Schwefel, D., Faelber, K., Rosenbaum, E., Mears, J., Rocks, O., and Daumke, O. (2013). Structural insights into oligomerization and mitochondrial remodelling of dynamin 1-like protein. EMBO J *32*, 1280–1292.

Fu, J., Yu, H.-M.I., Chiu, S.-Y., Mirando, A.J., Maruyama, E.O., Cheng, J.-G., and Hsu, W. (2014). Disruption of SUMO-Specific Protease 2 Induces Mitochondria Mediated Neurodegeneration. PLoS Genet *10*, e1004579.

Gallo-Payet, N., Grazzini, E., Coté, M., Chouinard, L., Chorvátová, A., Bilodeau, L., Payet, M.D., and Guillon, G. (1996). Role of Ca2+ in the action of adrenocorticotropin in cultured human adrenal glomerulosa cells. J. Clin. Invest. *98*, 460–466.

Gan, X., Wang, J., Xi, Y., Wu, Z., Li, Y., and Li, L. (2008). Nuclear Dvl, c-Jun, β-catenin, and TCF form a complex leading to stabiLization of β-catenin–TCF interaction. Journal of Cell Biology *180*, 1087–1100.

Ganichkin, O.M., Vancraenenbroeck, R., Rosenblum, G., Hofmann, H., Mikhailov, A.S., Daumke, O., and Noel, J.K. (2021). Quantification and demonstration of the collective constriction-by-ratchet mechanism in the dynamin molecular motor. Proc. Natl. Acad. Sci. U.S.A. *118*, e2101144118.

Gannon, A.-L., OHara, L., Mason, J.I., Jorgensen, A., Frederiksen, H., Milne, L., Smith, S., Mitchell, R.T., and Smi, L.B. (2019). Androgen receptor signalling in the male adrenal facilitates X-zone regression, cell turnover and protects against adrenal degeneration during ageing. Sci Rep *9*, 10457.

Gannon, A.-L., Hara, L.O., Mason, I.J., Jorgensen, A., Frederiksen, H., Curley, M., Milne, L., Smith, S., Mitchell, R.T., and Smi, L.B. (2021). Androgen Receptor Is Dispensable for X-Zone Regression in the Female Adrenal but Regulates Post-Partum Corticosterone Levels and Protects Cortex Integrity. Front. Endocrinol. *11*, 599869.

Gao, C., and Chen, Y.-G. (2010). Dishevelled: The hub of Wnt signaling. Cellular Signalling *22*, 717–727.

Gao, S., and Hu, J. (2021). Mitochondrial Fusion:

The Machineries In and Out. Trends in Cell Biology *31*, 62–74.

García-Gutiérrez, P., Juárez-Vicente, F., Gallardo-Chamizo, F., Charnay, P., and García-Dom'ınguez, M. (2011). The transcription factor Krox20 is an E3 ligase that sumoylates its Nab coregulators. EMBO Rep *12*, 1018–1023.

Garvin, A.J., Walker, A.K., Densham, R.M., Chauhan, A.S., Stone, H.R., Mackay, H.L., Jamshad, M., Starowicz, K., Daza-Martin, M., Ronson, G.E., et al. (2019). The deSUMOylase SENP2 coordinates homologous recombination and nonhomologous end joining by independent mechanisms. Genes Dev. *33*, 333–347.

Gerard, M., Hernandez, L., Wevrick, R., and Stewart, C.L. (1999). Disruption of the mouse necdin gene results in early post-natal lethality. Nat Genet *23*, 199–202.

Giordano, R., Picu, A., Bonelli, L., Balbo, M., Berardelli, R., Marinazzo, E., Corneli, G., Ghigo, E., and Arvat, E. (2008). Hypothalamus–pituitary–adrenal axis evaluation in patients with hypothalamo–pituitary disorders: Comparison of different provocative tests. Clin Endocrinol *68*, 935–941.

Girdwood, D.W.H., Tatham, M.H., and Hay, R.T. (2004). SUMO and transcriptional regulation. Seminars in Cell & Developmental Biology *15*, 201–210.

Goetz, S.C., and Anderson, K.V. (2010). The primary cilium: A signalling centre during vertebrate development. Nat Rev Genet *11*, 331–344.

Goldstein, J.L., DeBose-Boyd, R.A., and Brown, M.S. (2006). Protein Sensors for Membrane Sterols. Cell *124*, 35–46.

Gomez-Sanchez, E., and Gomez-Sanchez, C.E. (2014). The Multifaceted Mineralocorticoid Receptor. In Comprehensive Physiology, R. Terjung, ed. (Wiley), pp. 965–994.

Gong, L., and Yeh, E.T.H. (2006). Characterization of a Family of Nucleolar SUMO-specific Proteases with Preference for SUMO-2 or SUMO-3. Journal of Biological Chemistry *281*, 15869–15877.

González-Prieto, R., Eifler-Olivi, K., Claessens, L.A., Willemstein, E., Xiao, Z., Talavera Ormeno, C.M.P., Ovaa, H., Ulrich, H.D., and Vertegaal, A.C.O. (2021). Global non-covalent SUMO interaction networks reveal SUMO-dependent stabilization of the non-homologous end joining complex. Cell Reports *34*, 108691.

Grabek, A., Dolfi, B., Klein, B., Jian-Motamedi, F., Chaboissier, M.-C., and Schedl, A. (2019). The Adult Adrenal Cortex Undergoes Rapid Tissue Renewal in a Sex-Specific Manner. Cell Stem Cell *25*, 290–296.e2.

Grisolano, J.L., Wesselschmidt, R.L., Pelicci, P.G., and Ley, T.J. (1997). Altered Myeloid Development and Acute Leukemia in Transgenic Mice Expressing PML-RARα Under Control of Cathepsin G Regulatory Sequences. Blood *89*, 376–387.

Gross, M., Yang, R., Top, I., Gasper, C., and Shuai, K. (2004). PIASy-mediated repression of the androgen receptor is independent of sumoylation. Oncogene *23*, 3059–3066.

Grugni, G., Beccaria, L., Corrias, A., Crino, A., Cappa, M., De Medici, C., Di Candia, S., Gargantini, L., Ragusa, L., Salvatoni, A., et al. (2013). Central adrenal insufficiency in young adults with Prader-Willi Syndrome. Clin

Endocrinol *79*, 371–378.

Guagliardo, N.A., Klein, P.M., Gancayco, C.A., Lu, A., Leng, S., Makarem, R.R., Cho, C., Rusin, C.G., Breault, D.T., Barrett, P.Q., et al. (2020). Angiotensin II induces coordinated calcium bursts in aldosterone-producing adrenal rosettes. Nat Commun *11*, 1679.

Guasti, L., Cavlan, D., Cogger, K., Banu, Z., Shakur, A., Latif, S., and King, P.J. (2013a). Dlk1 Up-Regulates Gli1 Expression in Male Rat Adrenal Capsule Cells Through the Activation of β Integrin and ERK1/2. Endocrinology *154*, 4675–4684.

Guasti, L., Candy Sze, W.C., McKay, T., Grose, R., and King, P.J. (2013b). FGF signalling through Fgfr2 isoform IIIb regulates adrenal cortex development. Molecular and Cellular Endocrinology *371*, 182–188.

Guo, C., Hildick, K.L., Luo, J., Dearden, L., Wilkinson, K.A., and Henley, J.M. (2013). SENP3-mediated deSUMOylation of dynamin-related protein 1 promotes cell death following ischaemia. EMBO J *32*, 1514–1528.

Guo, C., Wilkinson, K.A., Evans, A.J., Rubin, P.P., and Henley, J.M. (2017). SENP3-mediated deSUMOylation of Drp1 facilitates interaction with Mff to promote cell death. Sci Rep *7*, 43811.

Guo, C., Hildick, K.L., Jiang, J., Zhao, A., Guo, W., Henley, J.M., and Wilkinson, K.A. (2021). SENP3 Promotes an Mff-Primed Bcl-xL-Drp1 Interaction Involved in Cell Death Following Ischemia. Front. Cell Dev. Biol. *9*, 752260.

Guo, D., Li, M., Zhang, Y., Yang, P., Eckenrode, S., Hopkins, D., Zheng, W., Purohit, S., Podolsky, R.H., Muir, A., et al. (2004). A functional variant of SUMO4, a new IκBα modifier, is associated with type 1 diabetes. Nat Genet *36*, 837–841.

Hadjidemetriou, I., Mariniello, K., Ruiz-Babot, G., Pittaway, J., Mancini, A., Mariannis, D., Gomez-Sanchez, C.E., Parvanta, L., Drake, W.M., Chung, T.-T., et al. (2019). DLK1/PREF1 marks a novel cell population in the human adrenal cortex. The Journal of Steroid Biochemistry and Molecular Biology *193*, 105422.

Häfner, R., Bohnenpoll, T., Rudat, C., Schultheiss, T.M., and Kispert, A. (2015). Fgfr2 is required for the expansion of the early adrenocortical primordium. Molecular and Cellular Endocrinology *413*, 168–177.

Halloun, R., Habib, C., Ekhilevitch, N., Weiss, R., Tiosano, D., and Cohen, M. (2021). Expanding the spectrum of endocrinopathies identified in Schaaf-Yang syndrome - A case report and review of the literature. European Journal of Medical Genetics *64*, 104252.

Hammer, G.D., Krylova, I., Zhang, Y., Darimont, B.D., Simpson, K., Weigel, N.L., and Ingraham, H.A. (1999). Phosphorylation of the Nuclear Receptor SF-1 Modulates Cofactor Recruitment. Molecular Cell *3*, 521–526.

Han, Y., Huang, C., Sun, X., Xiang, B., Wang, M., Yeh, E.T.H., Chen, Y., Li, H., Shi, G., Cang, H., et al. (2010). SENP3-mediated De-conjugation of SUMO2/3 from Promyelocytic Leukemia Is Correlated with Accelerated Cell Proliferation under Mild Oxidative Stress. Journal of Biological Chemistry *285*, 12906–12915.

Hanel, W., Lata, P., Youssef, Y., Tran, H., Tsyba, L., Sehgal, L., Blaser, B.W., Huszar, D., Helmig-Mason, J., Zhang, L., et al. (2022). A sumoylation program is essential for maintaining the mitotic

fidelity in proliferating mantle cell lymphoma cells. Exp Hematol Oncol *11*, 40.

Hao, H.-X., Xie, Y., Zhang, Y., Charlat, O., Oster, E., Avello, M., Lei, H., Mickanin, C., Liu, D., Ruffner, H., et al. (2012). ZNRF3 promotes Wnt receptor turnover in an R-spondin-sensitive manner. Nature *485*, 195–200.

Harder, Z., Zunino, R., and McBride, H. (2004). Sumo1 Conjugates Mitochondrial Substrates and Participates in Mitochondrial Fission. Current Biology *14*, 340–345.

Harding, M.J., McGraw, H.F., and Nechiporuk, A. (2014). The roles and regulation of multicellular rosette structures during morphogenesis. Development *141*, 2549–2558.

Hart, M., Concordet, J.P., Lassot, I., Albert, I., del los Santos, R., Durand, H., Perret, C., Rubinfeld, B., Margottin, F., Benarous, R., et al. (1999). The F-box protein β-TrCP associates with phosphorylated β-catenin and regulates its activity in the cell. Curr Biol *9*, 207–210.

Hartig, S.M., Bader, D.A., Abadie, K.V., Motamed, M., Hamilton, M.P., Long, W., York, B., Mueller, M., Wagner, M., Trauner, M., et al. (2015). Ubc9 Impairs Activation of the Brown Fat Energy Metabolism Program in Human White Adipocytes. Molecular Endocrinology *29*, 1320–1333.

Hasegawa, T., Zhao, L., Caron, K.M., Majdic, G., Suzuki, T., Shizawa, S., Sasano, H., and Parker, K.L. (2000). Developmental Roles of the Steroidogenic Acute Regulatory Protein (StAR) as Revealed by StAR Knockout Mice. Molecular Endocrinology *14*, 1462–1471.

Hatano, O., Takakusu, A., Nomura, M., and Morohash, K. (1996). Identical origin of adrenal cortex and gonad revealed by expression profiles of Ad4BP/SF-1. Genes to Cells *1*, 663–671.

Hay, R.T. (2005). SUMO : A History of Modification. Molecular Cell *18*, 1–12.

Hazell, G., Horn, G., Lightman, S.L., and Spiga, F. (2019). Dynamics of ACTH-Mediated Regulation of Gene Transcription in ATC1 and ATC7 Adrenal Zona Fasciculata Cell Lines. Endocrinology *160*, 587–604.

He, X., Riceberg, J., Soucy, T., Koenig, E., Minissale, J., Gallery, M., Bernard, H., Yang, X., Liao, H., Rabino, C., et al. (2017). Probing the roles of SUMOylation in cancer cell biology by using a selective SAE inhibitor. Nat Chem Biol *13*, 1164–1171.

Hecker, C.-M., Rabiller, M., Haglund, K., Bayer, P., and Dikic, I. (2006). Specification of SUMO1- and SUMO2-interacting Motifs. Journal of Biological Chemistry *281*, 16117–16127.

Heikkilä, M., Peltoketo, H., Leppäluoto, J., Ilves, M., Vuolteenaho, O., and Vainio, S. (2002). Wnt-4 Deficiency Alters Mouse Adrenal Cortex Function, Reducing Aldosterone Production. Endocrinology *143*, 4358–4365.

Heitzmann, D., Derand, R., Jungbauer, S., Bandulik, S., Sterner, C., Schweda, F., Wakil, A.E., Lalli, E., Guy, N., Mengual, R., et al. (2008). Invalidation of TASK1 potassium channels disrupts adrenal gland zonation and mineralocorticoid homeostasis. EMBO J *27*, 179–187.

Helfenberger, K.E., Castillo, A.F., Mele, P.G., Fiore, A., Herrera, L., Finocchietto, P., Podest'a, E.J., and Poderoso, C. (2019). Angiotensin II

stimulation promotes mitochondrial fusion as a novel mechanism involved in protein kinase compartmentalization and cholesterol transport in human adrenocortical cells. The Journal of Steroid Biochemistry and Molecular Biology *192*, 105413.

Hendriks, I.A., and Vertegaal, A.C.O. (2016). A comprehensive compilation of SUMO proteomics. Nat Rev Mol Cell Biol *17*, 581–595.

Hendriks, I.A., Lyon, D., Su, D., Skotte, N.H., Daniel, J.A., Jensen, L.J., and Nielsen, M.L. (2018). Site-specific characterization of endogenous SUMOylation across species and organs. Nat Commun *9*, 2456.

Hendriksen, J., Fagotto, F., van der Velde, H., van Schie, M., Noordermeer, J., and Fornerod, M. (2005). RanBP3 enhances nuclear export of active β-catenin independently of CRM1. J Cell Biol *171*, 785–797.

Heng, J.-C.D., Feng, B., Han, J., Jiang, J., Kraus, P., Ng, J.-H., Orlov, Y.L., Huss, M., Yang, L., Lufkin, T., et al. (2010). The Nuclear Receptor Nr5a2 Can Replace Oct4 in the Reprogramming of Murine Somatic Cells to Pluripotent Cells. Cell Stem Cell *6*, 167–174.

Hershkovitz, L., Beuschlein, F., Klammer, S., Krup, M., and Weinstein, Y. (2007). Adrenal 20alpha-Hydroxysteroid Dehydrogenase in the Mouse Catabolizes Progesterone and 11-Deoxycorticosterone and Is Restricted to the X-Zone. Endocrinology *148*, 976–988.

Herzog, M., Wendling, O., Guillou, F., Chambon, P., Mark, M., Losson, R., and Cammas, F. (2011). TIF1β association with HP1 is essential for post-gastrulation development, but not for Sertoli cell functions during spermatogenesis. Developmental Biology *350*, 548–558.

Hietakangas, V., Anckar, J., Blomster, H.A., Fujimoto, M., Palvimo, J.J., Nakai, A., and Sistonen, L. (2006). PDSM, a motif for phosphorylation-dependent SUMO modification. Proc. Natl. Acad. Sci. U.S.A. *103*, 45–50.

Higuchi, C., Yamamoto, M., Shin, S.-W., Miyamoto, K., and Matsumoto, K. (2019). Perturbation of maternal PIASy abundance disrupts zygotic genome activation and embryonic development via SUMOylation pathway. Biology Open *8*, bio048652.

Hill, M.A. (2010). Embryology carnegie stage comparison (https://embryology.med.unsw.edu.au/embryology/index.php/Carnegie_Stage_Comparison, consulté le 2/5/22).

Hinson, J.P., Cameron, L.A., Purbrick, A., and Kapas, S. (1994). The role of neuropeptides in the regulation of adrenal zona glomerulosa function: Effects of substance P, neuropeptide Y, neurotensin, Met-enkephalin, Leu-enkephalin and corticotrophin-releasing hormone on aldosterone secretion in the intact perfused rat adrenal. Journal of Endocrinology *140*, 91–96.

Hoekstra, M., and Van Eck, M. (2016). HDL is redundant for adrenal steroidogenesis in LDLR knockout mice with a human-like lipoprotein profile. Journal of Lipid Research *57*, 631–637.

Hoekstra, M., Meurs, I., Koenders, M., Out, R., Hildebrand, R.B., Kruijt, J.K., Van Eck, M., and Van Berkel, T.J.C. (2008). Absence of HDL cholesteryl ester uptake in mice via SR-BI impairs an adequate adrenal glucocorticoid-mediated stress response to fasting. Journal of Lipid Research *49*, 738–745.

Hoekstra, M., van der Sluis, R.J., Van Eck, M., and Van Berkel, T.J.C. (2013). Adrenal-Specific Scavenger Receptor BI Deficiency Induces Glucocorticoid Insufficiency and Lowers Plasma Very-Low-Density and Low-Density Lipoprotein Levels in Mice. ATVB *33*.

Hori, S., Nomura, T., and Sakaguchi, S. (2003). Control of Regulatory T Cell Development by the Transcription Factor *Foxp3*. Science *299*, 1057–1061.

Hu, J., Zhang, Z., Shen, W.-J., and Azhar, S. (2010). Cellular cholesterol delivery, intracellular processing and utilization for biosynthesis of steroid hormones. Nutr Metab (Lond) *7*, 47.

Hu, M.-M., Yang, Q., Xie, X.-Q., Liao, C.-Y., Lin, H., Liu, T.-T., Yin, L., and Shu, H.-B. (2016). Sumoylation Promotes the Stability of the DNA Sensor cGAS and the Adaptor STING to Regulate the Kinetics of Response to DNA Virus. Immunity *45*, 555–569.

Huang, C.-C.J., and Kang, Y. (2019). The transient cortical zone in the adrenal gland: The mystery of the adrenal X-zone. Journal of Endocrinology *241*, R51–R63.

Huang, C., Han, Y., Wang, Y., Sun, X., Yan, S., Yeh, E.T.H., Chen, Y., Cang, H., Li, H., Shi, G., et al. (2009). SENP3 is responsible for HIF-1 transactivation under mild oxidative stress via P300 de-SUMOylation. EMBO J *28*, 2748–2762.

Huang, C., Wu, D., Jiao, X., Khan, F.A., Xiong, C., Liu, X., Yang, J., Yin, T., and Huo, L. (2017). Maternal SENP7 programs meiosis architecture and embryo survival in mouse. Biochimica Et Biophysica Acta (BBA) - Molecular Cell Research *1864*, 1195–1206.

Huang, C.-C.J., Miyagawa, S., Matsumaru, D., Parker, K.L., and Yao, H.H.-C. (2010). Progenitor Cell Expansion and Organ Size of Mouse Adrenal Is Regulated by Sonic Hedgehog. Endocrinology *151*, 1119–1128.

Huang, C.-C.J., Liu, C., and Yao, H.H.-C. (2012). Investigating the role of adrenal cortex in organization and differentiation of the adrenal medulla in mice. Molecular and Cellular Endocrinology *361*, 165–171.

Huang, H.-J., Zhou, L.-L., Fu, W.-J., Zhang, C.-Y., Jiang, H., Du, J., and Hou, J. (2015). β-catenin SUMOylation is involved in the dysregulated proliferation of myeloma cells. Am J Cancer Res *5*, 309–320.

Huang, J., Xie, P., Dong, Y., and An, W. (2020). Inhibition of Drp1 SUMOylation by ALR protects the liver from ischemia-reperfusion injury. Cell Death Differ.

Hwang, J.R., Chou, C.-L., Medvar, B., Knepper, M.A., and Jung, H.J. (2017). Identification of β-catenin-interacting proteins in nuclear fractions of native rat collecting duct cells. American Journal of Physiology-Renal Physiology *313*, F30–F46.

Hyatt, P. (1987). Functional significance of the adrenal zones. In Recent Advances in Adrenal Regulation and Function, (Raven Press, New York), pp. 35–49.

Ikeda, S., Kishida, S., Yamamoto, H., Murai, H., Koyama, S., and Kikuchi, A. (1998). Axin, a negative regulator of the Wnt signaling pathway, forms a complex with GSK-3β and β-catenin and promotes GSK-3β-dependent phosphorylation of β-catenin. EMBO J *17*, 1371–1384.

Inomata, A., and Sasano, H. (2015). Practical

approaches for evaluating adrenal toxicity in nonclinical safety assessment. J Toxicol Pathol *28*, 125–132.

Ishii, T., Mitsui, T., Suzuki, S., Matsuzaki, Y., and Hasegawa, T. (2012). A Genome-Wide Expression Profile of Adrenocortical Cells in Knockout Mice Lacking Steroidogenic Acute Regulatory Protein. Endocrinology *153*, 2714–2723.

Itahana, Y., Yeh, E.T.H., and Zhang, Y. (2006). Nucleocytoplasmic Shuttling Modulates Activity and Ubiquitination-Dependent Turnover of SUMO-Specific Protease 2. Mol Cell Biol *26*, 4675–4689.

Ito, M., Ye, X., Wang, Q., Guo, L., Hao, D., Howatt, D., Daugherty, A., Cai, L., Temel, R., and Li, X.-A. (2020). SR-BI (Scavenger Receptor BI), Not LDL (Low-Density Lipoprotein) Receptor, Mediates Adrenal Stress Response. ATVB.

Itoh, K., Brott, B.K., Bae, G.-U., Ratcliffe, M.J., and Sokol, S.Y. (2005). Nuclear localization is required for Dishevelled function in Wnt/β-catenin signaling. J Biol *4*, 3.

Jaillard, S., Bell, K., Akloul, L., Walton, K., McElreavy, K., Stocker, W.A., Beaumont, M., Harrisson, C., Jääskeläinen, T., Palvimo, J.J., et al. (2020). New insights into the genetic basis of premature ovarian insufficiency: Novel causative variants and candidate genes revealed by genomic sequencing. Maturitas *141*, 9–19.

Jamieson, C., Mills, K.M., Lui, C., Semaan, C., Molloy, M.P., Sharma, M., Forwood, J.K., and Henderson, B.R. (2016). Characterization of a beta-catenin nuclear localization defect in MCF-7 breast cancer cells. Experimental Cell Research *341*, 196–206.

Jentsch, S., and Psakhye, I. (2013). Control of Nuclear Activities by Substrate-Selective and Protein-Group SUMOylation. Annu. Rev. Genet. *47*, 167–186.

Jiang, M., Chiu, S.-Y., and Hsu, W. (2011). SUMO-specific protease 2 in Mdm2-mediated regulation of P53. Cell Death Differ *18*, 1005–1015.

Jiang, Q.-F., Tian, Y.-W., Shen, Q., Xue, H.-Z., and Li, K. (2014). SENP2 regulated the stability of β-catenin through WWOX in hepatocellular carcinoma cell. Tumor Biology *35*, 9677–9682.

Jin, C., Shiyanova, T., Shen, Z., and Liao, X. (2001). Heteronuclear nuclear magnetic resonance assignments, structure and dynamics of SUMO-1, a human ubiquitin-like protein. International Journal of Biological Macromolecules *28*, 227–234.

Joels, M., Karst, H., Krugers, H.J., and Lucassen, P.J. (2007). Chronic stress: Implications for neuronal morphology, function and neurogenesis. Frontiers in Neuroendocrinology *28*, 72–96.

Johnson, E.S. (1997). The ubiquitin-like protein Smt3p is activated for conjugation to other proteins by an Aos1p/Uba2p heterodimer. The EMBO Journal *16*, 5509–5519.

Jones, M.C., Fusi, L., Higham, J.H., Abdel-Hafiz, H., Horwitz, K.B., Lam, E.W.-F., and Brosens, J.J. (2006). Regulation of the SUMO pathway sensitizes differentiating human endometrial stromal cells to progesterone. Proceedings of the National Academy of Sciences *103*, 16272–16277.

Jopek, K., Celichowski, P., Szyszka, M., Tyczewska, M., Milecka, P., Malendowicz, L.K., and Rucinski, M. (2017). Transcriptome Profile of Rat Adrenal Evoked by Gonadectomy

and Testosterone or Estradiol Replacement. Front Endocrinol (Lausanne) *8*, 26.

Jukam, D., Shariati, S.A.M., and Skotheim, J.M. (2017). Zygotic Genome Activation in Vertebrates. Developmental Cell *42*, 316–332.

Kadoya, T., Kishida, S., Fukui, A., Hinoi, T., Michiue, T., Asashima, M., and Kikuchi, A. (2000). Inhibition of Wnt Signaling Pathway by a Novel Axin-binding Protein. Journal of Biological Chemistry *275*, 37030–37037.

Kadoya, T., Yamamoto, H., Suzuki, T., Yukita, A., Fukui, A., Michiue, T., Asahara, T., Tanaka, K., Asashima, M., and Kikuchi, A. (2002). Desumoylation Activity of Axam, a Novel Axin-Binding Protein, Is Involved in Downregulation of β-Catenin. Mol Cell Biol *22*, 3803–3819.

Kagey, M.H., Melhuish, T.A., and Wotton, D. (2003). The Polycomb Protein Pc2 Is a SUMO E3. Cell *113*, 127–137.

Kahyo, T., Nishida, T., and Yasuda, H. (2001). Involvement of PIAS1 in the Sumoylation of Tumor Suppressor P53. Molecular Cell *8*, 713–718.

Kallen, C.B., Billheimer, J.T., Summers, S.A., Stayrook, S.E., Lewis, M., and Strauss, J.F. (1998). Steroidogenic Acute Regulatory Protein (StAR) Is A Sterol Transfer Protein. Journal of Biological Chemistry *273*, 26285–26288.

Kamilaris, C.D.C., Faucz, F.R., Voutetakis, A., and Stratakis, C.A. (2019). Carney Complex. Exp Clin Endocrinol Diabetes *127*, 156–164.

Kamilaris, C.D.C., Stratakis, C.A., and Hannah-Shmouni, F. (2021). Molecular Genetic and Genomic Alterations in Cushing's Syndrome and Primary Aldosteronism. Front. Endocrinol. *12*, 632543.

Kang, X., Qi, Y., Zuo, Y., Wang, Q., Zou, Y., Schwartz, R.J., Cheng, J., and Yeh, E.T.H. (2010). SUMO-Specific Protease 2 Is Essential for Suppression of Polycomb Group Protein-Mediated Gene Silencing during Embryonic Development. Molecular Cell *38*, 191–201.

Kaouane, N., Porte, Y., VallÃÂe, M., Brayda-Bruno, L., Mons, N., Calandreau, L., Marighetto, A., Piazza, P.V., and Desmedt, A. (2012). Glucocorticoids Can Induce PTSD-Like Memory Impairments in Mice. Science *335*, 1510–1513.

Karami, S., Lin, F.-M., Kumar, S., Bahnassy, S., Thangavel, H., Quttina, M., Li, Y., Ren, J., and Bawa-Khalfe, T. (2017). Novel SUMO-Protease SENP7S Regulates β-catenin Signaling and Mammary Epithelial Cell Transformation. Scientific Reports *7*, 46477.

Keller-Wood, M. (2015). Hypothalamic-Pituitary-Adrenal Axis—Feedback Control. In Comprehensive Physiology, R. Terjung, ed. (Wiley), pp. 1161–1182.

Kiel, C., and Serrano, L. (2006). The Ubiquitin Domain Superfold: Structure-based Sequence Alignments and Characterization of Binding Epitopes. Journal of Molecular Biology *355*, 821–844.

Kim, A.C., Reuter, A.L., Zubair, M., Else, T., Serecky, K., Bingham, N.C., Lavery, G.G., Parker, K.L., and Hammer, G.D. (2008). Targeted disruption of β-catenin in Sf1-expressing cells impairs development and maintenance of the adrenal cortex. Development *135*, 2593–2602.

Kim, H., Scimia, M.C., Wilkinson, D., Trelles, R.D., Wood, M.R., Bowtell, D., Dillin, A., Mercola, M., and Ronai, Z.A. (2011). Fine-Tuning

of Drp1/Fis1 Availability by AKAP121/Siah2 Regulates Mitochondrial Adaptation to Hypoxia. Molecular Cell *44*, 532–544.

Kim, K.I., Baek, S.H., Jeon, Y.-J., Nishimori, S., Suzuki, T., Uchida, S., Shimbara, N., Saitoh, H., Tanaka, K., and Chung, C.H. (2000). A New SUMO-1-specific Protease, SUSP1, That Is Highly Expressed in Reproductive Organs. J. Biol. Chem. *275*, 14102–14106.

Kim, Y., Bingham, N., Sekido, R., Parker, K.L., Lovell-Badge, R., and Capel, B. (2007). Fibroblast growth factor receptor 2 regulates proliferation and Sertoli differentiation during male sex determination. Proceedings of the National Academy of Sciences *104*, 16558–16563.

King, P., Paul, A., and Laufer, E. (2009). Shh signaling regulates adrenocortical development and identifies progenitors of steroidogenic lineages. Proceedings of the National Academy of Sciences *106*, 21185–21190.

Koirala, S., Guo, Q., Kalia, R., Bui, H.T., Eckert, D.M., Frost, A., and Shaw, J.M. (2013). Interchangeable adaptors regulate mitochondrial dynamin assembly for membrane scission. Proc. Natl. Acad. Sci. U.S.A. *110*.

Komatsu, T., Mizusaki, H., Mukai, T., Ogawa, H., Baba, D., Shirakawa, M., Hatakeyama, S., Nakayama, K.I., Yamamoto, H., Kikuchi, A., et al. (2004). Small Ubiquitin-Like Modifier 1 (SUMO-1) Modification of the Synergy Control Motif of Ad4 Binding Protein/Steroidogenic Factor 1 (Ad4BP/SF-1) Regulates Synergistic Transcription between Ad4BP/SF-1 and Sox9. Molecular Endocrinology *18*, 2451–2462.

Korinek, V., Barker, N., Morin, P.J., van Wichen, D., de Weger, R., Kinzler, K.W., Vogelstein, B., and Clevers, H. (1997). Constitutive Transcriptional Activation by a β-Catenin-Tcf Complex in APCmin Colon Carcinoma. Science *275*, 1784–1787.

Kotaja, N., Karvonen, U., Janne, O.A., and Palvimo, J.J. (2002). PIAS Proteins Modulate Transcription Factors by Functioning as SUMO-1 Ligases. Molecular and Cellular Biology *22*, 5222–5234.

Kotelevtsev, Y., Brown, R.W., Fleming, S., Kenyon, C., Edwards, C.R.W., Seckl, J.R., and Mullins, J.J. (1999). Hypertension in mice lacking 11beta-hydroxysteroid dehydrogenase type 2. J. Clin. Invest. *103*, 683–689.

Kozlov, S.V., Bogenpohl, J.W., Howell, M.P., Wevrick, R., Panda, S., Hogenesch, J.B., Muglia, L.J., Van Gelder, R.N., Herzog, E.D., and Stewart, C.L. (2007). The imprinted gene Magel2 regulates normal circadian output. Nat Genet *39*, 1266–1272.

Kraemer, F.B., Shen, W.-J., Patel, S., Osuga, J., Ishibashi, S., and Azhar, S. (2007). The LDL receptor is not necessary for acute adrenal steroidogenesis in mouse adrenocortical cells. American Journal of Physiology-Endocrinology and Metabolism *292*, E408–E412.

Krieghoff, E., Behrens, J., and Mayr, B. (2006). Nucleo-cytoplasmic distribution of β-catenin is regulated by retention. Journal of Cell Science *119*, 1453–1463.

Lacroix, A., Feelders, R.A., Stratakis, C.A., and Nieman, L.K. (2015). Cushing's syndrome. The Lancet *386*, 913–927.

Lallemand-Breitenbach, V., and de Thé, H.

(2018). PML nuclear bodies: From architecture to function. Current Opinion in Cell Biology *52*, 154–161.

Lambert-Langlais, S., Val, P., Guyot, S., Ragazzon, B., Sahut-Barnola, I., De Haze, A., Lefrançois-Martinez, A.-M., and Martinez, A. (2009). A transgenic mouse line with specific Cre recombinase expression in the adrenal cortex. Mol Cell Endocrinol *300*, 197–204.

Langston, S.P., Grossman, S., England, D., Afroze, R., Bence, N., Bowman, D., Bump, N., Chau, R., Chuang, B.-C., Claiborne, C., et al. (2021). Discovery of TAK-981, a First-in-Class Inhibitor of SUMO-Activating Enzyme for the Treatment of Cancer. J. Med. Chem. *64*, 2501–2520.

Laufer, E., Kesper, D., Vortkamp, A., and King, P. (2012). Sonic hedgehog signaling during adrenal development. Molecular and Cellular Endocrinology *351*, 19–27.

Le Moal, M. (2007). Historical approach and evolution of the stress concept: A personal account. Psychoneuroendocrinology *32*, S3–S9.

Lee, S. (2000). Expression and imprinting of MAGEL2 suggest a role in Prader-Willi syndrome and the homologous murine imprinting phenotype. Human Molecular Genetics *9*, 1813–1819.

Lee, F.Y., Faivre, E.J., Suzawa, M., Lontok, E., Ebert, D., Cai, F., Belsham, D.D., and Ingraham, H.A. (2011). Eliminating SF-1 (NR5A1) Sumoylation In Vivo Results in Ectopic Hedgehog Signaling and Disruption of Endocrine Development. Developmental Cell *21*, 315–327.

Lee, J., Yang, D.J., Lee, S., Hammer, G.D., Kim, K.W., and Elmquist, J.K. (2016). Nutritional conditions regulate transcriptional activity of SF-1 by controlling sumoylation and ubiquitination. Sci Rep *6*, 19143.

Lee, J.S., Chae, S., Nan, J., Koo, Y.D., Lee, S.-A., Park, Y.J., Hwang, D., Han, W., Lee, D.-S., Kim, Y.-B., et al. (2022). SENP2 suppresses browning of white adipose tissues by de-conjugating SUMO from C/EBPβ. Cell Reports *38*, 110408.

Lee, M.B., Lebedeva, L.A., Suzawa, M., Wadekar, S.A., Desclozeaux, M., and Ingraham, H.A. (2005). The DEAD-Box Protein DP103 (Ddx20 or Gemin-3) Represses Orphan Nuclear Receptor Activity via SUMO Modification. MCB *25*, 1879–1890.

Lefrançois-Martinez, A.-M., Tournaire, C., Martinez, A., Berger, M., Daoudal, S., Tritsch, D., Veyssiere, G., and Jean, C. (1999). Product of Side-chain Cleavage of Cholesterol, Isocaproaldehyde, Is an Endogenous Specific Substrate of Mouse Vas Deferens Protein, an Aldose Reductase-like Protein in Adrenocortical Cells. Journal of Biological Chemistry *274*, 32875–32880.

Leng, S., Pignatti, E., Khetani, R.S., Shah, M.S., Xu, S., Miao, J., Taketo, M.M., Beuschlein, F., Barrett, P.Q., Carlone, D.L., et al. (2020). β-Catenin and FGFR2 regulate postnatal rosette-based adrenocortical morphogenesis. Nat Commun *11*, 1680.

Levasseur, A. (en préparation).

Levasseur, A., Dumontet, T., and Martinez, A. (2019). Sexual dimorphism in adrenal gland development and tumorigenesis. Current Opinion in Endocrine and Metabolic Research *8*, 60–65.

Li, J., and Wang, C.-Y. (2008). TBL1–TBLR1 and β-catenin recruit each other to Wnt target-gene promoter for transcription activation and oncogenesis. Nat Cell Biol *10*, 160–169.

Li, H., Zhang, W., Yan, M., Qiu, J., Chen, J., Sun, X., Chen, X., Song, L., and Zhang, Y. (2019). Nucleolar and spindle associated protein 1 promotes metastasis of cervical carcinoma cells by activating Wnt/β-catenin signaling. J Exp Clin Cancer Res *38*, 33.

Li, J., Lu, D., Dou, H., Liu, H., Weaver, K., Wang, W., Li, J., Yeh, E.T.H., Williams, B.O., Zheng, L., et al. (2018). Desumoylase SENP6 maintains osteochondroprogenitor homeostasis by suppressing the P53 pathway. Nat Commun *9*, 143.

Li, M., Xu, X., Chang, C.-W., and Liu, Y. (2020). TRIM28 functions as the SUMO E3 ligase for PCNA in prevention of transcription induced DNA breaks. Proc Natl Acad Sci USA *117*, 23588–23596.

Li, V.S.W., Ng, S.S., Boersema, P.J., Low, T.Y., Karthaus, W.R., Gerlach, J.P., Mohammed, S., Heck, A.J.R., Maurice, M.M., Mahmoudi, T., et al. (2012). Wnt Signaling through Inhibition of β-Catenin Degradation in an Intact Axin1 Complex. Cell *149*, 1245–1256.

Li, X., Vadrevu, S., Dunlop, A., Day, J., Advant, N., Troeger, J., Klussmann, E., Jaffrey, E., Hay, R.T., Adams, D.R., et al. (2010). Selective SUMO modification of cAMP-specific phosphodiesterase-4D5 (PDE4D5) regulates the functional consequences of phosphorylation by PKA and ERK. Biochemical Journal *428*, 55–65.

Li, Y., Varejão, N., and Reverter, D. (2022). Structural basis for the SUMO protease activity of the atypical ubiquitin-specific protease USPL1. Nat Commun *13*, 1819.

Liang, Q., Zheng, Q., Zuo, Y., Chen, Y., Ma, J., Ni, P., and Cheng, J. (2019). SENP2 Suppresses Necdin Expression to Promote Brown Adipocyte Differentiation. Cell Reports *28*, 2004–2011.e4.

Liang, Y.-C., Lee, C.-C., Yao, Y.-L., Lai, C.-C., Schmitz, M.L., and Yang, W.-M. (2016). SUMO5, a Novel Poly-SUMO Isoform, Regulates PML Nuclear Bodies. Sci Rep *6*, 26509.

Lima, C.D., and Reverter, D. (2008). Structure of the Human SENP7 Catalytic Domain and Poly-SUMO Deconjugation Activities for SENP6 and SENP7. Journal of Biological Chemistry *283*, 32045–32055.

Lin, D., Sugawara, T., Strauss, J.F., Clark, B.J., Stocco, D.M., Saenger, P., Rogol, A., and Miller, W.L. (1995). Role of Steroidogenic Acute Regulatory Protein in Adrenal and Gonadal Steroidogenesis. Science *267*, 1828–1831.

Lin, D., Tatham, M.H., Yu, B., Kim, S., Hay, R.T., and Chen, Y. (2002). Identification of a Substrate Recognition Site on Ubc9. Journal of Biological Chemistry *277*, 21740–21748.

Lin, Y., Hou, X., Shen, W.-J., Hanssen, R., Khor, V.K., Cortez, Y., Roseman, A.N., Azhar, S., and Kraemer, F.B. (2016). SNARE-Mediated Cholesterol Movement to Mitochondria Supports Steroidogenesis in Rodent Cells. Molecular Endocrinology *30*, 234–247.

Liu, A. (2019). Proteostasis in the Hedgehog signaling pathway. Seminars in Cell & Developmental Biology *93*, 153–163.

Liu, B., Mink, S., Wong, K.A., Stein, N., Getman, C., Dempsey, P.W., Wu, H., and Shuai, K. (2004). PIAS1 selectively inhibits interferon-inducible genes and is important in innate immunity. Nat Immunol *5*, 891–898.

Liu, B., Tahk, S., Yee, K.M., Fan, G., and Shuai, K. (2010). The Ligase PIAS1 Restricts Natural Regulatory T Cell Differentiation by Epigenetic Repression. Science *330*, 521–525.

Liu, B., Wang, T., Mei, W., Li, D., Cai, R., Zuo, Y., and Cheng, J. (2014b). Small Ubiquitin-like Modifier (SUMO) Protein-specific Protease 1 De-SUMOylates Sharp-1 Protein and Controls Adipocyte Differentiation. J. Biol. Chem. *289*, 22358–22364.

Liu, B., Yee, K.M., Tahk, S., Mackie, R., Hsu, C., and Shuai, K. (2014a). PIAS1 SUMO ligase regulates the self-renewal and differentiation of hematopoietic stem cells. EMBO J *33*, 101–113.

Liu, S.Y., Ma, Y.L., and Lee, E.H.Y. (2013a). NMDA receptor signaling mediates the expression of protein inhibitor of activated STAT1 (PIAS1) in rat hippocampus. Neuropharmacology *65*, 101–113.

Liu, Y., Zhang, Y.-D., Guo, L., Huang, H.-Y., Zhu, H., Huang, J.-X., Liu, Y., Zhou, S.-R., Dang, Y.-J., Li, X., et al. (2013b). Protein Inhibitor of Activated STAT 1 (PIAS1) Is Identified as the SUMO E3 Ligase of CCAAT/Enhancer-Binding Protein beta (C/EBPbeta) during Adipogenesis. Mol. Cell. Biol. *33*, 4606–4617.

Loi, M., Sarabdjitsingh, R.A., Tsouli, A., Trinh, S., Arp, M., Krugers, H.J., Karst, H., van den Bos, R., and JoÃÂls, M. (2017). Transient Prepubertal Mifepristone Treatment Normalizes Deficits in Contextual Memory and Neuronal Activity of Adult Male Rats Exposed to Maternal Deprivation. eNeuro *4*, ENEURO.0253–17.2017.

Lopez, A.-G., Duparc, C., Wils, J., Naccache, A., Castanet, M., Lefebvre, H., and Louiset, E. (2021a). Steroidogenic cell microenvironment and adrenal function in physiological and pathophysiological conditions. Molecular and Cellular Endocrinology *535*, 111377.

Lopez, J.P., Brivio, E., Santambrogio, A., De Donno, C., Kos, A., Peters, M., Rost, N., Czamara, D., Bruckl, T.M., Roeh, S., et al. (2021b). Single-cell molecular profiling of all three components of the HPA axis reveals adrenal ABCB1 as a regulator of stress adaptation. Sci. Adv. *7*, eabe4497.

Losón, O.C., Song, Z., Chen, H., and Chan, D.C. (2013). Fis1, Mff, MiD49, and MiD51 mediate Drp1 recruitment in mitochondrial fission. MBoC *24*, 659–667.

Luo, X., Ikeda, Y., and Parker, K.L. (1994). A cell-specific nuclear receptor is essential for adrenal and gonadal development and sexual differentiation. Cell *77*, 481–490.

Luo, Z., Wijeweera, A., Oh, Y., Liou, Y.-C., and Melamed, P. (2010). Pin1 Facilitates the Phosphorylation-Dependent Ubiquitination of SF-1 To Regulate Gonadotropin-Subunit Gene Transcription. MCB *30*, 745–763.

Ma, R., Ma, L., Weng, W., Wang, Y., Liu, H., Guo, R., Gao, Y., Tu, J., Xu, T.-L., Cheng, J., et al. (2020). DUSP6 SUMOylation protects cells from oxidative damage via direct regulation of Drp1 dephosphorylation. Sci. Adv. *6*, eaaz0361.

MacDonald, H.R., and Wevrick, R. (1997). The Necdin Gene is Deleted in Prader-Willi Syndrome and is Imprinted in Human and Mouse. Human Molecular Genetics *6*, 1873–1878.

MacKenzie, S.M., van Kralingen, J.C., and Davies, E. (2019). Regulation of Aldosterone Secretion. In

Vitamins and Hormones, (Elsevier), pp. 241–263.

Mahajan, R., Delphin, C., Guan, T., Gerace, L., and Melchior, F. (1997). A Small Ubiquitin-Related Polypeptide Involved in Targeting RanGAP1 to Nuclear Pore Complex Protein RanBP2. Cell *88*, 97–107.

Malik, S., Dolan, T.M., Maben, Z.J., and Hinkle, P.M. (2015). Adrenocorticotropic Hormone (ACTH) Responses Require Actions of the Melanocortin-2 Receptor Accessory Protein on the Extracellular Surface of the Plasma Membrane. Journal of Biological Chemistry *290*, 27972–27985.

Manza, L.L., Codreanu, S.G., Stamer, S.L., Smith, D.L., Wells, K.S., Roberts, R.L., and Liebler, D.C. (2004). Global Shifts in Protein Sumoylation in Response to Electrophile and Oxidative Stress. Chem. Res. Toxicol. *17*, 1706–1715.

Marik, P.E., and Levitov, A. (2010). The koala stress syndrome and adrenal responsiveness in the critically ill. Intensive Care Med *36*, 1805–1806.

Marongiu, M., Deiana, M., Meloni, A., Marcia, L., Puddu, A., Cao, A., Schlessinger, D., and Crisponi, L. (2010). The Forkhead Transcription Factor Foxl2 Is Sumoylated in Both Human and Mouse: Sumoylation Affects Its Stability, Localization, and Activity. PLoS ONE *5*, e9477.

Mart'ın, M.G., Lindberg, I., SolorzanoVargas, R.S., Wang, J., Avitzur, Y., Bandsma, R., Sokollik, C., Lawrence, S., Pickett, L.A., Chen, Z., et al. (2013). Congenital Proprotein Convertase 1/3 Deficiency Causes Malabsorptive Diarrhea and Other Endocrinopathies in a Pediatric Cohort. Gastroenterology *145*, 138–148.

Maruyama, E.O., Lin, H., Chiu, S.-Y., Yu, H.-M.I., Porter, G.A., and Hsu, W. (2016). Extraembryonic but not embryonic SUMO-specific protease 2 is required for heart development. Sci Rep *6*, 20999.

Maruyama, K., Usami, M., Aizawa, T., and Yoshikawa, K. (1991). A novel brain-specific mRNA encoding nuclear protein (necdin) expressed in neurally differentiated embryonal carcinoma cells. Biochemical and Biophysical Research Communications *178*, 291–296.

Mateska, I., Nanda, K., Dye, N.A., Alexaki, V.I., and Eaton, S. (2020). Range of SHH signaling in adrenal gland is limited by membrane contact to cells with primary cilia. Journal of Cell Biology 24.

Mathieu, M., Drelon, C., Rodriguez, S., Tabbal, H., Septier, A., Damon-Soubeyrand, C., Dumontet, T., Berthon, A., Sahut-Barnola, I., Djari, C., et al. (2018). Steroidogenic differentiation and PKA signaling are programmed by histone methyltransferase EZH2 in the adrenal cortex. Proc Natl Acad Sci USA *115*, E12265–E12274.

Matic, I., van Hagen, M., Schimmel, J., Macek, B., Ogg, S.C., Tatham, M.H., Hay, R.T., Lamond, A.I., Mann, M., and Vertegaal, A.C.O. (2008). In Vivo Identification of Human Small Ubiquitin-like Modifier Polymerization Sites by High Accuracy Mass Spectrometry and an in Vitro to in Vivo Strategy. Molecular & Cellular Proteomics *7*, 132–144.

Matsuda, K., Uruno, A., Kogure, N., Sugawara, K., Shimada, H., Nezu, M., Saito-Ito, T., Iki, Y., Kudo, M., Shimizu, K., et al. (2014). Angiotensin II receptor blockers differentially affect CYP11B2 expression in human adrenal H295R cells. Molecular and Cellular Endocrinology *383*, 60–68.

Matunis, M.J., Coutavas, E., and Blobel, G. (1996). A novel ubiquitin-like modification modulates the

partitioning of the Ran-GTPase-activating protein RanGAP1 between the cytosol and the nuclear pore complex. Journal of Cell Biology *135*, 1457–1470.

McManus, J.M., Bohn, K., Alyamani, M., Chung, Y.-M., Klein, E.A., and Sharifi, N. (2019). Rapid and structure-specific cellular uptake of selected steroids. PLoS ONE *14*, e0224081.

Meimaridou, E., Goldsworthy, M., Chortis, V., Fragouli, E., Foster, P.A., Arlt, W., Cox, R., and Metherell, L.A. (2018). NNT is a key regulator of adrenal redox homeostasis and steroidogenesis in male mice. Journal of Endocrinology *236*, 13–28.

Méjat, A. (2010). LINC complexes in health and disease. Nucleus *1*, 40–52.

Mendoza, H.M., Shen, L., Botting, C., Lewis, A., Chen, J., Ink, B., and Hay, R.T. (2003). NEDP1, a Highly Conserved Cysteine Protease That deNEDDylates Cullins. Journal of Biological Chemistry *278*, 25637–25643.

Menzies, R.I., Zhao, X., Mullins, L.J., Mullins, J.J., Cairns, C., Wrobel, N., Dunbar, D.R., Bailey, M.A., and Kenyon, C.J. (2017). Transcription controls growth, cell kinetics and cholesterol supply to sustain ACTH responses. Endocrine Connections *6*, 446–457.

Mercer, R.E., and Wevrick, R. (2009). Loss of Magel2, a Candidate Gene for Features of Prader-Willi Syndrome, Impairs Reproductive Function in Mice. PLoS ONE *4*, e4291.

Metherell, L.A., Chapple, J.P., Cooray, S., David, A., Becker, C., Ruschendorf, F., Naville, D., Begeot, M., Khoo, B., Nurnberg, P., et al. (2005). Mutations in MRAP, encoding a new interacting partner of the ACTH receptor, cause familial glucocorticoid deficiency type 2. Nat Genet *37*, 166–170.

Migeon, C.J., Kenny, E.M., Kowarski, A., Snipes, C.A., Spaulding, J.S., Finkelstein, J.W., and Blizzard, R.M. (1968). The syndrome of congenital adrenocortical unresponsiveness to ACTH. Report of six cases. Pediatr Res *2*, 501–513.

Mikkonen, L., Hirvonen, J., and Jänne, O.A. (2013). SUMO-1 Regulates Body Weight and Adipogenesis via PPARγ in Male and Female Mice. Endocrinology *154*, 698–708.

Minguez, P., Parca, L., Diella, F., Mende, D.R., Kumar, R., Helmer-Citterich, M., Gavin, A.-C., van Noort, V., and Bork, P. (2012). Deciphering a global network of functionally associated post-translational modifications. Mol Syst Biol *8*, 599.

Minty, A., Dumont, X., Kaghad, M., and Caput, D. (2000). Covalent Modification of P73α by SUMO-1. Journal of Biological Chemistry *275*, 36316–36323.

Mitani, T., Watanabe, S., Yoshioka, Y., Katayama, S., Nakamura, S., and Ashida, H. (2017). Theobromine suppresses adipogenesis through enhancement of CCAAT-enhancer-binding protein beta degradation by adenosine receptor A1. Biochimica Et Biophysica Acta (BBA) - Molecular Cell Research *1864*, 2438–2448.

Mohan, D.R., Borges, K.S., Finco, I., LaPensee, C.R., Rege, J., Solon, A.L., Little, D.W., Else, T., Almeida, M.Q., Dang, D., et al. (2022). β-catenin programs a tissue-specific epigenetic vulnerability in aggressive adrenocortical carcinoma (Cancer Biology).

Monod, J., Wyman, J., and Changeux, J.-P. (1965). On the nature of allosteric transitions: A plausible model. Journal of Molecular Biology *12*, 88–118.

Morley, S.D., Viard, I., Chung, B.C., Ikeda, Y., Parker, K.L., and Mullins, J.J. (1996). Variegated expression of a mouse steroid 21-hydroxylase/β-galactosidase transgene suggests centripetal migration of adrenocortical cells. Molecular Endocrinology *10*, 585–598.

Moscogiuri, G., Formoso, G., Pugliese, G., Ruggeri, R.M., Scarano, E., and Colao, A. (2019). Prader-Willi syndrome: An uptodate on endocrine and metabolic complications. Rev Endocr Metab Disord *20*, 239–250.

Mukhopadhyay, D., and Dasso, M. (2017). The SUMO Pathway in Mitosis. In SUMO Regulation of Cellular Processes, V.G. Wilson, ed. (Cham: Springer International Publishing), pp. 171–184.

Mukhopadhyay, D., Ayaydin, F., Kolli, N., Tan, S.-H., Anan, T., Kametaka, A., Azuma, Y., Wilkinson, K.D., and Dasso, M. (2006). SUSP1 antagonizes formation of highly SUMO2/3-conjugated species. Journal of Cell Biology *174*, 939–949.

Muscatelli, F. (2000). Disruption of the mouse Necdin gene results in hypothalamic and behavioral alterations reminiscent of the human Prader-Willi syndrome. Human Molecular Genetics *9*, 3101–3110.

Nacerddine, K., Lehembre, F., Bhaumik, M., Artus, J., Cohen-Tannoudji, M., Babinet, C., Pandolfi, P.P., and Dejean, A. (2005). The SUMO Pathway Is Essential for Nuclear Integrity and Chromosome Segregation in Mice. Developmental Cell *9*, 769–779.

Nan, J., Lee, J.S., Moon, J.H., Lee, S.-A., Park, Y.J., Lee, D.-S., Chung, S.S., and Park, K.S. (2022). SENP2 regulates mitochondrial function and insulin secretion in pancreatic β cells. Exp Mol Med.

Naville, D., Barjhoux, L., Jaillard, C., Faury, D., Despert, F., Esteva, B., Durand, P., Saez, J.M., and Begeot, M. (1996). Demonstration by transfection studies that mutations in the adrenocorticotropin receptor gene are one cause of the hereditary syndrome of glucocorticoid deficiency. The Journal of Clinical Endocrinology & Metabolism *81*, 1442–1448.

Neyret-Kahn, H., Benhamed, M., Ye, T., Le Gras, S., Cossec, J.-C., Lapaquette, P., Bischof, O., Ouspenskaia, M., Dasso, M., Seeler, J., et al. (2013). Sumoylation at chromatin governs coordinated repression of a transcriptional program essential for cell growth and proliferation. Genome Research *23*, 1563–1579.

Nishida, T., and Yasuda, H. (2002). PIAS1 and PIASxα Function as SUMO-E3 Ligases toward Androgen Receptor and Repress Androgen Receptor-dependent Transcription. J. Biol. Chem. *277*, 41311–41317.

Nishida, T., Tanaka, H., and Yasuda, H. (2000). A novel mammalian Smt3-specific isopeptidase 1 (SMT3IP1) localized in the nucleolus at interphase: Mammalian Smt3-specific isopeptidase. European Journal of Biochemistry *267*, 6423–6427.

Nishida, T., Kaneko, F., Kitagawa, M., and Yasuda, H. (2001). Characterization of a Novel Mammalian SUMO-1/Smt3-specific Isopeptidase, a Homologue of Rat Axam, Which Is an Axin-binding Protein Promoting β-Catenin Degradation. J. Biol. Chem. *276*, 39060–39066.

Nishimoto, K., Rigsby, C.S., Wang, T., Mukai, K., Gomez-Sanchez, C.E., Rainey, W.E., and

Seki, T. (2012). Transcriptome Analysis Reveals Differentially Expressed Transcripts in Rat Adrenal Zona Glomerulosa and Zona Fasciculata. Endocrinology *153*, 1755–1763.

Niwa-Kawakita, M., Ferhi, O., Soilihi, H., Le Bras, M., Lallemand-Breitenbach, V., and de ThÃ, H. (2017). PML is a ROS sensor activating P53 upon oxidative stress. Journal of Experimental Medicine *214*, 3197–3206.

Novoselova, T.V., Hussain, M., King, P.J., Guasti, L., Metherell, L.A., Charalambous, M., Clark, A.J.L., and Chan, L.F. (2018). MRAP deficiency impairs adrenal progenitor cell differentiation and gland zonation. FASEB j. *32*, 6186–6196.

Nyunt, O., Cotterill, A.M., Archbold, S.M., Wu, J.Y., Leong, G.M., Verge, C.F., Crock, P.A., Ambler, G.R., Hofman, P., and Harris, M. (2010). Normal Cortisol Response on Low-Dose Synacthen Test in Children with Prader Willi Syndrome. The Journal of Clinical Endocrinology & Metabolism *95*, E464–E467.

Obrynba, K.S., Hoffman, R.P., Repaske, D.R., Anglin, K., and Kamboj, M.K. (2018). No central adrenal insufficiency found in patients with Prader-Willi syndrome with an overnight metyrapone test. Journal of Pediatric Endocrinology and Metabolism *31*, 809–814.

Odeh, H.M., Coyaud, E., Raught, B., and Matunis, M.J. (2018). The SUMO-specific isopeptidase SENP2 is targeted to intracellular membranes via a predicted N-terminal amphipathic α-helix. MBoC *29*, 1878–1890.

Ogawa, H., Komatsu, T., Hiraoka, Y., and Morohashi, K. (2009). Transcriptional Suppression by Transient Recruitment of ARIP4 to Sumoylated Nuclear Receptor Ad4BP/SF-1. MBoC *20*, 4235–4245.

Oitzl, M.S., Reichardt, H.M., Joels, M., and de Kloet, E.R. (2001). Point mutation in the mouse glucocorticoid receptor preventing DNA binding impairs spatial memory. Proceedings of the National Academy of Sciences *98*, 12790–12795.

Okuma, T., Honda, R., Ichikawa, G., Tsumagari, N., and Yasuda, H. (1999). In VitroSUMO-1 Modification Requires Two Enzymatic Steps, E1 and E2. Biochemical and Biophysical Research Communications *254*, 693–698.

Omar, M.H., and Scott, J.D. (2020). AKAP Signaling Islands: Venues for Precision Pharmacology. Trends in Pharmacological Sciences *41*, 933–946.

Orengo, C.A., Jones, D.T., and Thornton, J.M. (1994). Protein superfamilles and domain superfolds. Nature *372*, 631–634.

Osmanovic, A., Förster, A., Widjaja, M., Auber, B., Das, A.M., Christians, A., Brand, F., Petri, S., and Weber, R.G. (2022). A SUMO4 initiator codon variant in amyotrophic lateral sclerosis reduces SUMO4 expression and alters stress granule dynamics. J Neurol.

Oto, Y., Matsubara, K., Ayabe, T., Shiraishi, M., Murakami, N., Ihara, H., Matsubara, T., and Nagai, T. (2018). Delayed peak response of cortisol to insulin tolerance test in patients with Prader-Willi syndrome. Am J Med Genet *176*, 1369–1374.

Owen, D.R., Fan, J., Campioli, E., Venugopal, S., Midzak, A., Daly, E., Harlay, A., Issop, L., Libri, V., Kalogiannopoulou, D., et al. (2017). *TSPO* mutations in rats and a human polymorphism

impair the rate of steroid synthesis. Biochemical Journal *474*, 3985–3999.

Owerbach, D., McKay, E.M., Yeh, E.T.H., Gabbay, K.H., and Bohren, K.M. (2005). A proline-90 residue unique to SUMO-4 prevents maturation and sumoylation. Biochemical and Biophysical Research Communications *337*, 517–520.

Papadopoulos, V., Fan, J., and Zirkin, B. (2018). Translocator protein (18 kDa): An update on its function in steroidogenesis. Journal of Neuroendocrinology *30*, e12500.

Park, J.-E., Kim, Y.-J., Lee, S.G., Kim, J.Y., Chung, J.-Y., Jeong, S.-Y., Koh, H., Yun, J., Park, H.T., Yoo, Y.H., et al. (2019). Drp1 Phosphorylation Is Indispensable for Steroidogenesis in Leydig Cells. Endocrinology *160*, 729–743.

Park, J.H., Lee, S.W., Yang, S.W., Yoo, H.M., Park, J.M., Seong, M.W., Ka, S.H., Oh, K.H., Jeon, Y.J., and Chung, C.H. (2014). Modification of DBC1 by SUMO2/3 is crucial for P53-mediated apoptosis in response to DNA damage. Nat Commun *5*, 5483.

Patti, G., Guzzeti, C., Di Iorgi, N., Maria Allegri, A.E., Napoli, F., Loche, S., and Maghnie, M. (2018). Central adrenal insufficiency in children and adolescents. Best Practice & Research Clinical Endocrinology & Metabolism *32*, 425–444.

Petterino, C., Naylor, S., Mukaratirwa, S., and Bradley, A. (2015). Adrenal Gland Background Findings in CD-1 (Crl:CD-1(ICR)BR) Mice from 104-week Carcinogenicity Studies. Toxicol Pathol *43*, 816–824.

Pezzi, V., Clark, B.J., Ando, S., Stocco, D.M., and Rainey, W.E. (1996). Role of Calmodulin-dependent protein kinase II in the acute stimulation of aldosterone production. The Journal of Steroid Biochemistry and Molecular Biology *58*, 417–424.

Pichler, A., Gast, A., Seeler, J.S., Dejean, A., and Melchior, F. (2002). The Nucleoporin RanBP2 Has SUMO1 E3 Ligase Activity. Cell *108*, 109–120.

Pignatti, E., Leng, S., Yuchi, Y., Borges, K.S., Guagliardo, N.A., Shah, M.S., Ruiz-Babot, G., Kariyawasam, D., Taketo, M.M., Miao, J., et al. (2020). Beta-Catenin Causes Adrenal Hyperplasia by Blocking Zonal Transdifferentiation. Cell Reports *31*, 107524.

Pihlajoki, M., Gretzinger, E., Cochran, R., Kyrönlahti, A., Schrade, A., Hiller, T., Sullivan, L., Shoykhet, M., Schoeller, E.L., Brooks, M.D., et al. (2013). Conditional Mutagenesis of *Gata6* in SF1-Positive Cells Causes Gonadal-Like Differentiation in the Adrenal Cortex of Mice. Endocrinology *154*, 1754–1767.

Pilla, E., Möller, U., Sauer, G., Mattiroli, F., Melchior, F., and Geiss-Friedlander, R. (2012). A Novel SUMO1-specific Interacting Motif in Dipeptidyl Peptidase 9 (DPP9) That Is Important for Enzymatic Regulation. Journal of Biological Chemistry *287*, 44320–44329.

Plewes, M.R., Hou, X., Talbott, H.A., Zhang, P., Wood, J.R., Cupp, A.S., and Davis, J.S. (2020). Luteinizing hormone regulates the phosphorylation and localization of the mitochondrial effector dynamin-related protein-1 (DRP1) and steroidogenesis in the bovine corpus luteum. FASEB j. fj.201902958R.

Polex-Wolf, J., Yeo, G.S.H., and O'Rahilly, S. (2016). Impaired prohormone processing: A grand unified theory for features of Prader-Willi

syndrome? Journal of Clinical Investigation *127*, 98–99.

Potts, P.R., and Yu, H. (2005). Human MMS21/NSE2 Is a SUMO Ligase Required for DNA Repair. Mol Cell Biol *25*, 7021–7032.

Prudent, J., Zunino, R., Sugiura, A., Mattie, S., Shore, G.C., and McBride, H.M. (2015). MAPL SUMOylation of Drp1 Stabilizes an ER/Mitochondrial Platform Required for Cell Death. Molecular Cell *59*, 941–955.

Qi, Y., Wang, J., Bomben, V.C., Li, D.-P., Chen, S.-R., Sun, H., Xi, Y., Reed, J.G., Cheng, J., Pan, H.-L., et al. (2014). Hyper-SUMOylation of the Kv7 Potassium Channel Diminishes the M-Current Leading to Seizures and Sudden Death. Neuron *83*, 1159–1171.

Ragazzon, B., Cazabat, L., Rizk-Rabin, M., Assie, G., Groussin, L., Fierrard, H., Perlemoine, K., Martinez, A., and Bertherat, J. (2009). Inactivation of the Carney Complex Gene 1 (Protein Kinase A Regulatory Subunit 1A) Inhibits SMAD3 Expression and TGF -Stimulated Apoptosis in Adrenocortical Cells. Cancer Research *69*, 7278–7284.

Rainey, W.E., Shay, J.W., and Mason, J.I. (1986). ACTH induction of 3-hydroxy-3-methylglutaryl coenzyme A reductase, cholesterol biosynthesis, and steroidogenesis in primary cultures of bovine adrenocortical cells. J Biol Chem *261*, 7322–7326.

Rajan, S., Torres, J., Thompson, M.S., and Philipson, L.H. (2012). SUMO downregulates GLP-1-stimulated cAMP generation and insulin secretion. American Journal of Physiology-Endocrinology and Metabolism *302*, E714–E723.

Ramamoorthy, S., and Cidlowski, J.A. (2016). Corticosteroids. Rheumatic Disease Clinics of North America *42*, 15–31.

Reul, J.M.H.M., and Kloet, E.R.D. (1985). Two Receptor Systems for Corticosterone in Rat Brain: Microdistribution and Differential Occupation. Endocrinology *117*, 2505–2511.

Rigotti, A., Trigatti, B.L., Penman, M., Rayburn, H., Herz, J., and Krieger, M. (1997). A targeted mutation in the murine gene encoding the high density lipoprotein (HDL) receptor scavenger receptor class B type I reveals its key role in HDL metabolism. Proc. Natl. Acad. Sci. U.S.A. *94*, 12610–12615.

Riising, E.M., Boggio, R., Chiocca, S., Helin, K., and Pasini, D. (2008). The Polycomb Repressive Complex 2 Is a Potential Target of SUMO Modifications. PLoS ONE *3*, e2704.

Rodriguez, M.S., Dargemont, C., and Hay, R.T. (2001). SUMO-1 Conjugation *in Vivo* Requires Both a Consensus Modification Motif and Nuclear Targeting. J. Biol. Chem. *276*, 12654–12659.

Romero, D.G., Yanes, L.L., de Rodriguez, A.F., Plonczynski, M.W., Welsh, B.L., Reckelhoff, J.F., Gomez-Sanchez, E.P., and Gomez-Sanchez, C.E. (2007). Disabled-2 Is Expressed in Adrenal Zona Glomerulosa and Is Involved in Aldosterone Secretion. Endocrinology *148*, 2644–2652.

Rosenberg, A.G.W., Pellikaan, K., Poitou, C., Goldstone, A.P., Høybye, C., Markovic, T., Grugni, G., Crin'o, A., Caix'as, A., Coupaye, M., et al. (2020). Central Adrenal Insufficiency Is Rare in Adults With Prader–Willi Syndrome. The Journal of Clinical Endocrinology & Metabolism *105*, e2563–e2571.

Rosenfield, R.L. (2021). Normal and Premature

Adrenarche. Endocrine Reviews *42*, 783–814.

Rossitto, M., Déjardin, S., Rands, C.M., Gras, S.L., Migale, R., Rafiee, M.-R., Neirijnck, Y., Pruvost, A., Nguyen, A.L., Bossis, G., et al. (2022). TRIM28-dependent SUMOylation protects the adult ovary from the male pathway. Nature Communications.

Roth, W., Sustmann, C., Kieslinger, M., Gilmozzi, A., Irmer, D., Kremmer, E., Turck, C., and Grosschedl, R. (2004). PIASy-Deficient Mice Display Modest Defects in IFN and Wnt Signaling. J Immunol *173*, 6189–6199.

Rousseaux, M.W., Revelli, J.-P., Vázquez-Vélez, G.E., Kim, J.-Y., Craigen, E., Gonzales, K., Beckinghausen, J., and Zoghbi, H.Y. (2018). Depleting Trim28 in adult mice is well tolerated and reduces levels of α-synuclein and tau. eLife *7*, e36768.

Roy, K., and Pucadyil, T.J. (2022). Is Drp1 sufficient to catalyze membrane fission? Proc. Natl. Acad. Sci. U.S.A. *119*, e2201709119.

Sachdev, S. (2001). PIASy, a nuclear matrix-associated SUMO E3 ligase, represses LEF1 activity by sequestration into nuclear bodies. Genes & Development *15*, 3088–3103.

Sahut-Barnola, I., de Joussineau, C., Val, P., Lambert-Langlais, S., Damon, C., Lefrançois-Martinez, A.-M., Pointud, J.-C., Marceau, G., Sapin, V., Tissier, F., et al. (2010). Cushing's Syndrome and Fetal Features Resurgence in Adrenal Cortex–Specific Prkar1a Knockout Mice. PLoS Genetics *6*, e1000980.

Saitoh, H., and Hinchey, J. (2000). Functional Heterogeneity of Small Ubiquitin-related Protein Modifiers SUMO-1 versus SUMO-2/3. Journal of Biological Chemistry *275*, 6252–6258.

Sandhu, J., Li, S., Fairall, L., Pfisterer, S.G., Gurnett, J.E., Xiao, X., Weston, T.A., Vashi, D., Ferrari, A., Orozco, J.L., et al. (2018). Aster Proteins Facilitate Nonvesicular Plasma Membrane to ER Cholesterol Transport in Mammalian Cells. Cell *175*, 514–529.e20.

Santti, H., Mikkonen, L., Anand, A., Hirvonen-Santti, S., Toppari, J., Panhuysen, M., Vauti, F., Perera, M., Corte, G., Wurst, W., et al. (2005). Disruption of the murine PIASx gene results in reduced testis weight. Journal of Molecular Endocrinology *34*, 645–654.

Sasaki, G., Zubair, M., Ishii, T., Mitsui, T., Hasegawa, T., and Auchus, R.J. (2014). The Contribution of Serine 194 Phosphorylation to Steroidogenic Acute Regulatory Protein Function. Molecular Endocrinology *28*, 1088–1096.

Scagliotti, V., Esse, R., Willis, T.L., Howard, M., Carrus, I., Lodge, E., Andoniadou, C.L., and Charalambous, M. (2021). Dynamic Expression of Imprinted Genes in the Developing and Postnatal Pituitary Gland. Genes *12*, 509.

Schaaf, C.P., Gonzalez-Garay, M.L., Xia, F., Potocki, L., Gripp, K.W., Zhang, B., Peters, B.A., McElwain, M.A., Drmanac, R., Beaudet, A.L., et al. (2013). Truncating mutations of MAGEL2 cause Prader-Willi phenotypes and autism. Nat Genet *45*, 1405–1408.

Schaller, F., Watrin, F., Sturny, R., Massacrier, A., Szepetowski, P., and Muscatelli, F. (2010). A single postnatal injection of oxytocin rescues the lethal feeding behaviour in mouse newborns deficient for the imprinted Magel2 gene. Human Molecular Genetics *19*, 4895–4905.

Scheys, J.O., Heaton, J.H., and Hammer, G.D. (2011). Evidence of Adrenal Failure in Aging Dax1-Deficient Mice. Endocrinology *152*, 3430–3439.

Schulz, S., Chachami, G., Kozaczkiewicz, L., Winter, U., Stankovic-Valentin, N., Haas, P., Hofmann, K., Urlaub, H., Ovaa, H., Wittbrodt, J., et al. (2012). Ubiquitin-specific protease-like 1 (USPL1) is a SUMO isopeptidase with essential, non-catalytic functions. EMBO Rep *13*, 930–938.

Sebag, J.A., and Hinkle, P.M. (2009). Opposite Effects of the Melanocortin-2 (MC2) Receptor Accessory Protein MRAP on MC2 and MC5 Receptor Dimerization and Trafficking. Journal of Biological Chemistry *284*, 22641–22648.

Seckl, J.R. (2004). 11β-hydroxysteroid dehydrogenases: Changing glucocorticoid action. Curr Opin Pharmacol *4*, 597–602.

Seftel, A.D. (2005). Phosphodiesterase 11 (PDE11) Regulation of Spermatozoa Physiology. Journal of Urology *174*, 1043–1044.

Seibel, M.J., Cooper, M.S., and Zhou, H. (2013). Glucocorticoid-induced osteoporosis: Mechanisms, management, and future perspectives. The Lancet Diabetes & Endocrinology *1*, 59–70.

Selvaraj, V., Stocco, D.M., and Clark, B.J. (2018). Current knowledge on the acute regulation of steroidogenesis. Biology of Reproduction *99*, 13–26.

Selye, H. (1936). A Syndrome produced by Diverse Nocuous Agents. Nature *138*, 32–32.

Sen, B., Xie, Z., Howard, S., Styner, M., van Wijnen, A.J., Uzer, G., and Rubin, J. (2022). Mechanically Induced Nuclear Shuttling of β-Catenin Requires Co-transfer of Actin. Stem Cells sxac006.

Sha, Z., Blyszcz, T., González-Prieto, R., Vertegaal, A.C.O., and Goldberg, A.L. (2019). Inhibiting ubiquitination causes an accumulation of SUMOylated newly synthesized nuclear proteins at PML bodies. J. Biol. Chem. *294*, 15218–15234.

Shao, R., Zhang, F.-P., Rung, E., Palvimo, J.J., Huhtaniemi, I., and Billig, H. (2004). Inhibition of Small Ubiquitin-Related Modifier-1 Expression by Luteinizing Hormone Receptor Stimulation is Linked to Induction of Progesterone Receptor during Ovulation in Mouse Granulosa Cells. Endocrinology *145*, 384–392.

Sharma, M. (2003). hZimp10 is an androgen receptor co-activator and forms a complex with SUMO-1 at replication foci. The EMBO Journal *22*, 6101–6114.

Sharma, M., Jamieson, C., Lui, C., and Henderson, B.R. (2016). Distinct hydrophobic "patches" in the N- and C-tails of beta-catenin contribute to nuclear transport. Experimental Cell Research *348*, 132–145.

Sharma, P., Yamada, S., Lualdi, M., Dasso, M., and Kuehn, M.R. (2013). Senp1 Is Essential for Desumoylating Sumo1-Modified Proteins but Dispensable for Sumo2 and Sumo3 Deconjugation in the Mouse Embryo. Cell Reports *3*, 1640–1650.

Shen, H.-J., Zhu, H.-Y., Yang, C., and Ji, F. (2012). SENP2 Regulates Hepatocellular Carcinoma Cell Growth by Modulating the Stability of β-catenin. Asian Pacific Journal of Cancer Prevention *13*, 3583–3587.

Shen, W.-J., Azhar, S., and Kraemer, F.B. (2018). SR-B1: A Unique Multifunctional Receptor for Cholesterol Influx and Efflux. Annu. Rev. Physiol.

80, 95–116.

Shimano, H., Shimomura, I., Hammer, R.E., Herz, J., Goldstein, J.L., Brown, M.S., and Horton, J.D. (1997). Elevated levels of SREBP-2 and cholesterol synthesis in livers of mice homozygous for a targeted disruption of the SREBP-1 gene. J. Clin. Invest. *100*, 2115–2124.

Shimomura, I., Shimano, H., Horton, J.D., Goldstein, J.L., and Brown, M.S. (1997). Differential expression of exons 1a and 1c in mRNAs for sterol regulatory element binding protein-1 in human and mouse organs and cultured cells. J. Clin. Invest. *99*, 838–845.

Shin, E.J., Shin, H.M., Nam, E., Kim, W.S., Kim, J.-H., Oh, B.-H., and Yun, Y. (2012). DeSUMOylating isopeptidase: A second class of SUMO protease. EMBO Rep *13*, 339–346.

Shitashige, M., Satow, R., Honda, K., Ono, M., Hirohashi, S., and Yamada, T. (2008). Regulation of Wnt Signaling by the Nuclear Pore Complex. Gastroenterology *134*, 1961–1971.e4.

Shukur, H.H., de Rijke, Y.B., van Rossum, E.F.C., Hussain-Alkhateeb, L., and Höybye, C. (2020). Hair cortisol-a method to detect chronic cortisol levels in patients with Prader-Willi syndrome. BMC Endocr Disord *20*, 166.

Shyu, Y.-C., Liao, P.-C., Huang, T.-S., Yang, C.-J., Lu, M.-J., Huang, S.-M., Lin, X.-Y., Liou, C.-C., Kao, Y.-H., Lu, C.-H., et al. (2022). Genetic Disruption of KLF1 K74 SUMOylation in Hematopoietic System Promotes Healthy Longevity in Mice. Advanced Science 2201409.

Skalhegg, B.S., and Tasken, K. (2000). SPECIFICITY IN THE cAMP/PKA SIGNALING PATHWAY. DIFFERENTIAL EXPRESSION, REGULATION, AND SUBCELLULAR LOCALIZATION OF SUBUNITS OF PKA. Frontiers in Bioscience 16.

Smirnova, E., Shurland, D.-L., Ryazantsev, S.N., and van der Bliek, A.M. (1998). A Human Dynamin-related Protein Controls the Distribution of Mitochondria. Journal of Cell Biology *143*, 351–358.

Song, J., Durrin, L.K., Wilkinson, T.A., Krontiris, T.G., and Chen, Y. (2004). Identification of a SUMO-binding motif that recognizes SUMO-modified proteins. Proc. Natl. Acad. Sci. U.S.A. *101*, 14373–14378.

Speiser, P.W., and White, P.C. (2003). Congenital Adrenal Hyperplasia. N Engl J Med *349*, 776–788.

Spiga, F., Zavala, E., Walker, J.J., Zhao, Z., Terry, J.R., and Lightman, S.L. (2017). Dynamic responses of the adrenal steroidogenic regulatory network. Proc Natl Acad Sci USA *114*, E6466–E6474.

Steenblock, C., Rubin de Celis, M.F., Delgadillo Silva, L.F., Pawolski, V., Brennand, A., Werdermann, M., Berger, I., Santambrogio, A., Peitzsch, M., Andoniadou, C.L., et al. (2018). Isolation and characterization of adrenocortical progenitors involved in the adaptation to stress. Proc. Natl. Acad. Sci. U.S.A. *115*, 12997–13002.

Stefan, M., Ji, H., Simmons, R.A., Cummings, D.E., Ahima, R.S., Friedman, M.I., and Nicholls, R.D. (2005). Hormonal and Metabolic Defects in a Prader-Willi Syndrome Mouse Model with Neonatal Failure to Thrive. Endocrinology *146*, 4377–4385.

Stevens, A., and White, A. (2009). ACTH: Cellular Peptide Hormone Synthesis and Secretory

Pathways. In Cellular Peptide Hormone Synthesis and Secretory Pathways, J.F. Rehfeld, and J.R. Bundgaard, eds. (Berlin, Heidelberg: Springer Berlin Heidelberg), pp. 121–135.

Stevenson, D.A., Anaya, T.M., Clayton-Smith, J., Hall, B.D., Van Allen, M.I., Zori, R.T., Zackai, E.H., Frank, G., and Clericuzio, C.L. (2004). Unexpected death and critical illness in Prader-Willi syndrome: Report of ten individuals. Am. J. Med. Genet. *124A*, 158–164.

Stijnen, P., Ramos-Molina, B., O'Rahilly, S., and Creemers, J.W.M. (2016). PCSK1 Mutations and Human Endocrinopathies: From Obesity to Gastrointestinal Disorders. Endocrine Reviews *37*, 347–371.

Suh, H.-Y., Kim, J.-H., Woo, J.-S., Ku, B., Shin, E.J., Yun, Y., and Oh, B.-H. (2012). Crystal structure of DeSI-1, a novel deSUMOylase belonging to a putative isopeptidase superfamily. Proteins n/a–n/a.

Sun, H., and Hunter, T. (2012). Poly-Small Ubiquitin-like Modifier (PolySUMO)-binding Proteins Identified through a String Search. Journal of Biological Chemistry *287*, 42071–42083.

Sun, H., Leverson, J.D., and Hunter, T. (2007a). Conserved function of RNF4 family proteins in eukaryotes: Targeting a ubiquitin ligase to SUMOylated proteins. EMBO J *26*, 4102–4112.

Sun, L.-P., Seemann, J., Goldstein, J.L., and Brown, M.S. (2007b). Sterol-regulated transport of SREBPs from endoplasmic reticulum to Golgi: Insig renders sorting signal in Scap inaccessible to COPII proteins. Proc. Natl. Acad. Sci. U.S.A. *104*, 6519–6526.

Szarek, E., and Stratakis, C. (2014). Phosphodiesterases and Adrenal Cushing in Mice and Humans. Horm Metab Res *46*, 863–868.

Tago, K., Chiocca, S., and Sherr, C.J. (2005). Sumoylation induced by the Arf tumor suppressor: A P53-independent function. Proc. Natl. Acad. Sci. U.S.A. *102*, 7689–7694.

Taguchi, N., Ishihara, N., Jofuku, A., Oka, T., and Mihara, K. (2007). Mitotic Phosphorylation of Dynamin-related GTPase Drp1 Participates in Mitochondrial Fission. J. Biol. Chem. *282*, 11521–11529.

Tahk, S., Liu, B., Chernishof, V., Wong, K.A., Wu, H., and Shuai, K. (2007). Control of specificity and magnitude of NF-κB and STAT1-mediated gene activation through PIASy and PIAS1 cooperation. Proc. Natl. Acad. Sci. U.S.A. *104*, 11643–11648.

Tahmasebi, S., Ghorbani, M., Savage, P., Yan, K., Gocevski, G., Xiao, L., You, L., and Yang, X.-J. (2013). Sumoylation of Krüppel-like Factor 4 Inhibits Pluripotency Induction but Promotes Adipocyte Differentiation. Journal of Biological Chemistry *288*, 12791–12804.

Tahmasebi, S., Ghorbani, M., Savage, P., Gocevski, G., and Yang, X.-J. (2014). The SUMO Conjugating Enzyme Ubc9 Is Required for Inducing and Maintaining Stem Cell Pluripotency: Ubc9 in Pluripotency Induction and Maintenance. Stem Cells *32*, 1012–1020.

Takahashi, K., and Yamanaka, S. (2006). Induction of Pluripotent Stem Cells from Mouse Embryonic and Adult Fibroblast Cultures by Defined Factors. Cell *126*, 663–676.

Tan, J.-A., Hall, S.H., Hamil, K.G., Grossman, G., Petrusz, P., and French, F.S. (2002). Protein Inhibitors of Activated STAT Resemble Scaffold

Attachment Factors and Function as Interacting Nuclear Receptor Coregulators. Journal of Biological Chemistry *277*, 16993–17001.

Tan, J.H.L., Wollmann, H., van Pelt, A.M.M., Kaldis, P., and Messerschmidt, D.M. (2020). Infertility-Causing Haploinsufficiency Reveals TRIM28/KAP1 Requirement in Spermatogonia. Stem Cell Reports *14*, 818–827.

Tan, M., Gong, H., Wang, J., Tao, L., Xu, D., Bao, E., Liu, Z., and Qiu, J. (2015). SENP2 regulates MMP13 expression in a bladder cancer cell line through SUMOylation of TBL1/TBLR1. Sci Rep *5*, 13996.

Tan, S., Feng, B., Yin, M., Zhou, H.J., Lou, G., Ji, W., Li, Y., and Min, W. (2017). Stromal Senp1 promotes mouse early folliculogenesis by regulating BMP4 expression. Cell Biosci *7*, 36.

Tatham, M.H., Jaffray, E., Vaughan, O.A., Desterro, J.M.P., Botting, C.H., Naismith, J.H., and Hay, R.T. (2001). Polymeric Chains of SUMO-2 and SUMO-3 Are Conjugated to Protein Substrates by SAE1/SAE2 and Ubc9. Journal of Biological Chemistry *276*, 35368–35374.

Tauber, M., and Hoybye, C. (2021). Endocrine disorders in Prader-Willi syndrome: A model to understand and treat hypothalamic dysfunction. The Lancet Diabetes & Endocrinology *9*, 235–246.

Taylor, M.J., Ullenbruch, M.R., Frucci, E.C., Rege, J., Ansorge, M.S., Gomez-Sanchez, C.E., Begum, S., Laufer, E., Breault, D.T., and Rainey, W.E. (2019). Chemogenetic activation of adrenocortical Gq signaling causes hyperaldosteronism and disrupts functional zonation. Journal of Clinical Investigation *130*, 83–93.

Tee, M.-K., Lin, D., Sugawara, T., Holt, J.A., Guiguen, Y., Buckingham, B., Strauss, J.F., and Miller, W.L. (1995). T-A transversion 11 bp from a splice acceptor site in the human gene for steroidogenic acute regulatory protein causes congenital lipoid adrenal hyperplasia. Hum Mol Genet *4*, 2299–2305.

Tennese, A.A., and Wevrick, R. (2011). Impaired Hypothalamic Regulation of Endocrine Function and Delayed Counterregulatory Response to Hypoglycemia in Magel2-Null Mice. Endocrinology *152*, 967–978.

Thiruvalluvan, M., Barghouth, P.G., Tsur, A., Broday, L., and Oviedo, N.J. (2018). SUMOylation controls stem cell proliferation and regional cell death through Hedgehog signaling in planarians. Cell. Mol. Life Sci. *75*, 1285–1301.

Thomas, M., Keramidas, M., Monchaux, E., and Feige, J.-J. (2004). Dual hormonal regulation of endocrine tissue mass and vasculature by adrenocorticotropin in the adrenal cortex. Endocrinology *145*, 4320–4329.

Trzeciak, W.H., and Boyd, G.S. (1974). Activation of Cholesteryl Esterase in Bovine Adrenal Cortex. Eur J Biochem *46*, 201–207.

Tsai, L.-C.L., Shimizu-Albergine, M., and Beavo, J.A. (2011). The High-Affinity cAMP-Specific Phosphodiesterase 8B Controls Steroidogenesis in the Mouse Adrenal Gland. Mol Pharmacol *79*, 639–648.

Tsai, T.-F., Armstrong, D., and Beaudet, A.L. (1999). Necdin-deficient mice do not show lethality or the obesity and infertility of Prader-Willi syndrome. Nat Genet *22*, 15–16.

Tsigos, C., Arai, K., Hung, W., and Chrousos, G.P. (1993). Hereditary isolated glucocorticoid

deficiency is associated with abnormalities of the adrenocorticotropin receptor gene. J. Clin. Invest. *92*, 2458–2461.

Tu, L.N., Morohaku, K., Manna, P.R., Pelton, S.H., Butler, W.R., Stocco, D.M., and Selvaraj, V. (2014). Peripheral Benzodiazepine Receptor/Translocator Protein Global Knock-out Mice Are Viable with No Effects on Steroid Hormone Biosynthesis. Journal of Biological Chemistry *289*, 27444–27454.

Tucker, E.J. (2021). The Genetics and Biology of ***FOXL2***. Sex Dev 1–10.

Ulman, A., Levin, T., Dassa, B., Javitt, A., Kacen, A., Shmueli, M.D., Eisenberg-Lerner, A., Sheban, D., Fishllevich, S., Levy, E.D., et al. (2021). Altered Protein Abundance and Localization Inferred from Sites of Alternative Modification by Ubiquitin and SUMO. Journal of Molecular Biology *433*, 167219.

Uruno, A., Matsuda, K., Noguchi, N., Yoshikawa, T., Kudo, M., Satoh, F., Rainey, W.E., Hui, X.-G., Akahira, J.-i., Nakamura, Y., et al. (2011). Peroxisome proliferator-activated receptor-suppresses CYP11B2 expression and aldosterone production. Journal of Molecular Endocrinology *46*, 37–49.

Uzer, G., Bas, G., Sen, B., Xie, Z., Birks, S., Olcum, M., McGrath, C., Styner, M., and Rubin, J. (2018). Sun-mediated mechanical LINC between nucleus and cytoskeleton regulates β-catenin nuclear access. Journal of Biomechanics *74*, 32–40.

Val, P., Jeays-Ward, K., and Swain, A. (2006). Identification of a novel population of adrenal-like cells in the mammalian testis. Developmental Biology *299*, 250–256.

Val, P., Martinez-Barbera, J.-P., and Swain, A. (2007). Adrenal development is initiated by Cited2 and Wt1 through modulation of Sf-1 dosage. Development *134*, 2349–2358.

Valera-Alberni, M., Joffraud, M., Miro-Blanch, J., Capellades, J., Junza, A., Dayon, L., N'uñez Galindo, A., Sanchez-Garcia, J.L., Valsesia, A., Cercillieux, A., et al. (2021). Crosstalk between Drp1 phosphorylation sites during mitochondrial remodeling and their impact on metabolic adaptation. Cell Reports *36*, 109565.

Valles, S. (2020). Philosophy of Biomedicine. In The Stanford Encyclopedia of Philosophy, E.N. Zalta, ed. (https://plato.stanford.edu/archives/sum2020/entries/biomedicine/; Metaphysics Research Lab, Stanford University),.

van der Sluis, R.J., Van Eck, M., and Hoekstra, M. (2015). Adrenocortical LDL receptor function negatively influences glucocorticoid output. Journal of Endocrinology *226*, 145–154.

Vegiopoulos, A., and Herzig, S. (2007). Glucocorticoids, metabolism and metabolic diseases. Molecular and Cellular Endocrinology *275*, 43–61.

Vidal, V., Sacco, S., Rocha, A.S., da Silva, F., Panzolini, C., Dumontet, T., Doan, T.M.P., Shan, J., Rak-Raszewska, A., Bird, T., et al. (2016). The adrenal capsule is a signaling center controlling cell renewal and zonation through *Rspo3*. Genes & Development *30*, 1389–1394.

Vigodner, M., and Morris, P.L. (2005). Testicular expression of small ubiquitin-related modifier-1 (SUMO-1) supports multiple roles in spermatogenesis: Silencing of sex chromosomes in

spermatocytes, spermatid microtubule nucleation, and nuclear reshaping. Developmental Biology *282*, 480–492.

Viho, E.M.G., Buurstede, J.C., Berkhout, J.B., Mahfouz, A., and Meijer, O.C. (2021). Cell type specificity of glucocorticoid signaling in the adult mouse hippocampus. J Neuroendocrinology.

Visel, A. (2004). GenePaint.org: An atlas of gene expression patterns in the mouse embryo. Nucleic Acids Research *32*, 552D–556.

Walczak, E.M., Kuick, R., Finco, I., Bohin, N., Hrycaj, S.M., Wellik, D.M., and Hammer, G.D. (2014). Wnt Signaling Inhibits Adrenal Steroidogenesis by Cell-Autonomous and Non–Cell-Autonomous Mechanisms. Molecular Endocrinology *28*, 1471–1486.

Walker, A.K., Lanz, A.J., Jamshad, M., Garvin, A.J., Wotherspoon, P., Cooper, B.F., Knowles, T.J., and Morris, J.R. (2022). Modification of the SUMO activating enzyme subunit SAE2 directs SUMO isoform bias required for mitotic fidelity (Molecular Biology).

Walker, J.J., Terry, J.R., and Lightman, S.L. (2010). Origin of ultradian pulsatility in the hypothalamic–pituitary–adrenal axis. Proc. R. Soc. B. *277*, 1627–1633.

Walker, J.J., Spiga, F., Waite, E., Zhao, Z., Kershaw, Y., Terry, J.R., and Lightman, S.L. (2012). The Origin of Glucocorticoid Hormone Oscillations. PLoS Biol *10*, e1001341.

Wang, C.-M., Liu, R., Wang, L., and Yang, W.-H. (2013). Acidic Residue Glu199 Increases SUMOylation Level of Nuclear Hormone Receptor NR5A1. IJMS *14*, 22331–22345.

Wang, F., Sun, F., Luo, J., Yue, T., Chen, L., Zhou, H., Zhang, J., Yang, C., Luo, X., Zhou, Q., et al. (2019). Loss of ubiquitin-conjugating enzyme E2 (Ubc9) in macrophages exacerbates multiple low-dose streptozotocin-induced diabetes by attenuating M2 macrophage polarization. Cell Death Dis *10*, 892.

Wang, J., Chen, L., Wen, S., Zhu, H., Yu, W., Moskowitz, I.P., Shaw, G.M., Finnell, R.H., and Schwartz, R.J. (2011). Defective sumoylation pathway directs congenital heart disease. Birth Defects Research Part A: Clinical and Molecular Teratology *91*, 468–476.

Wang, L., Wansleeben, C., Zhao, S., Miao, P., Paschen, W., and Yang, W. (2014). SUMO2 is essential while SUMO 3 is dispensable for mouse embryonic development. EMBO Rep *15*, 878–885.

Wasiak, S., Zunino, R., and McBride, H.M. (2007). Bax/Bak promote sumoylation of DRP1 and its stable association with mitochondria during apoptotic cell death. Journal of Cell Biology *177*, 439–450.

Weber, A., Toppari, J., Harvey, R.D., Klann, R.C., Shaw, N.J., Ricker, A.T., Nanto-Salonen, K., Bevan, J.S., and Clark, A.J. (1995). Adrenocorticotropin receptor gene mutations in familial glucocorticoid deficiency: Relationships with clinical features in four families. The Journal of Clinical Endocrinology & Metabolism *80*, 65–71.

Weger, S., Hammer, E., and Heilbronn, R. (2005). Topors acts as a SUMO-1 E3 ligase for P53 in vitro and in vivo. FEBS Letters *579*, 5007–5012.

Weigand, I., Ronchi, C.L., Rizk-Rabin, M., Dalmazi, G.D., Wild, V., Bathon, K., Rubin, B., Calebiro, D., Beuschlein, F., Bertherat, J., et al. (2017). Differential expression of the protein

kinase A subunits in normal adrenal glands and adrenocortical adenomas. Sci Rep *7*, 49.

Wellman, K., Fu, R., Baldwin, A., Rege, J., Murphy, E., Rainey, W.E., and Mukherjee, N. (2021). Transcriptomic Response Dynamics of Human Primary and Immortalized Adrenocortical Cells to Steroidogenic Stimuli. Cells *10*, 2376.

Wenger, J., Klinglmayr, E., Fröhlich, C., Eibl, C., Gimeno, A., Hessenberger, M., Puehringer, S., Daumke, O., and Goettig, P. (2013). Functional Mapping of Human Dynamin-1-Like GTPase Domain Based on X-ray Structure Analyses. PLoS ONE *8*, e71835.

Westermann, B. (2008). Molecular Machinery of Mitochondrial Fusion and Fission. J. Biol. Chem. *283*, 13501–13505.

Wikstrom, J.D., Mahdaviani, K., Liesa, M., Sereda, S.B., Si, Y., Las, G., Twig, G., Petrovic, N., Zingaretti, C., Graham, A., et al. (2014). Hormone-induced mitochondrial fission is utilized by brown adipocytes as an amplification pathway for energy expenditure. EMBO J n/a–n/a.

Wilhelm, D., and Englert, C. (2002). The Wilms tumor suppressor WT1 regulates early gonad development by activation of *Sf1*. Genes Dev. *16*, 1839–1851.

Wilmot Roussel, H., Vezzosi, D., Rizk-Rabin, M., Barreau, O., Ragazzon, B., René-Corail, F., de Reynies, A., Bertherat, J., and Assié, G. (2013). Identification of Gene Expression Profiles Associated With Cortisol Secretion in Adrenocortical Adenomas. The Journal of Clinical Endocrinology & Metabolism *98*, E1109–E1121.

Wilmouth, J., Olabe, J., Roucher-Boulez, F., and Val, P. (2019). WNT pathway deregulation in adrenal cortex tumorigenesis. Current Opinion in Endocrine and Metabolic Research *8*, 174–182.

Wils, J., Duparc, C., Cailleux, A.-F., Lopez, A.-G., Guiheneuf, C., Boutelet, I., Boyer, H.-G., Dubessy, C., Cherifi, S., Cauliez, B., et al. (2020). The neuropeptide substance P regulates aldosterone secretion in human adrenals. Nat Commun *11*, 2673.

Winer, I.S., Bommer, G.T., Gonik, N., and Fearon, E.R. (2006). Lysine Residues Lys-19 and Lys-49 of β-Catenin Regulate Its Levels and Function in T Cell Factor Transcriptional Activation and Neoplastic Transformation. Journal of Biological Chemistry *281*, 26181–26187.

Wing, C.E., Fung, H.Y.J., and Chook, Y.M. (2022). Karyopherin-mediated nucleocytoplasmic transport. Nat Rev Mol Cell Biol *23*, 307–328.

Witchel, S.F. (2017). Congenital Adrenal Hyperplasia. Journal of Pediatric and Adolescent Gynecology *30*, 520–534.

Wong, K.A., Kim, R., Christofk, H., Gao, J., Lawson, G., and Wu, H. (2004). Protein Inhibitor of Activated STAT Y (PIASy) and a Splice Variant Lacking Exon 6 Enhance Sumoylation but Are Not Essential for Embryogenesis and Adult Life. Mol Cell Biol *24*, 5577–5586.

Wood, M.A., Acharya, A., Finco, I., Swonger, J.M., Elston, M.J., Tallquist, M.D., and Hammer, G.D. (2013). Fetal adrenal capsular cells serve as progenitor cells for steroidogenic and stromal adrenocortical cell lineages in M. musculus. Development *140*, 4522–4532.

Wu, H., Liu, X., Jaenisch, R., and Lodish, H.F. (1995). Generation of committed erythroid BFU-E and CFU-E progenitors does not require

erythropoietin or the erythropoietin receptor. Cell *83*, 59–67.

Wyllie, A.H., Kerr, J.F.R., Macaskill, I.A.M., Currie, A.R., and Currie, A.R. (1973). Adrenocortical cell deletion: The role of ACTH. J. Pathol. *111*, 85–94.

Xiao, M., Bian, Q., Lao, Y., Yi, J., Sun, X., Sun, X., and Yang, J. (2021). SENP3 loss promotes M2 macrophage polarization and breast cancer progression. Mol Oncol 1878–0261.12967.

Xiao, T.Z., Bhatia, N., Urrutia, R., Lomberk, G.A., Simpson, A., and Longley, B.J. (2011). MAGE I Transcription Factors Regulate KAP1 and KRAB Domain Zinc Finger Transcription Factor Mediated Gene Repression. PLoS ONE *6*, e23747.

Xiao, T.Z., Suh, Y., and Longley, B.J. (2014). MAGE proteins regulate KRAB zinc finger transcription factors and KAP1 E3 ligase activity. Archives of Biochemistry and Biophysics *563*, 136–144.

Xing, Y., Morohashi, K., Ingraham, H.A., and Hammer, G.D. (2017). Timing of adrenal regression controlled by synergistic interaction between Sf1 SUMOylation and Dax1. Development *144*, 3798–3807.

Xu, D., Wang, Z., Xia, Y., Shao, F., Xia, W., Wei, Y., Li, X., Qian, X., Lee, J.-H., Du, L., et al. (2020). The gluconeogenic enzyme PCK1 phosphorylates INSIG1/2 for lipogenesis. Nature *580*, 530–535.

Xu, H.-D., Liang, R.-P., Wang, Y.-G., and Qiu, J.-D. (2021). mUSP: A high-accuracy map of the in situ crosstalk of ubiquitylation and SUMOylation proteome predicted via the feature enhancement approach. Brief Bioinform.

Xu, Z., Lam, L.S.M., Lam, L.H., Chau, S.F., Ng, T.B., and Au, S.W.N. (2008). Molecular basis of the redox regulation of SUMO proteases: A protective mechanism of intermolecular disulfide linkage against irreversible sulfhydryl oxidation. FASEB j. *22*, 127–137.

Yadav, V.K., Berger, J.M., Singh, P., Nagarajan, P., and Karsenty, G. (2022). Embryonic osteocalcin signaling determines lifelong adrenal steroidogenesis and homeostasis in the mouse. The Journal of Clinical Investigation *132*.

Yamaguchi, T., Sharma, P., Athanasiou, M., Kumar, A., Yamada, S., and Kuehn, M.R. (2005). Mutation of SENP1/SuPr-2 Reveals an Essential Role for Desumoylation in Mouse Development. Mol Cell Biol *25*, 5171–5182.

Yamamoto, H. (2003). Sumoylation is involved in beta-catenin-dependent activation of Tcf-4. The EMBO Journal *22*, 2047–2059.

Yan, S., Sun, X., Xiang, B., Cang, H., Kang, X., Chen, Y., Li, H., Shi, G., Yeh, E.T.H., Wang, B., et al. (2010). Redox regulation of the stability of the SUMO protease SENP3 via interactions with CHIP and Hsp90. EMBO J *29*, 3773–3786.

Yan, Y.-L., Zhang, C., Hao, J., Wang, X.-L., Ming, J., Mi, L., Na, J., Hu, X., and Wang, Y. (2019). DPPA2/4 and SUMO E3 ligase PIAS4 opposingly regulate zygotic transcriptional program. PLoS Biol *17*, e3000324.

Yang, F.-M., Pan, C.-T., Tsai, H.-M., Chiu, T.-W., Wu, M.-L., and Hu, M.-C. (2009a). Liver receptor homolog-1 localization in the nuclear body is regulated by sumoylation and cAMP signaling in rat granulosa cells: LRH-1 subnuclear localization in granulosa cells. FEBS Journal *276*, 425–436.

Yang, S.-H., Galanis, A., Witty, J., and Sharrocks, A.D. (2006a). An extended consensus motif enhances the specificity of substrate modification by SUMO. EMBO J *25*, 5083–5093.

Yang, T., Espenshade, P.J., Wright, M.E., Yabe, D., Gong, Y., Aebersold, R., Goldstein, J.L., and Brown, M.S. (2002). Crucial step in cholesterol homeostasis: Sterols promote binding of SCAP to INSIG-1, a membrane protein that facilitates retention of SREBPs in ER. Cell *110*, 489–500.

Yang, W., Sheng, H., Thompson, J.W., Zhao, S., Wang, L., Miao, P., Liu, X., Moseley, M.A., and Paschen, W. (2014). Small Ubiquitin-Like Modifier 3–Modified Proteome Regulated by Brain Ischemia in Novel Small Ubiquitin-Like Modifier Transgenic Mice: Putative Protective Proteins/Pathways. Stroke *45*, 1115–1122.

Yang, W., Robichaux, W.G., Mei, F.C., Lin, W., Li, L., Pan, S., White, M.A., Chen, Y., and Cheng, X. (2022). Epac1 activation by cAMP regulates cellular SUMOylation and promotes the formation of biomolecular condensates. Sci. Adv. *8*, eabm2960.

Yang, W.-H., Heaton, J.H., Brevig, H., Mukherjee, S., IÃÂiguez-LluhÃÂ, J.A., and Hammer, G.D. (2009b). SUMOylation Inhibits SF-1 Activity by Reducing CDK7-Mediated Serine 203 Phosphorylation. MCB *29*, 613–625.

Yang, Y.-L., Chao, P.-K., and Lu, K.-T. (2006b). Systemic and Intra-Amygdala Administration of Glucocorticoid Agonist and Antagonist Modulate Extinction of Conditioned Fear. Neuropsychopharmacol *31*, 912–924.

Yazawa, T., Mizutani, T., Yamada, K., Kawata, H., Sekiguchi, T., Yoshino, M., Kajitani, T., Shou, Z., Umezawa, A., and Miyamoto, K. (2006). Differentiation of Adult Stem Cells Derived from Bone Marrow Stroma into Leydig or Adrenocortical Cells. Endocrinology *147*, 4104–4111.

Yazawa, T., Kawabe, S., Inaoka, Y., Okada, R., Mizutani, T., Imamichi, Y., Ju, Y., Yamazaki, Y., Usami, Y., Kuribayashi, M., et al. (2011). Differentiation of mesenchymal stem cells and embryonic stem cells into steroidogenic cells using steroidogenic factor-1 and liver receptor homolog-1. Molecular and Cellular Endocrinology *336*, 127–132.

Yoon, Y., Pitts, K.R., and McNiven, M.A. (2001). Mammalian Dynamin-like Protein DLP1 Tubulates Membranes. MBoC *12*, 2894–2905.

Yoshikawa, K. (2021). Necdin: A purposive integrator of molecular interaction networks for mammalian neuron vitality. Genes Cells *26*, 641–683.

Yu, C., Wen, Q., Ren, Q., Du, Y., and Xie, X. (2021). Polychlorinated biphenyl congener 180 (PCB 180) regulates mitotic clonal expansion and enhances adipogenesis through modulation of C/EBPβ SUMOylation in preadipocytes. Food Chem Toxicol *152*, 112205.

Yu, H.-M.I., Hsu, T., Maruyama, E.O., Paschen, W., Yang, W., and Hsu, W. (2020). The requirement of SUMO2/3 for SENP2 mediated extraembryonic and embryonic development. Developmental Dynamics *249*, 237–244.

Yu, L., Ji, W., Zhang, H., Renda, M.J., He, Y., Lin, S., Cheng, E., Chen, H., Krause, D.S., and Min, W. (2010). SENP1-mediated GATA1 deSUMOylation is critical for definitive erythropoiesis. The Journal of Experimental Medicine *207*, 1183–1195.

Yu, X., Lao, Y., Teng, X.-L., Li, S., Zhou, Y., Wang, F., Guo, X., Deng, S., Chang, Y., Wu, X., et al. (2018). SENP3 maintains the stability and function of regulatory T cells via BACH2 deSUMOylation. Nat Commun *9*, 3157.

Zhang, F.-P., Mikkonen, L., Toppari, J., Palvimo, J.J., Thesleff, I., and Janne, O.A. (2008). Sumo-1 Function Is Dispensable in Normal Mouse Development. Molecular and Cellular Biology *28*, 5381–5390.

Zhang, J.Z., Lu, T.-W., Stolerman, L.M., Tenner, B., Yang, J.R., Zhang, J.-F., Falcke, M., Rangamani, P., Taylor, S.S., Mehta, S., et al. (2020). Phase Separation of a PKA Regulatory Subunit Controls cAMP Compartmentation and Oncogenic Signaling. Cell *182*, 1531–1544.e15.

Zhang, J.Z., Mehta, S., and Zhang, J. (2021a). Liquid–liquid phase separation: A principal organizer of the cell's biochemical activity architecture. Trends in Pharmacological Sciences *42*, 845–856.

Zhang, N., Wei, P., Gong, A., Chiu, W.-T., Lee, H.-T., Colman, H., Huang, H., Xue, J., Liu, M., Wang, Y., et al. (2011). FoxM1 promotes β-catenin nuclear localization and controls Wnt target-gene expression and glioma tumorigenesis. Cancer Cell *20*, 427–442.

Zhang, Y., Chen, Y., Sun, H., Zhang, W., Zhang, L., Li, H., Huang, X., Yang, J., and Ye, Z. (2021b). SENP3-Mediated PPARγ2 DeSUMOylation in BM-MSCs Potentiates Glucocorticoid-Induced Osteoporosis by Promoting Adipogenesis and Weakening Osteogenesis. Front. Cell Dev. Biol. *9*, 693079.

Zhao, X., Sternsdorf, T., Bolger, T.A., Evans, R.M., and Yao, T.-P. (2005). Regulation of MEF2 by Histone Deacetylase 4- and SIRT1 Deacetylase-Mediated Lysine Modifications. Mol Cell Biol *25*, 8456–8464.

Zhao, X., Hendriks, I.A., Gras, S.L., Ye, T., Ramos-Alonso, L., P, A.N., Lien, G.F., Ghasemi, F., Klungland, A., Jost, B., et al. (2022). Waves of sumoylation support transcription dynamics during adipocyte differentiation. Nucleic Acids Research gkac027.

Zheng, F., Fang, P., Chang, J., Chen, M., Zhong, Q., Chen, T., Chen, C., and Zhang, Z. (2020). Methylene Blue Protects Against Sevoflurane-Induced Cognitive Dysfunction by Suppressing Drp1 deSUMOylation in Aged Mice. Neurochem Res *45*, 956–963.

Zheng, Q., Cao, Y., Chen, Y., Wang, J., Fan, Q., Huang, X., Wang, Y., Wang, T., Wang, X., Ma, J., et al. (2018). Senp2 regulates adipose lipid storage by de-SUMOylation of Setdb. 9.

Zhou, W., Ryan, J.J., and Zhou, H. (2004). Global Analyses of Sumoylated Proteins in Saccharomyces cerevisiae. Journal of Biological Chemistry *279*, 32262–32268.

Zhu, P.-P., Patterson, A., Stadler, J., Seeburg, D.P., Sheng, M., and Blackstone, C. (2004). Intra- and Intermolecular Domain Interactions of the C-terminal GTPase Effector Domain of the Multimeric Dynamin-like GTPase Drp1. Journal of Biological Chemistry *279*, 35967–35974.

Zhu, X., Zhou, A., Dey, A., Norrbom, C., Carroll, R., Zhang, C., Laurent, V., Lindberg, I., Ugleholdt, R., Holst, J.J., et al. (2002). Disruption of PC1/3 expression in mice causes dwarfism and multiple neuroendocrine peptide processing defects. Proc.

Natl. Acad. Sci. U.S.A. *99*, 10293–10298.

Zubair, M., Ishihara, S., Oka, S., Okumura, K., and Morohashi, K. (2006). Two-Step Regulation of *Ad4BP/SF-1* Gene Transcription during Fetal Adrenal Development: Initiation by a Hox-Pbx1-Prep1 Complex and Maintenance via Autoregulation by Ad4BP/SF-1. Mol Cell Biol *26*, 4111–4121.

Zubair, M., Parker, K.L., and Morohashi, K.-i. (2008). Developmental Links between the Fetal and Adult Zones of the Adrenal Cortex Revealed by Lineage Tracing. Molecular and Cellular Biology *28*, 7030–7040.

Zunino, R., Schauss, A., Rippstein, P., Andrade-Navarro, M., and McBride, H.M. (2007). The SUMO protease SENP5 is required to maintain mitochondrial morphology and function. Journal of Cell Science *120*, 1178–1188.

Zunino, R., Braschi, E., Xu, L., and McBride, H.M. (2009). Translocation of SenP5 from the Nucleoli to the Mitochondria Modulates DRP1-dependent Fission during Mitosis. J. Biol. Chem. *284*, 17783–17795.

ANNEXES

Experimental Gerontology 113 (2018) 228–236

Contents lists available at ScienceDirect

Experimental Gerontology

journal homepage: www.elsevier.com/locate/expgero

Metabolic memory of dietary restriction ameliorates DNA damage and adipocyte size in mouse visceral adipose tissue

Abbas Ishaq[1], Damien Dufour[1], Kerry Cameron, Thomas von Zglinicki, Gabriele Saretzki*

The Ageing Biology Centre, Newcastle Institute for Ageing, Institute for Cell and Molecular Biosciences, Campus of Ageing and Vitality, Newcastle upon Tyne, UK

ARTICLE INFO

Section Editor: Holly M. Brown-Borg

Keywords:
Dietary restriction
Adipose tissue
Senescence
DNA damage
Mice
Ageing
Metabolic

ABSTRACT

Dietary restriction (DR) is thought to exert its beneficial effects on healthspan at least partially by a senolytic and senostatic action, i.e. by reducing frequencies of cells with markers of DNA damage and senescence in multiple tissues. Due to its importance in metabolic and inflammation regulation, fat is a prime tissue for health span determination as well as a prime target for DR. We aimed to determine here whether the beneficial effects of DR would be retained over a subsequent period of ad libitum (AL) feeding.

Male mice were kept under either 40% DR or AL feeding regimes from 3 to 12 months of age and then either switched back to the opposite feeding regimen or kept in the same state for another 3 months. Visceral adipose tissue from 4 to 5 mice per group for all conditions was analysed for markers of senescence (adipocyte size, γH2A.X, p16, p21) and inflammation (e.g. IL-6, TNFα, IL-1β) using immuno-staining or qPCR. Macrophages were detected by immunohistochemistry.

We found that both 9 and 12 months DR (long term) as well as 3 month (short term, mid-life onset) DR reduced the number of cells harbouring DNA damage and adipocyte size (area and perimeter) in visceral adipocytes with similar efficiency. Importantly, beneficial health markers induced by DR such as small adipocyte size and low DNA damage were maintained for at least 3 month after termination of DR, demonstrating that the previously identified 'metabolic memory' of the DR state in male mice extends to senescence markers in visceral fat.

1. Introduction

Obesity is a major health problem world-wide. Consequently, weight reduction is an important field of research to combat obesity and to improve healthspan. Beneficial health effects of dietary restriction have been shown repeatedly in various animal models including non-human primates while lifespan was not always extended significantly (Shimokawa and Trindade, 2010; Fadini et al., 2011; Heestand et al., 2013; Metaxakis and Partridge, 2013; Colman et al., 2014; Shimokawa et al., 2015; Mattison et al., 2017). Intriguingly, fat reduction during DR correlated inversely to life extension in male mice (Liao et al., 2011). In humans however, a prolonged period of strict and substantial caloric restriction seems rather unfeasible (Speakman and Hambly, 2007) and weight is often quickly regained after ending a weight-loss diet (Wing and Hill, 2001). Thus, intensive research is directed at finding alternative ways for weight loss. For example, it has been shown that short term fasting or feeding every other day also promotes improved health for an extended period in humans, mice and rats, and could be maintained by a metabolic memory (Yu et al., 1985; Ceriello et al., 2009; Aschner and Ruiz, 2012; Selman and Hempenstall, 2012).

We have previously shown that male mice retained several beneficial physiological parameters of DR feeding such as reduced body mass and improved glucose tolerance after switch-back to AL condition (Cameron et al., 2012). DR induced a metabolic memory of increased glucose tolerance and lowered plasma insulin levels in male (but not in female) mice for at least 3 months (Cameron et al., 2012) and up to 10 months (Selman and Hempenstall, 2012) after reverting to ad-libitum feeding. DR-induced reduction of senescent cell frequencies in liver also lasted for at least 3 months after termination of the restriction (Ogrodnik et al., 2017). In contrast, others have found a quick reversion in gene expression around 2 months after switching back from DR to AL in mouse heart tissue (Dhahbi et al., 2006).

Adipose tissue is an important regulator of energy balance and

* Corresponding author at: The Ageing Biology Centre and Institute for Cell and Molecular Biosciences, Campus for Ageing and Vitality, Edwardson Building, Newcastle upon Tyne NE4 5PL, UK.
E-mail address: gabriele.saretzki@ncl.ac.uk (G. Saretzki).
[1] These authors contributed equally.

https://doi.org/10.1016/j.exger.2018.10.008
Received 13 June 2018; Received in revised form 24 September 2018; Accepted 8 October 2018
Available online 10 October 2018
0531-5565/

metabolism. It regulates storage and utilization of energy in triglycerides depots under the control of insulin. Visceral adipose tissue (VAT) is one of the main depots of excess calorie storage in humans and mice (Spalding et al., 2017). Additionally, VAT is active as an endocrine organ secreting various adipokines with multiple functions within the organism (Ibrahim, 2010). During accumulation of visceral fat adipocytes contribute to insulin resistance (Laviola et al., 2006) and a pro-inflammatory environment (Del Corno et al., 2016). Macrophage presence and inflammatory state fluctuate with VAT physiology (Boutens and Stienstra, 2016). Increased visceral adipocyte size correlates with infiltration of macrophages into the VAT (Osborn and Olefsky, 2012). Increased lipolysis as well as hypertrophy in adipocytes promote formation of macrophages into aggregates and crown-like structures (CLS) (Kosteli et al., 2010; Ebke et al., 2014). Macrophages are anti-inflammatory in healthy VAT, but become pro-inflammatory during removal of adipocytes containing excess lipids in VAT during obesity (Cinti et al., 2005; Heilbronn and Campbell, 2008; Kratz et al., 2014). Over-accumulation of lipids in VAT may promote leakage of fatty acids (Lelliott and Vidal-Puig, 2004), promoting hyperlipidaemia and accumulation of lipids in other tissues such as during liver steatosis.

Cellular senescence is a permanent cell cycle arrest, characterised by telomere shortening, uncapping or damage, as well as a senescence-associated secretory phenotype (SASP) (Campisi and d'Adda di Fagagna, 2007). Senescence has been best investigated in dividing cells such as fibroblasts and endothelial cells but not much is known about senescence in adipocytes (Brown et al., 1997; d'Adda di Fagagna et al., 2003; Herbig et al., 2004; Erusalimsky and Skene, 2009; Passos et al., 2010). Importantly, cell cycle-independent senescence has also been identified in terminally differentiated and post-mitotic cells (Jurk et al., 2012; Ogrodnik et al., 2017; Ishaq et al., 2018). Senescence-targeted cell ablation experiments have confirmed the causal role of senescence for ageing-related dysfunction and disease in a multitude of tissues including fat (Baker et al., 2016; Kirkland and Tchkonia, 2017; Musi et al., 2018). DR is able to reduce senescent cell frequencies in multiple tissues (Wang et al., 2010; Ogrodnik et al., 2017; Ishaq et al., 2018). In liver, DR did not only reduce hepatocyte senescence but also suppressed steatosis by improving mitochondrial function, and these beneficial effects were maintained for at least 3 months after DR termination (Ogrodnik et al., 2017).

In humans, increased fat mass in particular increased abdominal obesity due to deposition of visceral fat is associated with the metabolic syndrome and ageing (Das et al., 2004). An association between increased lifespan and a decrease in fat mass has been demonstrated previously in various model organisms. A reduction in fat mass in Drosophila due to expression of a forkhead transcription factor as well as a fat-specific disruption of the insulin receptor (FIRKO) resulting in reduced adiposity increased longevity independently of food intake (Giannakou et al., 2004). However, the underlying molecular mechanisms of how adipose tissue might be linked to longevity are not well understood. Decreased triglyceride storage in fat tissue as well as a reduced size of adipocytes are consequences of caloric restriction and might increase lifespan (Blüher, 2008) while increased fat mass is associated with changes in substrate oxidation and glucose homeostasis, partly via the effects of free fatty acids (FFA) and glycerol (Barzilai and Gupta, 1999). Thus, systemic benefits of DR on metabolism have been attributed to decreased fat reservoirs (Barzilai and Gupta, 1999). In male rhesus monkeys, 18 m of DR specifically decreased total fat body mass (Colman et al., 1998). Several studies also showed a decrease in inflammatory markers in fat tissue after DR (Sierra Rojas et al., 2016; Park et al., 2017).

In addition, we demonstrated previously that DR was able to reduce multiple markers of senescence (adipocyte size, DNA damage, p21 expression) in mouse visceral adipocytes (Ishaq et al., 2018).

The main aim of the current study was to investigate whether the protective effect of DR in visceral adipose tissue could be maintained after a switch to AL-feeding. Our study focused on parameters of senescence such as adipocyte size, DNA damage, expression of senescence and inflammation markers as well as the accumulation of macrophages. We found that some, but not all of these features were maintained after switching back from DR to AL and thus are in line with a selective metabolic memory.

2. Materials and methods

2.1. Mouse DR experiment

Male inbred C57BL/6 (Harlan, Blackthorn UK) were used. Ethical approval was granted by the LERC Newcastle University, UK. Mice were housed in same-sex cages in groups of 4 to 6 and identified by ear notches. They were provided with sawdust, paper bedding and environmental enrichment. Mice were housed at 20 ± 2 °C under a 12 h light/12 h dark photoperiod with lights on at 7.00 am. Mice were fed standard rodent pelleted chow (Special Diets Services, Witham, UK). Smaller pellets amounting to 60% of AL intake (calculated based on average food intake in 90 control AL mice between 5 and 12 months of age) were fed to DR mice. At the age of 12 months, mice from the AL and DR groups had their dietary regime changed to the opposite feeding type AL to DR or DR to AL for 3 months (see Fig. 1 for details). AL-fed and DR mice were sacrificed at 12 and 15 months, while the switched back mice were sacrificed at 15 months. All mice were dissected and macroscopically examined for tumor prevalence at death. For more details of husbandry please see (Cameron et al., 2012). Visceral fat was fixed in 4% PFA and embedded in paraffin. Frozen tissue was obtained by snap-freezing in liquid nitrogen and storage at −80 °C. Retroperitoneal fat was used throughout this study.

2.2. Dewaxing and antigen retrieval for paraffin sections

Paraffin sections were cut at 5 µm thickness. Slides were dewaxed and hydrated in Histoclear, 100%, 90% and 70% methanol and dH_2O for 5 min each, twice. The slides were then microwaved in citrate buffer for 4 min at high power and 10 min at 40% power.

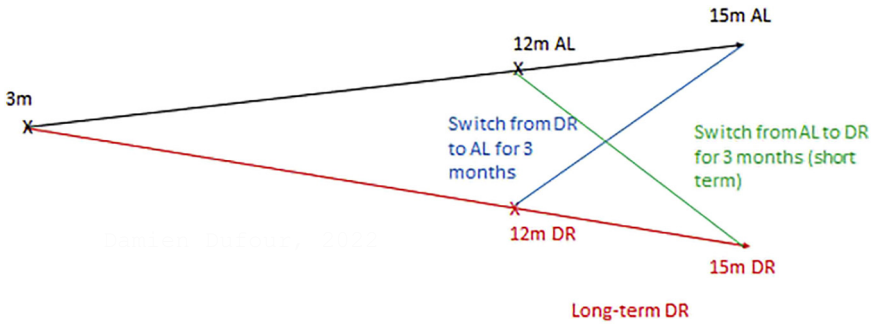

Fig. 1. Schematic representation of the study protocol. At the age of 3 months, male mice were split into two groups, one fed ad libitum (AL) and the other dietary restricted (DR). At the age of 12 months a switch in diet was performed from DR to AL or AL to DR while other mice continued till 15 months in their original feeding regimen.

2.3. Determination of adipocyte size using H&E staining

Following antigen retrieval, Mayer's haematoxylin (Sigma-Aldrich) was applied to the samples for 2 min, washed off with water, and eosin (RAL Diagnostics) was applied for 20s. The samples were washed with water again. After drying, slides were mounted with DPX mounting agent (Leica Biosystems, Germany) and visualised using a Nikon Eclipse E800 microscope (Nikon, Japan) at 200× magnification. 7–14 images were taken from different areas on each slide. To measure adipocyte size ImageJ software was used by drawing an outline around each fat droplet containing cell (adipocyte) on each image. Adipocytes with border damage from sectioning were disregarded. The area within and perimeter of the outline were determined using the 'measure' function in ImageJ (https://imagej.nih.gov/ij/).

Frequency distribution histograms for adipocyte area were made in Graphpad Prism (GraphPad Software, USA). Due to size differences, AL-treated adipocyte areas were binned by 1000 μm increments, DR and AL to DR -treated adipocyte areas were binned by 200 μm increments and DR to AL-treated adipocyte areas are binned by 500 μm increments. Mode, mean and median were determined and are presented for each graph and condition.

2.4. CD68/Nova red staining, imaging and analysis

The full methods used for staining and quantifying macrophage numbers with CD68 and Nova Red staining (SP-2001, Vector Laboratories, USA) have previously been described (Ishaq et al., 2018). Following antigen retrieval, the samples were washed with PBS and placed in 0.9% H_2O_2 for 30 min. The samples were washed and blocked for 30 min (5% normal goat serum (NGS), 1% BSA in PBS). The samples were then rinsed with PBS and blocked with an avidin/biotin solution (Vector Laboratories, USA). The samples were then incubated overnight at 4 °C in 1:100 of CD68 primary antibody (ab125212, Abcam, UK) in blocking solution (5% NGS, 1% BSA in PBS). The samples were then washed thrice with PBS and incubated for 1 h at room temperature in 1:200 of biotinylated anti-rabbit antibody (PK-4000, Vectastain ABC kit, Vector laboratories, USA) in blocking solution. The AB complex (Vectastain, ABC kit) was then applied to the samples for 30 min. The samples were then washed thrice with PBS. Nova Red (Vector Laboratories, USA) was then applied to the samples for exactly 2 min. Nova Red was rinsed off with water and methyl green (0.2% in dH_2O, Sigma-Aldrich) was applied to the samples for 10 min. The samples were then briefly rinsed with water and dehydrated in 70%, 95%, 100% methanol and Histoclear for 30 s at each step. The samples were mounted in DPX (Leica Biosystems, Germany) and stored at room temperature. Images were acquired using a 200× magnification in a Nikon Eclipse E800 microscope (Nikon, Japan) and analysed using ImageJ (https://imagej.nih.gov/ij/).

2.5. Immunofluorescence analysis

The full methods used for immunofluorescence (IF) staining on paraffin-embedded sections and their analysis have been previously described (Ishaq et al., 2018). The samples were washed and blocked for 30 min (5% NGS, 1% BSA in PBS). Rabbit monoclonal primary antibody to γH2A.X (9718, Cell Signaling Technologies, USA) in blocking solution (1:1000) was then applied to the samples for 1 h at room temperature. The samples were then washed thrice in PBS for 5 min. Fluorescently labeled AlexaFluor 488 goat anti-rabbit secondary antibody (A11008, Molecular Probes, UK) in blocking solution was then applied for 1 h at room temperature. The samples were then washed thrice in PBS for 5 min. DAPI (Partec, Germany) was then applied to the samples for 10 min at room temperature. The samples were then washed in PBS once for 10 min. The samples were then mounted in Vectashield anti-fade fluorescence mounting solution (Vector Laboratories, USA). 63× and 1000× magnification images were acquired using a Leica DMi8 microscope (Leica Microsystems, Germany) and analysed using ImageJ.

For IF double-staining with rabbit-anti-γH2A.X (9718, Cell Signaling Technologies, USA) and rat-anti-CD68 (14-0681-80, Invitrogen, USA) on 40 μm frozen sections were thawed and fixed with 4% PFA for 20 min. The samples were then washed and blocked (5% NGS, 1% BSA in PBS) for 1 h at room temperature. Rabbit monoclonal primary antibody to γH2A.X (9718, Cell Signaling Technologies, USA) and rat monoclonal primary antibody to CD68 (14-0681-80, Invitrogen, USA) in blocking solution (γH2A.X: 1:200, CD68: 1:2000) were then simultaneously applied to the samples for 24 h at 4 °C. The samples were then washed thrice in PBS for 5 min. Fluorescently labeled goat anti-rabbit secondary antibody (A11008, AlexaFluor 488; Molecular Probes, UK) and goat anti-rat secondary antibody (A11007, AlexaFluor 594; Molecular Probes, UK) in blocking solution (1:1000 for each) were applied to the samples for 1 h at room temperature. The samples were then washed thrice in PBS for 5 min. DAPI was then applied to the samples for 10 min at room temperature. The samples were then washed in PBS once for 10 min. The samples were then mounted in Vectashield anti-fade fluorescence mounting solution (Vector Laboratories, USA).

2.6. RNA extraction, reverse transcription and qPCR

Up to 100 mg of whole frozen tissue samples were ground in liquid nitrogen before RNA extraction using the Qiagen RNeasy Lipid Tissue Mini Kit (Qiagen, Belgium). Concentrations of RNA obtained from the fat tissue were quantified using a Nanodrop spectrophotometer (ND-1000, Thermo Scientific, USA). Reverse transcription and qPCR were then performed as previously described (Ishaq et al., 2018). 1 μg of RNA was added to 1 μl of random primers (Thermo Scientific, USA) and made up to a final volume of 11 μl in nuclease-free water. RNA was denatured for 7 min at 75 °C in a PCR Sprint Thermal Cycler (Hybaid, Germany) and briefly cooled on ice. 4 μl of 5× First Strand Buffer (Invitrogen, UK) and 2 μl of 0.1 M DTT (Invitrogen, UK) were then added to the PCR tube, along with 1 μl 10 mM dNTP mix (Biolabs, USA), 1 μl RNase Inhibitor (Promega, USA) and 1 μl Reverse Transcriptase (Catalogue no. 18080093, Superscript III; Invitrogen, USA) to a final volume of 20 μl. The reverse transcriptase mixture was then incubated at 42 °C for 90 min in the Thermal Cycler, inactivated at 95 °C, and the resulting cDNA stored at −70 °C. For qPCR, each sample and negative control was measured in triplicate. For each well on a 96-well qPCR plate (Applied Biosystems, USA), 5 μl of Sybr Green (Catalogue no. BIO-92005, SensiFAST SYBR Hi-ROX kit, Bioline, UK), 0.5 μl each of 10 μM forward and reverse primers (Table 1) diluted 1:10 in nuclease free water, and 3 μl of nuclease free water was added to a

Table 1
Primer sequences used in qPCR. Annealing temperatures for all primer pairs were 60 °C.

Primer Name	Forward primer	Reverse primer
Nono (Arsenijevic et al., 2012)	TGCTCCTGTGCCACCTGGTACTC	CCGGAGCTGGACGGTTGAATGC
p16 (Edwards et al., 2007)	CCCAACGCCCCGAACT	GCAGAAGAGCTGCTACGTGAA
p21 (Scoumanne et al., 2011)	GCCTTAGCCCTCACTCTGTG	AGCTGGCCTTAGAGGTGACA
TNF-α (Wang et al., 2015)	ACGTGGAACTGGCAGAAGA	CTCCTCCACTTGGTGGTTTG
IL-6 (Holl et al., 2014)	TGTATGAACAACGATGATGCACTT	ACTCTGGCTTTGTCTTTCTTGTTATCT

500 µl microfuge tube. 9 µl of this mastermix was added to each well, along with 1 µl of sample cDNA. Amplification was performed with the following program: 1 cycle at 95 °C for 2 min, 50 cycles at 95 °C for 5 s and 60 °C for 30 s, 1 cycle at 95 °C for 15 s, 60 °C for 1 min, and 95 °C for 15 s. Non-POU domain-containing octamer binding protein, encoded by *Nono*, was used as the fat-specific internal housekeeping gene. Values were expressed as a $2^{-\Delta\Delta Ct}$ average for each sample, as previously described (Ishaq et al., 2018).

2.7. Statistical analysis

Statistical analysis was performed using SigmaPlot 12.5 (Systat Software Inc., USA). All data sets were tested for normal distribution using Shapiro-Wilks test, then analysed with One Way ANOVA. F- and *p*-values for ANOVA are reported. F-values were reported with degrees of freedom of each sample and cumulative sample size in subscript ($F_{x,y}$). A Holm-Sidak post hoc test was used for pairwise comparisons of different groups in multiple comparisons. Unless stated in figure legends, post hoc tests were not significant (n.s.). For multiple comparisons, *p*-values for post hoc test at $p < 0.05$ except for adipocyte area were not significant at a lower *p*-value threshold. Graphs are presented using GraphPad Prism (GraphPad Software, USA). Bars on all bar graphs represent means and SEM of 4–6 mice as stated in the figure legends.

3. Results

3.1. Visceral adipocyte size decreases after switch from AL to DR and remains low after switch-back from DR to AL

We used both parameters, area and perimeter, to characterize adipocyte size. Histological analysis (Fig. 2) showed that adipocytes were consistently and significantly larger in area after 12 (4535 ± 702 µm^2) and 15 months (4813 ± 1109 µm^2) of AL feeding, compared to visceral adipocytes from mice under DR for the same durations (1466 ± 485 µm^2 and 1195 ± 527 µm^2 for 12 and 15 months respectively, Fig. 2B). There was no change in adipocyte area between the two time-points (12 and 15 months) of the same feeding conditions (Fig. 1 B, C). There was no significant reduction, only a trend for lower adipocyte area after switch from AL to DR (689 ± 117 µm^2 vs 1466 ± 485 µm^2, Fig. 2B) Likewise, there was no increase in adipocyte area after 3 months switch to AL feeding after long-term DR (1398 ± 517 µm^2, Fig. 2B).

Adipocyte perimeter (Fig. 2C) showed similar trends as adipocyte area, but there were no significant changes in perimeter size between 12 m AL and DR. However, the decrease in perimeter size from 15 m AL to 15 m DR, 15 m AL-DR, and 15 m DR-AL (259 ± 31 µm to 125 ± 33 µm, 96 ± 9 µm, and 138 ± 25 µm respectively) was significant and similar to their changes in adipocyte area, but more muted as a result of squared vs linear size measurements.

The distribution analysis of adipocyte area (Fig. 2D) with mode, mean and median shifted to lower values for the DR samples as well as the AL to DR and DR to AL switches. These results confirm the mean values from Fig. 2B of smaller adipocyte area in the 9 and 12 months DR as well as for the two switches.

3.2. DNA damage decreases after switch from AL to DR and remains low after switch-back from DR to AL

Using γH2A.X as a marker for DNA damage and analysing the average number of DNA damage foci (Fig. 3B) as well as the average number of cells harbouring these foci (Fig. 3C), we found that the amount of cells with DNA damage in the VAT during AL feeding was significantly higher than in that of long-term DR which started at 3 months of age. As expected from our previous study on a late-onset, short-term DR experiment in C57BL/6 ICFRa mice (Ishaq et al., 2018), the switch from AL to DR at the age of 12 months for 3 months decreased the amount of cells bearing DNA damage to similar levels as for

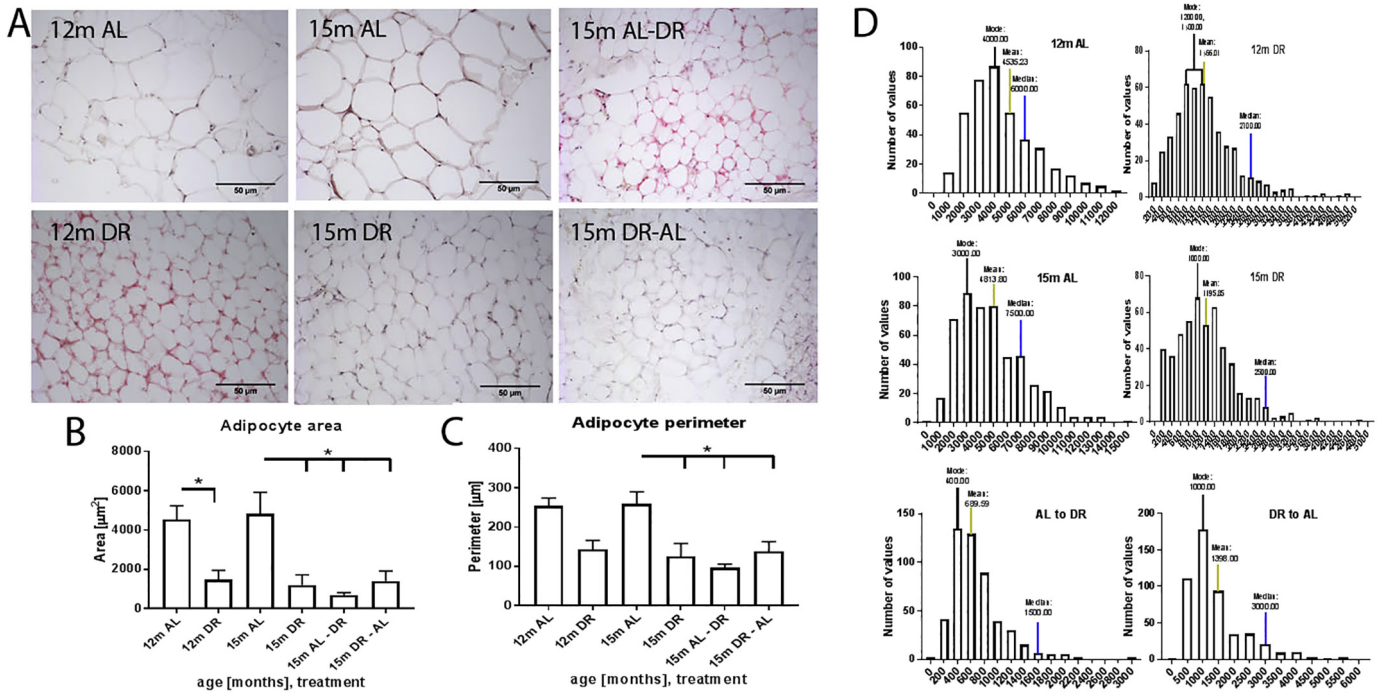

Fig. 2. Determination of adipocyte size under AL and DR conditions as well as after switches from AL to DR and DR to AL. A: Representative images of indicated conditions. B: Adipocyte area as a measure of adipocyte size. $F_{1,5} = 7.652$, $p < 0.001$ by ANOVA. *$p < 0.05$ comparing 12 m AL vs 12 m DR, and 15 m AL to 15 m DR, 15 m AL-DR, and 15 m DR-AL by Holm-Sidak pairwise post hoc test. C: Adipocyte perimeter as a measure of adipocyte size. $F_{1,5} = 7.508$, $p < 0.001$ by ANOVA. * $p < 0.05$ comparing 15 m AL to 15 m DR, 15 m AL-DR, and 15 m DR-AL by Holm-Sidak pairwise post hoc test. n = 4 for 12 m AL, 12 m DR. n = 5 for 15 m AL, 15 m DR, and AL-DR. n = 6 for DR-AL. D: Area distribution for all 6 conditions. Mode, mean and median have been added to each graph.

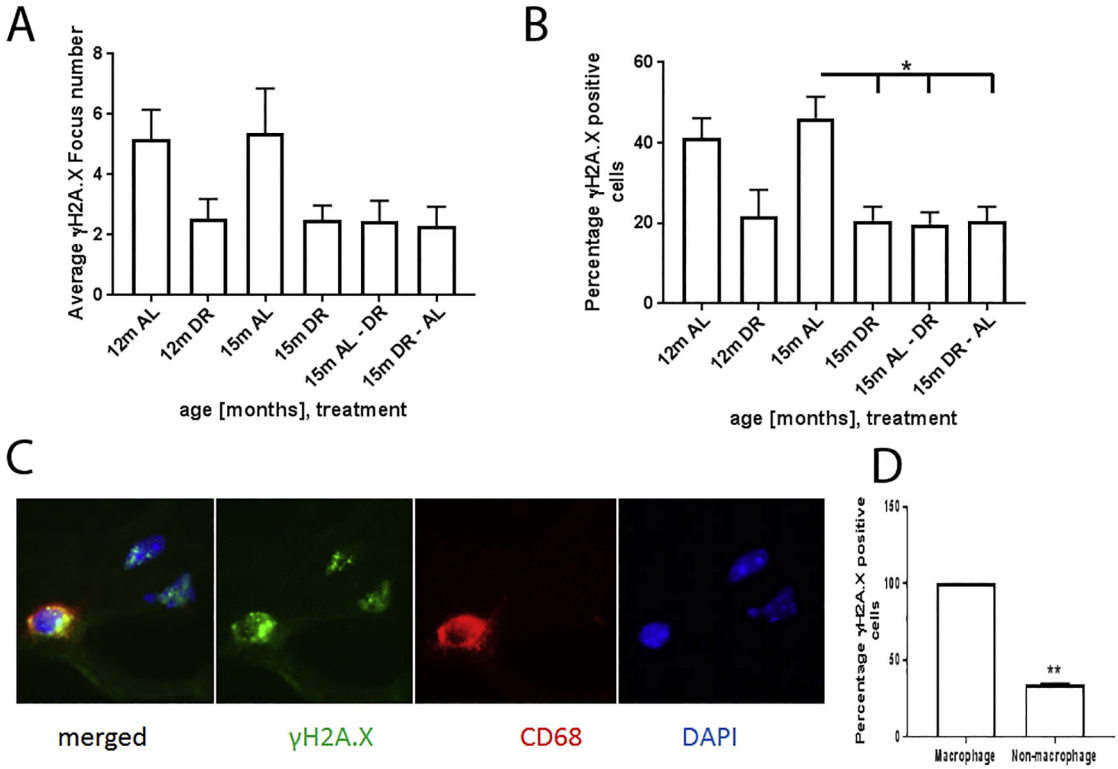

Fig. 3. Analysis of γH2A.X DNA damage foci. A: average γH2A.X focus number per nucleus. $F_{1,5} = 2.725$, $p = 0.045$ by ANOVA. B: Percentage of γH2A.X-positive cells. $F_{1,5} = 6.628$, $p < 0.001$ by ANOVA. *$p < 0.05$ comparing 15 m AL to 15 m DR, 15 m AL-DR, and 15 m DR-AL pairwise by Holm-Sidak pairwise post hoc test. n = 4 for 12 m AL, 12 m DR. n = 5 for 15 m AL, 15 m DR, AL-DR, and DR-AL. C: Representative image of CD68 and γH2A.X co-localisation on frozen tissue. Green: γH2A.X, red: CD68, blue: DAPI. Image was acquired at 400× magnification. D) Quantification of number of macrophages vs non-macrophages (mainly adipocytes) positive for foci. **$p < 0.001$ by *t*-test, n = 15 macrophages, 54 non-macrophages. (For interpretation of the references to colour in this figure legend, the reader is referred to the web version of this article.)

long-term DR starting at 3 months (Fig. 3B). Importantly, the switch-back from DR to AL at the age of 12 months for 3 months did not increase the amount of foci (Fig. 3B) and showed a trend for low percentage of damaged cells (Fig. 3C). However, there was only a trend for the number of DNA damage foci (Fig. 2B) that paralleled the results for the fraction of cells with damage, but without reaching statistical significance.

In order to address the question of what cell type within the fat tissue was predominantly damaged we performed immunofluorescence co-staining with CD68 and γH2A.X (Fig. 3C, D) which showed that 100% of macrophages were damaged while only 34.4% of other cells (mainly adipocytes) were damaged. As determined in Fig. 5B there are around 50 macrophages for each 100 adipocytes, giving a ratio of 1:2 for these 2 cell types and their respective contribution to the DNA damage. However, it is important to mention that this analysis was performed on frozen tissue due to technical issues with the CD68 antibody not working on paraffin-embedded tissue. Thus, the absolute numbers of damaged cells might not correspond to the ones found in paraffin-embedded tissue. We did not find any differences between AL and DR samples (data not shown) for the damage distribution between both cell types. Thus, we suggest that both cell types contribute to the reduction of DNA damage during DR.

3.3. Senescence and inflammatory markers

P16 and p21 were used as senescence markers. There were no significant changes in p16 expression between any samples (Fig. 4A). P21 expression was consistently low in all samples except in adipose tissue from 15 months AL-fed mice (Fig. 4B). P21 expression significantly decreased after 3 months of DR after switching from AL after 12 months corresponding to our previous data (Ishaq et al., 2018). Importantly, p21 did not increase after switching back from DR to AL in line with a possible metabolic memory of the DR condition (Fig. 4B).

There were no significant changes in the expression of any of the analysed inflammatory markers (TNFα, IL-6, or IL-1β). However, TNFα and IL-1β expression displayed a trend towards decreased values in the 15 months DR adipose tissue as well as in both switch directions (Fig. 4C-E).

3.4. Analysis of macrophage numbers and aggregates

Using CD68 as a general macrophage marker (representative images are shown in Fig. 5A), there were no differences in single macrophage counts between the different feeding conditions including the 2 switches in feeding state (Fig. 5B). However, there was a trend for a decrease of macrophage aggregates in 12 and 15 months DR and the shift from DR to AL also showed rather low aggregate amounts. In contrast, the shift from AL to DR at 12 months did not show any tendency for a decrease (Fig. 5C).

4. Discussion

Our results presented here confirm previous findings that dietary restriction is beneficial in mouse visceral adipose tissue, reducing visceral adipocyte size and DNA damage (Ishaq et al., 2018), while others have shown beneficial effects of DR in VAT on insulin sensitivity and alleviation of VAT inflammation (Barzilai et al., 1998; Barzilai and Gupta, 1999; Masoro, 2006; Sierra Rojas et al., 2016). Importantly, some of our analysed parameters also confirm the occurrence of a "metabolic memory" of the DR condition even after switching back to AL feeding for 3 months. We had previously examined various physiological parameters in the same mouse cohort as used in this study and

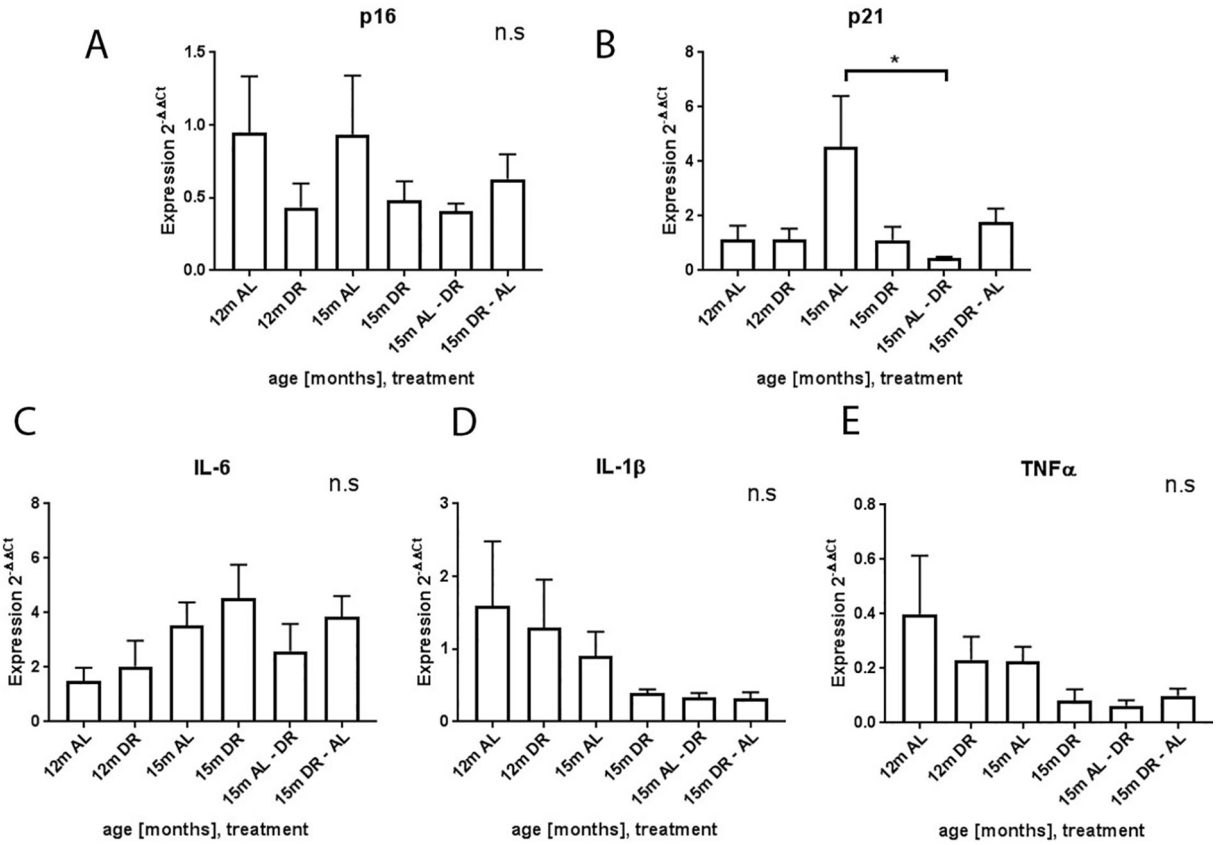

Fig. 4. Gene expression analysis of visceral adipose tissue under the indicated conditions. A: p16, $F_{1,\ 5} = 0.963$, $p = 0.461$ for ANOVA. B: p21, $F_{1,\ 5} = 2.723$, $p = 0.045$ for ANOVA. *$p < 0.05$ comparing 15 m AL to 15 m AL-DR only by Holm-Sidak pairwise post hoc test. C: IL-6, $F_{1,\ 5} = 1.494$, $p = 0.230$ for ANOVA. D: IL-1β, $F_{1,\ 5} = 1.787$, $p = 0.155$ for ANOVA. E: TNFα, $F_{1,\ 5} = 2.216$, $p = 0.087$ for ANOVA. n = 4 for 12 m AL, 12 m DR. n = 5 for 15 m AL, 15 m DR, and AL-DR. n = 6 for DR-AL.

had found a metabolic memory for improved glucose tolerance specifically in male mice after switching back from DR to AL (Cameron et al., 2012).

Here we found a decrease in adipocyte size under DR which remained low after switching back to AL. Our data here confirms that short-term, mid-life onset DR for 3 months is sufficient to alleviate AL-feeding-induced DNA damage in adipose tissue corresponding to our previous findings (Ishaq et al., 2018). It seems that changes in visceral adipocyte size are associated with the amount of cells with DNA damage under the different conditions analysed. While DNA damage is a well-established general stress-and senescence marker in many tissue types, cell size seems to be more specific for differentiated adipocytes. However, an increase in cell size is also a feature of senescent cells. Thus, both parameters seem to point into a similar direction. Low amounts of telomere-associated DNA damage in liver tissue and significantly decreased liver steatosis was found after switching back from DR to AL for 3 months in the same mouse cohort as used here, suggesting a "metabolic memory" in this tissue as well (Ogrodnik et al., 2017). Interestingly, we found a higher amount of DNA damage in macrophages than in non-macrophages that are most likely in the majority adipocytes. Fat tissue composition according to our results shows an approximate ratio of macrophages to adipocytes under AL condition of 1:2 while under DR there is a trend for a slightly smaller fraction of macrophages. However, we did not find any changes of the damage fractions between AL and DR (data not shown) which suggests that both cell types seem to have a decrease in DNA damage under DR treatment. However, the role of macrophages during senescence is not without controversy. Recently, Hall et al. (2017) demonstrated that macrophages can be p16 and senescence-associates beta-galactosidase positive as part of their physiological programme of polarization during immune-stimulation which could be reversible (Hall et al., 2016, 2017). Although the role of DNA damage in those macrophages have not been analysed, data about macrophage senescence have to be interpreted with caution.

We did not find any significant changes in the expression of p16, while for p21 there was a significant decrease after 3 months of DR compared to 15 months AL. This decrease corresponds well with our previous findings of a decrease in p21 in a late-onset, short-term DR in 17 month old mice (Ishaq et al., 2018) while long-term DR did only show a trend for a decrease.

DR is known to decrease the amount of body fat and the reduced fat content is thought to induce some of the beneficial effects of DR such as decrease in inflammation in different tissues (Gerbase-Delima et al., 1975; Masoro, 2003; Fontana, 2009; Ye and Keller, 2010). However, we did not find any significant changes in inflammatory markers under DR or any switch-condition although the expression levels for TNFα and IL-1β had a tendency towards decreased levels under these conditions. However, we only analysed 3 inflammatory markers while the SASP phenotype includes a large number of other markers. Thus, it is possible that other markers of the SASP phenotype are changed. We had found a decrease in IL-6 in our previous study on a short-term, late-onset DR regimen (Ishaq et al., 2018), but could not detect any changes in IL-6 in this study.

Changes in body weight after switching from DR to AL and AL to DR in our mouse cohort were proportional to changes in fat mass with no depot-specific changes as published in a previous study on the same mouse cohort (Cameron et al., 2012), similar to other studies in C57BL/6 male mice (Selman and Hempenstall, 2012; Schmitz et al., 2016).

The amounts, distribution and function of adipose tissue macrophage and their inflammatory states in lean adipose tissue versus obese

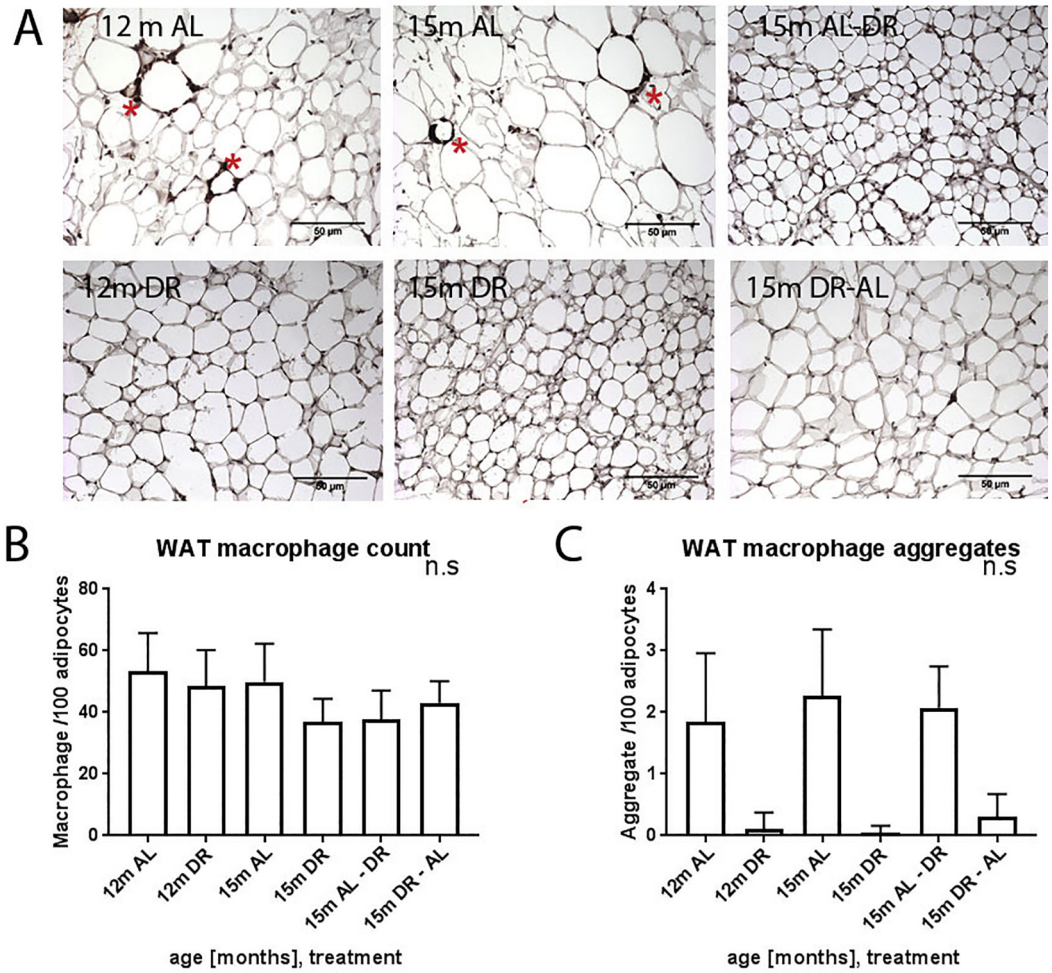

Fig. 5. Analysis of macrophage numbers and aggregates. A: Representative images of CD68/Nova Red staining for the indicated conditions. Red asterisks show macrophage aggregates B: Numbers of macrophages per 100 adipocytes, $F_{1,\ 5} = 0.399$, $p = 0.844$ for ANOVA. C: Number of macrophage aggregates, $F_{1,5} = 2.018$, $p = 0.116$ for ANOVA. n = 4 m for 12 DR, DR-AL. n = 5 for 15 m AL, 15 m DR, and AL-DR.

adipose tissue are well characterised (Boutens and Stienstra, 2016). Hypertrophy of adipocytes, caloric restriction and pharmacologically-induced lipolysis promotes adipose tissue macrophage aggregation (Kosteli et al., 2010; Lee et al., 2013; Ebke et al., 2014). Here we found no changes in general macrophage numbers in any group of the analysed conditions. However, there was a trend towards increase in macrophage aggregates in 12 and 15 months old mice under AL condition, in line with the other studies (Ebke et al., 2014). However, switching to 3 months of DR at mid-life did not reduce the amount of aggregates, but the adipocytes were no longer hypertrophic (as characterised by a smaller size), suggesting an increased lipolysis. In contrast, mice under DR had a tendency towards low numbers of aggregates that remained low after the switch to AL but did not reach statistical significance due to large variations between analysed tissues. While our study followed changes after nutritional switches for only 3 months, another study has monitored DR to AL and AL to DR nutritional switches in mice at 1, 6 and 10 months (Selman and Hempenstall, 2012). That latter study found a “glycaemic memory” with improved glucose tolerance still persisting 10 months after switch from DR to AL despite body mass while fasting insulin levels and insulin sensitivity were all reversed back to the AL phenotype by that time (Selman and Hempenstall, 2012). Thus, there can be a lasting beneficial metabolic effect in systemic physiological parameters (Cameron et al., 2012; Selman and Hempenstall, 2012) as well as in different tissues such as liver (Ogrodnik et al., 2017) and visceral fat of DR in mice even when switched back to AL feeding. In contrast, others describe a “gorging effect” and even higher fat deposition after re-feeding in rodents (Kirchner et al., 2012; Kliewer et al., 2015).

Taken together, our results demonstrate that some beneficial changes during long-term dietary restriction can be maintained in fat tissue as a “metabolic memory” even after switching back from DR to ad libitum feeding. This applies mainly to parameters such as adipocyte size and the amount of cells with DNA damage while other factors like the amount of macrophage aggregates and the expression of senescence and inflammatory markers showed a trend towards a similar effect but were not statistically significant.

Acknowledgement

The work was supported by BBSRC grant BB/C008200/1 to TvZ and from a Grant from Newcastle University Institute for Ageing (BH161774) to GS.

Disclosure statement

None of the authors have anything to disclose.

References

Arsenijevic, T., Grégoire, F., Delforge, V., Delporte, C., Perret, J., 2012. Murine 3T3-L1 adipocyte cell differentiation model: validated reference genes for qPCR gene expression analysis. PLoS One 7 (5), e37517.
Aschner, P.J., Ruiz, A.J., 2012. Metabolic memory for vascular disease in diabetes.

Diabetes Technol. Ther. 14 (Suppl. 1), S68–S74.
Baker, D.J., Childs, B.G., Durik, M., Wijers, M.E., Sieben, C.J., Zhong, J., Saltness, R.A., Jeganathan, K.B., Verzosa, G.C., Pezeshki, A., Khazaie, K., Miller, J.D., van Deursen, J.M., 2016. Naturally occurring p16(Ink4a)-positive cells shorten healthy lifespan. Nature 530 (7589), 184–189.
Barzilai, N., Gupta, G., 1999. Revisiting the role of fat mass in the life extension induced by caloric restriction. J. Gerontol. A Biol. Sci. Med. Sci. 54 (3), B89–B96 (discussion B97–8).
Barzilai, N., Banerjee, S., Hawkins, M., Chen, W., Rossetti, L., 1998. Caloric restriction reverses hepatic insulin resistance in aging rats by decreasing visceral fat. J. Clin. Invest. 101 (7), 1353–1361.
Blüher, M., 2008. Fat tissue and long life. Obes. Facts 1 (4), 176–182.
Boutens, L., Stienstra, R., 2016. Adipose tissue macrophages: going off track during obesity. Diabetologia 59, 879–894.
Brown, J.P., Wei, W., Sedivy, J.M., 1997. Bypass of senescence after disruption of p21CIP1/WAF1 gene in normal diploid human fibroblasts. Science 277 (5327), 831–834.
Cameron, K.M., Miwa, S., Walker, C., von Zglinicki, T., 2012. Male mice retain a metabolic memory of improved glucose tolerance induced during adult onset, short-term dietary restriction. Longev. Healthspan 1, 3.
Campisi, J., d'Adda di Fagagna, F., 2007. Cellular senescence: when bad things happen to good cells. Nat. Rev. Mol. Cell Biol. 8 (9), 729–740.
Ceriello, A., Ihnat, M.A., Thorpe, J.E., 2009. The "metabolic memory": is more than just tight glucose control necessary to prevent diabetic complications? J. Clin. Endocrinol. Metab. 94 (2), 410–415.
Cinti, S., Mitchell, G., Barbatelli, G., Murano, I., Ceresi, E., Faloia, E., Wang, S., Fortier, M., Greenberg, A.S., Obin, M.S., 2005. Adipocyte death defines macrophage localization and function in adipose tissue of obese mice and humans. J. Lipid Res. 46 (11), 2347–2355.
Colman, R.J., Roecker, E.B., Ramsey, J.J., Kemnitz, J.W., 1998. The effect of dietary restriction on body composition in adult male and female rhesus macaques. Aging (Milano) 10 (2), 83–92.
Colman, R.J., Beasley, T.M., Kemnitz, J.W., Johnson, S.C., Weindruch, R., Anderson, R.M., 2014. Caloric restriction reduces age-related and all-cause mortality in rhesus monkeys. Nat. Commun. 5, 3557.
d'Adda di Fagagna, F., Reaper, P.M., Clay-Farrace, L., Fiegler, H., Carr, P., Von Zglinicki, T., Saretzki, G., Carter, N.P., Jackson, S.P., 2003. A DNA damage checkpoint response in telomere-initiated senescence. Nature 426 (6963), 194–198.
Das, M., Gabriely, I., Barzilai, N., 2004. Caloric restriction, body fat and ageing in experimental models. Obes. Rev. 5 (1), 13–19.
Del Corno, M., DArchivio, M., Conti, L., Scazzocchio, B., Vari, R., Donninelli, G., Varano, B., Giammarioli, S., De Meo, S., Silecchia, G., Pennestri, F., Persiani, R., Masella, R., Gessani, S., 2016. Visceral fat adipocytes from obese and colorectal cancer subjects exhibit distinct secretory and omega6 polyunsaturated fatty acid profiles and deliver immunosuppressive signals to innate immunity cells. Oncotarget 7 (39), 63093–63105.
Dhahbi, J.M., Tsuchiya, T., Kim, H.J., Mote, P.L., Spindler, S.R., 2006. Gene expression and physiologic responses of the heart to the initiation and withdrawal of caloric restriction. J. Gerontol. A Biol. Sci. Med. Sci. 61 (3), 218–231.
Ebke, L.A., Nestor-Kalinoski, A.L., Slotterbeck, B.D., Al-Dieri, A.G., Ghosh-Lester, S., Russo, L., Najjar, S.M., von Grafenstein, H., McInerney, M.F., 2014. Tight association between macrophages and adipocytes in obesity: implications for adipocyte preparation. Obesity (Silver Spring) 22 (5), 1246–1255.
Edwards, M.G., Anderson, R.M., Yuan, M., Kendziorski, C.M., Weindruch, R., Prolla, T.A., 2007. Gene expression profiling of aging reveals activation of a p53-mediated transcriptional program. BMC Genomics 8, 80.
Erusalimsky, J.D., Skene, C., 2009. Mechanisms of endothelial senescence. Exp. Physiol. 94 (3), 299–304.
Fadini, G.P., Ceolotto, G., Pagnin, E., de Kreutzenberg, S., Avogaro, A., 2011. At the crossroads of longevity and metabolism: the metabolic syndrome and lifespan determinant pathways. Aging Cell 10 (1), 10–17.
Fontana, L., 2009. Neuroendocrine factors in the regulation of inflammation: excessive adiposity and calorie restriction. Exp. Gerontol. 44 (1), 41–45.
Gerbase-Delima, M., Liu, R.K., Cheney, K.E., Mickey, R., Walford, R.L., 1975. Immune function and survival in a long-lived mouse strain subjected to undernutrition. Gerontologia 21 (4), 184–202.
Giannakou, M.E., Goss, M., Junger, M.A., Hafen, E., Leevers, S.J., Partridge, L., 2004. Long-lived Drosophila with overexpressed dFOXO in adult fat body. Science 305 (5682), 361.
Hall, B.M., Balan, V., Gleiberman, A.S., Strom, E., Krasnov, P., Virtuoso, L.P., Rydkina, E., Vujcic, S., Balan, K., Gitlin, I., Leonova, K., Polinsky, A., Chernova, O.B., Gudkov, A.V., 2016. Aging of mice is associated with p16(Ink4a)- and beta-galactosidase-positive macrophage accumulation that can be induced in young mice by senescent cells. Aging (Albany NY) 8 (7), 1294–1315.
Hall, B.M., Balan, V., Gleiberman, A.S., Strom, E., Krasnov, P., Virtuoso, L.P., Rydkina, E., Vujcic, S., Balan, K., Gitlin, I.I., Leonova, K.I., Consiglio, C.R., Gollnick, S.O., Chernova, O.B., Gudkov, A.V., 2017. p16(Ink4a) and senescence-associated beta-galactosidase can be induced in macrophages as part of a reversible response to physiological stimuli. Aging (Albany NY) 9 (8), 1867–1884.
Heestand, B.N., Shen, Y., Liu, W., Magner, D.B., Storm, N., Meharg, C., Habermann, B., Antebi, A., 2013. Dietary restriction induced longevity is mediated by nuclear receptor NHR-62 in *Caenorhabditis elegans*. PLoS Genet. 9 (7), e1003651.
Heilbronn, L.K., Campbell, L.V., 2008. Adipose tissue macrophages, low grade inflammation and insulin resistance in human obesity. Curr. Pharm. Des. 14 (12), 1225–1230.
Herbig, U., Jobling, W.A., Chen, B.P., Chen, D.J., Sedivy, J.M., 2004. Telomere shortening triggers senescence of human cells through a pathway involving ATM, p53, and p21(CIP1), but not p16(INK4a). Mol. Cell 14 (4), 501–513.
Holl, E.K., Bond, J.E., Selim, M.A., Ehanire, T., Sullenger, B., Levinson, H., 2014. The nucleic acid scavenger polyamidoamine third-generation dendrimer inhibits fibroblast activation and granulation tissue contraction. Plast. Reconstr. Surg. 134 (3), 420e-33e.
Ibrahim, M.M., 2010. Subcutaneous and visceral adipose tissue: structural and functional differences. Obes. Rev. 11 (1), 11–18.
Ishaq, A., Schroder, J., Edwards, N., von Zglinicki, T., Saretzki, G., 2018. Dietary restriction ameliorates age-related increase in DNA damage, senescence and inflammation in mouse adipose tissue. J. Nutr. Health Aging 22 (4), 555–561.
Jurk, D., Wang, C., Miwa, S., Maddick, M., Korolchuk, V., Tsolou, A., Gonos, E.S., Thrasivoulou, C., Saffrey, M.J., Cameron, K., von Zglinicki, T., 2012. Postmitotic neurons develop a p21-dependent senescence-like phenotype driven by a DNA damage response. Aging Cell 11 (6), 996–1004.
Kirchner, H., Hofmann, S.M., Fischer-Rosinsky, A., Hembree, J., Abplanalp, W., Ottaway, N., Donelan, E., Krishna, R., Woods, S.C., Muller, T.D., Spranger, J., Perez-Tilve, D., Pfluger, P.T., Tschop, M.H., Habegger, K.M., 2012. Caloric restriction chronically impairs metabolic programming in mice. Diabetes 61 (11), 2734–2742.
Kirkland, J.L., Tchkonia, T., 2017. Cellular senescence: a translational perspective. EBioMedicine 21, 21–28.
Kosteli, A., Sugaru, E., Haemmerle, G., Martin, J.F., Lei, J., Zechner, R., Ferrante Jr., A.W., 2010. Weight loss and lipolysis promote a dynamic immune response in murine adipose tissue. J. Clin. Invest. 120 (10), 3466–3479.
Kliewer, K.L., Ke, J.Y., Lee, H.Y., Stout, M.B., Cole, R.M., Samuel, V.T., Shulman, G.I., Belury, M.A., 2015. Short-term food restriction followed by controlled refeeding promotes gorging behavior, enhances fat deposition, and diminishes insulin sensitivity in mice. J. Nutr. Biochem. 26 (7), 721–728.
Kratz, M., Coats, B.R., Hisert, K.B., Hagman, D., Mutskov, V., Peris, E., Schoenfelt, K.Q., Kuzma, J.N., Larson, I., Billing, P.S., Landerholm, R.W., Crouthamel, M., Gozal, D., Hwang, S., Singh, P.K., Becker, L., 2014. Metabolic dysfunction drives a mechanistically distinct proinflammatory phenotype in adipose tissue macrophages. Cell Metab. 20 (4), 614–625.
Laviola, L., Perrini, S., Cignarelli, A., Giorgino, F., 2006. Insulin signalling in human adipose tissue. Arch. Physiol. Biochem. 112 (2), 82–88.
Lee, Y.H., Petkova, A.P., Granneman, J.G., 2013. Identification of an adipogenic niche for adipose tissue remodeling and restoration. Cell Metab. 18 (3), 355–367.
Lelliott, C., Vidal-Puig, A.J., 2004. Lipotoxicity, an imbalance between lipogenesis de novo and fatty acid oxidation. Int. J. Obes. 28, S22.
Liao, C.Y., Rikke, B.A., Johnson, T.E., Gelfond, J.A., Diaz, V., Nelson, J.F., 2011. Fat maintenance is a predictor of the murine lifespan response to dietary restriction. Aging Cell 10 (4), 629–639.
Masoro, E.J., 2003. Subfield history: caloric restriction, slowing aging, and extending life. Sci. Aging Knowl. Environ. 2003 (8), Re2.
Masoro, E.J., 2006. Caloric restriction and aging: controversial issues. J. Gerontol. A Biol. Sci. Med. Sci. 61 (1), 14–19.
Mattison, J.A., Colman, R.J., Beasley, T.M., Allison, D.B., Kemnitz, J.W., Roth, G.S., Ingram, D.K., Weindruch, R., de Cabo, R., Anderson, R.M., 2017. Caloric restriction improves health and survival of rhesus monkeys. Nat. Commun. 8, 14063.
Metaxakis, A., Partridge, L., 2013. Dietary restriction extends lifespan in wild-derived populations of Drosophila melanogaster. PLoS One 8 (9), e74681.
Musi, N., Valentine, J.M., Sickora, K.R., Baeuerle, E., Thompson, C.S., Shen, Q., Orr, M.E., 2018. Tau protein aggregation is associated with cellular senescence in the brain. Aging Cell, e12840.
Ogrodnik, M., Miwa, S., Tchkonia, T., Tiniakos, D., Wilson, C.L., Lahat, A., Day, C.P., Burt, A., Palmer, A., Anstee, Q.M., Grellscheid, S.N., Hoeijmakers, J.H.J., Barnhoorn, S., Mann, D.A., Bird, T.G., Vermeij, W.P., Kirkland, J.L., Passos, J.F., von Zglinicki, T., Jurk, D., 2017. Cellular senescence drives age-dependent hepatic steatosis. Nat. Commun. 8, 15691.
Osborn, O., Olefsky, J.M., 2012. The cellular and signaling networks linking the immune system and metabolism in disease. Nat. Med. 18 (3), 363–374.
Park, C.Y., Park, S., Kim, M.S., Kim, H.K., Han, S.N., 2017. Effects of mild calorie restriction on lipid metabolism and inflammation in liver and adipose tissue. Biochem. Biophys. Res. Commun. 490 (3), 636–642.
Passos, J.F., Nelson, G., Wang, C., Richter, T., Simillion, C., Proctor, C.J., Miwa, S., Olijslagers, S., Hallinan, J., Wipat, A., Saretzki, G., Rudolph, K.L., Kirkwood, T.B.L., von Zglinicki, T., 2010. Feedback between p21 and reactive oxygen production is necessary for cell senescence. Mol. Syst. Biol. 6, 347.
Schmitz, J., Evers, N., Awazawa, M., Nicholls, H.T., Bronneke, H.S., Dietrich, A., Mauer, J., Bluher, M., Bruning, J.C., 2016. Obesogenic memory can confer long-term increases in adipose tissue but not liver inflammation and insulin resistance after weight loss. Mol. Metab. 5 (5), 328–339.
Scoumanne, A., Cho, S.J., Zhang, J., Chen, X., 2011. The cyclin-dependent kinase inhibitor p21 is regulated by RNA-binding protein PCBP4 via mRNA stability. Nucleic Acids Res. 39 (1), 213–224.
Selman, C., Hempenstall, S., 2012. Evidence of a metabolic memory to early-life dietary restriction in male C57BL/6 mice. Longev. Healthspan 1 (1), 2.
Shimokawa, I., Trindade, L.S., 2010. Dietary restriction and aging in rodents: a current view on its molecular mechanisms. Aging Dis. 1 (2), 89–107.
Shimokawa, I., Komatsu, T., Hayashi, N., Kim, S.E., Kawata, T., Park, S., Hayashi, H., Yamaza, H., Chiba, T., Mori, R., 2015. The life-extending effect of dietary restriction requires Foxo3 in mice. Aging Cell 14 (4), 707–709.
Sierra Rojas, J.X., Garcia-San Frutos, M., Horrillo, D., Lauzurica, N., Oliveros, E., Carrascosa, J.M., Fernandez-Agullo, T., Ros, M., 2016. Differential development of inflammation and insulin resistance in different adipose tissue depots along aging in Wistar rats: effects of caloric restriction. J. Gerontol. A Biol. Sci. Med. Sci. 71 (3),

310–322.
Spalding, K.L., Bernard, S., Näslund, E., Salehpour, M., Possnert, G., Appelsved, L., Fu, K.-Y., Alkass, K., Druid, H., Thorell, A., Rydén, M., Arner, P., 2017. Impact of fat mass and distribution on lipid turnover in human adipose tissue. Nat. Commun. 8, 15253.
Speakman, J.R., Hambly, C., 2007. Starving for life: what animal studies can and cannot tell us about the use of caloric restriction to prolong human lifespan. J. Nutr. 137 (4), 1078–1086.
Wang, C., Maddick, M., Miwa, S., Jurk, D., Czapiewski, R., Saretzki, G., Langie, S.A., Godschalk, R.W., Cameron, K., von Zglinicki, T., 2010. Adult-onset, short-term dietary restriction reduces cell senescence in mice. Aging (Albany NY) 2 (9), 555–566.
Wang, T.-S., Gao, F., Qi, Q.-R., Qin, F.-N., Zuo, R.-J., Li, Z.-L., Liu, J.-L., Yang, Z.-M., 2015. Dysregulated LIF-STAT3 pathway is responsible for impaired embryo implantation in a Streptozotocin-induced diabetic mouse model. Biol. Open 4 (7), 893–902.
Wing, R.R., Hill, J.O., 2001. Successful weight loss maintenance. Annu. Rev. Nutr. 21, 323–341.
Ye, J., Keller, J.N., 2010. Regulation of energy metabolism by inflammation: a feedback response in obesity and calorie restriction. Aging (Albany NY) 2 (6), 361–368.
Yu, B.P., Masoro, E.J., McMahan, C.A., 1985. Nutritional influences on aging of Fischer 344 rats: I. Physical, metabolic, and longevity characteristics. J. Gerontol. 40 (6), 657–670.

THE FASEB JOURNAL • RESEARCH • www.fasebj.org

Hormonal and spatial control of SUMOylation in the human and mouse adrenal cortex

Typhanie Dumontet,* Isabelle Sahut-Barnola,* Damien Dufour,* Anne-Marie Lefrançois-Martinez,* Annabel Berthon,* Nathanaëlle Montanier,*,† Bruno Ragazzon,‡ Cyril Djari,* Jean-Christophe Pointud,* Florence Roucher-Boulez,*,§ Marie Batisse-Lignier,*,¶ Igor Tauveron,*,¶ Jérôme Bertherat,‡,‖ Pierre Val,* and Antoine Martinez*,[1]

*Génétique Reproduction and Dévelopement (GReD), Centre National de la Recherche Scientifique (CNRS), INSERM, and ¶Service d'Endocrinologie, Faculté de Médecine, Centre Hospitalier Universitaire (CHU), Université Clermont-Auvergne, Clermont-Ferrand, France; †Service d'Endocrinologie, Centre Hospitalier Régional (CHR), Hôpital de la Source, Orléans, France; ‡Institut Cochin, Centre National de la Recherche Scientifique (CNRS), INSERM, Université Paris Descartes, Paris, France; §Endocrinologie Moléculaire et Maladies Rares, CHU, Université Claude Bernard Lyon 1, Bron, France; and ‖Centre Maladies Rares de la Surrénale, Service d'Endocrinologie, Hôpital Cochin, Assistance Publique Hôpitaux de Paris, Paris, France

ABSTRACT: SUMOylation is a highly conserved and dynamic post-translational mechanism primarily affecting nuclear programs for adapting organisms to stressful challenges. Alteration of SUMOylation cycles leads to severe developmental and homeostatic defects and malignancy, but signals coordinating SUMOylation are still unidentified. The adrenal cortex is a zonated endocrine gland that controls body homeostasis and stress response. Here, we show that in human and in mouse adrenals, SUMOylation follows a decreasing centripetal gradient that mirrors cortical differentiation flow and delimits highly and weakly SUMOylated steroidogenic compartments, overlapping glomerulosa, and fasciculata zones. Activation of PKA signaling by acute hormonal treatment, mouse genetic engineering, or in Carney complex results in repression of small ubiquitin-like modifier (SUMO) conjugation in the inner cortex by coordinating expression of SUMO pathway inducers and repressors. Conversely, genetic activation of canonical wingless-related integration site signaling maintains high SUMOylation potential in the outer neoplastic cortex. Thus, SUMOylation is tightly regulated by signaling pathways that orchestrate adrenal zonation and diseases.—Dumontet, T., Sahut-Barnola, I., Dufour, D., Lefrançois-Martinez, A.-M., Berthon, A., Montanier, N., Ragazzon, B., Djari, C., Pointud, J.-C., Roucher-Boulez, F., Batisse-Lignier, M., Tauveron, I., Bertherat, J., Val, P., Martinez, A. Hormonal and spatial control of SUMOylation in the human and mouse adrenal cortex. FASEB J. 33, 10218–10230 (2019). www.fasebj.org

KEY WORDS: endocrine diseases · PKA · SENP1/2 · PIAS3.β-catenin · mouse models

The adrenal cortex is divided into structurally and functionally distinct concentric zones (1). Under the capsule, the zona glomerulosa (zG) ensures production of aldosterone under the control of angiotensin II and potassium, mainly through calcium signaling (2). The zona fasciculata (zF), located just below, forms a wide layer of cells responsible for the secretion of glucocorticoids in response to ACTH, acting through cAMP/PKA signaling pathway (3). The zona reticularis (zR), located in the inner part of the cortex close to the medulla, supports the secretion of adrenal androgen precursors in response to ACTH (4). In rodents, the adult cortex only consists of zG and zF (5). However, in mice, a third and transient zone termed the X-zone is located in the innermost part of the cortex and is considered to be a remnant of the fetal cortex (6, 7). By its capacity to rapidly release hormones acting both on blood pressure control and glucido-lipidic metabolism, the adrenal gland is considered to be the endocrine gland for stress response.

The zonal organization and cellular renewal of the adrenal cortex are maintained through the recruitment of progenitor cells from the periphery of the gland that migrate centripetally and differentiate successively into zG and zF cells (8, 9). Hormonal signals that control adrenal function also participate in the zonation of the

ABBREVIATIONS: AKR1B7, aldo-keto reductase 1B7; ATC1, adrenocortical tumor cell line 1; CNC, Carney complex; Cre, cyclization recombinase; CREB, cAMP responsive element binding protein; DESI1, deSUMOylating isopeptidase 1; HPA, hypothalamic-pituitary-adrenal; PIAS, protein inhibitor of activated signal transducer; PPNAD, primary pigmented nodular adrenocortical disease; PRKAR1A, R1α/ PKA-dependent type 1 regulatory subunit α; qRT-PCR, quantitative RT-PCR; SAE, SUMO-activating enzyme; SENP, SUMO/sentrin specific peptidase; SF-1, steroidogenic factor-1; SIK, salt-inducible kinase; SUMO, small ubiquitin-like modifier; UBE2I, ubiquitin-conjugating enzyme E2 I; WNT, wingless-related integration site; WT, wild type; zF, zona fasciculata; zG, zona glomerulosa; zR, zona reticularis

[1] Correspondence: GReD, CNRS UMR6293, INSERM U1103, Faculté de Médecine, CRBC, Université Clermont-Auvergne, 28 place Henri Dunant, BP38, 63001 Clermont-Ferrand, France. E-mail: antoine.martinez@uca.fr

doi: 10.1096/fj.201900557R

This article includes supplemental data. Please visit *http://www.fasebj.org* to obtain this information.

0892-6638/19/0033-10218 © FASEB

cortex. The R-spondin/wingless-related integration site (WNT)/β-catenin signaling pathway contributes to the acquisition of zG identity (10, 11), whereas ACTH/cAMP/PKA signaling is essential for zF and zR differentiation (12, 13). Maintaining adequate zonation during the unidirectional renewal of the cortex is ensured at least by the antagonistic interactions between these 2 signaling pathways and through epigenetic programming of newly recruited cells (14–16).

PKA is a tetramer composed of 2 catalytic and 2 cAMP-binding regulatory subunits. When intracellular levels of cAMP increase, following activation of the G-protein–coupled ACTH receptor, the regulatory subunits release the catalytic subunits, which become active and phosphorylate downstream effectors (17). These targets include transcription factors stimulating the expression of steroidogenic genes. Inactivating mutations of the PKA-dependent type 1 regulatory subunit α gene (*PRKAR1A*) encoding the regulatory subunit R1α leads to constitutive activation of PKA and development of Carney complex (CNC), a multiple endocrine neoplasia syndrome (18, 19). Primary pigmented nodular adrenocortical disease (PPNAD), the most frequent endocrine tumor in these patients, is a benign adrenal hyperplasia responsible for ACTH-independent hypercortisolism (Cushing syndrome) (20). We have shown that the adrenal inactivation of *Prkar1a* in developing mice is sufficient to induce ACTH-independent Cushing syndrome and formation of apoptosis-resistant hyperplasia in the inner zF (21, 22). Moreover, by tracing the lineage of *Prkar1a* mutant cells in the adult gland, we have established that PKA signaling is a driving force for sexually dimorphic cortex replenishment and for the conversion of zF into zR identity (13).

SUMOylation has emerged as a critical mechanism for modulating fundamental cellular and developmental processes whose dysregulation can lead to severe diseases. SUMOylation regulates the activity of various proteins involved in DNA replication and repair, chromosome dynamics, genome integrity, nuclear shuttling, cell signaling, and proliferation. Its involvement in tissue morphogenesis (23) has been demonstrated in enterocytes (24), keratinocytes (25), and adipocytes (26, 27). However, it also participates in human malignancy by favoring cancer cell stemness (28, 29). Post-translational modification of target proteins by the covalent addition of small ubiquitin-like modifier (SUMO) 1–3 peptides to specific lysine residues involves an enzymatic cascade requiring the sequential action of the E1 heterodimer SUMO-activating enzyme (SAE) 1/2 for the activation step, the unique E2 enzyme ubiquitin-conjugating enzyme E2 I (UBE2I or UBC9) for the conjugation step, and various E3 ligation enzymes including protein inhibitor of activated signal transducer and activator of transcription-1 (PIAS) 1–4, Ran GTPase binding protein 2, structural maintenance of chromosome 5–6 complex SUMO ligase, and chromobox 4 proteins that increases efficiency of the conjugation step (30). Preserving the balance between SUMOylated and unSUMOylated proteins is a critical point for maintaining cellular physiology. Therefore, the dynamics and reversibility of the reaction are ensured by SUMO/sentrin specific peptidase (SENP) 1–7 and deSUMOylating isopeptidase 1 (DESI1) proteases that cleave and recycle SUMO peptides from their substrates (31, 32).

One of the major roles of SUMOylation cycles is the control of transcription processes through the individual modification of *trans*-acting factors and chromatin remodeling (33–35). The properties of the transcription factors Wilms tumor protein 1, nuclear receptor related-1 protein (also known as NR4A2), and steroidogenic factor-1 (SF-1, also known as NR5A1) that are essential for development and function of adrenal cortex are also regulated by SUMOylation (36–40). However, physiologic evidence of the impact of SUMOylation on adrenal cortex function remains scarce but was elegantly brought into light by a knock-in experiment from Lee *et al*. (41). Indeed, the complete lack of SUMO-conjugated SF-1 in these mice was shown to affect adrenal cortex homeostasis, disturbing cell identities and resulting in mild endocrine hypofunction. This highlighted the importance of SF-1 SUMOylation in fine-tuning the genetic programs of endocrine differentiation, but many other potential SUMO targets should influence adrenal function. As a first step in understanding this vast question, it requires a better knowledge of the overall SUMOylation patterns in the adrenal gland and the exploration of their sensitivity to hormonal regulation. Interestingly, increased cAMP levels were shown to influence the expression of members of the SUMO pathway in ovarian granulosa cells (42).

Here, we hypothesized that SUMOylation, cortex architecture, and hormonal regulation of adrenocortical function should be coordinated. To test this hypothesis, we analyzed the influence of ACTH/PKA signaling on the SUMOylation process in cell culture, wild-type (WT) mice, genetic mouse models of adrenal diseases, and in human PPNAD tissues. This enabled us to propose that cell signalings critical for adrenal cortex homeostasis and stress response tightly coordinate the SUMOylation pathway, which in turn is found altered in cortical diseases.

MATERIALS AND METHODS

Adrenocortical cell cultures

Adrenocortical tumor cell line 1 (ATC1) cells were established from an adrenal tumor derived from a mouse expressing the Simian Virus 40 large T (SV40 T) antigen under the control of the aldo-keto reductase 1b7 (*Akr1b7*) gene promoter specific to the adrenal cortex (43, 44). The primary cultures were obtained from adrenals of 3-wk-old female mice following the protocol previously described (45). The cells were cultured on poly-D-lysine–coated dishes (MilliporeSigma, Burlington, MA, USA) in a DMEM-F12 medium (Thermo Fisher Scientific, Waltham, MA, USA) at 37°C in the presence of 5% CO_2, insulin (10 μg/ml), transferrin (5.5 μg/ml), selenium (6.7 ng/ml) (Thermo Fisher Scientific), L-glutamine (2 mM), penicillin 0.1 U/ml), streptomycin (0.1 μg/ml), 2.5% horse serum, and 2.5% fetal calf serum (43). For PKA induction experiments, cells were seeded in 6-well plates at a density of 2.10^5 cells per well, cultured to subconfluence, and then weaned 12 h (serum-free medium) prior to the addition of forskolin, ACTH, cycloheximide, and actinomycin at the times and concentrations indicated in the legends of the figures.

Animals and treatments

Two-month-old CD-1 mice received an intraperitoneal injection of immediate ACTH (0.05 mg/30 g, Synacthene 0.25 mg/ml; Novartis, Basel, Switzerland) 2 or 4 h before adrenal sampling. Others received an i.m. injection of long-acting ACTH (12 μg/30 g, Synacthene Retard 1 mg/ml; Novartis), and the adrenals were dissected 6 or 24 h later. For the 24 h point, the mice received a second injection 12 h before sampling. Immediate ACTH, with a short half-life, allows the observation of the early effects of stimulation. The delayed ACTH is stabilized because, complexed with zinc salts, the diffusion is slowed, which allows the observation of long-term effects. Alternatively, 6-mo-old females were injected s.c. with dexamethasone 21-acetate for 5 d in order to deplete endogenous ACTH production (75 μg twice daily in corn oil) and were injected with immediate ACTH for 2 or 6 h. The female *Sf-1-Cre::Prkar1a*$^{fl/fl}$ and ΔCat [*Akr1b7-Cre::Catnb*$^{lox(ex3)}$] mice used (where Cre is cyclization recombinase, fl or lox is loxP site, ex3 is exon3 of *Ctnnb1* gene encoding beta-catenin, Catnblox(ex3) is the exon3 floxed allele of *Ctnnb1* gene and deltaCat is the name of the transgenic mouse line expressing exon3-deleted form of *Ctnnb1* gene) were 2.5- and 18-mo-old, respectively (11, 14). The mice were euthanized by decapitation, and the adrenals were immediately frozen in liquid nitrogen.

Protein extraction and Western blot

Cell and tissue samples were lysed in RIPA buffer (50 mM Tris-HCl, pH 7.4, 1% Nonidet P-40, 0.25% Na-deoxycholate, 150 mM NaCl, 1 mM EDTA) supplemented extemporaneously with phosphatase inhibitors (1 mM Na_3VO_4, 0.5 mM NaF), protease inhibitors (Roche, Basel, Switzerland), and SUMO inhibitor proteases N-ethylmaleimide (MilliporeSigma) (3.13 mg/ml). The cell debris was removed by centrifugation at 13,000 rpm for 15 min at 4°C. The protein concentration was determined by the Bradford method (Bio-Rad, Hercules, CA, USA), and 50 μg of proteins was denatured for 5 min at 95°C in Læmmli (50 mM Tris, 100 mM DTT, 2% SDS, 0.1% bromophenol blue, 12% glycerol). The proteins were then separated on a 7% SDS-PAGE or precast gels 4–15% (Bio-Rad) (Supplemental Fig. 3*D*) and transferred to a nitrocellulose membrane (Hybond ECL; Amersham Biosciences, Little Chalfont, United Kingdom) overnight at 4°C at 50 V followed by 1 h at 120 V. Nonspecific protein binding sites were saturated for 1 h at room temperature by incubation in Tris-buffered saline and Tween 20 [50 mM Tris-HCl (pH 8), 150 mM NaCl, and 0.1% Tween 20] containing 5% Regilait. Incubation with the appropriate primary antibody (Supplemental Table 1*A*) was carried out in the same buffer overnight at 4°C with gentle stirring. After rinsing in Tris-buffered saline and Tween 20, the membranes were incubated for 1 h at room temperature with the appropriate secondary antibody conjugated with peroxidase. The specific complexes were revealed by chemiluminescence (ECL) system (Amersham Biosciences). The fluorescence signals were quantified using the MultiGauge v.3.2 software (Fujifilm, Tokyo, Japan).

Quantitative RT-PCR analyses

The cell samples were lysed in Trizol (Thermo Fisher Scientific), and the total RNAs were extracted according to the manufacturer's recommendations. Tissue samples were ground in RNA II lysis buffer (Thermo Fisher Scientific), and total RNAs were extracted using the NucleoSpin RNA II kit as recommended by the manufacturer. Five hundred nanograms of mRNA were reverse-transcribed for 1 h at 37°C with 5 pmol (reverse transcriptase), 2.5 mM deoxynucleoside triphosphate, and 20 U of RNAse inhibitors (recombinant RNAsin, N2615; Promega, Madison, WI, USA) in a final volume of 25 μl. The cDNAs obtained were used (at one-fourth dilution) as template for quantitative RT-PCR (qRT-PCR) analysis using the qPCR Sybr (TAKRR820W; Takara Bio, Kyoto, Japan) premix under standard conditions (40 cycles at 95°C for 15 s, 60°C for 15 s, and 72°C for 20 s). The relative accumulation of mRNAs was determined from the average of duplicates by the $\Delta\Delta C_t$ method (46) using the actin household gene. The primers are listed in Supplemental Table 1*B*.

Immunohistochemistry

After collection, the adrenals were fixed in 4% paraformaldehyde for 24 h, dehydrated in an increasing gradient of ethanol, and then placed in Histoclear (HS200; National Diagnostics, Atlanta, GA, USA) for 2 h before being included in paraffin. Five-micrometer-thick sections were made using a microtome (HM 340E; Thermo Fisher Scientific). The tissue sections were then dewaxed by passing through the Histoclear and progressively rehydrated in an increasing gradient of ethanol. Immunohistological analyses were performed according to the conditions described in Supplemental Table 1C. The tissues were photographed using an Axioplan2 imaging microscope (Carl Zeiss, Oberkochen, Germany). In order to evaluate the presence of non-SUMOylated nuclei, a counterstaining with hematoxylin was performed on the same sections previously used for SUMO1 immunohistochemistry. Quantification of SUMO signals were performed using Zen Software (Carl Zeiss).

Patients

Adrenal tissue analysis and genetic diagnosis was obtained from patients after signed consent. The study was approved by an institutional review committee (Advisory Committee for the Protection of Persons in Biomedical Research, Cochin Hospital, Paris, France). PPNAD paraffin sections were performed from adrenal samples of patients with PPNAD who underwent bilateral adrenalectomy for ACTH-independent Cushing syndrome. Most patients were carriers of *PRKAR1A* inactivating germinal mutations.

Statistical analysis

Statistical analyses were performed using a Student's *t* test or Mann-Whitney test depending on Gaussian values distribution to compare 2 groups. For multiple comparisons, 1-way ANOVA (Gaussian values distribution) test or Kruskal-Wallis (non-Gaussian values distribution) test followed by Dunett's, Dunn's, or Tukey's *post hoc* tests were performed. A value of $P \leq 0.05$ was considered statistically significant ($^*P \leq 0.05$, $^{**}P \leq 0.01$, $^{***}P \leq 0.001$, $^{****}P \leq 0.0001$).

Study approval

All animal work was conducted according to French and European directives for the use and care of animals for research purposes and was approved by the local ethics committee, C2E2A (Comité d'Ethique pour l'Expérimentation Animale en Auvergne).

RESULTS

SUMO conjugation is repressed by ACTH/PKA signaling in adrenocortical cells *in vitro*

To evaluate the role of PKA signaling on adrenocortical protein SUMOylation, we analyzed the effects of forskolin,

an adenylate cyclase activator, on the formation of SUMO conjugates in lysates of ATC1 mouse adrenocortical cells (43). Immunoblotting with either anti-SUMO1 (**Fig. 1*A***) or anti-SUMO2/3 (Fig. 1*B*) showed that SUMOylated proteins in cell extracts were represented by a smear of bands of high molecular mass whose intensity decreased with forskolin, reaching a nadir after 6–12 h of treatment. Quantification of the Western blots showed that steady-state levels of Sumo1- and Sumo2/3-conjugated proteins were reduced by 54 and 40%, respectively, after 6 h of forskolin treatment.

To explore the mechanism leading to PKA-mediated inhibition of protein SUMOylation, the hormonal responsiveness of genes encoding SUMO modules and enzymes of the SUMO conjugation-deconjugation pathway (Fig. 1*C*) was assessed by qRT-PCR in an ATC1 cell line and primary adrenocortical cells (Fig. 1*D*). In both cell types, strong induction of *Akr1b7* mRNA levels, a well-characterized ACTH/PKA-responsive gene (43), validated treatments at all time points, including the expected more robust effect of forskolin compared with ACTH, the physiologic inducer (Supplemental Fig. S1*A*). In both cell culture systems, PKA stimulation down-regulated mRNA accumulation of *Sumo1*, *Sae1*, *Pias3*, and to a lesser extent, *Ube2i*, with a maximal effect occurring between 6 and 12 h (Fig. 1*D*). Conversely, these treatments induced a 200% increase in *Senp2* mRNA expression that culminated between 2 and 6 h. This positive PKA responsiveness was also observed at protein levels (Fig. 1*E*), suggesting that *Senp2* gene regulation by ACTH/PKA was mainly transcriptional, as confirmed by the sensitivity to actinomycin D and resistance to cycloheximide (Supplemental Fig. S1*B*). Mechanisms of PKA-dependent repression of genes involved in SUMO conjugation (*Sumo1*, *Ube2i*, *Sae1*, and *Pias3*) were less clear but presumably required *de novo* expression of a labile repressor as suggested by *Pias3* mRNA sensitivity to both actinomycin D and cycloheximide (Supplemental Fig. S1*B*). Interestingly, although *Ube2i* transcript levels were still elevated 6 h postinduction in ATC1 cells, protein levels declined between 2 and 6 h (Fig. 1*E*). Therefore, this further suggests that PKA-dependent repression might also be achieved by post-translational mechanisms. The responsiveness of the other effectors of SUMOylation appeared either unaffected by PKA stimulation or not reproduced under ACTH treatment (Supplemental Fig. S1*C*). Taken together, these results indicate that the PKA-induced overall decrease of SUMO-conjugated protein substrates in adrenocortical cells could be the consequence of 2 coordinated and convergent mechanisms: increased gene transcription of deSUMOylating enzyme (here, *Senp2*) and repression of genes encoding SUMOylating proteins including SUMO peptides.

Acute and chronic effects of ACTH/PKA repress SUMOylation in mouse adrenal glands

To evaluate *in vivo* the hormonal responsiveness of genes of the SUMOconjugation or -deconjugation pathways, WT young adult mice were injected with rapid- or long-acting forms of ACTH and sacrificed after 2–4 or 6–24 h, respectively. qRT-PCR analyses in the adrenal cortex showed that activation of PKA signaling repressed mRNA levels of *Sumo1*, *Sumo2*, and *Sumo3* by 50, 25, and 30% after 4 h of treatment, respectively (Fig. 2*A, B*). Extended ACTH treatments showed that this decline was transient and could be maintained over 6 h. However, expression reincreased at 24 h (Supplemental Fig. S2*A*). A similar repression pattern was observed for *Pias3* mRNA levels that reached a nadir after 2–4 h of treatment (75% drop) and reincreased at 24 h (Fig. 2*B* and Supplemental Fig. S2*A*). In contrast, transcript levels for the SUMO protease *Senp2* were increased by 200% after 2 h, returning to pretreatment values after 4 h (Fig. 2*B*). Remarkably, mRNA levels for SUMO protease Desi1 remained stable for the first 6 h of treatment and were increased more than 150% after 24 h (Fig. 2*B* and Supplemental Fig. S2*A*). Regardless of the treatment duration, the expression of *Ube2i* transcripts was unaltered (Fig. 2*B* and Supplemental Fig. S2*A*). We next investigated the effect of chronic activation of PKA signaling on genes ensuring SUMO conjugation/deconjugation dynamics. For this, we used *Sf1-Cre::Prkar1a*$^{fl/fl}$ mice with adrenal-specific deletion of PKA regulatory R1α subunit (14). qRT-PCR analysis revealed a 38% reduction of *Pias3* expression compared with WT levels, whereas *Senp2* and *Desi1* expression was induced by 150 and 200%, respectively. *Senp3* and *Senp5* mRNA levels also showed a modest but significant increase (Fig. 2*C*). Interestingly, under these chronic stimulation conditions, there was no down-regulation of *Sumo* genes, and expression levels of all other conjugating/deconjugating genes were unaltered or only slightly increased (Supplemental Fig. S2*B*). In agreement with the repression of *Pias3* and simultaneous stimulation of genes for deSUMOylating isopeptidases, Western blot analysis of adrenal lysates showed that Sumo2/3 conjugation levels in mutant mice were ~30% of WT (Fig. 2*D*).

Taken together, these data suggest that ACTH stimulation *in vivo* limits the SUMOylation process in the adrenal gland through both acute (≤4 h) and chronic (≥24 h) transcriptional effects. These lead to the simultaneous and opposite regulation of a subset of PKA-responsive genes of the SUMOylation pathway, with repression of actors of the conjugation process (*Sumo1–3* and *Pias3*) and stimulation of deconjugation enzymes (*Senp2*, *Senp3*, *Senp5*, and *Desi1*).

Regionalization of SUMOylation in the adrenal cortex is dependent on ACTH/PKA signaling

In the adrenal cortex, ACTH/PKA signaling is required for differentiation, maintenance, and function of the zF (12, 13). Active SUMOylation processes can be assessed in tissue sections by monitoring changes in the intensity of nuclear SUMO signal (47, 48). Immunohistochemical staining of mouse adrenal samples revealed a cortical gradient of Sumo1 and Sumo2/3 staining in steroidogenic cells, with high nuclear signal in the peripheral subcapsular/glomerulosa region, intermediate signal at the glomerulosa-fasciculata junction, and low labeling in

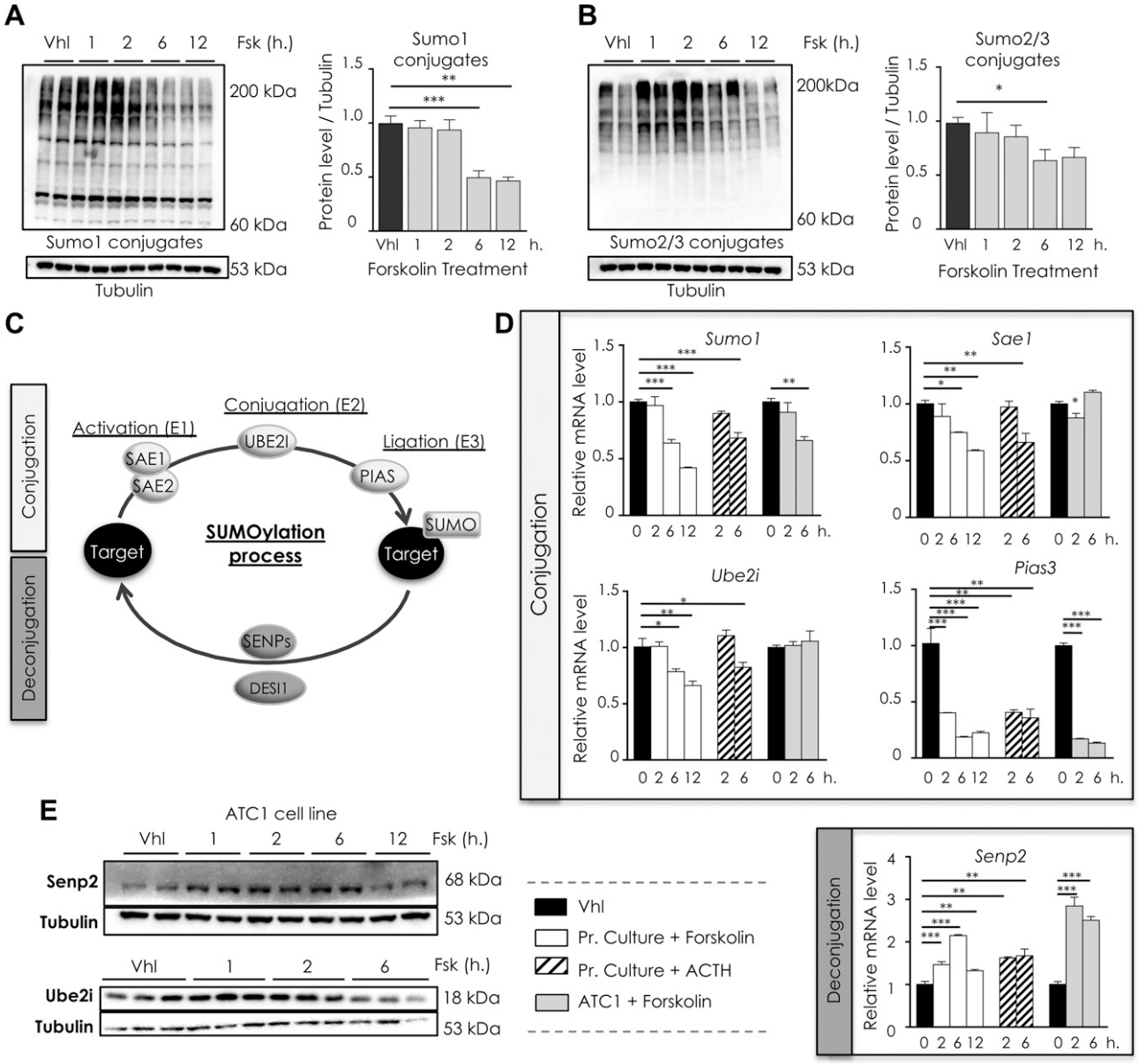

Figure 1. Activation of PKA signaling decreases global SUMOylation in adrenocortical cell cultures. *A*, *B*) Time course effects of PKA activation on the accumulation of adrenocortical proteins conjugated to Sumo1 (*A*) and Sumo2/3 (*B*). Murine adrenocortical ATC1 cell line was treated with forskolin (10^{-5} M) for the indicated time (h) or with vehicle (Veh) (DMSO) for the longest treatment time. The accumulation of Sumo1 and Sumo2/3 conjugates was analyzed by Western blot (representative figure) and quantified (histograms). Tubulin signal was used to normalize the quantification of SUMO signals. *C*) Schematic representation of the SUMOylation cycle. Sumo1, Sumo2, and Sumo3 peptides are conjugated to their substrate proteins by an enzymatic process involving E1, E2, and E3 enzymes. The dynamism of the SUMOylation is ensured by the proteases Senp and Desi1, which allow the removal of the SUMO peptide from the targeted protein. *D*) Time course effects of PKA activation on the mRNA expression of SUMOylation pathway genes. Primary cultured cells from mouse adrenal cortex and ATC1 cell line were treated with forskolin (10^{-5} M) for the indicated time or with DMSO (Vhl) for the longest treatment time. Primary cultures were also treated with ACTH (10^{-9} M). qRT-PCR analyses were normalized with respect to actin gene expression. *E*) PKA responsiveness of Senp2 and Ube2i protein levels. ATC1 cells were treated with forskolin (10^{-5} M) for the indicated time (h) or with DMSO (Vhl) for the longest treatment time. Protein accumulation of Senp2 and Ube2i was analyzed by Western blot. Tubulin signal serves as loading control. Fsk, forskolin; Pr. Culture, primary culture. Quantification histograms represent means ± SEM from 3 to 4 experiments. Statistical analyses were conducted by 1-way ANOVA followed by Dunett's test. $^{*}P < 0.05$, $^{**}P < 0.01$, $^{***}P < 0.005$.

fasciculata cells (**Fig. 3*A, B*** and Supplemental Fig. S3*A*). Sumo1 and Sumo2/3 staining pattern was similar in both sexes, although the decreased SUMOylation levels between zG to zF appeared more pronounced in females (Supplemental Fig. S3*B*). Interestingly, SUMO labeling was not restricted to steroidogenic cells. Indeed, capsular as well as endothelial cell nuclei were strongly positive for Sumo2/3, whereas Sumo1 staining was much less pronounced in these cell populations (Fig. 3*A, B* and Supplemental Fig. S3*B*).

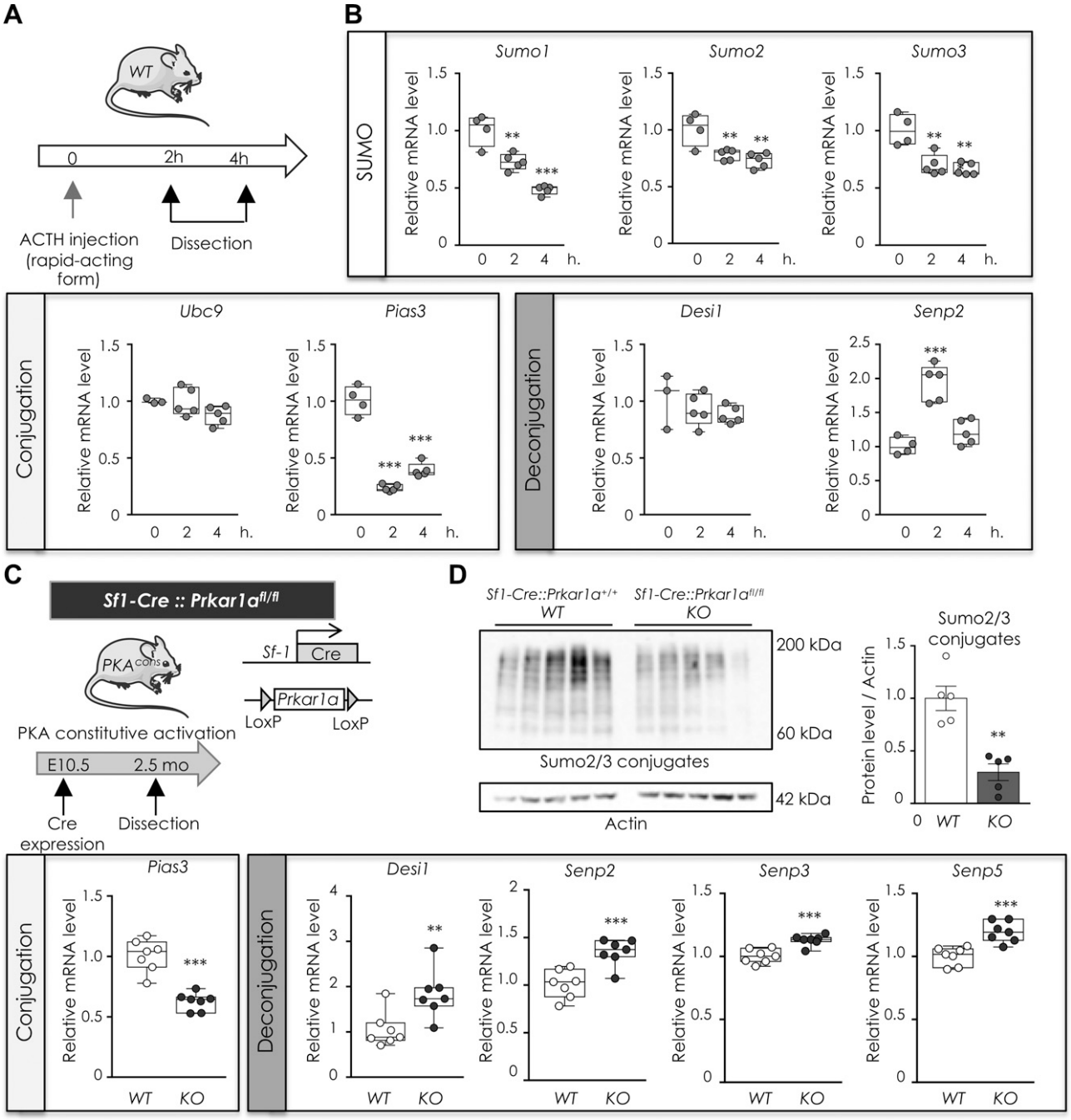

Figure 2. Acute hormonal induction or constitutive activation of PKA signaling affects protein SUMOylation and SUMO pathway gene expression in mouse adrenals. *A*, *B*) WT mice were injected with immediate ACTH, and adrenals were removed 2 or 4 h later; control adrenals were dissected from untreated mice (0 h) and subjected to RNA extraction: experimental setup (*A*); qRT-PCR analyses (*B*) of SUMOylation pathway gene expression normalized with respect to actin gene expression. Statistical analyses were conducted by 1-way ANOVA followed by Dunett's test. *C*) CNC mouse model with constitutive activation of PKA following adrenal inactivation of *Prkar1a* (*Sf-1-Cre::Prkar1a*$^{fl/fl}$ mice): experimental setup. Adrenals from *Sf-1-Cre::Prkar1a*$^{+/+}$ (*WT*) and *Sf-1-Cre::Prkar1a*$^{fl/fl}$ [*knock-out* (*KO*)] mice were removed and subjected to RNA and protein extraction. qRT-PCR analyses of SUMOylation pathway gene expression normalized with respect to actin gene expression; *D*) Western blot analyses of Sumo2/3 conjugates in adrenal protein extracts and quantification (histogram). Tubulin signal was used to normalize the quantification of SUMO signals. Statistical analyses were conducted by Student's *t* test. Quantification histograms represent means ± SEM. $^{*}P < 0.05$, $^{**}P < 0.01$, $^{***}P < 0.001$.

In order to evaluate the consequences of changes in the hypothalamic-pituitary-adrenal (HPA) axis on SUMO staining profile, mice were either treated for 5 d with dexamethasone to block endogenous ACTH secretion or supplemented with (rapid-acting) ACTH injection on the last day (Fig. 3C). Compared with basal conditions, HPA axis blockade had no significant effect on either Sumo1 or Sumo2/3 nuclear staining patterns. In contrast, ACTH supplementation resulted in a transient decrease in SUMO nuclear labeling that affected all cortical zones after 2 h and

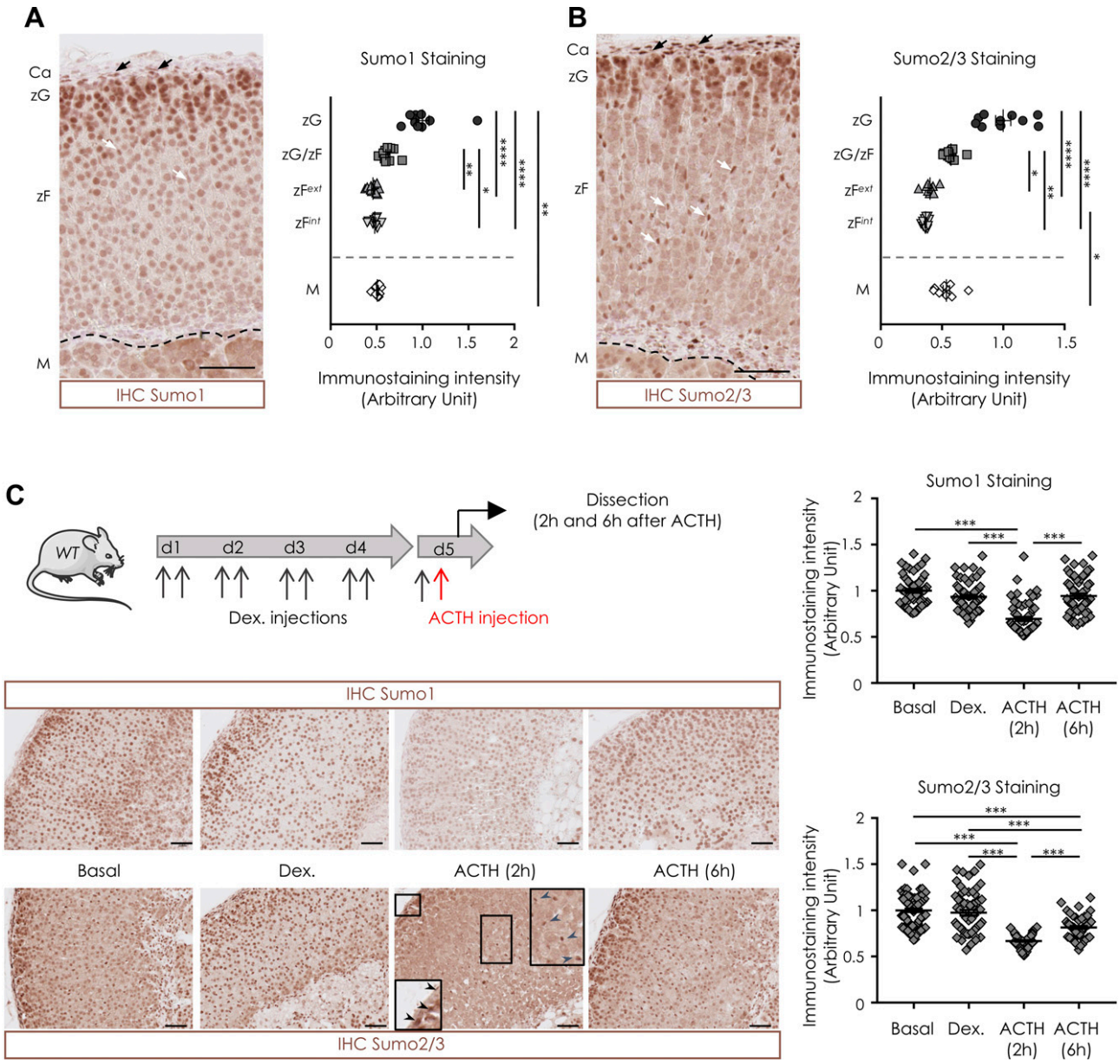

Figure 3. SUMOylation is regionalized in mouse adrenal cortex and modulated by ACTH/PKA signaling. *A*, *B*) SUMOylation profile forms a decreasing gradient of intensity from the outer to the inner cortex. The accumulation of conjugated proteins to Sumo1 (*A*) and Sumo2/3 (*B*) was analyzed by immunohistochemistry (IHC) in adrenals of 6-mo-old female mice. The quantification graphs represent means ± SEM of SUMO nuclear staining intensity in each histologic zone and interzone all along the cortex and in medulla for 3 adrenals from 3 different animals and 50–60 nuclei per adrenal. Black and white arrows: nuclear Sumo staining in capsular and endothelial cells, respectively. Statistical analyses were conducted by Kruskal-Wallis followed by Dunn's test. Ca, capsule; M, medulla; zF^{ext}, external zF; zF^{init}, internal zF. *C*) Stimulation of the corticotropic axis changes the cortical SUMOylation profile. Six-month-old female mice were treated with dexamethasone (Dex.) for 5 d, injected or not the last morning with ACTH, and euthanized 2 or 6 h later. Basal conditions correspond to untreated mice. The accumulation of conjugated nuclear proteins to Sumo1 and Sumo2/3 was analyzed by IHC. The quantification graphs represent means ± SEM of SUMO nuclear staining intensity in zF cells for 6 adrenals from 6 different animals and 10 nuclei per adrenal. Insets, black and gray arrows: nuclear Sumo staining in capsular and endothelial cells, respectively. Statistical analyses were conducted by 1-way ANOVA followed by Tukey's *post hoc* test. Scale bars, 50 μm. $*P < 0.05$, $**P < 0.01$, $***P < 0.001$, $****P < 0.0001$.

almost returned to pretreatment labeling after 6 h. Interestingly, the negative effect of ACTH was restricted to steroidogenic cells because nuclear Sumo2/3 staining intensity was unaltered in capsular or endothelial cells. In agreement with histologic data, Western blotting analysis of the corresponding adrenal extracts showed a parallel change of Sumo2/3 and Sumo1 conjugate levels (Supplemental Fig. S3*D*). General staining pattern for SUMO was also assessed in adrenal sections from *Sf-1-Cre::Prkar1a*$^{fl/fl}$ mice. This showed that chronic stimulation of PKA signaling in the cortex resulted in the relative loss of centripetal gradient of nuclear Sumo1 labeling typical of WT cortex (Supplemental Fig. S3*C*). Altogether, these results indicate that there is a centripetally decreasing

gradient of SUMOylation throughout adrenal cortical zones that relies on the activity of ACTH/PKA signaling, which maintains relative hypoSUMOylation context in steroidogenic cells of the zF.

Differential SUMOylation pattern of adrenal cortex is conserved in human adrenal and is altered in primary pigmented nodular adrenal hyperplasia (PPNAD) from CNC patients

To assess whether our observations were transferable to humans, we analyzed by immunohistochemistry the SUMOylation pattern of adrenal samples from either healthy patients or from hypercortisolic patients suffering from pathologic activation of PKA due to CNC. The SUMO1 and SUMO2/3 immunolabeling performed on normal human adrenal sections revealed a centripetally decreasing gradient of steroidogenic cell nuclear staining intensity similar to that found in mice (**Fig. 4*A***) and Supplemental Fig. S4*A*). Accordingly, nuclear staining intensity was maximal in cells of the outer cortex (zG and zG/zF transition zone) and weaker in the zF and zR. Interestingly, SUMO1 immunolabeling of adrenal samples from patients with CNC ($n = 3 + 3$) revealed obvious hypoSUMOylation of cells forming the hyperplastic nodules (as evidenced by hematoxylin counterstaining). This contrasted with the intense SUMO1 nuclear staining found in adjacent internodular tissue (Fig. 4*B* and Supplemental Fig. S4*B*). Reciprocally, the signal for SUMO protease SENP1 was more pronounced within nodules (Fig. 4*C* and Supplemental Fig. S4*C*). Altogether, these data suggest that the SUMOylation potential was inhibited in a context of constitutive PKA activity that is expected to occur through R1α loss within PPNAD nodules (*PRKAR1A* loss of heterozygosity) and was maintained or even increased in a context of blunted PKA activity, as found in the atrophic internodular fasciculata tissue [due to repressed ACTH levels (49)]. We conclude that, as suggested by mouse studies, SUMOylation follows a centripetally decreasing gradient in human adrenal cortex that seems to negatively correlate with activation of PKA signaling in normal gland (zF) and in adrenal nodules from patients suffering from CNC.

WNT/β-catenin signaling favors SUMOylation in the adrenal cortex

We have previously established that WNT and PKA signaling pathways exert complementary and antagonistic actions to maintain adrenal cortex zonation: WNT signaling is essential for zG identity, whereas PKA signaling drives identity of the inner cortex (zF and zR) (13, 14). Therefore, we hypothesized that relative hyperSUMOylation of the outer cortex could rely on WNT/β-catenin signaling. To evaluate this hypothesis, we analyzed changes in SUMO and β-catenin immunofluorescent staining in adrenal sections of ΔCat mice that present stochastic constitutive activation of β-catenin (encoded by *Ctnnb1* gene) due to *Ctnnb1* exon 3 excision (*Akr1b7-Cre::Catnb*$^{fl(ex3)}$) (11) (**Fig. 5*A***). As previously described, constitutive activation of WNT signaling resulted in expansion of the nucleo-cytoplasmic staining of β-catenin beyond zG and throughout the cortex. This resulted in the formation of large hyperplastic cells clusters (Fig. 5*B*) in which β-catenin staining intensity was massively increased compared with the adjacent nonrecombined tissue (Supplemental Fig. S5*A*). Coimmunofluorescent detection of either Sumo1 or Sumo2/3 revealed that hyperplastic clusters (β-catenin positive) and areas with highest Sumo nuclear labeling overlap. This was confirmed by quantifying Sumo nuclear signals in hyperplastic area (β-catenin high) and intact adjacent cortex (β-catenin low). This showed that increased SUMOylation correlated with β-catenin activation (Fig. 5*C*, *D*). We assessed possible concurrent changes in SUMO pathway gene expression in ΔCat adrenal glands using qRT-PCR. As illustrated in Fig. 5*E*, mRNA levels for genes involved in SUMO conjugation (*Sumo2*, *Sumo3*, *Pias1*, and *Pias2*) were induced, whereas mRNA expression of SUMO protease *Desi1* was reduced by 50% in adrenals from ΔCat mice. With the exception of genes for SUMO protease *Senp1* and *Senp6*, which were upregulated, expression of all other tested genes was unaltered in ΔCat adrenals (Supplemental Fig. S5*B*). We conclude that WNT/β-catenin signaling pathway activation favors SUMOylation *in vivo* and can participate in establishing the centripetally decreasing gradient of SUMOylation in the adrenal cortex by maintaining high SUMOylation potential in the outer cortex.

DISCUSSION

The results presented here show that there is a negative correlation between the activation of PKA signaling (genetically or hormonally induced) and the SUMOylation of adrenocortical proteins in cell culture and *in vivo*. This PKA-dependent hypoSUMOylation relies on the coordinated transcriptional stimulation of deSUMOylating isopeptidase genes (Senp2, Desi1, SENP1) and repression of genes encoding SUMO peptides and SUMO (Pias3) ligase. In agreement with this inhibitory effect, we show that in both human and mouse adrenal cortices, the SUMOylation pattern appears as a centripetally decreasing gradient. This is inversely correlated with PKA sensitivity of the cells, as emphasized by strong nuclear staining in zG and weaker staining in zF/zR. Activation of PKA signaling by ACTH injections leads to a transient decrease in SUMOylation in zF, which suggests a possible active role of this post-translational modification in zonation and/or stress response. Conversely, this gradient seems less sensitive to ACTH suppression, as dexamethasone treatment leads to a slight though nonsignificantly increased SUMOylation (Supplemental Fig. S3*D*). Moreover, the hypoSUMOylating effect of PKA signaling could participate in the etiology of PPNAD. Indeed, we show that global SUMOylation is reduced in the nodules of patients with PPNAD as well as in the adrenals of a mouse model of PPNAD (*Sf-1-Cre::Prkar1a*$^{fl/fl}$).

In adrenocortical cells, kinetics of SUMO pathway gene expression in response to PKA stimulation are similar to that of steroidogenic genes (43). This observation suggests

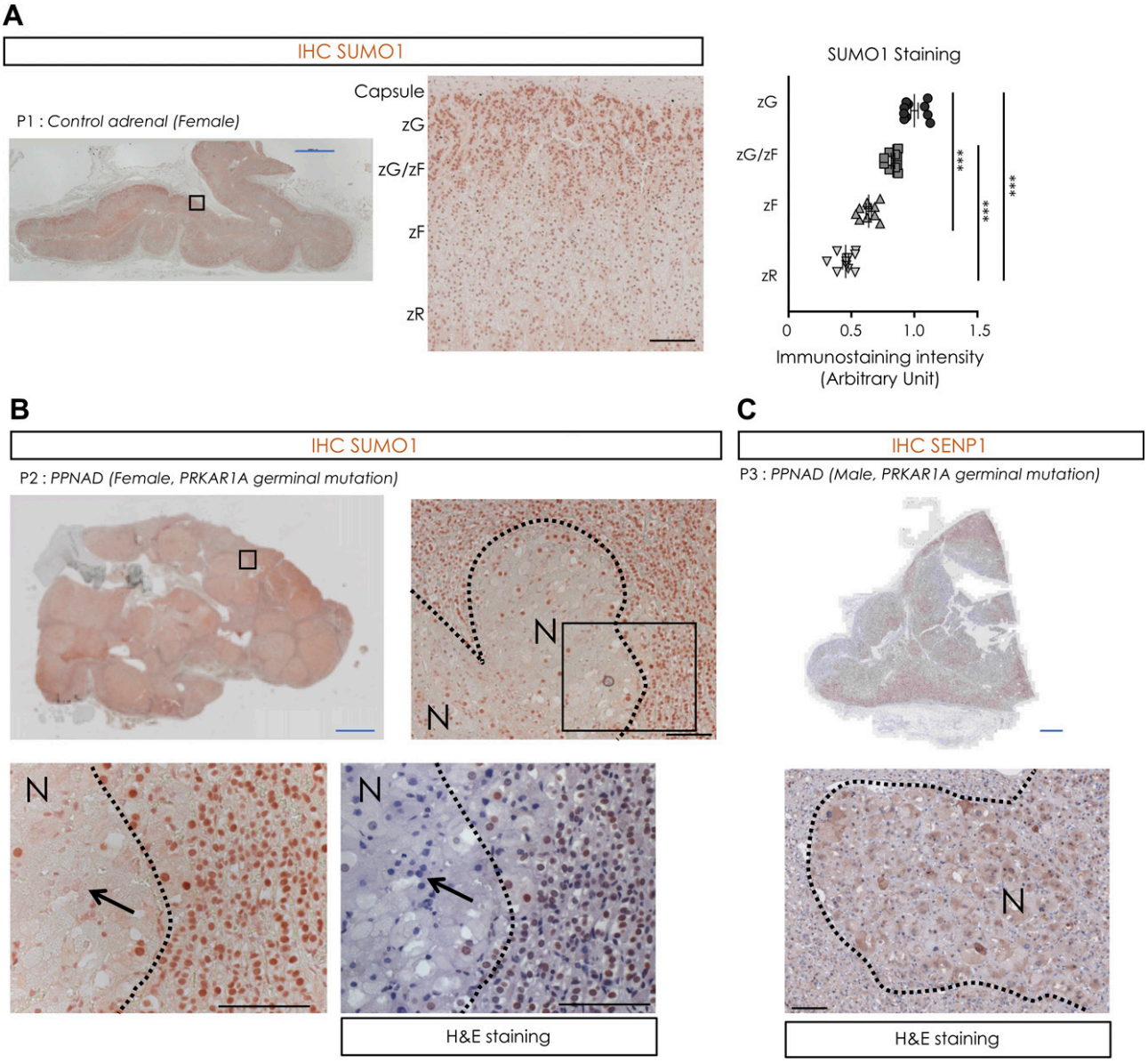

Figure 4. SUMOylation is regionalized in human adrenal cortex and altered in nodular hyperplasia from patients with CNC. *A*) SUMOylation profile forms a decreasing gradient of intensity from the outer to the inner cortex. The accumulation of conjugated proteins to SUMO1 was analyzed by immunohistochemistry in a control human adrenal. The quantification graph represents means ± SEM of SUMO1 nuclear staining intensity in steroidogenic cells in each histologic zone and interzone all along the cortex. Statistical analyses were conducted by 1-way ANOVA followed by Dunett's test. ***$P < 0.001$. *B*, *C*) HypoSUMOylation of PPNAD nodules. PPNAD sections from patients with *PRKAR1A* germinal mutation were immunostained for SUMO1 (*B*) or for SENP1 (*C*) and counterstained with hematoxylin (H&E). HypoSUMOylated nuclei (black arrow). N, nodule. Blue scale bars, 2 cm; black scale bars, 100 μm.

that the SUMOylation process may be subordinated to the same regulatory mechanisms as steroidogenesis. Although PKA-mediated transcriptional activation is well documented, data on mechanisms relaying its repressive effects are scarce, even though they are quite prominent. Indeed, our transcriptome analyses of mice with adrenal *Prkar1a* gene inactivation with various Cre drivers (13, 14) showed similar numbers of down- and up-regulated genes following constitutive PKA activation. The only negative molecular mechanism identified to date in the adrenal gland mobilizes the oscillating salt-inducible kinase (SIK)–cAMP responsive element binding protein (CREB)-regulated transcription coactivator cascade, in which SIK represses the activity of CREB in a transient PKA-dependent manner (50–52). The participation of SIK–CREB-regulated transcription coactivator in the transcriptional repression of *Sumo1–3* and *Pias3* genes will require further investigation.

In contrast to SUMO-conjugating genes, and in agreement with the overall hypoSUMOylation induced by PKA, expression of deSUMOylases Senp2 and Desi1 is stimulated by activation of PKA signaling in the same way as steroidogenic genes. The induction of *Senp2* mRNA expression by ACTH/PKA might rely on the recruitment of CREB to a functional cAMP responsive element located in the proximal promoter region that was described to

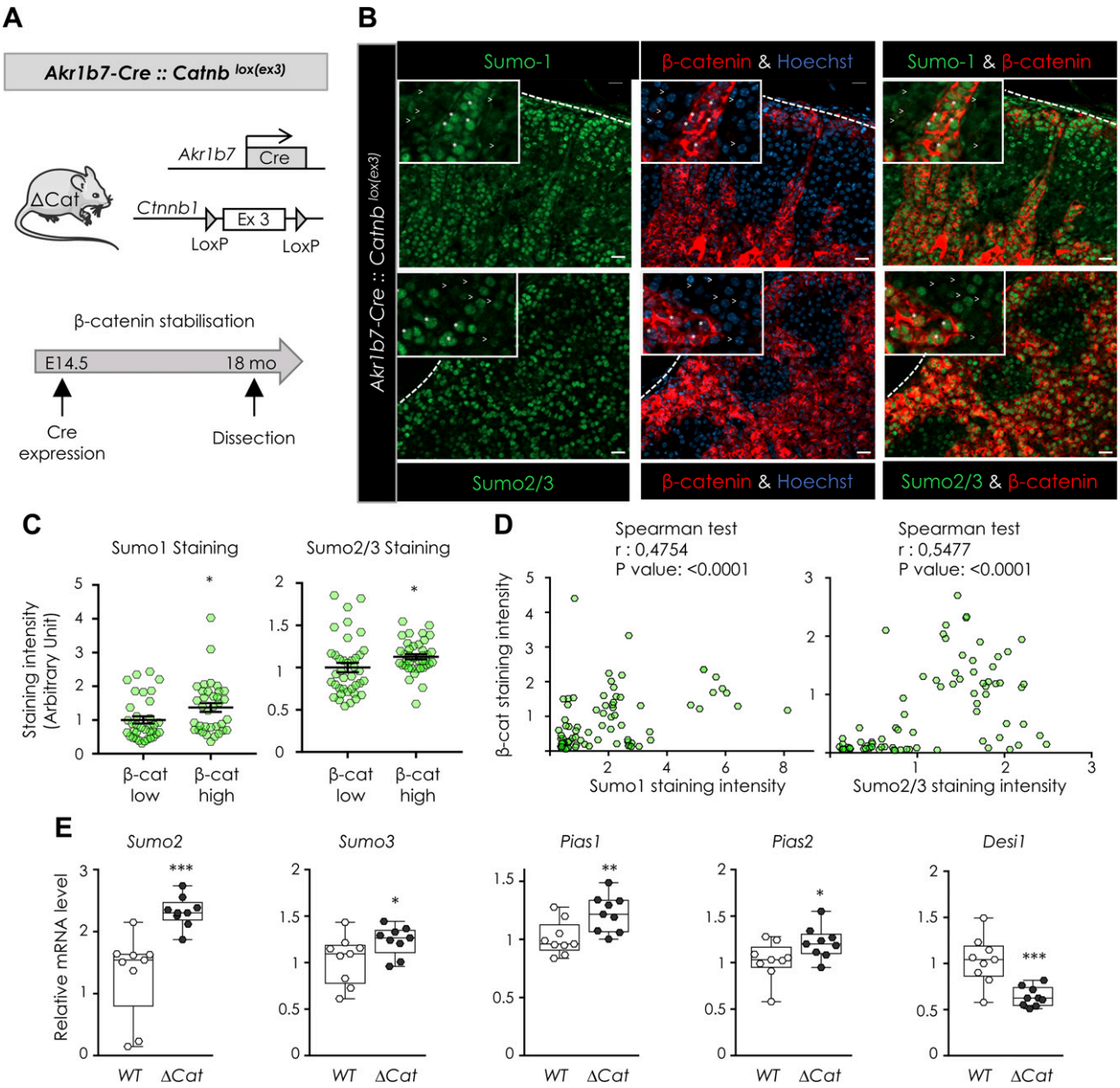

Figure 5. Adrenal cortex SUMOylation is enhanced by constitutive activation of WNT/β-catenin (β-cat) signaling. *A*) Experimental setup. β-cat (endoded by *Ctnnb1* gene) stabilization in adrenal cortex was allowed by deletion of exon 3 of *Ctnnb1 [Catnb*$^{lox(ex3)}$ *allele]* using *Akr1b7-Cre* line (referred to as ΔCat mice). *B*) Coimmunofluorescent labeling of Sumo1 (upper) or Sumo2/3 (bottom) (green), β-cat (red) and merged signals in adrenal sections from ΔCat female mice of 18 mo. *Inset*, magnification view showing nuclei from cells with low (white arrowheads) or high (white asterisk) β-cat staining. Scale bar, 20 μm. *C*) The quantification graphs represent means ± SEM of SUMO nuclear Sumo1 and Sumo2/3 staining intensity in cells that express low or high levels of β-cat (3 adrenals from 3 different animals and 10–15 nuclei per adrenal). *D*) Sumo1 or Sumo2/3 nuclear staining is correlated with β-cat activation. Spearman correlation between staining intensity values of Sumo1 or Sumo2/3 nuclear signal and staining intensity of β-cat nucleo-cytoplasmic signal. *E*) Adrenals from *Akr1b7-Cre::Catnb*$^{+/+}$ *(WT)* and *Akr1b7-Cre::Catnb*$^{lox(ex3)/+}$ (*ΔCat*) mice were removed and subjected to RNA extraction. qRT-PCR analyses of SUMOylation pathway gene expression normalized with respect to actin gene expression. Statistical analyses were conducted by Student's *t* test. Quantification histograms represent means ± SEM. $^{*}P < 0.05$, $^{**}P < 0.01$, $^{***}P < 0.001$.

mediate PKA responsiveness in 3T3L1 preadipocytes (53). No functional data are available for the *Desi1* regulatory regions. However, the kinetics of ACTH responsiveness *in vivo*, with fast up-regulation of *Senp2* transcripts (2 h) and slow up-regulation of *Desi1* (24 h), suggests that mechanisms contributing to their regulation by PKA may differ. In addition, Senp2 and Desi1 proteins are supposed to diverge in their subcellular localization. Indeed, whereas Senp2 is mainly nuclear (54) Desi1 is cytoplasmic (32). This suggests that their target substrates may differ.

The centripetal decreasing gradient of SUMOylation within the adrenal cortex (zG > zF/zR) together with its sensitivity to the HPA axis is suggestive of a role for SUMOylation in the response to stress. Accordingly,

requirement of SUMO pathway for adaptative response to stress seems to have been conserved in evolution (55). Indeed, proteomic analyses have demonstrated the coordinated SUMOylation of protein groups involved in the same biochemical pathway after genotoxic stress in yeast (56). SENP2-dependent deSUMOylation is required to adapt cells to etoposide-induced genotoxic stress, whereas SENP1-mediated deSUMOylation is required to counteract colon tumor growth induced by genotoxic *E. coli* strains (57, 58). In agreement with this concept, the repressor effect of PKA signaling on the SUMOylation process could participate in the transcriptional response of adrenocortical cells following stress. The constitutive hypoSUMOylation in zF could exert a permissive action on the response to stress by lifting the tonic repression exerted by SUMOylation on transcription factors such as SF-1 and nuclear receptor related-1 protein (37, 59). Under stress conditions, ACTH-induced transient hypoSUMOylation would further facilitate steroidogenic response. Furthermore, activation of some phosphodiesterases (PDEs) following their SUMOylation (60) suggests that such an intracellular feedback mechanism would allow the adrenal cortex to sustain elevated intracellular levels of cAMP and promote activation of PKA. The hypoSUMOylation observed in PPNAD nodules suggests the involvement of this modification in the etiology of the disease. These results are consistent with the increasing number of studies involving SUMOylation in tumor mechanisms (61).

Finally, the decreasing gradient of SUMOylation in the adrenal cortex also suggests its possible involvement in the establishment and/or maintenance of cortical zonation. Increased SUMOylation consecutive to depletion of SENP1/2/7 proteins was reported in various models to activate the WNT/β-catenin pathway by increasing β-catenin stability (62, 63) and by promoting its nuclear translocation (64, 65). The ability of SUMOylation to activate the WNT pathway is likely to explain the intense staining observed in zG. Reciprocally, we report here that constitutive β-catenin activation in mouse adrenals not only induces zG tumor formation (11, 66) but also expands the hyperSUMOylation domain. This suggests that a positive feedback loop between SUMO-induced WNT pathway and β-catenin–dependent SUMOylation increase could allow maintaining higher SUMO staining in the zG. Conversely, the hypoSUMOylating effects of PKA signaling activation could participate (*e.g.*, through *Senp2/SENP1* up-regulated expression) in the antagonism between WNT/β-catenin and ACTH/PKA pathways, which is needed to establish proper functional zonation and to counteract β-catenin–induced tumor formation (13, 14).

In summary, our findings reveal that protein SUMOylation follows a conserved centripetally decreasing gradient within the adrenal cortex. This relies on antagonistic actions of ACTH/PKA and WNT/β-catenin signaling pathways: ACTH/PKA signaling acutely reduces SUMOylation in zF by coordinating the expression of both SUMO pathway inducers and repressors, whereas WNT/β-catenin induces hyperSUMOylation. Our data suggest that programming of the SUMOylation pattern could play a role in endocrine function and stress response and maintenance of zonation and pathology (hypersecretion syndromes and cancer). FJ

ACKNOWLEDGMENTS

The authors thank Kaitlin J. Basham (University of Michigan, Ann Arbor, MI, USA) for critical reading of the manuscript. The authors also wish to thank Sandrine Plantade, Philippe Mazuel, and Khirredine Ouchen (all from the Université Clermont-Auvergne, Clermont-Ferrand, France) for care of the transgenic mice. This work was funded through institutional support from Centre national de la Recherche Scientifique, INSERM, Université Clermont-Auvergne, and the French government Initiative d'EXcellence-Initiative Science Innovation Territoires Economie (IDEX-ISITE) initiative 16-IDEX-0001 (CAP 20-25) and supported by grants from Région Auvergne-Rhône-Alpes to T.D., Fondation Association pour la Recherche sur le Cancer to T.D., and Agence Nationale pour la Recherche (ANR-14-CE12-000) to A.M. Human adrenal samples were collected by the French Cortico et Médullosurrénale: les Tumeurs Endocrines (COMETE) network. The authors declare no conflicts of interest.

AUTHOR CONTRIBUTIONS

T. Dumontet, I. Sahut-Barnola, D. Dufour, A.-M. Lefrançois-Martinez, P. Val, and A. Martinez conceived of and designed the experiments; T. Dumontet, I. Sahut-Barnola, D. Dufour, A.-M. Lefrançois-Martinez, A. Berthon, N. Montanier, C. Djari, J.-C. Pointud, and F. Roucher-Boulez performed the experiments; T. Dumontet, I. Sahut-Barnola, D. Dufour, A.-M. Lefrançois-Martinez, and A. Martinez analyzed the data; B. Ragazzon, M. Batisse-Lignier, I. Tauveron, and J. Bertherat provided human samples; A. Martinez supervised the project; T. Dumontet and A. Martinez wrote the manuscript; and P. Val and all authors edited the manuscript.

REFERENCES

1. Vinson, G. P. (2016) Functional zonation of the adult mammalian adrenal cortex. *Front. Neurosci.* **10**, 238
2. Bollag, W. B. (2014) Regulation of aldosterone synthesis and secretion. *Compr. Physiol.* **4**, 1017–1055
3. Gorrigan, R. J., Guasti, L., King, P., Clark, A. J., and Chan, L. F. (2011) Localisation of the melanocortin-2-receptor and its accessory proteins in the developing and adult adrenal gland. *J. Mol. Endocrinol.* **46**, 227–232
4. Auchus, R. J., and Rainey, W. E. (2004) Adrenarche - physiology, biochemistry and human disease. *Clin. Endocrinol. (Oxf.)* **60**, 288–296
5. Yates, R., Katugampola, H., Cavlan, D., Cogger, K., Meimaridou, E., Hughes, C., Metherell, L., Guasti, L., and King, P. (2013) Adrenocortical development, maintenance, and disease. *Curr. Top. Dev. Biol.* **106**, 239–312
6. Morohashi, K., and Zubair, M. (2011) The fetal and adult adrenal cortex. *Mol. Cell. Endocrinol.* **336**, 193–197
7. Zubair, M., Parker, K. L., and Morohashi, K. (2008) Developmental links between the fetal and adult zones of the adrenal cortex revealed by lineage tracing. *Mol. Cell. Biol.* **28**, 7030–7040
8. Freedman, B. D., Kempna, P. B., Carlone, D. L., Shah, M., Guagliardo, N. A., Barrett, P. Q., Gomez-Sanchez, C. E., Majzoub, J. A., and Breault, D. T. (2013) Adrenocortical zonation results from lineage conversion of differentiated *zona glomerulosa* cells. *Dev. Cell* **26**, 666–673
9. King, P., Paul, A., and Laufer, E. (2009) Shh signaling regulates adrenocortical development and identifies progenitors of steroidogenic lineages. *Proc. Natl. Acad. Sci. USA* **106**, 21185–21190

10. Vidal, V., Sacco, S., Rocha, A. S., da Silva, F., Panzolini, C., Dumontet, T., Doan, T. M. P., Shan, J., Rak-Raszewska, A., Bird, T., Vainio, S., Martinez, A., and Schedl, A. (2016) The adrenal capsule is a signaling center controlling cell renewal and zonation through Rspo3. *Genes Dev.* **30**, 1389–1394
11. Berthon, A., Sahut-Barnola, I., Lambert-Langlais, S., de Joussineau, C., Damon-Soubeyrand, C., Louiset, E., Taketo, M. M., Tissier, F., Bertherat, J., Lefrançois-Martinez, A. M., Martinez, A., and Val, P. (2010) Constitutive beta-catenin activation induces adrenal hyperplasia and promotes adrenal cancer development. *Hum. Mol. Genet.* **19**, 1561–1576
12. Chida, D., Nakagawa, S., Nagai, S., Sagara, H., Katsumata, H., Imaki, T., Suzuki, H., Mitani, F., Ogishima, T., Shimizu, C., Kotaki, H., Kakuta, S., Sudo, K., Koike, T., Kubo, M., and Iwakura, Y. (2007) Melanocortin 2 receptor is required for adrenal gland development, steroidogenesis, and neonatal gluconeogenesis. *Proc. Natl. Acad. Sci. USA* **104**, 18205–18210
13. Dumontet, T., Sahut-Barnola, I., Septier, A., Montanier, N., Plotton, I., Roucher-Boulez, F., Ducros, V., Lefrançois-Martinez, A.-M., Pointud, J.-C., Zubair, M., Morohashi, K.-I., Breault, D. T., Val, P., and Martinez, A. (2018) PKA signaling drives reticularis differentiation and sexually dimorphic adrenal cortex renewal. *JCI Insight* **3**, 98394
14. Drelon, C., Berthon, A., Sahut-Barnola, I., Mathieu, M., Dumontet, T., Rodriguez, S., Batisse-Lignier, M., Tabbal, H., Tauveron, I., Lefrançois-Martinez, A.-M., Pointud, J.-C., Gomez-Sanchez, C. E., Vainio, S., Shan, J., Sacco, S., Schedl, A., Stratakis, C. A., Martinez, A., and Val, P. (2016) PKA inhibits WNT signalling in adrenal cortex zonation and prevents malignant tumour development. *Nat. Commun.* **7**, 12751
15. Mathieu, M., Drelon, C., Rodriguez, S., Tabbal, H., Septier, A., Damon-Soubeyrand, C., Dumontet, T., Berthon, A., Sahut-Barnola, I., Djari, C., Batisse-Lignier, M., Pointud, J.-C., Richard, D., Kerdivel, G., Calméjane, M.-A., Boeva, V., Tauveron, I., Lefrançois-Martinez, A.-M., Martinez, A., and Val, P. (2018) Steroidogenic differentiation and PKA signaling are programmed by histone methyltransferase EZH2 in the adrenal cortex. *Proc. Natl. Acad. Sci. USA* **115**, E12265–E12274
16. Walczak, E. M., Kuick, R., Finco, I., Bohin, N., Hrycaj, S. M., Wellik, D. M., and Hammer, G. D. (2014) Wnt signaling inhibits adrenal steroidogenesis by cell-autonomous and non-cell-autonomous mechanisms. *Mol. Endocrinol.* **28**, 1471–1486
17. Sunahara, R. K., Dessauer, C. W., and Gilman, A. G. (1996) Complexity and diversity of mammalian adenylyl cyclases. *Annu. Rev. Pharmacol. Toxicol.* **36**, 461–480
18. Carney, J. A., Gordon, H., Carpenter, P. C., Shenoy, B. V., and Go, V. L. (1985) The complex of myxomas, spotty pigmentation, and endocrine overactivity. *Medicine (Baltimore)* **64**, 270–283
19. Kirschner, L. S., Carney, J. A., Pack, S. D., Taymans, S. E., Giatzakis, C., Cho, Y. S., Cho-Chung, Y. S., and Stratakis, C. A. (2000) Mutations of the gene encoding the protein kinase A type I-alpha regulatory subunit in patients with the Carney complex. *Nat. Genet.* **26**, 89–92
20. Bertherat, J., Horvath, A., Groussin, L., Grabar, S., Boikos, S., Cazabat, L., Libe, R., René-Corail, F., Stergiopoulos, S., Bourdeau, I., Bei, T., Clauser, E., Calender, A., Kirschner, L. S., Bertagna, X., Carney, J. A., and Stratakis, C. A. (2009) Mutations in regulatory subunit type 1A of cyclic adenosine 5′-monophosphate-dependent protein kinase (PRKAR1A): phenotype analysis in 353 patients and 80 different genotypes. *J. Clin. Endocrinol. Metab.* **94**, 2085–2091
21. Sahut-Barnola, I., de Joussineau, C., Val, P., Lambert-Langlais, S., Damon, C., Lefrançois-Martinez, A. M., Pointud, J. C., Marceau, G., Sapin, V., Tissier, F., Ragazzon, B., Bertherat, J., Kirschner, L. S., Stratakis, C. A., and Martinez, A. (2010) Cushing's syndrome and fetal features resurgence in adrenal cortex-specific Prkar1a knockout mice. *PLoS Genet.* **6**, e1000980
22. De Joussineau, C., Sahut-Barnola, I., Tissier, F., Dumontet, T., Drelon, C., Batisse-Lignier, M., Tauveron, I., Pointud, J.-C., Lefrançois-Martinez, A.-M., Stratakis, C. A., Bertherat, J., Val, P., and Martinez, A. (2014) mTOR pathway is activated by PKA in adrenocortical cells and participates in vivo to apoptosis resistance in primary pigmented nodular adrenocortical disease (PPNAD). *Hum. Mol. Genet.* **23**, 5418–5428
23. Deyrieux, A. F., and Wilson, V. G. (2017) Sumoylation in development and differentiation. *Adv. Exp. Med. Biol.* **963**, 197–214
24. Demarque, M. D., Nacerddine, K., Neyret-Kahn, H., Andrieux, A., Danenberg, E., Jouvion, G., Bomme, P., Hamard, G., Romagnolo, B., Terris, B., Cumano, A., Barker, N., Clevers, H., and Dejean, A. (2011) Sumoylation by Ubc9 regulates the stem cell compartment and structure and function of the intestinal epithelium in mice. *Gastroenterology* **140**, 286–296
25. Deyrieux, A. F., Rosas-Acosta, G., Ozbun, M. A., and Wilson, V. G. (2007) Sumoylation dynamics during keratinocyte differentiation. *J. Cell Sci.* **120**, 125–136
26. Liu, B., Wang, T., Mei, W., Li, D., Cai, R., Zuo, Y., and Cheng, J. (2014) Small ubiquitin-like modifier (SUMO) protein-specific protease 1 de-SUMOylates Sharp-1 protein and controls adipocyte differentiation. *J. Biol. Chem.* **289**, 22358–22364
27. Liu, Y., Zhang, Y.-D., Guo, L., Huang, H.-Y., Zhu, H., Huang, J.-X., Liu, Y., Zhou, S.-R., Dang, Y.-J., Li, X., and Tang, Q.-Q. (2013) Protein inhibitor of activated STAT 1 (PIAS1) is identified as the SUMO E3 ligase of CCAAT/enhancer-binding protein β (C/EBPβ) during adipogenesis. *Mol. Cell. Biol.* **33**, 4606–4617
28. Zhang, Z., Du, J., Wang, S., Shao, L., Jin, K., Li, F., Wei, B., Ding, W., Fu, P., van Dam, H., Wang, A., Jin, J., Ding, C., Yang, B., Zheng, M., Feng, X.-H., Guan, K.-L., and Zhang, L. (2019) OTUB2 promotes cancer metastasis via hippo-independent activation of YAP and TAZ. *Mol. Cell* **73**, 7–21.e7
29. Cui, C.-P., Wong, C. C.-L., Kai, A. K.-L., Ho, D. W.-H., Lau, E. Y.-T., Tsui, Y.-M., Chan, L.-K., Cheung, T.-T., Chok, K. S.-H., Chan, A. C. Y., Lo, R. C.-L., Lee, J. M.-F., Lee, T. K.-W., and Ng, I. O. L. (2017) SENP1 promotes hypoxia-induced cancer stemness by HIF-1α deSUMOylation and SENP1/HIF-1α positive feedback loop. *Gut* **66**, 2149–2159
30. Geiss-Friedlander, R., and Melchior, F. (2007) Concepts in sumoylation: a decade on. *Nat. Rev. Mol. Cell Biol.* **8**, 947–956
31. Nayak, A., and Müller, S. (2014) SUMO-specific proteases/isopeptidases: SENPs and beyond. *Genome Biol.* **15**, 422
32. Shin, E. J., Shin, H. M., Nam, E., Kim, W. S., Kim, J.-H., Oh, B.-H., and Yun, Y. (2012) DeSUMOylating isopeptidase: a second class of SUMO protease. *EMBO Rep.* **13**, 339–346
33. Verger, A., Perdomo, J., and Crossley, M. (2003) Modification with SUMO. A role in transcriptional regulation. *EMBO Rep.* **4**, 137–142
34. Heun, P. (2007) SUMOrganization of the nucleus. *Curr. Opin. Cell Biol.* **19**, 350–355
35. Neyret-Kahn, H., Benhamed, M., Ye, T., Le Gras, S., Cossec, J.-C., Lapaquette, P., Bischof, O., Ouspenskaia, M., Dasso, M., Seeler, J., Davidson, I., and Dejean, A. (2013) Sumoylation at chromatin governs coordinated repression of a transcriptional program essential for cell growth and proliferation. *Genome Res.* **23**, 1563–1579
36. Smolen, G. A., Vassileva, M. T., Wells, J., Matunis, M. J., and Haber, D. A. (2004) SUMO-1 modification of the Wilms' tumor suppressor WT1. *Cancer Res.* **64**, 7846–7851
37. Galleguillos, D., Vecchiola, A., Fuentealba, J. A., Ojeda, V., Alvarez, K., Gómez, A., and Andrés, M. E. (2004) PIASgamma represses the transcriptional activation induced by the nuclear receptor Nurr1. *J. Biol. Chem.* **279**, 2005–2011
38. Komatsu, T., Mizusaki, H., Mukai, T., Ogawa, H., Baba, D., Shirakawa, M., Hatakeyama, S., Nakayama, K. I., Yamamoto, H., Kikuchi, A., and Morohashi, K. (2004) Small ubiquitin-like modifier 1 (SUMO-1) modification of the synergy control motif of Ad4 binding protein/steroidogenic factor 1 (Ad4BP/SF-1) regulates synergistic transcription between Ad4BP/SF-1 and Sox9. *Mol. Endocrinol.* **18**, 2451–2462
39. Chen, W. Y., Lee, W. C., Hsu, N. C., Huang, F., and Chung, B. C. (2004) SUMO modification of repression domains modulates function of nuclear receptor 5A1 (steroidogenic factor-1). *J. Biol. Chem.* **279**, 38730–38735
40. Lee, M. B., Lebedeva, L. A., Suzawa, M., Wadekar, S. A., Desclozeaux, M., and Ingraham, H. A. (2005) The DEAD-box protein DP103 (Ddx20 or Gemin-3) represses orphan nuclear receptor activity via SUMO modification. *Mol. Cell. Biol.* **25**, 1879–1890
41. Lee, F. Y., Faivre, E. J., Suzawa, M., Lontok, E., Ebert, D., Cai, F., Belsham, D. D., and Ingraham, H. A. (2011) Eliminating SF-1 (NR5A1) sumoylation in vivo results in ectopic hedgehog signaling and disruption of endocrine development. *Dev. Cell* **21**, 315–327
42. Yang, F. M., Pan, C. T., Tsai, H. M., Chiu, T. W., Wu, M. L., and Hu, M. C. (2009) Liver receptor homolog-1 localization in the nuclear body is regulated by sumoylation and cAMP signaling in rat granulosa cells. *FEBS J.* **276**, 425–436
43. Ragazzon, B., Lefrançois-Martinez, A. M., Val, P., Sahut-Barnola, I., Tournaire, C., Chambon, C., Gachancard-Bouya, J. L., Begue, R. J., Veyssière, G., and Martinez, A. (2006) Adrenocorticotropin-dependent changes in SF-1/DAX-1 ratio influence steroidogenic genes expression in a novel model of glucocorticoid-producing adrenocortical cell lines derived from targeted tumorigenesis. *Endocrinology* **147**, 1805–1818

44. Batisse-Lignier, M., Sahut-Barnola, I., Tissier, F., Dumontet, T., Mathieu, M., Drelon, C., Pointud, J.-C., Damon-Soubeyrand, C., Marceau, G., Kemeny, J.-L., Bertherat, J., Tauveron, I., Val, P., Martinez, A., and Lefrançois-Martinez, A.-M. (2017) P53/Rb inhibition induces metastatic adrenocortical carcinomas in a preclinical transgenic model. *Oncogene* **36**, 4445–4456
45. Lefrancois-Martinez, A.-M., Blondet-Trichard, A., Binart, N., Val, P., Chambon, C., Sahut-Barnola, I., Pointud, J.-C., and Martinez, A. (2011) Transcriptional control of adrenal steroidogenesis: novel connection between Janus kinase (JAK) 2 protein and protein kinase A (PKA) through stabilization of cAMP response element-binding protein (CREB) transcription factor. *J. Biol. Chem.* **286**, 32976–32985
46. Winer, J., Jung, C. K., Shackel, I., and Williams, P. M. (1999) Development and validation of real-time quantitative reverse transcriptase-polymerase chain reaction for monitoring gene expression in cardiac myocytes in vitro. *Anal. Biochem.* **270**, 41–49
47. Yang, W., Sheng, H., Warner, D. S., and Paschen, W. (2008) Transient focal cerebral ischemia induces a dramatic activation of small ubiquitin-like modifier conjugation. *J. Cereb. Blood Flow Metab.* **28**, 892–896
48. Tirard, M., Hsiao, H.-H., Nikolov, M., Urlaub, H., Melchior, F., and Brose, N. (2012) In vivo localization and identification of SUMOylated proteins in the brain of His6-HA-SUMO1 knock-in mice. *Proc. Natl. Acad. Sci. USA* **109**, 21122–21127
49. Tirosh, A., Valdés, N., and Stratakis, C. A. (2018) Genetics of micronodular adrenal hyperplasia and Carney complex. *Presse Med.* **47**, e127–e137
50. Lin, X., Takemori, H., Doi, J., Katoh, Y., and Okamoto, M. (2000) SIK (Salt-inducible kinase): regulation of ACTH-mediated steroidogenic gene expression and nuclear/cytosol redistribution. *Endocr. Res.* **26**, 995–1002
51. Takemori, H., and Okamoto, M. (2008) Regulation of CREB-mediated gene expression by salt inducible kinase. *J. Steroid Biochem. Mol. Biol.* **108**, 287–291
52. Jagannath, A., Butler, R., Godinho, S. I. H., Couch, Y., Brown, L. A., Vasudevan, S. R., Flanagan, K. C., Anthony, D., Churchill, G. C., Wood, M. J. A., Steiner, G., Ebeling, M., Hossbach, M., Wettstein, J. G., Duffield, G. E., Gatti, S., Hankins, M. W., Foster, R. G., and Peirson, S. N. (2013) The CRTC1-SIK1 pathway regulates entrainment of the circadian clock. *Cell* **154**, 1100–1111
53. Chung, S. S., Ahn, B. Y., Kim, M., Choi, H. H., Park, H. S., Kang, S., Park, S. G., Kim, Y. B., Cho, Y. M., Lee, H. K., Chung, C. H., and Park, K. S. (2010) Control of adipogenesis by the SUMO-specific protease SENP2. *Mol. Cell. Biol.* **30**, 2135–2146
54. Hang, J., and Dasso, M. (2002) Association of the human SUMO-1 protease SENP2 with the nuclear pore. *J. Biol. Chem.* **277**, 19961–19966
55. Tempé, D., Piechaczyk, M., and Bossis, G. (2008) SUMO under stress. *Biochem. Soc. Trans.* **36**, 874–878
56. Psakhye, I., and Jentsch, S. (2012) Protein group modification and synergy in the SUMO pathway as exemplified in DNA repair. *Cell* **151**, 807–820
57. Lee, M. H., Mabb, A. M., Gill, G. B., Yeh, E. T. H., and Miyamoto, S. (2011) NF-κB induction of the SUMO protease SENP2: a negative feedback loop to attenuate cell survival response to genotoxic stress. *Mol. Cell* **43**, 180–191
58. Cougnoux, A., Dalmasso, G., Martinez, R., Buc, E., Delmas, J., Gibold, L., Sauvanet, P., Darcha, C., Déchelotte, P., Bonnet, M., Pezet, D., Wodrich, H., Darfeuille-Michaud, A., and Bonnet, R. (2014) Bacterial genotoxin colibactin promotes colon tumour growth by inducing a senescence-associated secretory phenotype. *Gut* **63**, 1932–1942
59. Campbell, L. A., Faivre, E. J., Show, M. D., Ingraham, J. G., Flinders, J., Gross, J. D., and Ingraham, H. A. (2008) Decreased recognition of SUMO-sensitive target genes following modification of SF-1 (NR5A1). *Mol. Cell. Biol.* **28**, 7476–7486
60. Li, X., Vadrevu, S., Dunlop, A., Day, J., Advant, N., Troeger, J., Klussmann, E., Jaffrey, E., Hay, R. T., Adams, D. R., Houslay, M. D., and Baillie, G. S. (2010) Selective SUMO modification of cAMP-specific phosphodiesterase-4D5 (PDE4D5) regulates the functional consequences of phosphorylation by PKA and ERK. *Biochem. J.* **428**, 55–65
61. Seeler, J.-S., and Dejean, A. (2017) SUMO and the robustness of cancer. *Nat. Rev. Cancer* **17**, 184–197
62. Karami, S., Lin, F.-M., Kumar, S., Bahnassy, S., Thangavel, H., Quttina, M., Li, Y., Ren, J., and Bawa-Khalfe, T. (2017) Novel SUMO-protease SENP7S regulates β-catenin signaling and mammary epithelial cell transformation. *Sci. Rep.* **7**, 46477
63. Huang, H.-J., Zhou, L.-L., Fu, W.-J., Zhang, C.-Y., Jiang, H., Du, J., and Hou, J. (2014) β-catenin SUMOylation is involved in the dysregulated proliferation of myeloma cells. *Am. J. Cancer Res.* **5**, 309–320
64. Choi, H.-K., Choi, K.-C., Yoo, J.-Y., Song, M., Ko, S. J., Kim, C. H., Ahn, J.-H., Chun, K.-H., Yook, J. I., and Yoon, H.-G. (2011) Reversible SUMOylation of TBL1-TBLR1 regulates β-catenin-mediated Wnt signaling. *Mol. Cell* **43**, 203–216
65. Tan, M., Gong, H., Wang, J., Tao, L., Xu, D., Bao, E., Liu, Z., and Qiu, J. (2015) SENP2 regulates MMP13 expression in a bladder cancer cell line through SUMOylation of TBL1/TBLR1. *Sci. Rep.* **5**, 13996
66. Berthon, A., Drelon, C., Ragazzon, B., Boulkroun, S., Tissier, F., Amar, L., Samson-Couterie, B., Zennaro, M. C., Plouin, P. F., Skah, S., Plateroti, M., Lefèbvre, H., Sahut-Barnola, I., Batisse-Lignier, M., Assié, G., Lefrançois-Martinez, A. M., Bertherat, J., Martinez, A., and Val, P. (2014) WNT/β-catenin signalling is activated in aldosterone-producing adenomas and controls aldosterone production. *Hum. Mol. Genet.* **23**, 889–905

Received for publication February 27, 2019.
Accepted for publication May 13, 2019.

JCI The Journal of Clinical Investigation

Protein kinase A drives paracrine crisis and WNT4-dependent testis tumor in Carney complex

Cyril Djari, … , Antoine Martinez, Anne-Marie Lefrançois-Martinez

J Clin Invest. 2021;131(23):e146910. https://doi.org/10.1172/JCI146910.

Research Article | Endocrinology | Reproductive biology

Graphical abstract

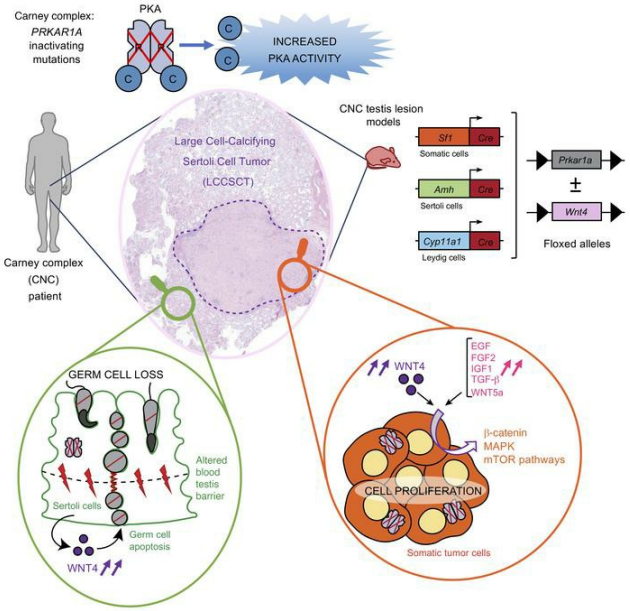

Protein kinase A drives paracrine crisis and WNT4-dependent testis tumor in Carney complex

Cyril Djari,[1] Isabelle Sahut-Barnola,[1] Amandine Septier,[1] Ingrid Plotton,[2] Nathanaëlle Montanier,[1,3] Damien Dufour,[1] Adrien Levasseur,[1] James Wilmouth Jr.,[1] Jean-Christophe Pointud,[1] Fabio R. Faucz,[4] Crystal Kamilaris,[4] Antoine-Guy Lopez,[5] Florian Guillou,[6] Amanda Swain,[7] Seppo J. Vainio,[8] Igor Tauveron,[1,3] Pierre Val,[1] Hervé Lefebvre,[5] Constantine A. Stratakis,[4] Antoine Martinez,[1] and Anne-Marie Lefrançois-Martinez[1]

[1]iGReD, Université Clermont-Auvergne, CNRS6293, INSERM U1103, Clermont-Ferrand, France. [2]UM Pathologies Endocriniennes Rénales Musculaires et Mucoviscidose, Hospices Civils de Lyon, Bron, France. [3]Université Clermont-Auvergne, CHU Clermont-Ferrand, Clermont-Ferrand, France. [4]Section on Endocrinology and Genetics, Eunice Kennedy Shriver National Institute of Child Health and Human Development (NICHD), NIH, Bethesda, Maryland, USA. [5]Normandie University, UNIROUEN, INSERM U1239, Rouen University Hospital, Department of Endocrinology, Diabetology and Metabolic Diseases and CIC-CRB 1404h4, Rouen, France. [6] PRC, INRAE, CNRS, IFCE, Tours University, Nouzilly, France. [7]Division of Cancer Biology, Institute of Cancer Research, London, United Kingdom. [8]Laboratory of Developmental Biology, Faculty of Biochemistry and Molecular Medicine, Biocenter Oulu, University of Oulu, Oulu, Finland.

Large-cell calcifying Sertoli cell tumors (LCCSCTs) are among the most frequent lesions occurring in male Carney complex (CNC) patients. Although they constitute a key diagnostic criterion for this rare multiple neoplasia syndrome resulting from inactivating mutations of the tumor suppressor *PRKAR1A*, leading to unrepressed PKA activity, LCCSCT pathogenesis and origin remain elusive. Mouse models targeting *Prkar1a* inactivation in all somatic populations or separately in each cell type were generated to decipher the molecular and paracrine networks involved in the induction of CNC testis lesions. We demonstrate that the *Prkar1a* mutation was required in both stromal and Sertoli cells for the occurrence of LCCSCTs. Integrative analyses comparing transcriptomic, immunohistological data and phenotype of mutant mouse combinations led to the understanding of human LCCSCT pathogenesis and demonstrated PKA-induced paracrine molecular circuits in which the aberrant WNT4 signal production is a limiting step in shaping intratubular lesions and tumor expansion both in a mouse model and in human CNC testes.

Introduction

Carney complex (CNC) is a rare multiple neoplasia syndrome mainly associated with inactivating mutations of the *PRKAR1A* gene encoding the R1α subunit of the PKA, which results in overactive PKA signaling (1). It is characterized by pigmented lesions of the skin and mucosae, cardiac, cutaneous, and other myxomatous tumors, and multiple other endocrine and nonendocrine neoplasms (2, 3). Approximatively 70% of patients are estimated to develop large-cell calcifying Sertoli cell tumors (LCCSCTs) (2, 4). LCCSCT is a testicular sex cord stromal tumor (SCST) subtype characterized by bilateral and multifocal masses caused by inactivating mutations of *PRKAR1A* (17q22–24) associated with CNC, but is also described in Peutz-Jeghers syndrome (PJS) caused by inactivating mutations of *STK11* (19p13.3) (5, 6). LCCSCTs developing in the case of CNC (CNC-LCCSCTs) are mostly benign tumors with low malignant potential, may be diagnosed from childhood by sonographic examination, and are associated with precocious puberty in some cases (7, 8). In engineered *Prkar1a*$^{+/-}$ mice, loss of heterozygosity for the *Prkar1a* locus has been implicated in the tumorigenesis process for CNC-related neoplasia (9), indicating that the resulting constitutive PKA activity plays an oncogenic role in specific tissues (10). The current management for LCCSCTs consists of the resection of the primary tumor due to the limited effect of chemotherapy and radiation treatments. However, the tumor discriminant markers are insufficient to allow early detection of a potential recurrence and to distinguish LCCSCTs from other SCSTs. Histological analyses highlight various tissue alterations (11). Moderate tubular damages characterized by spermatogenesis defects, calcifications, peritubular fibrosis, and composite tumor mass combined with Sertoli cell (SC) proliferating nodules have been described (12, 13). LCCSCT presence is systematically associated with increased production of inhibin-α, S100, calretinin, and β-catenin, but its molecular status is still incompletely determined due to low LCCSCT incidence (11, 14, 15). Therefore the molecular mechanisms and the cellular events involved in LCCSCT pathogenesis remain to be understood to improve their management. Moreover, the reproductive alterations have been poorly investigated in male CNC patients, especially concerning their fertility as well as their testis endocrine activity.

In embryo, SCs and Leydig cells (LCs) arise from a common pool of SF1^{+} (also called NR5A1) progenitor cells under the control of coordinate genetic and paracrine mechanisms triggered by the male-determining SRY- and SOX9-induced programs to counteract the female RSPO1/WNT4/β-catenin and FOXL2 pathways (16). At adulthood, testicular physiology carries out exocrine and endocrine functions: SCs support germ cell (GC) nursing, includ-

Conflict of interest: The authors have declared that no conflict of interest exists.

Submitted: December 15, 2020; **Accepted:** October 1, 2021; **Published:** December 1, 2021.
Reference information: *J Clin Invest*. 2021;131(23):e146910.
https://doi.org/10.1172/JCI146910.

ing growth and differentiation in seminiferous tubules (STs), and LCs produce androgens in the interstitial compartment. Pituitary follicle-stimulating hormone (FSH) and luteinizing hormone (LH) are the main regulators of the adult SC and LC functions through their respective specific G protein–coupled receptors, FSH-R and LH-R, both interacting with a number of intracellular effectors, among which the cAMP/PKA pathway plays a central role. Activating mutations of human FSH-R and LH-R resulting in permanent PKA activity have been described for several years, and their physiological outcomes have been extensively studied through biochemical and functional approaches, including mutant mouse models (17–20). Whether activating mutations of the gonadotropin receptors are involved in tumor development is not yet clear, and their pathological outcomes do not overlap with the testis CNC lesions etiology. The objective of our work was to identify the molecular networks (deregulated by PKA activation) that cause the resulting cellular alterations found in the CNC testis. We generated several genetic mouse models lacking *Prkar1a*, either in all somatic testicular cells arising from fetal somatic progenitors (prKO model) or exclusively in SC (srKO model) or LC (lrKO model). The ontogenetic follow-up of the mutant mouse testes, together with genetic manipulation of the catalytic PKA subunit and WNT4 signal, should provide a readout of the sequence of histological, molecular, and endocrine modifications arising in human LCCSCTs from CNC patients.

Results

Prkar1a loss in mouse testicular somatic cells induces LCCSCT-like lesions. *Sf1:Cre,Prkar1a*$^{fl/fl}$ mice (prKO mice) were generated to identify the underlying mechanisms of CNC-LCCSCT lesions by targeting early *Prkar1a* inactivation (E10.5) in somatic testis cells (Supplemental Figure 1, A and B; supplemental material available online with this article; https://doi.org/10.1172/JCI146910DS1). The use of the *Rosa26R-mtmg* reporter locus confirmed that the recombination affected all somatic testis cell types, excluding the GC population as previously described (ref. 21 and Supplemental Figure 1, A–C), and reverse-transcription quantitative PCR (RT-qPCR) analyses confirmed a robust reduction in *Prkar1a* mRNA levels in prKO testes (Supplemental Figure 1D). The mutant mouse colony setup revealed that prKO male mice were sterile beginning with the onset of puberty due to a lack of spermatozoa production and displayed a disrupted gonadotropic axis, with collapsed FSH and LH levels associated with hypertestosteronemia (Supplemental Figure 1, E–G). In contrast, 2-month-old *Sf1:cre,Prkar1a*$^{fl/fl}$,*Prkaca*$^{-/+}$ male mice, harboring *Prkaca* haploinsufficiency with decreased PKA catalytic activity, retained healthy testis histology, indicating that testis failures in prKO mice were mostly due to PKA overactivation (Supplemental Figure 2, A–E). Masson's trichrome and H&E staining revealed that 2- and 4-month-old prKO mice exhibited a severe gonadic dysplasia with seminiferous compartment disorganization. Further analyses highlighted calcification areas using alizarin red S coloration, peritubular basal lamina thickening attested by laminin B1 immunostaining, and GC loss in close similarity with human CNC-LCCSCT histology (Figure 1, A and B, Supplemental Figure 1, H–J, and Supplemental Figure 3). Transcript levels for the SCST current molecular markers, i.e., *Calb2*, *Ctnnb1*, *Inha*, and *S100a1*, were strongly increased in the 4-month-old prKO testes compared with that of WT (Figure 1C). Moreover, hypertrophic blood vessels and early bilateral proliferative stromal tumor mass expansion, attested by the increased stromal proliferating cell nuclear antigen (PCNA) index, were observed in 4-month-old mutant testes, whereas only limited stromal hyperplastic areas arose without tubular defect in 2-week-old mutant testes (Figure 1, A, D, and E, and Supplemental Figure 1K). In contrast, heterozygous *Sf1:Cre,Prkar1a*$^{fl/+}$ littermates displayed a healthy testicular phenotype, similarly to that of the *Prkar1a*$^{fl/fl}$ mice. All these observations demonstrated that loss of *Prkar1a* in mice phenocopied all tissue defects found in testes from CNC patients. To gain insight into the gene expression profiles associated with the prKO testis lesion setup, we conducted comparative microarray analyses on gene expression in 2-week-old and 2-month-old prKO and WT testes. Transcriptomic analyses revealed 1328 significantly deregulated genes in adult prKO mice (676 up- and 652 downregulated genes), whereas only 93 genes were deregulated at 2 weeks in mutant testes: 90 up- and 3 downregulated genes compared with WT (abs[$\log_2$ fold change (FC)] > 1, adj. $P < 0.05$; Figure 1, F and G, and Supplemental Data File 2). These data emphasized the delayed functional response to *Prkar1a* inactivation that was triggered from the early fetal gonadal stage (Supplemental Figure 1B). Gene Ontology (GO) analyses performed on transcriptomic data from 2-week-old testes highlighted an increased expression in genes involved in steroid metabolism, whereas gene signatures associated with intratubular cell homeostasis were virtually unaffected (Supplemental Data Files 1–3). Consistent with these observations, hormonal assays revealed significant 134-fold increased testosterone levels in 17-day-old prKO testes (5.39 ng/organ) compared with WT (0.04 ng/organ) (plasma testosterone levels = 16.01 ng/mL ± 5.12 in prKO vs. 0.16 ng/mL ± 0.04 in WT), whereas testosterone levels were unchanged in the plasma of 5-day-old prKO mice (0.27 ng/mL ± 0.12) compared with WT (0.14 ng/mL ± 0.04). In 2-month-old prKO mice, unbiased GO and Kyoto Encyclopedia of Genes and Genomes (KEGG) analyses revealed a negative enrichment in signatures associated with spermatogenesis and sperm motility and a positive enrichment in gene expression involved in tissue reorganization and metabolic processes (Figure 1H), indicating that *Prkar1a* gene inactivation resulted in complex and deep disruption of adult testis function and somatic cell tumor formation.

ST defects are associated with Prkar1a loss in SCs. *Sf1:Cre*-mediated recombination in testis targeted both supporting and stromal cells and resulted in a complex phenotype in adult prKO mice with intratubular and stromal compartment alterations that could be amplified by reciprocal dysregulated paracrine signals. To unravel the impact of cell-specific *Prkar1a* loss in global LCCSCT pathogenesis, we generated lrKO (*Scc-Cre,Prkar1a*$^{fl/fl}$) and srKO (*Amh-Cre,Prkar1a*$^{fl/fl}$) mouse models with either LC- or SC-specific *Prkar1a* invalidation triggered from E13.5 and E15, respectively, using *Cyp11a1:Cre* or *Amh:Cre* drivers (22, 23). The cell specificity of recombination was confirmed by analyzing *Rosa26R-mtmg* reporter activity (Supplemental Figure 4, A–D). Similarly to WT, 2-month-old lrKO mice were fertile and showed healthy testicular histology (Figure 2, A–E) devoid of stromal hyperplasia or tumor expansion. However, like prKO mice, adult lrKO male mice developed hypertestosteronemia (Supplemental Figure 4G). Transcrip-

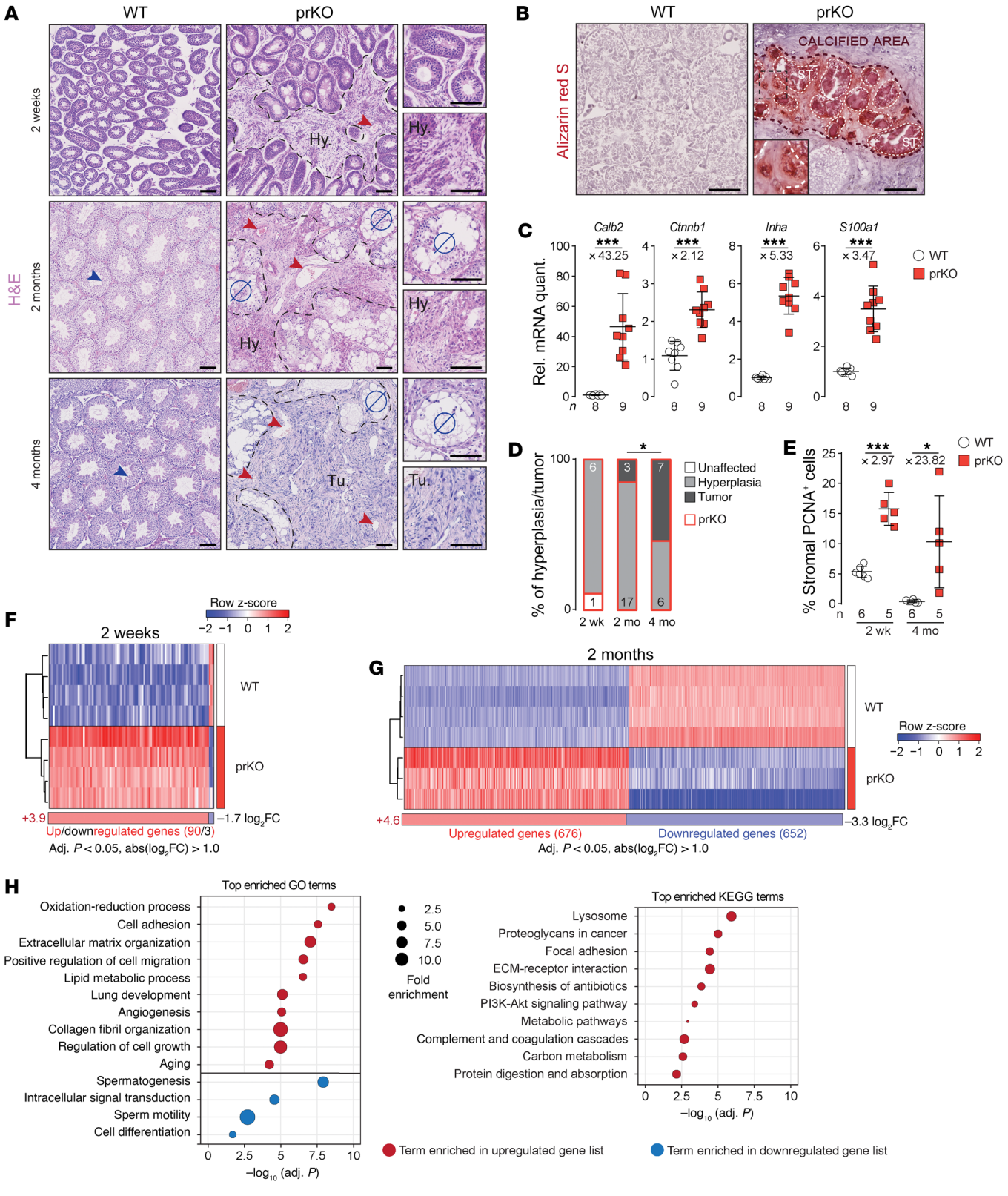
A
WT
prKO
2 weeks
2 months
4 months
H&E
Hy.
Tu.
B
WT
prKO
Alizarin red S
CALCIFIED AREA
ST
C
Calb2
Ctnnb1
Inha
S100a1
Rel. mRNA quant.
× 43.25
× 2.12
× 5.33
× 3.47
WT
prKO
D
% of hyperplasia/tumor
Unaffected
Hyperplasia
Tumor
prKO
2 wk
2 mo
4 mo
E
% Stromal PCNA+ cells
× 2.97
× 23.82
F
2 weeks
Row z-score
WT
prKO
+3.9
−1.7 log2FC
Up/downregulated genes (90/3)
Adj. P < 0.05, abs(log2FC) > 1.0
G
2 months
+4.6
−3.3 log2FC
Upregulated genes (676)
Downregulated genes (652)
H
Top enriched GO terms
Oxidation-reduction process
Cell adhesion
Extracellular matrix organization
Positive regulation of cell migration
Lipid metabolic process
Lung development
Angiogenesis
Collagen fibril organization
Regulation of cell growth
Aging
Spermatogenesis
Intracellular signal transduction
Sperm motility
Cell differentiation
−log10 (adj. P)
Fold enrichment
Top enriched KEGG terms
Lysosome
Proteoglycans in cancer
Focal adhesion
ECM-receptor interaction
Biosynthesis of antibiotics
PI3K-Akt signaling pathway
Metabolic pathways
Complement and coagulation cascades
Carbon metabolism
Protein digestion and absorption
Term enriched in upregulated gene list
Term enriched in downregulated gene list

Figure 1. *Prkar1a* loss in mouse testicular somatic cells induces LCCSCTs-like lesions. (**A**) H&E staining of 2-week-old, 2-month-old, and 4-month-old WT and *Prkar1a* somatic progenitor cell KO testes (noted as prKO, *Sf1:Cre,Prkar1a*$^{fl/fl}$). Red arrowheads indicate prKO hypervascularization. Blue arrowheads indicate spermatozoa. Hy., hyperplasia; Tu., tumor; Ø, absence of spermatozoa. (**B**) Alizarin red S staining in 2-month-old prKO testis. Dashed lines delineate calcium accumulation areas in both ST and stroma (inset). (**C**) RT-qPCR analysis for LCCSCT marker transcripts (*Calb2*, *Ctnnb1*, *Inha*, *S100a1*) in 4-month-old WT and prKO testes. Statistical analysis was performed using Student's *t* test or Welch's *t* test. Rel, relative; quant, quantification. (**D**) Relative proportion of hyperplasia and tumor from 2-week-old to 4-month-old prKO testes evaluated following H&E staining. Number of each histological defect is indicated in bars. Statistical analysis was performed using 2-proportion Fisher's test (hyperplasia/tumor proportions between 2-month-old and 4-month-old prKO testes). $P = 0.0259$. (**E**) Stromal PCNA$^+$ cell quantification represented as percentages of cells in 2-week-old and 4-month-old WT and prKO testes. Statistical analysis was performed using Welch's *t* test. (**F** and **G**) Heatmap representing the median-centered expression of significantly deregulated genes (abs[$\log_2$ FC > 1] and adj. $P < 0.05$) in 2-week-old (**F**) and 2-month-old (**G**) prKO testes ($n = 3$–4) compared with WT ($n = 4$). (**H**) Top 10 enriched GO and KEGG terms using 2-month-old prKO significant deregulated genes. Bars represent mean per group ± SD. Scale bars: 100 μm. Original magnification, ×2.12 (inset, **B**). $^*P < 0.05$; $^{***}P < 0.001$.

tomic data from comparative lrKO versus WT testes microarray analyses confirmed fewer molecular deregulations in 2-month-old lrKO testes, with only 22 significantly deregulated genes (17 up- and 5 downregulated genes; Figure 2G). In contrast, loss of *Prkar1a* in SC (srKO model) was sufficient to reproduce intratubular and peritubular LCCSCT lesions and led to infertility (Figure 2, A–D, and Supplemental Figure 4, E and F). The unbiased transcriptomic analyses revealed a huge deregulation of the molecular networks in 2-month-old srKO testes (560 deregulated, 150 up- and 410 downregulated genes; Figure 2, F and G). Comparative heatmap analyses among WT, prKO, srKO, and lrKO model data highlighted a main cluster of 473 genes (84.4 % of srKO deregulated genes) exhibiting deregulations in both 2-month-old prKO and srKO mutant testes (114 up- and 359 downregulated genes) compared with WT. Consistent with the GC population decrease, 75.5% of these cluster genes were significantly downregulated and strongly associated with spermatogenesis alteration in gene set enrichment analyses (GSEA) (Figure 2, G and H, and Figure 3A). Unlike the prKO model, adult srKO mice had normal testosterone plasma levels and never developed tumors (up to 12 months of age; Supplemental Figure 4, G and H). In agreement with the delayed *Prkar1a* loss impact previously observed in the prKO model, transcriptomic analyses of both 2-week-old lrKO and srKO testes revealed very little divergence from WT molecular signatures (Figure 2F). Together, data from srKO mice demonstrated that SC-specific loss of *Prkar1a* failed to initiate tumorigenesis, although ST functions were altered.

PKA overactivation in SCs triggers increased GC apoptosis from prepubertal age. Adult prKO and srKO mice shared common deregulated molecular signatures associated with nonautonomous GC loss that could be attributed to disturbed SC nursing capacities. Hallmark GSEA showed a robust negative enrichment for a "spermatogenesis" gene set and a positive enrichment for an "apoptosis" gene set in srKO and prKO testes compared with WT (Figure 3, A and B, and Supplemental Data File 3). In order to specify the nature of the cellular events leading to the GC loss at adulthood in response to Sertoli *Prkar1a* inactivation, developing GC types in srKO testes were evaluated. Significantly increased TUNEL staining over the entire width of the germinal epithelium from 5-week-old and 2-month-old srKO testes confirmed that apoptosis induced by *Prkar1a* loss occurred at different spermatogenesis stages and contributed to decreases in germinal epithelium thickness (Figure 3, C–F). Although a complete lack of spermatozoa was evidenced in 2-month-old srKO ST (Figure 3G), immunostaining analyses only identified a significant 1.8-fold decrease in ZBTB16$^+$ spermatogonia and a 1.6-fold decrease in G9A$^+$ cell numbers (Figure 3, H–K), corresponding to the undifferentiated spermatogonia up to early leptotene spermatocyte populations. Moreover, SYCP3$^+$ spermatocyte numbers were unchanged in srKO compared with WT (Figure 3, L and M), suggesting the occurrence of compensatory events counteracting increased apoptotic GC counts. Indeed, further time-course analyses revealed a transient growing number of ZBTB16$^+$ cells, G9A$^+$ cells, and SYCP3$^+$ meiotic cells from 2 up to 5 weeks of age, which paralleled a significant increased srKO testis weight from PND9 to 5 weeks compared with WT (Supplemental Figure 5, A and B). This enhanced germ-line expansion, including elongated spermatid formation, resulted in an abnormal overfilling of the srKO ST as attested by testis weight that culminated at 5 weeks of age before being drastically drained thereafter (Supplemental Figure 5, C–E). SOX9 immunostaining analyses revealed that SC numbers were significantly increased, 1.17-fold, in 2-week-old srKO testis compared with WT and 0.85-fold decreased at 7 weeks (Supplemental Figure 6, A and B). However, these slight variations were unlikely to fully account for the magnitude of the alterations affecting the germ line. Together, these data suggest that the lack of germ line in adult srKO testis was rather due to chronic apoptosis events overlapping with a deregulated increase of GC population instead of a meiosis commitment blockade in response to SC *Prkar1a* gene inactivation. These observations are consistent with DDX4 immunostaining in human CNC-LCCSCT biopsies, which reveal a strong decrease in GC numbers (Figure 3, N–P).

PKA overactivation alters SC polarity. The formation of vacuoles inside the germinal epithelium associated with round clusters of GCs that are released in the lumen was another phenomena, specifically occurring in the testes of CNC patients and prKO and srKO mice, that resulted, together with apoptosis, in the loss of spermatogenic cells (Supplemental Figure 7, A and B). Comparative time-course analyses of srKO and prKO histological intratubular alterations indicated a more precocious prKO increase in vacuolated tubules into the germinal epithelium compared with the srKO model that could contribute to worsen GC depletion (Supplemental Figure 7, A and D). Consistent with these observations, GSEA of the transcriptome of 2-month-old srKO testis revealed extended modification of the molecular networks supporting tubule architecture, including cytoskeleton, adhesion, or junctional proteins (Figure 4A). To gain insight into the modulators of the germinal epithelium integrity, we extracted expression levels of 32 genes involved in Sertoli-Sertoli junctions or Sertoli-GC interactions. Fifteen of these 32 genes were significantly upregulated, and 3 genes were downregulated both in srKO and prKO testes compared with WT (Figure 4B). RT–qPCR conduct-

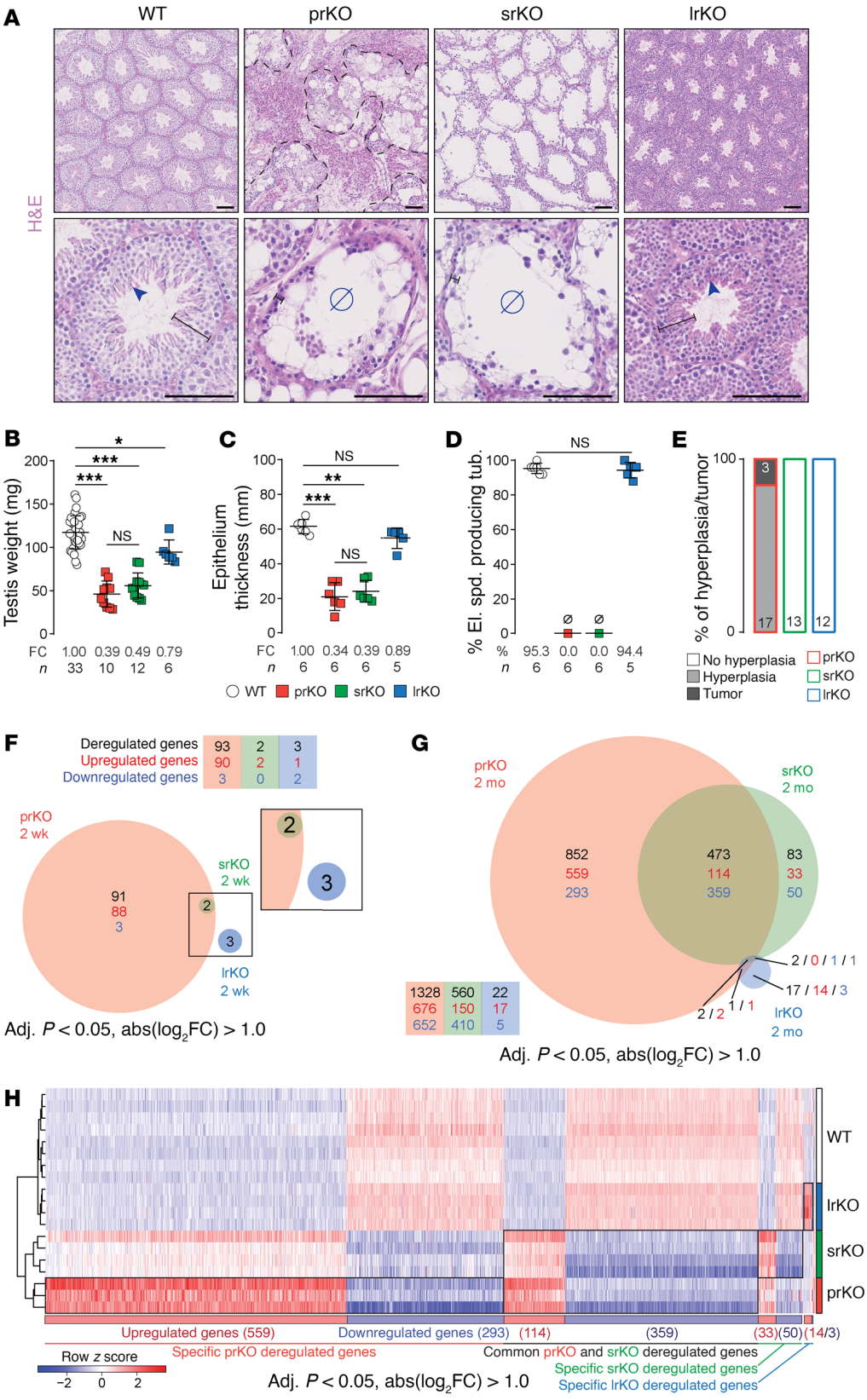

Figure 2. Seminiferous defects are associated with *Prkar1a* loss in SCs. (**A**) H&E staining of 2-month-old WT, prKO (*Sf1:Cre,Prkar1a*$^{fl/fl}$; somatic progenitor cell *Prkar1a* inactivation) (already presented in Figure 1A), srKO (*Amh:Cre,Prkar1a*$^{fl/fl}$; SC *Prkar1a* inactivation), and lrKO (*Cyp11a1:Cre,Prkar1a*$^{fl/fl}$; LC *Prkar1a* inactivation) testes. Dashed black lines delineate the tumor developed in prKO testis, blue arrowheads show spermatozoa, and black lines limit seminiferous epithelium thickness. Ø, absence of spermatozoa. Scale bars: 100 μm. (**B**) Testis weight of 4-month-old WT, prKO, srKO,and lrKO mice. One-way ANOVA was followed by Tukey's multiple-correction test. (**C**) Epithelium thickness quantified following H&E staining in 2-month-old WT, prKO, srKO, and lrKO testes. Kruskal-Wallis test was followed by Dunn's multiple-correction test. (**D**) Quantification of ST with elongated spermatids (el. spd.) represented as a percentage of positive tubules (tub.) quantified following H&E staining in 2-month-old WT, prKO, srKO, and lrKO testes. Statistical analysis was performed using Student's *t* test. (**E**) Relative proportion of hyperplasia and tumor in 2-month-old prKO, srKO, and lrKO testes. Numbers for each histological defect and genotype are indicated in bars. (**F** and **G**) Venn diagrams of the significantly deregulated genes (abs[$\log_2$] FC > 1 and adj. $P < 0.05$) in 2-week-old (**F**) and 2-month-old (**G**) prKO, srKO, and lrKO testes compared with WT (n = 3–4 mice per group). (**H**) Heatmap representing the median-centered expression of significantly deregulated genes in 2-month-old prKO, srKO, and lrKO testes compared with WT. Bars represent the mean per group ± SD. $^*P < 0.05$; $^{**}P < 0.01$; $^{***}P < 0.001$.

ed on independent WT, srKO, and prKO samples confirmed these results (Supplemental Figure 7E). Immunohistological analyses of Claudin11 (*Cldn11*) and β-catenin (*Ctnnb1*) specified that these junction proteins involved in blood-testis barrier (BTB) establishment were delocalized to the entire membrane perimeter in both srKO and prKO mutant testes (5 weeks) and that β-catenin staining was also diffused into the cytoplasm (Figure 4, C–E). These delocalizations were associated with a SC cytoskeleton alteration attested by tubulin β3 densification and vimentin disorganization (Supplemental Figure 7F). The junctional defects were also

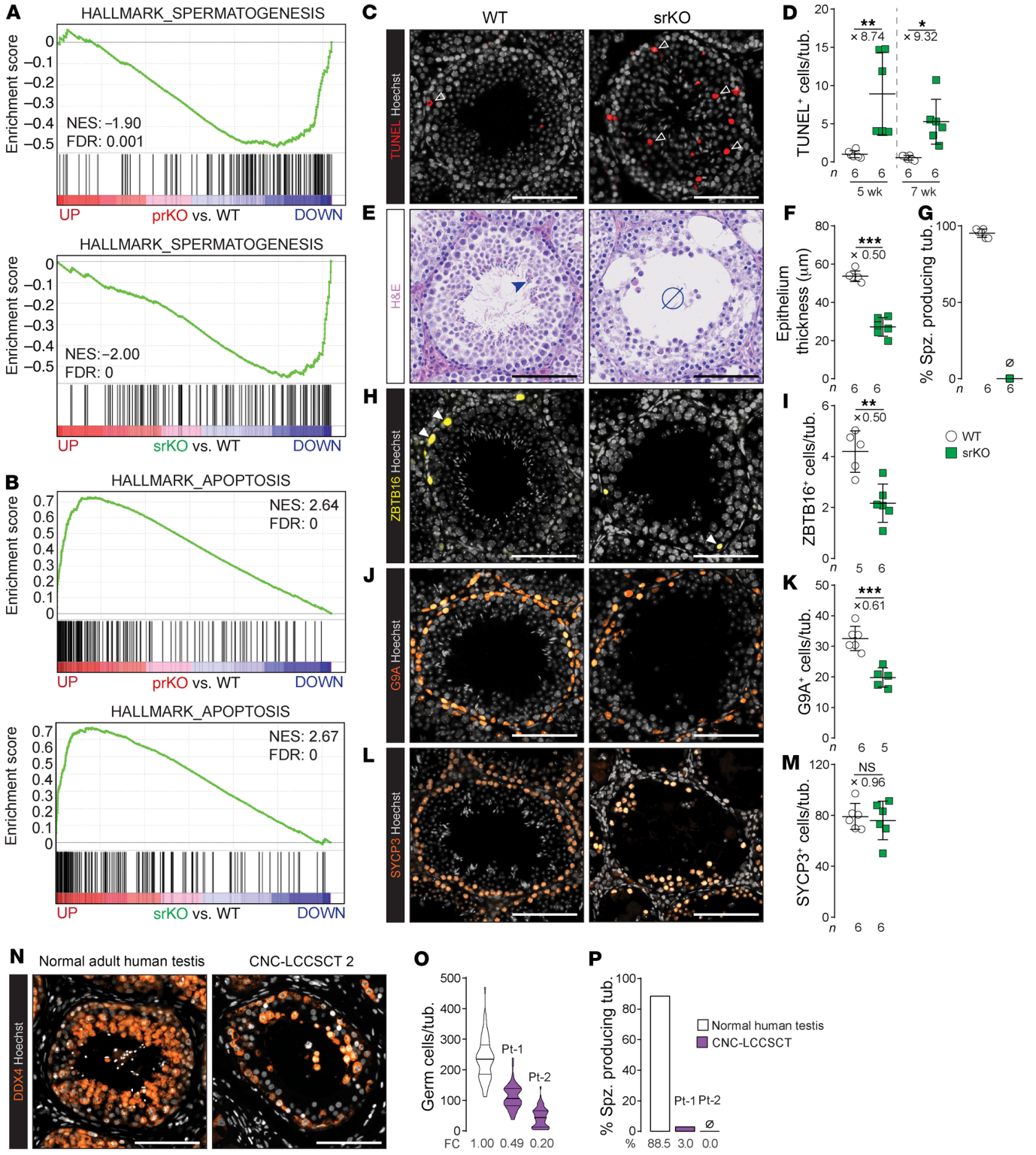

Figure 3. PKA overactivation in SCs triggers increased GC apoptosis from prepubertal age. (**A** and **B**) GSEA of microarray gene expression data of hallmark-spermatogenesis gene list (**A**) and hallmark-apoptosis gene list (**B**) in both 2-month-old prKO and srKO testes compared with WT. NES, normalized enrichment score. (**C**) TUNEL staining in 5-week-old WT and srKO testes. White open arrowheads indicate TUNEL$^+$ cells. (**D**) Quantification of TUNEL$^+$ cells in 5-week-old and 7-week-old srKO testes compared with WT. Statistical analysis was performed using Welch's *t* test or Mann-Whitney *U* test. (**E**) H&E staining of 7-week-old WT and srKO testes. Blue arrowhead indicates spermatozoa; Ø indicates absence of spermatozoa. (**F** and **G**) Epithelium thickness quantification (**F**) and percentage of ST with elongated spermatids (**G**) in 7-week-old WT and srKO testes. Statistical analysis was performed using Student's *t* test. (**H**–**M**) Immunohistochemical detection and quantification of ZBTB16 (spermotogonia-A) (**H** and **I**), G9A (spermotogonia-B) (**J** and **K**), and SYCP3 (spermotocytes) (**L** and **M**) in 7-week-old WT and srKO testes. White arrowheads indicate ZBTB16$^+$ cells. Quantification is based on the number of positive cells per tubule. Statistical analysis was performed using Student's *t* test. (**N** and **O**) DDX4 immunohistochemical detection (**N**) and GC loss quantification in CNC-LCCSCTs compared with normal adult human testis (**O**). (**P**) Percentages of ST with elongated spermatids quantified following H&E staining in CNC-LCCSCTs compared with normal adult human testis. Bars represent the mean per group ± SD. Scale bars: 100 µm. $^*P < 0.05$; $^{**}P < 0.01$; $^{***}P < 0.001$.

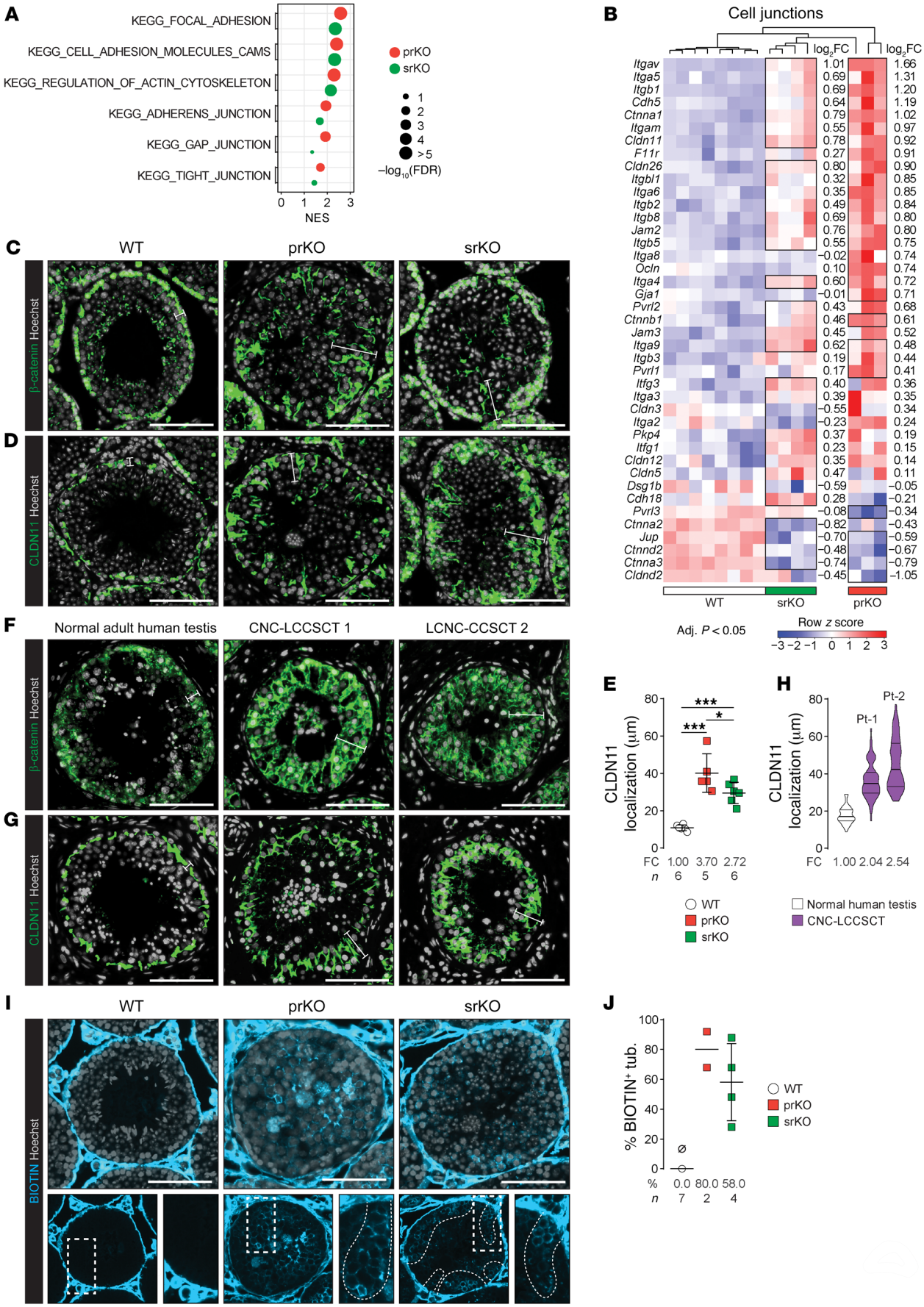
A
KEGG_FOCAL_ADHESION
KEGG_CELL_ADHESION_MOLECULES_CAMS
KEGG_REGULATION_OF_ACTIN_CYTOSKELETON
KEGG_ADHERENS_JUNCTION
KEGG_GAP_JUNCTION
KEGG_TIGHT_JUNCTION
0 1 2 3
NES
prKO
srKO
1
2
3
4
>5
−log10(FDR)
B
Cell junctions
log2FC
log2FC
Itgav 1.01 1.66
Itga5 0.69 1.31
Itgb1 0.69 1.20
Cdh5 0.64 1.19
Ctnna1 0.79 1.02
Itgam 0.55 0.97
Cldn11 0.78 0.92
F11r 0.27 0.91
Cldn26 0.80 0.90
Itgbl1 0.32 0.85
Itga6 0.35 0.85
Itgb2 0.49 0.84
Itgb8 0.69 0.80
Jam2 0.76 0.80
Itgb5 0.55 0.75
Itga8 −0.02 0.74
Ocln 0.10 0.74
Itga4 0.60 0.72
Gja1 −0.01 0.71
Pvrl2 0.43 0.68
Ctnnb1 0.46 0.61
Jam3 0.45 0.52
Itga9 0.62 0.48
Itgb3 0.19 0.44
Pvrl1 0.17 0.41
Itfg3 0.40 0.36
Itga3 0.39 0.35
Cldn3 −0.55 0.34
Itga2 −0.23 0.24
Pkp4 0.37 0.19
Itfg1 0.23 0.15
Cldn12 0.35 0.14
Cldn5 0.47 0.11
Dsg1b −0.59 −0.05
Cdh18 0.28 −0.21
Pvrl3 −0.08 −0.34
Ctnna2 −0.82 −0.43
Jup −0.70 −0.59
Ctnnd2 −0.48 −0.67
Ctnna3 −0.74 −0.79
Cldnd2 −0.45 −1.05
WT srKO prKO
Adj. P < 0.05
Row z score
−3 −2 −1 0 1 2 3
C
WT
prKO
srKO
β-catenin Hoechst
D
CLDN11 Hoechst
F
Normal adult human testis
CNC-LCCSCT 1
LCNC-CCSCT 2
β-catenin Hoechst
G
CLDN11 Hoechst
E
CLDN11 localization (μm)
***
*
***
0 20 40 60 80
FC 1.00 3.70 2.72
n 6 5 6
WT
prKO
srKO
H
CLDN11 localization (μm)
Pt-1
Pt-2
0 20 40 60 80
FC 1.00 2.04 2.54
Normal human testis
CNC-LCCSCT
I
WT
prKO
srKO
BIOTIN Hoechst
J
% BIOTIN+ tub.
0 20 40 60 80 100
% 0.0 80.0 58.0
n 7 2 4
WT
prKO
srKO

Figure 4. PKA overactivation alters SC polarity. (**A**) GSEA enrichment scores of microarray gene expression data using KEGG gene lists associated with junction/cytoskeleton in 2-month-old prKO or srKO testes compared with WT. (**B**) Heatmap representing the median centered expression of significantly deregulated regulators of cell junctions (for black boxes, adj. $P < 0.05$) in 2-month-old prKO and srKO testes ($n = 3–4$) compared with WT ($n = 4$). (**C–H**) Immunohistochemical detection of β-catenin and CLDN11 and quantification of CLDN11 expression domain based on the distance between basal lamina and apical CLDN11 in 5-week-old WT, prKO, and srKO testes and in normal adult human testis and CNC-LCCSCTs. White lines delineate β-catenin or CLDN11 expression domain. One-way ANOVA was followed by Tukey's multiple-correction test. (**I**) Biotin tracer detection after injection underneath the testis capsule in 6-week-old WT, prKO, and srKO testes. White dashed lines mark intraseminiferous biotin diffusion in prKO and srKO testes. (**J**) BTB integrity loss evaluation based on the percentage of tubule with intraseminiferous biotin accumulation. Scale bars: 100 μm. $^*P < 0.05$; $^{***}P < 0.001$.

present in the human CNC ST located out of the tumor mass, as attested by Claudin11 and β-catenin IHC analyses (Figure 4, F–H). These data suggested a compromised setting of the adluminal compartment by the BTB junctions, which is critical to spermatogenesis achievement (24). Therefore, BTB functional integrity was tested in the srKO and prKO mutant mice by intratesticular injection of a fluorescent tracker (Figure 4, I and J). The tracker signal confirmed a drastic loss of BTB sealing in both srKO and prKO (6 weeks of age), demonstrating that SC failed to provide an appropriate structural dynamic for GC maturation across the seminiferous epithelium. Moreover, transcriptomic and RT-qPCR analyses highlighted an upregulation of *Dpt* expression in 2-week-old prKO and in 2-month-old srKO and prKO testes (Supplemental Figure 7G), indicating increased dermatopontin production by both altered adult STs and the hyperplastic stromal compartment. Our results are consistent with previous data demonstrating that the dermatopontin excessive production in SCs induced BTB alterations, vacuole formation, and GC loss (25). However, srKO and prKO comparative analyses also revealed precocious and higher growing *Dpt* transcript levels associated with tumor expansion in prKO testes. These latest observations are consistent with previous data highlighting cAMP controlled expression of *Dpt* and its involvement in tumor growth (26, 27).

PKA overactivation modifies Sertoli signals involved in the control of spermatogenesis. The maintenance of GCs within the spermatogenic cycle is supported by mature SCs through appropriate production of mitogens and differentiation factors that could be affected by *Prkar1a* gene inactivation. The interaction of the growth factor Kit-ligand (KIT-L) produced by SCs with its specific c-KIT receptor expressed on GCs from differentiating spermatogonia causes the PI3K-AKT pathway activation that is required for proliferation and survival of mitotic GCs in both the embryonic and postnatal testes (28–30). KIT-L also triggers PI3K/AKT and Ras/MAPK crosstalk that plays a critical role in the development of GC cancers (31). In addition, the KIT-L/c-KIT/JAK/STAT pathway is the main promoter of mast cell growth and differentiation from bone marrow and peripheral progenitors (32). Cyclic AMP/PKA-driven mechanisms leading to increased *Kitl* transcription in SCs have been previously described (33, 34). Consistent with these previous observations, transcriptomic and RT-qPCR analyses in prKO/srKO testes showed that *Prkar1a* loss led to a significant and early upregulation of *Kitl* transcripts associated with a positive enrichment of Reactome signaling by the SCF (alias KIT-L)/KIT gene set as well as an increase in mast cell recruitment in interstitial tissue (Figure 5, A–D).

Surprisingly, further transcriptomic and RT-qPCR analyses highlighted a significant upregulation of *Wnt4* gene expression that was listed in the common deregulated gene cluster from adult prKO and srKO models, indicating that most of the WNT4 overproduction originated from adult SCs in response to *Prkar1a* inactivation (Figure 5, E and F). Heatmap of a WNT signaling gene set showed a robust positive enrichment of these molecular signatures in adult srKO and prKO testes compared with WT, suggesting a functional significance of WNT pathway activation. This observation was confirmed by RT-qPCR analysis of *Axin2*, *c-Myc*, *Ccdc80*, and *Nr0b1* target gene expression (Figure 5G and refs. 35, 36). Together, these data reveal that constitutive PKA activation leads to upregulation of *Wnt4* in SCs, whereas PKA-dependent *Wnt4* gene expression was only previously demonstrated in other tissue differentiations, such as kidney tubulogenesis or uterine stromal cell decidualization (37, 38).

Wnt4 inactivation decreases GC apoptosis induced by Prkar1a loss. The WNT4/β-catenin pathway is involved in stem cell proliferation of several tissues (39). Although WNT4/β-catenin has been shown to be an essential modulator of female ovary differentiation (40), *Ctnnb1* expression is dispensable for testis development (41). Moreover, Boyer et al. demonstrated that an excessive WNT4 signal repressed the normal activity of spermatogonial stem cells by inducing their apoptosis (42), while forced expression of active β-catenin in fetal gonocytes deregulated spermatogonial proliferation and apoptosis (43, 44). Our analyses indicated that the increase in GC apoptosis together with disturbed BTB establishment impaired the spermatozoa accumulation in prKO and srKO mice. In order to assess the role of WNT4 in GC-altered homeostasis triggered by *Prkar1a* gene loss, we generated double-KO mice for *Prkar1a* and *Wnt4* in somatic cells (prwKO model; *Sf1:Cre,Prkar1a*$^{fl/fl}$*,Wnt4*$^{fl/fl}$) or restricted to SCs (srwKO model; *Amh:Cre,Prkar1a*$^{fl/fl}$, *Wnt4*$^{fl/fl}$; Supplemental Figure 8, A–D). As expected, simple mutant mice bearing targeted *Wnt4* inactivation in SC (swKO) or in somatic cells (pwKO) were fertile and had normal testicular development and physiology (Supplemental Figure 8E). Unlike the srKO testis, ST from 8-week-old double-mutant srwKO testes maintained a complete germinal epithelium containing all GC types, including spermatozoa and were associated with a significant decrease in intratubular apoptosis events compared with srKO testes (Figure 6, A–J). This indicates that *Wnt4* loss in a PKA activation context allowed the achievement of a complete GC lineage, whereas SC junction disorganization, vacuole, and infertility were still maintained (Figure 6, J–M). Therefore, SC-specific PKA constitutive activity upregulated *Wnt4* expression, which increased GC apoptosis. Nevertheless, several spermatocytes with abnormal mitotic features not only persisted in srwKO, but also were accentuated in prwKO testes, despite normalization of the germ-line marker gene *Ddx4* (Figure 6A and Supplemental Figure 8F). These data revealed a critical role of SC-specific PKA signaling on spermatogenesis that impaired long-term maintenance of GCs, which is independent of the WNT4 signal. Transcriptomic and RT-qPCR analyses highlighted increased *Ctnnb1*

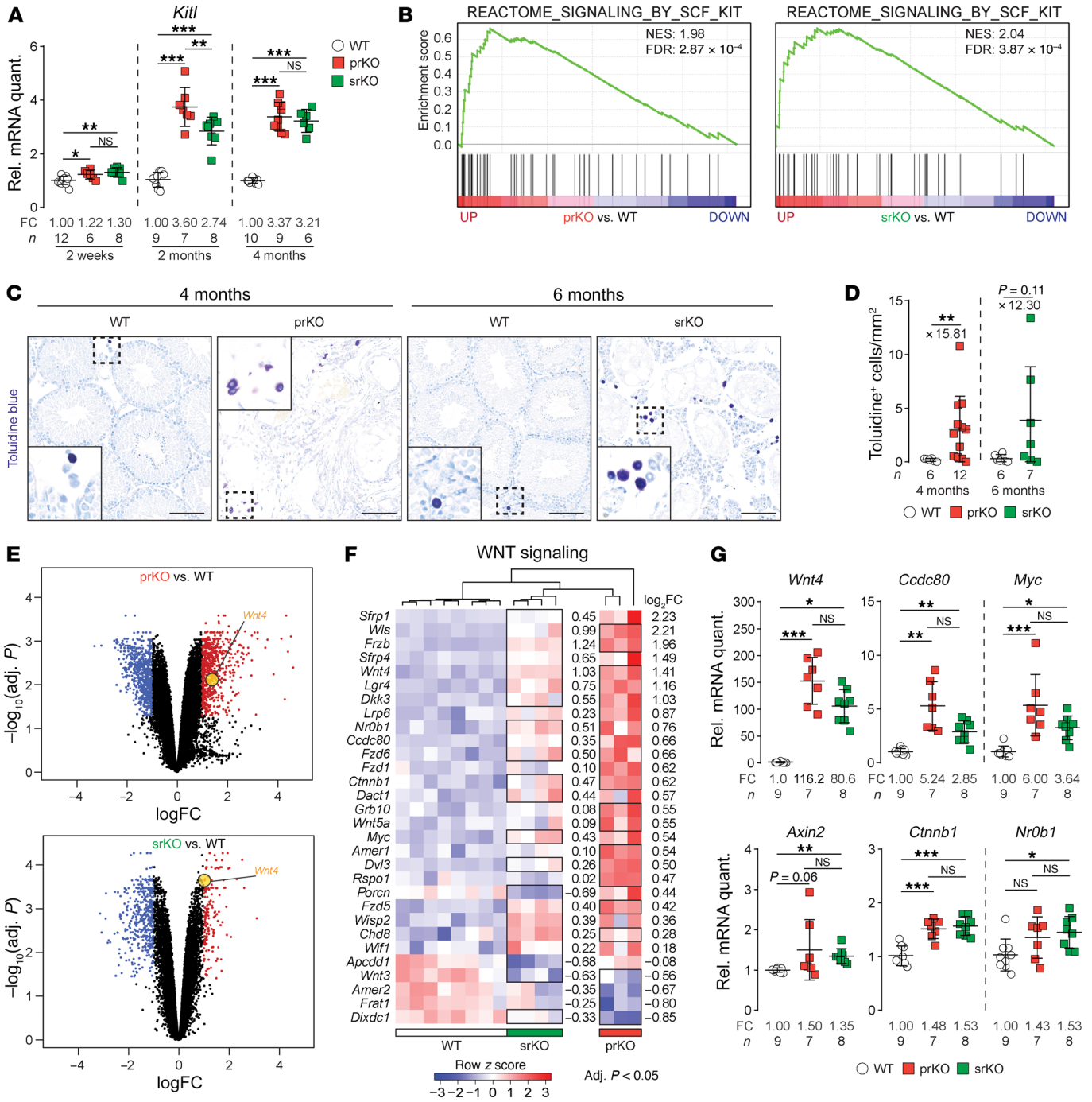

Figure 5. PKA overactivation modifies Sertoli signals involved in control of spermatogenesis. (**A**) *Kitl* transcripts of RT-qPCR analysis in 2-week-old, 2-month-old, and 4-month-old WT, prKO, and srKO testes. One-way ANOVA was followed by Tukey's multiple-correction test, and Welch's 1-way ANOVA was followed by Games-Howell multiple-correction test. (**B**) GSEA of microarray gene expression data using Reactome signaling by the SCF KIT gene list in 2-month-old prKO and srKO testes compared with WT. (**C**) Toluidine blue staining showing mast cell recruitment in 4-month-old prKO and 6-month-old srKO testes. Scale bars: 100 μm. Original magnification, ×2.65 (insets, **C**). (**D**) Mast cell quantification based on the toluidine⁺ cell number per histological section. Statistical analysis was performed using Welch's *t* test. (**E**) Volcano plot showing differential gene expression in 2-month-old prKO and srKO testes compared with WT. Significantly deregulated genes (abs[$\log_2$ FC > 1 and adj. $P < 0.05$) are highlighted in blue (down) or in red (up). *Wnt4* (yellow point) is an upregulated gene. (**F**) Heatmap representing the median centered expression of significantly deregulated WNT pathway regulators and target genes (for black boxes, adj. $P < 0.05$) in 2-month-old prKO and srKO testes (n = 3-4) compared with WT (n = 4). (**G**) RT-qPCR analysis of WNT pathway regulators (*Wnt4*, *Ctnnb1*) and target gene (*Axin2*, *Ccdc80*, *Myc*, *Nr0b1*) expression in 2-month-old WT, prKO, and srKO testes. One-way ANOVA was followed by Tukey's multiple-correction test, Welch's 1-way ANOVA was followed by Games-Howell multiple-correction test, and Kruskal-Wallis test was followed by Dunn's multiple-correction test. Bars represent the mean per group ± SD. *$P < 0.05$; **$P < 0.01$; ***$P < 0.001$.

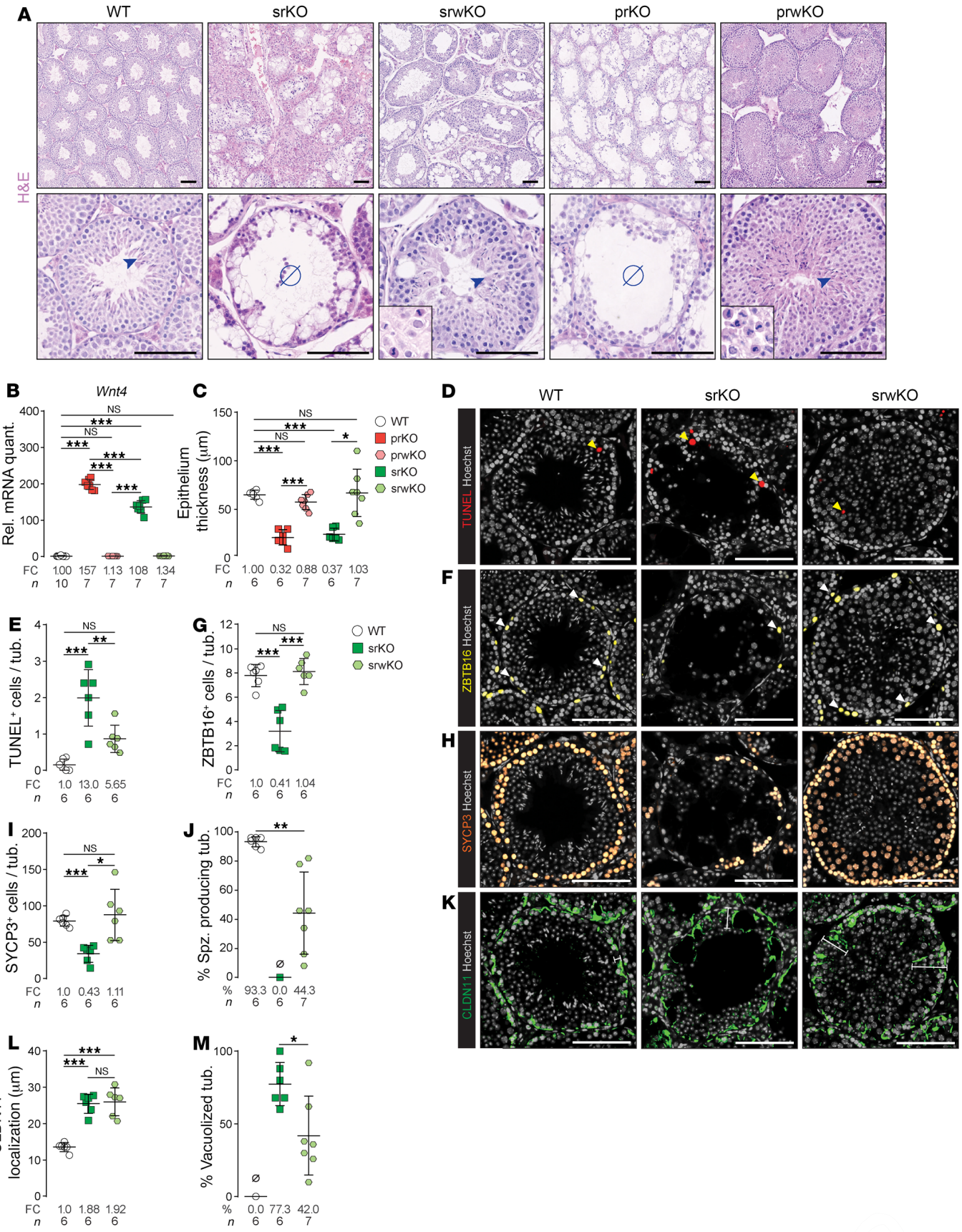
A
WT
srKO
srwKO
prKO
prwKO
H&E
B
Wnt4
Rel. mRNA quant.
FC 1.00 157 1.13 108 1.34
n 10 7 7 7 7
C
Epithelium thickness (µm)
WT
prKO
prwKO
srKO
srwKO
FC 1.00 0.32 0.88 0.37 1.03
n 6 6 7 6 7
D
WT
srKO
srwKO
TUNEL Hoechst
E
TUNEL+ cells / tub.
FC 1.0 13.0 5.65
n 6 6 6
F
ZBTB16 Hoechst
G
ZBTB16+ cells / tub.
H
SYCP3 Hoechst
I
SYCP3+ cells / tub.
FC 1.0 0.43 1.11
n 6 6 6
J
% Spz. producing tub.
% 93.3 0.0 44.3
n 6 6 7
K
CLDN11 Hoechst
L
CLDN11 localization (µm)
FC 1.0 1.88 1.92
n 6 6 6
M
% Vacuolized tub.
% 0.0 77.3 42.0
n 6 6 7

Figure 6. *Wnt4* inactivation decreases GC apoptosis induced by *Prkar1a* loss. (**A**) H&E staining of 2-month-old WT, prKO, double-mutant prwKO testes (*Sf1:Cre,Prkar1a*$^{fl/fl}$,*Wnt4*$^{fl/fl}$), and srKO and srwKO testes (*Amh:Cre,Prkar1a*$^{fl/fl}$,*Wnt4*$^{fl/fl}$). Arrowheads indicate spermatozoa; Ø indicates absence of spermatozoa; insets show abnormal mitotic features. (**B**) RT-qPCR analysis of *Wnt4* transcripts in 2-month-old WT, prKO, prwKO, srKO, and srwKO testes. Welch's 1-way ANOVA was followed by Games-Howell multiple-correction test. (**C**) Epithelium thickness quantified following H&E staining in 2-month-old WT, prKO, prwKO, srKO, and srwKO testes. Welch's 1-way ANOVA was followed by Games-Howell multiple-correction test. (**D** and **E**) TUNEL staining in 2-month-old WT, srKO, and srwKO testes (**D**) and TUNEL$^+$ cell quantification (**E**) in 2-month-old srwKO testes compared with WT and srKO testes. Yellow arrowheads indicate TUNEL$^+$ cells. One-way ANOVA was followed by Tukey's multiple-correction test. (**F**–**I**) Immunohistochemical detection of ZBTB16 (**F**) and SYCP3 (**H**) in 2-month-old WT, srKO, and srwKO testes and quantification of ZBTB16 (**G**) and SYCP3 (**I**) based on the number of positive cells per tubule. White arrowheads indicate ZBTB16$^+$ cells. Welch's 1-way ANOVA was followed by Games-Howell multiple-correction test. (**J**) Percentage of ST with elongated spermatids quantified following H&E staining in 2-month-old WT, srKO, and srwKO testes. Statistical analysis was performed by Welch's *t* test. (**K**) Immunohistochemical detection of CLDN11 in 2-month-old WT, srKO, and srwKO testes. (**L** and **M**) Quantification of CLDN11 expression domain (**L**) and percentage of vacuolized tubules (**M**) in 2-month-old srwKO testis compared with WT and srKO. Statistical analysis was performed using Student's *t* test or 1-way ANOVA followed by Tukey's multiple-correction test. Bars represent the mean per group ± SD. Scale bars: 100 μm. Original magnification, ×1.41. (insets, **A**). $^*P < 0.05$; $^{**}P < 0.01$; $^{***}P < 0.001$.

mRNA levels in the adult testes of both prKO and srKO mice, which remained elevated in srwKO and prwKO (Supplemental Figure 8G), demonstrating that PKA induced *Ctnnb1* expression independently of the WNT4 signal.

Wnt4 inactivation impaired tumor mass formation induced by Prkar1a loss. Human CNC-LCCSCT masses are the site of proliferative activity mediated by molecular pathways that, to our knowledge, had not been identified until now. Consistent with LCCSCTs in the CNC context, from 8 weeks of age, prKO testis developed early proliferative tumor masses arising from neonatal stromal hyperplasia. RT-qPCR and IHC analyses highlighted an upregulation of *Wnt4* and *Ctnnb1* expression in 2-month-old prKO mice, suggesting, together with the WNT-signaling heatmap analysis (Figure 5, F and G, and Supplemental Figure 8, C and D), that PKA-induced WNT/β-catenin signaling could be involved in the LCCSCT promotion in CNC patients and prKO mice. In addition to *Wnt4* upregulation, further analyses indicated that the loss of *Prkar1a* led to a chronic increase of both active β-catenin accumulation and gene expression of *Fzd6* and *Wnt5a* in 4-month-old prKO testes (Figure 5F and Figure 7, A–C). Interestingly, increased expression of *Fzd6* and *Wnt5a* were previously associated with tumor expansion through canonical and noncanonical WNT pathway activity in various cancers (45). Histological examination of mutant testes revealed that, although the oldest double-mutant prwKO testes were still the site of stromal fibrosis, they were devoid of tumors compared with single-mutant prKO testes (Figure 7, D–F, and Supplemental Figure 8E). Comparative PCNA IHC analyses confirmed that *Wnt4* inactivation strongly decreased the stromal proliferation that was triggered by *Prkar1a* loss in somatic testis cells (Figure 7, G and H). Moreover, whole-testis RT-qPCR analyses confirmed that in these prwKO testes, *Ccdc80*, *Axin2*, and *Ki67* transcripts were reduced compared with those in 4-month-old prKO testes (Figure 7, I and J). Together, these results demonstrate that WNT4 is a testis tumor signal in response to *Prkar1a* inactivation. Consistent with our murine models, IHC analyses confirmed that human CNC-LCCSCT cells retained WNT4 staining that colocalized with cytoplasmic β-catenin accumulation. This demonstrates that WNT/β-catenin activation is likely associated with human CNC-LCCSCT expansion (Figure 7K).

PKA constitutive activation in somatic cells activates growth factor signaling pathways in CNC-LCCSCTs. Unbiased GO and GSEA highlighted additional prKO-specific enrichment in signatures associated with proliferative pathways that could participate in tumor formation, including upregulated expression for *Fgf2*, *Egf*, *Igf1*, and *Tgfb1-3* (Figure 8, A–D). These increased *Fgf2*, *Egf*, *Igf1*, and *Tgfb1-3* transcript levels in prKO testes remained unaffected by *Wnt4* loss, suggesting that their PKA-induced upregulation was not sufficient to trigger precocious tumor formation (Figure 8E). Proliferative/oncogenic activities of the growth factors (IGF1, EGF, FGF2, KIT-L) overexpressed in prKO testes are mainly mediated by converging signaling pathways, including RAS/MAPK and PI3K/AKT/mTOR (46–49). Immunodetection of activated MAPK modulators and mTOR targets in Western blot revealed significantly increased levels of phosphorylated forms of ERK, 4EBP1, and S6K in 4-month-old prKO testes compared with WT (Figure 8, F and G). These increases persisted after *Wnt4* inactivation in the 4-month-old prwKO testes, revealing that the loss of *Wnt4* did not affect the p4EBP1, pERK, and pS6K relative protein levels compared with their respective increased levels in *Prkar1a*-KO testes. In testis, the mTOR pathway was previously shown to control SC polarity and spermatogenesis (50, 51). Additionally, its overactivity was demonstrated to mediate SC disruption in a mouse model lacking the *Lkb1* gene in SCs (52). In prKO testes, IHC analyses revealed increased p4EBP1 accumulation in the tubular compartment and tumor mass compared with WT, demonstrating that the mTOR pathway was activated in tumor cells in response to *Prkar1a* loss (Figure 8H). Consistent with these observations, IHC analyses revealed that the human LCCSCT samples retained strong p4EBP1 immunostaining restricted to the majority of tumor cells and absent from nontumor areas (Figure 8I). Moreover, to a lesser extent, the human LCCSCT masses also displayed numerous foci of pERK accumulation, demonstrating that these 2 proliferative pathways are activated in CNC-LCCSCTs in response to *PRKAR1A* inactivation (Figure 8J). LCCSCTs are solid tumors; this implies they could be the site of hypoxia. This hypothesis was strongly suggested in 2-month-old prKO testes by GO and GSEA analyses highlighting positive enrichment in hypoxia-responsive genes (Figure 8, A and K). RT-qPCR analyses in 4-month-old prKO mice confirmed increased mRNA levels of *Hif1a*, *Hif1b*, and *Hif2a* genes that played a central role in O_2-dependent transcriptional response (Figure 8L). Consistent with these observations, IHC analyses in human LCCSCTs revealed increased cytoplasmic and nuclear HIF2A protein accumulation restricted to tumor cells (Figure 8M). Together, our data reveal that LCCSCTs are the site of multiple proliferative pathways, including mTOR, MAPK, and hypoxia, acting with the active WNT/β-catenin pathway to promote tumor growth.

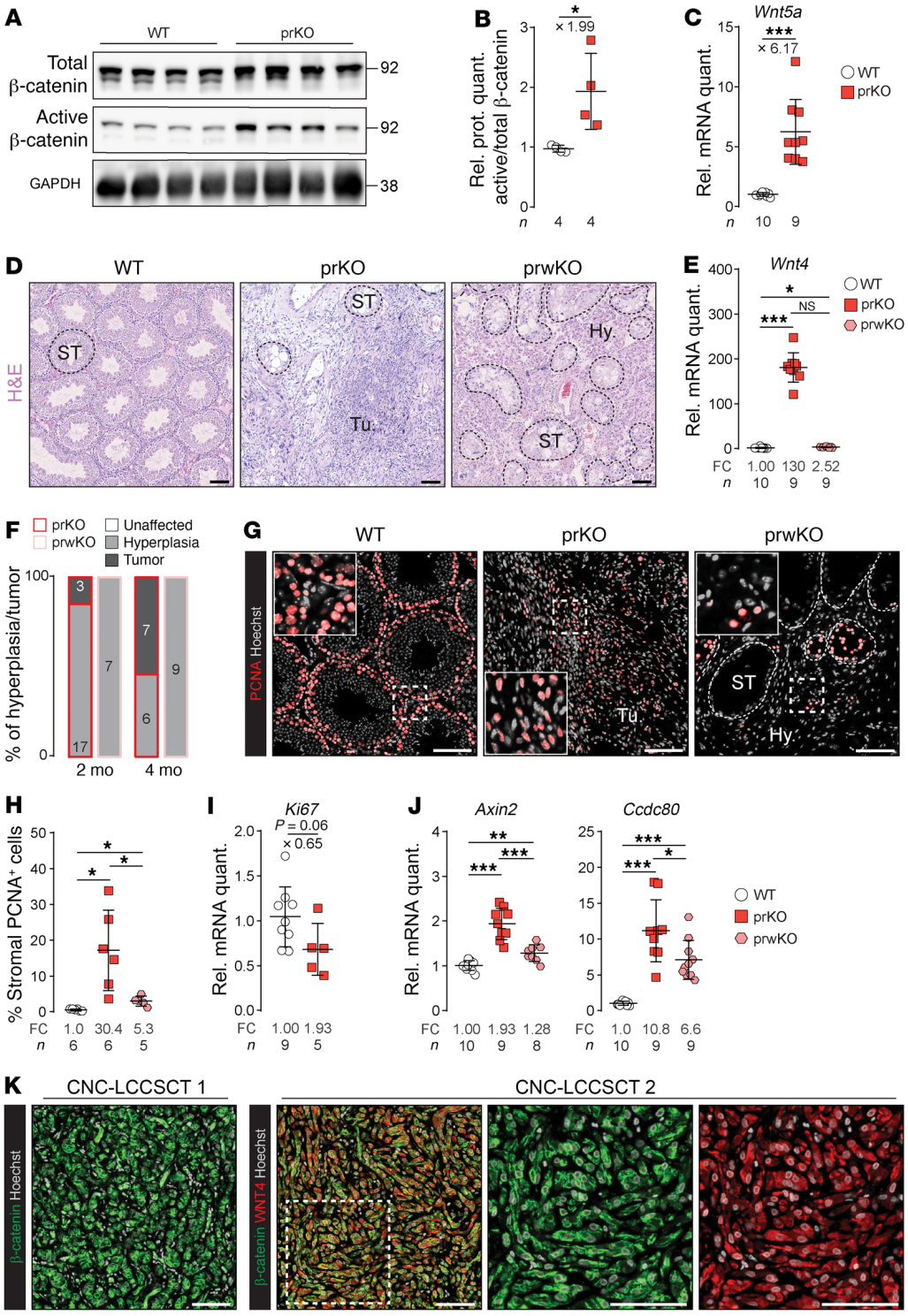

Figure 7. *Wnt4* inactivation impairs tumor mass formation induced by *Prkar1a* loss. (**A**) Active β-catenin accumulation in 4-month-old WT and prKO testes. (**B**) Active β-catenin quantification over total β-catenin. Statistical analysis was performed using Student's *t* test. prot., protein.(**C**) *Wnt5a* transcripts in 4-month-old WT and prKO testes. Statistical analysis was performed using Welch's *t* test. (**D**) H&E staining of 4-month-old WT, prKO, and prwKO testes. Dashed lines delineate ST. (**E**) *Wnt4* transcripts in 4-month-old WT, prKO, and prwKO testes. One-way ANOVA was followed by Tukey's multiple-correction test. (**F**) Relative proportion of testicular hyperplasia and tumor in 2-month-old and 4-month-old prKO and prwKO testes was evaluated following H&E staining. Numbers for each histological defect and genotype are indicated in bars. (**G**) Immunohistochemical analysis of PCNA in 4-month-old WT, prKO, and prwKO testes. (**H**) Quantification of stromal PCNA⁺ cells represented as a percentage of cells in 4-month-old WT, prKO, and prwKO testes. Welch's 1-way ANOVA was followed by Games-Howell multiple-correction test. (**I**) *Ki67* transcripts of RT-qPCR analysis in 4-month-old prKO and prwKO testes. Statistical analysis was performed using Student's *t* test. (**J**) *Axin2* and *Ccdc80* transcripts of RT-qPCR analysis in 4-month-old WT, prKO, and prwKO testes. One-way ANOVA was followed by Tukey's multiple-correction test, and Welch's 1-way ANOVA was followed by Games-Howell multiple-correction test. (**K**) Coimmunostaining for β-catenin and WNT4 in CNC-LCCSCTs. Bars represent the mean per group ± SD. Scale bars: 100 μm. Original magnification, ×2.65 (insets, **G**); ×2.00 (insets, **K**). $^*P < 0.05$; $^{**}P < 0.01$; $^{***}P < 0.001$.

Discussion

To gain a better understanding of CNC-LCCSCT pathogenesis, we performed *Prkar1a* inactivation either targeted in the entire somatic compartment or in main subtypes of testicular somatic cells in mice. These unique mouse models, offering a more homogeneous sampling than human biopsies, provide access to early stages of pathology as well as advanced stages of tumor development. In addition, they constitute invaluable tools for deciphering crosstalks between deregulated molecular circuits.

The prKO mice develop all the alterations identified in CNC-LCCSCT patients (bilateral tumors arranged in solid cords, fibrosis, and calcifications associated with the increased expression of sex cord tumor markers [*Calb2*, *Ctnnb1*, *Inha*, and *S100*]), and therefore, they constitute a reliable model for exhaustive analyses of the molecular alterations caused by lack of the R1α subunit.

The ontogenetic analysis of the prKO model showed that major changes in endocrine activities, histological features, and the testicular transcriptome did not appear before the prepubertal stage; thus

they occurred with a delay compared with early fetal inactivation of the *Prkar1a* gene. This suggests that lack of the R1α subunit has little impact on testicular ontogeny during the fetal and perinatal periods. Conversely, in the princeps CNC mouse model carrying a constitutive homozygous *Prkar1a* deletion, lethality occurred as early as E8.5 due to growth defects in mesoderm-derived cardiac tissues, which can be rescued by further inactivation of the *Prkaca* gene encoding the Cα catalytic subunit of PKA (10). Possible compensatory mechanisms involving other PKA regulatory subunits, PKA inhibitor peptides, or phosphodiesterases in the developing fetal prKO testis remain to be determined. It should be noted that, although the occurrence of LCCSCTs in CNC patients may be observed as early as the first decade (5, 6, 53), no cases of testicular abnormalities have been reported at birth, suggesting that in humans, as in our mouse models, the *Prkar1a* mutation does not cause abnormal fetal gonadal development. In our models, the total absence of tumors in the double-mutant testis *Sf1:Cre,Prkar1a*$^{fl/fl}$*, Prkaca*$^{+/-}$ demonstrates that the induction of testicular lesions of prKO mice relies on the unrepressed catalytic activity of PKA rather than on a defect of the R1α subunit per se, in agreement with previous observations in other tissue lesions of the CNC (9, 54, 55). The prKO testes transcriptomic analysis revealed a modified expression profile for more than 1328 genes in the 2-month-old testis associated with tissue and functional homeostasis disruption, which reflects the complexity of the mechanisms resulting from *Prkar1a* loss in all gonadal somatic cells. In addition, molecular signatures and histological analyses revealed germ-line damages resulting from paracrine/nonautonomous cell actions. Very few studies have looked at the infertilities associated with *PRKAR1A* mutations in CNC patients; nevertheless, previous studies showed alterations in male GCs (55, 56) as a consequence of *PRKAR1A* loss in somatic cells and GCs. The comparison of gene signatures of prKO testis with those of lrKO and srKO models allowed for demonstration that *Prkar1a* inactivation restricted to SCs led to a progressive germ-line loss from the prepubertal stages, resulting in infertility at puberty. In both prKO and srKO STs, the underlying mechanisms include an increase in GC apoptosis and formation of GC syncytia containing vacuoles reminiscent of those observed at the LCCSCT periphery in CNC patients. The massive apoptosis and desquamation mask the exacerbated increase in germ population that occurs in the first spermatogenesis waves in srKO testis compared with littermate control mice. These apoptotic events differ from the phenotypes observed in mouse models bearing FSH-R signaling upregulation (tgFSH/hpg and MT-hFSH-R mice) in which, at best, only an enhancement of spermatogonia proliferation and meiotic/postmeiotic cell survival was observed (57, 58). Likewise, the activating mutations of FSH signaling described in human species do not affect the fertility of male patients (59, 60). Notably, an activating mutation of the FSH-R has been shown to autonomously sustain spermatogenesis in a hypophysectomized man, and this has been further validated in mouse models (61, 62). While it is well documented that the FSH/FSH-R/PKA pathway exerts its effects on the germ line via the production of SC growth signals, such as FGF2, GDNF, or KIT-L (33, 34, 63–67), our data indicate that constitutive activation of PKA in the SC triggers additional circuits that oppose actions normally arising from FSH/FSH-R signaling. Indeed, the transcriptomic analysis of prKO and srKO testes allowed us to point out a very strong WNT4 signal overproduction by mutant SCs. This observation is reminiscent of a previously described mouse model showing that SC-specific β-catenin constitutive activation leads to WNT4 overproduction and a subsequent decrease in the spermatogonial stem cell activity responsible for apoptosis and loss of GCs (42). In a report analyzing the testis of *E2f1-Wnt4* double-KO mice, Jorgez et al. specified that germ-line maintenance was dependent on *Wnt4* repression by *E2f1*, supporting a role of *Wnt4* in GC survival (68). Interestingly, in response to *Prkar1a* inactivation, our models also show WNT/β-catenin activation attested by upregulation of *Wnt4* and *Ctnnb1* expression and by increased accumulation of the β-catenin active form (i.e., dephosphorylated). In CNC patients, we also observed intracytoplasmic accumulation of β-catenin in SCs from testicular biopsies. Moreover, we found that about 36% of the genes upregulated in SCs from the *Ctnnb1*$^{tm1Mmt/+}$*; Amhr2*$^{tm3(cre)Bhr/+}$ model (42) are also upregulated in srKO testis, indicating the establishment of partially common molecular alterations resulting from the mobilization of the WNT/β-catenin signaling pathway in the two models. Finally, by suppressing germ-line apoptosis in srwKO mice via *Wnt4* inactivation, we confirmed the hypothesis of a converging phenotype between these different mutant models and demonstrated the cooperation between overactive PKA and WNT/β-catenin signaling in triggering germ-line alterations. However, unlike the observations of Boyer and colleagues, our analyses of prKO and srKO mutants indicate that PKA-induced *Wnt4* upregulation is not associated with acquisition of the granulosa *Fst* marker. Moreover, SCs maintain high *Sox9* expression, while both *Foxl2* and *Rspo1* expression are absent from all *Prkar1a* mutant testis (42). Together, the comparison of *Ctnnb1*$^{tm1Mmt/+}$*;Amhr2*$^{tm3(cre)Bhr/+}$ and prKO or srKO models suggests that constitutive activation of PKA both triggers massive overexpression of *Wnt4* and opposes the *Wnt4* female identity programming function, possibly by reinforcing the maintenance of protesticular factors such as SOX9, which regulates its own expression and represses *Foxl2* expression (16, 69–72). Transcriptomic and IHC analyses reveal an increased production of the BTB proteins and SC-associated cytoskeleton components in both mutant murine and CNC human STs. These junctional proteins are known to be positively controlled by various factors, including SOX9 and also the androgen and mTOR-signaling pathways, both of which are enhanced in our models (51, 69, 73). However, an alteration of GC progression into the adluminal tubular compartment due to paracellular extension of SC BTB proteins is unlikely to contribute to GC apoptosis in *PRKAR1A*/*Prkar1a* mutant human and murine testes. Indeed, in double-mutant prwKO STs, the extended distribution of BTB proteins persists, while the GC apoptosis blockade partially restores the accumulation of elongated spermatids. This indicates that structural changes in the BTB induced by *Prkar1a* loss are mostly independent of WNT4 action and do not prevent spermatogenesis. Nevertheless, the SC nuclei delocalization and BTB functional failure are loss of polarity criteria suggestive of SC maturity disturbance in the srKO and prKO testes. However, unlike in the *Ctnnb1*$^{tm1Mmt/+}$*; Amhr2*$^{tm3(cre)Bhr/+}$ model (74), in srKO and prKO STs, SCs do not proliferate and no overproduction of AMH persists at adulthood. These data indicate that activation of PKA in SCs induces specific prodifferentiating actions that counteract some exacerbated effects of WNT/β-catenin signaling observed in mouse mod-

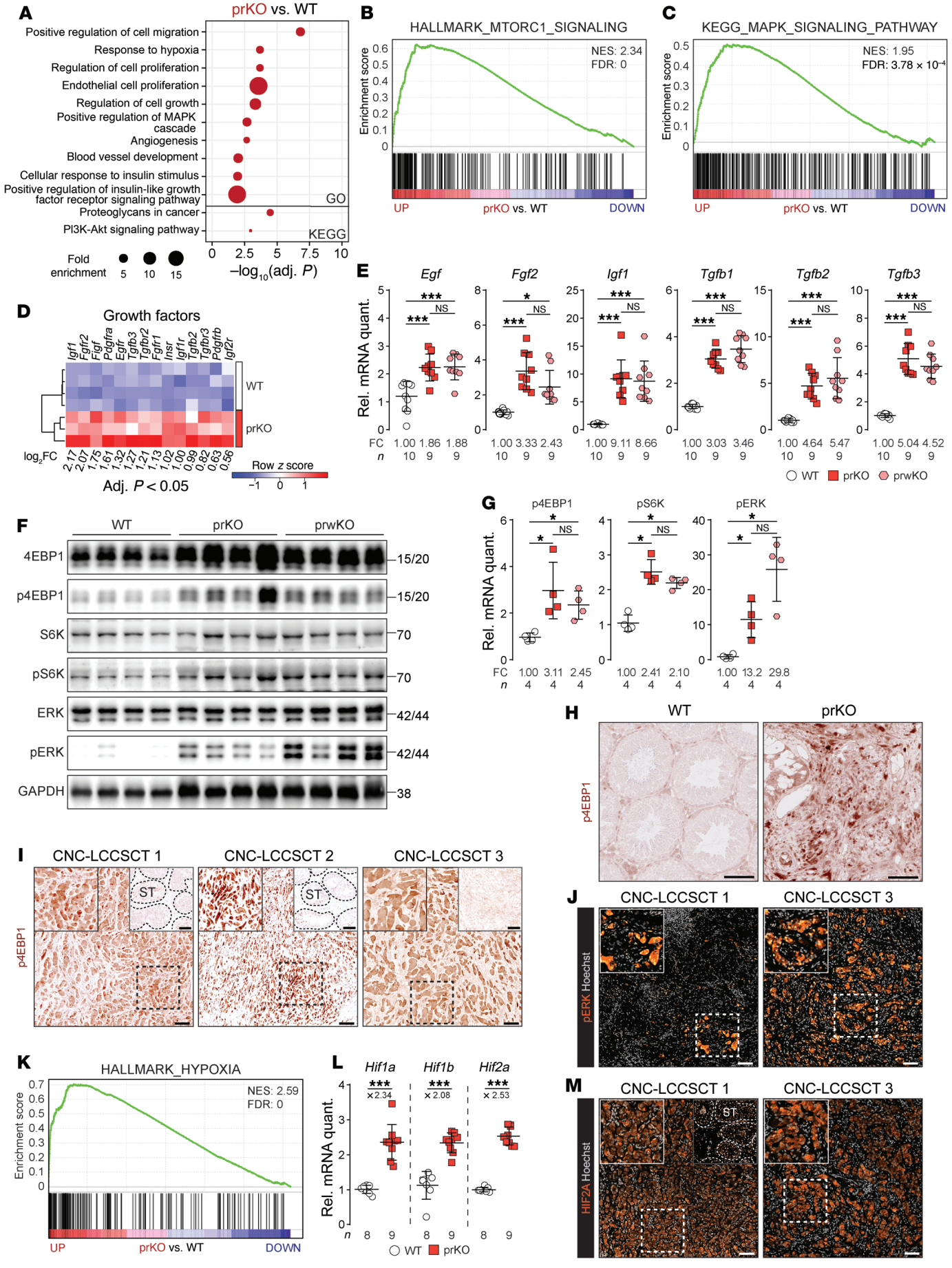
A
prKO vs. WT
Positive regulation of cell migration
Response to hypoxia
Regulation of cell proliferation
Endothelial cell proliferation
Regulation of cell growth
Positive regulation of MAPK cascade
Angiogenesis
Blood vessel development
Cellular response to insulin stimulus
Positive regulation of insulin-like growth factor receptor signaling pathway
Proteoglycans in cancer
PI3K-Akt signaling pathway
GO
KEGG
Fold enrichment 5 10 15
0 2.5 5 7.5 10
–log10(adj. P)
B
HALLMARK_MTORC1_SIGNALING
NES: 2.34
FDR: 0
Enrichment score
UP
prKO vs. WT
DOWN
C
KEGG_MAPK_SIGNALING_PATHWAY
NES: 1.95
FDR: 3.78 × 10−4
Enrichment score
UP
prKO vs. WT
DOWN
D
Growth factors
Igf1 Fgfr2 Figf Pdgfra Egfr Tgfb3 Tgfbr2 Fgfr1 Insr Igf1r Tgfb2 Tgfbr3 Pdgfrb Igf2r
WT
prKO
log2FC
2.17 2.07 1.75 1.61 1.32 1.27 1.21 1.13 1.02 1.00 0.99 0.82 0.63 0.56
Row z score
−1 0 1
Adj. P < 0.05
E
Egf Fgf2 Igf1 Tgfb1 Tgfb2 Tgfb3
Rel. mRNA quant.
***
NS
FC 1.00 1.86 1.88 | 1.00 3.33 2.43 | 1.00 9.11 8.66 | 1.00 3.03 3.46 | 1.00 4.64 5.47 | 1.00 5.04 4.52
n 10 9 9 | 10 9 9 | 10 9 9 | 10 9 9 | 10 9 9 | 10 9 9
WT prKO prwKO
F
WT prKO prwKO
4EBP1
p4EBP1
S6K
pS6K
ERK
pERK
GAPDH
15/20
15/20
70
70
42/44
42/44
38
G
p4EBP1 pS6K pERK
Rel. mRNA quant.
*
NS
FC 1.00 3.11 2.45 | 1.00 2.41 2.10 | 1.00 13.2 29.8
n 4 4 4 | 4 4 4 | 4 4 4
H
WT
prKO
p4EBP1
I
CNC-LCCSCT 1
CNC-LCCSCT 2
CNC-LCCSCT 3
ST
p4EBP1
J
CNC-LCCSCT 1
CNC-LCCSCT 3
pERK Hoechst
K
HALLMARK_HYPOXIA
NES: 2.59
FDR: 0
Enrichment score
UP
prKO vs. WT
DOWN
L
Hif1a Hif1b Hif2a
***
×2.34 ×2.08 ×2.53
Rel. mRNA quant.
n 8 9 | 8 9 | 8 9
WT prKO
M
CNC-LCCSCT 1
CNC-LCCSCT 3
ST
HIF2A Hoechst

Figure 8. PKA activation induces mTOR, MAPK, and hypoxia pathways in tumor of human LCCSCTs. (**A**) GO enrichment scores of tumor development–associated pathways based on gene list specifically deregulated in 2-month-old prKO testis compared with srKO and lrKO testes. (**B** and **C**) GSEA of microarray gene expression data showing positive enrichment of hallmark-MTORC1 signaling gene list (**B**) and KEGG-MAPK signaling pathway gene list (**C**) in 2-month-old prKO testis compared with WT. (**D**) Heatmap representing the median-centered expression of significantly deregulated growth factors and associated receptors (adj. $P < 0.05$) in 2-month-old prKO ($n = 3$–4) compared with WT ($n = 4$). (**E**) RT-qPCR analysis of *Egf*, *Fgf2*, *Igf1*, *Tgfb1*, *Tgfb2*, and *Tgfb3* transcripts in 4-month-old WT, prKO, and prwKO testes. One-way ANOVA was followed by Tukey's multiple-correction test, Welch's 1-way ANOVA was followed by Games-Howell multiple-correction test, and Kruskal-Wallis test was followed by Dunn's multiple-correction test. (**F**) Western blot analysis of p4EBP1, pS6K, and pERK accumulation in 4-month-old WT, prKO, and prwKO testes. (**G**) Phosphorylated protein quantification over total proteins. Statistical analysis was performed using Student's *t* test. (**H**) Immunohistochemical detection of p4EBP1 in 4-month-old WT and prKO testes. (**I** and **J**) Immunohistochemical detection of p4EBP1 and pERK in CNC-LCCSCTs. Insets at the top right (**I**) correspond to areas adjacent to the tumor characterized by low p4EBP1 staining. (**K**) GSEA of microarray gene expression data showing positive enrichment of hallmark-hypoxia gene list (genes upregulated in response to hypoxia) in 2-month-old prKO testis compared with WT. (**L**) *Hif1a*, *Hif1b*, and *Hif2a* transcript analysis in 4-month-old WT and prKO testes. Statistical analysis was performed using Welch's or Student's *t* test. (**M**) Immunohistochemical detection of HIF2A in CNC-LCCSCTs. Bars represent the mean per group ± SD. Scale bars: 100 μm. Original magnification, ×1.60 (left insets, **I**, **J**, and **M**); ×0.80 (right insets, **I** and **M**). $^{*}P < 0.05$; $^{***}P < 0.001$.

els developed by Tanwar and colleagues and Boyer and colleagues (42, 74). In particular, the *Prkar1a* mutant SCs display an early and much higher increase of *Inha* transcripts than any other TGF-β family genes. This could play a major role in limiting SC proliferation induced by the WNT/β-catenin pathway, as suggested by previous studies on inhibin-α autocrine actions (75, 76). In addition, previously defined molecular signatures attesting to SC maturation under the control of androgens (73, 77, 78) and thyroid hormone (79, 80) remain unchanged in srKO and prKO transcriptomes at the prepubertal stage (2 weeks), but increase at adulthood. Finally, whether PKA-induced *Wnt4* expression results from PKA-dependent increased *Ctnnb1* expression and/or PKA-mediated β-catenin activation mechanisms, as described in ovarian granulosa and luteal cells (81–83), remains to be explored for *Prkar1a*$^{-/-}$ SCs. In contrast to the srKO and lrKO models, prKO mice develop testicular tumors with histological and molecular characteristics similar to those of LCCSCTs of CNC patients. This indicates that tumor onset is dependent on both SC and stromal proliferative signals activated by *Prkar1a* loss in both testicular compartments. This unprecedented situation in genetic models of testicular tumors underlines the role of paracrine interactions in CNC-LCCSCT pathogenesis. Among the upregulated signals in response to *Prkar1a* loss, *Wnt4* expression is present at significantly higher levels in the prKO than in the srKO model and increases in parallel with tumor development, suggesting that tumor cells could be an additional source of the WNT4 signal. Indeed, our IHC analyses on human CNC-LCCSCT biopsies confirm that WNT4 is accumulated in cells within the tumor mass. This increase in the WNT4 signal is associated with an increase in the expression of WNT/β-catenin responsive genes and therefore raises the question of its involvement in tumor promotion of LCCSCTs. The double-mutant prwKO model study demonstrates that the WNT4 signal is a limiting component in the growth factor set that conditions CNC-LCCSCT development. Indeed, in the prwKO testis, *Wnt4* loss abolishes tumor formation and drastically reduces the stromal proliferation rate compared with in the prKO testis. Importantly, *Wnt4* loss does not prevent the overall WNT/β-catenin pathway activation in the prwKO testis, given that the WNT5A ligand remains produced in excess and that PKA-dependent phosphorylation can directly favor β-catenin stabilization (84). In this context, it can be assumed that *Wnt4* inactivation sufficiently reduces the strength of the pathway to slow down stromal proliferation below a limiting threshold for tumor formation. Residual stromal hyperplasia in the double-mutant testis also confirms the impact of additional PKA-activated growth signals independently of *Wnt4* expression. Previously, a mouse model (*Ctnnb1*$^{tm1Mmt/+}$*; Tg[AMH-cre]1Flor*) expressing a stabilized form of β-catenin targeted in SCs developed testicular cancers with molecular and invasive characteristics different from those found in tumors of the prKO model and human CNC-LCCSCT and that arose independently of the influence of the stromal compartment (85). In humans, while *WNT4* duplications have been associated with chromosome 46, XY testicular dysgenesis and ambiguous external genitalia occur beginning with fetal development, and despite the recurrent *CTNNB1*-activating mutations in SCST cells (86), WNT4-activating mutations remain poorly documented in testicular cancer, unlike in other tissues, i.e., ovaries (87). These observations reinforce the idea that, although the WNT4 signal is a mandatory actor, it does not support on its own the formation of the LCCSCT.

Although *Fgf2*, *Egf*, *Igf1*, and *Tgfb1-3* gene expression was also strongly upregulated in prKO testes, it remained elevated in prwKO testes, suggesting that it could participate in maintaining the moderate proliferation observed in the prwKO residual stromal hyperplasia. A functional cooperation of WNT4 and TGF-β pathways in tumor growth and in its fibrotic enrichment is not excluded. Indeed, studies showed that the TGF-β/SMAD3 pathway mobilized the WNT/β-catenin pathway in smooth muscle cell proliferation (88) and in the development of pathological dermal fibrosis in a p38-dependent manner by decreasing the accumulation of WNT pathway negative regulators (89). In the prwKO testis, tumor suppression is associated with a systematic reduction in the fibrotic areas that characterizes LCCSCTs. Consistent with the increase of FGF2, EGF, IGF1, and KIT-L, their converging signaling pathways (MAPK and PI3K/AKT/mTOR; ref. 90) are activated in the LCCSCTs of CNC patients and prKO mice, supporting their involvement in tumoral expansion. In addition, several studies in different tissues have shown that TGF-β signaling activates the expression of *miR-21* targeting PTEN production and activity, lifting the inhibition of AKT/mTORC1 signaling, which in turn amplifies the oncogenic signal, matrix protein synthesis, and fibrosis (91, 92). As revealed by the prKO transcriptomic analyses, *miR-21* upregulation argues in favor of such a TGF-β/mTOR crosstalk in the development of CNC-LCCSCTs (NCBI's Gene Expression Omnibus [GEO] GSE159150). The mTOR pathway was previously shown to be activated in SCs in response to *Lkb1* inactivation in a study aiming to understand the molecular mechanisms involved in testicular alterations in PJS (52). In this study, mTOR pathway activation induced by disruption

of the LKB1/AMPK pathway resulted in SC polarity and BTB alterations, resumption of their proliferative activities, and loss of germ cells. However, no LCCSCT-type tumorigenesis was shown in this work, suggesting that, as in CNC-LCCSCTs, PJS-LCCSCT development could be dependent on signals activated by the mutation that should be present both in SCs and other testicular compartments. In the prKO model, PKA-induced mTORC1 pathway activation in both the tumor and in SCs does not imply any alteration of the expression nor activity of AMPK, indicating that *Prkar1a* and *Lkb1* mutations lead to mTOR pathway mobilization by a different way. In previous work examining the molecular consequences of *Prkar1a* loss in the adrenal cortex leading to primary pigmented nodular adrenocortical disease (PPNAD) lesions, we showed that PKA activity triggers an increase in TGF-β family member expression and directly activates mTORC1 to promote cell survival (93, 94). Intriguingly and in contrast with our present results in testis, we previously showed a marked reciprocal antagonism of the WNT/β-catenin and PKA pathways in adrenocortical zonation and tumorigenesis (95), since *Prkar1a* inactivation in the adrenal cortex represses zona glomerulosa identity and opposes the prooncogenic action of WNT/β-catenin signaling. Our work suggests that in the CNC, the molecular modalities of PKA action in PPNAD and LCCSCT expansion do not fully overlap. This incomplete overlap would probably rely on nonidentical PKA-controlled key networks involved in tissue homeostasis of adrenal and testis that yet arise from common primordium. In this context, the question of WNT-PKA cooperation in the pathogenesis of the CNC ovary remains unanswered.

In conclusion, our data demonstrate that the chronic unrepressed PKA activity in somatic testis cells of CNC patients unbalances testicular homeostasis by generating a gonadal paracrine network crisis that includes an aberrant postnatal WNT4 signal acting as a driving force for shaping intratubular lesions and tumor expansion.

Methods

Mice. *Sf1:Cre* (95), *Amh:Cre* (22), or *Scc:Cre* (23), *Prkar1a*$^{fl/fl}$ (9), *Wnt4*$^{fl/fl}$ (96), and *Prkaca*$^{+/-}$ mice (97) have been described previously. The following mouse crossings were enabled to generate multiple models: prKO (*Sf1:Cre,Prkar1a*$^{fl/fl}$, progenitor cell *R1a* KO), prKO/*Prkaca*$^{+/-}$ (*Sf1:Cre,Prkar1a*$^{fl/fl}$,*Prkaca*$^{+/-}$ with global *Prkaca* haploinsufficiency), srKO (*Amh:Cre,Prkar1a*$^{fl/fl}$, SC *R1a* KO), lrKO (*Scc:Cre,Prkar1a*$^{fl/fl}$, LC *R1a* KO), double-mutant prwKO (*Sf1:Cre,Prkar1a*$^{fl/fl}$,*Wnt4*$^{fl/fl}$), and srwKO (*Amh:Cre,Prkar1a*$^{fl/fl}$,*Wnt4*$^{fl/fl}$). Mouse models used are listed in Supplemental Table 1. Mouse models were enriched with the *Rosa26R-mtmg* system to follow recombination events. Control animals were *Prkar1a*$^{fl/fl}$ or *Prkar1a*$^{fl/fl}$,*Wnt4*$^{fl/fl}$ littermates, depending on experiments.

Samples from patients. Histological slides of testis lesions were obtained from 3 CNC patients. Human adult healthy testis sections were used as controls for histological analyses (UM-HuFPT151, CliniSciences). The clinical data summary of CNC patients is provided in Supplemental Table 2.

Hormonal measurements. Mice were euthanized by decapitation, and blood was collected between 9:00 am and 10:00 am, since animals were maintained on a 12-hour light (07:00 am to 7:00 pm)/12-hour dark cycle. Plasma testosterone concentrations were determined using an ELISA kit. Plasma LH and FSH concentrations were determined using a multiplex assay (MPTMAG-49K, Merck Millipore).

Histology. Testes were embedded in paraffin, and 5 μm sections were prepared. H&E, Masson's trichrome, alizarin red S, and toluidine blue stainings were performed depending on experiments. Detailed descriptions of immunohistochemistry and TUNEL staining are provided in the Supplemental Methods and Supplemental Table 3.

Microarray analyses. Gene expression profiles for 2-week-old and 2-month-old WT, prKO, srKO, and lrKO testes were analyzed using Affymetrix Mouse Gene 2.0 ST arrays. Raw and processed data have been deposited in NCBI's GEO database (GSE159150). Further description of methods is provided in Supplemental Methods.

RT-qPCR. Total mRNAs were extracted and reverse transcribed as previously described (95). Primers used are listed in Supplemental Table 4. Relative gene expression was obtained by the ΔΔCt method with normalization to average expression of actin.

Western blot. Thirty micrograms of total proteins were loaded on 8% SDS-PAGE gel, transferred on nitrocellulose, and detected with primary antibodies (Supplemental Table 3). Signals were quantified with the ChemiDoc MP Imaging System camera system and Image Lab software (Bio-Rad).

Statistics. Statistical analyses were performed using R and GraphPad Prism 8. Numbers of mice per group are reported in the figures. All bars represent the mean ± SD. Normality of data was assessed using the Shapiro-Wilk normality test. For comparison of 2 groups, variance equality was tested using the *F* test. Statistical analysis of 2 groups was performed by 2-tailed Student's *t* test with or without Welch's correction (as a function of variance) for normally distributed data or by Mann-Whitney *U* test for not normally distributed data. For comparison of multiple groups, variance equality was tested using the Brown-Forsythe test. Statistical analysis of multiple groups was performed by 1-way ANOVA followed by Tukey's multiple-correction test or Welch's 1-way ANOVA followed by the Games-Howell multiple-correction test (as a function of variance) for normally distributed data or by Kruskal-Wallis test followed by Dunn's multiple-correction test for not normally distributed data. Statistical analysis of hyperplasia/tumor proportion was performed by 2-proportion Fisher's test.

Study approval. All patients underwent tumor resection and gave informed consent for the use of their resected tissues for research purposes. Mouse experiments were conducted according to French and European directives for the use and care of animals for research purposes and were approved by the Comité d'Éthique pour l'Expérimentation Animale en Auvergne, C2EA-02, at Institut National de Recherche pour l'Agriculture, l'Alimentation et l'Environnement, Research Center Clermont-Theix, France (C2E2A).

Author contributions

CD, AMLM, and AM designed research. FG, A Swain, and SJV provided *Cre*-expressing and *Wnt4*-floxed mice. CAS, CK, FRF, HL, and AGL provided human tumor samples and clinical data. CD, DD, AL, AMLM, NM, IP, JCP, ISB, and JW performed experiments. CD, AMLM, AM, ISB, and A Septier analyzed data. CD and AMLM wrote the paper. AM, IT, and PV edited the paper.

Acknowledgments

We acknowledge C. Lyssikatos (now at the University of Indiana, Indianapolis, Indiana, USA) and E. Belyavskaya (NICHD, NIH, Bethesda, Maryland, USA) for the coordination of clinical studies

and sample retrieval and shipment under protocol 95CH0059. We thank A. François and J.C. Sabourin (head of the CRB-TMT in Rouen) for providing human tumor samples and N. Ghyselinck (Institut de Génétique et de Biologie Moléculaire et Cellulaire [IGBMC], Illkirch, France) for his expertise and advice on the germ line. We thank K. Ouchen, S. Plantade, and P. Mazuel for animal care, C. Damon-Soubeyrand (Anipath-Clermont) and J.P. Saru for their technical assistance, and Y. Renaud for management of the bioinformatic platform. This work was funded through institutional support from Université Clermont-Auvergne, CNRS, INSERM, the French government IDEX-ISITE initiative 16-IDEX-0001 (CAP 20-25), and grants from Fondation Association pour la Recherche sur le Cancer (to CD), Agence Nationale pour la Recherche (ANR-14-CE12-0007-01-DevMiCar to AM), and the NICHD, NIH intramural research program (to CAS).

Address correspondence to: Anne-Marie Lefrançois-Martinez, GReD Institute, 28 place Henri Dunant, Faculté de Médecine-CRBC 63001 Clermont Ferrand CEDEX 01, France. Phone: 33.0.4.73.40.77.59; Email: a-marie.lefrancois-martinez@uca.fr.

1. Bertherat J, et al. Mutations in regulatory subunit type 1A of cyclic adenosine 5′-monophosphate-dependent protein kinase (PRKAR1A): phenotype analysis in 353 patients and 80 different genotypes. *J Clin Endocrinol Metab*. 2009;94(6):2085–2091.
2. Stratakis CA, et al. Clinical and molecular features of the Carney complex: diagnostic criteria and recommendations for patient evaluation. *J Clin Endocrinol Metab*. 2001;86(9):4041–4046.
3. Boikos SA, Stratakis CA. Carney complex: the first 20 years. *Curr Opin Oncol*. 2007;19(1):24–29.
4. Correa R, et al. Carney complex: an update. *Eur J Endocrinol*. 2015;173(4):M85–M97.
5. Ulbright TM, et al. Intratubular large cell hyalinizing Sertoli cell neoplasia of the testis: a report of 8 cases of a distinctive lesion of the Peutz-Jeghers syndrome. *Am J Surg Pathol*. 2007;31(6):827–835.
6. Gourgari E, et al. Large-cell calcifying Sertoli cell tumors of the testes in pediatrics. *Curr Opin Pediatr*. 2012;24(4):518–522.
7. Carney JA, et al. The complex of myxomas, spotty pigmentation, and endocrine overactivity. *Medicine (Baltimore)*. 1985;64(4):270–283.
8. Kratzer SS, et al. Large cell calcifying Sertoli cell tumor of the testis: contrasting features of six malignant and six benign tumors and a review of the literature. *Am J Surg Pathol*. 1997;21(11):1271–1280.
9. Kirschner LS, et al. A mouse model for the Carney complex tumor syndrome develops neoplasia in cyclic AMP-responsive tissues. *Cancer Res*. 2005;65(11):4506–4514.
10. Amieux PS, McKnight GS. The essential role of RI alpha in the maintenance of regulated PKA activity. *Ann N Y Acad Sci*. 2002;968:75–95.
11. Mesa H, et al. Comparative immunomorphology of testicular Sertoli and sertoliform tumors. *Hum Pathol*. 2017;61:181–189.
12. Idrees MT, et al. The World Health Organization 2016 classification of testicular non-germ cell tumours: a review and update from the International Society of Urological Pathology Testis Consultation Panel. *Histopathology*. 2017;70(4):513–521.
13. Roth LM, et al. Perspectives on testicular sex cord-stromal tumors and those composed of both germ cells and sex cord-stromal derivatives with a comparison to corresponding ovarian neoplasms. *Hum Pathol*. 2017;65:1–14.
14. Toppari J, et al. Inhibin gene expression in a large cell calcifying Sertoli cell tumour and serum inhibin and activin levels. *APMIS*. 1998;106(1):101–112.
15. Sato K, et al. Large cell calcifying Sertoli cell tumor of the testis: comparative immunohistochemical study with Leydig cell tumor. *Pathol Int*. 2005;55(6):366–371.
16. Rotgers E, et al. At the crossroads of fate-somatic cell lineage specification in the fetal gonad. *Endocr Rev*. 2018;39(5):739–759.
17. Nordhoff V, et al. Constitutively active mutations of G protein-coupled receptors: the case of the human luteinizing hormone and follicle-stimulating hormone receptors. *Arch Med Res*. 1999;30(6):501–509.
18. Huhtaniemi I, et al. Genetically modified mouse models in studies of luteinising hormone action. *Mol Cell Endocrinol*. 2006;252(1–2):126–135.
19. Casarini L, et al. Effects of polymorphisms in gonadotropin and gonadotropin receptor genes on reproductive function. *Rev Endocr Metab Disord*. 2011;12(4):303–321.
20. McGee SR, Narayan P. Precocious puberty and Leydig cell hyperplasia in male mice with a gain of function mutation in the LH receptor gene. *Endocrinology*. 2013;154(10):3900–3913.
21. Bingham NC, et al. Development of a steroidogenic factor 1/Cre transgenic mouse line. *Genesis*. 2006;44(9):419–424.
22. Lécureuil C, et al. Sertoli and granulosa cell-specific Cre recombinase activity in transgenic mice. *Genesis*. 2002;33(3):114–118.
23. Buaas FW, et al. In vivo evidence for the crucial role of SF1 in steroid-producing cells of the testis, ovary and adrenal gland. *Development*. 2012;139(24):4561–4570.
24. Mruk DD, Cheng CY. The mammalian blood-testis barrier: its biology and regulation. *Endocr Rev*. 2015;36(5):564–591.
25. Cai J,et al. Increased expression of dermatopontin and its implications for testicular dysfunction in mice. *Mol Med Rep*. 2016;13(3):2431–2438.
26. Takeuchi T, et al. Extracellular matrix dermatopontin modulates prostate cell growth in vivo. *J Endocrinol*. 2006;190(2):351–361.
27. Zhou W, et al. Changes in gene expression in somatic cells of rat testes resulting from hormonal modulation and radiation-induced germ cell depletion. *Biol Reprod*. 2010;82(1):54–65.
28. Ohta H, et al. Regulation of proliferation and differentiation in spermatogonial stem cells: the role of c-kit and its ligand SCF. *Development*. 2000;127(10):2125–2131.
29. Dolci S, et al. Signaling through extracellular signal-regulated kinase is required for spermatogonial proliferative response to stem cell factor. *J Biol Chem*. 2001;276(43):40225–40233.
30. Sato T, et al. Testis tissue explantation cures spermatogenic failure in c-Kit ligand mutant mice. *Proc Natl Acad Sci U S A*. 2012;109(42):16934–16938.
31. Cardoso HJ, et al. The stem cell factor (SCF)/c-KIT signalling in testis and prostate cancer. *J Cell Commun Signal*. 2017;11(4):297–307.
32. Morales JK, et al. Mast cell homeostasis and the JAK-STAT pathway. *Genes Immun*. 2010;11(8):599–608.
33. Yan W, et al. Stage-specific regulation of stem cell factor gene expression in the rat seminiferous epithelium. *Endocrinology*. 1999;140(3):1499–1504.
34. Grimaldi P, et al. Cyclic adenosine monophosphate (cAMP) stimulation of the kit ligand promoter in sertoli cells requires an Sp1-binding region, a canonical TATA box, and a cAMP-induced factor binding to an immediately downstream GC-rich element. *Biol Reprod*. 2003;69(6):1979–1988.
35. Walczak EM, et al. Wnt signaling inhibits adrenal steroidogenesis by cell-autonomous and non-cell-autonomous mechanisms. *Mol Endocrinol*. 2014;28(9):1471–1486.
36. Mizusaki H, et al. Dax-1 (dosage-sensitive sex reversal-adrenal hypoplasia congenita critical region on the X chromosome, gene 1) gene transcription is regulated by wnt4 in the female developing gonad. *Mol Endocrinol*. 2003;17(4):507–519.
37. Gallegos TF, et al. A protein kinase A and Wnt-dependent network regulating an intermediate stage in epithelial tubulogenesis during kidney development. *Dev Biol*. 2012;364(1):11–21.
38. Yu HF, et al. Bmp2 regulates Serpinb6b expression via cAMP/PKA/Wnt4 pathway during uterine decidualization. *J Cell Mol Med*. 2020;24(12):7023–7033.
39. Rajaram RD, et al. Progesterone and Wnt4 control mammary stem cells via myoepithelial crosstalk. *EMBO J*. 2015;34(5):641–652.
40. Vainio S, et al. Female development in mammals is regulated by Wnt-4 signalling. *Nature*. 1999;397(6718):405–409.
41. Liu CF, et al. Sex-specific roles of beta-catenin in mouse gonadal development. *Hum Mol Genet*. 2009;18(3):405–417.
42. Boyer A, et al. CTNNB1 signaling in sertoli cells downregulates spermatogonial stem cell activity via WNT4. *PLoS One*. 2012;7(1):e29764.
43. Kimura T, et al. The stabilization of beta-catenin leads to impaired primordial germ cell development via aberrant cell cycle progression. *Dev Biol*. 2006;300(2):545–553.

44. Chassot AA, et al. Constitutive WNT/CTNNB1 activation triggers spermatogonial stem cell proliferation and germ cell depletion. *Dev Biol*. 2017;426(1):17–27.
45. Corda G, Sala A. Non-canonical WNT/PCP signalling in cancer: Fzd6 takes centre stage. *Oncogenesis*. 2017;6(7):e364.
46. Pitetti JL, et al. An essential role for insulin and IGF1 receptors in regulating sertoli cell proliferation, testis size, and FSH action in mice. *Mol Endocrinol*. 2013;27(5):814–827.
47. Khan SA, et al. Follicle-stimulating hormone amplifies insulin-like growth factor I-mediated activation of AKT/protein kinase B signaling in immature rat Sertoli cells. *Endocrinology*. 2002;143(6):2259–2267.
48. Wandzioch E, et al. Activation of the MAP kinase pathway by c-Kit is PI-3 kinase dependent in hematopoietic progenitor/stem cell lines. *Blood*. 2004;104(1):51–57.
49. Cannarella R, et al. Effects of the insulin-like growth factor system on testicular differentiation and function: a review of the literature. *Andrology*. 2018;6(1):3–9.
50. Boyer A, et al. mTOR regulates gap junction alpha-1 protein trafficking in sertoli cells and is required for the maintenance of spermatogenesis in mice. *Biol Reprod*. 2016;95(1):13.
51. Mok KW, et al. Regulation of blood-testis barrier (BTB) dynamics during spermatogenesis via the "Yin" and "Yang" effects of mammalian target of rapamycin complex 1 (mTORC1) and mTORC2. *Int Rev Cell Mol Biol*. 2013;301:291–358.
52. Tanwar PS, et al. Altered LKB1/AMPK/TSC1/TSC2/mTOR signaling causes disruption of Sertoli cell polarity and spermatogenesis. *Hum Mol Genet*. 2012;21(20):4394–4405.
53. Washecka R, et al. Testicular tumors in Carney's complex. *J Urol*. 2002;167(3):1299–1302.
54. Griffin KJ, et al. Down-regulation of regulatory subunit type 1A of protein kinase A leads to endocrine and other tumors. *Cancer Res*. 2004;64(24):8811–8815.
55. Burton KA, et al. Haploinsufficiency at the protein kinase A RI alpha gene locus leads to fertility defects in male mice and men. *Mol Endocrinol*. 2006;20(10):2504–2513.
56. Wieacker P, et al. Male infertility as a component of Carney complex. *Andrologia*. 2007;39(5):196–197.
57. Kumar TR, et al. Transgenic models to study gonadotropin function: the role of follicle-stimulating hormone in gonadal growth and tumorigenesis. *Mol Endocrinol*. 1999;13(6):851–865.
58. Haywood M, et al. An activated human follicle-stimulating hormone (FSH) receptor stimulates FSH-like activity in gonadotropin-deficient transgenic mice. *Mol Endocrinol*. 2002;16(11):2582–2591.
59. Huhtaniemi IT, Aittomäki K. Mutations of follicle-stimulating hormone and its receptor: effects on gonadal function. *Eur J Endocrinol*. 1998;138(5):473–481.
60. Siegel ET, et al. The molecular basis of impaired follicle-stimulating hormone action: evidence from human mutations and mouse models. *Reprod Sci*. 2013;20(3):211–233.
61. Gromoll J, et al. An activating mutation of the follicle-stimulating hormone receptor autonomously sustains spermatogenesis in a hypophysectomized man. *J Clin Endocrinol Metab*. 1996;81(4):1367–1370.
62. Oduwole OO, et al. Role of follicle-stimulating hormone in spermatogenesis. *Front Endocrinol*. 2018;9:763.
63. Mullaney BP, Skinner MK. Basic fibroblast growth factor (bFGF) gene expression and protein production during pubertal development of the seminiferous tubule: follicle-stimulating hormone-induced Sertoli cell bFGF expression. *Endocrinology*. 1992;131(6):2928–2934.
64. Rossi P, et al. Follicle-stimulating hormone induction of steel factor (SLF) mRNA in mouse Sertoli cells and stimulation of DNA synthesis in spermatogonia by soluble SLF. *Dev Biol*. 1993;155(1):68–74.
65. Tadokoro Y, et al. Homeostatic regulation of germinal stem cell proliferation by the GDNF/FSH pathway. *Mech Dev*. 2002;113(1):29–39.
66. Plotton I, et al. Decrease of both stem cell factor and clusterin mRNA levels in testicular biopsies of azoospermic patients with constitutive or idiopathic but not acquired spermatogenic failure. *Hum Reprod*. 2006;21(9):2340–2345.
67. Bhattacharya I, et al. A switch in Sertoli cell responsiveness to FSH may be responsible for robust onset of germ cell differentiation during prepubartal testicular maturation in rats. *Am J Physiol Endocrinol Metab*. 2012;303(7):E886–E898.
68. Jorgez CJ, et al. E2F1 regulates testicular descent and controls spermatogenesis by influencing WNT4 signaling. *Development*. 2021;148(1):dev191189.
69. Li Y, et al. The sex-determining factors SRY and SOX9 regulate similar target genes and promote testis cord formation during testicular differentiation. *Cell Rep*. 2014;8(3):723–733.
70. Barrionuevo F, et al. Homozygous inactivation of Sox9 causes complete XY sex reversal in mice. *Biol Reprod*. 2006;74(1):195–201.
71. Moniot B, et al. The PGD2 pathway, independently of FGF9, amplifies SOX9 activity in Sertoli cells during male sexual differentiation. *Development*. 2009;136(11):1813–1821.
72. Gonen N, et al. Sex reversal following deletion of a single distal enhancer of *Sox9*. *Science*. 2018;360(6396):1469–1473.
73. Willems A, et al. Selective ablation of the androgen receptor in mouse sertoli cells affects sertoli cell maturation, barrier formation and cytoskeletal development. *PLoS One*. 2010;5(11):e14168.
74. Tanwar PS, et al. Constitutive WNT/beta-catenin signaling in murine Sertoli cells disrupts their differentiation and ability to support spermatogenesis. *Biol Reprod*. 2010;82(2):422–432.
75. Cai K, et al. Action mechanism of inhibin α-subunit on the development of Sertoli cells and first wave of spermatogenesis in mice. *PLoS One*. 2011;6(10):e25585.
76. Namwanje M, Brown CW. Activins and inhibins: roles in development, physiology, and disease. *Cold Spring Harb Perspect Biol*. 2016;8(7):a021881.
77. Vija L, et al. Ligand-dependent stabilization of androgen receptor in a novel mouse ST38c Sertoli cell line. *Mol Cell Endocrinol*. 2014;384(1–2):32–42.
78. Edelsztein NY, Rey RA. Importance of the androgen receptor signaling in gene transactivation and transrepression for pubertal maturation of the testis. *Cells*. 2019;8(8):861.
79. Meroni SB, et al. Molecular mechanisms and signaling pathways involved in sertoli cell proliferation. *Front Endocrinol (Lausanne)*. 2019;10:224.
80. Hernandez A, Martinez ME. Thyroid hormone action in the developing testis: intergenerational epigenetics. *J Endocrinol*. 2020;244(3):R33–R46.
81. Parakh TN, et al. Follicle-stimulating hormone/cAMP regulation of aromatase gene expression requires beta-catenin. *Proc Natl Acad Sci U S A*. 2006;103(33):12435–12440.
82. Roy L, et al. Convergence of 3′,5′-cyclic adenosine 5′-monophosphate/protein kinase A and glycogen synthase kinase-3beta/beta-catenin signaling in corpus luteum progesterone synthesis. *Endocrinology*. 2009;150(11):5036–5045.
83. Boyer A, et al. WNT4 is required for normal ovarian follicle development and female fertility. *FASEB J*. 2010;24(8):3010–3025.
84. Hino S, et al. Phosphorylation of beta-catenin by cyclic AMP-dependent protein kinase stabilizes beta-catenin through inhibition of its ubiquitination. *Mol Cell Biol*. 2005;25(20):9063–9072.
85. Chang H, et al. Overactive beta-catenin signaling causes testicular sertoli cell tumor development in the mouse. *Biol Reprod*. 2009;81(5):842–849.
86. Perrone F, et al. Frequent mutation and nuclear localization of β-catenin in sertoli cell tumors of the testis. *Am J Surg Pathol*. 2014;38(1):66–71.
87. McMellen A, et al. Wnt signaling in gynecologic malignancies. *Int J Mol Sci*. 2020;21(12):4272.
88. DiRenzo DM, et al. A crosstalk between TGF-β/Smad3 and Wnt/β-catenin pathways promotes vascular smooth muscle cell proliferation. *Cell Signal*. 2016;28(5):498–505.
89. Akhmetshina A, et al. Activation of canonical Wnt signalling is required for TGF-β-mediated fibrosis. *Nat Commun*. 2012;3:735.
90. Witsch E, et al. Roles for growth factors in cancer progression. *Physiology (Bethesda)*. 2010;25(2):85–101.
91. Woodcock HV, et al. The mTORC1/4E-BP1 axis represents a critical signaling node during fibrogenesis. *Nat Commun*. 2019;10(1):6.
92. Dey N, et al. microRNA-21 governs TORC1 activation in renal cancer cell proliferation and invasion. *PLoS One*. 2012;7(6):e37366.
93. Sahut-Barnola I, et al. Cushing's syndrome and fetal features resurgence in adrenal cortex-specific Prkar1a knockout mice. *PLoS Genet*. 2010;6(6):e1000980.
94. de Joussineau C, et al. mTOR pathway is activated by PKA in adrenocortical cells and participates in vivo to apoptosis resistance in primary pigmented nodular adrenocortical disease (PPNAD). *Hum Mol Genet*. 2014;23(20):5418–5428.
95. Drelon C, et al. PKA inhibits WNT signalling in adrenal cortex zonation and prevents malignant tumour development. *Nat Commun*. 2016;7(1):1–14.
96. Shan J, et al. Generation of an allele to inactivate Wnt4 gene function conditionally in the mouse. *Genesis*. 2009;47(11):782–788.
97. Skålhegg BS, et al. Mutation of the Calpha subunit of PKA leads to growth retardation and sperm dysfunction. *Mol Endocrinol*. 2002;16(3):630–639.

Steroidogenic Factor-1 Lineage Origin of Skin Lesions in Carney Complex Syndrome

Isabelle Sahut-Barnola[1], Anne-Marie Lefrançois-Martinez[1], Damien Dufour[1], Jean-Marie Botto[2], Crystal Kamilaris[3], Fabio R. Faucz[3], Constantine A. Stratakis[3], Pierre Val[1] and Antoine Martinez[1]

Carney complex is a rare familial multineoplastic syndrome predisposing to endocrine and nonendocrine tumors due to inactivating mutations of *PRKAR1A,* leading to perturbations of the cAMP–protein kinase A signaling pathway. Skin lesions are the most common manifestation of Carney complex, including lentigines, blue nevi, and cutaneous myxomas in unusual locations such as oral and genital mucosa. Unlike endocrine disorders, the pathogenesis of skin lesions remains unexplained. In this study, we show that embryonic invalidation of the *Prkar1a* gene in steroidogenic factor-1–expressing cells leads to the development of familial skin pigmentation alterations, reminiscent of those in patients with Carney complex. Immunohistological and molecular analyses, coupled with genetic monitoring of recombinant cell lineages in mouse skin, suggest that familial lentiginosis and myxomas occur in skin areas specifically enriched in dermal melanocytes. In lentigines- and blue nevi–prone areas from mutant mice and patients, *Prkar1a/PRKAR1A* invalidation occurs in a subset of dermal fibroblasts capable of inducing, under the influence of protein kinase A signaling, the production of promelanogenic EDN3 and hepatocyte GF signals. Our model strongly suggests that the origin of the typical Carney complex cutaneous lesions is the result of noncell-autonomous promelanogenic activity of a dermal fibroblast population sharing a community of origin with steroidogenic factor-1 lineage.

Journal of Investigative Dermatology (2022) ■, ■–■; doi:10.1016/j.jid.2022.04.019

INTRODUCTION

Carney complex (CNC) is a rare multiple endocrine neoplasia and lentiginosis syndrome that is familial in 70% of cases with autosomal dominant inheritance. CNC is characterized by pigmented lesions of the skin and mucosal tumors, myxomas (of the heart, skin, and breast), and various endocrine and nonendocrine tumors. Endocrine manifestations of CNC affect the adrenal cortex (25–68% of cases), gonads (testes, 35–41% ovaries, 14%), and pituitary and thyroid (up to 70%). Patients with CNC may also present with cardiac myxoma (20–40%) and skin myxoma (20–50%). The most common clinical manifestation is abnormal skin pigmentation (60–80%), ranging from lentigines or so-called freckles to blue nevi (Correa et al., 2015; Espiard et al., 2020; Stratakis, 2016). Lentigines observed in patients with CNC are found in unusual places such as the cheeks, vermilion border, ears, eyelids, and/or genitals. In contrast to endocrine manifestations, the pathogenesis of cutaneous disorders remains unexplained. CNC is primarily caused by inactivating mutations of the *PRKAR1A* gene, encoding the R1α subunit of protein kinase A (PKA), resulting in constitutive activation of the cAMP–PKA signaling pathway (Carney et al., 1985; Casey et al., 2000; Kirschner et al., 2000).

We have previously developed genetic mouse models carrying conditional *Prkar1a* invalidation using different Cre drivers (*Akr1b7-Cre*, AS^{Cre}, and *Sf1-Cre*), allowing a spatiotemporal R1α loss in steroidogenic cells (Amaya et al., 2021; Drelon et al., 2016; Dumontet et al., 2018; Sahut-Barnola et al., 2010). These models recapitulated the primary bilateral adrenocortical hyperplasia observed in patients with CNC, associated with chronic glucocorticoid excess (Cushing's syndrome), which resulted in metabolic comorbidities and alterations of brain structure. Remarkably, spotty skin pigmentation, the most common and earliest clinical manifestation of CNC, was only observed when *Prkar1a* was invalidated using the *Sf1-Cre* driver (*Prkar1a*$^{fl/fl}$*::Sf1-Cre/+*, named $AdKO_{2.0}$), which was active in steroidogenic cell lineage from embryonic days 10.5–11.5 onward (Bingham et al., 2006). In this study, we show that $AdKO_{2.0}$ mice exhibit skin alterations characterized by hyperpigmentation in skin areas mirroring those of patients with CNC, including lentigines, blue nevi, and development of cutaneous myxomas. We used immunohistological and molecular approaches as well as cell lineage tracing studies to characterize the origin and pathogenesis of these cutaneous lesions in the skin of $AdKO_{2.0}$ mice and compared them with skin biopsies from patients with CNC. We further show that $AdKO_{2.0}$ mice recapitulate the skin lesions found in patients with CNC and allow us to identify the noncell-autonomous mechanisms involving specific dermal cell populations.

[1]Institut *Genetics, Reproduction & Development (iGReD), CNRS, Inserm, University of Clermont-Auvergne, France;* [2]*Ashland - Global Skin Research Center, Sophia Antipolis, France; and* [3]*Section on Endocrinology and Genetics, Eunice Kennedy Shriver National Institute of Child Health and Human Development, National Institutes of Health, Bethesda, Maryland, USA*

Correspondence: Antoine Martinez, Institut Génétique, Reproduction et Développement (iGReD), CNRS UMR6293, INSERM U1103, Faculté de Médecine, CRBC, Université Clermont-Auvergne, 28 place Henri Dunant, TSA 50400, Clermont-Ferrand 63001, France. E-mail: antoine.martinez@uca.fr

Abbreviations: CNC, Carney complex; eGFP, enhanced GFP; HGF, hepatocyte GF; KITL, kit ligand; mTmG, membrane-targeted Tomato/membrane-targeted eGFP; PKA, protein kinase A; SF-1, steroidogenic factor-1; WB, western blot; WT, wild-type

Received 23 September 2021; revised 28 March 2022; accepted 16 April 2022; accepted manuscript published online XXX; corrected proof published online XXX

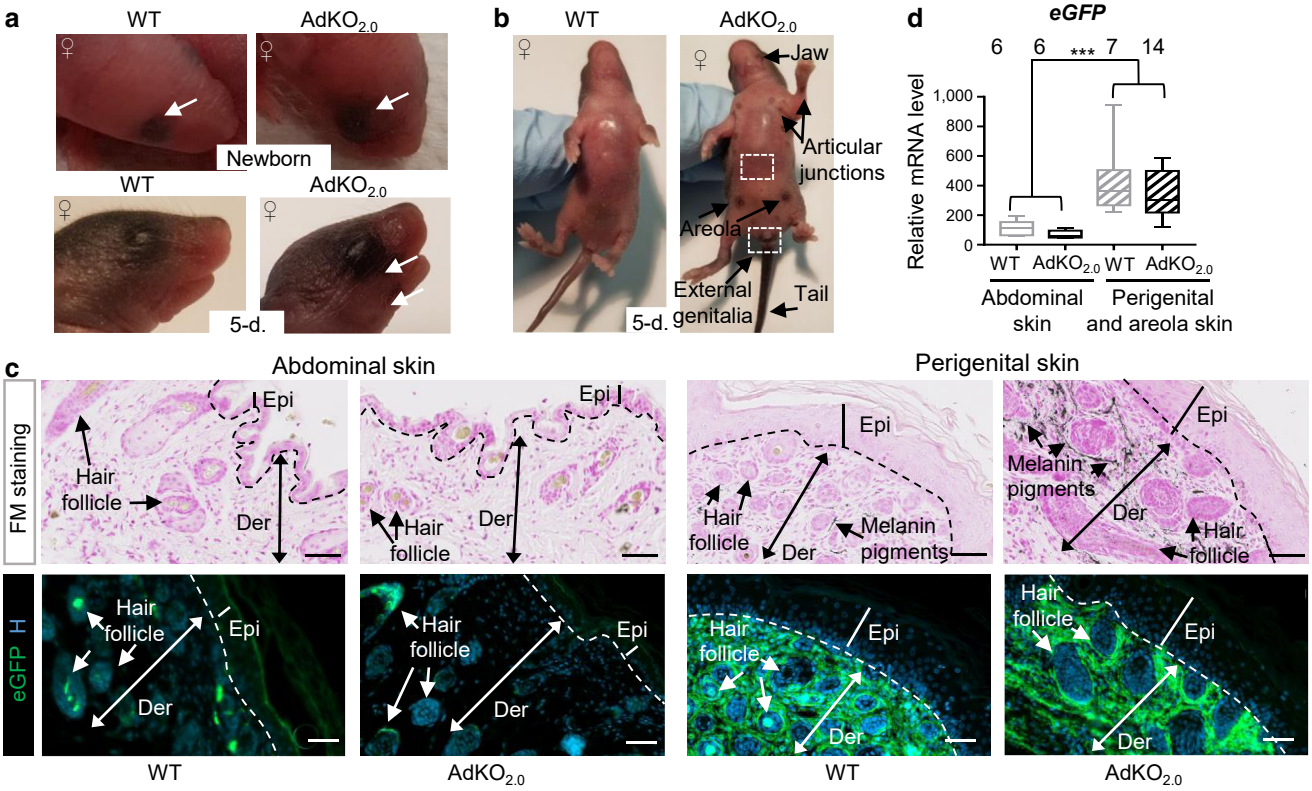

Figure 1. Skin pigmentation abnormalities in $AdKO_{2.0}$ mice are associated with *Sf1-Cre* dermal activity. (**a, b**) $AdKO_{2.0}$ newborns (arrows in **a**, top) show a pigmentation ring around the eye (arrows). At 5 days, pigmentation defects appear as black spots under the eye (arrows in **a**, bottom) and in specific locations (arrows in **b**) (details are in Supplementary Figure S1). (**c**) FM staining (melanin) and eGFP immunodetection in WT (*Prkar1a*$^{fl/+}$*::Sf1-Cre/+::R26R*$^{mTmG/+}$) and $AdKO_{2.0}$ (*Prkar1a*$^{fl/fl}$*::Sf1-Cre/+::R26R*$^{mTmG/+}$) (aged 5 days) abdominal (top square in **b**) and perigenital (bottom square in **b**) skin sections. Hoechst nuclei staining is indicated with H. Bars = 50 μm. (**d**) qPCR analysis of eGFP (a proxy for recombination) in perigenital and/or areola skin compared with that in the WT and $AdKO_{2.0}$ abdominal skin (aged 5 days). n is indicated above the graph. Statistical analyses were performed with Mann–Whitney test. ***$P < 0.001$. 5-d, 5 days; Der, dermis; eGFP, enhanced GFP; Epi, epidermis; FM, Fontana–Masson; WT, wild-type.

RESULTS

Pigmented skin lesions in $AdKO_{2.0}$ mice are correlated with *Sf1-Cre* driver activity

The skin pigmentation phenotype of $AdKO_{2.0}$ mice was detected at birth as a pigmented ring around the eyes. In $AdKO_{2.0}$ mice aged 5 days, hyperpigmentation was found in the perigenital skin, in the tail, and around the nipples in females. Hyperpigmentation also formed discrete symmetrical patches under the jaw and on the joints of the upper limbs (Figure 1a and b and Supplementary Figure S1a). These skin manifestations, reminiscent of lentigines, were fully penetrant and were always found in these specific areas. Because adult $AdKO_{2.0}$ mice had glucocorticoid-induced alopecia, this pattern of lentiginosis remained visible despite hair growth as large areas around the nipples, as spotty pigmentation on the scrotum, and at the upper limb junctions (Supplementary Figure S1b). Fontana–Masson staining was carried out on skin sections from differentially pigmented areas in mice aged 5 days. As expected, there were no melanin pigments or histological alterations in the abdominal skin, regardless of wild-type (WT) and $AdKO_{2.0}$ mice. By contrast, melanin staining in the dermis (at least in the papillary and upper reticular dermis) was strongly increased in genitalia skin sections from $AdKO_{2.0}$ mice compared with that in WT (Figure 1c, top panels). The specific hyperpigmentation of $AdKO_{2.0}$ mutants does not rely on the systemic action of excess glucocorticoids because the other two adrenal-specific *Prkar1a* invalidation models using *Akr1b7-Cre* (AdKO) or *AS*^{Cre} (DAdKO) drivers do not show any phenotype in the skin (Dumontet et al., 2018; Sahut-Barnola et al., 2010). This is in agreement with the observation that lentiginosis usually appears very early (at birth or during childhood) in patients with CNC, independently from endocrine manifestations (Stratakis, 2016). Therefore, the skin phenotype of $AdKO_{2.0}$ mice should solely be the consequence of the recombinase activity of the *Sf1-Cre* driver. To evaluate this hypothesis, we traced *Sf1-Cre* lineage in the skin by introducing the Cre recombinase membrane-targeted Tomato/membrane-targeted eGFP (mTmG) membrane reporter transgene (Muzumdar et al., 2007) into WT and mutant mice. In compound transgenic mice, Cre-mediated recombination fixes definitive enhanced GFP (eGFP) expression in cells expressing the *Sf1-Cre* transgene and in all their descending lineages. In abdominal skin sections, eGPF immunostaining was limited to hair follicles (details in Supplementary Figure S1c), whereas strong eGFP expression was shown in the perigenital dermis of WT and $AdKO_{2.0}$ mice (Figure 1c, bottom panels). In developing embryos, direct eGFP fluorescence progressed anteroposteriorly from the telencephalon on embryonic day 9.5 to specific areas of the skin, first at

the upper limb-bud joint from embryonic day 12.5, around the eyes and genitalia from embryonic day 14.5, and finally on the tail from embryonic day 16.5 (Supplementary Figure S2a). As a control, we confirmed that eGFP fluorescence was adequately detected in embryonic tissues with high steroidogenic factor-1 (SF-1) expression such as the adrenal gland, gonads, and spleen (Supplementary Figure S2b and c) (Bingham et al., 2006). This shows that the skin areas where postnatal pigmentation occurs in the case of *Prkar1a* mutation have been programmed during embryonic development and consist of specific cell lineages currently expressing or having expressed the *Sf1-Cre* transgene early. This enrichment of eGFP expression in pigmentation-prone skin areas was confirmed at the mRNA level by RT-qPCR analyses in WT and mutant mice aged 5 days (Figure 1d). Although the steroidogenic activity of the skin has been well-documented (Ceruti et al., 2018; Slominski et al., 2013), SF-1 expression has been reported in only one study (Patel et al., 2001). To determine the timeline expression of *Sf1* in the developing skin, we conducted embryonic and perinatal immunohistological studies that revealed an apparent decrease in the density of SF-1–labeled nuclei in the dermis of genital skin from embryonic day 14.5 to embryonic day 18.5, becoming virtually undetectable at birth (Supplementary Figure S2d). Because we never detected a parallel induction or a significant expression of *Sf1* in postnatal skin (aged 5 days and adult) samples, either using RT-qPCR or immunostaining (not shown), we conclude that skin eGFP-positive cells derived from dermal *Sf1* lineage that definitely loses *Sf1* expression shortly after embryonic day 18.5.

As expected, we showed that in $AdKO_{2.0}$ perigenital skin, *Prkar1a* mRNA levels were decreased, whereas the transcripts for genes involved in melanosome biogenesis (*Mlana/Mart1*) and melanogenesis (*Tryp1* and *Tryp2*) were increased compared with those in the skin of WT mice (Supplementary Figure S1d). Surprisingly, no change in mRNA levels was observed for genes encoding melanogenic transcription factors (*Mitf, Sox9, Sox10*) or dermal fibroblastic markers (*Vimentin* and *Col1a1*) (Supplementary Figure S1d). The lack of variation in *Mitf* expression (a major melanocyte marker and regulator of genes involved in melanogenesis) despite the marked increase in melanogenesis has previously been described in transgenic mouse models with dermal hyperpigmentation (Wolnicka-Glubisz et al., 2013). In addition, the unaltered expression of *Mitf* in $AdKO_{2.0}$ perigenital skin samples was consistent with the unaltered expression of its positive upstream regulators *Sox9* and *Sox10* (Supplementary Figure S1d) (Passeron et al., 2007; Verastegui et al., 2000).

In summary, these results show a direct correlation between the location of lentigines in $AdKO_{2.0}$ mice and *Sf1-Cre* activity in the dermis. *Prkar1a* inactivation in these lentigines-prone areas is expected to increase PKA activity, which in turn will enhance the melanogenic activity of dermal melanocytes.

Dermal *Sf1-Cre* lineages of the lentigines-prone areas are not melanocytes

To identify the dermal cells of the *Sf1-Cre* lineage, we carried out double immunohistochemical analyses using, on the one hand, eGFP immunostaining, which marks *Prkar1a*-negative recombined cells, and on the other hand, MLAN-A or vimentin staining for melanocyte and fibroblast immunodetection, respectively (Figure 2a and b). In the lentigines from $AdKO_{2.0}$ mice, there was no colocalization of eGFP and MLAN-A staining, although eGFP cells were in close vicinity of MLAN-A–positive cells. In contrast, eGFP-positive cells were all positive for vimentin, indicating that *Prkar1a* invalidation occurred in dermal fibroblasts but not in dermal melanocytes.

Fibroblasts play an important role in regulating the activities of melanocytes by secreting a number of paracrine factors, which bind to their receptors and modulate the intracellular signaling cascades linked to melanocytic functions (Wang et al., 2017). We focused on three, whose corresponding receptors are expressed on melanocytes, which were well-characterized for the promelanogenic actions: hepatocyte GF (HGF) and mesenchymal–epithelial transition receptor (Kapoor et al., 2020; Kunisada et al., 2000; Matsumoto et al., 1991), EDN-3 and EDNRB (Baynash et al., 1994; Bondurand et al., 2018; Hosoda et al., 1994), and kit ligand (KITL) and c-Kit receptor (Copeland et al., 1990; Geissler et al., 1988; Kasamatsu et al., 2008).

qPCR analyses showed an increase in the mRNA levels of *Hgf* and *Edn3* and for their cognate receptors mesenchymal–epithelial transition gene *Met* and *Ednrb* in $AdKO_{2.0}$ lentigines, whereas mRNA for *Kitl* and its receptor were not regulated (Figure 2c).

To assess the paracrine action of mutant fibroblasts in the $AdKO_{2.0}$ skin phenotype, we performed primary cultures of fibroblasts from eGFP-positive WT and $AdKO_{2.0}$ skin (Figure 2d). These virtually pure fibroblast cultures solely consisted of vimentin-positive cells and, irrespective of the genotype, contained at least one third of eGFP/vimentin double-positive cells. This confirms that *Prkar1a* mutation does not influence the contingent of dermal cells descending from the *Sf1* lineage in lentigines-prone skin areas (Figure 1c and d). Therefore, *Prkar1a* mRNA levels were decreased in $AdKO_{2.0}$ primary culture compared with those in WT, whereas *eGFP* transcripts remained unchanged (Supplementary Figure S3a). In contrast to WT fibroblasts, $AdKO_{2.0}$ fibroblasts secreted large amounts of HGF and expressed high levels of *Edn3* and *Hgf* mRNAs (Figure 2e and f). Importantly, *Hgf* and *Edn3* gene expression as well as HGF secretion could be further enhanced by forskolin-induced PKA stimulation in mutant primary cultures; however, PKA responsiveness (at 48 hours) in WT cultures did not reach significance (Supplementary Figure S3b and c). Consistent with our result, HGF is a known target of the cAMP–PKA pathway in human fibroblasts (Matsunaga et al., 1994). On the other hand, primary melanocytes (MLAN-A positive) were subjected to conditioned media from either WT or $AdKO_{2.0}$ fibroblasts (Supplementary Figure S3d and e). After 14 days of culture, $AdKO_{2.0}$-conditioned media specifically increased the number of melanocytes and possibly their melanogenic activity (as suggested by the increased density of melanosomes) (Supplementary Figure S3d). In addition, the effects were not homogeneous in all melanocytes culture wells, likely owing to the low inoculation density of primary melanocytes (5.10^3 per well) and the drastic decrease of HGF production in conditioned media with each passage of $AdKO_{2.0}$ fibroblasts (Supplementary Figure S3e).

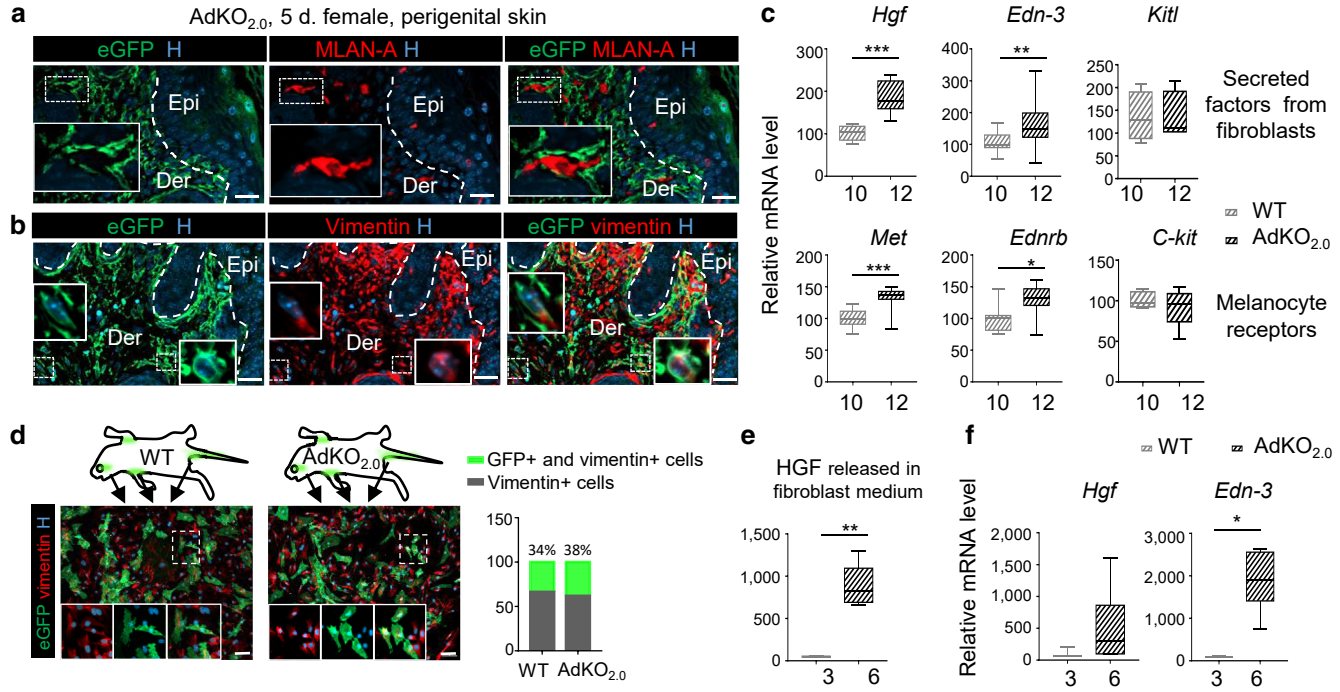

Figure 2. eGFP+ dermal cells (*Prkar1a*-KO) are PKA-reprogrammed fibroblasts producing melanogenic signals. (**a**) eGFP (*Prkar1a*-KO cells) and MLAN-A (melanocytes) or (**b**) vimentin (mesenchymal cells) colabeling in $AdKO_{2.0}$ perigenital skin (aged 5 days). Hoechst nuclei staining is indicated with H. Insets shows the dotted frames magnification. Bars = 20 μm. (**c**) qPCR analyses of WT/$AdKO_{2.0}$ perigenital skin samples (aged 5 days) for fibroblast secreted factors and corresponding receptors on melanocytes. (**d**) Primary cultured fibroblasts from eGFP+ skin samples dissected from mice aged 4 days. Colabeling of eGFP and vimentin (Insets show the magnification) shows a similar proportion of eGFP+ cells in WT and $AdKO_{2.0}$ cultures (quantification, right graph). Bars = 100 μm. (**e**) HGF released in WT and $AdKO_{2.0}$ fibroblasts media. (**f**) qPCR analyses of primary cultured fibroblasts. n is indicated under the graphs. Statistical analyses were performed by Mann–Whitney test. $*P < 0.05$, $**P < 0.01$, and $***P < 0.001$. 5-d, 5 days; Der, dermis; eGFP, enhanced GFP; Epi, epidermis; HGF, hepatocyte GF; KO, knockout; PKA, protein kinase A; WT, wild-type.

In summary, the invalidation of *Prkar1a* in a subset of dermal fibroblast progenitors, descending from a cell lineage that has expressed *Sf1* at least until embryonic day 18.5, induces the expression of the promelanogenic factor HGF (and likely EDN3), which in turn increases the number of dermal melanocytes and/or stimulates melanogenesis in lentigines-prone areas (Figure 3d).

Dermal *Sf1-Cre* lineages induce nevi formation and promote the occurrence of cutaneous myxomas in $AdKO_{2.0}$ mice

As early as age 2 months, all $AdKO_{2.0}$ mice developed nevi symmetrically located on the posterior aspect of the thighs. These appeared deeply embedded in the dermis and took on a blue color (Figure 3a). Histological staining and eGFP immunostaining of blue nevi sections showed that melanin pigment deposits were found in the vicinity of dermal cells that had lost *Prkar1a*-conditional allele (eGFP positive) (Figure 3b). Note that clusters of sebaceous glands (positive for cytokeratin 7, not shown) formed of eGFP-negative cells with large cytoplasm and were detected close to these pigmented formations. Double immunostaining for eGFP/MLAN-A and eGFP/vimentin confirmed that *Prkar1a*-knockout cells were fibroblasts (vimentin positive) but not melanocytes (MLAN-A negative) (Supplementary Figure S4a). As expected, qPCR analyses of the nevi formed in $AdKO_{2.0}$ mice showed an increased expression of genes involved in melanogenesis (*Mlan-A, Tyrp1*, and *Tyrp2*) and of fibroblastic promelanogenic factors (*Hgf* and *Edn3*) (Supplementary Figure S4b). The association between HGF and MLAN-A protein accumulation was further confirmed in western blots (WBs) (Figure 3c). This increase in local HGF should also promote the differentiation of sebaceous glands in the nevus area, which have been shown to express high levels of mesenchymal–epithelial transition receptors (Wu et al., 2014, Zouboulis, 2009). Our results indicate that as with the lentigines described earlier, blue nevi formation in $AdKO_{2.0}$ mice arises from activation of a promelanogenic fibroblast population after *Prkar1a* loss (Figures 3d and 4a for a diagram of pigmented skin areas in $AdKO_{2.0}$ mice).

In 20–50% of patients with CNC, cutaneous myxomas were found localized in specific areas such as the eyelid, external ear canal, areola, and genitals (Correa et al., 2015; Espiard et al., 2020). Approximately 44% of $AdKO_{2.0}$ mice from age 6 months developed large skin tumors localized either on the thighs or on the shoulder joint (where nevi occur) (Figure 4b). The tumor masses always appeared dense, poorly vascularized, nonmelanic, and encapsulated. Hematoxylin staining showed an epidermal delineation of the tumor (Figure 4c). CNC skin myxomas are composed of spindle-shaped cells and polygonal cells (Hachisuka et al., 2006). Similar histological features were also observed in skin tumor masses of $AdKO_{2.0}$ mice. The eGFP-labeled cells (*Prkar1a*-knockout cells) were found scattered throughout the entire tumor and accounted for at least 10% of the total cell population, which consisted mainly of mesenchymal cells (vimentin positive), indicating the myxomatous nature of these cutaneous tumors (Figure 4d). qPCR analyses suggested

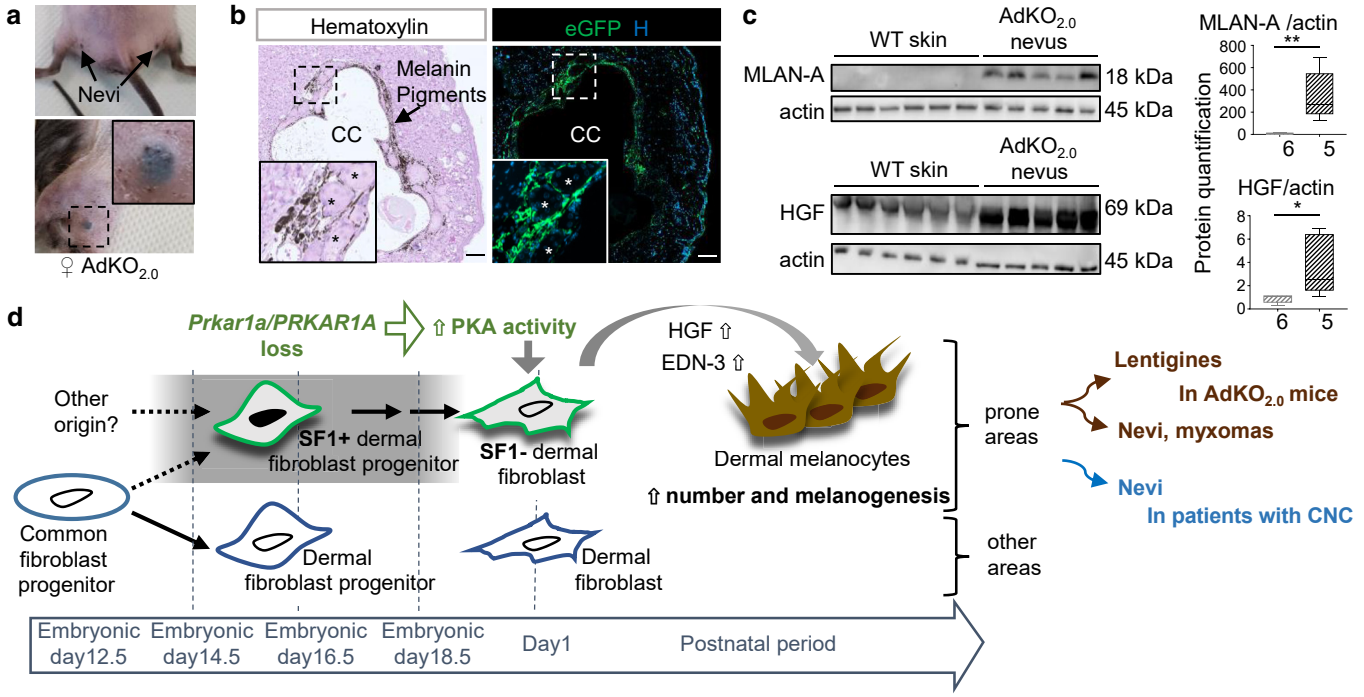

Figure 3. Increased PKA activity is associated with blue nevi in AdKO$_{2.0}$ skin. (**a**) View of symmetrical nevi (top) and magnification (bottom) in female mice aged 4–6 months. (**b**) Hematoxylin staining and eGFP immunodetection of blue nevus section from AdKO$_{2.0}$ female mice aged 6 months. In the section, the central cavity represents where melanin accumulates (eliminated by histological treatments). The cavity periphery is lined by melanin pigments, eGFP-positive cells, and clusters of sebaceous glands formed from eGFP-negative cells with large cytoplasm (Asterisk [*] is shown in magnifications). Bars = 100 µm. (**c**) Western blot analyses of MLAN-A and HGF protein accumulation in skin extracts from wild-type and AdKO$_{2.0}$ (nevi) mice. Graphs show the quantification normalized to actin. n is indicated under the graphs. Statistical analyses were performed by Mann–Whitney test. *$P < 0.05$ and **$P < 0.01$. (**d**) Scheme summarizing the skin effects of *Prkar1a/PRKAR1A* loss (AdKO$_{2.0}$ mice/patients with CNC). Increased production of diffusible factors (HGF, EDN-3) in response to PKA activation in dermal fibroblasts descending from a cell lineage that has activated *Sf1-Cre* (shaded box, period during which SF-1 was experimentally detected in embryonic dermis) increases the number and melanogenic activity of dermal melanocytes, favoring lentigines/nevi formation in prone areas. CNC, Carney complex; eGFP, enhanced GFP; HGF, hepatocyte GF; PKA, protein kinase A; SF-1, steroidogenic factor-1.

that the formation of skin myxomas could involve a dramatic increase (×100) in *Hgf* gene expression, whereas as expected, *Edn3* mRNA levels were not increased in these nonpigmented lesions compared with those in blue nevi (Figure 4e). In conclusion, AdKO$_{2.0}$ mice develop cutaneous tumors that are hallmarks of skin lesions found in patients

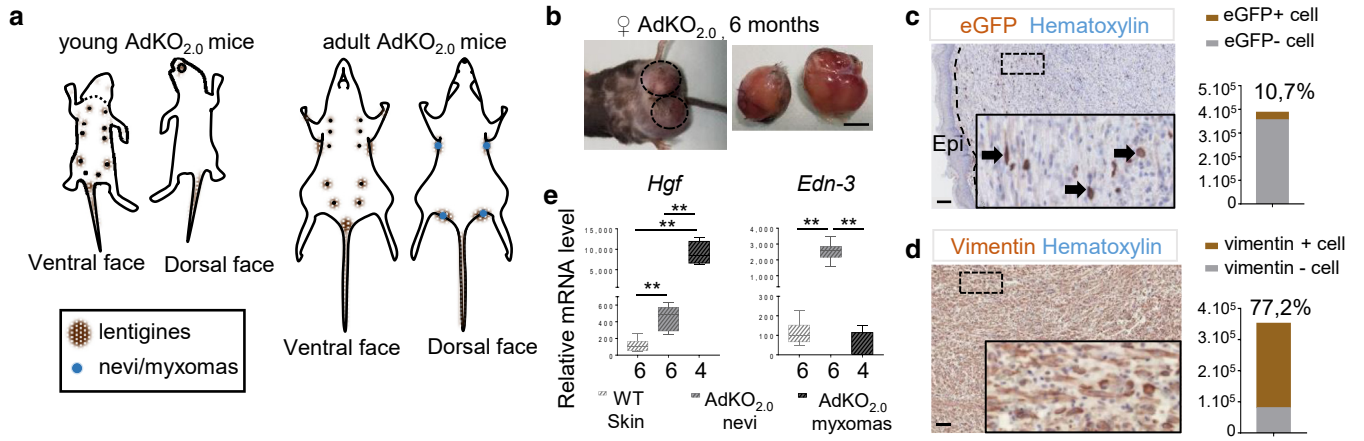

Figure 4. Cutaneous myxomas in AdKO$_{2.0}$ mice. (**a**) Skin lesions maps in mice aged 5 days and 2 months. Head lentigines are no longer seen in adults owing to hair growth. Nevi form symmetrically on the back of thighs and shoulders. (**b**) Myxomas emerge in 44% of AdKO$_{2.0}$ mice (aged ≥6 months) in areas where nevi form. Bar = 1 cm. (**c, d**) The tumor is delimited by the Epi. (**c**) eGFP or (**d**) vimentin immunodetections (insets show the frame magnification) and hematoxylin counterstaining. Percentages of eGFP-positive (*Prkar1a*-KO) and vimentin-positive cells are calculated from counts of four different tumors. Bar = 100 µm. (**e**) qPCR analyses of fibroblastic-secreted factors in wild-type skin (sampling located where nevi form in mutants) and AdKO$_{2.0}$ nevi (females aged 3 months) and in AdKO$_{2.0}$ myxomas. n is indicated under the graphs. Statistical analyses were performed by Mann–Whitney test. **$P < 0.01$. eGFP, enhanced GFP; Epi, epidermis; KO, knockout.

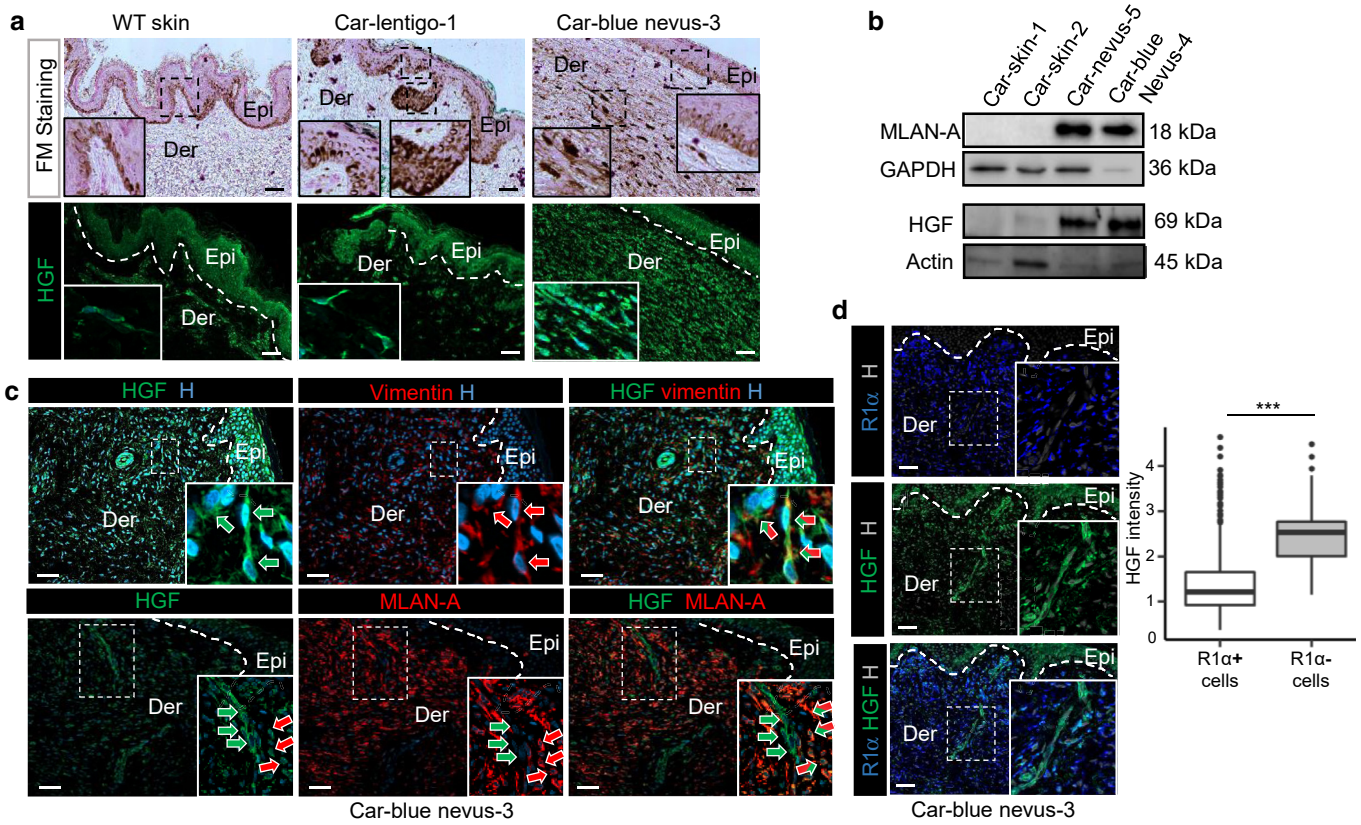

Figure 5. Increased HGF is associated with dermal melanin in blue nevi from patients with CNC. (**a**) FM staining and HGF immunodetection of normal human skin and lentigines/blue nevi from patients with CNC. (**b**) Western blot analysis of MLAN-A and HGF protein in skin extracts from patients with CNC. (**c**) Coimmunolabeling of HGF (green arrows) and vimentin (mesenchymal cells, red arrows) in top panels or MLAN-A (melanocytes, red arrows) in bottom panels in blue nevus from patients with CNC (striped arrows, colabeled cells). (**d**) Coimmunofluorescent labeling of R1α and HGF in blue nevus from patients with CNC. Quantification of HGF labeling intensity in R1α+ (n = 1,103) and R1α− cells (n = 33). Statistical analyses were performed by Mann−Whitney test. ***$P = 9.10^{-15}$. Hoechst nuclei staining is indicated with H. Insets are a magnification of dotted frames. Bars = 50 μm. CNC, Carney complex; Der, dermis; Epi, epidermis; FM, Fontana−Masson; HGF, hepatocyte GF.

with CNC. The occurrence of myxomas in sites where blue nevi initially develop suggests a possible continuity between these pigmented lesions and myxoma formation.

Lentigines and blue nevi from patients with CNC

With access to some rare skin samples from patients with CNC, we characterized the sites of melanin accumulation using Fontana−Masson or hematoxylin staining (Figure 5a and Supplementary Figure S5a). Lentigines (Car-lentigo-1, Car-lentigo-2) showed high levels of melanin pigments in the basal layer of the epidermis as previously described (Courcoutsakis et al., 2013), whereas the pigmentation in blue nevi (Car-blue nevus-3, Car-blue nevus-4) was rather concentrated in the dermis. In normal skin and lentigines, HGF immunostaining was present in the epidermis and in scattered cells in the dermis, in agreement with the literature showing HGF production in keratinocytes and fibroblasts (Serre et al., 2018). In contrast, in blue nevi, HGF labeling was strong in the dermis (Figure 5a and Supplementary Figure S5a). WB analyses confirmed that HGF contents were high in pigmented skin lesions from patients with CNC that expressed high levels of the melanosome biogenesis marker MLAN-A (Figure 5b).

HGF/vimentin and HGF/MLAN-A double immunostaining was performed in blue nevi sections (Figure 5c), with similar results for Car-blue nevus-4 (not shown). These experiments showed colocalization of HGF staining with most of the numerous dermal fibroblasts (vimentin positive). Using HGF/MLAN-A costaining, two cell types could be identified: (i) strongly HGF-positive/MLAN-A−negative cells that should be HGF-producing fibroblasts and (ii) double-positive cells that should be dermal melanocytes on which HGF binds to enhance melanogenesis.

We then interrogated the expression pattern of *PRKAR1A* in CNC skin samples. As expected, in CNC adrenal gland, R1α immunostaining was only detected in the internodular cortex where *PRKAR1A* is expressed from the intact allele and was absent from nodules owing to loss of heterozygosity (Supplementary Figure S5c). In normal skin or CNC lentigines, R1α staining was detected in both the dermis and in epidermal melanocytes (MLAN-A−positive cells) (Supplementary Figure S5b, bottom right). In blue nevi, R1α staining was present in most dermal cells, with the exception of a few clusters of fibroblasts that strongly expressed HGF, presumably owing to increased PKA activity (Figure 5d). The lentigines formation in patients with CNC did not appear to be associated with an increase in HGF (Figure 5a and Supplementary Figure S5a).

DISCUSSION

We have shown that the invalidation of *Prkar1a* in a subset of dermal fibroblasts induces the expression of the

promelanogenic factors HGF and EDN3, which in turn increases the number of dermal melanocytes and/or stimulates melanogenesis in lentigines-prone areas. These data are consistent with previous observations from transgenic mice overexpressing HGF or EDN3 in the epidermis, which displayed skin hyperpigmentation associated with an increase in dermal melanocytes (Aoki et al., 2009; Kunisada et al., 2000; Wolnicka-Glubisz et al., 2013). The mitogenic effect of HGF has also been described in primary cultures of human melanocytes (Matsumoto et al., 1991). Under physiological conditions, HGF production seemed to be linked to the pigmentation of certain skin regions. Indeed, areas of the mouse skin with little hair, such as the tail, nose, ear, and genitalia, were shown to contain far more dermal melanocytes than hairy regions, and this was associated, at least in part, with increased expression of HGF (Kunisada et al., 2000).

Our results also showed increased mRNA expression of *Edn3* and its receptor *Ebnrb*. These were in agreement with data showing that *Edn3* overexpression from embryonic day 13.5 induced an increased proliferation of melanoblasts, resulting in the presence of numerous dermal melanocytes and dark skin at birth (Garcia et al., 2008). Similar mechanisms involving the factors identified in our animal model could also be relevant in humans. Indeed, mutations in either *EDN3* or *EDNRB* genes have been associated with diminished pigmentation in patients with Waardenburg syndrome (Mccallion and Chakravarti, 2001). Furthermore, in patients with neurofibromatosis type 1, skin hyperpigmentation was associated with increased production of HGF by dermal fibroblasts (Okazaki et al., 2003).

In $AdKO_{2.0}$ model, the mRNA encoding KITL and its receptor were not deregulated. Interestingly, mouse models that overexpressed HGF or EDN3 in the skin under the control of the human keratin gene *K14* promoter displayed hyperpigmentation that was not influenced by KITL. Indeed, blocking KITL signaling in these mice using either antibodies or a genetic approach did not affect skin hyperpigmentation, whereas it completely inhibited that of the coat. These previous findings and our present $AdKO_{2.0}$ model provide independent and converging arguments establishing a clear distinction between the maintenance of dermal (and non-cutaneous) melanocytes and epidermal melanocytes (contributing to hair pigmentation) on the basis of their differential requirement toward kit signaling (Aoki et al., 2009; Kunisada et al., 2000).

In the skin samples of patients with CNC, the lentigines showed a strong accumulation of melanin in the basal layer of the epidermis that was not associated with an increase in HGF (Figure 5a and Supplementary Figure S5a). This discrepancy with the $AdKO_{2.0}$ model could rely on species specificity because unlike humans, the adult mouse epidermis lacks melanocytes (present mainly in hair follicles), and therefore, skin pigmentation solely relies on dermal melanocytes. Other differences characterize human and murine skin. The epidermis and dermis are thicker in human skin, and the boundary between these two areas undulates in humans, whereas it remains rather flat in mice. Finally, in most body sites, mice have a greater density of hair follicles (Lynch and Watt, 2018).

Nonetheless, beyond these species differences, we present converging evidence that loss of R1α in some dermal fibroblasts induces PKA-dependent production of secreted GFs, including HGF, which in turn stimulate the growth and melanogenic activity of dermal melanocytes. In this paper, we propose a noncell-autonomous mechanism of *PRKAR1A*-dependent blue nevus pathogenesis in patients with CNC that is consistent with what we showed in the skin lesions of $AdKO_{2.0}$ mice, which ultimately might evolve into massive skin myxomas (Figure 3d). Unexpectedly, this pathogenic mechanism relies on a specific population of fibroblasts belonging to the *Sf1* lineage. There is great heterogeneity in the origin, location, and functions of skin fibroblasts. For example, cell fate mapping analyses performed on the avian or mouse embryo revealed that skin fibroblasts of the dorsal, ventral, lateral, or craniofacial dermis are derived from different embryonic tissues (Thulabandu et al., 2018). Our cell lineage tracing experiments in mice suggest that the pigmented skin lesions typical of CNC form through the *Prkar1a*-dependent activation of a specific subpopulation of dermal fibroblast progenitors sharing a common origin with the steroidogenic lineage but having lost the ability to express *Sf1* in late embryos. Most recent studies investigating the lineage diversity of fibroblast populations have focused primarily on the mechanisms of hair follicle formation and repair (Driskell et al., 2013; Joost et al., 2020). Therefore, we hypothesize that the specific distribution of cutaneous pigmented lesions in CNC may rely on the paracrine activity of specific dermal fibroblast populations, preferentially located in areas enriched in dermal melanocytes, sharing possible common origins with SF-1 lineage and having increased sensitivity to changes in PKA activity.

MATERIALS AND METHODS

Mouse

The $Prkar1a^{fl/fl}$::*Sf1-Cre*/+::$R26R^{mTmG/+}$ mouse line has been described previously (Drelon et al., 2016; Muzumdar et al., 2007). Mice were all maintained and bred on a mixed background. Throughout, WT refers to $Prkar1a^{fl/+}$::*Sf1-Cre*/+::$R26R^{mTmG/+}$ in which we did not observe any discernible phenotype. Littermate control mice were used in all experiments.

Histology and immunostaining

For general morphology and melanin detection, sections were stained with H&E and with Fontana–Masson staining (MF-100-T; Biognost, Zagreb, Croatia), following the manufacturer's instructions. Immunohistological methods for tissues have been previously described (Drelon et al., 2016). See Supplementary Table S1 for the conditions used. Immunofluorescence analyses in primary cultured cells were preceded by a 4% paraformaldehyde fixation for 15 minutes and permeabilization for 3 minutes in 0.1% NP40. Cell count in tissue samples and fluorescence intensity measurements were performed using the QuPath software (Bankhead et al., 2017).

WB

A total of 25 μg (mouse WB) or 12 μg (human WB) of total proteins were loaded on 4/15% SDS-PAGE gel, transferred on nitrocellulose, and detected with primary antibodies (Supplementary Table S1). Signals were quantified with ChemiDoc MP Imaging System camera system (Bio-Rad Laboratories, Hercules, CA) and Image Lab software

(Bio-Rad Laboratories). Expression of proteins was normalized to the expression of the actin or GAPDH proteins.

Real-time PCR analysis

Total RNAs were extracted from skin samples or primary cultured fibroblasts using the RNAII nucleotide extraction kit (Macherey-Nagel, Duren, Germany) or RNAzol (Molecular Research Center, Cincinnati, OH), respectively, following the manufacturers' instructions. A total of 1 μg of total mRNAs was reverse transcribed for 1 hour at 37 °C with 5 pmol of random hexamers primers, 200 units reverse transcriptase (M-MLV RT, M1701, Promega, Madison, WI), 2 mM deoxynucleoside triphosphates, and 20 units of RNAsin (N2615, Promega). A total of 1 μl of a one-fourth dilution of cDNA was used in each qPCR. PCR reactions were conducted with SYBR qPCR Premix Ex Taq II Tli RNaseH+ (TAKRR820W, Takara Bio, Shiga, Japan). Primer pairs are listed in Supplementary Table S2. For each experiment and primer pair, the efficiency of PCR reactions was evaluated by amplification of serial dilutions of a mixture of cDNAs. Relative gene expression was obtained by the ΔΔCt method after normalization to actin.

Primary cultures and HGF dosage

Primary cultures of fibroblasts and melanocytes were performed according to the protocol described by Murphy et al. (2019). A brief description is in Supplementary Materials and Methods. HGF assays were performed according to the instructions of the supplier (ELISA Kit, E-EL-M3033, Elabscience Biotechnology, Houston, TX).

Samples from patients

Histological slides of skin lesions from patients with CNC and skin biopsies were obtained from Stratakis's laboratory, National Institutes of Health (Bethesda, MD). Human adult normal skin sections were used as a control for histological analyses (UM-HuFPT136, CliniSciences, Nanterre, France). Sample information is available in Supplementary Tables S3 and S4.

Statistics

Statistical analyses were conducted by Mann–Whitney test or Kruskal–Wallis tests, followed by uncorrected Dunn's test. $P < 0.05$ was considered significant. All the data are represented by Box and Whiskers plots with the minimum and maximum value and the median.

Study approval

All animal studies were approved by Ethics Committee for Animal Experimentation in Auvergne (number 21153-2019061912044646V2) and were conducted in agreement with international standards for animal welfare.

All patients gave written informed consent for the use of their resected tissues for research purposes. All human study procedures were approved by the Eunice Kennedy Shriver National Institute of Child Health and Human Development Institutional Review Board.

Data availability statement

No datasets were generated or analyzed during this study.

ORCIDs

Isabelle Sahut-Barnola: http://orcid.org/0000-0001-7004-8577
Anne-Marie Lefrancois-Martinez: http://orcid.org/0000-0003-2021-2548
Damien Dufour: http://orcid.org/0000-0002-1220-1745
Jean-Marie Botto: http://orcid.org/0000-0002-6182-4236
Crystal Kamilaris: http://orcid.org/0000-0002-3872-0447
Fabio R. Faucz: http://orcid.org/0000-0001-7959-9842
Constantine A. Stratakis: http://orcid.org/0000-0002-4058-5520
Pierre Val: http://orcid.org/0000-0001-7648-5567
Antoine Martinez: http://orcid.org/0000-0001-9304-5061

CONFLICT OF INTEREST

The authors state no conflict of interest.

ACKNOWLEDGMENTS

This work was funded through institutional support from Centre National de la Recherche Scientifique, INSERM, Université Clermont-Auvergne (Clermont-Ferrand, France) and by Agence Nationale de la Recherche (ANR-18-CE14-0012-02). We wish to thank Sandrine Plantade, Philippe Mazuel, and Khirredine Ouchen for caring for the transgenic mice.

AUTHOR CONTRIBUTIONS

Supervision: ISB, AM; Writing – Original Draft Preparation: ISB, AMLM, PV, AM; Writing – Review and Editing: ISB, AMLM, DD, JMB, CK, FRF, CAS, PV, AM

SUPPLEMENTARY MATERIAL

Supplementary material is linked to the online version of the paper at www.jidonline.org, and at https://doi.org/10.1016/j.jid.2022.04.019

REFERENCES

Amaya JM, Suidgeest E, Sahut-Barnola I, Dumontet T, Montanier N, Pagès G, et al. Effects of long-term endogenous corticosteroid exposure on brain volume and glial cells in the AdKO mouse. Front Neurosci 2021;15:604103.

Aoki H, Yamada Y, Hara A, Kunisada T. Two distinct types of mouse melanocyte: differential signaling requirement for the maintenance of non-cutaneous and dermal versus epidermal melanocytes. Development 2009;136:2511–21.

Bankhead P, Loughrey MB, Fernández JA, Dombrowski Y, McArt DG, Dunne PD, et al. QuPath: open source software for digital pathology image analysis. Sci Rep 2017;7:16878.

Baynash AG, Hosoda K, Giaid A, Richardson JA, Emoto N, Hammer RE, et al. Interaction of endothelin-3 with endothelin-B receptor is essential for development of epidermal melanocytes and enteric neurons. Cell 1994;79:1277–85.

Bingham NC, Verma-Kurvari S, Parada LF, Parker KL. Development of a steroidogenic factor 1/Cre transgenic mouse line. Genesis 2006;44:419–24.

Bondurand N, Dufour S, Pingault V. News from the endothelin-3/EDNRB signaling pathway: role during enteric nervous system development and involvement in neural crest-associated disorders. Dev Biol 2018;444(Suppl 1):S156–69.

Carney JA, Gordon H, Carpenter PC, Shenoy BV, Go VL. The complex of myxomas, spotty pigmentation, and endocrine overactivity. Medicine (Baltimore) 1985;64:270–83.

Casey M, Vaughan CJ, He J, Hatcher CJ, Winter JM, Weremowicz S, et al. Mutations in the protein kinase A R1α regulatory subunit cause familial cardiac myxomas and Carney complex [published correction appears in J Clin Invest 2001;107:235]. J Clin Invest 2000;106: R31–8.

Ceruti JM, Leirós GJ, Balañá ME. Androgens and androgen receptor action in skin and hair follicles. Mol Cell Endocrinol 2018;465:122–33.

Copeland NG, Gilbert DJ, Cho BC, Donovan PJ, Jenkins NA, Cosman D, et al. Mast cell growth factor maps near the steel locus on mouse chromosome 10 and is deleted in a number of steel alleles. Cell 1990;63:175–83.

Correa R, Salpea P, Stratakis CA. Carney complex: an update. Eur J Endocrinol 2015;173: M85–97.

Courcoutsakis NA, Tatsi C, Patronas NJ, Lee CC, Prassopoulos PK, Stratakis CA. The complex of myxomas, spotty skin pigmentation and endocrine overactivity (Carney complex): imaging findings with clinical and pathological correlation. Insights Imaging 2013;4:119–33.

Drelon C, Berthon A, Sahut-Barnola I, Mathieu M, Dumontet T, Rodriguez S, et al. PKA inhibits WNT signalling in adrenal cortex zonation and prevents malignant tumour development. Nat Commun 2016;7:12751.

Driskell RR, Lichtenberger BM, Hoste E, Kretzschmar K, Simons BD, Charalambous M, et al. Distinct fibroblast lineages determine dermal architecture in skin development and repair. Nature 2013 (cited 2021 Apr 28);504:277–81.

Dumontet T, Sahut-Barnola I, Septier A, Montanier N, Plotton I, Roucher-Boulez F, et al. PKA signaling drives reticularis differentiation and sexually dimorphic adrenal cortex renewal. JCI Insight 2018;3:e98394.

Espiard S, Vantyghem MC, Assié G, Cardot-Bauters C, Raverot G, Brucker-Davis F, et al. Frequency and incidence of Carney complex manifestations:

A prospective multicenter study with a three-year follow-Up. J Clin Endocrinol Metab 2020;105:dgaa002.

Garcia RJ, Ittah A, Mirabal S, Figueroa J, Lopez L, Glick AB, et al. Endothelin 3 induces skin pigmentation in a keratin-driven inducible mouse model. J Invest Dermatol 2008;128:131–42.

Geissler EN, Ryan MA, Housman DE. The dominant-white spotting (W) locus of the mouse encodes the c-kit proto-oncogene. Cell 1988;55:185–92.

Hachisuka J, Ichikawa M, Moroi Y, Urabe K, Furue M. A case of Carney complex. Int J Dermatol 2006;45:1406–7.

Hosoda K, Hammer RE, Richardson JA, Baynash AG, Cheung JC, Giaid A, et al. Targeted and natural (piebald-lethal) mutations of endothelin-B receptor gene produce megacolon associated with spotted coat color in mice. Cell 1994;79:1267–76.

Joost S, Annusver K, Jacob T, Sun X, Dalessandri T, Sivan U, et al. The molecular anatomy of mouse skin during hair growth and rest. Cell Stem Cell 2020;26:441–57.e7.

Kapoor R, Dhatwalia SK, Kumar R, Rani S, Parsad D. Emerging role of dermal compartment in skin pigmentation: comprehensive review. J Eur Acad Dermatol Venereol 2020;34:2757–65.

Kasamatsu S, Hachiya A, Higuchi K, Ohuchi A, Kitahara T, Boissy RE. Production of the soluble form of KIT, s-KIT, abolishes stem cell factor-induced melanogenesis in human melanocytes. J Invest Dermatol 2008;128:1763–72.

Kirschner LS, Carney JA, Pack SD, Taymans SE, Giatzakis C, Cho YS, et al. Mutations of the gene encoding the protein kinase A type I-alpha regulatory subunit in patients with the Carney complex. Nat Genet 2000;26:89–92.

Kunisada T, Yamazaki H, Hirobe T, Kamei S, Omoteno M, Tagaya H, et al. Keratinocyte expression of transgenic hepatocyte growth factor affects melanocyte development, leading to dermal melanocytosis. Mech Dev 2000;94:67–78.

Lynch MD, Watt FM. Fibroblast heterogeneity: implications for human disease. J Clin Invest 2018;128:26–35.

Matsumoto K, Tajima H, Nakamura T. Hepatocyte growth factor is a potent stimulator of human melanocyte DNA synthesis and growth. Biochem Biophys Res Commun 1991;176:45–51.

Matsunaga T, Gohda E, Takebe T, Wu YL, Iwao M, Kataoka H, et al. Expression of hepatocyte growth factor is up-regulated through activation of a cAMP-mediated pathway. Exp Cell Res 1994;210:326–35.

Mccallion AS, Chakravarti A. *EDNRB*/*EDN3* and Hirschsprung disease type II. Pigment Cell Res 2001;14:161–9.

Murphy BM, Weiss TJ, Burd CE. Rapid generation of primary murine melanocyte and fibroblast cultures. J Vis Exp 2019;148:59468.

Muzumdar MD, Tasic B, Miyamichi K, Li L, Luo L. A global double-fluorescent Cre reporter mouse. Genesis 2007;45:593–605.

Okazaki M, Yoshimura K, Suzuki Y, Uchida G, Kitano Y, Harii K, et al. The mechanism of epidermal hyperpigmentation in café-au-lait macules of neurofibromatosis type 1 (von Recklinghausen's disease) may be associated with dermal fibroblast-derived stem cell factor and hepatocyte growth factor. Br J Dermatol 2003;148:689–97.

Passeron T, Valencia JC, Bertolotto C, Hoashi T, Le Pape E, Takahashi K, et al. SOX9 is a key player in ultraviolet B-induced melanocyte differentiation and pigmentation. Proc Natl Acad Sci USA 2007;104:13984–9.

Patel MV, McKay IA, Burrin JM. Transcriptional regulators of steroidogenesis, DAX-1 and SF-1, are expressed in human skin. J Invest Dermatol 2001;117:1559–65.

Sahut-Barnola I, de Joussineau C, Val P, Lambert-Langlais S, Damon C, Lefrançois-Martinez AM, et al. Cushing's syndrome and fetal features resurgence in adrenal cortex–specific Prkar1a knockout mice. PLoS Genet 2010;6:e1000980.

Serre C, Busuttil V, Botto JM. Intrinsic and extrinsic regulation of human skin melanogenesis and pigmentation. Int J Cosmet Sci 2018;40:328–47.

Slominski A, Zbytek B, Nikolakis G, Manna PR, Skobowiat C, Zmijewski M, et al. Steroidogenesis in the skin: implications for local immune functions. J Steroid Biochem Mol Biol 2013;137:107–23.

Stratakis CA. Carney complex: A familial lentiginosis predisposing to a variety of tumors. Rev Endocr Metab Disord 2016;17:367–71.

Thulabandu V, Chen D, Atit RP. Dermal fibroblast in cutaneous development and healing. Wiley Interdiscip Rev Dev Biol 2018;7: 10.1002/wdev.307.

Verastegui C, Bille K, Ortonne JP, Ballotti R. Regulation of the microphthalmia-associated transcription factor gene by the Waardenburg syndrome type 4 gene, SOX10. J Biol Chem 2000;275:30757–60.

Wang Y, Viennet C, Robin S, Berthon JY, He L, Humbert P. Precise role of dermal fibroblasts on melanocyte pigmentation. J Dermatol Sci 2017;88:159–66.

Wolnicka-Glubisz A, Pecio A, Podkowa D, Plonka PM, Grabacka M. HGF/SF increases number of skin melanocytes but does not alter quality or quantity of follicular melanogenesis. PLoS One 2013;8:e74883.

Wu BY, Lee SP, Hsiao HC, Chiu H, Chen CY, Yeo YH, et al. Matriptase expression and zymogen activation in human pilosebaceous unit. J Histochem Cytochem 2014;62:50–9.

Zouboulis CC. Sebaceous gland receptors. Dermatoendocrinol 2009;1:77–80.

SUPPLEMENTARY MATERIALS AND METHODS

Primary murine skin cell cultures and immunostaining

Primary cultures of fibroblasts and melanocytes were dispersed from enhanced GFP−positive skin samples dissected under a fluorescent binocular loupe (from the external genitalia, tail, base of the forelimbs, and around the eyes) on mice aged 4 days: 6 wild-type (*Prkar1a*$^{fl/+}$*::Sf1-Cre/+::R26R*$^{mTmG/+}$) and 11 $AdKO_{2.0}$ (*Prkar1a*$^{fl/fl}$*::Sf1-Cre/+::R26R*$^{mTmG/+}$) mice were used. The skin samples were cut into small pieces of about 1 mm^3 using a scalpel. Digestion of tissue pieces and differential cultures of fibroblasts and melanocytes were performed according to the protocol described by Murphy et al. (2019).

At the first passage, fibroblasts were cultured for 3 days (66,000 cells per well, 6 wells for wild-type cells, and 12 for knockout cells); then, serum was weaned for 6 hours and treated with 3.10^{-5} M forskolin or vehicle (DMSO) for 48 hours. A fraction of the conditioned media was collected after 24 and 48 hours, and forskolin or vehicle treatments were performed for hepatocyte GF ELISA dosages. At 48 hours, the cells were harvested for RNA extraction. At the first passage, wild-type melanocytes were seeded (5,000 cells per well, eight wells in total) and grown until day 14 without any passage in conditioned media from either wild-type or $AdKO_{2.0}$ fibroblasts. In parallel, fibroblast cultures were split every 3−4 days, and their media were enriched with protein kinase A and protein kinase C activators used in melanocyte medium conditions as described by Murphy et al. (2019). Fractions of these media were collected for hepatocyte GF assays. On day 14, melanocytes were photographed in regions with the most cell density. Not enough melanocytes were present in the cultures for RNA extraction. The number of passages of fibroblast cultures did not exceed passage 5.

At passage 1, a fraction of fibroblast and melanocyte suspensions was seeded on coverslips to perform vimentin/enhanced GFP labeling for fibroblasts and MLAN-A labeling for melanocytes.

SUPPLEMENTARY REFERENCES

Duverger O, Morasso MI. Epidermal patterning and induction of different hair types during mouse embryonic development. Birth Defects Res C Embryo Today 2009;87:263−72.

Murphy BM, Weiss TJ, Burd CE. Rapid generation of primary murine melanocyte and fibroblast cultures. J Vis Exp 2019;148:59468.

Slominski A, Zbytek B, Nikolakis G, Manna PR, Skobowiat C, Zmijewski M, et al. Steroidogenesis in the skin: implications for local immune functions. J Steroid Biochem Mol Biol 2013;137:107−23.

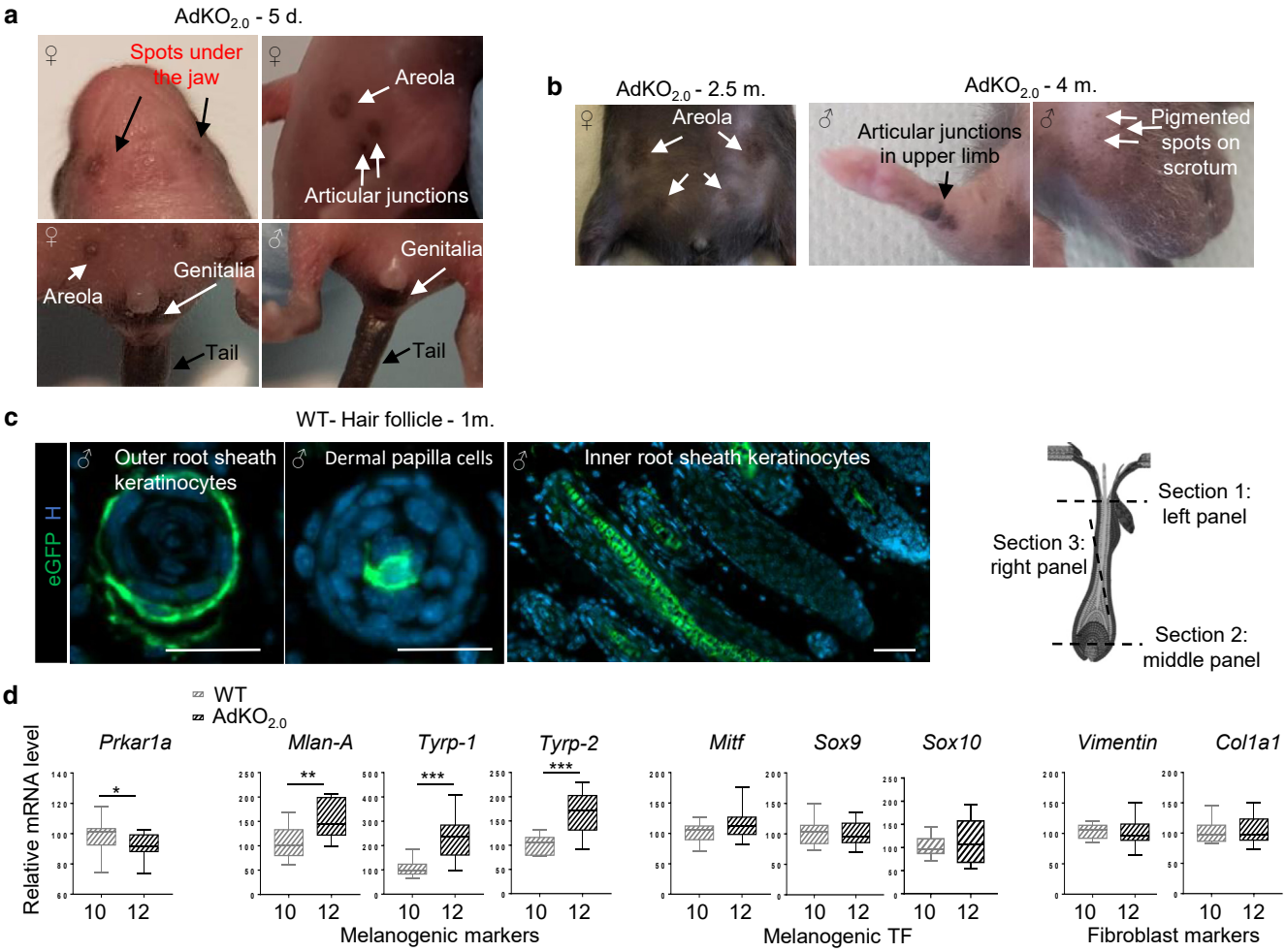

Supplementary Figure S1. *Sf1-Cre* activity in AdKO$_{2.0}$ and WT mice. (**a, b**) Pigmentation in (**a**) young and (**b**) adult AdKO$_{2.0}$ mice. (**c**) In various skin types, Cre is also active in hair follicles: representative picture from a WT male skin section aged 1 month (follicle drawing was inspired by Slominski et al., 2013). Bars = 50 μm. (**d**) QPCR analyses from WT and AdKO$_{2.0}$ perigenital skins (aged 5 days) confirm melanogenic markers–increased expression. As expected, regarding restricted Cre activity, *Prkar1a* mRNA level is only slightly decreased in AdKO$_{2.0}$. mRNA expression of melanogenic transcription factors or fibroblast markers is unchanged. n is indicated under the graphs. Statistical analyses were performed by Mann–Whitney test. *$P < 0.05$, **$P < 0.01$, and ***$P < 0.001$. 1m, 1 month; 2.5 m, 2.5 months; 4 m, 4 months; 5 d, 5 days; eGFP, enhanced GFP; WT, wild-type.

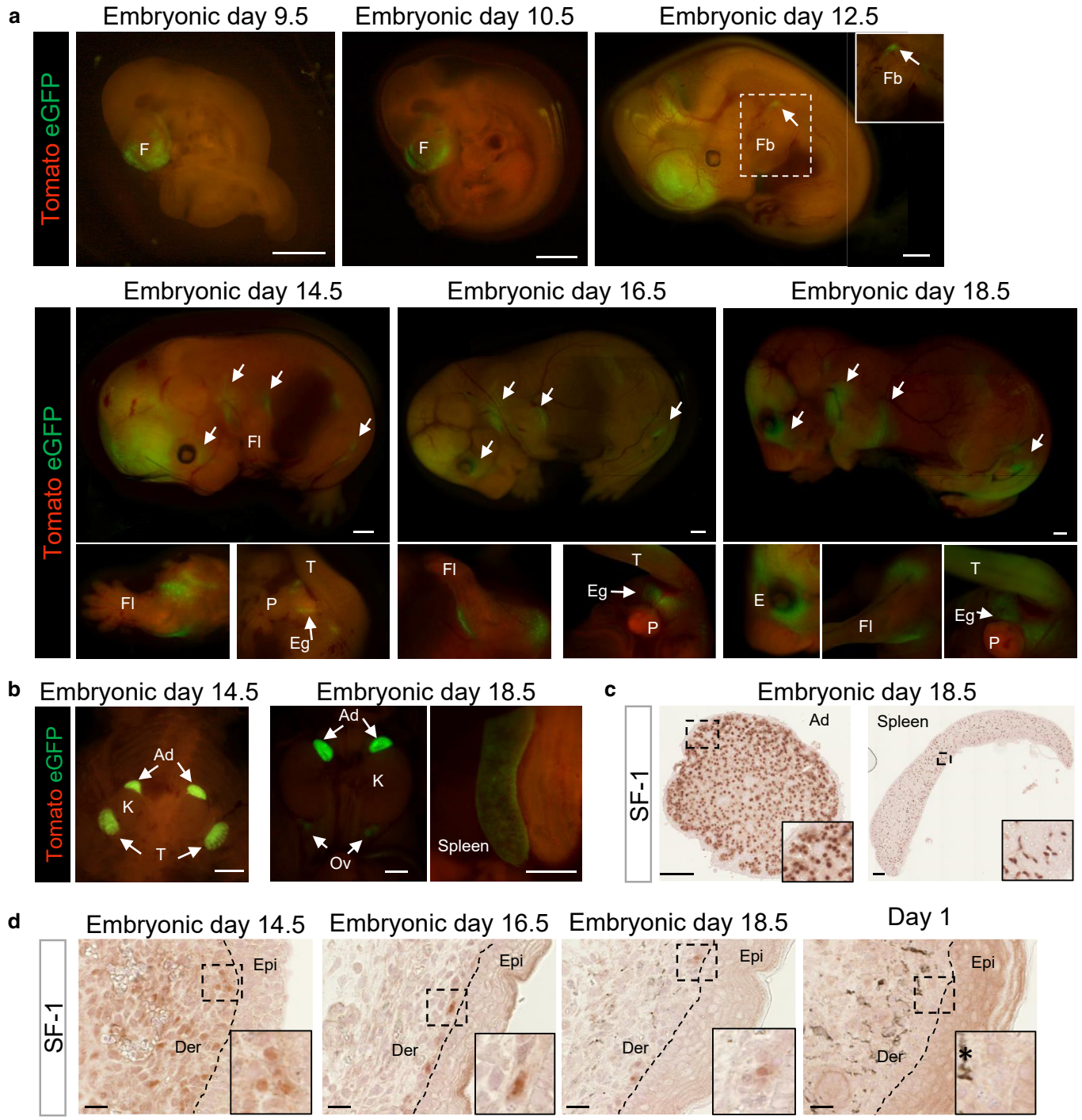

Supplementary Figure S2. *Sf1-Cre* activity and SF-1 endogenous expression in mouse embryonic skin. (**a**) *Prkar1a*$^{fl/+}$*::Sf1-Cre/+::R26R*$^{mTmG/+}$ (referred to as WT) mice allow tracking eGFP expression sites that report *Sf1-Cre* driver activity. From embryonic day 12.5 onward, direct eGFP fluorescence highlights Cre cutaneous activity (arrows), which corresponded to melanic areas in the $AdKO_{2.0}$ mice. Magnifications of the different eGFP-positive areas are presented either in a white square (embryonic day 12.5) or under the embryo images (embryonic days 14.5, 16.5, and 18.5). From embryonic day 14.5, eGFP signal appears as a symmetrical dotted pattern, typical of the planar view of a primary placode (the first sign of hair follicle induction). In the later stages, this symmetrical eGFP pattern becomes denser as the waves of hair follicle induction progress to secondary (embryonic day 16.5) and tertiary (embryonic day 18.5) placodes (Duverger and Morasso, 2009). F is the same as telencephalon. (**b**) Detection of eGFP (*Sf1-Cre* recombined) and Tomato (nonrecombined) fluorescent signals in reference tissues for SF-1 expression. Bars = 1 mm. (**c**) SF-1 immunodetection in embryonic adrenal and spleen (magnification is shown in a black square). Bars = 100 μm. (**d**) Immunodetection of nuclear SF-1 signal in some cells of the dermis (magnification is shown in a black square) from embryonic day 14.5 to embryonic day 18.5 in the genital skin. On day 1, SF-1 staining is no longer detected, whereas dermal melanin pigments (*) are normally detected. Bars = 20 μm. Ad, adrenal; Der, dermis; E, eye; Eg, external genitalia; eGFP, enhanced GFP; Epi, epidermis; F, forebrain; Fb, forelimb bud; Fl, forelimb; K, kidney; Ov, ovary; P, penis; SF-1, steroidogenic factor-1; T, tail; Ts, testis; WT, wild-type.

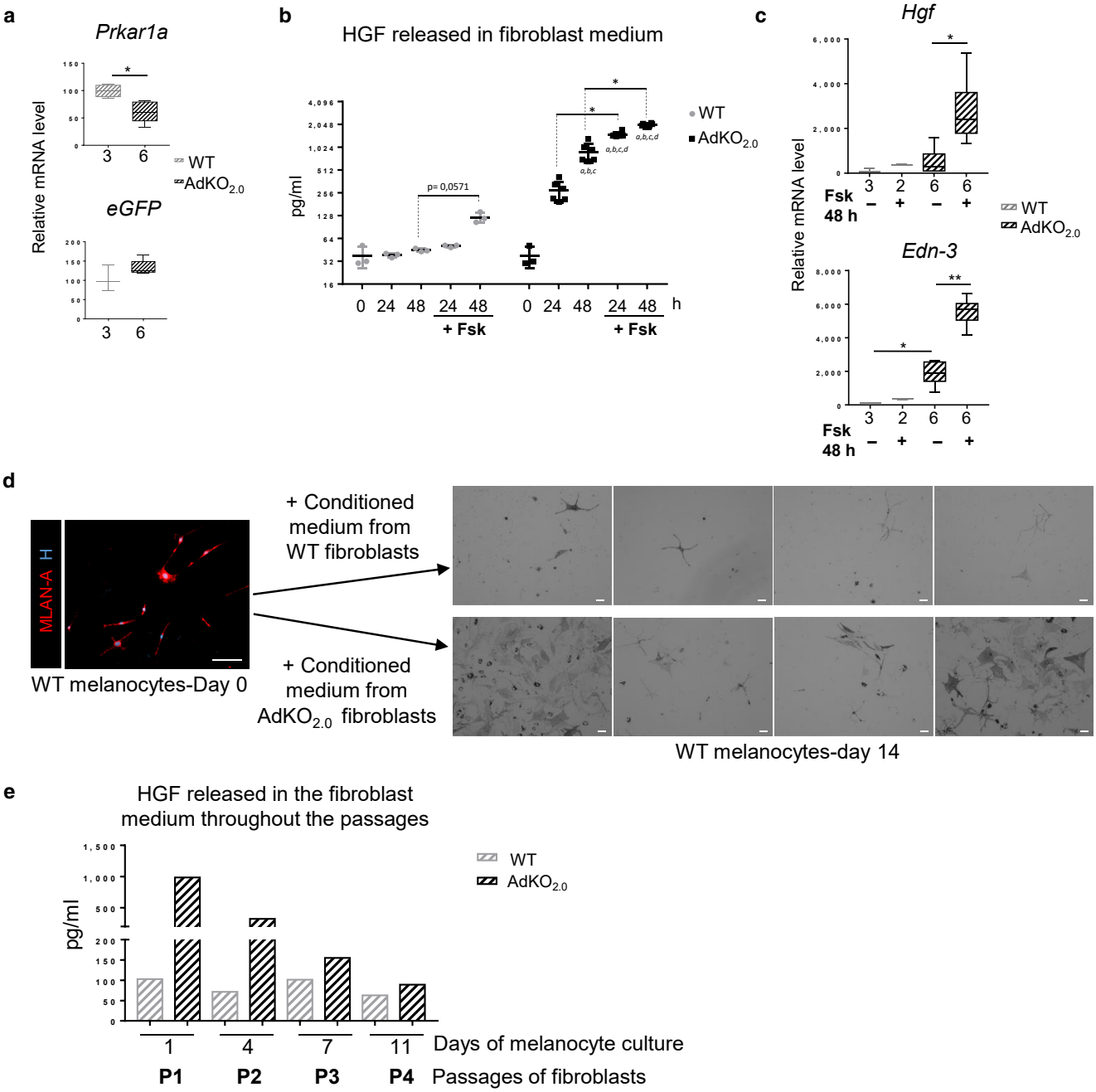

Supplementary Figure S3. Primary cultures of AdKO$_{2.0}$ fibroblasts produce melanogenic and proliferative signals and respond to Fsk. (**a**) qPCR analyses (*Prkar1a* and *eGFP*) of WT and AdKO$_{2.0}$ primary cultures of fibroblasts. n is indicated under the graphs. Statistical analyses were performed by Mann–Whitney test. *$P < 0.05$. (**b**) Detection of HGF in the culture medium from WT and AdKO$_{2.0}$ fibroblasts at 0, 24, and 48 hours with or without Fsk treatment. Statistical analysis was conducted by Kruskal–Wallis tests followed by uncorrected Dunn's test. **a–d** indicates significant differences (at least $P < 0.05$) compared respectively with the WT at 24 hours, WT at 48 hours, WT at 24 hours + Fsk, and WT at 48 hours + Fsk. Mann–Whitney test (* or *P*-value) was used to assess the effect of Fsk treatment for the same time point in each genotype. *$P < 0.05$. (**c**) qPCR analyses of melanogenic signals of WT and AdKO$_{2.0}$ primary cultures of fibroblasts with or without Fsk treatment (48 hours). n is indicated under the graphs. Statistical analyses were performed by Mann–Whitney test. *$P < 0.05$ and **$P < 0.01$. (**d**) Immunofluorescent labeling of MLAN-A in WT primary cultures of melanocytes on the first day of the experiment before treatment (14 days) with conditioned medium from either WT or AdKO$_{2.0}$ fibroblast primary cultures. Nuclei are stained with Hoechst (indicated with H, blue). The four pictures (right panels) taken in four different wells show the fields in which the highest density of melanocytes is observed. Note that the clusters of melanocytes present a dark brown color. Bars = 100 μm. (**e**) The concentrations of HGF in the conditioned media decrease with each P of AdKO$_{2.0}$ fibroblast cultures. eGFP, enhanced GFP; Fsk, forskolin; h, hour; HGF, hepatocyte GF; P, passage; WT, wild-type.

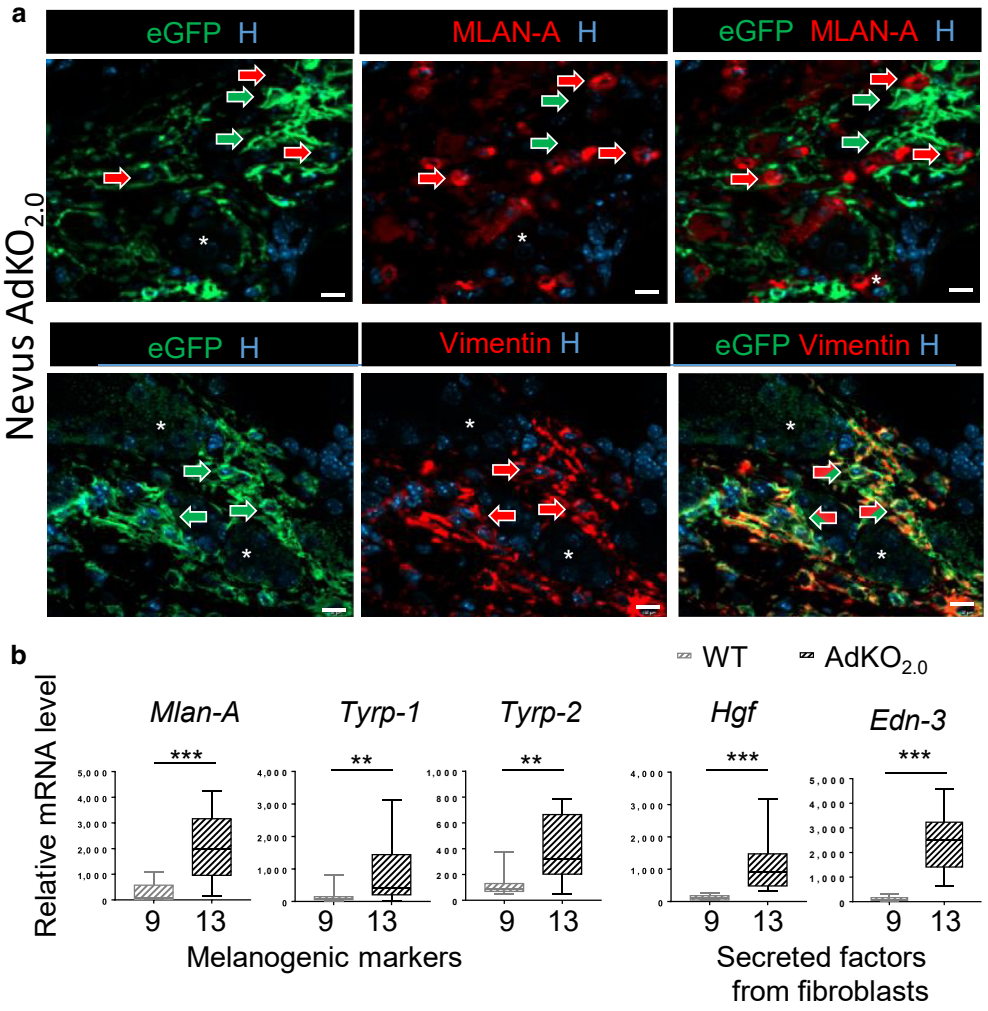

Supplementary Figure S4. PKA increase affects dermal fibroblasts in AdKO$_{2.0}$ blue nevi. (**a**) Coimmunofluorescent labeling of eGFP (*Prkar1a*-KO cells, green arrows) and MLAN-A (melanocytes, red arrows) in top panels or vimentin (mesenchymal cells, red arrows) in bottom panels, in the blue nevus shown in Figure 3a. Cells colabeled with eGFP and vimentin are identified by striped arrows. Hoechst nuclei staining is indicated with H. Sebaceous glands are indicated with an asterisk (*). Bars = 10 μm. (**b**) qPCR analyses of melanogenic markers and fibroblastic-secreted factors in WT skin (sampling located where nevi form in mutants) and AdKO$_{2.0}$ nevi from females aged 3–4 months. n is indicated under the graphs. Statistical analyses were performed by Mann–Whitney test. $^{**}P < 0.01$ and $^{***}P < 0.001$. eGFP, enhanced GFP; KO, knockout; PKA, protein kinase A; WT, wild-type.

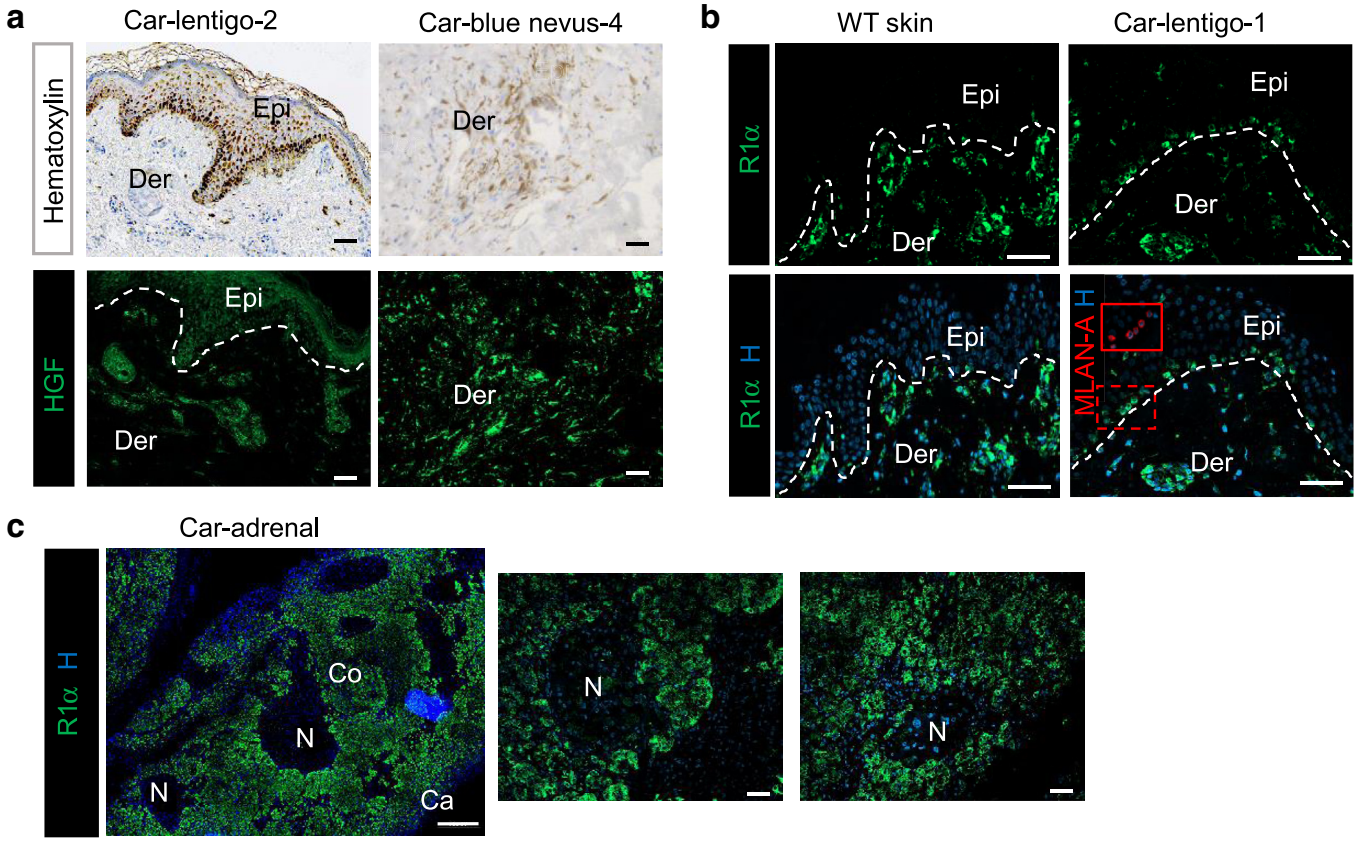

Supplementary Figure S5. Lentigines, blue nevi, and adrenal glands in patients with CNC. (**a**) Hematoxylin staining (black staining is melanin pigments) and immunostaining of HGF in lentigines and in blue nevus from patients with CNC. Bars = 50 μm. (**b**) Immunofluorescent labeling of R1α in lentigines from patients with CNC. Hoechst nuclei staining is indicated with H. The red inset (corresponding to the dotted red frame) shows the immunolabeling of MLAN-A. Bars = 50 μm. (**c**) Immunolabeling of R1α in micronodular hyperplastic adrenal gland from patients with CNC. Ns are negative for R1α, confirming the specificity of the antibody. Bars = 500 μm in the left panel and 50 μm in the two right-hand panels. Ca, capsule; CNC, Carney complex; Co, cortex; Der, dermis; Epi, epidermis; HGF, hepatocyte GF; N, nodule; WT, wild-type.

Supplementary Table S1. Immunohistological and Western Blot Conditions

Immunohistochemistry and Immunofluorescence

Antibody	Supplier	Reference	Host	Dilution	Epitope Retrieval
GFP	Invitrogen	A11122	Rabbit	1/1,500	25 minutes boiling in TE solution (10 mM Tris, 1 mM EDTA, pH = 9.0)
GFP	Abcam	5450	Goat	1/1,000	
HGF	R&D Systems	AB-294-NA	Goat	1/100	
MLAN-A	Abclonal	A6290	Rabbit	1/200	
PRKAR1A	BD Biosciences	610610	Mouse	1/400	
Vimentin	Cell Signaling Technology	5741	Rabbit	1/1,000	
SF-1	Cosmo Bio	KAL-KO611	Rabbit	1/100	

Western Blot

Antibody	Supplier	Reference	Host	Dilution	Blocking
Actin	Sigma-Aldrich	A2066	Rabbit	1/5,000	10% milk
GAPDH	Sigma-Aldrich	G9545	Rabbit	1/10,000	
HGF	R&D Systems	AB-294-NA	Goat	1/250	
MLAN-A	Abclonal	A6290	Rabbit	1/1,000	

Abbreviations: HGF, hepatocyte GF; SF-1, steroidogenic factor-1.

Supplementary Table S2. Sequences of the Primers Used for RT-qPCR

Target	Forward (5′–3′)	Reverse (5′–3′)
Actin	TCATCACTATTGGCAACGAGC	AGTTTCATGGATGCCACAGG
C-kit	AGGTGTACCACTCCTGTCT	TCCTCGACAACCTTCCATTG
Edn3	GCTGCACGTGCTTCACTTAC	TTTCTGGAACTGGCCCCAAG
Ednrb	TCGCTCTGTATTTGGTGAGCA	ATTCGGCGAGTGTTCTTGC
eGFP	GAAGCAGCACGACTTCTTCAAG	AAGTCGATGCCCTTCAGCTC
Hgf	GGGACCCTGGTGTTTCACAA	CATCAAAGCCCTTGTCGGGA
Kitl	ACGTCTGAGTGCTGAAAACCC	CACCATCCAGGCTGAAATCTAC
Mlana	GCACAGACGCTCCTATGTCA	AGTACCAGCAGCCGATAAGC
Col1A1	CGACCTCAAGATGTGCCACT	CCATCGGTCATGCTCTCTCC
Met	ACCCCAAGGTACAAACTCCAG	AAGCGTTCTGCTACACCGTC
Mitf	CCAGGCCTTACCATCAGCAA	AGCTCCTTAATGCGGTCGTT
Prkar1a	CGGGAATGCGAGCTCTATGT	CTCGAGTCAGTACGGATGCC
Sox10	ATGTCAGATGGGAACCCAGA	GTCTTTGGGGTGGTTGGAG
Sox9	GCGGAGCTCAGCAAGACTCTG	ATCGGGGTGGTCTTTCTTGTG
Tyrp1	GGATTCATGGTACTGGTGAGCA	TGGAAACTGAGCCCAAACCT
Tyrp2	TAAGCAGTATGGCTGGAGCAC	CTTCTCGCCAGTCTTCCTTGT
Vim	GGATCAGCTCACCAACGACA	AAGGTCAAGACGTGCCAGAG

Supplementary Table S3. Human skin Information

Number	Identification Number	Diagnosis	Sample
Car-skin-1	CAR 27.04	Skin myxoma	Sample for WB
Car-skin-2	CMC.01	Spitz nevus	Sample for WB
Car-nevus-5	CAR46.01	Nevus	Sample for WB
Car-nevus-4	CAR 20.15	Blue nevus	Sample for WB and histological slides
Car-nevus-3	CAR 742.01	Blue nevus	Histological slides
Car-lentigo-1	CAR 58.02	Benign lentigo	Histological slides
Car-lentigo-2	CAR 510.01	Benign lentigo	Histological slides

Abbreviation: WB, western blot.

Supplementary Table S4. Clinical Data of Patients with CNC

Sample Identifier	*PRKAR1A* Mutation	Age, y	Sex	CNC-Associated Manifestations	Hormonal Data
CAR27.04	c.124C>T/ p.Arg42X	Data not available	Female	Data not available	Data not available
CMC.01	Suspected somatic defect	Data not available	Male	Data not available	Data not available
CAR46.01	No mutation	46	Male	GH excess, thyroid nodules, LCCSCT, PPNAD, nevus	410 mg/ml IGF-1 (110–267) 0.9 ng/dl Free T4 (0.7–1.5) 0.98 uIU/ml TSH (0.4–4) 274 ng/dl testosterone (240–871) 3 µg/dl midnight serum cortisol 2.5 µg/l prolactin (1–25) GH at 2 hours of 2.8 ng/ml OGTT 8 µg/24 h, 4.8 µg/24 h, 6.7 µg/24 h, and 6.8 µg/24 h (3.5–45) of urinary free cortisol
CAR20.15	c.491_492delTG/p. Val164fsX4	32	Female	lentigines, blue nevi, growth hormone excess, PPNAD, breast myxomas, pituitary adenoma, breast ductal adenoma, ovarian cyst	3.3 mcg/dl midnight cortisol 1.44 uIU/ml TSH (0.4–4) 0.8 ng/dl free T4 (0.7–1.5) 1.64 mcg/ml DHEAS (18–244) GH at 2 hours of 4.9 ng/ml OGTT 486 ng/ml IGF-1 (110–267) 4 U/l FSH (3–11 for follicular, 6–21 for midcycle, 1–9 for luteal) LH <1 U/l (1–12 for follicular, 17–77 for midcycle, 0–15 for luteal)
CAR742.01	No mutation		Male	Lentigines, blue nevus, pigmented epithelioid melanocytoma. The patient also has a history of multiple myeloma	Data not available
CAR58.01	Exon 2 deletion	43	Female	Benign lentigo, cardiac myxoma, PPNAD, hyperprolactinemia, thyroid nodules, lentigines	7.2 mcg/dl midnight serum cortisol 7 U/l FSH (3–11 for follicular, 6–21 for midcycle, 1–9 for luteal) 1.27 mcIU/ml TSH (0.4–4) DHEAS <15 µg/dl (18–244) 79 pg/ml estradiol (15–350) 25.5 pg/ml ACTH (9–52) 8.4 mcg/dl thyroxine (4.5–12.5) 4 U/l LH (follicular 1–12, midcycle 17–77, luteal 0–15) 117 ng/ml IGF-1 (110–267) 30.9 mcg/l prolactin (1–25) GH at 2 hours of 0.3 ng/ml OGTT
CAR510.01	No mutation	57	Female	benign lentigo, pituitary adenoma, GH excess, hyperprolactinemia, lentigines. The patient also has a history of infiltrating ductal breast carcinoma and a schwannoma.	218 ng/ml IGF-1 (after TSS) (110–267) 18 pg/ml estradiol (after TSS) (15–350) 2 U/l LH (after TSS) (11–40) 1.2 ng/dl Free T4 (after TSS) (0.7–1.5) 0.95 uIU/ml TSH (after TSS) (0.4–4) GH at 2 hours of 6.3 ng/ml OGTT (before TSS) 7 pg/ml ACTH (after TSS) (9–52) 9 U/l FSH (after TSS) (22–153) 11 µg/l Prolactin (after TSS) (1–25) 1.4 mcg/dl midnight serum cortisol (after TSS) UFC: 52 mcg/24 h and 25 mcg/24 h

Abbreviations: ACTH, adrenocorticotropic hormone; CNC, Carney complex; DHEAS, dehydroepiandrosterone sulfate; FSH, follicular-stimulating hormone; GH, growth hormone; h, hour; IGF-1, insulin-like GF 1; LCCSCT, large cell calcifying sertoli cell tumor; LH, luteinizing hormone; OGTT, oral glucose tolerance test; PPNAD, primary pigmented nodular adrenocortical disease; TSH, thyroid-stimulating hormone; TSS, transsphenoidal surgery; UFC, urinary-free cortisol.

Sexually dimorphic activation of innate antitumour immunity prevents adrenocortical carcinoma development

James J Wilmouth JR[1#], Julie Olabe[1#], Diana Garcia-Garcia[1], Cécily Lucas[1], Rachel Guiton[1], Florence Roucher-Boulez[1,2,3], Damien Dufour[1], Christelle Damon-Soubeyrand[1], Isabelle Sahut-Barnola[1], Jean-Christophe Pointud[1], Yoan Renaud[1], Adrien Levasseur[1], Igor Tauveron[1,4], Anne-Marie Lefrançois-Martinez[1], Antoine Martinez[1] and Pierre Val[1*]

1- Institut GReD (Genetics, Reproduction and Development), CNRS UMR 6293, Inserm U1103, Université Clermont Auvergne, 28 Place Henri Dunant 63000 Clermont-Ferrand, France
2- Laboratoire de Biochimie et Biologie Moléculaire, UM Pathologies Endocriniennes, Groupement Hospitalier Est, Hospices Civils de Lyon, Bron, France
3- Univ Lyon, Université Claude Bernard Lyon 1, Lyon, France
4- Endocrinologie Diabétologie CHU Clermont Ferrand 58 rue Montalembert F63000 Clermont Fd France

# These authors contributed equally to this work
* Lead author, to whom correspondence should be addressed (pierre.val@uca.fr)

Summary

In contrast with most cancers, adrenocortical carcinomas (ACC) are more frequent in women than men, but the underlying mechanisms of this sexual dimorphism remain elusive. Homozygous deletion of the negative WNT pathway regulator *ZNRF3* is the most frequent alteration in ACC patients. Here, we show that Cre-mediated inactivation of *Znrf3* in steroidogenic cells of the mouse adrenal cortex is associated with sexually dimorphic tumour progression. Indeed, although most knockout female mice develop metastatic carcinomas over an 18 month-time course, adrenal hyperplasia gradually regresses in male knockout mice. This male-specific regression is associated with induction of senescence and recruitment of macrophages, which differentiate as active phagocytes that clear-out senescent preneoplastic cells. Macrophage recruitment is also observed in female mice. However, it is delayed and dampened compared to males, which allows for tumour progression. Interestingly, testosterone treatment of female knockouts is sufficient to induce senescence, recruitment of phagocytic macrophages and regression of hyperplasia. We further show that although macrophages are present within adrenal tumours at 18 months, MERTK^{high} active phagocytes are mostly found in indolent lesions in males but not in aggressive tumours in females. Consistent with our observations in mice, analysis of RNA sequencing data from the TCGA cohort of ACC shows that phagocytic macrophages are more prominent in men than women and associated with better

prognosis. Altogether, these data establish that phagocytic macrophages prevent aggressive ACC development in male mice and suggest that they may play a key role in the unusual sexual dimorphism of ACC in patients.

Keywords: sexual dimorphism, cancer, macrophages, antitumour immunity, phagocytosis, senescence, senescence associated secretory phenotype, adrenocortical carcinoma, androgens, ZNRF3, WNT signalling

Introduction

Apart from reproductive tissues, cancer incidence and mortality are higher in males than females[1,2]. Adrenocortical carcinoma (ACC), which arises from steroidogenic cells of the adrenal cortex is one of the rare exceptions to this rule. Indeed, ACC female-to-male ratios range from 1.5 to 2.5:1 and women are generally diagnosed at a younger age (Fig S1A)[3–7]. Although the higher rate of steady state proliferation and more efficient adrenal cortex renewal in females [5,8,9] may play a role in sexually dimorphic tumorigenesis, the mechanisms underlying female prevalence of ACC remain elusive.

ACC is an aggressive cancer, with half of the patients presenting with metastatic disease at diagnosis. Overall, 5 year survival rates range between 16 and 47% and decrease to around 10% for metastatic patients[10]. In line with the steroidogenic activity of the adrenal cortex, ACC is associated with hormonal hypersecretion in more than 50% of patients[11]. A vast majority of secreting ACC produce excess glucocorticoids, but some tumours also produce sex steroids or a combination of both [12].

Radical surgical resection of ACC is the most effective therapeutic strategy for localized tumours, but the risk of recurrence remains high[12]. In patients with advanced inoperable or metastatic ACC, the adrenolytic compound mitotane, a derivate of the insecticide DDT, remains the standard of care, used as a single agent or in combination with an etoposide-doxorubicin-platin polychemotherapy[13–15]. Although these treatments can improve recurrence free survival, their benefit on overall survival is still debated[12,13,16–18]. Several phase I/II clinical trials of immune checkpoint inhibitors targeting PD1 and PD-L1, have also been conducted in ACC patients[19–22]. Unfortunately, these were associated with low response rates and have failed to

improve patient outcome significantly. One potential reason for these modest results is the low level of lymphocyte infiltration in ACC[23], which seems associated with local production of glucocorticoids[24].

Understanding the molecular underpinnings of ACC pathogenesis is thus of utmost importance to develop novel therapeutic approaches. Large scale pan-genomic studies have identified homozygous deletion of *ZNRF3* as the most frequent genetic alteration in ACC[25,26]. This gene encodes a membrane E3 ubiquitin-ligase that inhibits WNT signalling by inducing ubiquitination and degradation of Frizzled receptors[27,28]. We previously showed that conditional ablation of *Znrf3* within steroidogenic cells of the adrenal cortex, resulted in moderate WNT pathway activation and adrenal zona fasciculata hyperplasia up to 6 weeks, suggesting that ZNRF3 was a potential tumour suppressor in the adrenal cortex[29]. However, we did not evaluate later stages of tumour progression.

Here, we show that tumour progression following ablation of *Znrf3* within steroidogenic cells of the adrenal cortex is sexually dimorphic. Whereas most female mice develop full-fledged metastatic carcinomas over an 18 month-time course, adrenal hyperplasia gradually regresses in male knockout mice. We show that male-specific regression of hyperplasia is associated with induction of senescence, recruitment of macrophages and differentiation of active phagocytes that clear out senescent steroidogenic cells. Although some degree of macrophage recruitment is observed in female mice, it is delayed and dampened compared to males, which allows for tumour progression. This phenomenon is dependent on androgens and can be triggered by testosterone treatment in females. Interestingly, even though macrophages are present within adrenal tumours at 18 months, active phagocytes, characterised by expression of the TAM receptor MERTK are mostly found in males but not females. Consistent with our observations in mice, analysis of RNA sequencing data from the TCGA cohort of ACC shows that phagocytic macrophages are more prominent in men than women and associated with better prognosis. Altogether, these data establish that phagocytic macrophages prevent aggressive ACC development in male mice and suggest that they may play a key role in the unusual sexual dimorphism of ACC in patients.

Results

Sexually dimorphic tumour progression in *Znrf3 cKO* adrenals

We previously showed that adrenal targeted ablation of *Znrf3* resulted in massive zona fasciculata hyperplasia at 6 weeks of age, but we did not evaluate the phenotype at later stages[29]. To gain further insight into the potential tumour suppressor function of ZNRF3 in the adrenal cortex, we conducted a kinetic analysis from 4 to 78 weeks (Fig 1). In female *Znrf3 cKO* mice (ZKO), adrenal weight increased progressively from 4 to 6 weeks and plateaued from 9 to 24 weeks. By 52 weeks, *Znrf3 cKO* average adrenal weight was still significantly increased and some adrenals were massively enlarged with weights up to 534mg. This trend was further amplified at 78 weeks with a majority of female *Znrf3 cKO* adrenals showing over a 10-fold increase in weight compared to controls (Fig 1A). This suggested malignant transformation of adrenals over time. Consistent with this idea, introduction of the mTmG reporter in the breeding scheme allowed identification of multiple micro and macro-metastases in the local lymph nodes, peritoneal cavity, liver and lungs of 75% of female *Znrf3 cKO* mice at 78 weeks (Fig 1B and Fig S1B). Histological analysis of adrenals that were associated with metastatic development (Fig 1C) showed complete disorganisation of the cortex that was mostly composed of densely packed small basophilic cells. This was associated with a significant increase in Ki67 labelling index (Fig 1C & D), although proliferation was rather heterogeneous throughout the tumour with areas showing up to 25% Ki67 labelling (Fig S1C). In contrast, in the few mutant mice where no metastases were found at 78 weeks (indolent ZKO), adrenals were largely hyperplastic, but cells retained a relatively normal morphology and Ki67 labelling was similar to control (Fig 1C). Altogether, these data suggested that ZNRF3 behaved as a classical tumour suppressor in female mice, its ablation resulting in a high frequency of aggressive adrenocortical carcinoma formation at 78 weeks. In sharp contrast, although male *Znrf3 cKO* adrenals were also larger at 4 and 6 weeks, adrenal weight steadily declined thereafter, almost returning to normal at 78 weeks (Fig 1E). This was associated with lack of metastatic progression (Fig 1F), benign histology and low Ki67 labelling index (Fig 1G & H), although some patches of higher proliferation could be detected in some adrenals (Fig S1C). This suggested that overall tumour development was rapidly blunted in males, although the initial hyperplastic phase was equivalent to females.

To further gain insight into this sexually dimorphic phenotype, we evaluated proliferation from 4 to 52 weeks. Analysis of Ki67 labelling index showed that following an early significant increase, both males and females had a rapid arrest in proliferation at 6 weeks (Fig 1I & Fig S1D). This remained at low levels up to 52 weeks, although male adrenals displayed a mild but significant rebound at this stage (Fig 1I). The steady decline in adrenal weight, although

proliferation in male knockout adrenals was comparable to controls after 4 weeks, suggested that an active mechanism counteracted tumour progression in males. Surprisingly though, there was no increase in apoptosis, measured by cleaved caspase 3 staining, in either female or male adrenals at 6 and 12 weeks (Fig S1E). To try to further understand the sexually dimorphic phenotype, we conducted a careful kinetic evaluation of adrenal histology. This showed a similar hyperplastic phenotype in males and females at 4 and 6 weeks (Fig 1J). Hyperplasia progressed in females with accumulation of small basophilic cells that composed most of the gland by 52 weeks (Fig 1J). Strikingly, starting at 12 weeks, we observed progressive thinning of the cortex (eosinophilic cells) and concomitant appearance and expansion of multinucleated giant cells (MGCs containing up to 12 nuclei per cell) that progressively took over a large proportion of the male *Znrf3 cKO* gland (up to 40%) (Fig 1J). In females some MGCs were also observed. However, they were first visible at 24 weeks and only represented a small proportion of the gland, even at 52 weeks (Fig 1J). Interestingly, MGCs were reminiscent of fused macrophages that are observed in granulomatous inflammatory diseases, which suggested a potential involvement of innate immune cells in preventing tumour progression in male *Znrf3 cKO* adrenals.

Regression in male *Znrf3 cKO* adrenals is correlated with macrophage infiltration and fusion

To further gain insight into the underpinnings of the regression phenomenon, we analysed global gene expression by bulk RNA sequencing of control and *Znrf3 cKO* male adrenals at 4, 6 and 12 weeks. Gene set enrichment analysis (GSEA) of the RNA sequencing data using the C5 Gene Ontology database (MSigDB) showed that at 12 weeks, the 34 most significantly enriched gene sets were all related with immune response and inflammation (Fig 2A). Most of these gene sets were either not (FDR >0.05) or negatively enriched at 4 weeks and showed an intermediate enrichment score at 6 weeks. This suggested that ablation of Znrf3 resulted in the progressive establishment of a proinflammatory environment. Consistent with this idea, a large number of proinflammatory cytokines and chemokines genes were progressively upregulated at 6 and 12 weeks (Fig 2B and Fig S2A). Establishment of an inflammatory environment was further evaluated by immunohistochemistry for the pan leukocyte marker CD45. In control male adrenals, a few CD45-positive cells were found scattered throughout the cortex. Four-week-old male *Znrf3 cKO* adrenals were quite similar to controls, although more mononucleated leukocytes were present in the inner cortex. At 6 and 12 weeks, the number of CD45 positive cells dramatically increased in KO adrenals (Fig 2C and Fig S2B). These

177 comprised both mononuclear cells (stars) and the multinucleated giant cells (arrowheads) that
178 accumulated in the inner cortex (Fig 2C). To further identify the immune cell types that
179 composed the infiltrate, we deconvoluted RNA sequencing data with CibersortX using immune
180 cell signatures from ImmuCC (Fig 2D) and mMCP (Fig S2C). Both approaches showed a
181 significant increase in macrophages populations, which represented 63% of all immune
182 populations at 12 weeks. This was further confirmed by GSEA, showing a highly significant
183 positive enrichment of multiple macrophages signatures at 12 weeks (Fig 2E) and by RTqPCR
184 showing a progressive accumulation of the macrophage marker transcripts *Cd68*, *Adgre1* and
185 *Cd11b* (Fig S2D). Altogether, these data strongly suggested that regression of adrenal cortex
186 hyperplasia in *Znrf3 cKO* males was associated with establishment of a proinflammatory
187 environment and massive recruitment of macrophages.
188 To further confirm the nature of infiltrating cells, adrenals from control and *Znrf3 cKO* males
189 were dissociated and analysed by flow cytometry (Fig 2F and Fig S2E). In wild-type adrenals,
190 $CD64^+/F4/80^+$ macrophages represented ~30 to 36% of all live $CD45^+$ cells at 4 and 6 weeks.
191 In *Znrf3 cKO* adrenals, this proportion was significantly increased up to ~49%-54% at these
192 two stages, demonstrating increased macrophage infiltration as early as 4 weeks. Flow
193 cytometry analyses further showed that at 4 weeks, almost 80% of $CD45^+/CD64^+$ macrophages
194 co-expressed the M1 markers CD38 and MHC-II, together with the M2 marker CD206, both in
195 wild-type and *Znrf3 cKO* adrenals (Fig S3A). Although there was a very mild but significant
196 increase in both $MHC\text{-}II^+/CD206^+$ and $CD38^+/CD206^+$ double-positive macrophages in 6-week
197 *Znrf3 cKO* adrenals, there was no significant difference in either M1 or M2 macrophages
198 proportions, following ablation of *Znrf3* at the two analysed stages (Fig S3A). RTqPCR (Fig
199 S3B) and RNA sequencing analyses (Fig S3C-D) further confirmed deregulation of both M1
200 and M2 markers in *Znrf3cKO* adrenals, indicating that infiltrating macrophages had mixed M1
201 and M2 characteristics at 4 and 6 weeks.
202 Unfortunately, the majority of $CD45^+$ MGCs that accumulated from 12 weeks onward, had a
203 cell diameter larger than 40 µm, which precluded their characterisation by flow cytometry (Fig
204 S4A). To further characterise immune infiltration during the regression period, we thus resorted
205 to immunohistochemical analysis. Staining with pan-macrophages markers IBA-1 and F4/80
206 confirmed progressive infiltration from 4 to 12 weeks (Fig 2G). Interestingly, although
207 mononuclear cells appeared equivalently labelled by both IBA-1 and F4/80, IBA-1 staining of
208 MGCs was weak compared to F4/80 (Fig 2G). However, MGCs displayed high levels of
209 cytoplasmic CD68 staining, suggesting that they were derived from the fusion of mononuclear
210 macrophages (Fig 2G). Macrophage fusion has been shown to rely on TREM2, an activating

receptor of the Ig-superfamily and on TYROBP/DAP12, its transmembrane signalling adaptor [30,31]. Interestingly, expression of *Trem2* and *Tyrobp/Dap12* was strongly increased in RTqPCR at 12 weeks (Fig S4B) and IHC analyses showed a strong up-regulation of both TREM2 and TYROBP protein accumulation in MGCs (Fig 2H). High magnification images further showed TREM2/TYROBP-positive mononuclear macrophages actively fusing with MGCs (Fig 2I, arrowheads).

Altogether, this suggested that *Znrf3* ablation in steroidogenic cells resulted in macrophage infiltration and fusion to form MGCs in male adrenals.

Infiltrating macrophages actively phagocytose steroidogenic cells

Macrophages have been suggested to play a role in the early response to oncogenic insult, by clearing out preneoplastic cells[7,32]. Interestingly, GSEA of RNA sequencing data showed a progressive significant enrichment of gene sets associated with phagocytosis and clearance of apoptotic cells in male *Znrf3 cKO* adrenals, suggesting a potential role of phagocytosis in regression of hyperplasia (Fig 3A). Phagocytosis involves chemotaxis of macrophages towards target cells that express "find-me" signals and recognition of target cells through "eat-me" signals that can be received directly by phagocytic receptors, or indirectly after opsonization. Detailed analysis of RNA sequencing data showed significant up-regulation of genes coding the potential "find-me" chemokine CX3CL1[33], and of the GPR132/G2A and P2RY2/P2RY6 metabotropic receptors that recognize lysophosphatidylcholine (GPR132)[34] and nucleotides (P2RY2/P2RY6)[35], released by target cells (Fig 3B). Among potential "eat-me" signals, we found significant overexpression of C1Q complement components *C1qa*, *C1qb* and *C1qc* which have been shown to decorate the surface of apoptotic cells to target them for phagocytosis [35,36] (Fig 3B), and of *Slamf7*, which is involved in phagocytosis of hematopoietic tumour cells [37]. There was also upregulation of the gene coding MFGE8, which opsonizes apoptotic cells and is recognised by the integrin receptors $\alpha_v\beta_3$ and $\alpha_v\beta_5$ at the membrane of macrophages [38,39] (Fig 3B & 3C). Interestingly, TREM2 and TYROBP, which we found overexpressed both at the mRNA and protein level (Fig 2G, Fig 3B & Fig S4B), can also be involved in the phagocytic process through recognition of lipids and ApoE-opsonized cells [38,40,41]. Among the three TAM receptor tyrosine kinases, which play a central role in phagocytosis (TYRO3, MERTK, AXL)[35,42], *Mertk* was expressed at high levels and showed the most significant upregulation in *Znrf3 cKO* adrenals (Fig 3B &C). Although there was no upregulation of *Gas6* and *Pros1*, the natural TAM receptors ligands [35], there was a strong overexpression of *Lgals3* (27-fold), which

encodes Galectin-3, a phosphatidylserine-independent MERTK-specific opsonin [38,43] (Fig 3B). This was further confirmed by RTqPCR (Fig 3C), suggesting that engagement of MERTK by Galectin-3 may trigger phagocytosis of *Znrf3 cKO* hyperplastic steroidogenic cells.

To further gain insight into a potential phagocytic process in *Znrf3 cKO* adrenals, we analysed expression of the TAM receptor MERTK by IHC. Although some positive cells were found in wild-type adrenals, they were rather scarce and expressed low levels of MERTK (Fig 3D). In contrast, increased numbers of mononuclear MERTK^{high} cells were found in *Znrf3 cKO* adrenals as early as 6 weeks (Fig 3D). Most of these cells also stained for IBA-1, confirming their macrophage identity (Fig S4C). At 6 and 12 weeks, the number of mononuclear MERTK-high cells dramatically increased in *Znrf3 cKO* (Fig3D & Fig S4C). Interestingly, multinucleated fused macrophages expressed very high levels of MERTK (Fig 3D), which was associated with reduced IBA-1 expression (Fig S4C). MERTK^{high} and in particular, fused macrophages, were also positive for TREM2 (Fig S4D). However, TREM2 was expressed in a larger number of macrophages, including mononucleated MERTK^{-} macrophages (Fig S4D). Altogether, this suggested that macrophages infiltration in *Znrf3 cKO* male adrenals was associated with differentiation into active phagocytes.

To test this hypothesis, we evaluated phagocytosis by confocal microscopy. For this, we colocalised expression of 3βHSD and SF-1, two markers of steroidogenic cells with IBA-1 (from 4 to 9 weeks) and MERTK (at 12 weeks). We then counted 3βHSD and SF-1 positive cells that were found within the boundaries of IBA-1^{+} or MERTK^{high} macrophages throughout the confocal Z-stack (Fig 3E). A few IBA-1^{+} macrophages contained 3βHSD positive cells in control adrenals at 4, 6 and 9 weeks, indicating that phagocytosis of steroidogenic cells was taking place at homeostasis in the adrenal (Fig 3E). Interestingly, the number of phagocytic IBA-1^{+} cells was markedly increased in *Znrf3 cKO* adrenals at these three timepoints (Fig 3E), indicating that mononuclear IBA-1^{+} macrophages were actively involved in phagocytosis of *Znrf3 cKO* steroidogenic cells. Increased phagocytosis was also observed for MERTK^{high} macrophages at 12 weeks (Fig 3F).

Altogether, these data show that both IBA-1^{+} and MERTK^{high} macrophages are involved in a dramatic increase in phagocytosis of mutant steroidogenic cells in male *Znrf3 cKO* adrenals.

To further confirm the key role of macrophages in regression of adrenal hyperplasia, we depleted macrophages using a diet enriched with 290mg/kg Pexidartinib, a pharmacological inhibitor of CSF1R. This tyrosine kinase receptor plays a central role for survival of macrophages within their tissue niches, through stimulation by CSF1 and/or IL-34. Consistent

with the key function of CSF1R, flow cytometry analyses showed that 1 week of pexidartinib chow was sufficient to deplete almost all $CD45^+/CD64^+/F4/80^+$ macrophages within the adrenal cortex of control male mice (Fig S4E). We then evaluated the impact of macrophages depletion in male *Znrf3 cKO* mice by feeding them with standard chow or Pexidartinib chow from 3 to 12 weeks (Fig 3G). This resulted in a very strong decrease in the number of IBA-1^+ (Fig S4F) and $MERTK^{high}$ macrophages (Fig 3G) in IHC analyses. Consistent with these findings, H&E staining showed a remarkable decrease in the number of fused macrophages and concomitant expansion of presumptive eosinophilic steroidogenic cells (Fig 3G). This was further confirmed by a significant increase in SF-1 positive cells in the cortices of pexidartinib-treated mice (Fig 3G) and an inverse correlation between MERTK-positive and SF-1-positive cells (Fig S4G). Altogether, these data show that *Znrf3* ablation induces sustained recruitment of $IBA1^+$ and $MERTK^{high}$ macrophages, which results in phagocytic clearance of mutant steroidogenic cells and regression of adrenal hyperplasia in male mice.

Recruitment of phagocytic macrophages is delayed in females

In contrast with males, female *Znrf3 cKO* adrenals progress from hyperplasia at 4 weeks to development of full-fledged metastatic carcinomas at 78 weeks (Fig 1). Interestingly, analysis of the overall mononuclear macrophage population by IHC for IBA-1, showed increased recruitment of IBA-1-positive macrophages in *Znrf3 cKO* females from 4 to 52 weeks (Fig 4A). However, counting of IBA-1-positive cells suggested that macrophages recruitment was milder than in males from 4 to 12 weeks (Fig 4A&B). This was confirmed by GSEA (Fig 4C), showing a robust enrichment in macrophages signatures in male knockouts compared with female knockouts at 12 weeks and RTqPCR analyses of *Cd68*, *Adgre1* and *Cd11b* (Fig S5A). Milder inflammatory response in female knockouts was also confirmed by the absence of cytokine signature enrichment at 12 weeks, compared with male knockouts (Fig 4D). By 24 and up to 52 weeks, the number of IBA-1-positive cells significantly increased in female *Znrf3 cKO* adrenals, which was accompanied by a mild but significant increase in mRNA accumulation of *Adgre1* at 24 weeks and *Cd68* at 52 weeks (Fig 4A-B &Fig S5A). However, this was still not associated with enrichment of cytokines (Fig S5B). Altogether, this showed that macrophage recruitment was delayed in female *Znrf3 cKO* adrenals and was not associated with robust inflammation. In males, regression of hyperplasia is associated with fusion of mononuclear macrophages to form MGCs (Fig 3). Whereas fused macrophages were already present in large numbers in 12 weeks *Znrf3 cKO* males, they did not appear before 24 weeks in females (Fig 4E). Consistent with delayed fusion, fused macrophages harboured less nuclei (Fig S5C) and

were smaller than in males at this stage (Fig S5D). In male *Znrf3 cKO* adrenals, acquisition of high phagocytic capacities is associated with infiltration of MERTK^{high} macrophages as early as 6 weeks (Fig 3D & Fig 4G). In contrast, these were scarce until 24 weeks in female *Znrf3 cKO* adrenals (Fig 4F-G). They mostly represented fused macrophages (Fig 4F) and were only significantly increased in numbers at 52 weeks (Fig 4G). This suggested that phagocytosis of hyperplastic mutant cells may be impaired in female knockouts. Indeed, although there was trend for increased phagocytosis by IBA-1^{+} macrophages, it did not reach significance, from 4 to 9 weeks (Fig 4H). Furthermore, the rate of phagocytosis was much lower than in males, barely reaching 12 events per high power field in female knockouts, compared with over 40 in male knockouts (Fig 3E). The low phagocytic capacity in females was even more evident when analysed within MERTK^{high} macrophages at 12 weeks (Fig 4H). This was supported by the lack of enrichment of phagocytosis-related gene signatures at any time point (Fig 4I), which was further confirmed by RTqPCR at 12 weeks (Fig 4J).

Altogether, these data strongly suggest that delayed recruitment and impaired function of phagocytic macrophages allows progression of hyperplasia in *Znrf3 cKO* females.

Androgens are sufficient to trigger early recruitment of phagocytic macrophages and regression of hyperplasia

Sexually dimorphic phenotypic differences in phagocytic macrophage recruitment and regression of hyperplasia occur between 6 and 12 weeks, which coincides with onset of puberty in mice. To evaluate a potential contribution of androgens to this phenomenon, *Znrf3 cKO* females were implanted with placebo or testosterone pellets from 4 to 12 weeks and their adrenals were then harvested (Fig 5A). As expected, placebo treated female adrenals were almost completely devoid of MERTK^{high} macrophages (Fig 5B-C). In sharp contrast, testosterone-treated females displayed massive infiltration of both mononuclear and fused MERTK^{high} macrophages, which was almost equivalent to 12-week-old males (Fig 5B-C). Infiltration of macrophages was further confirmed by RTqPCR showing increased expression of *Cd68*, *Adgre1* and *Cd11b*, following androgen treatment (Fig 5D). Interestingly, RTqPCR analysis of phagocytosis-associated gene expression also showed increased accumulation of *Axl*, *Mertk*, *Mfge8*, *Trem2*, *Tyrobp* and *Lgals3*, suggesting that testosterone treatment stimulated recruitment of phagocytic macrophages (Fig 5E). Consistent with this hypothesis, testosterone treatment was associated with a marked decrease in *Znrf3 cKO* female adrenal weight, which returned to control levels (Fig 5F). Altogether, these experiments show that androgens are

sufficient to induce recruitment of phagocytic macrophages, which results in regression of hyperplasia.

Recruitment of phagocytic macrophages in male *Znrf3 cKO* mice is associated with sexually dimorphic induction of senescence

Recruitment of myeloid cells to preneoplastic lesions has been associated with induction of senescence [7,32]. To evaluate a potential role of senescence in the sexually dimorphic recruitment of phagocytes in the adrenal cortex of *Znrf3 cKO* mice, we evaluated enrichment of senescence-associated signatures in males and females from 4 to 12 weeks. Whereas most of these signatures were significantly enriched in *Znrf3 cKO* males at 6 and 12 weeks, there was no or negative enrichment in females (Fig 6A). This suggested that ablation of *Znrf3* resulted in male-specific induction of senescence. To further evaluate this hypothesis, we first analysed expression of the cell-cycle inhibitor p21. In these experiments, steroidogenic cells were labelled by GFP, which was expressed by the mTmG locus following SF-1:Cre-mediated recombination. Consistent with induction of senescence, there was a significant increase in p21 labelling-index within GFP^+ steroidogenic cells in *Znrf3 cKO* males at 4 weeks (Fig 6B and S6A-B). Levels of $P21^+$ cells accumulation returned to normal at 6 weeks in *Znrf3 cKO* males and were significantly reduced at 12 weeks, consistent with phagocytosis of senescent cells (Fig 6B). Surprisingly, a significant increase in P21 labelling was also observed in *Znrf3 cKO* females at 4 weeks and maintained up to 12 weeks (Fig 6B and S6B). This suggested that cell cycle was arrested in both males and females, following *Znrf3* ablation. To further assess induction of senescence, we analysed activity of the prototypic senescence-associated acidic β-galactosidase (SA-βGal). This showed a few positive cells in the subcapsular area and at the cortical-medullary junction in control males and females, which was further increased in control females at 12 weeks. This suggested that spontaneous senescence was taking place in these regions (Fig 6C). Strikingly, SA-βGal staining was increased within the inner cortex of male *Znrf3 cKO* mice at 6 weeks and to a lesser extent at 12 weeks, consistent with phagocytic clearance of senescent cells in male adrenals (Fig 6C). In contrast, there was no increase in SA-βGal staining in *Znrf3 cKO* females, which displayed a similar pattern to controls (Fig 6C). This suggested that although proliferation was arrested in both males and females, senescence was only induced in male *Znrf3 cKO* adrenals. To further confirm this, we evaluated expression of a senescence associated secretory phenotype (SASP) in our RNA sequencing data. This analysis showed that the 23 SASP-coding genes that were significantly deregulated in 12-week-

old *Znrf3 cKO* male adrenals were not deregulated in females (Fig 6D), suggesting that establishment of a SASP was male-specific. This was further confirmed by RTqPCR analyses showing significant up-regulation of *Mmp12* and *Il1a* at 6 weeks and *Cxcl2*, *Mmp12*, *Il1a* and *Tnfrsf1b* at 12 weeks in male, but not female adrenals (Fig 6E & Fig S6C), as well as male-specific enrichment of gene sets for NFkB signalling, which plays a key role in SASP induction[44,45] (Fig S6D). Interestingly, *Znrf3 cKO* female mice that received testosterone (Fig 5) also showed induction of senescence-associated β-galactosidase after 1 week of treatment (from 4 to 5 weeks, Fig 6F). This was associated with up-regulation of the SASP factors *Mmp12*, *Il1a* and *Tnfrsf1b* (Fig 6G), which was concomitant with recruitment of MERTK^{high} macrophages and regression of hyperplasia after testosterone treatment from 4 to 12 weeks (Fig 5). This suggested that testosterone played a key role in senescence induction, which in turn, allowed recruitment of macrophages through SASP factors. Consistent with this hypothesis, F4/80-positive macrophages were found in very close proximity to SA-βGalactosidase- and GFP-positive steroidogenic cells in the adrenal cortex of male *Znrf3 cKO* mice at 6 weeks (Fig 6H).

Altogether, these data strongly suggest that male-specific androgen-driven induction of senescence and SASP, results in recruitment, activation and fusion of highly efficient phagocytes that prevent tumour progression in male *Znrf3 cKO* mice.

Aggressive tumourigenesis is associated with infiltration of non-phagocytic macrophages in female adrenals

To further gain insight into the role of macrophages at late stages of tumourigenesis, we evaluated infiltration of macrophages in 78-week-old adrenal lesions in both male and female mice. At this stage, male *Znrf3 cKO* adrenals were still infiltrated by IBA-1-positive macrophages that were scattered throughout the cortex (Fig 7A). However, quantification of the IBA-1 index showed that in contrast with earlier stages, infiltration was equivalent to control males (Fig 7B). In female *Znrf3 cKO*, IBA-1-positive infiltration was somewhat heterogenous within the tissue, with areas of high infiltration and zones that were almost devoid of macrophages (Fig 7A). There was also interindividual heterogeneity. Indeed, some tumours were still infiltrated at levels comparable to controls, whereas others showed much less IBA-1-positive cells or virtually no macrophages (Fig 7A & B). There was no overall difference between indolent and aggressive (metastatic) tumours with respect to IBA-1 index (Fig 7B).

However, macrophages exclusion was only observed in a subset of 2/10 aggressive tumours (Fig 7A & B). Consistent with IHC analyses, accumulation of mRNA encoding macrophages markers were unaltered (*Cd68*, *Adgre1*) or decreased (*Cd11b*) in female *Znrf3 cKO* compared to controls (Fig 7C). Interestingly, although accumulation of *Adgre1* and *Cd11b* mRNA was unaltered, *Cd68* was still strongly accumulated in male *Znrf3 cKO* adrenals (Fig 7C). Since we showed high expression of CD68 in fused macrophages at earlier stages (Fig 2G), this suggested that active phagocytes may still be accumulating in male KO adrenals at 78 weeks. Consistent with this idea, there were still large numbers of MERTK^{high} fused macrophages in 78-week-old *Znrf3 cKO* male adrenals (Fig 7A &B), which was correlated with overexpression of *Mfge8*, *Trem2* and *Tyrobp* in qPCR (Fig 7D). In contrast, female *Znrf3 cKO* adrenals showed scarce infiltration of MERTK^{high} fused macrophages, although a few of them could still be observed in indolent tumours (Fig 7A & B). Consistent, with these observations, there was no deregulation of phagocytosis/fusion markers in *Znrf3 cKO* female adrenals at this stage (Fig 7D). Interestingly, gene set enrichment analyses showed strong enrichment of phagocytosis-associated signatures, but no enrichment of DNA proliferation / cell-cycle pathways in male *Znrf3 cKO* RNA sequencing data at 78 weeks (Fig 7E). In contrast, female knockouts showed high enrichment of proliferation signatures, but no enrichment of phagocytosis (Fig 7E).
Altogether, these data strongly suggest that even though macrophages are still present within tumour tissues at 78 weeks in both males and females, the lack of phagocytic activity is associated with aggressive tumour progression in females.

Phagocytic macrophages signatures are prominent in male ACC patients and associated with better prognosis

To further evaluate the role of macrophages in ACC progression, we evaluated their infiltration within human ACC. For this, we used RNA sequencing data from the TCGA consortium (79 sequenced ACCs) and evaluated expression of a 10-gene signature (based on single cell RNA sequencing data from mouse adrenals) as a proxy to general macrophages infiltration. Interestingly, tumours of the good prognosis group, defined as C1B, had significantly higher expression of the macrophages signature than tumours of the bad prognosis C1A group (Fig 8A). Consistent with our data showing similar infiltration of IBA-1^{+} macrophages in male and female *Znrf3 cKO* adrenals at 78 weeks (Fig 7B), there was no difference in the general macrophage signature expression between ACC in men (n=31) and women (n=48) (Fig 8B). However, a three gene phagocytic macrophage signature (*CD68*, *TREM2*, *TYROBP*) was significantly expressed at higher levels in men (Fig 8C), and in the good prognosis C1B group

of ACC (Fig 8D). High expression of the phagocytic signature (above median) was also associated with better survival, compared with low expression (below median) in Kaplan-Meier analysis (Fig 8E). Altogether, this suggested that infiltration with phagocytic macrophages was more frequent in men than in women and associated with better prognosis.

Detailed analysis of RNA sequencing data identified 365 genes that were significantly deregulated (FDR <0.01, abs(Log2FC>2)) between the groups of high and low expression of the phagocytic signature (Fig 8F). As expected, macrophages-associated genes such as *CD68*, *CSF1R*, *ITGAM*, *LAPTM5*, *CYBB* and *SIGLEC9* were up-regulated in phagocytic-high patients (Fig 8F). Gene set enrichment analyses confirmed enrichment of macrophages (Fig S7A) and phagocytosis signatures (Fig 8G). Consistent with data in our mouse models, phagocytic signatures were also associated with enrichment of senescence and NFkB signalling gene sets (Fig 8G), suggesting that these pathways may also play a role in phagocytic macrophages recruitment in ACC patients. Gene ontology analysis using the C5 GO database (MsigDB) showed that the top 35 positively enriched gene sets were all related with immune response and inflammation in patients with high expression of the phagocytic signature, suggesting that this subgroup was mounting a more profound immune response than patients with low expression of the signature (Fig S7B). Deconvolution of RNAseq data using Cibersort X showed that macrophages were the most prominent immune cell population in the two groups of patients, consistent with mouse adrenals (Fig 8H). Interestingly, it also showed that enrichment of macrophages signatures in the phagocytic-high subgroup of patients was associated with increased cytotoxic $CD8^+$ T lymphocytes signatures (Fig 8H). However, this was also correlated with lower B cells, plasma cells and NK cells and higher T-regulatory cells infiltration (Fig 8H), suggesting that the phagocytic-high subgroup of patients had a broad alteration of the immune tumour microenvironment.

Altogether, these observations suggest that phagocytic macrophages, which are more prominent in male than female ACC patients, are associated with senescence, global innate and adaptive immune response and better prognosis.

Discussion

Apart from reproductive tissues, cancers are generally more frequent and aggressive in men than in women, even after adjusting for known risk factors[1,2]. Although adrenocortical carcinoma is one of the rare exceptions to this rule, the mechanisms underlying the higher incidence and aggressiveness in women remain elusive. Here, we show that conditional deletion

of *Znrf3* within steroidogenic cells of the adrenal cortex, results in sexually dimorphic development of full-fledged metastatic ACC in female mice over an 18-month time course, whereas the initial hyperplasia gradually regresses in males. By a combination of RNA sequencing, flow cytometry and immunohistochemical analyses, we show that *Znrf3 cKO* males efficiently recruit macrophages from early stages of preneoplastic transformation, following induction of senescence. We further show that these macrophages, which differentiate as potent phagocytes are required for clearance of preneoplastic cells. Although females also mount an innate immune response to preneoplastic transformation, it is delayed compared to males and never achieves efficient clearance of preneoplastic cells. This phenomenon is maintained up to 78 weeks, when indolent lesions in male *Znrf3 cKO* adrenals are still infiltrated with large amounts of phagocytic macrophages, as opposed to aggressive female tumours. Consistent with our findings in mice, we show that a phagocytic macrophage signature is more prominent in male than in female ACC patients, where it is associated with better prognosis. This strongly suggests that the sexual dimorphism of ACC may result from differential recruitment and activation of phagocytic tumour associated macrophages (TAMs), which prevent both tumour initiation and progression in the adrenal cortex.

This is in contrast with most data of the literature showing that TAMs are generally associated with tumour progression and poor prognosis in many cancers, even though they may initially prevent tumour initiation[7,32,46–48]. Plasticity and diversity of TAMs explain their divergent functions. The standard dual classification of macrophages postulates that M1 macrophages that differentiate in response to proinflammatory cytokines (*e.g.* interferons and tumour necrosis factors) are involved in anti-tumour activities, whereas M2 macrophages that differentiate in response to immunomodulatory signals (*e.g.* IL-4, IL-10 and TGF-β) are associated with tumour promotion [49]. However, recent single cell RNA sequencing analyses of tumour infiltrating myeloid cells showed that M1 and M2 gene signatures were co-expressed in macrophage subsets from almost all cancer types[47]. Consistent with this idea, our RNA sequencing and flow cytometry analyses suggested that macrophages that accumulate in the adrenals of *Znrf3 cKO* males had mixed characteristics of the M1 and M2 phenotypes. Furthermore, we did not find evidence of overexpression of canonical tumoricidal macrophages markers such as the pro-inflammatory cytokines IL-1β, IL-2, IL-6, IL-12 and IL-23 (Fig 2B) or iNOS, which metabolizes arginine into the killer molecule nitric oxide (not shown). This suggests that the tumoricidal function of adrenal macrophages relies on alternative activities.

Consistent with this idea, we show a very strong increase in the phagocytic activity of macrophages in *Znrf3 cKO* male adrenals compared with their wild-type littermates and *Znrf3 cKO* females. This activity is associated with cytoplasmic accumulation of CD68 and high membrane expression of MERTK, TYROBP and TREM2, which play a central role in the phagocytic process [35,38,40–42]. Although *MERTK* expression did not correlate with the presence of macrophages in ACC patients (not shown), we show that increased expression of the phagocytic *CD68/TREM2/TYROBP* signature is correlated with better prognosis, within the TCGA cohort. This strongly suggests that phagocytosis plays a central role in the tumoricidal activity of macrophages in ACC. Interestingly, scRNA sequencing in human and mouse colorectal cancer identified a population of C1QC^{+} TAMs, characterised by high levels of *C1QA/B/C*, *TREM2* and *MERTK* expression, which were associated with potential recruitment and activation of T cells, phagocytosis and better prognosis[47,50]. Although we did not analyse macrophages by single cell RNA sequencing in *Znrf3 cKO* adrenals, our bulk RNA sequencing data show strong up-regulation of all these markers (Fig 3B), which are mostly expressed by macrophages in scRNA seq datasets from wild-type mouse adrenals (Fig S8A). This strongly suggests that tumoricidal TAMs found in ACC may be related with the phagocytic C1QC^{+} TAMs identified in other cancers[47,50].

Interestingly, we could find large numbers of macrophages (up to 15% of total cells in the tumour) in aggressive tumours in 78-week-old *Znrf3 cKO* female mice (Fig 7B), even though they were not differentiated as MERTK-hi active phagocytes. The presence of macrophages was further confirmed in ACC patients, where Cibersort X deconvolution suggested that they represented 31% of all immune cells, even in the tumours expressing low levels of the phagocytic signature (40% in phagocytic high tumours, Fig 8H). These data suggest that even in aggressive phagocytic-low lesions, macrophages may be reprogrammed to stimulate their tumoricidal potential. A large panel of molecules targeting macrophages is now available. Most of these pharmacological compounds or monoclonal antibodies aim at reducing macrophages infiltration within the tumour microenvironment, which our data suggest is not the best approach in ACC. However, strategies that stimulate tumoricidal activity and particularly phagocytosis of tumour cells by macrophages are currently being investigated[49]. Particularly interesting is the approach that aims at inhibiting the CD47 “don’t-eat-me” signal produced by cancer cells and/or the SIRPα receptor for CD47 on macrophages. In preclinical mouse models, this approach allowed stimulation of phagocytosis and tumour regression and also enhanced tumour antigen cross-presentation, resulting in adaptive immune responses[51,52]. It is currently

evaluated in a number of cancers such as non-hodgkin lymphomas and acute myeloid leukaemia, where it results in good overall response rates in the absence of overt toxicities[49]. Another interesting approach aims at stimulating Toll-Like Receptor signalling (TLR) with TLR agonists, which stimulates macrophages tumoricidal activity and allows for secretion of IL-12 and TNF, which promotes a cytotoxic $CD8^+$ T cell response. Agonists such as FDA-approved imiquimod (TLR7) or vidotilimod (TLR9) provide interesting responses in the context of basal cell carcinoma and metastatic melanoma, respectively[49]. Monophosphoryl lipid A (MPLA) a TLR4 agonist that is used as an FDA-approved vaccine adjuvant, was also demonstrated to trigger efficient innate and adaptive immune responses in association with IFN-γ, in the context of preclinical mouse models of breast and ovarian tumours[53]. One important factor that these therapeutic approaches will have to consider in the context of ACC, is the presence of high levels of glucocorticoids produced by adrenal steroidogenic cells, in particular within hormonally active tumours. Although glucocorticoids do not have the same detrimental impact on macrophages that they have on lymphocytes, they are generally associated with M2-like tolerogenic differentiation[54]. Therefore, therapeutics targeting macrophages in ACC, should probably consider combining macrophage activation with inhibition of glucocorticoid production or signalling, which would also favour recruitment of adaptive immune cells to the lesion. Availability of our clinically relevant mouse model will allow evaluation of these novel options.

An intriguing feature of the immune response following *Znrf3* deletion, is the formation of multinucleated giant cells (MGCs), resulting from the fusion of mononucleated macrophages. MGCs were first described in tuberculosis but are also present in sterile chronic inflammatory conditions and in response to macroscopic foreign bodies [55,56]. Literature on their association with tumours is rather scarce. However, they have been observed at high frequency in squamous cell carcinomas of multiple tissues[57] and papillary thyroid carcinomas[58]. They can either be correlated with good[57] or poor prognosis[58] depending on the tumour type and in vitro studies have associated MGCs with increased capacity for complement-mediated phagocytosis of large targets and amyloid deposits[55]. In *Znrf3 cKO* adrenals, MGCs are characterised by high levels of CD68, F4/80, MERTK, TYROBP and TREM2 expression and drastically reduced expression of IBA-1 (Fig 2G-I & Fig S4C-D). They appear early in male adrenals, almost concomitant with regression of hyperplasia and are maintained up to 78 weeks. In contrast, they only appear at late stages in females, are less frequent than in males and are mostly found

associated with indolent non-metastatic lesions at 78 weeks. Although we did not analyse macrophages *in situ* in ACC samples from patients, we further observed enrichment of a gene signature associated with development of MGCs from monocyte progenitors[59], within the high-phagocytosis group of patients. Altogether, this suggests that MGCs may play a role in clearing out neoplastic cells within both mouse and human tumours. Alternatively, their appearance may be a by-product of phagocytic clearance of neoplastic cells by mononuclear macrophages that would then fuse to form MGCs. This scenario could be facilitated by the high expression of TYROBP and TREM2 which have been shown to establish a fusion-competent state for macrophages[31]. Progressive cholesterol accumulation resulting from phagocytosis of cholesterol-laden steroidogenic cells, may also play a role in this phenomenon. Indeed, cholesterol is an essential and rate-limiting factor for formation of MGCs[59] and oil-red-o staining of *Znrf3 cKO* male adrenals at 12 weeks showed a strong accumulation of lipids within MGCs (Fig S8B).

Another striking feature of the phenotype is the strong sexual dimorphism in immune response to neoplasia. It culminates with the robust and early recruitment of tumoricidal phagocytic macrophages in male mice, which results in regression of hyperplasia and prevents aggressive tumorigenesis, specifically in this gender. We further show that testosterone treatment of females from 4 to 12 weeks is sufficient to trigger a response which is comparable to males and results in regression of hyperplasia (Fig 5). This strongly suggests a role of male hormones in this phenomenon and raises the question of the underlying mechanisms. One possibility is an intrinsic sexual dimorphism of macrophages within the adrenal, which would result in differential responses to oncogenic transformation of steroidogenic cells. Indeed, recruitment, replenishment and activation mechanisms of macrophages have been shown to diverge between males and females, resulting in sexually dimorphic responses to infection and proinflammatory stimuli. However, in most instances, female macrophages are more responsive to stimuli, mount a more robust response and have higher phagocytic capacities than male macrophages[60–65]. This suggests that the stronger inflammatory response observed in male *Znrf3 cKO* adrenals may result from indirect effects of sex hormones. Consistent with this, single cell sequencing data suggest that the androgen receptor *Ar* is only expressed in a small subset of adrenal macrophages, characterized by lower expression of *Trem2* and *Mertk,* which is unlikely to represent the major population of macrophages in *Znrf3c KO* adrenals (Fig S8A&C). Our data showing a strong association between induction of SASP and recruitment of macrophages suggest that androgens may stimulate the tumoricidal response by inducing release of

612 senescence associated cytokines by *Znrf3 cKO* cells (Fig 6). In line with this hypothesis, AR
613 activation was shown to induce p53-independent senescence in prostate cancer cells[66,67] and a
614 short-term testosterone treatment was sufficient to induce SA-βgalactosidase activity in female
615 *Znrf3 cKO* adrenals (Fig 6). This raises the question of the links between *Znrf3* inactivation,
616 AR signalling and senescence induction. One may speculate that the recently documented
617 sexual dimorphism in cortical cell proliferation, renewal and progenitor populations [8,9] may
618 result in sexually dimorphic response to *Znrf3* inactivation. In this context, the
619 hyperproliferation observed in both male and female *Znrf3 cKO* adrenals may result in faster
620 exhaustion of progenitor pools in males and subsequent induction of senescence. However, the
621 rapid induction of SA-βgalactosidase in testosterone-treated *Znrf3 cKO* females suggests that
622 this is an unlikely scenario. Alternatively, these findings may reflect a novel function of ZNRF3
623 in the control of cellular homeostasis. Interestingly, although we were able to show a mild
624 induction of *Axin2* accumulation in *Znrf3 cKO* adrenals by RNA in-situ hybridization[29],
625 analysis of our RNA sequencing data did not show evidence of canonical WNT signalling
626 induction in either male or female knockouts (Fig S8D), when compared with a previously
627 published model of constitutive β-catenin activation[68]. This suggests that the impact of *Znrf3*
628 inactivation on senescence induction may involve WNT-independent mechanisms.
629 Interestingly, inactivation of *Znrf3* and its homologue *Rnf43* in hepatocytes results in
630 hyperplasia, followed by cell death and senescence induction. This is associated with
631 deregulation of lipid and phospholipid metabolism through both canonical and non-canonical
632 WNT pathway activation[69]. Whether similar mechanisms resulting in accumulation of toxic
633 lipids are involved in senescence induction in the adrenal cortex, remains to be investigated.
634
635 In conclusion, we describe a novel interaction between tumour suppressor inactivation,
636 senescence induction and recruitment of tumoricidal macrophages, which results in sexually
637 dimorphic adrenal cancer development. This provides novel insight into the strong gender bias
638 of this particularly aggressive cancer and may help develop novel macrophage-centric
639 therapeutic approaches.
640
641 **Acknowledgments**
642 We thank Sandrine Plantade, Khirredine Ouchen and Philippe Mazuel for animal care and Dr
643 Laura Bousset (LMS, London) for fruitful discussions. The TREM2 antibody was supplied by
644 the Haass Lab at Ludwig Maximilians University Munich, specifically by Alice Suelzen and

Dr Kai Schlepckow. Single cell RNA sequencing data from mouse adrenals were kindly provided by Dr Cynthia Andoniadou and Val Yianni (King's College London). Protocol for mouse adrenal tissue dissociation for flow cytometry and flow cytometry parameters were kindly provided by Dr Marc Bajénoff and Dr Mitchell Bijnen (CIML, Marseille). This work was supported by grants from Worldwide Cancer Research (#16-1052), la Ligue Nationale Contre le Cancer ("Equipe Labellisée Ligue" and individual grant to JJW), Fondation ARC (individual grant to JO) and Agence Nationale pour la Recherche (ANR-21-CE14-0044-ADREMAC).

Authors contributions

JJW performed experiments, analysed data, prepared the manuscript
JO performed experiments, analysed data, prepared the manuscript
DGG performed experiments, analysed data, prepared the manuscript
CL performed experiments
RG conceived experiments
FRB performed experiments
DD performed experiments
CDS performed experiments
ISB performed experiments
JCP performed experiments
YR analysed data
AL performed experiments
IT conceived experiments, discussed findings
AMLM conceived experiments, discussed findings
AM conceived experiments, discussed findings
PV conceived experiments, performed experiments, analysed data, wrote the manuscript

Declaration of interests

The authors declare no competing interests

Figure legends

Figure 1. Sexually dimorphic tumour progression in *Znrf3 cKO* adrenals. A- Female adrenal weights measured from 4 to 78 weeks in wild-type and *Znrf3 cKO* (ZKO) adrenals. **B-**

679 Rate of metastasis in 78-week-old *Znrf3 cKO* females. **C-** Histology (upper panels) and
680 immunohistochemical analysis of Ki67 expression (lower panels) in 78-week-old female
681 controls, *Znrf3 cKO* adrenals associated with metastasis formation or indolent *Znrf3 cKO*
682 adrenals. **D-** Quantification of the Ki67 proliferation index as the ratio of positive cells over
683 total nuclei in the cortex of 78-week-old control and *Znrf3 cKO* females. **E-** Male adrenal
684 weights measured from 4 to 78 weeks in wild-type and *Znrf3 cKO* (ZKO) adrenals. **F-** Rate of
685 metastasis in 78-week-old *Znrf3 cKO* males. **G-** Histology (upper panels) and
686 immunohistochemical analysis of Ki67 expression (lower panels) in 78-week-old male controls
687 and *Znrf3 cKO* adrenals. **H-** Quantification of the Ki67 proliferation index as the ratio of
688 positive cells over total nuclei in the cortex of 78-week-old control and Znrf3 cKO males. **I-**
689 Kinetic analysis of the Ki67 proliferation index from 4 to 52 weeks in male and female control
690 and *Znrf3 cKO* adrenals. **J-** Kinetic analysis of the histological phenotype from 4 to 52 weeks
691 in male and female control and *Znrf3 cKO* adrenals. Arrowheads in insets show multinucleated
692 giant cells that accumulate in the inner cortex of mutant male mice and to a lesser extent mutant
693 female mice. M: medulla; zF: zona fasciculata ; zG zona glomerulosa ; Tu: tumour. Scale bar
694 = 200µm. Graphs represent mean +/- SEM. Statistical analyses in A, D, E, H and I were
695 conducted by Mann-Whitney tests. ns : not significant; * $p<0.05$; ** $p<0.01$; *** $p<0.001$; ****
696 $p<0.0001$.
697
698 **Figure 2. Regression in male *Znrf3 cKO* adrenals is correlated with macrophages**
699 **infiltration and fusion. A-** Gene Set Enrichment Analysis (GSEA) of gene expression data
700 (RNA sequencing) from 4, 6 and 12-week-old control and *Znrf3 cKO* male adrenals. The plot
701 represents the 35 gene sets from the C5 Gene Ontology database (MSigDB), with the highest
702 enrichment score in *Znrf3 cKO* adrenals compared with controls at 12 weeks. **B-** Heatmap
703 representing median-centred expression of cytokines/chemokines-coding genes in control and
704 *Znrf3 cKO* adrenals at 4, 6 and 12 weeks. Only genes significantly deregulated at 12 weeks
705 (FDR<0.05) are represented. They are sorted by decreasing Log2-fold-change. **C-**
706 Immunohistochemical analysis of CD45 expression in adrenals from control and *Znrf3 cKO*
707 (ZKO) mice at 4, 6 and 12 weeks. Arrowheads show multinucleated giant cells. Stars show
708 mononucleated leukocytes. **D-** Stacked bar plots representing immune cell populations
709 deconvoluted using CibersortX and the LM22 expression matrix, from gene expression data in
710 control and *Znrf3 cKO* adrenals at 4, 6 and 12 weeks. **E-** Enrichment analysis (GSEA) of
711 macrophages signatures derived from ImmuCC, LM22, and single cell RNA sequencing of
712 mouse adrenals, in 12-week-old male *Znrf3 cKO* adrenals compared to controls. **F-** Left,

representative dot plots of flow cytometry analysis of macrophages infiltration in 4 and 6-week-old control (top panels) and *Znrf3 cKO* (bottom panels) adrenals. Macrophages were defined as $CD45^+/CD64^+/F4/80^+$ live cells. Right panel, quantification of flow cytometry experiments. **G-** Immunohistochemical analysis of pan-macrophages markers IBA-1, F4/80 and CD68 in 4, 6 and 12-week-old control and *Znrf3 cKO* adrenals. Arrowheads show multinucleated giant cells. Stars show mononucleated macrophages. **H-** Immunohistochemical analysis of macrophage fusion-associated markers TREM2 and TYROBP in 6 and 12-week-old control and *Znrf3 cKO* adrenals. Arrowheads show multinucleated macrophages. Stars show mononucleated macrophages. **I-** High-magnification images of TREM2 and TYROBP staining showing fusion of mononucleated with multinucleated macrophages in *Znrf3 cKO* adrenals at 12 weeks (arrowheads). Co: cortex; M: medulla; scale bar =200µm. Graphs represent mean +/- SEM. Statistical analyses in F, were conducted by Mann-Whitney tests. * $p<0.05$; ** $p<0.01$.

Figure 3. Infiltrating macrophages actively phagocytose steroidogenic cells. A- Gene Set Enrichment Analysis (GSEA) of gene expression data (RNA sequencing) from 4, 6 and 12-week-old control and *Znrf3 cKO* male adrenals. The plot represents enrichment of phagocytosis/efferocytosis gene sets in *Znrf3 cKO* male adrenals compared with controls. **B-** Heatmap representing median-centred expression of key regulators of the phagocytic pathway in control and *Znrf3 cKO* male adrenals at 4, 6 and 12 weeks. **C-** RTqPCR analysis of the expression of phagocytosis-associated genes in control and *Znrf3 cKO* male adrenals at 12 weeks. **D-** Immunohistochemical analysis of the expression of the phagocytosis receptor MERTK in control and *Znrf3 cKO* male adrenals at 4, 6 and 12 weeks. Arrowheads show multinucleated macrophages. Stars show mononucleated macrophages. **E-F** Evaluation of phagocytosis by immunohistochemistry for 3βHSD (steroidogenic cells) and IBA-1 (E) or SF-1 (steroidogenic cells) and MERTK (F). Images were acquired by confocal microscopy and phagocytic events were counted when steroidogenic markers were found within the boundaries of macrophages markers along the Z-stack. Panels show representative zoomed-in images (x120) in 9-week-old (IBA-1) and 12-week-old (MERTK) *Znrf3 cKO* adrenals. White boxes show phagocytic events on the 2D projection of Z-stack and within the orthogonal projections (side images). Bottom graphs represent quantification of phagocytic events on 10 high power fields (HPF, x40) per individual mouse from 4 to 9 weeks ($IBA\text{-}1^+$ phagocytosis) and at 12 weeks (MERTK-hi phagocytosis). **G-** Immunohistochemical (MERTK & SF-1) and histological (H&E) analysis of *Znrf3 cKO* male mice that received control or Pexidartinib-enriched chow from 9 to 12 weeks (left panels). Percentages of MERTK-positive and SF-1-

positive cells, relative to total cortical cell numbers ($DAPI^+$) are displayed on the graphs (right panel). Co: cortex; M: medulla; scale bar =200µm. Graphs represent mean +/- SEM. Statistical analyses in C, E, F and G were conducted by Mann-Whitney tests. * $p<0.05$; ** $p<0.01$; *** $p<0.001$; **** $p<0.0001$.

Figure 4. Recruitment of phagocytic macrophages is delayed in females. A- Immunohistochemical analysis of IBA-1 expression in female control and *Znrf3 cKO* adrenals from 4 to 52 weeks. **B-** Quantification of the IBA-1 index as the ratio of IBA-1-positive cells over total nuclei in the cortex of control and *Znrf3 cKO* male (blue) and female (pink) mice from 4 to 52 weeks. **C-** GSEA of macrophages gene sets in male *Znrf3 cKO* compared with female *Znrf3 cKO* adrenals at 12 weeks. **D-** GSEA of the cytokine gene set in *Znrf3 cKO* males and females compared with their respective control adrenals at 12 weeks. **E-** Quantification of the number of fused macrophages (at least 2 nuclei) in control and *Znrf3 cKO* male and female adrenals from 4 to 52 weeks. **F-** Immunohistochemical analysis of MERTK expression in control and *Znrf3 cKO* female adrenals from 4 to 52 weeks. **G-** Quantification of the $MERTK^+$ index as the ratio of MERTK-positive cells over total nuclei in the cortex of control and *Znrf3 cKO* male (blue) and female (pink) mice from 4 to 52 weeks. **H-** Quantification of phagocytic events following immunohistochemistry for IBA-1 and 3βHSD ($IBA\text{-}1^+$ phagocytosis) or MERTK and SF-1 ($MERTK^{high}$ phagocytosis) in control and *Znrf3 cKO* females from 4 to 12 weeks. Quantification was performed on 10 high power fields (HPF, x40) per individual mouse. **I-** Gene Set Enrichment Analysis (GSEA) of gene expression data (RNA sequencing) from 4, 6, 12 and 52-week-old control and *Znrf3 cKO* female adrenals. The plot represents enrichment of phagocytosis/efferocytosis gene sets in *Znrf3 cKO* female adrenals compared with controls. **J-** RTqPCR analysis of the expression of phagocytosis and macrophages fusion-associated genes in control and *Znrf3 cKO* female adrenals at 12 weeks. Co: cortex; Tu: tumor; Scale bar = 200µm. Graphs represent mean +/- SEM. Statistical analyses in B, E, G, H and J were conducted by Mann-Whitney tests. ns: not significant; * $p<0.05$; ** $p<0.01$; *** $p<0.001$; **** $p<0.0001$.

Figure 5. Androgens are sufficient to trigger early recruitment of phagocytic macrophages and regression of hyperplasia. A- Cartoon of the experimental setup. **B-** Immunohistochemical analysis of MERTK expression in 12-week-old placebo and testosterone-treated *Znrf3 cKO* females. An untreated 12-week-old *Znrf3 cKO* male was included as a reference. **C-** Quantification of the $MERTK^+$ index as the ratio of MERTK-

positive cells over total nuclei in the cortex of placebo and testosterone-treated females at 12 weeks. **D-** RTqPCR analysis of the expression of macrophages-related genes in placebo and testosterone-treated *Znrf3 cKO* female adrenals at 12 weeks. **E-** RTqPCR analysis of the expression of phagocytosis and macrophages fusion-associated genes in placebo and testosterone-treated *Znrf3 cKO* female adrenals at 12 weeks. **F-** Adrenal weights from placebo and testosterone-treated 12-week-old *Znrf3 cKO* females. 12-week-old untreated control males/females *and Znrf3 cKO* males/females from Fig 1A&E were included as a reference. Co : cortex; Scale bar = 200 µm. Graphs represent mean +/- SEM. Statistical analyses in D and E were conducted by Mann-Whitney tests. In F, statistical analyses were conducted by one-way ANOVA followed by a Kruskal-Wallis *post-hoc* test. ns: not significant; * $p<0.05$; ** $p<0.01$; *** $p<0.001$.

Figure 6. Recruitment of phagocytic macrophages in male *Znrf3 cKO* mice is associated with sexually dimorphic induction of senescence. A- Gene Set Enrichment Analysis (GSEA) of gene expression data (RNA sequencing) from 4, 6 and 12 control and *Znrf3 cKO* male and female adrenals. The plot represents enrichment of senescence-associated gene sets in *Znrf3 cKO* compared with controls (sex matched). **B-** Quantification of the $P21^+$ index as the ratio of P21-positive cells over total nuclei in the cortex of male and female control and *Znrf3 cKO* mice from 4 to 12 weeks. **C-** Detection of the senescence associated acidic β-galactosidase activity on frozen tissue sections from male and female control and *Znrf3 cKO* mice at 4, 6and 12 weeks. Sections were counterstained with hematoxylin. **D-** Heatmap showing expression of senescence associated secretory phenotype (SASP) genes in 12-week-old male and female control and *Znrf3 cKO* adrenals. Genes were selected on the basis of significant deregulation in 12-week-old male *Znrf3 cKO* adrenals (FDR<0.1) and sorted by Log2 fold-change. **E-** RTqPCR analysis of the expression of SASP genes in control and *Znrf3 cKO* males (E - top panel) control and *Znrf3 cKO* females (E- bottom panel). **F-** Detection of SAβ-Galactosidase activity in the adrenals of Znrf3 cKO females that received placebo or testosterone treatment from 4 to 5 weeks. An untreated 6-week-old *Znrf3 cKO* male was included as a reference. **G-** RTqPCR analysis of the expression of SASP genes in placebo and testosterone-treated *Znrf3 cKO* females from Fig 5. **H-** Immunohistochemical analysis of GFP (marking SF-1:Cre-mediated recombination of mTmG in steroidogenic cells), F4/80 and SAβGalactosidase activity. Right panels show a high-magnification crop of the area delineated in white in left panels. Blue arrowheads show senescent GFP^+ cells; brown arrowheads show $F4/80^+$ macrophages. Co:

cortex; Scale bar = 200 µm (C-F) ; 100 µm (H). Graphs represent mean +/- SEM. Statistical analyses in B and E were conducted by Mann-Whitney tests. ns: not significant; * $p<0.05$; ** $p<0.01$; *** $p<0.001$; **** $p<0.0001$.

Figure 7. Aggressive tumourigenesis is associated with infiltration of non-phagocytic macrophages in female adrenals. A- Immunohistochemical analysis of IBA-1 and MERTK expression in control males/females and *Znrf3 cKO* males/females at 78 weeks. For *Znrf3 cKO* females, the panels represent indolent tumours (no metastases) and aggressive tumours with or without macrophages infiltration. **B-** Quantification of the IBA-1$^+$ and MERTK$^+$ index as the ratio of IBA-1 (left) or MERTK-positive (right) cells over total nuclei in the cortex of male and female control and *Znrf3 cKO* mice at 78 weeks. Values for primary tumours associated with metastases are shown as black dots. **C-** RTqPCR analysis of the expression of macrophages-related genes in control and *Znrf3 cKO* males (top panel) and control and *Znrf3 cKO* females (bottom panel) at 78 weeks. **D-** RTqPCR analysis of the expression of phagocytosis and macrophages fusion-associated genes in control and *Znrf3 cKO* males (top panel) and control and *Znrf3 cKO* females (bottom panel) at 78 weeks. **E-** Gene Set Enrichment Analysis (GSEA) of gene expression data (RNA sequencing) from 78 weeks control and *Znrf3 cKO* male and female adrenals. The plot represents enrichment of phagocytosis-associated gene sets and DNA replication-associated gene sets in *Znrf3 cKO* compared with controls (sex matched). Co: cortex; Tu: tumour; Scale bar = 200 µm. Graphs represent mean +/- SEM. Statistical analyses in B and E were conducted by Mann-Whitney tests. ns: not significant; * $p<0.05$.

Figure 8. Phagocytic macrophages signatures are prominent in male ACC patients and associated with better prognosis. A- Expression of a global macrophage gene signature in ACC patients from the TCGA program, dichotomised as patients with good (C1B) and poor (C1A) prognosis. **B-** Expression of a global macrophage gene signature in ACC patients from the TCGA program, dichotomised as men and women. **C-** Expression of a phagocytic macrophage gene signature in ACC patients from the TCGA program, dichotomised as men and women. **D-** Expression of a phagocytic macrophage gene signature in ACC patients from the TCGA program, dichotomised as patients with good (C1B) and poor (C1A) prognosis. **E-** Survival analysis of patients of the TCGA program dichotomised as patients with high (red) or low (green) expression of the phagocytic signature. **F-** Volcano plot displaying differential gene expression between patients with high and low expression of the phagocytic signature. Red dots represent genes with a Log2 fold-change> 2 and FDR<0.01. Green dots represent genes with

Log2 fold-change<-2 and FDR<0.01. **G-** GSEA of phagocytosis, senescence and NFkB-associated gene sets in patients with high expression of the phagocytic signature, compared with patients with low expression of the signature.

Materials and Methods

Mice

All experiments with mice were in accordance with protocols approved by the Auvergne Ethics Committee (CEMEAA). They were conducted in agreement with international standards for animal welfare in order to minimize animal suffering. *Znrf3 cKO* mice (ZKO) were generated by mating *Znrf3*$^{fl/fl}$ mice[27] with *SF1-Cre*^{high} mice[70]. Mice were bred and maintained on a C57Bl/6 genetic background. Mice were euthanized by decapitation at the end of experiments and blood collected in vacuum blood collection tubes (VFD053STK, Terumo). Adrenals were extracted, cleaned of excess fat, weighed and immediately fixed in 4% paraformaldehyde or stored at − 80 °C. Littermate control animals were used in all experiments.

Immunohistology

Adrenals were fixed in 4% paraformaldehyde overnight at 4°C, then washed two times in PBS. For the paraffin embedding, adrenals were dehydrated through an ethanol gradient. Then they were incubated for 2 h in Histoclear (HS200; National Diagnostics, Fisher Scientific, Illkirch, France) and embedded in paraffin. For frozen sections, adrenals were successively placed into 10% and 15% PBS-sucrose solutions for 20 minutes, then 20% PBS-sucrose solution for 1 hour, and in 50/50 OCT-Sucrose 20% solution overnight. Lastly, they were embedded in pure OCT solution and stored at -80°C. Paraffin and OCT samples were cut into 5 & 10µm sections, respectively. Haematoxylin/eosin staining was performed with a Microm HMS70 automated processor (Microm Microtech, Francheville, France), according to standard procedures. Antibody information, dilutions and unmasking conditions are listed in Supplementary Table 1. Notably, the TREM2 antibody [71], was supplied from the Haass Lab at Ludwig Maximilians University Munich. After deparaffinization with Histoclear and rehydration in decreasing ethanol gradients, unmasking was performed by boiling slides for 20 min in the appropriate unmasking solution. Next, endogenous peroxidases were inactivated by incubating slides with 0.3% hydrogen peroxide for 30 min at room temperature. After blocking for 1h, slides were incubated overnight at room temperature with primary antibodies at the indicated concentrations (Supplementary Table 1). Primary antibodies were detected with appropriate species polymers (ImmPress Polymer Detection Kit, Vector Laboratories). Polymer-coupled

HRP activity was then detected with either Novared (SK-4800, Vector Laboratories) for brightfield images or TSA-Alexa-coupled fluorochromes for fluorescence (Thermo Fisher, Alexa_488 B40953, Alexa_555 B40955, Alexa_647 B40958). For double-immunohistochemistry experiments, HRP was inactivated by incubation with 0.02% HCl for 20 min after detection of the first antibody to avoid cross-reaction. Nuclei were counterstained with Haematoxylin for brightfield images or Hoechst for fluorescence (Thermo Fisher 33342). Slides were mounted using a 50/50 PBS-Glycerol solution. Images were acquired with a Zeiss AxioImager with Apotome2 or Zeiss Axioscan Z1 slide scanner. Images were minimally processed for global levels and white balance using Affinity Photo® and Affinity Designer®. Image settings and processing were identical across genotypes.

Quantifications were performed on scanned whole adrenals (Axio Scan Zeiss scanner, 20× images) using the QuPath software version 0.3.1 (Bankhead et al 2017). Briefly, annotations were made of whole adrenals or just the adrenal cortex, and the positive cell detection feature was used to identify positive cells. The threshold for identifying positive cells was set to avoid quantification of background on each image.

For quantification of phagocytosis, confocal images were acquired on a Zeiss LSM 800 Airyscan confocal microscope with 40X magnification. Phagocytic events were identified and counted as the presence of steroidogenic cell markers (3βHSD or SF-1) within the boundaries of macrophages, defined by IBA-1 or MERTK staining. This was evaluated by a single operator, by manually scanning through Z-stacks of ten 40X images per adrenal. The operator was blinded to the genotype.

Senescence-associated beta-galactosidase (SA-β-galactosidase) staining

SA-β-galactosidase staining was conducted following the protocol of Debacq et al (4) on frozen adrenal 10µm-sections. After drying for 15 min under a vacuum, the sections were rehydrated with PBS and then incubated overnight at 37°C in a humid atmosphere in a pH 6.0 staining solution composed of 7.4mM citric acid, 25.3mM dibasic sodium phosphate, 5mM $K_4[Fe(CN)_6]$, 5mM $K_3[Fe(CN)_6]$, 150mM sodium chloride, 2mM $MgCl_2$ and 1mg/mL X-gal. Slides were mounted using a 50/50 PBS-Glycerol solution and imaged on a Zeiss ApoTome microscope with an AxioCam MRm camera and/or a Axio Scan Zeiss scanner.

Testosterone supplementation experiment

Testosterone or placebo implants were placed under gas anesthesia, in the interscapular region of 4-week-old *Znrf3 cKO* female mice for 60 days. These testosterone implants (T-M/60 Belma)

are designed to release daily doses of testosterone (from 51.9 to 154.5 µg/24hr for plasma concentrations of 0.9-3.7 ng/ml) to produce physiological plasma concentrations in mice.

Pexidartinib experiment

Chow was purchased from SAFE Nutrition Services (Augy, France). Male Control & ZKO mice were fed either control chow (E8220A01R 00000 v0025 A04 Pur) or pexidartinib chow (E8220A01R 00000 v0398 A04 +0.29g/kg Pexidartinib) from 3-12 weeks of age. Pexidartinib (HY16749) was purchased from MedChemExpress and incorporated in the chow by SAFE Nutrition Services. Chow was replaced every 3-4 days, renewed weekly and stored at 4°C when not in use.

FACS

Adrenals were harvested and excess fat was removed under a dissecting microscope. Adrenals were immediately placed into 900µL of digestion medium (Supplementary Table 2) and placed on ice until the end of the harvest. Adrenals were digested by incubating with a thermomixer set at 37°C – 900 rpm- for 37 min, stopping to pipette up and down at 10, 20, 30, 35, & 37min. Digested samples were filtered through 100µm nylon mesh and centrifuged at 400g for 5 min at 4°C. Cells were resuspended in wash buffer (PBS – EDTA 2.5mM – DNAse 100µg/ml – BSA 0.5%)) and stained appropriately. Cells were stained with Fixable Near-IR live/dead stain (L34975, Invitrogen) for 30min at room temperature (RT), blocked with CD16/CD32 & TrueStain (426102, BioLegend) for 15 min at RT, and stained with the appropriate antibody panel for 20 min at RT (Supplementary Table 3). All staining/blocking steps were preceded and followed by wash steps which included centrifugation at 200g for 4 min, followed by resuspension of the pellet with either wash buffer or the appropriate solution. Cells were immediately analyzed on the Attune NxT Flow Cytometer (Reference: A24858). Detailed analyses of the results were done using FlowJo® software.

Reverse-transcription quantitative PCR

Adrenals were flash-frozen and stored at -80°C post-harvest. RNAs were extracted using the Macherey-Nagel Nucleospin RNA kit (REF #740955.250). After reverse transcription of 500ng of total RNAs, cDNAs were diluted 1/10 and PCR reactions were conducted using SYBR qPCR Premix Ex Taq II Tli RNase H+ (TAKRR820W, Takara). Primers can be found in Supplementary Table 4. Relative expression was calculated using the 2^-ΔΔCT method.

RNA sequencing for gene expression analysis

Library preparation and sequencing

RNA sequencing was performed by the GenomEast platform, a member of the 'France Genomique' consortium (ANR-10-INBS-0009). Library preparation was performed using TruSeq Stranded mRNA Reference Guide - PN 1000000040498. RNA-Seq libraries were generated from 300 ng of total RNA using TruSeq Stranded mRNA Library Prep Kit and IDT for Illumina - TruSeq RNA UD Indexes (96 Indexes, 96 Samples) (Illumina, San Diego, USA), according to manufacturer's instructions. Briefly, following purification with poly-T oligo attached magnetic beads, the mRNA was fragmented using divalent cations at 94oC for 2 minutes. The cleaved RNA fragments were copied into first strand cDNA using reverse transcriptase and random primers. Strand specificity was achieved by replacing dTTP with dUTP during second strand cDNA synthesis using DNA Polymerase I and RNase H. Following addition of a single 'A' base and subsequent ligation of the adapter on double stranded cDNA fragments, the products were purified and enriched with PCR (30 sec at 98°C; [10 sec at 98°C, 30 sec at 60°C, 30 sec at 72°C] x 12 cycles; 5 min at 72°C) to create the cDNA library. Surplus PCR primers were further removed by purification using SPRI select beads (Beckman-Coulter, Villepinte, France) and the final cDNA libraries were checked for quality and quantified using capillary electrophoresis. Libraries were sequenced on an Illumina HiSeq 4000 sequencer as single read 50 base reads. Image analysis and base calling were performed using RTA version 2.7.7 and bcl2fastq version 2.20.0.422.

Genome mapping and differential gene expression analyses

Reads were filtered and trimmed to remove adapter-derived or low-quality bases using cutadapt v 3.2 and checked again with FASTQC v 0.11.7. Illumina reads were aligned to Mouse reference genome (mm10) with Hisat2 v 2.2.1. Read counts were generated for each annotated gene using R function "SummarizeOverlaps()" and RPKM were calculated for each gene. Differential expression analysis with multiple testing correction was conducted using the R Bioconductor DESeq2 package v 1.34.0.

Generation of heatmaps

Heatmaps to represent differential gene expression were generated with the *Biobase* and *gplots* packages in R. They represent median centered RPKM levels. Genes are either sorted by Log2 fold-change or by unsupervised clustering.

Reanalysis of single cell sequencing of adult mouse adrenals

The Seurat R package[72] was used to perform clustering analysis of single-cell data from Lopez et al. [73], available in the Gene Expression Omnibus GSE161751 (control adrenals from 10 week-old male mice). Raw sequencing data and annotated gene–barcode matrices were used for the input. Cells with more than 20 genes and genes expressed in more than 3 cells were selected for further analysis. After studying the distribution of count depth, number of genes, and mitochondrial read fraction, low-quality cells with less than 1000 counts, less than 400 genes detected, and percentage of mitochondrial gene counts higher than 25% were removed. Gene expression in each cell was then normalized by the total number of counts in the cell, multiplied by 10000 to get counts per 10000 (TP10K) and log-transformed to report gene expression as $E = \log(\text{TP10K} + 1)$.

The top 2,000 highly variable genes with a z-score cutoff of 0.5 were then centred and scaled to have a mean of zero and standard deviation of one, and used as inputs for initial principal component analysis (PCA). The number of principal components (PCs) was chosen according to the PCElbowPlot function and JackStrawPlot function. Next, the Louvain algorithm implemented in Seurat was used to iteratively group cells together, with the goal of optimizing the standard modularity function. The resolution parameter for clustering was set at $r = 1$. The default Wilcoxon rank-sum test was used by running FindAllMarkers function in Seurat to find differentially expressed markers in each cluster. Finally, each cell type was annotated after extensive literature reading and searching for specific gene expression patterns. Violin plot representations were used for visualizing expression of the different markers.

TCGA adrenocortical carcinoma data

TCGA gene expression and clinical ACC data were extracted from the TCGA database (The Cancer Genome Atlas). Distribution in the good (C1B) and poor prognosis (C1A) groups were previously defined, based on unsupervised clustering[26]. Expression data were standardized by the Relative Standard Error of the Mean (RSEM) algorithm and transformed into Log2 in order to refocus and symmetrize values' distribution. The macrophage signature was defined as the mean expression (Z-score) of *CD74*, *CXCL2*, *CCL4*, *APOE*, *CCL3*, *CTSS*, *C1QA*, *C1QB*, *C1QC* and *AIF1*. These were found as highly up-regulated genes in macrophages in single cell RNA sequencing analyses of adult mouse adrenals[73] (see above). For gene set enrichment analyses, TCGA ACC patients were dichotomized based on the expression of a phagocytic signature (mean expression (Z-score) of *TYROBP*, *TREM2* and *CD68*) with patients classified as high (expression above median) or low (expression below median). Differential gene expression between patients from the phagocytic high and phagocytic low groups was computed using the

limma R package. The volcano plot representing differential expression between these two groups was generated in R with the *calibrate* library. Kaplan Meier analysis was conducted in GraphPad prism after dichotomization of patients according to expression of the phagocytic signature.

Gene Set enrichment analyses

Gene set enrichment analyses were conducted on gene expression data from mouse models and TCGA ACC patients, using GSEA 4.1.0 with gene sets from the MsigDB and MGI Gene Ontology databases and with custom curated gene sets (Supplementary Table 5). Permutations were set to 1000 and were performed on gene sets. Phagocytosis gene sets were curated from an extensive search of the literature, including papers by Park et al.[74], Lecoultre et al.[75] and Janda et al[76] and extracted from the MGI gene ontology database. Senescence gene sets were extracted from papers by Eggert et al.[32], Kuilman et al.[77], özcan et al.[78], Acosta et al.[79], Fridman et al.[80], Coppé et al.[81,82], Buhl et al.[83] and Saul et al. [84]. LM22 and ImmuCC gene sets were derived from gene expression signatures published in Newman et al.[85] and Chen et al.[86]. To reduce the gene expression matrix into simple gene identifier lists for GSEA, genes in each of the lists were attributed to their cognate immune cell type based on their maximum of expression across all cell types. This resulted in gene signatures for each immune cell type that were then used in GSEA (Table). M0, M1 and M2 macrophages gene sets were further concatenated to result in global LM22 and ImmuCC macrophages gene sets. The mouse adrenal macrophages gene set was defined as the 100 most significantly upregulated genes within the two macrophages clusters (compared to all other clusters) in our reanalysis of the single-cell sequencing study of adult mouse adrenals by Lopez et al.[73]. The cytokine gene set was curated from an extensive search of the literature. NFκB and DNA replication gene sets were extracted from MsigDB C2, Hallmarks and C5 datasets.

GSEA output was either displayed as dot plots or enrichment curves. Dot plots represent the normalized enrichment score (NES) and FDR (size of dots defined as -log10(FDR)) and were drawn using the *ggplot2* library in R. Enrichment curves were drawn by feeding GSEA output to the *GSEA_replot* R function, developed by Thomas Kuilman (https://github.com/PeeperLab/Rtoolbox/blob/master/R/ReplotGSEA.R). Dot plots and enrichment curves were further processed in Affinity Designer® for colour matching and superimposition.

CibersortX and mMCP analyses

CibersortX analyses were run on the CibersortX server (https://cibersortx.stanford.edu) using the LM22 matrix and a mixture file representing gene expression data in control and *Znrf3 cKO* adrenals at 4, 6 and 12 weeks or TCGA ACC patients' data, dichotomized on the basis of high or low expression of the phagocytic signature (see TCGA adrenocortical carcinoma data). Output of CibersortX was then processed in R to concatenate subpopulations of macrophages, B cells, T-CD4, NK cells, DCs and mast cells. *Ggplot2* was then used to generate stacked bar plots representing the percentage of each immune cell population. Statistical analyses between genotypes or patients' groups were computed using the Mann-Whitney test.

mMCP analyses were run in R using the mMCP counter package (https://github.com/cit-bioinfo/mMCP-counter), following instructions in Petitprez et al.[87] Stacked bar plots were generated by *ggplot2* and statistical analyses conducted as above.

Statistical analyses

Minimal sample size was set at n=3 allowing for detection of 40% increases/decreases with α=0.05, δ=0.4 and sd=1.0. Statistical analyses were conducted with R and GraphPad Prism 9. Normality of data was assessed using D'Agostino & Pearson normality test. Statistical analysis of normally distributed data was performed by two-tailed Student's *t*- test (two groups) with or without Welch's correction (as a function of variance) or one-way ANOVA (multiple groups), followed by Tukey's multiple comparisons test. Analysis of non-normally distributed data was performed by two-tailed Mann & Whitney test (two groups) or Kruskal-Wallis test followed by Dunn's multiple comparisons test (multiple groups). All bars represent the mean ± SEM.

References

1. Dart, A. Sexual dimorphism in cancer. *Nat. Rev. Cancer* **20**, 627 (2020).
2. Clocchiatti, A., Cora, E., Zhang, Y. & Dotto, G. P. Sexual dimorphism in cancer. *Nat. Rev. Cancer* **16**, 330–339 (2016).
3. Audenet, F., Méjean, A., Chartier-Kastler, E. & Rouprêt, M. Adrenal tumours are more predominant in females regardless of their histological subtype: a review. *World J. Urol.* **31**, 1037–1043 (2013).
4. Else, T. *et al.* Adrenocortical Carcinoma. *Endocr. Rev.* **35**, 282–326 (2014).
5. Lyraki, R. & Schedl, A. The Sexually Dimorphic Adrenal Cortex: Implications for Adrenal Disease. *Int. J. Mol. Sci.* **22**, 4889 (2021).
6. Ayala-Ramirez, M. *et al.* Adrenocortical carcinoma: clinical outcomes and prognosis of 330 patients at a tertiary care center. *Eur. J. Endocrinol.* **169**, 891–899 (2013).
7. Kang, T.-W. *et al.* Senescence surveillance of pre-malignant hepatocytes limits liver cancer development. *Nature* **479**, 547–551 (2011).
8. Dumontet, T. *et al.* PKA signaling drives reticularis differentiation and sexually dimorphic adrenal cortex renewal. *JCI Insight* **3**, (2018).
9. Grabek, A. *et al.* The Adult Adrenal Cortex Undergoes Rapid Tissue Renewal in a

Sex-Specific Manner. *Cell Stem Cell* **25**, 290-296.e2 (2019).
10. Baudin, E. & Endocrine Tumor Board of Gustave Roussy. Adrenocortical carcinoma. *Endocrinol. Metab. Clin. North Am.* **44**, 411–434 (2015).
11. Sada, A. *et al.* Comparison between functional and non-functional adrenocortical carcinoma. *Surgery* **167**, 216–223 (2020).
12. Shariq, O. A. & McKenzie, T. J. Adrenocortical carcinoma: current state of the art, ongoing controversies, and future directions in diagnosis and treatment. *Ther. Adv. Chronic Dis.* **12**, 20406223211033104 (2021).
13. Fassnacht, M. *et al.* Combination chemotherapy in advanced adrenocortical carcinoma. *N. Engl. J. Med.* **366**, 2189–2197 (2012).
14. Lo Iacono, M. *et al.* Molecular Mechanisms of Mitotane Action in Adrenocortical Cancer Based on In Vitro Studies. *Cancers* **13**, 5255 (2021).
15. Puglisi, S. *et al.* New perspectives for mitotane treatment of adrenocortical carcinoma. *Best Pract. Res. Clin. Endocrinol. Metab.* **34**, 101415 (2020).
16. Terzolo, M. *et al.* Adjuvant mitotane treatment for adrenocortical carcinoma. *N. Engl. J. Med.* **356**, 2372–2380 (2007).
17. Berruti, A. *et al.* Long-Term Outcomes of Adjuvant Mitotane Therapy in Patients With Radically Resected Adrenocortical Carcinoma. *J. Clin. Endocrinol. Metab.* **102**, 1358–1365 (2017).
18. Calabrese, A. *et al.* Adjuvant mitotane therapy is beneficial in non-metastatic adrenocortical carcinoma at high risk of recurrence. *Eur. J. Endocrinol.* **180**, 387–396 (2019).
19. Le Tourneau, C. *et al.* Avelumab in patients with previously treated metastatic adrenocortical carcinoma: phase 1b results from the JAVELIN solid tumor trial. *J. Immunother. Cancer* **6**, 111 (2018).
20. Carneiro, B. A. *et al.* Nivolumab in Metastatic Adrenocortical Carcinoma: Results of a Phase 2 Trial. *J. Clin. Endocrinol. Metab.* **104**, 6193–6200 (2019).
21. Habra, M. A. *et al.* Phase II clinical trial of pembrolizumab efficacy and safety in advanced adrenocortical carcinoma. *J. Immunother. Cancer* **7**, 253 (2019).
22. Raj, N. *et al.* PD-1 Blockade in Advanced Adrenocortical Carcinoma. *J. Clin. Oncol. Off. J. Am. Soc. Clin. Oncol.* **38**, 71–80 (2020).
23. Thorsson, V. *et al.* The Immune Landscape of Cancer. *Immunity* **51**, 411–412 (2019).
24. Landwehr, L.-S. *et al.* Interplay between glucocorticoids and tumor-infiltrating lymphocytes on the prognosis of adrenocortical carcinoma. *J. Immunother. Cancer* **8**, e000469 (2020).
25. Assié, G. *et al.* Integrated genomic characterization of adrenocortical carcinoma. *Nat. Genet.* (2014) doi:10.1038/ng.2953.
26. Zheng, S. *et al.* Comprehensive Pan-Genomic Characterization of Adrenocortical Carcinoma. *Cancer Cell* **29**, 723–736 (2016).
27. Koo, B.-K. *et al.* Tumour suppressor RNF43 is a stem-cell E3 ligase that induces endocytosis of Wnt receptors. *Nature* **488**, 665–669 (2012).
28. Hao, H.-X. *et al.* ZNRF3 promotes Wnt receptor turnover in an R-spondin-sensitive manner. *Nature* **485**, 195–200 (2012).
29. Basham, K. J. *et al.* A ZNRF3-dependent Wnt/β-catenin signaling gradient is required for adrenal homeostasis. *Genes Dev.* **33**, 209–220 (2019).
30. Lucas, M. *et al.* Massive inflammatory syndrome and lymphocytic immunodeficiency in KARAP/DAP12-transgenic mice. *Eur. J. Immunol.* **32**, 2653–2663 (2002).
31. Helming, L. *et al.* Essential role of DAP12 signaling in macrophage programming into a fusion-competent state. *Sci. Signal.* **1**, ra11 (2008).
32. Eggert, T. *et al.* Distinct Functions of Senescence-Associated Immune Responses in Liver Tumor Surveillance and Tumor Progression. *Cancer Cell* **30**, 533–547 (2016).

33. Truman, L. A. *et al.* CX3CL1/fractalkine is released from apoptotic lymphocytes to stimulate macrophage chemotaxis. *Blood* **112**, 5026–5036 (2008).
34. Yang, L. V., Radu, C. G., Wang, L., Riedinger, M. & Witte, O. N. Gi-independent macrophage chemotaxis to lysophosphatidylcholine via the immunoregulatory GPCR G2A. *Blood* **105**, 1127–1134 (2005).
35. Lemke, G. How macrophages deal with death. *Nat. Rev. Immunol.* **19**, 539–549 (2019).
36. Galvan, M. D., Greenlee-Wacker, M. C. & Bohlson, S. S. C1q and phagocytosis: the perfect complement to a good meal. *J. Leukoc. Biol.* **92**, 489–497 (2012).
37. Chen, J. *et al.* SLAMF7 is critical for phagocytosis of haematopoietic tumour cells via Mac-1 integrin. *Nature* **544**, 493–497 (2017).
38. Cockram, T. O. J., Dundee, J. M., Popescu, A. S. & Brown, G. C. The Phagocytic Code Regulating Phagocytosis of Mammalian Cells. *Front. Immunol.* **12**, 2144 (2021).
39. Hanayama, R. *et al.* Autoimmune disease and impaired uptake of apoptotic cells in MFG-E8-deficient mice. *Science* **304**, 1147–1150 (2004).
40. Atagi, Y. *et al.* Apolipoprotein E Is a Ligand for Triggering Receptor Expressed on Myeloid Cells 2 (TREM2). *J. Biol. Chem.* **290**, 26043–26050 (2015).
41. Nugent, A. A. *et al.* TREM2 Regulates Microglial Cholesterol Metabolism upon Chronic Phagocytic Challenge. *Neuron* **105**, 837-854.e9 (2020).
42. Lu, Q. *et al.* Tyro-3 family receptors are essential regulators of mammalian spermatogenesis. *Nature* **398**, 723–728 (1999).
43. Caberoy, N. B., Alvarado, G., Bigcas, J.-L. & Li, W. Galectin-3 is a new MerTK-specific eat-me signal. *J. Cell. Physiol.* **227**, 401–407 (2012).
44. Meyer, P. *et al.* A model of the onset of the senescence associated secretory phenotype after DNA damage induced senescence. *PLoS Comput. Biol.* **13**, e1005741 (2017).
45. Salminen, A., Kauppinen, A. & Kaarniranta, K. Emerging role of NF-κB signaling in the induction of senescence-associated secretory phenotype (SASP). *Cell. Signal.* **24**, 835–845 (2012).
46. Vesely, M. D., Kershaw, M. H., Schreiber, R. D. & Smyth, M. J. Natural innate and adaptive immunity to cancer. *Annu. Rev. Immunol.* **29**, 235–271 (2011).
47. Cheng, S. *et al.* A pan-cancer single-cell transcriptional atlas of tumor infiltrating myeloid cells. *Cell* **184**, 792-809.e23 (2021).
48. Xue, W. *et al.* Senescence and tumour clearance is triggered by p53 restoration in murine liver carcinomas. *Nature* **445**, 656–660 (2007).
49. Pittet, M. J., Michielin, O. & Migliorini, D. Clinical relevance of tumour-associated macrophages. *Nat. Rev. Clin. Oncol.* (2022) doi:10.1038/s41571-022-00620-6.
50. Zhang, L. *et al.* Single-Cell Analyses Inform Mechanisms of Myeloid-Targeted Therapies in Colon Cancer. *Cell* **181**, 442-459.e29 (2020).
51. Weiskopf, K. *et al.* CD47-blocking immunotherapies stimulate macrophage-mediated destruction of small-cell lung cancer. *J. Clin. Invest.* **126**, 2610–2620 (2016).
52. von Roemeling, C. A. *et al.* Therapeutic modulation of phagocytosis in glioblastoma can activate both innate and adaptive antitumour immunity. *Nat. Commun.* **11**, 1508 (2020).
53. Sun, L. *et al.* Activating a collaborative innate-adaptive immune response to control metastasis. *Cancer Cell* **39**, 1361-1374.e9 (2021).
54. Diaz-Jimenez, D., Kolb, J. P. & Cidlowski, J. A. Glucocorticoids as Regulators of Macrophage-Mediated Tissue Homeostasis. *Front. Immunol.* **12**, 669891 (2021).
55. Milde, R. *et al.* Multinucleated Giant Cells Are Specialized for Complement-Mediated Phagocytosis and Large Target Destruction. *Cell Rep.* **13**, 1937–1948 (2015).
56. Helming, L. & Gordon, S. Molecular mediators of macrophage fusion. *Trends Cell Biol.* **19**, 514–522 (2009).

57. de Medeiros, V. A. *et al.* Absence of multinucleated giant cell reaction as an indicator of tumor progression in oral tongue squamous cell carcinoma. *Eur. Arch. Oto-Rhino-Laryngol. Off. J. Eur. Fed. Oto-Rhino-Laryngol. Soc. EUFOS Affil. Ger. Soc. Oto-Rhino-Laryngol. - Head Neck Surg.* (2021) doi:10.1007/s00405-021-07139-z.

58. Brooks, E., Simmons-Arnold, L., Naud, S., Evans, M. F. & Elhosseiny, A. Multinucleated giant cells' incidence, immune markers, and significance: a study of 172 cases of papillary thyroid carcinoma. *Head Neck Pathol.* **3**, 95–99 (2009).

59. Lösslein, A. K. *et al.* Monocyte progenitors give rise to multinucleated giant cells. *Nat. Commun.* **12**, 2027 (2021).

60. Gal-Oz, S. T. *et al.* ImmGen report: sexual dimorphism in the immune system transcriptome. *Nat. Commun.* **10**, 4295 (2019).

61. Thion, M. S. *et al.* Microbiome Influences Prenatal and Adult Microglia in a Sex-Specific Manner. *Cell* **172**, 500-516.e16 (2018).

62. Hanamsagar, R. *et al.* Generation of a microglial developmental index in mice and in humans reveals a sex difference in maturation and immune reactivity. *Glia* **65**, 1504–1520 (2017).

63. Bain, C. C. *et al.* Rate of replenishment and microenvironment contribute to the sexually dimorphic phenotype and function of peritoneal macrophages. *Sci. Immunol.* **5**, (2020).

64. Klein, S. L. & Flanagan, K. L. Sex differences in immune responses. *Nat. Rev. Immunol.* **16**, 626–638 (2016).

65. Scotland, R. S., Stables, M. J., Madalli, S., Watson, P. & Gilroy, D. W. Sex differences in resident immune cell phenotype underlie more efficient acute inflammatory responses in female mice. *Blood* **118**, 5918–5927 (2011).

66. Mirochnik, Y. *et al.* Androgen receptor drives cellular senescence. *PloS One* **7**, e31052 (2012).

67. Mirzakhani, K. *et al.* The androgen receptor-lncRNASAT1-AKT-p15 axis mediates androgen-induced cellular senescence in prostate cancer cells. *Oncogene* **41**, 943–959 (2022).

68. Leng, S. *et al.* β-Catenin and FGFR2 regulate postnatal rosette-based adrenocortical morphogenesis. *Nat. Commun.* **11**, 1680 (2020).

69. Belenguer, G. *et al.* RNF43/ZNRF3 loss predisposes to hepatocellular-carcinoma by impairing liver regeneration and altering the liver lipid metabolic ground-state. *Nat. Commun.* **13**, 334 (2022).

70. Bingham, N. C., Verma-Kurvari, S., Parada, L. F. & Parker, K. L. Development of a steroidogenic factor 1/Cre transgenic mouse line. *Genesis* **44**, 419–24 (2006).

71. Xiang, X. *et al.* TREM2 deficiency reduces the efficacy of immunotherapeutic amyloid clearance. *EMBO Mol. Med.* **8**, 992–1004 (2016).

72. R, S., Ja, F., D, G., Af, S. & A, R. Spatial reconstruction of single-cell gene expression data. *Nat. Biotechnol.* **33**, (2015).

73. Lopez, J. P. *et al.* Single-cell molecular profiling of all three components of the HPA axis reveals adrenal ABCB1 as a regulator of stress adaptation. *Sci. Adv.* **7**, (2021).

74. Park, S.-Y. & Kim, I.-S. Engulfment signals and the phagocytic machinery for apoptotic cell clearance. *Exp. Mol. Med.* **49**, e331 (2017).

75. Lecoultre, M., Dutoit, V. & Walker, P. R. Phagocytic function of tumor-associated macrophages as a key determinant of tumor progression control: a review. *J. Immunother. Cancer* **8**, e001408 (2020).

76. Janda, E., Boi, L. & Carta, A. R. Microglial Phagocytosis and Its Regulation: A Therapeutic Target in Parkinson's Disease? *Front. Mol. Neurosci.* **11**, (2018).

77. Kuilman, T. *et al.* Oncogene-induced senescence relayed by an interleukin-dependent inflammatory network. *Cell* **133**, 1019–1031 (2008).

78. Özcan, S. *et al.* Unbiased analysis of senescence associated secretory phenotype (SASP) to identify common components following different genotoxic stresses. *Aging* **8**, 1316–1329 (2016).
79. Acosta, J. C. *et al.* A complex secretory program orchestrated by the inflammasome controls paracrine senescence. *Nat. Cell Biol.* **15**, 978–990 (2013).
80. Fridman, A. L. & Tainsky, M. A. Critical pathways in cellular senescence and immortalization revealed by gene expression profiling. *Oncogene* **27**, 5975–5987 (2008).
81. Coppé, J.-P. *et al.* Senescence-associated secretory phenotypes reveal cell-nonautonomous functions of oncogenic RAS and the p53 tumor suppressor. *PLoS Biol.* **6**, 2853–2868 (2008).
82. Coppé, J.-P., Desprez, P.-Y., Krtolica, A. & Campisi, J. The senescence-associated secretory phenotype: the dark side of tumor suppression. *Annu. Rev. Pathol.* **5**, 99–118 (2010).
83. Buhl, J. L. *et al.* The Senescence-associated Secretory Phenotype Mediates Oncogene-induced Senescence in Pediatric Pilocytic Astrocytoma. *Clin. Cancer Res. Off. J. Am. Assoc. Cancer Res.* **25**, 1851–1866 (2019).
84. Saul, D. *et al.* A New Gene Set Identifies Senescent Cells and Predicts Senescence-Associated Pathways Across Tissues. 2021.12.10.472095 (2021) doi:10.1101/2021.12.10.472095.
85. Newman, A. M. *et al.* Robust enumeration of cell subsets from tissue expression profiles. *Nat. Methods* **12**, 453–457 (2015).
86. Chen, Z. *et al.* seq-ImmuCC: Cell-Centric View of Tissue Transcriptome Measuring Cellular Compositions of Immune Microenvironment From Mouse RNA-Seq Data. *Front. Immunol.* **9**, 1286 (2018).
87. Petitprez, F. *et al.* The murine Microenvironment Cell Population counter method to estimate abundance of tissue-infiltrating immune and stromal cell populations in murine samples using gene expression. *Genome Med.* **12**, 86 (2020).

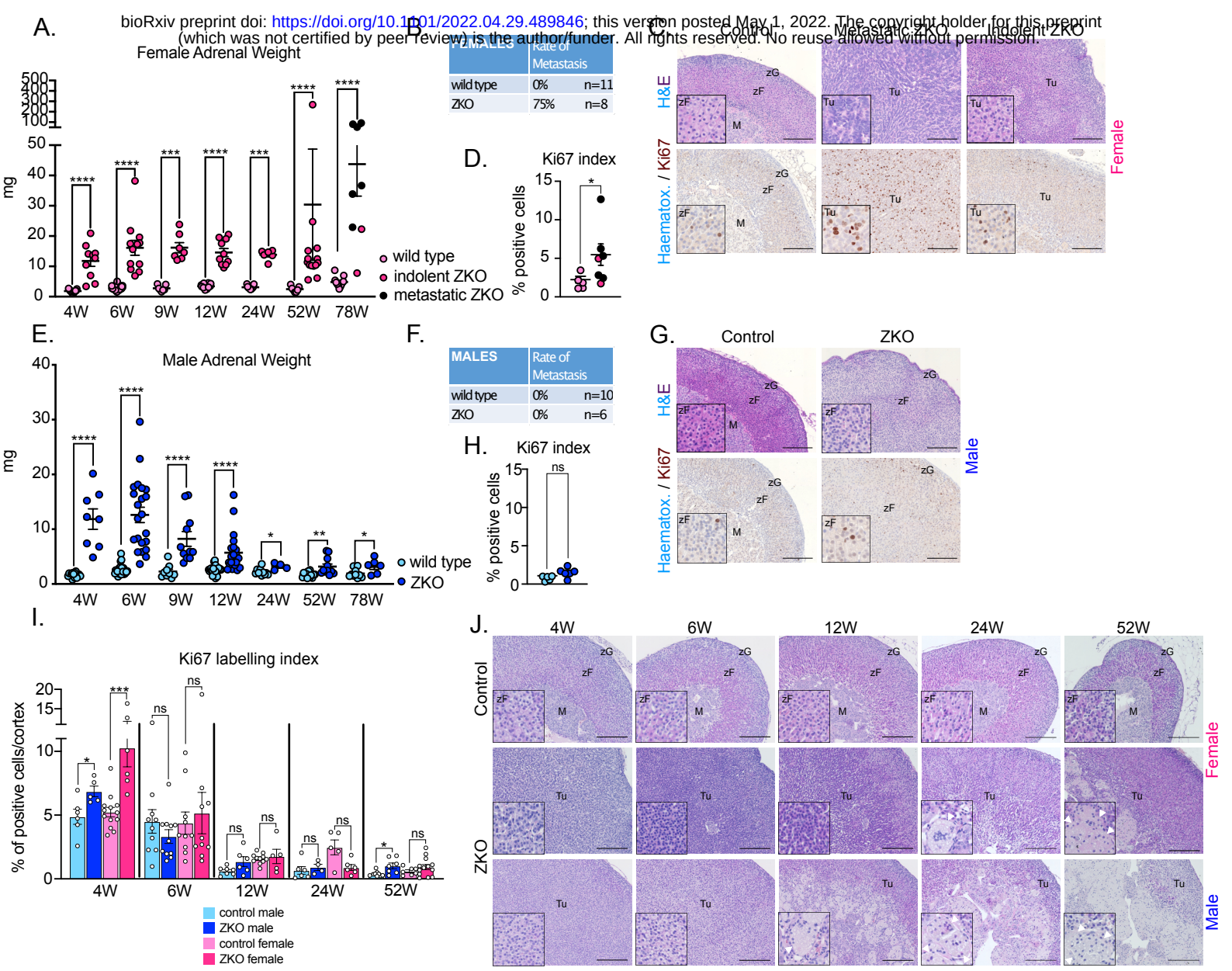

Figure 1

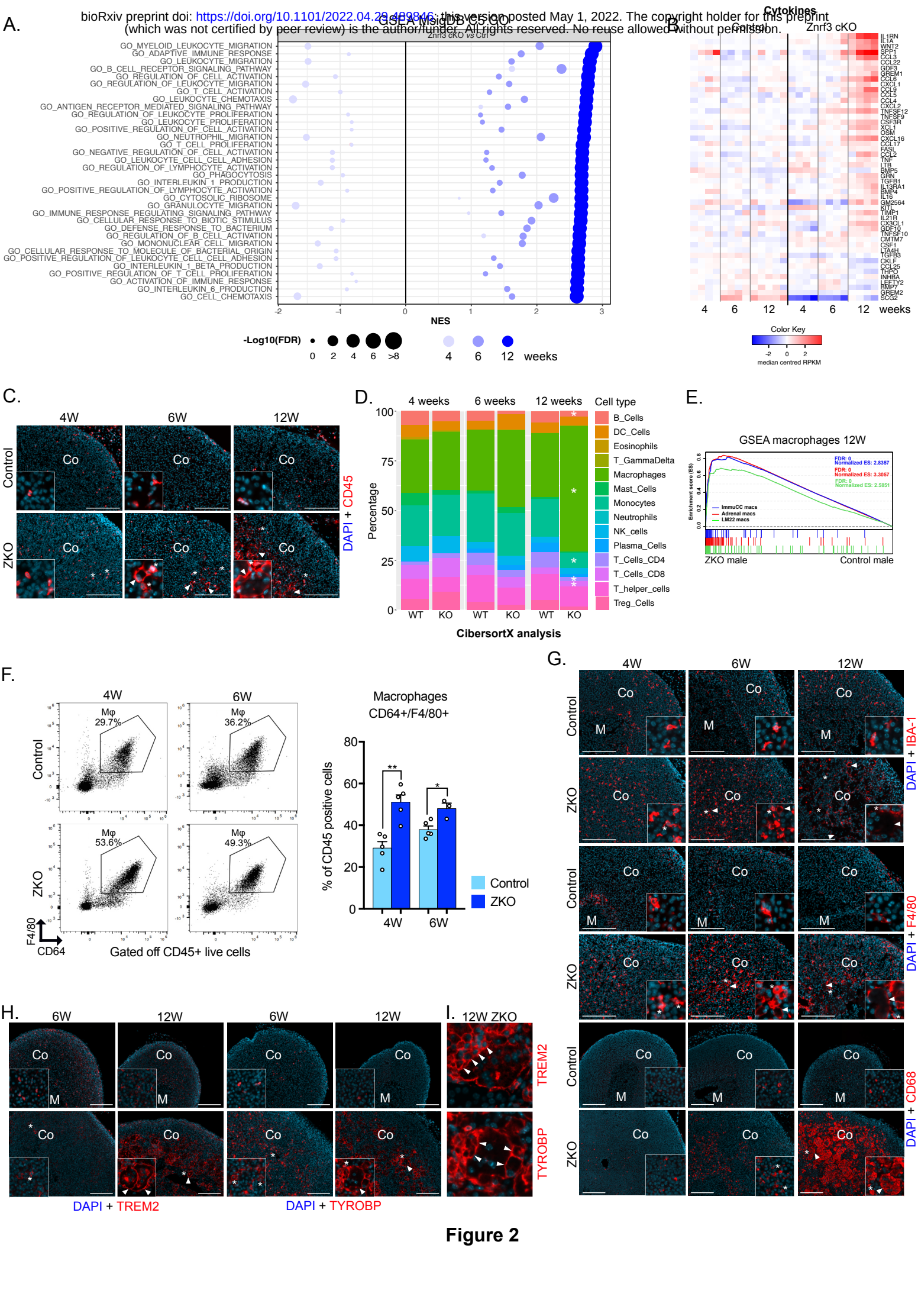

Figure 2

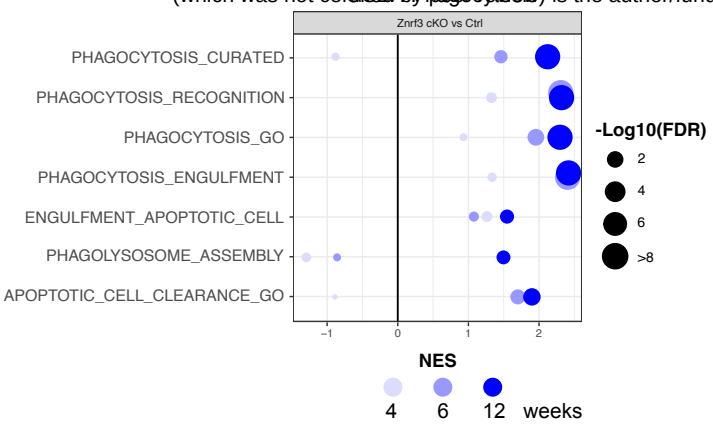

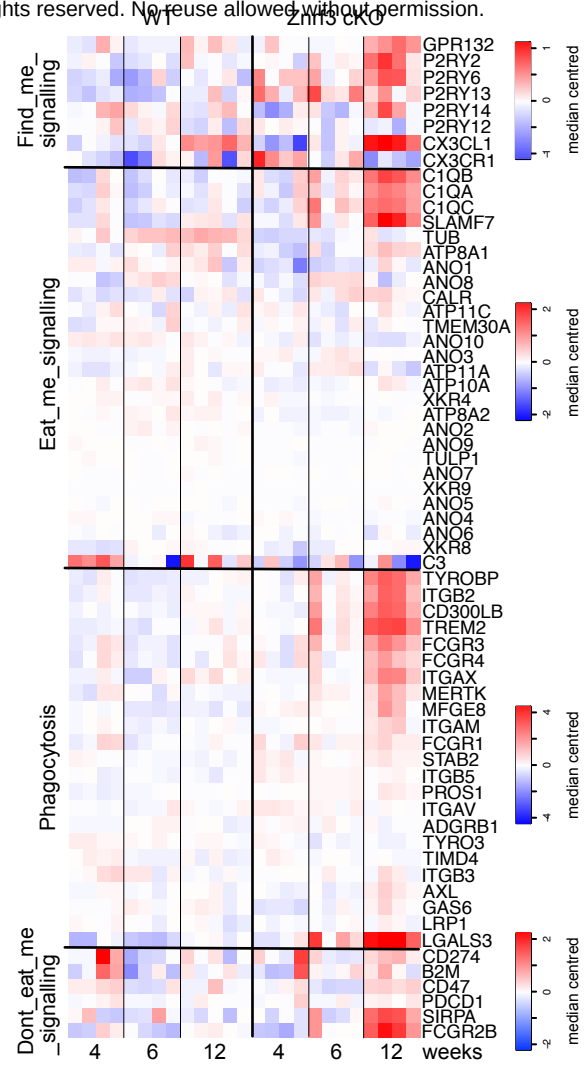

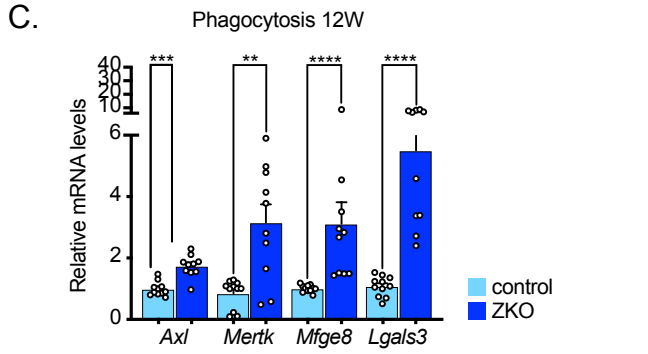

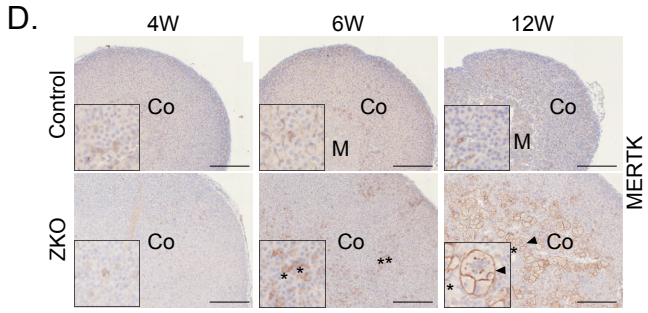

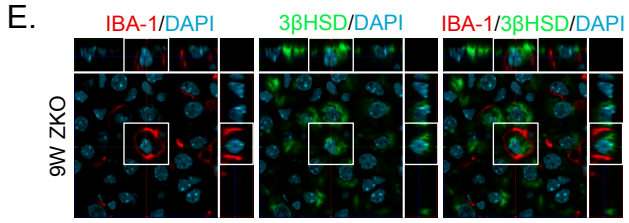

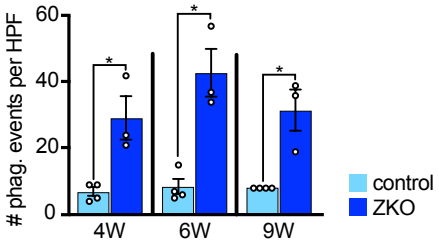

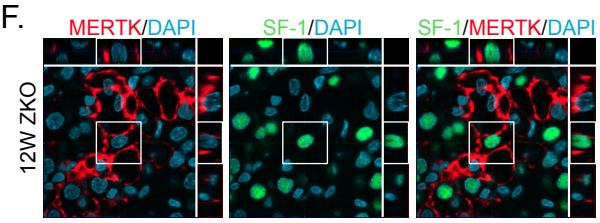

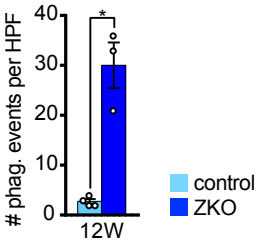

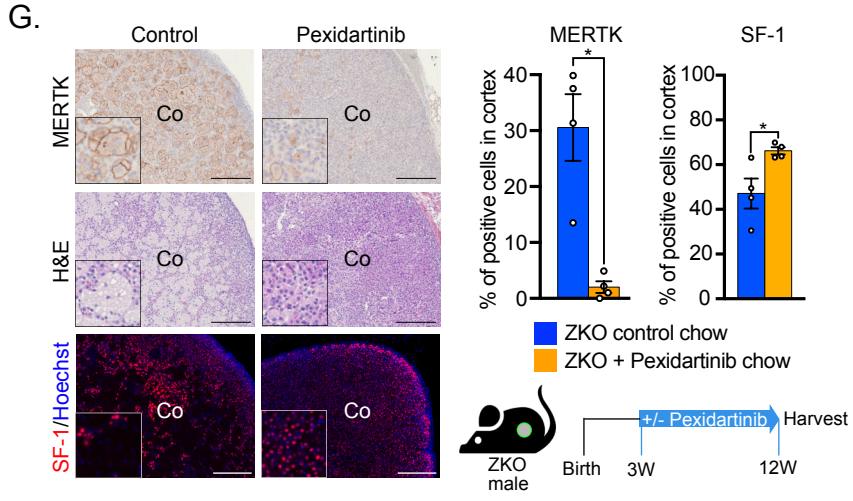

Figure 3

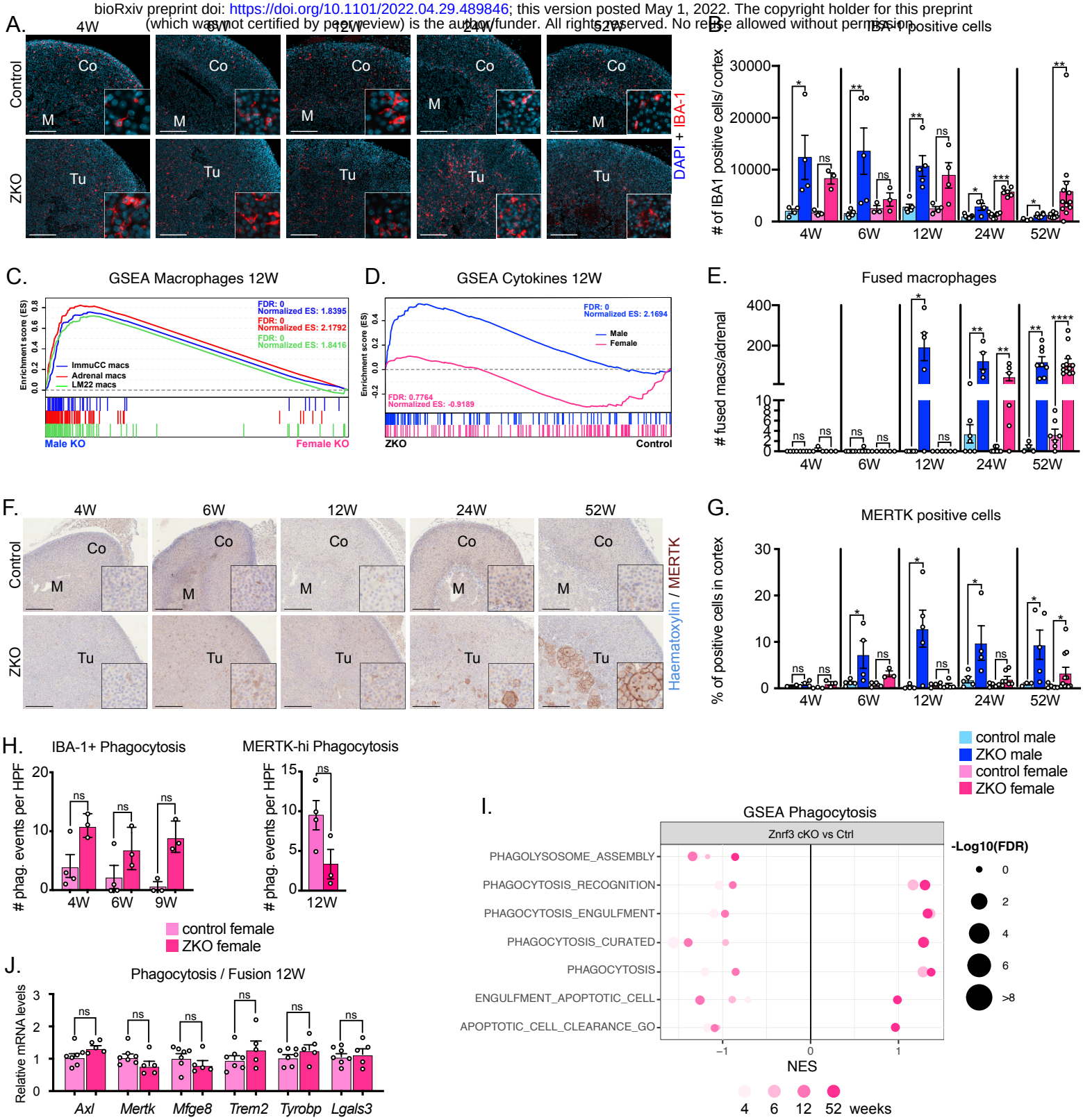

Figure 4

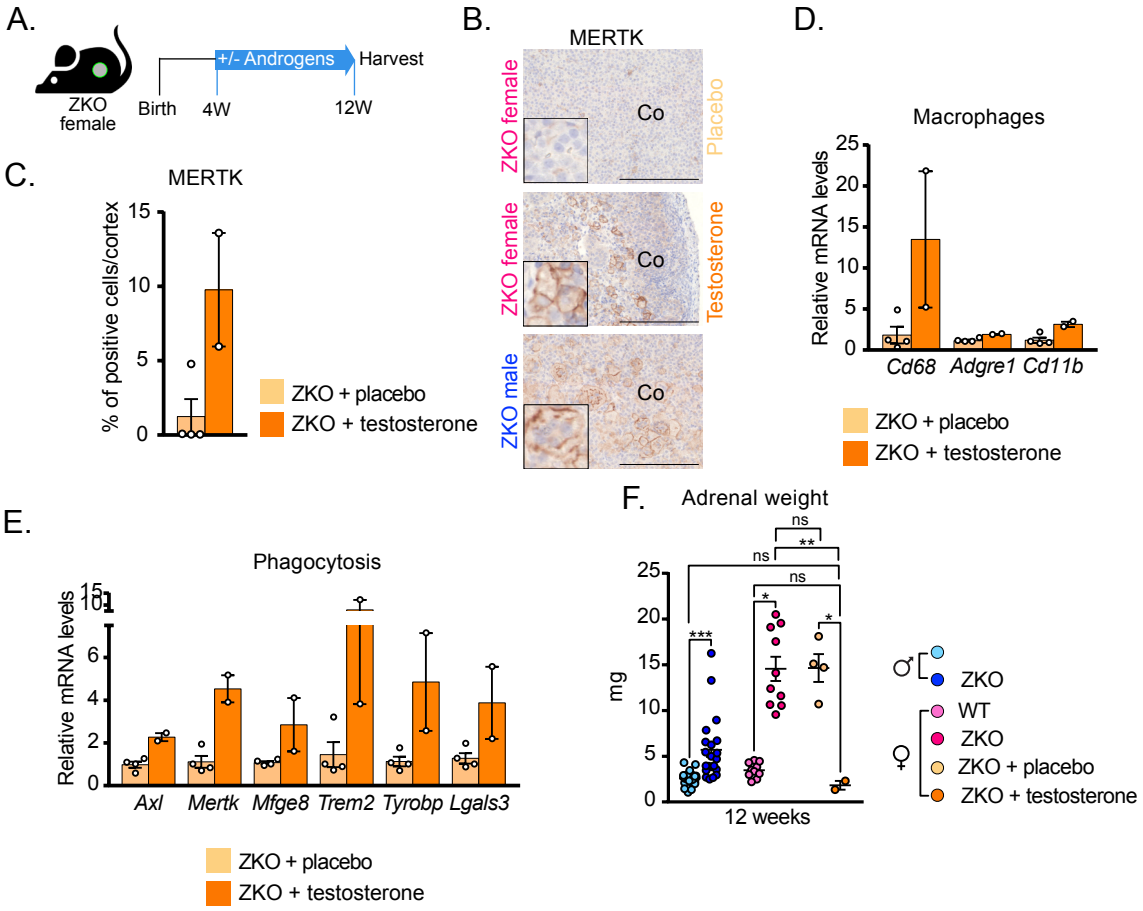

Figure 5

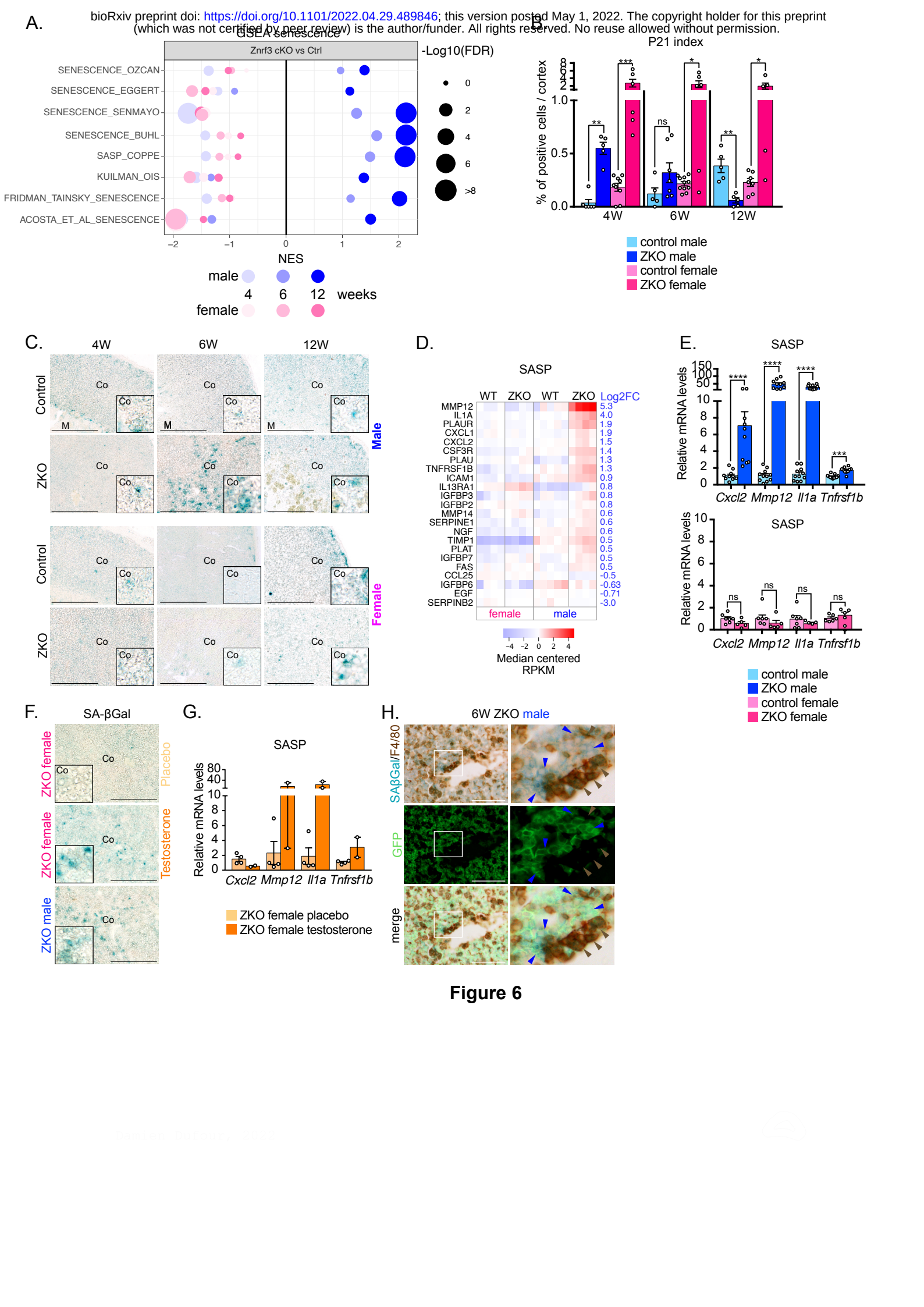

Figure 6

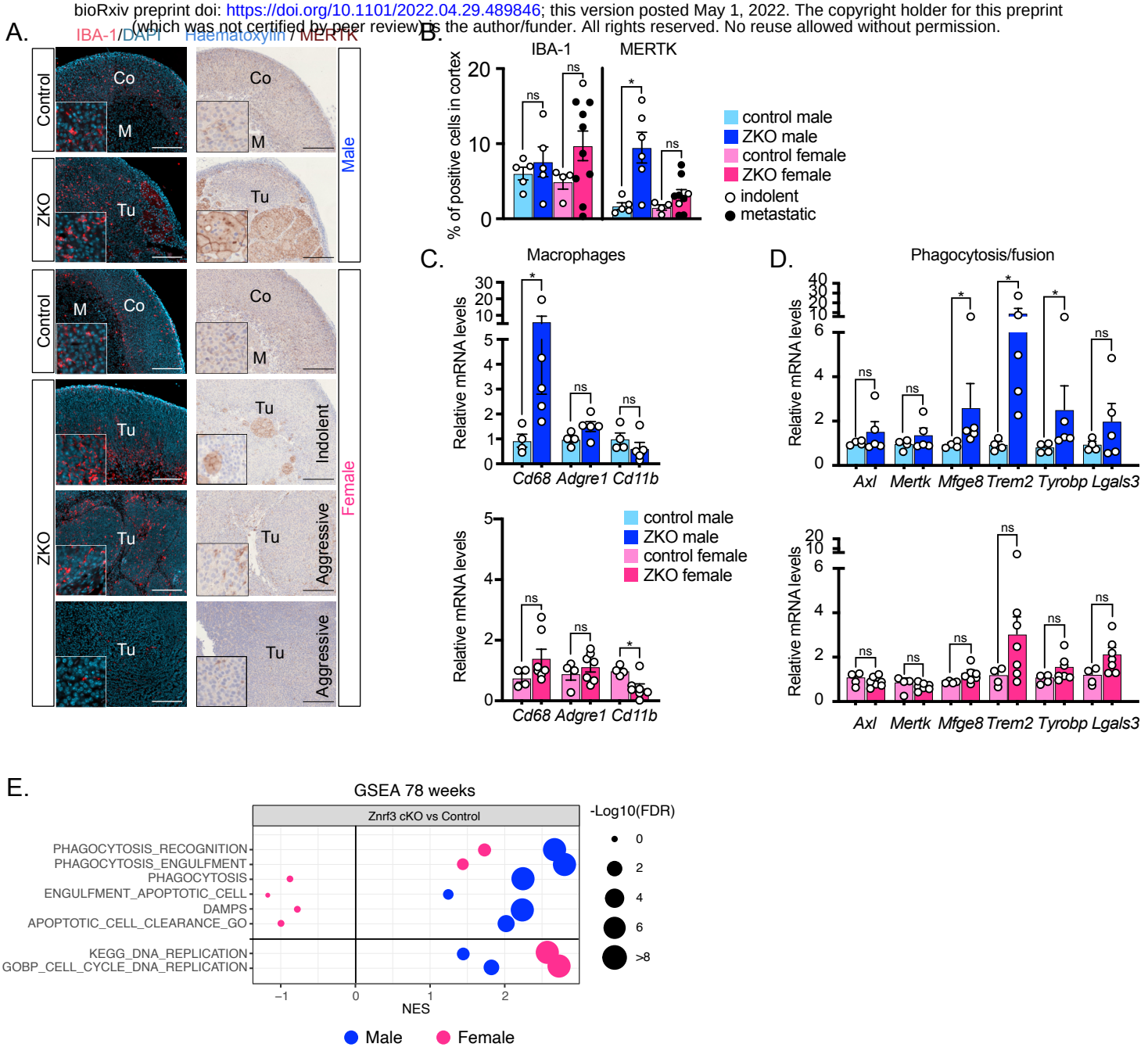

Figure 7

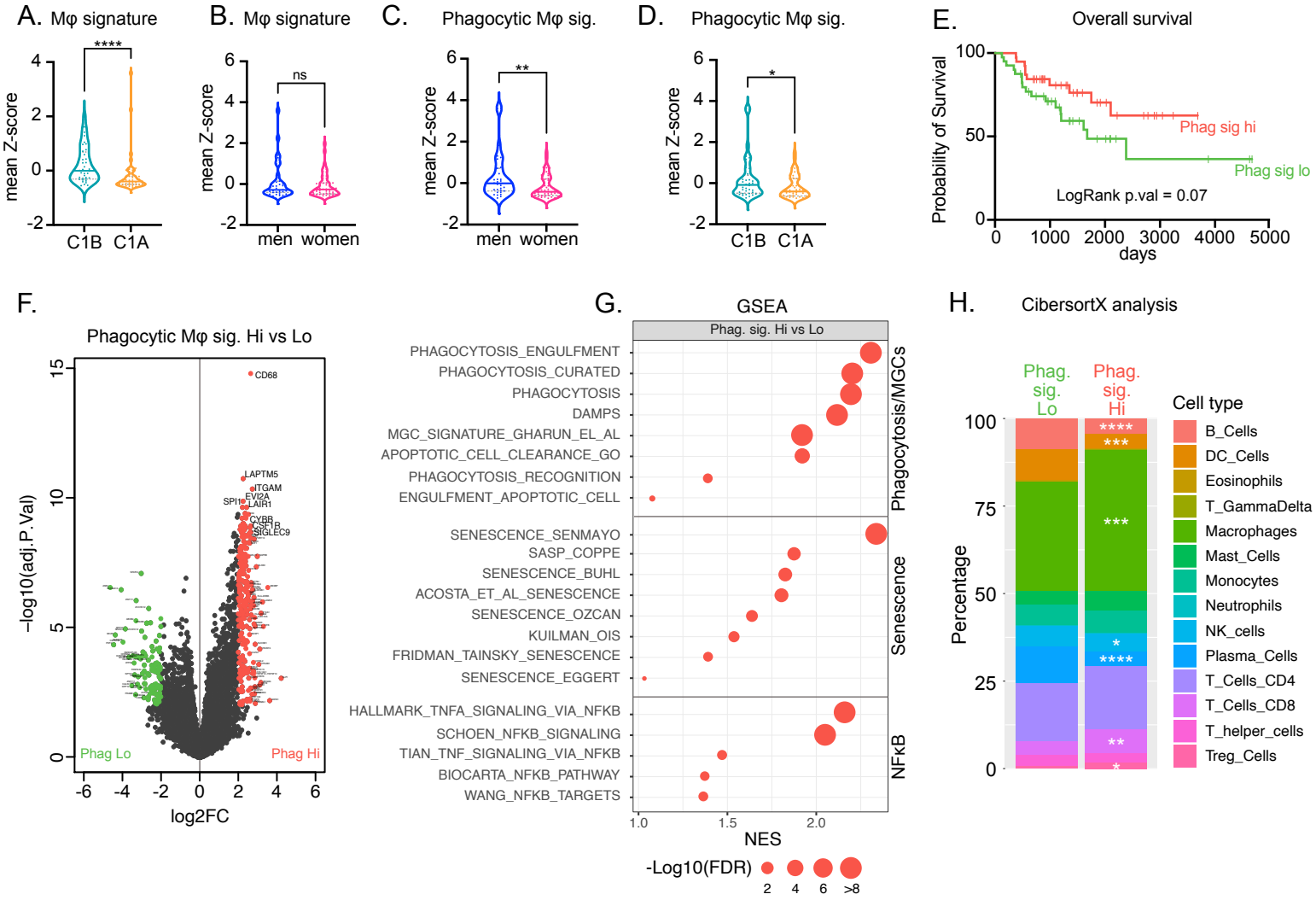

Figure 8